Mathematical Problems in Engineering

Recent Advances on the Theory and Applications of Networked Control Systems

Guest Editors: Yun-Bo Zhao, Xi-Ming Sun, Jinhui Zhang, and Peng Shi

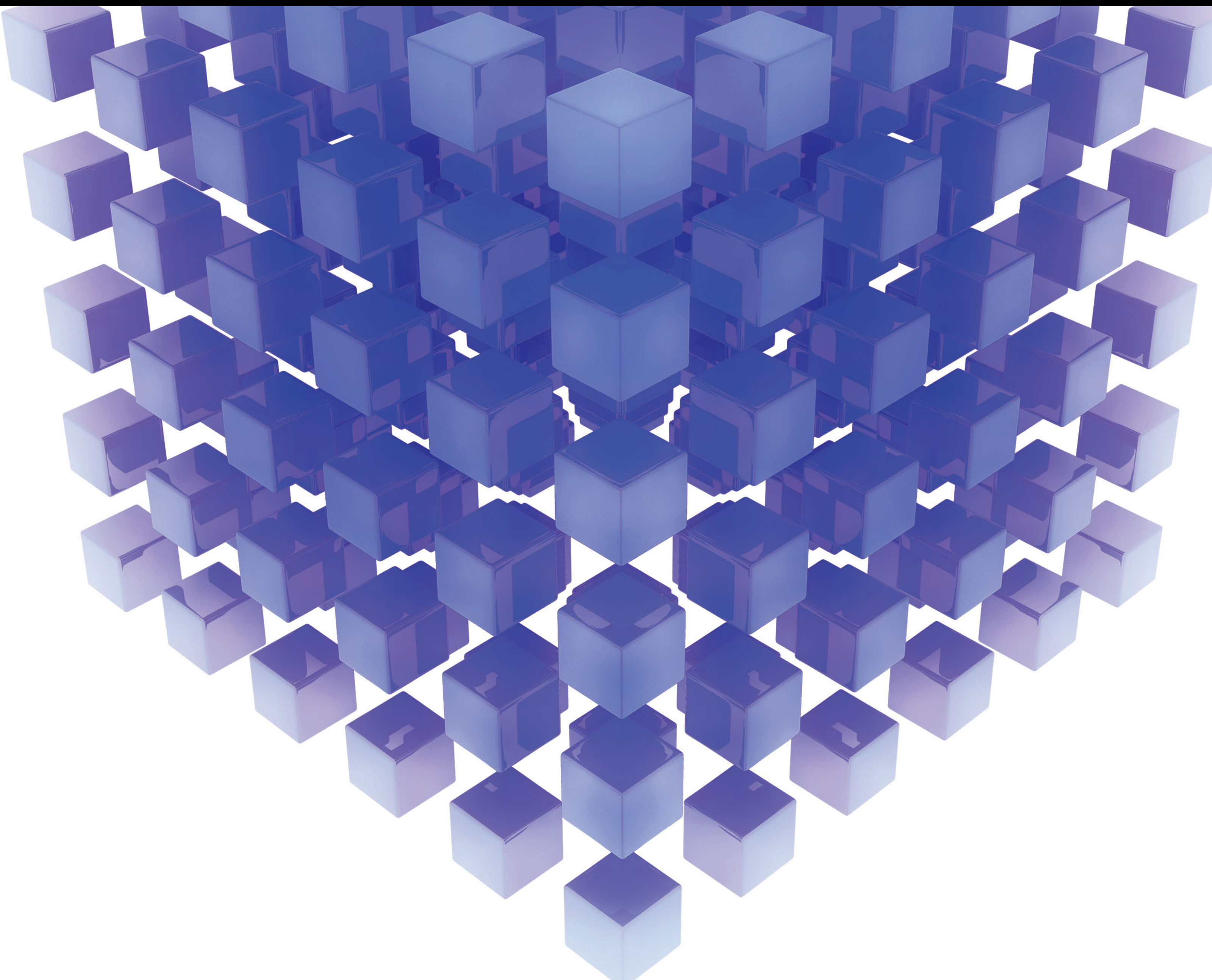

Recent Advances on the Theory and Applications of Networked Control Systems

Mathematical Problems in Engineering

Recent Advances on the Theory and Applications of Networked Control Systems

Guest Editors: Yun-Bo Zhao, Xi-Ming Sun, Jinhui Zhang, and Peng Shi

Editorial Board

Contents

Hindawi Publishing Corporation
Mathematical Problems in Engineering
Volume 2015, Article ID 239620, 2 pages
http://dx.doi.org/10.1155/2015/239620

Editorial

Recent Advances on the Theory and Applications of Networked Control Systems

Yun-Bo Zhao,[1] Xi-Ming Sun,[2] Jinhui Zhang,[3] and Peng Shi[4,5]

[1] *Department of Automation, Zhejiang University of Technology, Hangzhou 310023, China*
[2] *Research Center of Information and Control, Dalian University of Technology, Dalian 116024, China*
[3] *College of Information Science and Technology, Beijing University of Chemical Technology, Beijing 100029, China*
[4] *College of Automation, Harbin Engineering University, Harbin, Heilongjiang 150001, China*
[5] *School of Electrical and Electronic Engineering, University of Adelaide, Adelaide, SA 5005, Australia*

Correspondence should be addressed to Yun-Bo Zhao; yunbo.zhao@imperial.ac.uk

Received 10 March 2015; Accepted 10 March 2015

Networked control systems (NCSs) are control systems whose control links are closed via some form of communication networks [1, 2]. These communication networks can be either control-oriented, such as the control area network and the DeviceNet, or data networks such as the Internet which are not particularly optimized for real-time control systems. The former type of NCSs, often referred to as remote control systems, has long been an active topic in control theory and has already been successfully implemented in various industrial applications. However, it is the latter that has made NCSs an emerging research field in the recent decades, posing a number of great challenges for the control community as well as proposing even more potentially exciting applications in the future [3, 4]. Indeed, the data networks used in NCSs are featured by ubiquitous access and high throughput but have no real-time transmission or data consistency guarantee. These features have made NCSs cost-effective, maintainness-friendly, readily extendible, and reconfigurable but left a number of open questions to deal with as well [5–7].

The interest in NCSs originates with the control community, and therefore it is no wonder why NCSs have usually been regarded as control systems with only some special features, that is, the use of the data networks. With this perspective, various conventional control methods have found their applications to NCSs, contributing a major part in the early days to the research on NCSs [8]. People soon realized that the communication networks should not be only modelled as given parameters to the control systems. The active use of, or even the modification of, the communication networks can potentially give rise to much better systems performance. In fact, the codesign approach, that is, the integration of both control and communication, can be the ideal approach to NCSs [9–12].

In this special issue, a dozen of research works on NCSs and the related topics are reported. We are proud to notice that these limited numbers of research works have shown a great variety and in a sense give a fairly complete picture of the state-of-the-art research on NCSs. In addition, a brief tutorial on NCSs from the Editorial Board is also included in this special issue.

This special issue is organized in the following way.

First, theoretical studies constitute the major part of the works reported here. Various control methods have been used, for example, H_∞ output feedback control (S. H. Kim), guaranteed cost fault tolerant control (Y. Zhu et al.), and model predictive control (Q. Chen et al. and M. Li et al.). The authors have also considered different design and analysis issues in NCSs, for example, the stability of the closed-loop system (S. W. Yun et al. and A. F. Khalil and J. Wang), the robust design of NCSs (Z. Lu et al.), and the quantization effect (S. W. Yun et al.).

These theoretical studies from mainly the control perspective are then balanced with research works that have taken active consideration of the communication networks in NCSs. These include, for example, a codesign approach which integrates an event generator and a dynamic output feedback controller (D. Ma et al.) and the energy balanced redeployment algorithm for the wireless version of NCSs (G. Ye et al.). This type of works then further leads to a more network-based perspective, as seen in the works done by M. Manzano et al. and L. Du et al., where access control in ad hoc networks and pinning synchronization of switched complex dynamical networks are considered.

Finally, the special issue is concluded by the exciting applications of NCSs, which include, for example, distributed fault estimation applied to robotic manipulator (J. Chen et al.), banknote validation using RFID and NFC techniques (M. H. Eldefrawy and M. K. Khan), and the control and optimization of smart homes (J. Lai et al.).

To conclude, we believe that this Special Issue contains sufficiently interesting materials on NCSs and the related topics, both in theory and in applications. We hope this special issue will be a useful reference for people working on NCSs, and more fruitful results will be obtained in the time ahead based on the published works.

Acknowledgment

We are very grateful to the great support and encouragement from publishing and Editorial Board of this journal, which have made this project possible and successful.

Yun-Bo Zhao
Xi-Ming Sun
Jinhui Zhang
Peng Shi

References

[1] J. P. Hespanha, P. Naghshtabrizi, and Y. Xu, "A survey of recent results in networked control systems," *Proceedings of the IEEE*, vol. 95, no. 1, pp. 138–172, 2007.

[2] F.-Y. Wang and D. Liu, Eds., *Networked Control Systems: Theory and Applications*, Springer, London, UK, 1st edition, 2008.

[3] J. Baillieul and P. J. Antsaklis, "Control and communication challenges in networked real-time systems," *Proceedings of the IEEE*, vol. 95, no. 1, pp. 9–28, 2007.

[4] G. N. Nair, F. Fagnani, S. Zampieri, and R. J. Evans, "Feedback control under data rate constraints: an overview," *Proceedings of the IEEE*, vol. 95, no. 1, pp. 108–137, 2007.

[5] R. A. Gupta and M.-Y. Chow, "Networked control system: overview and research trends," *IEEE Transactions on Industrial Electronics*, vol. 57, no. 7, pp. 2527–2535, 2010.

[6] Y.-B. Zhao and G.-P. Liu, "Packet-based communication and control co-design for networked control systems," in *Frontiers of Intelligent Control and Information Processing*, chapter 5, pp. 151–174, World Scientific Publishing, Singapore, 2014.

[7] M. Zhu and S. Martinez, "On the performance analysis of resilient networked control systems under replay attacks," *IEEE Transactions on Automatic Control*, vol. 59, no. 3, pp. 804–808, 2014.

[8] T. C. Yang, "Networked control system: a brief survey," *IEE Proceedings: Control Theory and Applications*, vol. 153, no. 4, pp. 403–412, 2006.

[9] Y. B. Zhao, G. P. Liu, and D. Rees, "Integrated predictive control and scheduling co-design for networked control systems," *IET Control Theory & Applications*, vol. 2, no. 1, pp. 7–15, 2008.

[10] S.-L. Dai, H. Lin, and S. S. Ge, "Scheduling-and-control codesign for a collection of networked control systems with uncertain delays," *IEEE Transactions on Control Systems Technology*, vol. 18, no. 1, pp. 66–78, 2010.

[11] S. Longo, G. Herrmann, and P. Barber, "Robust scheduling of sampled-data networked control systems," *IEEE Transactions on Control Systems Technology*, vol. 20, no. 6, pp. 1613–1621, 2012.

[12] R. Postoyan and D. Nesic, "A framework for the observer design for networked control systems," *IEEE Transactions on Automatic Control*, vol. 57, no. 5, pp. 1309–1314, 2012.

Hindawi Publishing Corporation
Mathematical Problems in Engineering
Volume 2015, Article ID 724389, 10 pages
http://dx.doi.org/10.1155/2015/724389

Research Article

$\mathscr{H}_\infty$ Output-Feedback Tracking Control for Networked Control Systems

Sung Hyun Kim

School of Electrical Engineering, University of Ulsan, Daehak-ro 93, Nam-Gu, Ulsan 680-749, Republic of Korea

Correspondence should be addressed to Sung Hyun Kim; shnkim@ulsan.ac.kr

Received 27 May 2014; Revised 8 August 2014; Accepted 12 August 2014

Academic Editor: Yun-Bo Zhao

This paper investigates the observer-based $\mathscr{H}_\infty$ tracking problem of networked output-feedback control systems with consideration of data transmission delays, data-packet dropouts, and sampling effects. Different from other approaches, this paper offers a single-step procedure to handle nonconvex terms that appear in the process of designing observer-based output-feedback control, and then establishes a set of linear matrix inequality conditions for the solvability of the tracking problem. Finally, two numerical examples are given to illustrate the effectiveness of our result.

1. Introduction

Recently, the research on networked control systems (NCSs) has been rapidly growing due to both the fast development of technology of communication networks and the benefits of NCSs that include (1) overcoming the spatial limits of the traditional control system, (2) expanding system setups, (3) increasing flexibility, (4) multitasking, and (5) improving system diagnosis and maintenance (see [1–4]). In particular, more recently, the development of the embedded system that has various communication modules and digital signal processing (DPS) core has confirmed the necessity of further investigations on NCSs. However, it is worth noticing here that the signal transmission over communication channels inevitably gives rise to data transmission delay problem, data-packet dropout problem, and sampling problem (see [3, 5–8]), which may cause instability or serious deterioration in the performance of the resultant control systems. Thus, exploring such problems has been recognized as one of the most important issues in the application of control theory.

Over the past several years, numerous researchers have made considerable efforts to propose methods for solving the aforementioned problems, especially based on Lyapunov-Krasovskii functional approach (see [9–11] for stabilization of NCSs (S-NCSs); [12, 13] for stabilization of NOCSs (S-NOCSs); and [5, 14–16] for tracking control of NCSs (T-NCSs), where NOCSs is the abbreviation of networked output-feedback control systems). In addition, [17] investigated the problem of output tracking for NCSs on the basis of the Lyapunov function approach. However, it is worth pointing out here that, regardless of such abundant literature, little progress has been made toward solving the tracking problem of NOCSs (T-NOCSs) in light of the Lyapunov-Krasovskii functional approach. In fact, all states of the controlled plant are not fully measurable in many engineering applications, and thus the tracking problem has emerged as a topic of significant interest in parallel to the stabilization problem. Thus, it is quite meaningful to study the method of designing T-NOCSs, especially by establishing a set of linear matrix inequality (LMI) conditions for the solvability of the tracking problem.

Motivated by the above concern, we investigate the problem of designing an observer-based T-NOCS with consideration of data transmission delays, data-packet dropouts, and sampling effects. Specifically, the attention is focused on designing an observer-based NOCS in such a way that the plant state tracks the reference signal in the $\mathscr{H}_\infty$ sense. The contributions of this paper are mainly threefold.

(1) The problem of designing T-NOCSs is systematically covered with the help of the Lyapunov-Krasovskii functional approach, which helps our results to have more wide applications.

(2) A single-step procedure is proposed to handle nonconvex terms that inherently appear in the process of designing observer-based output-feedback control, which allows the derived sufficient conditions for the solvability of the tracking problem to be established in terms of LMIs.

(3) Through the control synthesis process, this paper shows that the stability criteria derived from the reciprocally convex approach [18] can be clearly applied to the problem of designing T-NOCSs, which offers the possibilities for the extension of the results [19, 20] on the stability analysis toward the design of T-NOCSs.

Finally, two numerical examples are given to illustrate the effectiveness of our result.

Notation. The Lebesgue space $\mathscr{L}_{2+} = \mathscr{L}_2[0,\infty)$ consists of square-integrable functions on $[0,\infty)$. Throughout this paper, standard notions will be adopted. The notations $X \geq Y$ and $X > Y$ mean that $X - Y$ is positive semidefinite and positive definite, respectively. In symmetric block matrices, $(*)$ is used as an ellipsis for terms that are induced by symmetry. For a square matrix $\mathcal{Q}$, the notation $\mathbf{He}(\mathcal{Q})$ denotes $\mathcal{Q}+\mathcal{Q}^T$, where $\mathcal{Q}^T$ is the transpose of $\mathcal{Q}$. $\mathbf{col}(q_1, q_2)$ is a column vector with entries q_1 and q_2 and $\mathbf{diag}(\mathcal{Q}_1, \mathcal{Q}_2)$ is a diagonal matrix with diagonal entries $\mathcal{Q}_1$ and $\mathcal{Q}_2$. All matrices, if their dimensions are not explicitly stated, are assumed to be compatible with algebraic operation.

2. System Description and Preliminaries

Consider a continuous-time plant of the following form:

$$\begin{aligned} \dot{x}(t) &= Ax(t) + Bu(t) + Dw(t), \\ y(t) &= Cx(t), \end{aligned} \tag{1}$$

where $x(t) \in \mathbb{R}^{n_x}$, $u(t) \in \mathbb{R}^{n_u}$, and $y(t) \in \mathbb{R}^{n_y}$ denote the state to be estimated, the control input, and the output, respectively, and $w(t) \in \mathbb{R}^{n_w}$ denotes the disturbance input such that $w(t) \in \mathscr{L}_{2+}$. Here, as a way to estimate the immeasurable state variables of (1), we employ the following usual state observer:

$$\begin{aligned} \dot{\hat{x}}(t) &= A\hat{x}(t) + Bu(t) - L\left(y(t) - \hat{y}(t)\right), \\ \hat{y}(t) &= C\hat{x}(t), \end{aligned} \tag{2}$$

where $\hat{x}(t) \in \mathbb{R}^{n_x}$ denotes the estimated state and $L \in \mathbb{R}^{n_x \times n_y}$ is the observer gain to be designed. Further, in parallel to (1) and (2), we incorporate the following dynamic system that generates the reference signal $x_r(t) \in \mathbb{R}^{n_x}$:

$$\dot{x}_r(t) = A_r x_r(t) + r(t), \tag{3}$$

where $r(t) \in \mathbb{R}^{n_x}$ denotes the reference input such that $r(t) \in \mathscr{L}_{2+}$ and A_r is constructed to be an asymptotically stable matrix. In this paper, our interest is to design an observer-based networked output-feedback control system (NOCS), based on (1)–(3), such that

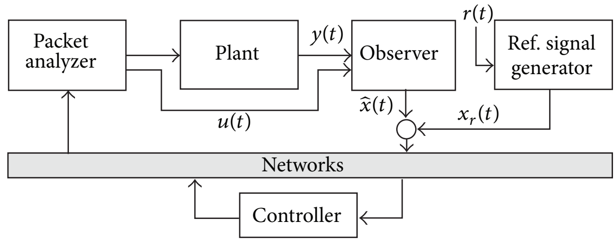

Figure 1: Networked output-feedback control systems (NOCSs) with observer-based controller.

(1) the estimated state $\hat{x}(t)$ can approach the real state $x(t)$ asymptotically;

(2) the estimated state $\hat{x}(t)$ can track a reference signal $x_r(t)$ over a communication network; that is, the state $x(t)$ can track $x_r(t)$ by (1);

(3) a guaranteed $\mathscr{H}_\infty$ tracking performance can be achieved.

To this end, we first employ the networked control system (NCS) architecture proposed in [3], which contains an observer with time-driven sampler, an event-driven controller, and a packet analyzer with event-driven holder (see Figure 1). For brevity, this paper omits the sophisticated description for the NCS under consideration since it is analogue to that of [3]. However, different from [3], we assume that the initial condition of (2) is given as $\hat{x}(t) = \phi(t)$, for $t \in [t_0 - d_M, t_0]$, and the initial condition of (3) is given as $x_r(t) = \varphi(t)$, for $t \in [t_0 - d_M, t_0]$, where t_0 denotes the initial time.

Remark 1. Here, it should be noted that, by the NCS architecture of [3], the communication constraints, such as data transmission delays and packet dropouts, can be represented in terms of piecewise continuous-time-varying delays with the lower and upper bounds.

Next, let us consider the following control law, inferred by [3]:

$$u(t) = F\left(\hat{x}(t - d(t)) - x_r(t - d(t))\right), \tag{4}$$

where $d(t) \in [d_m, d_M]$ corresponds to the piecewise continuous-time-varying delay that occurs from data transmission delays and packet dropouts. Then, by letting $e(t) = x(t) - \hat{x}(t)$ and $e_r(t) = x(t) - x_r(t)$, the control law (4) can be rewritten as

$$u(t) = F\left(e_r(t - d(t)) - e(t - d(t))\right). \tag{5}$$

Further, by setting $\tilde{x}(t) = \mathbf{col}(x_r(t), e_r(t), e(t)) \in \mathbb{R}^{3n_x}$ and $\widetilde{w}(t) = \mathbf{col}(w(t), r(t)) \in \mathbb{R}^{n_w+n_x}$ and by combining (1), (2), (3), and (5), the closed-loop system is described as

$$\begin{aligned} \dot{\tilde{x}}(t) &= \widetilde{A}\tilde{x}(t) + \widetilde{A}_d\tilde{x}(t - d(t)) + \widetilde{D}\widetilde{w}(t), \\ \tilde{z}(t) &= \widetilde{C}\tilde{x}(t) \left(= Ce_r(t)\right), \end{aligned} \tag{6}$$

where $\widetilde{z}(t) \in \mathbb{R}^{n_x}$ denotes the desired output,

$$\widetilde{A} = \begin{bmatrix} A_r & 0 & 0 \\ A - A_r & A & 0 \\ 0 & 0 & A + LC \end{bmatrix}, \qquad \widetilde{A}_d = \begin{bmatrix} 0 & 0 & 0 \\ 0 & BF & -BF \\ 0 & 0 & 0 \end{bmatrix},$$
$$\widetilde{C}^T = \begin{bmatrix} 0 \\ C^T \\ 0 \end{bmatrix}, \qquad \widetilde{D} = \begin{bmatrix} 0 & I \\ D & -I \\ D & 0 \end{bmatrix}. \tag{7}$$

Before ending this section, we present the following lemma that will be used in the proof of our main results.

Lemma 2 (see [21]). *For real matrices X, Y, and $S > 0$ with appropriate dimensions, it is satisfied that $0 \leq (X - SY)^T S^{-1}(X - SY)$ and thus the following inequality holds: $Y^T SY \geq \mathbf{He}(X^T Y) - X^T S^{-1} X$. Further if $X = \mu I$, then*

$$Y^T SY \geq \mathbf{He}(\mu Y) - \mu^2 S^{-1}, \tag{8}$$

where μ is a scalar. On the other hand, if $S < 0$, then

$$Y^T SY \leq -\mathbf{He}(\mu Y) - \mu^2 S^{-1}. \tag{9}$$

3. Main Results

Choose a Lyapunov-Krasovskii functional of the following form:

$$\begin{aligned} V(t) &= V_1(t) + V_2(t) + V_3(t), \\ V_1(t) &= \widetilde{x}^T(t) P \widetilde{x}(t), \\ V_2(t) &= \int_{t-d_m}^{t} \widetilde{x}^T(\alpha) Q_1 \widetilde{x}(\alpha)\, d\alpha + \int_{t-d_M}^{t} \widetilde{x}^T(\alpha) Q_2 \widetilde{x}(\alpha)\, d\alpha, \\ V_3(t) &= d_m \int_{-d_m}^{0} \int_{t+\alpha}^{t} \dot{\widetilde{x}}^T(\beta) R_1 \dot{\widetilde{x}}(\beta)\, d\beta d\alpha \\ &\quad + d_I \int_{-d_M}^{-d_m} \int_{t+\alpha}^{t} \dot{\widetilde{x}}^T(\beta) R_2 \dot{\widetilde{x}}(\beta)\, d\beta d\alpha, \end{aligned} \tag{10}$$

where P, Q_1, Q_2, R_1, and $R_2 \in \mathbb{R}^{3n_x \times 3n_x}$ are positive definite matrices and $d_I = d_M - d_m$. For later convenience, we define an augmented state $\zeta(t) = \mathbf{col}(\widetilde{x}(t), \widetilde{x}(t-d_m), \widetilde{x}(t-d(t)), \widetilde{x}(t-d_M), \widetilde{w}(t)) \in \mathbb{R}^{n_\eta}$, $n_\eta = 13n_x + n_w$, and then establish some block entry matrices $\mathbf{e}_i$ such that $\widetilde{x}(t) = \mathbf{e}_1\zeta(t)$, $\widetilde{x}(t - d_m) = \mathbf{e}_2\zeta(t)$, $\widetilde{x}(t - d(t)) = \mathbf{e}_3\zeta(t)$, $\widetilde{x}(t - d_M) = \mathbf{e}_4\zeta(t)$, and $\widetilde{w}(t) = \mathbf{e}_5\zeta(t)$. Then the closed-loop system (6) can be rewritten as $\dot{\widetilde{x}}(t) = \Phi_t\zeta(t)$, where $\Phi_t = \widetilde{A}\mathbf{e}_1 + \widetilde{A}_d\mathbf{e}_3 + \widetilde{D}\mathbf{e}_5$. As a result, the time derivative of $V_i(t)$ along the trajectories of (6) is given by

$$\begin{aligned} \dot{V}_1(t) &= \zeta^T(t)\, \mathbf{He}\left(\mathbf{e}_1^T P \Phi_t\right) \zeta(t), \\ \dot{V}_2(t) &= \zeta^T(t) \left(\mathbf{e}_1^T (Q_1 + Q_2)\mathbf{e}_1 - \mathbf{e}_2^T Q_1 \mathbf{e}_2 - \mathbf{e}_4^T Q_2 \mathbf{e}_4\right) \zeta(t), \\ \dot{V}_3(t) &= \zeta^T(t)\, \Phi_t^T \left(d_m^2 R_1 + d_I^2 R_2\right) \Phi_t \zeta(t) + \mathcal{O}, \end{aligned} \tag{11}$$

where

$$\begin{aligned} \mathcal{O} = &- d_m \int_{t-d_m}^{t} \dot{\widetilde{x}}^T(\alpha) R_1 \dot{\widetilde{x}}(\alpha)\, d\alpha \\ &- d_I \int_{t-d(t)}^{t-d_m} \dot{\widetilde{x}}^T(\alpha) R_2 \dot{\widetilde{x}}(\alpha)\, d\alpha \\ &- d_I \int_{t-d_M}^{t-d(t)} \dot{\widetilde{x}}^T(\alpha) R_2 \dot{\widetilde{x}}(\alpha)\, d\alpha. \end{aligned} \tag{12}$$

By (11), the time derivative of $V(t)$ becomes

$$\dot{V}(t) = \zeta^T(t)\, \Pi_0 \zeta(t) + \mathcal{O}, \tag{13}$$

where $\Pi_0 = \mathbf{He}(\mathbf{e}_1^T P \Phi_t) + \mathbf{e}_1^T(Q_1 + Q_2)\mathbf{e}_1 - \mathbf{e}_2^T Q_1 \mathbf{e}_2 - \mathbf{e}_4^T Q_2 \mathbf{e}_4 + \Phi_t^T(d_m^2 R_1 + d_I^2 R_2)\Phi_t$. To deal with $\mathcal{O}$, we apply the Jensen inequality [22] to $\mathcal{O}$, which results in

$$\begin{aligned} \mathcal{O} \leq &- \left(\int_{t-d_m}^{t} \dot{\widetilde{x}}(\alpha) d\alpha\right)^T R_1 \left(\int_{t-d_m}^{t} \dot{\widetilde{x}}(\alpha)\, d\alpha\right) \\ &- \frac{1}{\theta_1(t)} \left(\int_{t-d(t)}^{t-d_m} \dot{\widetilde{x}}(\alpha) d\alpha\right)^T R_2 \left(\int_{t-d(t)}^{t-d_m} \dot{\widetilde{x}}(\alpha)\, d\alpha\right) \\ &- \frac{1}{\theta_2(t)} \left(\int_{t-d_M}^{t-d(t)} \dot{\widetilde{x}}(\alpha) d\alpha\right)^T R_2 \left(\int_{t-d_M}^{t-d(t)} \dot{\widetilde{x}}(\alpha)\, d\alpha\right) \\ = &- \zeta^T(t) (\mathbf{e}_1 - \mathbf{e}_2)^T R_1 (\mathbf{e}_1 - \mathbf{e}_2) \zeta(t) \\ &- \frac{1}{\theta_1(t)} \zeta^T(t) (\mathbf{e}_2 - \mathbf{e}_3)^T R_2 (\mathbf{e}_2 - \mathbf{e}_3) \zeta(t) \\ &- \frac{1}{\theta_2(t)} \zeta^T(t) (\mathbf{e}_3 - \mathbf{e}_4)^T R_2 (\mathbf{e}_3 - \mathbf{e}_4) \zeta(t), \end{aligned} \tag{14}$$

where $\theta_1(t) = (d(t) - d_m)/d_I \geq 0$, $\theta_2(t) = (d_M - d(t))/d_I \geq 0$, and $\theta_1(t) + \theta_2(t) = 1$; that is, the set of $\theta_i(t)$ is convex. Furthermore, by taking the convexity of $\theta_i(t)$ into account, we can get the following equality:

$$\begin{aligned} &\text{RHS of (14)} \\ &= \zeta^T(t) \left((\mathbf{e}_1 - \mathbf{e}_2)^T R_1 (\mathbf{e}_2 - \mathbf{e}_1) + (\mathbf{e}_2 - \mathbf{e}_3)^T R_2 (\mathbf{e}_3 - \mathbf{e}_2) \right. \\ &\qquad \left. + (\mathbf{e}_3 - \mathbf{e}_4)^T R_2 (\mathbf{e}_4 - \mathbf{e}_3)\right) \zeta(t) \\ &\quad - \frac{\theta_2(t)}{\theta_1(t)} \zeta^T(t) (\mathbf{e}_2 - \mathbf{e}_3)^T R_2 (\mathbf{e}_2 - \mathbf{e}_3) \zeta(t) \\ &\quad - \frac{\theta_1(t)}{\theta_2(t)} \zeta^T(t) (\mathbf{e}_3 - \mathbf{e}_4)^T R_2 (\mathbf{e}_3 - \mathbf{e}_4) \zeta(t) \end{aligned}$$

$$= \zeta^T(t)\Pi_1\zeta(t) - \begin{bmatrix} \sqrt{\frac{\theta_2}{\theta_1}}(\mathbf{e}_2 - \mathbf{e}_3)\zeta(t) \\ \sqrt{\frac{\theta_1}{\theta_2}}(\mathbf{e}_3 - \mathbf{e}_4)\zeta(t) \end{bmatrix}^T \times \Pi_2 \begin{bmatrix} \sqrt{\frac{\theta_2}{\theta_1}}(\mathbf{e}_2 - \mathbf{e}_3)\zeta(t) \\ \sqrt{\frac{\theta_1}{\theta_2}}(\mathbf{e}_3 - \mathbf{e}_4)\zeta(t) \end{bmatrix}, \tag{15}$$

where $\Pi_1 = (\mathbf{e}_1 - \mathbf{e}_2)^T R_1(\mathbf{e}_2 - \mathbf{e}_1) + (\mathbf{e}_2 - \mathbf{e}_3)^T R_2(\mathbf{e}_3 - \mathbf{e}_2) + (\mathbf{e}_3 - \mathbf{e}_4)^T R_2(\mathbf{e}_4 - \mathbf{e}_3) + \mathbf{He}((\mathbf{e}_2 - \mathbf{e}_3)^T S(\mathbf{e}_3 - \mathbf{e}_4))$,

$$\Pi_2 = \begin{bmatrix} R_2 & S \\ (*) & R_2 \end{bmatrix}. \tag{16}$$

Hence, we can see that the time derivative of $V(t)$ satisfies that $\dot{V}(t) \leq \zeta^T(t)(\Pi_0 + \Pi_1)\zeta(t) - (\star)^T\Pi_2(\star)$, where $(\star) = \mathbf{col}(\sqrt{\theta_2/\theta_1}(\mathbf{e}_2 - \mathbf{e}_3)\zeta(t), \sqrt{\theta_1/\theta_2}(\mathbf{e}_3 - \mathbf{e}_4)\zeta(t))$. As a result, based on this derivation, the following stability criteria can be established.

Lemma 3 (stability criterion). *For $\widetilde{w}(t) = 0$, the stability criterion is given by*

$$0 > \Pi_0 + \Pi_1, \qquad 0 \leq \Pi_2, \tag{17}$$

where $\Phi_t = \widetilde{A}\mathbf{e}_1 + \widetilde{A}_d\mathbf{e}_3$.

Proof. If $\Pi_2 \geq 0$ holds, then $\dot{V}(t) \leq \zeta^T(t)(\Pi_0 + \Pi_1)\zeta(t)$. □

Lemma 4 (stability criterion in the $\mathscr{H}_\infty$ sense). *The stability criterion in the $\mathscr{H}_\infty$ sense is given by*

$$0 > \Pi_0 + \Pi_1 + \Pi_3, \qquad 0 \leq \Pi_2, \tag{18}$$

where $\Phi_t = \widetilde{A}\mathbf{e}_1 + \widetilde{A}_d\mathbf{e}_3 + \widetilde{D}\mathbf{e}_5$, $\Pi_3 = \mathbf{e}_1^T\widetilde{C}^T\widetilde{C}\mathbf{e}_1 - \gamma^2\mathbf{e}_5^T\mathbf{e}_5$.

Proof. Let us consider the $\mathscr{H}_\infty$ tracking performance such that $\sup_{\widetilde{w}}(\|\widetilde{z}\|_2/\|\widetilde{w}\|_2) < \gamma$. Then, as reported in [19], the $\mathscr{H}_\infty$ stability criterion can be readily derived by $\dot{V}(t) + \widetilde{z}^T(t)\widetilde{z}(t) - \gamma^2\widetilde{w}^T(t)\widetilde{w}(t) < 0$, which is assured by (18). □

Based on Lemma 3, the stabilization problem of (6) with $\widetilde{w}(t) = 0$ will be addressed in Section 3.1, and further, based on Lemma 4, the $\mathscr{H}_\infty$ stabilization problem of (6) with $\widetilde{w}(t) \neq 0$ will be investigated in Section 3.2. Here, to derive a set of linear matrix inequalities (LMIs), we first set $P = \mathbf{diag}(P_1, P_2, P_3)$ and $\overline{P} = P^{-1} = \mathbf{diag}(\overline{P}_1, \overline{P}_2, \overline{P}_3)$, where $\overline{P}_1 = P_1^{-1}$, $\overline{P}_2 = P_2^{-1}$, and $\overline{P}_3 = P_3^{-1}$. Then, from (7), it follows that

$$P\widetilde{A} = \begin{bmatrix} P_1A_r & 0 & 0 \\ P_2A - P_2A_r & P_2A & 0 \\ 0 & 0 & P_3A + \overline{L}C \end{bmatrix},$$

$$P\widetilde{A}_d = \begin{bmatrix} 0 & 0 & 0 \\ 0 & P_2B\overline{F}P_2 & -P_2B\overline{F}P_2 \\ 0 & 0 & 0 \end{bmatrix}, \qquad P\widetilde{D} = \begin{bmatrix} 0 & P_1 \\ P_2D & -P_2 \\ P_3D & 0 \end{bmatrix}, \tag{19}$$

where $\overline{L} = P_3L$ and $\overline{F} = F\overline{P}_2$. Accordingly, the term $P\Phi_t$ becomes

$$P\Phi_t = X\breve{A}X\mathbf{e}_1 + X\breve{A}_dX\mathbf{e}_3 + X\breve{D}\mathbf{e}_5, \tag{20}$$

where $X = \mathbf{diag}(I, P_2, P_2)$,

$$\breve{A} = \begin{bmatrix} P_1A_r & 0 & 0 \\ A - A_r & A\overline{P}_2 & 0 \\ 0 & 0 & \overline{P}_2\left(P_3A + \overline{L}C\right)\overline{P}_2 \end{bmatrix},$$

$$\breve{A}_d = \begin{bmatrix} 0 & 0 & 0 \\ 0 & B\overline{F} & -B\overline{F} \\ 0 & 0 & 0 \end{bmatrix}, \qquad \breve{D} = \begin{bmatrix} 0 & P_1 \\ D & -I \\ \overline{P}_2P_3D & 0 \end{bmatrix}. \tag{21}$$

Remark 5. Inspired by the work of [18], this paper also applied the reciprocally convex approach to reduce the computational complexity and the conservatism of the delay-dependent stability criteria that will be used to derive our main results.

3.1. Control Design for $\widetilde{w}(t) = 0$

Lemma 6. *Let $\mu_1 > 0$, $\mu_2 > 0$, and $\epsilon > 0$ be prescribed. Suppose that there exist matrices $\overline{F} \in \mathbb{R}^{n_u \times n_x}$, $\overline{L} \in \mathbb{R}^{n_x \times n_y}$, and $\widetilde{S} \in \mathbb{R}^{3n_x \times 3n_x}$ and symmetric matrices $0 < P_1, \overline{P}_2, P_3 \in \mathbb{R}^{n_x \times n_x}$, $0 < \widetilde{Q}_1, \widetilde{Q}_2 \in \mathbb{R}^{3n_x \times 3n_x}$, $0 < \widetilde{R}_1, \widetilde{R}_2 \in \mathbb{R}^{3n_x \times 3n_x}$ such that*

$$0 > \left[\begin{array}{cc|ccccc|c} (1,1) & 0 & d_m\overline{A} & 0 & d_m\breve{A}_d & 0 & \epsilon E_1 \\ 0 & (2,2) & d_I\overline{A} & 0 & d_I\breve{A}_d & 0 & \epsilon E_2 \\ \hline (*) & (*) & (3,3) & \widetilde{R}_1 & \breve{A}_d & 0 & \epsilon E_3 \\ 0 & 0 & (*) & (4,4) & \widetilde{R}_2 + \widetilde{S} & -\widetilde{S} & 0 \\ (*) & (*) & (*) & (*) & (5,5) & \widetilde{R}_2 + \widetilde{S} & 0 \\ 0 & 0 & 0 & (*) & (*) & (6,6) & 0 \\ \hline (*) & (*) & (*) & 0 & 0 & 0 & (7,7) \end{array}\right], \tag{22}$$

$$0 \leq \begin{bmatrix} \widetilde{R}_2 & \widetilde{S} \\ (*) & \widetilde{R}_2 \end{bmatrix}, \tag{23}$$

where

$$(1,1) = \mu_1^2\widetilde{R}_1 + \mathbf{diag}\left(-2\mu_1P_1, -2\mu_1\overline{P}_2, -2\epsilon\overline{P}_2\right),$$

$$(2,2) = \mu_2^2\widetilde{R}_2 + \mathbf{diag}\left(-2\mu_2P_1, -2\mu_2\overline{P}_2, -2\epsilon\overline{P}_2\right),$$

$$(3,3) = \overline{\overline{A}} + \widetilde{Q}_1 + \widetilde{Q}_2 - \widetilde{R}_1,$$

$$(4,4) = -\widetilde{Q}_1 - \widetilde{R}_1 - \widetilde{R}_2,$$

$$(5,5) = -2\widetilde{R}_2 - \mathbf{He}\left(\widetilde{S}\right), \qquad (6,6) = -\widetilde{Q}_2 - \widetilde{R}_2,$$

$$(7,7) = \begin{bmatrix} -2\mu_1P_3 & 0 & d_m\left(P_3A + \overline{L}C\right) \\ 0 & -2\mu_2P_3 & d_I\left(P_3A + \overline{L}C\right) \\ (*) & (*) & \mathbf{He}\left(P_3A + \overline{L}C\right) \end{bmatrix},$$

$$\breve{A}_d = \begin{bmatrix} 0 & 0 & 0 \\ 0 & B\overline{F} & -B\overline{F} \\ 0 & 0 & 0 \end{bmatrix},$$

$$\overline{A} = \begin{bmatrix} P_1A_r & 0 & 0 \\ A - A_r & A\overline{P}_2 & 0 \\ 0 & 0 & 0 \end{bmatrix},$$

$$\overline{\overline{A}} = \begin{bmatrix} \mathbf{He}\left(P_1A_r\right) & \left(A - A_r\right)^T & 0 \\ (*) & \mathbf{He}\left(A\overline{P}_2\right) & 0 \\ 0 & 0 & -2\epsilon\overline{P}_2 \end{bmatrix},$$

$$E_1 = \begin{bmatrix} 0 & 0 & 0 \\ 0 & 0 & 0 \\ I & 0 & 0 \end{bmatrix}, \qquad E_2 = \begin{bmatrix} 0 & 0 & 0 \\ 0 & 0 & 0 \\ 0 & I & 0 \end{bmatrix},$$

$$E_3 = \begin{bmatrix} 0 & 0 & 0 \\ 0 & 0 & 0 \\ 0 & 0 & I \end{bmatrix}. \tag{24}$$

Then the closed-loop system (6) *is asymptotically stable in the absence of $\widetilde{w}(t)$ for any time-varying delay $d(t)$ satisfying $d_m \le d(t) \le d_M$. Moreover, the control and observer gain matrices can be reconstructed as follows:*

$$F = \overline{F}\,\overline{P}_2^{-1}, \qquad L = P_3^{-1}\overline{L}. \tag{25}$$

Proof. From Lemma 3, the stabilization condition is given as follows: (i) $0 \le \Pi_2$ and (ii) $0 > \Pi_0 + \Pi_1 = \mathbf{He}(\mathbf{e}_1^T P\Phi_t) + \mathbf{e}_1^T(Q_1 + Q_2)\mathbf{e}_1 - \mathbf{e}_2^T Q_1\mathbf{e}_2 - \mathbf{e}_4^T Q_2\mathbf{e}_4 + \Phi_t^T(d_m^2R_1 + d_I^2R_2)\Phi_t + (\mathbf{e}_1-\mathbf{e}_2)^T R_1(\mathbf{e}_2-\mathbf{e}_1) + (\mathbf{e}_2-\mathbf{e}_3)^T R_2(\mathbf{e}_3-\mathbf{e}_2) + (\mathbf{e}_3-\mathbf{e}_4)^T R_2(\mathbf{e}_4-\mathbf{e}_3) + \mathbf{He}((\mathbf{e}_2-\mathbf{e}_3)^T S(\mathbf{e}_3-\mathbf{e}_4))$, where $\Phi_t = \widetilde{A}\mathbf{e}_1 + \widetilde{A}_d\mathbf{e}_3$ and thus $P\Phi_t = X\breve{A}X\mathbf{e}_1 + X\breve{A}_dX\mathbf{e}_3$. Let us consider the condition given in (ii). Then, by letting $\overline{R}_1 = X\overline{P}R_1\overline{P}X$ and $\overline{R}_2 = X\overline{P}R_2\overline{P}X$, we can rewrite the condition, $0 > \Pi_0 + \Pi_1$, as follows:

$$\begin{aligned} 0 > {} & \mathbf{He}\left(\mathbf{e}_1^T X\breve{A}X\mathbf{e}_1 + \mathbf{e}_1^T X\breve{A}_dX\mathbf{e}_3\right) + \mathbf{e}_1^T\left(Q_1 + Q_2\right)\mathbf{e}_1 \\ & - \mathbf{e}_2^T Q_1\mathbf{e}_2 - \mathbf{e}_4^T Q_2\mathbf{e}_4 + \left(X\breve{A}X\mathbf{e}_1 + X\breve{A}_dX\mathbf{e}_3\right)^T \\ & \times \overline{X}\left(d_m^2\overline{R}_1 + d_I^2\overline{R}_2\right)\overline{X}\left(X\breve{A}X\mathbf{e}_1 + X\breve{A}_dX\mathbf{e}_3\right) \\ & + \left(\mathbf{e}_1 - \mathbf{e}_2\right)^T P\overline{X}R_1\overline{X}P\left(\mathbf{e}_2 - \mathbf{e}_1\right) \\ & + \left(\mathbf{e}_2 - \mathbf{e}_3\right)^T P\overline{X}R_2\overline{X}P\left(\mathbf{e}_3 - \mathbf{e}_2\right) \\ & + \left(\mathbf{e}_3 - \mathbf{e}_4\right)^T P\overline{X}R_2\overline{X}P\left(\mathbf{e}_4 - \mathbf{e}_3\right) \\ & + \mathbf{He}\left(\left(\mathbf{e}_2 - \mathbf{e}_3\right)^T S\left(\mathbf{e}_3 - \mathbf{e}_4\right)\right), \end{aligned} \tag{26}$$

where $\overline{X} = X^{-1}$. Further, since $\mathbf{diag}(\overline{X},\overline{X},\overline{X},\overline{X})\mathbf{e}_i^T = \mathbf{e}_i^T\overline{X}$ $(i = 1, 2, 3, 4)$, pre- and postmultiplying both sides of (26) by $\mathbf{diag}(\overline{X},\overline{X},\overline{X},\overline{X})$ and its transpose yield

$$0 > \mathcal{Q} + \left(\breve{A}\mathbf{e}_1 + \breve{A}_d\mathbf{e}_3\right)^T\left(d_m^2\overline{R}_1 + d_I^2\overline{R}_2\right)\left(\breve{A}\mathbf{e}_1 + \breve{A}_d\mathbf{e}_3\right), \tag{27}$$

where $\mathcal{Q} = \mathbf{He}(\mathbf{e}_1^T\breve{A}\mathbf{e}_1 + \mathbf{e}_1^T\breve{A}_d\mathbf{e}_3) + \mathbf{e}_1^T(\widetilde{Q}_1 + \widetilde{Q}_2)\mathbf{e}_1 - \mathbf{e}_2^T\widetilde{Q}_1\mathbf{e}_2 - \mathbf{e}_4^T\widetilde{Q}_2\mathbf{e}_4 + (\mathbf{e}_1-\mathbf{e}_2)^T\widetilde{R}_1(\mathbf{e}_2-\mathbf{e}_1) + (\mathbf{e}_2-\mathbf{e}_3)^T\widetilde{R}_2(\mathbf{e}_3-\mathbf{e}_2) + (\mathbf{e}_3-\mathbf{e}_4)^T\widetilde{R}_2(\mathbf{e}_4-\mathbf{e}_3) + \mathbf{He}((\mathbf{e}_2-\mathbf{e}_3)^T\widetilde{S}(\mathbf{e}_3-\mathbf{e}_4))$ in which $\widetilde{Q}_1 = \overline{X}Q_1\overline{X}$, $\widetilde{Q}_2 = \overline{X}Q_2\overline{X}$, $\widetilde{R}_1 = \overline{X}\,\overline{R}_1\overline{X}$, $\widetilde{R}_2 = \overline{X}\,\overline{R}_2\overline{X}$, $\widetilde{S} = \overline{X}S\overline{X}$, and $\widetilde{X} = \overline{X}P\overline{X} = \mathbf{diag}(P_1, \overline{P}_2, \overline{P}_2P_3\overline{P}_2) > 0$. That is, by applying the Schur complement to (27), we can get

$$0 > \left[\begin{array}{cc|c} -\overline{R}_1^{-1} & 0 & d_m\left(\breve{A}\mathbf{e}_1 + \breve{A}_d\mathbf{e}_3\right) \\ 0 & -\overline{R}_2^{-1} & d_I\left(\breve{A}\mathbf{e}_1 + \breve{A}_d\mathbf{e}_3\right) \\ \hline (*) & (*) & \mathcal{Q} \end{array}\right]. \tag{28}$$

Here, since $\overline{R}_1^{-1} = \widetilde{X}\widetilde{R}_1^{-1}\widetilde{X}$ and $\overline{R}_2^{-1} = \widetilde{X}\widetilde{R}_2^{-1}\widetilde{X}$, it follows from Lemma 2 that $\overline{R}_1^{-1} \ge 2\mu_1\widetilde{X} - \mu_1^2\widetilde{R}_1$ and $\overline{R}_2^{-1} \ge 2\mu_2\widetilde{X} - \mu_2^2\widetilde{R}_2$. In this sense, it is clear that (28) holds if

$$0 > \left[\begin{array}{cc|cccc} (1,1)' & 0 & (1,3)' & 0 & d_m\breve{A}_d & 0 \\ 0 & (2,2)' & (2,3)' & 0 & d_I\breve{A}_d & 0 \\ \hline (*) & (*) & (3,3)' & \widetilde{R}_1 & \breve{A}_d & 0 \\ 0 & 0 & (*) & (4,4) & \widetilde{R}_2 + \widetilde{S} & -\widetilde{S} \\ (*) & (*) & (*) & (*) & (5,5) & \widetilde{R}_2 + \widetilde{S} \\ 0 & 0 & 0 & (*) & (*) & (6,6) \end{array}\right], \tag{29}$$

where

$$\begin{aligned} (1,1)' &= \mu_1^2\widetilde{R}_1 + \mathbf{diag}\left(-2\mu_1P_1, -2\mu_1\overline{P}_2, \overline{P}_2\left(-2\mu_1P_3\right)\overline{P}_2\right), \\ (2,2)' &= \mu_2^2\widetilde{R}_2 + \mathbf{diag}\left(-2\mu_2P_1, -2\mu_2\overline{P}_2, \overline{P}_2\left(-2\mu_2P_3\right)\overline{P}_2\right), \\ (3,3)' &= \mathbf{He}\left(\breve{A}\right) + \widetilde{Q}_1 + \widetilde{Q}_2 - \widetilde{R}_1, \\ (1,3)' &= d_m\breve{A}, \qquad (2,3)' = d_I\breve{A}. \end{aligned} \tag{30}$$

However, as shown in (29), there exist some nonconvex terms in $(1,1)'$, $(1,3)'$, $(2,2)'$, $(2,3)'$, and $(3,3)'$ as follows:

$$\begin{aligned} (1,1)' &= \begin{bmatrix} (\star) & (\star) & (\star) \\ (\star) & (\star) & (\star) \\ (\star) & (\star) & (\star) + \overline{P}_2\left(-2\mu_1P_3\right)\overline{P}_2 \end{bmatrix}, \\ (2,2)' &= \begin{bmatrix} (\star) & (\star) & (\star) \\ (\star) & (\star) & (\star) \\ (\star) & (\star) & (\star) + \overline{P}_2\left(-2\mu_2P_3\right)\overline{P}_2 \end{bmatrix}, \\ (1,3)' &= \begin{bmatrix} (\star) & 0 & 0 \\ (\star) & (\star) & 0 \\ 0 & 0 & \overline{P}_2\left(d_m\left(P_3A + \overline{L}C\right)\right)\overline{P}_2 \end{bmatrix}, \\ (2,3)' &= \begin{bmatrix} (\star) & 0 & 0 \\ (\star) & (\star) & 0 \\ 0 & 0 & \overline{P}_2\left(d_I\left(P_3A + \overline{L}C\right)\right)\overline{P}_2 \end{bmatrix}, \\ (3,3)' &= \begin{bmatrix} (\star) & (\star) & (\star) \\ (\star) & (\star) & (\star) \\ (\star) & (\star) & (\star) + \overline{P}_2\left(\mathbf{He}\left(P_3A + \overline{L}C\right)\right)\overline{P}_2 \end{bmatrix}. \end{aligned} \tag{31}$$

Here, note that all terms associated with $\overline{P}_2(\star)\overline{P}_2$ in

$$\begin{bmatrix} (1,1)' & 0 & (1,3)' \\ 0 & (2,2)' & (2,3)' \\ (*) & (*) & (3,3)' \end{bmatrix} \tag{32}$$

can be separated as follows:

$$\begin{bmatrix} E_1 \\ E_2 \\ E_3 \end{bmatrix} \underbrace{\begin{bmatrix} \overline{P}_2 & 0 & 0 \\ 0 & \overline{P}_2 & 0 \\ 0 & 0 & \overline{P}_2 \end{bmatrix} \begin{bmatrix} -2\mu_1 P_3 & 0 & d_m(P_3 A + \overline{L}C) \\ 0 & -2\mu_2 P_3 & d_I(P_3 A + \overline{L}C) \\ (*) & (*) & \mathbf{He}(P_3 A + \overline{L}C) \end{bmatrix} \begin{bmatrix} \overline{P}_2 & 0 & 0 \\ 0 & \overline{P}_2 & 0 \\ 0 & 0 & \overline{P}_2 \end{bmatrix}}_{\Psi} \begin{bmatrix} E_1 \\ E_2 \\ E_3 \end{bmatrix}^T . \tag{33}$$

Furthermore, from Lemma 2, it follows that

$$\begin{aligned} \Psi \le & -2\epsilon \begin{bmatrix} \overline{P}_2 & 0 & 0 \\ 0 & \overline{P}_2 & 0 \\ 0 & 0 & \overline{P}_2 \end{bmatrix} \\ & -\epsilon^2 \begin{bmatrix} -2\mu_1 P_3 & 0 & d_m(P_3 A + \overline{L}C) \\ 0 & -2\mu_2 P_3 & d_I(P_3 A + \overline{L}C) \\ (*) & (*) & \mathbf{He}(P_3 A + \overline{L}C) \end{bmatrix}^{-1}, \end{aligned} \tag{34}$$

which allows that (22) implies (29), based on the Schur complement. Next, we need to convert the given condition in (i), that is, $0 \le \Pi_2$, into an LMI. To this end, let us pre- and postmultiply both sides of $0 \le \Pi_2$ by $\mathbf{diag}(\overline{X}, \overline{X})$ and its transpose. Then we can get

$$0 \le \begin{bmatrix} \overline{X} R_2 \overline{X} & \widetilde{S} \\ (*) & \overline{X} R_2 \overline{X} \end{bmatrix}, \tag{35}$$

which becomes (23) due to $\widetilde{R}_2 = \overline{X}\,\overline{R}_2 \overline{X} = (\overline{X} P \overline{X})(X \overline{P} R_2 \overline{R} X)(\overline{X} P \overline{X}) = \overline{X} R_2 \overline{X}$. □

3.2. Control Design for $\overline{w}(t) \neq 0$

Theorem 7. *Let $\mu_1 > 0$, $\mu_2 > 0$, $\epsilon_p > 0$ be prescribed. Suppose that there exist scalars $\epsilon_q > 0$, $\gamma > 0$; matrices $\overline{F} \in \mathbb{R}^{n_u \times n_x}$, $\overline{L} \in \mathbb{R}^{n_x \times n_y}$, $\widetilde{S} \in \mathbb{R}^{3n_x \times 3n_x}$; and symmetric matrices $0 < P_1$, $\overline{P}_2, P_3 \in \mathbb{R}^{n_x \times n_x}$, $0 < \widetilde{Q}_1, \widetilde{Q}_2 \in \mathbb{R}^{3n_x \times 3n_x}$, $0 < \widetilde{R}_1, \widetilde{R}_2 \in \mathbb{R}^{3n_x \times 3n_x}$ such that*

$$0 > \left[\begin{array}{cc|cccccc|c} (1,1) & 0 & d_m \overline{A} & 0 & d_m \breve{A}_d & 0 & d_m \overline{D} & \epsilon_p E_1 & 0 \\ 0 & (2,2) & d_I \overline{A} & 0 & d_I \breve{A}_d & 0 & d_I \overline{D} & \epsilon_p E_2 & 0 \\ \hline (*) & (*) & (3,3) & \widetilde{R}_1 & \breve{A}_d & 0 & \overline{D} & \epsilon_p E_3 & \overline{X}\widetilde{C}^T \\ 0 & 0 & (*) & (4,4) & \widetilde{R}_2 + \widetilde{S} & -\widetilde{S} & 0 & 0 & 0 \\ (*) & (*) & (*) & (*) & (5,5) & \widetilde{R}_2 + \widetilde{S} & 0 & 0 & 0 \\ 0 & 0 & 0 & (*) & (*) & (6,6) & 0 & 0 & 0 \\ (*) & (*) & (*) & 0 & 0 & 0 & (7,7) & \epsilon_q E_4 & 0 \\ (*) & (*) & (*) & 0 & 0 & 0 & (*) & (8,8) & 0 \\ \hline 0 & 0 & (*) & 0 & 0 & 0 & 0 & 0 & -I \end{array}\right], \tag{36}$$

$$0 \le \begin{bmatrix} \widetilde{R}_2 & \widetilde{S} \\ (*) & \widetilde{R}_2 \end{bmatrix}, \tag{37}$$

where

$$(1,1) = \mu_1^2 \widetilde{R}_1 + \mathbf{diag}\left(-2\mu_1 P_1, -2\mu_1 \overline{P}_2, -2\epsilon_p \overline{P}_2\right),$$

$$(2,2) = \mu_2^2 \widetilde{R}_2 + \mathbf{diag}\left(-2\mu_2 P_1, -2\mu_2 \overline{P}_2, -2\epsilon_p \overline{P}_2\right),$$

$$(3,3) = \overline{\overline{A}} + \widetilde{Q}_1 + \widetilde{Q}_2 - \widetilde{R}_1,$$

$$(4,4) = -\widetilde{Q}_1 - \widetilde{R}_1 - \widetilde{R}_2,$$

$$(5,5) = -2\widetilde{R}_2 - \mathbf{He}\left(\widetilde{S}\right),$$

$$(6,6) = -\widetilde{Q}_2 - \widetilde{R}_2, \qquad (7,7) = \mathbf{diag}\left(-2\epsilon_q I, -\gamma^2 I\right),$$

$$(8,8) = \begin{bmatrix} -2\mu_1 P_3 & 0 & d_m\left(P_3 A + \overline{L}C\right) & d_m P_3 D \\ 0 & -2\mu_2 P_3 & d_I\left(P_3 A + \overline{L}C\right) & d_I P_3 D \\ (*) & (*) & \mathbf{He}\left(P_3 A + \overline{L}C\right) & P_3 D \\ (*) & (*) & (*) & -\gamma^2 I \end{bmatrix},$$

$$\breve{A}_d = \begin{bmatrix} 0 & 0 & 0 \\ 0 & B\overline{F} & -B\overline{F} \\ 0 & 0 & 0 \end{bmatrix},$$

$$\overline{A} = \begin{bmatrix} P_1 A_r & 0 & 0 \\ A - A_r & A\overline{P}_2 & 0 \\ 0 & 0 & 0 \end{bmatrix},$$

$$\overline{\overline{A}} = \begin{bmatrix} \mathbf{He}\left(P_1 A_r\right) & \left(A - A_r\right)^T & 0 \\ (*) & \mathbf{He}\left(A\overline{P}_2\right) & 0 \\ 0 & 0 & -2\epsilon_p \overline{P}_2 \end{bmatrix},$$

$$\overline{D} = \begin{bmatrix} 0 & P_1 \\ D & -I \\ 0 & 0 \end{bmatrix}, \qquad \widetilde{C}^T = \begin{bmatrix} 0 \\ C^T \\ 0 \end{bmatrix},$$

$$E_1 = \begin{bmatrix} 0 & 0 & 0 & 0 \\ 0 & 0 & 0 & 0 \\ I & 0 & 0 & 0 \end{bmatrix}, \qquad E_2 = \begin{bmatrix} 0 & 0 & 0 & 0 \\ 0 & 0 & 0 & 0 \\ 0 & I & 0 & 0 \end{bmatrix},$$

$$E_3 = \begin{bmatrix} 0 & 0 & 0 & 0 \\ 0 & 0 & 0 & 0 \\ 0 & 0 & I & 0 \end{bmatrix}, \qquad E_4 = \begin{bmatrix} 0 & 0 & 0 & I \\ 0 & 0 & 0 & 0 \end{bmatrix}. \tag{38}$$

Then the closed-loop system (6) *is asymptotically stable and satisfies* $\|\widetilde{z}\|_2 < \gamma\|\widetilde{w}\|_2$ *for all nonzero* $\widetilde{w}(t) \in \mathscr{L}_{2+}$ *and for any time-varying delay* $d(t)$ *satisfying* $d_m \leq d(t) \leq d_M$. *Moreover, the control and observer gain matrices can be reconstructed as follows:*

$$F = \overline{F}\,\overline{P}_2^{-1}, \qquad L = P_3^{-1}\overline{L}. \tag{39}$$

Proof. From Lemma 4, the $\mathscr{H}_\infty$ stabilization condition is given as follows: (i) $0 \leq \Pi_2$ and (ii) $0 > \Pi_0 + \Pi_1 + \Pi_3 = \mathbf{He}(\mathbf{e}_1^T P\Phi_t) + \mathbf{e}_1^T(Q_1 + Q_2)\mathbf{e}_1 - \mathbf{e}_2^T Q_1 \mathbf{e}_2 - \mathbf{e}_4^T Q_2 \mathbf{e}_4 + \Phi_t^T(d_m^2 R_1 + d_I^2 R_2)\Phi_t + (\mathbf{e}_1 - \mathbf{e}_2)^T R_1(\mathbf{e}_2 - \mathbf{e}_1) + (\mathbf{e}_2 - \mathbf{e}_3)^T R_2(\mathbf{e}_3 - \mathbf{e}_2) + (\mathbf{e}_3 - \mathbf{e}_4)^T R_2(\mathbf{e}_4 - \mathbf{e}_3) + \mathbf{He}((\mathbf{e}_2 - \mathbf{e}_3)^T S(\mathbf{e}_3 - \mathbf{e}_4)) + \mathbf{e}_1^T \widetilde{C}^T \widetilde{C}\mathbf{e}_1 - \gamma^2 \mathbf{e}_5^T \mathbf{e}_5$, where $\Phi_t = \widetilde{A}\mathbf{e}_1 + \widetilde{A}_d \mathbf{e}_3 + \widetilde{D}\mathbf{e}_5$. As in the proof of Lemma 6, we first consider the condition given in (ii) by letting $\overline{R}_1 = X\overline{P}R_1\overline{P}X$ and $\overline{R}_2 = X\overline{P}R_2\overline{P}X$. Then the condition, $0 > \Pi_0 + \Pi_1 + \Pi_3$, can be converted by (20) into

$$\begin{aligned} 0 > {} & \mathbf{He}\left(\mathbf{e}_1^T X\breve{A}X\mathbf{e}_1 + \mathbf{e}_1^T X\breve{A}_d X\mathbf{e}_3 + \mathbf{e}_1^T X\breve{D}\mathbf{e}_5\right) \\ & + \mathbf{e}_1^T\left(Q_1 + Q_2\right)\mathbf{e}_1 - \mathbf{e}_2^T Q_1 \mathbf{e}_2 - \mathbf{e}_4^T Q_2 \mathbf{e}_4 \\ & + \left(X\breve{A}X\mathbf{e}_1 + X\breve{A}_d X\mathbf{e}_3 + X\breve{D}\mathbf{e}_5\right)^T \overline{X}\left(d_m^2 \overline{R}_1 + d_I^2 \overline{R}_2\right) \\ & \times \overline{X}\left(X\breve{A}X\mathbf{e}_1 + X\breve{A}_d X\mathbf{e}_3 + X\breve{D}\mathbf{e}_5\right) \\ & + \left(\mathbf{e}_1 - \mathbf{e}_2\right)^T P\overline{X}\overline{R}_1\overline{X}P\left(\mathbf{e}_2 - \mathbf{e}_1\right) \\ & + \left(\mathbf{e}_2 - \mathbf{e}_3\right)^T P\overline{X}\overline{R}_2\overline{X}P\left(\mathbf{e}_3 - \mathbf{e}_2\right) + \mathbf{e}_1^T \widetilde{C}^T \widetilde{C}\mathbf{e}_1 \\ & + \left(\mathbf{e}_3 - \mathbf{e}_4\right)^T P\overline{X}\overline{R}_2\overline{X}P\left(\mathbf{e}_4 - \mathbf{e}_3\right) \\ & + \mathbf{He}\left(\left(\mathbf{e}_2 - \mathbf{e}_3\right)^T S\left(\mathbf{e}_3 - \mathbf{e}_4\right)\right) - \gamma^2 \mathbf{e}_5^T \mathbf{e}_5, \end{aligned} \tag{40}$$

where $\overline{X} = X^{-1}$. Further, since $\mathbf{diag}(\overline{X}, \overline{X}, \overline{X}, \overline{X}, I)\mathbf{e}_i^T = \mathbf{e}_i^T \overline{X}$, for $i = 1, 2, 3, 4$, and $\mathbf{diag}(\overline{X}, \overline{X}, \overline{X}, \overline{X}, I)\mathbf{e}_5^T = \mathbf{e}_5^T I$, pre- and postmultiplying both sides of (40) by $\mathbf{diag}(\overline{X}, \overline{X}, \overline{X}, \overline{X}, I)$ and its transpose yield

$$\begin{aligned} 0 > {} & \mathcal{Q} + \left(\breve{A}\mathbf{e}_1 + \breve{A}_d \mathbf{e}_3 + \breve{D}\mathbf{e}_5\right)^T \\ & \times \left(d_m^2 \overline{R}_1 + d_I^2 \overline{R}_2\right)\left(\breve{A}\mathbf{e}_1 + \breve{A}_d \mathbf{e}_3 + \breve{D}\mathbf{e}_5\right), \end{aligned} \tag{41}$$

where $\mathcal{Q} = \mathbf{He}(\mathbf{e}_1^T \breve{A}\mathbf{e}_1 + \mathbf{e}_1^T \breve{A}_d \mathbf{e}_3 + \mathbf{e}_1^T \breve{D}\mathbf{e}_5) + \mathbf{e}_1^T(\widetilde{Q}_1 + \widetilde{Q}_2)\mathbf{e}_1 - \mathbf{e}_2^T \widetilde{Q}_1 \mathbf{e}_2 - \mathbf{e}_4^T \widetilde{Q}_2 \mathbf{e}_4 + (\mathbf{e}_1 - \mathbf{e}_2)^T \widetilde{R}_1(\mathbf{e}_2 - \mathbf{e}_1) + (\mathbf{e}_2 - \mathbf{e}_3)^T \widetilde{R}_2(\mathbf{e}_3 - \mathbf{e}_2) + (\mathbf{e}_3 - \mathbf{e}_4)^T \widetilde{R}_2(\mathbf{e}_4 - \mathbf{e}_3) + \mathbf{He}((\mathbf{e}_2 - \mathbf{e}_3)^T \widetilde{S}(\mathbf{e}_3 - \mathbf{e}_4)) + \mathbf{e}_1^T \overline{X}\widetilde{C}^T \widetilde{C}\overline{X}\mathbf{e}_1 - \gamma^2 \mathbf{e}_5^T \mathbf{e}_5$, in which $\widetilde{Q}_1 = \overline{X}Q_1\overline{X}$, $\widetilde{Q}_2 = \overline{X}Q_2\overline{X}$, $\widetilde{R}_1 = \widetilde{X}R_1\widetilde{X}$, $\widetilde{R}_2 = \widetilde{X}R_2\widetilde{X}$, $\widetilde{S} = \widetilde{X}S\widetilde{X}$, $\widetilde{X} = \overline{X}P\overline{X} = \mathbf{diag}(P_1, \overline{P}_2, \overline{P}_2 P_3 \overline{P}_2) > 0$. That is, by applying the Schur complement to (41), we can get

$$0 > \left[\begin{array}{cc|c} -\overline{R}_1^{-1} & 0 & d_m\left(\breve{A}\mathbf{e}_1 + \breve{A}_d \mathbf{e}_3 + \breve{D}\mathbf{e}_5\right) \\ 0 & -\overline{R}_2^{-1} & d_I\left(\breve{A}\mathbf{e}_1 + \breve{A}_d \mathbf{e}_3 + \breve{D}\mathbf{e}_5\right) \\ \hline (*) & (*) & \mathcal{Q} \end{array}\right]. \tag{42}$$

Here, since $\overline{R}_1^{-1} = \widetilde{X}\widetilde{R}_1^{-1}\widetilde{X}$ and $\overline{R}_2^{-1} = \widetilde{X}\widetilde{R}_2^{-1}\widetilde{X}$, it follows from Lemma 2 that $\overline{R}_1^{-1} \geq 2\mu_1\widetilde{X} - \mu_1^2\widetilde{R}_1$ and $\overline{R}_2^{-1} \geq 2\mu_2\widetilde{X} - \mu_2^2\widetilde{R}_2$. In this sense, it is clear that (42) holds if

$$0 > \left[\begin{array}{cc|ccccc} (1,1)' & 0 & (1,3)' & 0 & d_m\breve{A}_d & 0 & (1,7)' \\ 0 & (2,2)' & (2,3)' & 0 & d_I\breve{A}_d & 0 & (2,7)' \\ \hline (*) & (*) & (3,3)'' & \widetilde{R}_1 & \breve{A}_d & 0 & (3,7)' \\ 0 & 0 & (*) & (4,4) & \widetilde{R}_2 + \widetilde{S} & -\widetilde{S} & 0 \\ (*) & (*) & (*) & (*) & (5,5) & \widetilde{R}_2 + \widetilde{S} & 0 \\ 0 & 0 & 0 & (*) & (*) & (6,6) & 0 \\ (*) & (*) & (*) & 0 & 0 & 0 & (7,7)' \end{array}\right], \tag{43}$$

where

$$\begin{aligned} (1,1)' &= \mu_1^2\widetilde{R}_1 + \mathbf{diag}\left(-2\mu_1 P_1, -2\mu_1\overline{P}_2, \overline{P}_2\left(-2\mu_1 P_3\right)\overline{P}_2\right), \\ (2,2)' &= \mu_2^2\widetilde{R}_2 + \mathbf{diag}\left(-2\mu_2 P_1, -2\mu_2\overline{P}_2, \overline{P}_2\left(-2\mu_2 P_3\right)\overline{P}_2\right), \\ (3,3)'' &= \mathbf{He}\left(\breve{A}\right) + \widetilde{Q}_1 + \widetilde{Q}_2 - \widetilde{R}_1 + \overline{X}\widetilde{C}^T\widetilde{C}\overline{X}, \\ (1,3)' &= d_m\breve{A}, \qquad (1,7)' = d_m\breve{D}, \\ (2,3)' &= d_I\breve{A}, \qquad (2,7)' = d_I\breve{D}, \qquad (3,7)' = \breve{D}, \\ (7,7)' &= \mathbf{diag}\left(-\gamma^2 I, -\gamma^2 I\right). \end{aligned} \tag{44}$$

However, as shown in (43), there exist some nonconvex terms in $(1,1)'$, $(1,3)'$, $(1,7)'$, $(2,2)'$, $(2,3)'$, $(2,7)'$, $(3,3)''$, $(3,7)'$, and $(7,7)'$ as follows: $(1,1)'$, $(1,3)'$, $(2,2)'$, and $(2,3)'$ are the same as those defined in the proof of Lemma 6, and

$$(1,7)' = \begin{bmatrix} 0 & (\star) \\ (\star) & (\star) \\ \overline{P}_2 (d_m P_3 D) I & 0 \end{bmatrix},$$

$$(2,7)' = \begin{bmatrix} 0 & (\star) \\ (\star) & (\star) \\ \overline{P}_2 (d_I P_3 D) I & 0 \end{bmatrix},$$

$$(3,7)' = \begin{bmatrix} 0 & (\star) \\ (\star) & (\star) \\ \overline{P}_2 (P_3 D) I & 0 \end{bmatrix},$$

$$(7,7)' = \begin{bmatrix} -\gamma^2 I & 0 \\ 0 & (\star) \end{bmatrix},$$

$$(3,3)'' = \begin{bmatrix} (\star) & (\star) & (\star) \\ (\star) & (\star) & (\star) \\ (\star) & (\star) & (\star) + \overline{P}_2 \left(\mathbf{He}\left(P_3 A + \overline{L} C\right)\right) \overline{P}_2 \end{bmatrix} + \overline{X}\widetilde{C}^T \widetilde{C} \overline{X}, \tag{45}$$

where I denotes the identity matrix. As in the proof of Lemma 6, to deal with the nonconvex terms, we apply Lemma 2 to (43), which boils down to

$$0 > \left[\begin{array}{cc|ccccc|c} (1,1) & 0 & d_m \overline{A} & 0 & d_m \breve{A}_d & 0 & d_m \overline{D} & E_1 \\ 0 & (2,2) & d_I \overline{A} & 0 & d_I \breve{A}_d & 0 & d_I \overline{D} & E_2 \\ \hline (*) & (*) & (3,3)' & \widetilde{R}_1 & \breve{A}_d & 0 & \overline{D} & E_3 \\ 0 & 0 & (*) & (4,4) & \widetilde{R}_2 + \widetilde{S} & -\widetilde{S} & 0 & 0 \\ (*) & (*) & (*) & (*) & (5,5) & \widetilde{R}_2 + \widetilde{S} & 0 & 0 \\ 0 & 0 & 0 & (*) & (*) & (6,6) & 0 & 0 \\ (*) & (*) & (*) & 0 & 0 & 0 & (7,7) & E_4 \\ \hline (*) & (*) & (*) & 0 & 0 & 0 & (*) & (8,8) \end{array}\right], \tag{46}$$

where $(3,3)' = \overline{\overline{A}} + \widetilde{Q}_1 + \widetilde{Q}_2 - \widetilde{R}_1 + \overline{X}\widetilde{C}^T \widetilde{C} \overline{X}$. As a result, by applying the Schur complement to $\overline{X}\widetilde{C}^T \widetilde{C} \overline{X}$ in $(3,3)'$, we can obtain (36). The next step is to convert the given condition in (i), that is, $0 \le \Pi_2$, into an LMI. To this end, let us pre- and postmultiply both sides of $0 \le \Pi_2$ by $\mathbf{diag}(\overline{X}, \overline{X})$ and its transpose. Then we can get

$$0 \le \begin{bmatrix} \overline{X} R_2 \overline{X} & \widetilde{S} \\ (*) & \overline{X} R_2 \overline{X} \end{bmatrix}, \tag{47}$$

which becomes (23) due to $\widetilde{R}_2 = \overline{X} R_2 \overline{X}$. □

4. Numerical Example

We provide two examples to verify the effectiveness of the proposed methods in Lemma 6 and Theorem 7. For the networked output-feedback control system (NOCS), we assume that the sampling period $h = 0.01$ and the data transmission delay bounds are given by $\tau_m = 0.005$ and $\tau_M = 0.01$. As a result, from [3], it follows that $d_m = \tau_m = 0.005[s]$ and $d_M = (\overline{o} + 1)h + \tau_M = 0.01\overline{o} + 0.02[s]$, where $\overline{o}$ denotes the maximum number of data-packet dropouts.

4.1. Example 1. Consider a continuous-time system of the following form:

$$\dot{x}(t) = \begin{bmatrix} 0 & 1 \\ -1 & \alpha \end{bmatrix} x(t) + \begin{bmatrix} 0 \\ 1 \end{bmatrix} u(t) + \begin{bmatrix} 0 \\ 1 \end{bmatrix} w(t),$$
$$y(t) = \begin{bmatrix} 1 & 0 \end{bmatrix} x(t), \tag{48}$$

where $\alpha > 0$ is a variable element. First of all, to show the applicability of the proposed method in Lemma 6, we search the maximum allowable upper bounds (MAUBs) for (48) with $\widetilde{w}(t) = \mathbf{col}(w(t), r(t)) = 0 \in \mathbb{R}^{n_x + n_w}$. To this end, let us set $\mu_1 = \mu_2 = 0.1$, $\epsilon = 10$, and $A_r = \mathbf{diag}(1,1)$. Then, from Lemma 6, we can obtain the MAUBs for $\alpha = 1, 2, 3$, which are tabulated in Table 1. Now, let us analyze the behavior of the tracking response for $x(t)$ and $x_r(t)$ of the NOCS in the case where $\widetilde{w}(t) \neq 0$ by using the derived condition in Theorem 7. For this purpose, we set $\alpha = 1$, $\overline{o} = 10$, $\mu_1 = \mu_2 = 0.1$, $\epsilon = 10$, and $A_r = \mathbf{diag}(1,1)$. Then, from Theorem 7, we can obtain the following control and observer gain matrices: $F = [-5.5501 \; -4.9075]$, $L = [-31.1609 \; -179.7242]^T$. In addition, the disturbance attenuation is given by $\gamma = 1.1679$. Here we assume that $w(t) = e^{-0.5t}\sin(2\pi t)$, $x(0) = \mathbf{col}(\pm 0.5, \pm 0.5)$, $x_r(t) = \hat{x}(t) = 0$, for $t \in [-d_M, 0]$, and $r(t) = \mathbf{col}(0.2\sin 0.2\pi t, 0.04\pi\cos 0.2\pi t)$, for $t \ge 0$, where the initial time t_0 is set to zero. Figure 2(a) shows the x_1-x_2 trajectories for four different initial conditions $x(0)$, which form a specific ellipse, made by the given reference input $r(t)$, as the time t increases. Further, the behavior of the estimation error $e_1(t) = y(t) - \hat{y}(t)$ is depicted in Figure 2(d), from which we can see that the estimation error goes to zero as the time t increases. Figures 2(b) and 2(c) show the behavior of the state $x(t)$ of (49) for initial condition $x(0) = (0.5, -0.5)$, where the network-induced delay $d(t)$ is generated as shown in Figure 2(e) such that the data transmission delay $\tau(t) \in [0.005, 0.01]$ and the data-packet dropouts $\overline{o} = 10$. From Figures 2(b) and 2(c), we can see that the state $x(t)$ tracks the reference signal $x_r(t)$ well; that is, the tracking response of

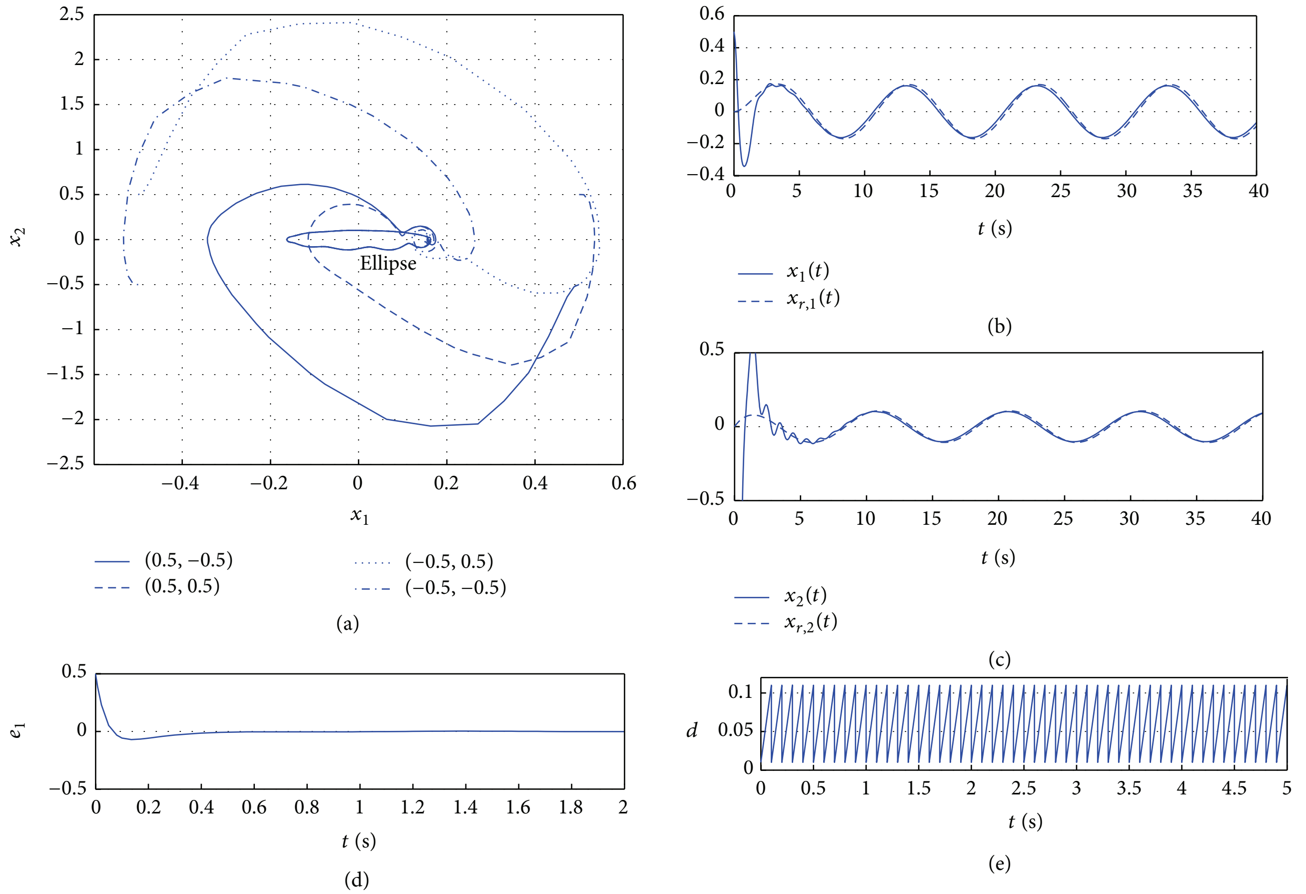

Figure 2: (a) The x_1-x_2 trajectory for each different initial condition $x(0)$; (b) the tracking response of $x_1(t)$ for $x_{r,1}(t)$; (c) the tracking response of $x_2(t)$ for $x_{r,2}(t)$; (d) the estimation error $e_1(t) = y(t) - \hat{y}(t)$; and (e) the network-induced delay $d(t)$. Here, x_i, $\hat{x}_i$, e_i, and $x_{r,i}$ denote the ith element of x, $\hat{x}$, e, and x_r, respectively.

Table 1: Maximum allowable upper bounds (MAUBs) for α of Example 1.

α	1	2	3
τ_M	0.32 ($\bar{o} = 30$)	0.19 ($\bar{o} = 17$)	0.09 ($\bar{o} = 7$)

Table 2: $\mathscr{H}_\infty$ performance for each upper bound d_M.

d_M	0.02	0.03	0.05	0.1
γ	0.8265	0.9072	1.1337	2.3290

the NOCS with (2), (5), and (48) is in a good shape with respect to our control goal.

4.2. Example 2. Consider the following satellite system, modified from [5]: $A_r = \mathbf{diag}(-1, -1, -1, -1)$,

$$A = \begin{bmatrix} 0.000 & 0.000 & 1.000 & 0.000 \\ 0.000 & 0.000 & 0.000 & 1.000 \\ -0.300 & 0.300 & -0.004 & 0.004 \\ 0.300 & -0.300 & 0.004 & -0.004 \end{bmatrix}, \quad B = \begin{bmatrix} 0 \\ 0 \\ 1 \\ 0 \end{bmatrix}, \quad C^T = \begin{bmatrix} 0 \\ 1 \\ 0 \\ 0 \end{bmatrix}, \quad D = \begin{bmatrix} 0 \\ 0 \\ 0 \\ 1 \end{bmatrix}. \tag{49}$$

Through this example, we will achieve the $\mathscr{H}_\infty$ performance for (49) based on Theorem 7 to design an observer-based NOCS in such a way that the state $x(t)$ of (49) tracks the reference signal $x_r(t)$ in the $\mathscr{H}_\infty$ sense. The obtained $\mathscr{H}_\infty$ performance for each upper bound d_M is tabulated in Table 2, where $\mu_1 = \mu_2 = 0.1$ and $\epsilon_p = 10$ are assumed. From Table 2, we can see that the $\mathscr{H}_\infty$ performance is improved as d_M decreases from 0.1 to 0.02, which is reasonable.

5. Concluding Remarks

This paper has addressed the observer-based $\mathscr{H}_\infty$ tracking problem of NOCSs with network-induced delays. In the derivation, a single-step procedure is proposed to handle nonconvex terms that appear in the process of designing observer-based output-feedback control, and then a set of linear matrix inequality conditions are established for the solvability of the tracking problem.

Conflict of Interests

The author declares that there is no conflict of interests regarding the publication of this paper.

Acknowledgment

This work was supported by the National Research Foundation of Korea Grant funded by the Korean Government (NRF-2012R1A1A1013687).

References

[1] G. Xie and L. Wang, "Stabilization of NCSs: asynchronous partial transfer approach," in *Proceedings of the American Control Conference (ACC '05)*, pp. 1226–1230, Portland, Ore, USA, June 2005.

[2] Q. Zhu, B. Xie, and Y. Zhu, "Guaranteed cost control for multirate networked control systems with both time-delay and packet-dropout," *Mathematical Problems in Engineering*, Article ID 637329, Art. ID , 9 pages, 2014.

[3] S. H. Kim, P. Park, and C. Jeong, "Robust H_∞ stabilisation of networked control systems with packet analyser," *IET Control Theory and Applications*, vol. 4, no. 9, pp. 1828–1837, 2010.

[4] L. Zhang, H. Gao, and O. Kaynak, "Network-induced constraints in networked control systems—a survey," *IEEE Transactions on Industrial Informatics*, vol. 9, no. 1, pp. 403–416, 2013.

[5] H. Gao and T. Chen, "Network-based H_∞ output tracking control," *IEEE Transactions on Automatic Control*, vol. 53, no. 3, pp. 655–667, 2008.

[6] Y.-L. Wang and G.-H. Yang, "Output tracking control for networked control systems with time delay and packet dropout," *International Journal of Control*, vol. 81, no. 11, pp. 1709–1719, 2008.

[7] V. Suplin, E. Fridman, and U. Shaked, "H_∞ sampled data control of systems with time-delays," *International Journal of Control*, vol. 82, no. 2, pp. 298–309, 2009.

[8] Y. L. Wang and G. H. Yang, "Robust H_∞ model reference tracking control for networked control systems with communication constraints," *International Journal of Control, Automation and Systems*, vol. 7, no. 6, pp. 992–1000, 2009.

[9] C. Huang, Y. Bai, and X. Liu, "H-infinity state feedback control for a class of networked cascade control systems with uncertain delay," *IEEE Transactions on Industrial Informatics*, vol. 6, no. 1, pp. 62–72, 2010.

[10] Y. Sun and S. Qin, "Stability analysis and controller design for networked control systems with random time delay," *International Journal of Systems Science*, vol. 42, no. 3, pp. 359–367, 2011.

[11] L. Qiu, Q. Luo, F. Gong, S. Li, and B. Xu, "Stability and stabilization of networked control systems with random time delays and packet dropouts," *Journal of the Franklin Institute*, vol. 350, no. 7, pp. 1886–1907, 2013.

[12] F. Hao and X. Zhao, "Linear matrix inequality approach to static output-feedback stabilisation of discrete-time networked control systems," *IET Control Theory & Applications*, vol. 4, no. 7, pp. 1211–1221, 2010.

[13] J. Qiu, G. Feng, and H. Gao, "Fuzzy-model-based piecewise H_∞ static-output-feedback controller design for networked nonlinear systems," *IEEE Transactions on Fuzzy Systems*, vol. 18, no. 5, pp. 919–934, 2010.

[14] X. Jia, D. Zhang, X. Hao, and N. Zheng, "Fuzzy H_∞ tracking control for nonlinear networked control systems in T-S fuzzy model," *IEEE Transactions on Systems, Man, and Cybernetics B: Cybernetics*, vol. 39, no. 4, pp. 1073–1079, 2009.

[15] S. K. Nguang, "Comments on 'Fuzzy H_∞ tracking control for nonlinear networked control systems in TS fuzzy model'," *IEEE Transactions on Systems, Man, and Cybernetics B: Cybernetics*, vol. 40, no. 3, p. 957, 2010.

[16] Y. Shi, J. Huang, and B. Yu, "Robust tracking control of networked control systems: application to a networked DC motor," *IEEE Transactions on Industrial Electronics*, vol. 60, no. 12, pp. 5864–5874, 2013.

[17] Z.-H. Pang, G.-P. Liu, D. Zhou, and M. Chen, "Output tracking control for networked systems: a model-based prediction approach," *IEEE Transactions on Industrial Electronics*, vol. 61, no. 9, pp. 4867–4877, 2014.

[18] P. Park, J. W. Ko, and C. Jeong, "Reciprocally convex approach to stability of systems with time-varying delays," *Automatica*, vol. 47, no. 1, pp. 235–238, 2011.

[19] C. Jeong, P. Park, and S. H. Kim, "Improved approach to robust stability and H_∞ performance analysis for systems with an interval time-varying delay," *Applied Mathematics and Computation*, vol. 218, no. 21, pp. 10533–10541, 2012.

[20] H. Shao and Q. Han, "Less conservative delay-dependent stability criteria for linear systems with interval time-varying delays," *International Journal of Systems Science*, vol. 43, no. 5, pp. 894–902, 2012.

[21] K. Zhou and P. P. Khargonekar, "Robust stabilization of linear systems with norm-bounded time-varying uncertainty," *Systems & Control Letters*, vol. 10, no. 1, pp. 17–20, 1988.

[22] K. Gu, V. L. Kharitonov, and J. Chen, *Stability of Time-Delay Systems*, Birkhäuser, Lausanne, Switzerland, 2003.

Hindawi Publishing Corporation
Mathematical Problems in Engineering
Volume 2015, Article ID 154158, 10 pages
http://dx.doi.org/10.1155/2015/154158

Research Article

Robust Output Feedback Model Predictive Control for a Class of Networked Control Systems with Nonlinear Perturbation

Qiuxia Chen,[1] Ying Liu,[2] and Haoqi Zhu[1]

[1] *Designing Institute, Hangzhou Hangyang Co., Ltd., Hangzhou 310014, China*
[2] *Department of Information Engineering, Research Center for Smart Agriculture and Forestry, Zhejiang A&F University, Lin'an 311300, China*

Correspondence should be addressed to Ying Liu; zafuliuying@gmail.com

Received 20 June 2014; Revised 27 August 2014; Accepted 29 August 2014

Academic Editor: Yun-Bo Zhao

This paper is concerned with the design problem of robust dynamic output feedback model predictive controllers for a class of discrete-time systems with time-varying network-induced delays and nonlinear perturbation. The designed controllers achieve on-line suboptimal receding horizon guaranteed cost such that the system can be stabilized for all admissible uncertainties. A novel delay compensation strategy is proposed to eliminate the effects of the time-varying network-induced delays. By using multistep prediction and the receding optimization, the delay-dependent sufficient condition is derived for the existence of delay compensation controllers. By employing the cone complementarity linearization (CCL) idea, a nonlinear minimization problem with linear matrix inequality (LMI) constraints is formulated to design the desired output feedback controllers, and an iterative algorithm involving convex optimization is presented to solve the nonlinear minimization problem. Finally, an example is given to illustrate the feasibility and effectiveness of the proposed results.

1. Introduction

With the rapid development of digital systems and communication networks, more and more control engineers would like to use a real-time communication channel interfaced to a digital system to exchange information and to complete the control task. Such networked control systems (NCSs) have received increasing attention in recent years because of their many advantages, such as lower cost and more convenience for installation and maintenance. Industrial applications of NCSs include automobiles, vehicle systems, robotic systems, jacking systems for trains, and process control systems [1–3]. However, the streams of data exchange between NCS components are prone to delay, losses, and missynchronization, which degrade the performance and even cause the instability of the systems [4, 5]. Network-induced delays typically have negative effects on the NCS's stability and performance. So far, different techniques have been presented to deal with the problem of network-induced delays, such as the stochastic system approach [6, 7], the hybrid system approach [8, 9], and the time-delay system approach [10, 11]. It is noted that, in the aforementioned results, all the proposed controllers are operated in an off-line fashion, and the controllers are designed such that the overall closed-loop NCSs can tolerate certain amount of network-induced delays. Another constructive scheme is to use future control sequences to directly eliminate the negative effects of the network-induced delays, and model predictive control (MPC) which can provide future control sequences and operate in an on-line fashion is such a desired algorithm.

Model predictive control is probably one of the most successful modern control technologies during recent years. This is due to several thousand applications in process control because of its many advantages, including ease of computation, good tracking performance, and I/O constraint handling capability. Recently, MPC has received increasing attention in NCSs for its ability to on-line compensate time delays as well as its good tracking performance. Reference [12] proposed a new approach of predictive compensation for simultaneous network-induced delays and packet losses and addressed the codesign of both network and controller. In [13], a model-based networked predictive output tracking control scheme is proposed to actively compensate for the random round-trip time delay. Reference [14] proposed a data-driven networked predictive control scheme which consisted of the control prediction generator and network delay compensator for MIMO NCSs with random network delays. However, all the above designed model predictive controllers are state feedback controllers which are quite difficult for implementation when the system states cannot be directly measured for availability. Therefore, it is necessary to design a feedback controller using the measured output. To the best of the authors' knowledge, few results have been reported on the dynamic output feedback MPC for NCSs [15]. Besides, the above approaches are not applicable to the case that there are parameter uncertainties in the model. Since the uncertainties are frequently the sources of instability and performance deterioration, the stability analysis and controller synthesis for NCSs with model uncertainty and external disturbances have been some of the most challenging issues. Up to now, a few robust MPC algorithms have been presented to improve the robustness of the networked control systems [16, 17].

Taking the network-induced delay into consideration, the NCSs can be modeled as an uncertain discrete-time system with time-varying delays, and this motivates us to apply the theory of time-delay systems and robust MPC strategy to design the feedback controllers for such NCSs. The main results of this paper will contribute to the development of the delay-dependent dynamic output feedback robust MPC for a class of NCSs with norm-bounded nonlinear perturbation and time-varying communication delays. A sufficient delay-dependent condition that guarantees the robust stability of the closed-loop NCS is derived. An optimization problem is also formulated to construct the dynamic output feedback MPC controllers subject to a set of nonlinear matrix inequalities. Based on the linearization idea [18], an iterative algorithm involving convex optimization is proposed to solve the nonlinear matrix inequality system, and the iterative optimization algorithm is guaranteed to be feasible at each time step if it is feasible at the first step. The control inputs applied to the system from the solutions of the MPC optimization problems guarantee an on-line suboptimal receding horizon guaranteed cost. Finally, an example is given to illustrate the effectiveness of the proposed results.

Notation. Throughout the paper, $\mathfrak{R}^n$ stands for the set of all real n-dimensional vectors and $\mathfrak{R}^{n\times m}$ is the set of all $n \times m$-dimensional matrices. $\mathbf{I}$ denotes identity matrix of appropriate dimensions; diag$\{\cdot\}$ denotes the block diagonal matrix. $\mathbf{G} > 0$ ($\mathbf{G} \geq 0$, $\mathbf{G} < 0$, $\mathbf{G} \leq 0$) means that $\mathbf{G}$ is a real symmetric positive-definite matrix (positive-semidefinite, negative-definite, and negative-semidefinite). $*$ denotes the symmetric part.

2. Problem Formulation and Preliminaries

The detailed assumptions about the NCS studied in this paper are described as follows.

(1) The sensor is clock-driven and has the sampling period h, and the controller and the actuator are event-driven.

(2) The sensor-to-controller delay τ_k^{sc} and the controller-to-actuator delay τ_k^{ca} are both uncertain but bounded and can be obtained by best case analysis and worst case analysis. The total time delay $\tau_k^{sa} = \tau_k^{sc} + \tau_k^{ca}$ satisfies $\underline{\tau} \leq \tau_k^{sa} \leq \overline{\tau}$, where $\overline{\tau}$ and $\underline{\tau}$ are known positive integers corresponding to maximum and minimum of τ_k^{sa}.

(3) Controller computational delay can be absorbed into either τ_k^{sc} or τ_k^{ca} [19].

The uncertain discrete-time system with nonlinear perturbation is described by the following state space model:

$$\begin{aligned}\mathbf{x}(k+1) &= (\mathbf{A}+\Delta\mathbf{A}(k))\,\mathbf{x}(k)+(\mathbf{B}+\Delta\mathbf{B}(k))\,\mathbf{u}(k)\\ &\quad+\mathbf{f}(\mathbf{x}(k),\mathbf{u}(k)),\\ \mathbf{y}(k) &= \mathbf{C}\mathbf{x}(k),\end{aligned} \tag{1}$$

where $\mathbf{x}(k) \in \mathfrak{R}^n$ is the state, $\mathbf{u}(k) \in \mathfrak{R}^l$ is the control input, $\mathbf{y}(k) \in \mathfrak{R}^v$ is the measured output, and $\mathbf{A}$, $\mathbf{B}$, and $\mathbf{C}$ are known real constant matrices of appropriate dimensions. $\Delta\mathbf{A}(k)$ and $\Delta\mathbf{B}(k)$ are unknown matrices representing time-varying parameter uncertainties in the system model. It is assumed that the uncertainties are norm-bounded and can be described as $[\Delta\mathbf{A}\quad\Delta\mathbf{B}] = \mathbf{D}\mathbf{F}(k)[\mathbf{E}_1\quad\mathbf{E}_2]$, where $\mathbf{F}(k) \in \mathfrak{R}^{i\times j}$ is an unknown matrix satisfying $\mathbf{F}^T(k)\mathbf{F}(k) \leq \mu\mathbf{I}$ and μ is a known positive scalar representing the upper bound of the unknown matrix $\mathbf{F}(k)$, and $\mathbf{D}$, $\mathbf{E}_1$, and $\mathbf{E}_2$ are known constant matrices of appropriate dimensions. The nonlinear function $\mathbf{f}$ satisfies the following:

$$\mathbf{f}^T\mathbf{f} \leq \alpha^2 \begin{bmatrix}\mathbf{x}(k)\\ \mathbf{u}(k)\end{bmatrix}^T \begin{bmatrix}\mathbf{H}_1^T\mathbf{H}_1 & 0\\ 0 & \mathbf{H}_2^T\mathbf{H}_2\end{bmatrix} \begin{bmatrix}\mathbf{x}(k)\\ \mathbf{u}(k)\end{bmatrix}, \tag{2}$$

where $\mathbf{H}_1$ and $\mathbf{H}_2$ are known constant matrices and $\alpha > 0$ is the bounding parameter on the uncertain function $\mathbf{f}$.

The physical system consisting of sensor and actuator nodes is connected to the controller through a communication medium. For the convenience of system analysis and controller design, the sensor-to-controller delay τ_k^{sc} and the controller-to-actuator delay τ_k^{ca} are lumped up as the feed-forward delay $\tau(k)h$. Considering the delay effect, the input of the controller can be given as $\mathbf{y}(k) = \mathbf{y}(k-\tau(k))$, and then the full-order dynamic output feedback controller to be determined has the following form:

$$\begin{aligned}\widehat{\mathbf{x}}(k+1) &= \mathbf{A}_c\widehat{\mathbf{x}}(k)+\mathbf{B}_c\mathbf{y}(k-\tau(k))\\ \mathbf{u}(k) &= \mathbf{C}_c\widehat{\mathbf{x}}(k),\end{aligned} \tag{3}$$

where $\widehat{\mathbf{x}}(k) \in \mathfrak{R}^{\mathbf{n}}$ is the controller state.

Applying controller (3) to the system (1) results in the following networked closed-loop system:

$$\overline{\mathbf{x}}(k+1) = \widetilde{\mathbf{A}}\overline{\mathbf{x}}(k)+\overline{\mathbf{A}}_d\mathbf{x}(k-\tau(k))+\overline{\mathbf{I}}^T\mathbf{f}(\mathbf{x}(k),\mathbf{u}(k)), \tag{4}$$

where

$$\overline{\mathbf{x}}(k)=\begin{bmatrix}\mathbf{x}(k)\\ \hat{\mathbf{x}}(k)\end{bmatrix},\qquad \overline{\mathbf{A}}=\begin{bmatrix}\mathbf{A} & \mathbf{B}\mathbf{C}_c\\ 0 & \mathbf{A}_c\end{bmatrix},$$
$$\overline{\mathbf{A}}_d=\begin{bmatrix}0\\ \mathbf{B}_c\mathbf{C}\end{bmatrix},\qquad \overline{\mathbf{D}}=\begin{bmatrix}\mathbf{D}\\ 0\end{bmatrix},\tag{5}$$
$$\widetilde{\mathbf{A}}=\overline{\mathbf{A}}+\overline{\mathbf{D}}\mathbf{F}(k)\overline{\mathbf{E}},$$
$$\overline{\mathbf{E}}=\left[\mathbf{E}_1\quad \mathbf{E}_2\mathbf{C}_c\right],\qquad \overline{\mathbf{I}}=\left[\mathbf{I}\quad 0\right].$$

In this way, the NCS (1) and (3) with nonlinear perturbation and communication delays is modeled as the uncertain discrete-time system (4) with time-varying state delay, which enables us to apply the theory of time-delay systems and the receding optimization of the MPC to deal with the analysis and design problem of such NCS.

Remark 1. Equation (4) is used to express the mathematical model of the networked control systems when the transmitted data is single packet. For the multiple-packet transmission case, since the arrival time of the sensor messages at the controller or the arrival time of the controller messages at the actuator may be different, especially for the case when the sampling times of the sensors are different, a buffer before the controller and actuator is needed. By employing the buffer technology on the network, model (4) can also be used to express the NCS with multiple-packet transmission.

The objective of this paper is to find a stabilizing dynamic output feedback controller of the form (3) for the uncertain system (1) with time-varying delays by MPC strategy. To this end, we define the following min-max optimization problem, which is considered at each sampling time k:

$$\min_{\mathbf{u}_{k+i|k},i=0,1,\ldots,m}\ \max_{[\mathbf{A}(k+i),\mathbf{B}(k+i)],i\geq 0} J(k),$$
$$J(k)=\sum_{i=0}^{p}\mathbf{x}_{k+i|k}^{T}S_1\mathbf{x}_{k+i|k}+\sum_{i=0}^{m}\mathbf{u}_{k+i|k}^{T}\mathbf{S}_2\mathbf{u}_{k+i|k},\tag{6}$$

where m is the control horizon, p is the prediction horizon, $\mathbf{S}_1>0$ and $\mathbf{S}_2>0$ are given weighting matrices, and $\mathbf{x}_{k+i|k}$ and $\mathbf{u}_{k+i|k}$ denote the predicted variables of the state and the input, respectively, with $\mathbf{x}_{k|k}=\mathbf{x}(k)$, $\hat{\mathbf{x}}_{k|k}=\hat{\mathbf{x}}(k)$, and $\mathbf{x}_{k-i|k}=\mathbf{x}(k-i)$ for $i\geq 1$. Besides, we have the terminal constraints $\mathbf{u}_{k+i|k}=0$ for $i>m$.

Associated with the closed-loop system (4), the min-max optimization problem (6) becomes of the following form:

$$\min_{\mathbf{u}_{k+i|k},i=0,1,\ldots,m}\ \max_{[\mathbf{A}(k+i),\mathbf{B}(k+i)],i\geq 0} J(k),$$
$$J(k)=\sum_{i=0}^{p}\overline{\mathbf{x}}_{k+i|k}^{T}\widetilde{\mathbf{S}}\overline{\mathbf{x}}_{k+i|k},\tag{7}$$

where $\hat{\mathbf{x}}_{k+i|k}=0$, $i>m$, and $\widetilde{\mathbf{S}}=\operatorname{diag}\{\mathbf{S}_1,\mathbf{C}_c^T\mathbf{S}_2\mathbf{C}_c\}$.

The future control sequence can be obtained by solving the above optimization problem. In order to eliminate the delay effects, the control input should be $\mathbf{u}(k)=u_{k+\tau_k^{sa}/h|k}$ but not $u_{k+\tau(k)|k}$. By using the multistep prediction and the linear interpolation method, the control sequence $\Pi_k=\{u_{k+\tau_k^{sa}/h|k},u_{k+1+\tau_k^{sa}/h|k},\ldots,u_{k+\omega+\tau_k^{sa}/h|k}\}$ can be obtained. In the receding horizon framework, only the first control variable $u_{k+\tau_k^{sa}/h|k}$ actuates the system in time.

Lemma 2 (see [20]). *Let $\hat{\mathbf{J}}=\hat{\mathbf{J}}^T>0$ and $\widehat{\mathbf{H}}$, $\widehat{\mathbf{L}}$ be given matrices with appropriate dimensions. Then, it follows that*

$$\hat{\mathbf{J}}+\widehat{\mathbf{H}}\mathbf{F}\widehat{\mathbf{L}}+\widehat{\mathbf{L}}\mathbf{F}\widehat{\mathbf{H}}<0\tag{8}$$

holds for any matrix $\mathbf{F}$ satisfying $\mathbf{F}^T\mathbf{F}\leq\mu\mathbf{I}$, if and only if there exists a scalar $\varepsilon>0$ such that

$$\mu\widehat{\mathbf{H}}\widehat{\mathbf{H}}^T+\varepsilon\hat{\mathbf{J}}+\varepsilon^2\widehat{\mathbf{L}}^T\widehat{\mathbf{L}}<0.\tag{9}$$

3. Main Results

In this section, we first derive an upper bound on the worst value of the cost $J(k)$.

Theorem 3. *Consider the uncertain system (1) and the cost function $J(k)$. If there exist a controller of the form (3), a scalar $\varepsilon\geq\sqrt{\mu}$, $\mathbf{P}>0\in\mathfrak{R}^{2n\times 2n}$, $\mathbf{Q}>0\in\mathfrak{R}^{n\times n}$, $\mathbf{R}>0\in\mathfrak{R}^{n\times n}$, and matrices $\mathbf{M}_0\in\mathfrak{R}^{n\times n}$, $\mathbf{M}_1\in\mathfrak{R}^{n\times n}$, such that the following matrix inequality holds*

$$\begin{bmatrix}\mathbf{M}_a & * & * & * & * & * & * & *\\ \mathbf{M}_b & \mathbf{M}_c & * & * & * & * & * & *\\ 0 & 0 & \lambda\mathbf{I} & * & * & * & * & *\\ \overline{\mathbf{A}} & \overline{\mathbf{A}}_d & \overline{\mathbf{I}}^T & \mathbf{P}^{-1} & * & * & * & *\\ \overline{\mathbf{A}}_f & 0 & \mathbf{I} & 0 & \overline{\tau}^{-1}\mathbf{R}^{-1} & * & * & *\\ \widetilde{\mathbf{M}}_0 & \mathbf{M}_1 & 0 & 0 & 0 & \overline{\tau}^{-1}\mathbf{R} & * & *\\ 0 & 0 & 0 & \overline{\mathbf{D}}^T & \mathbf{D}^T & 0 & \varepsilon^{-1}\mathbf{I} & *\\ \overline{\mathbf{E}} & 0 & 0 & 0 & 0 & 0 & 0 & \varepsilon^{-1}\mathbf{I}\end{bmatrix}>0,\tag{10}$$

where

$$\begin{aligned}\mathbf{M}_a&=\mathbf{P}-\widetilde{\mathbf{S}}-\mathbf{M}_d-\lambda\alpha^2\widetilde{\mathbf{H}},\\ \mathbf{M}_d&=\operatorname{diag}\left\{\mathbf{M}_0+\mathbf{M}_0^T-d_c\mathbf{Q},0\right\},\\ d_c&=\underline{\tau}-\overline{\tau}-1,\\ \widetilde{\mathbf{H}}&=\operatorname{diag}\left\{\mathbf{H}_1^T\mathbf{H}_1,\mathbf{C}_c^T\mathbf{H}_2^T\mathbf{H}_2\mathbf{C}_c\right\},\\ \mathbf{M}_b&=\left[\mathbf{M}_1^T-\mathbf{M}_0 0\right],\\ \mathbf{M}_c&=\mathbf{Q}+\mathbf{M}_1+\mathbf{M}_1^T,\\ \overline{\mathbf{A}}_f&=\left[\mathbf{A}-\mathbf{I}\quad \mathbf{B}\mathbf{C}_c\right],\\ \widetilde{\mathbf{M}}_0&=\left[\mathbf{M}_0\quad 0\right]\end{aligned}\tag{11}$$

then the closed-loop system (4) *is asymptotically stable and the cost function* $J(k)$ *satisfies the following:*

$$\begin{aligned}\max_{[\mathbf{A}(k+i),\mathbf{B}(k+i)],i\geq 0} J(k) < \overline{\mathbf{x}}_{k|k}^{T}\mathbf{P}\overline{\mathbf{x}}_{k|k} + \sum_{\theta=k-\overline{\tau}}^{k-1}\mathbf{x}_{\theta|k}^{T}\mathbf{Q}\mathbf{x}_{\theta|k} \\ + \sum_{j=-\overline{\tau}}^{-1}\sum_{\theta=k+j}^{k-1}\eta_{\theta|k}^{T}\mathbf{R}\eta_{\theta|k} \\ + \sum_{j=-\overline{\tau}+2}^{-\underline{\tau}+1}\sum_{\theta=k+j-1}^{k-1}\mathbf{x}_{\theta|k}^{T}\mathbf{Q}\mathbf{x}_{\theta|k},\end{aligned} \tag{12}$$

where $\eta_{\theta|k} = \mathbf{x}_{\theta+1|k} - \mathbf{x}_{\theta|k}$.

Proof. Choose the following candidate Lyapunov functional:

$$\overline{V}(\overline{\mathbf{x}}_{k+i|k}) = V_1(\overline{\mathbf{x}}_{k+i|k}) + V_2(\overline{\mathbf{x}}_{k+i|k}) + V_3(\overline{\mathbf{x}}_{k+i|k}), \tag{13}$$

where

$$\begin{aligned}V_1(\overline{\mathbf{x}}_{k+i|k}) &= \overline{\mathbf{x}}_{k+i|k}^{T}\mathbf{P}\overline{\mathbf{x}}_{k+i|k}, \\ V_2(\overline{\mathbf{x}}_{k+i|k}) &= \sum_{\theta=k+i-\tau(k)}^{k+i-1}\mathbf{x}_{\theta|k}^{T}\mathbf{Q}\mathbf{x}_{\theta|k}, \\ V_3(\overline{\mathbf{x}}_{k+i|k}) &= \sum_{j=-\overline{\tau}}^{-1}\sum_{\theta=k+j}^{k+i-1}\eta_{\theta|k}^{T}\mathbf{R}\eta_{\theta|k} + \sum_{j=-\overline{\tau}+2}^{-\underline{\tau}+1}\sum_{\theta=k+i+j-1}^{k+i-1}\mathbf{x}_{\theta|k}^{T}\mathbf{Q}\mathbf{x}_{\theta|k}, \\ & \qquad i = 0,1,\ldots,p.\end{aligned} \tag{14}$$

Taking the forward difference for the Lyapunov functional $V_1(\overline{\mathbf{x}}_{k+i|k})$, one obtains

$$\Delta V_1(\overline{\mathbf{x}}_{k+i|k}) = \boldsymbol{\psi}^{T}(k)\left\{\Gamma^{T}\mathbf{P}\Gamma + \operatorname{diag}\{-\mathbf{P},0,0\}\right\}\boldsymbol{\psi}(k), \tag{15}$$

where

$$\begin{aligned}\Gamma &= \begin{bmatrix}\widetilde{\mathbf{A}} & \overline{\mathbf{A}}_d & \overline{\mathbf{I}}^{T}\end{bmatrix}, \\ \psi^{T}(k) &= \begin{bmatrix}\overline{\mathbf{x}}_{k+i|k}^{T}\mathbf{x}_{k+i-\tau(k)|k}^{T} & \mathbf{f}^{T}(\mathbf{x}_{k+i|k},\mathbf{u}_{k+i|k})\end{bmatrix}.\end{aligned} \tag{16}$$

Direct computation gives

$$\begin{aligned}\Delta V_2(\overline{\mathbf{x}}_{k+i|k}) = \mathbf{x}_{k+i|k}^{T}\mathbf{Q}\mathbf{x}_{k+i|k} - \mathbf{x}_{k+i-\tau(k)|k}^{T}\mathbf{Q}\mathbf{x}_{k+i-\tau(k)|k} \\ + \sum_{\theta=k+i+1-\tau(k+1)}^{k+i-1}\mathbf{x}_{\theta|k}^{T}\mathbf{Q}\mathbf{x}_{\theta|k} \\ - \sum_{\theta=k+i+1-\tau(k)}^{k+i-1}\mathbf{x}_{\theta|k}^{T}\mathbf{Q}\mathbf{x}_{\theta|k}.\end{aligned} \tag{17}$$

Note that

$$\begin{aligned}&\sum_{\theta=k+i+1-\tau(k+1)}^{k+i-1}\mathbf{x}_{\theta|k}^{T}\mathbf{Q}\mathbf{x}_{\theta|k} \\ &= \sum_{\theta=k+i+1-\underline{\tau}}^{k+i-1}\mathbf{x}_{\theta|k}^{T}\mathbf{Q}\mathbf{x}_{\theta|k} + \sum_{\theta=k+i+1-\tau(k+1)}^{k+i-\underline{\tau}}\mathbf{x}_{\theta|k}^{T}\mathbf{Q}\mathbf{x}_{\theta|k} \\ &\leq \sum_{\theta=k+i+1-\tau(k)}^{k+i-1}\mathbf{x}_{\theta|k}^{T}\mathbf{Q}\mathbf{x}_{\theta|k} + \sum_{\theta=k+i+1-\overline{\tau}}^{k+i-\underline{\tau}}\mathbf{x}_{\theta|k}^{T}\mathbf{Q}\mathbf{x}_{\theta|k}.\end{aligned} \tag{18}$$

Hence, we have

$$\begin{aligned}\Delta V_2(\overline{\mathbf{x}}_{k+i|k}) \leq \mathbf{x}_{k+i|k}^{T}\mathbf{Q}\mathbf{x}_{k+i|k} - \mathbf{x}_{k+i-\tau(k)|k}^{T}\mathbf{Q}\mathbf{x}_{k+i-\tau(k)|k} \\ + \sum_{\theta=k+i+1-\overline{\tau}}^{k+i-\underline{\tau}}\mathbf{x}_{\theta|k}^{T}\mathbf{Q}\mathbf{x}_{\theta|k}.\end{aligned} \tag{19}$$

$\Delta\mathbf{V}_3(\overline{\mathbf{x}}_{k+i|k})$ is computed as follows:

$$\begin{aligned}\Delta\mathbf{V}_3(\overline{\mathbf{x}}_{k+i|k}) = \overline{\tau}\eta_{k+i|k}^{T}\mathbf{R}\eta_{k+i|k} + (\overline{\tau}-\underline{\tau})\,\mathbf{x}_{k+i|k}^{T}\mathbf{Q}\mathbf{x}_{k+i|k} \\ - \sum_{\theta=k+i-\overline{\tau}}^{k+i-1}\eta_{\theta|k}^{T}\mathbf{R}\eta_{\theta|k} - \sum_{\theta=k+i+1-\overline{\tau}}^{k+i-\underline{\tau}}\mathbf{x}_{\theta|k}^{T}\mathbf{Q}\mathbf{x}_{\theta|k}.\end{aligned} \tag{20}$$

By the well-known inequality $-2\mathbf{a}^{T}\mathbf{b} \leq \mathbf{a}^{T}\mathbf{R}\mathbf{a} + \mathbf{b}^{T}\mathbf{R}^{-1}\mathbf{b}$, we obtain

$$-\sum_{\theta=k+i-\overline{\tau}}^{k+i-1}\eta_{\theta|k}^{T}\mathbf{R}\eta_{\theta|k} \leq \psi^{T}(k)\,\Delta_1\psi(k), \tag{21}$$

where $\Delta_1 = 2[\widetilde{\mathbf{I}} \quad -\mathbf{I} \quad 0]^{T}\widetilde{\mathbf{Y}}+\widetilde{\mathbf{Y}}^{T}\overline{\tau}\mathbf{R}^{-1}\widetilde{\mathbf{Y}}$, $\widetilde{\mathbf{Y}} = [\widetilde{\mathbf{M}}_0 \quad \mathbf{M}_1 \quad 0]$.

Combining (15)–(21) yields

$$\Delta\overline{V}(\overline{\mathbf{x}}_{k+i|k}) \leq \psi^{T}(k)\,\Pi_1\psi(k) - \overline{\mathbf{x}}_{k+i|k}^{T}\widetilde{\mathbf{S}}\overline{\mathbf{x}}_{k+i|k}, \tag{22}$$

where

$$\begin{aligned}\widetilde{\mathbf{A}}_f &= \overline{\mathbf{A}}_f + \mathbf{D}\mathbf{F}(k)\,\overline{\mathbf{E}}, \\ \Pi_1 &= \Delta_1 + \Delta_2 + \Delta_3, \\ \Delta_2 &= \begin{bmatrix}-\mathbf{P}+\widetilde{\mathbf{S}}+\mathbf{M}_d & \mathbf{M}_b^{T} & 0 \\ \mathbf{M}_b & -\mathbf{M}_c & 0 \\ 0 & 0 & 0\end{bmatrix}, \\ \Delta_3 &= \Gamma^{\mathbf{T}}\mathbf{P}\Gamma + \begin{bmatrix}\widetilde{\mathbf{A}}_f & 0 & \mathbf{I}\end{bmatrix}^{T}\overline{\tau}\mathbf{R}\begin{bmatrix}\widetilde{\mathbf{A}}_f & 0 & \mathbf{I}\end{bmatrix},\end{aligned} \tag{23}$$

and $\psi^{T}(k)\Pi_1\psi(k) < 0$ implies that $\Delta\overline{V}(\overline{\mathbf{x}}_{k+i|k}) < -\overline{\mathbf{x}}_{k+i|k}^{T}\widetilde{\mathbf{S}}\overline{\mathbf{x}}_{k+i|k} \leq 0$; that is, $\overline{V}(\overline{\mathbf{x}}_{k+i|k})$ is degenerated. Therefore, the closed-loop system (4) is asymptotically stable. Besides, for any integer $K > 0$, we have

$$\begin{aligned}\sum_{i=0}^{K}\overline{\mathbf{x}}_{k+i|k}^{T}\widetilde{\mathbf{S}}\overline{\mathbf{x}}_{k+i|k} &\leq -\sum_{i=0}^{K}\Delta\overline{V}(\overline{\mathbf{x}}_{k+i|k}) \\ &= -\overline{V}(\overline{\mathbf{x}}_{k+K+1|k}) + \overline{V}(\overline{\mathbf{x}}_{k|k}) \\ &< \overline{V}(\overline{\mathbf{x}}_{k|k}).\end{aligned} \tag{24}$$

To guarantee the existence of the upper bound on the robust performance index $J(k)$, we must have $\mathbf{x}_{k+K|k} = 0$, $K \geq p$; hence, $\overline{V}(\overline{\mathbf{x}}_{k+K+1|k}) = 0$, $K \geq p$. Let $K \rightarrow p$, and then $\max_{[\mathbf{A}(k+i),\mathbf{B}(k+i)],i\geq 0} J(k) \leq \overline{V}(\overline{\mathbf{x}}_{k|k})$; we get (12).

By Schur complement, (2) is equivalent to the following matrix inequality:

$$\psi^T(k)\,\Pi_2\psi(k) \geq 0, \tag{25}$$

where $\Pi_2 = \mathrm{diag}\{\alpha^2\widetilde{\mathbf{H}}, 0, -\mathbf{I}\}$.

By S-procedure, $\psi^T(k)\Pi_1\psi(k) < 0$ is equivalent to the existence of matrices $\mathbf{P} > 0$, $\mathbf{Q} > 0$, $\mathbf{R} > 0$, $\mathbf{M}_0$, and $\mathbf{M}_1$ and a scalar $\lambda \geq 0$ such that

$$\begin{bmatrix} -\mathbf{M}_a & \mathbf{M}_b^T & 0 & \widetilde{\mathbf{A}}^T & \widetilde{\mathbf{A}}_f^T & \widetilde{\mathbf{M}}_0^T \\ \mathbf{M}_b & -\mathbf{M}_c & 0 & \overline{\mathbf{A}}_d^T & 0 & \mathbf{M}_1^T \\ 0 & 0 & -\lambda\mathbf{I} & \overline{\mathbf{I}} & \mathbf{I} & 0 \\ \widetilde{\mathbf{A}} & \overline{\mathbf{A}}_d & \overline{\mathbf{I}}^T & -\mathbf{P}^{-1} & 0 & 0 \\ \widetilde{\mathbf{A}}_f & 0 & \mathbf{I} & 0 & -\overline{\tau}^{-1}\mathbf{R}^{-1} & 0 \\ \widetilde{\mathbf{M}}_0 & \mathbf{M}_1 & 0 & 0 & 0 & -\overline{\tau}^{-1}\mathbf{R} \end{bmatrix} < 0. \tag{26}$$

Define matrix

$$\widehat{\mathbf{J}} = \begin{bmatrix} -\mathbf{M}_a & \mathbf{M}_b^T & 0 & \overline{\mathbf{A}}^T & \overline{\mathbf{A}}_f^T & \widetilde{\mathbf{M}}_0^T \\ \mathbf{M}_b & -\mathbf{M}_c & 0 & \overline{\mathbf{A}}_d^T & 0 & \mathbf{M}_1^T \\ 0 & 0 & -\lambda\mathbf{I} & \overline{\mathbf{I}} & \mathbf{I} & 0 \\ \overline{\mathbf{A}} & \overline{\mathbf{A}}_d & \overline{\mathbf{I}}^T & -\mathbf{P}^{-1} & 0 & 0 \\ \overline{\mathbf{A}}_f & 0 & \mathbf{I} & 0 & -\overline{\tau}^{-1}\mathbf{R}^{-1} & 0 \\ \widetilde{\mathbf{M}}_0 & \mathbf{M}_1 & 0 & 0 & 0 & -\overline{\tau}^{-1}\mathbf{R} \end{bmatrix}, \tag{27}$$

and then inequality (26) can be rewritten as

$$\begin{aligned} &\widehat{\mathbf{J}} + \begin{bmatrix} 0 & 0 & 0 & \overline{\mathbf{D}}^T & \mathbf{D}^T & 0 \end{bmatrix}^T \mathbf{F} \begin{bmatrix} \overline{\mathbf{E}} & 0 & 0 & 0 & 0 & 0 \end{bmatrix} \\ &\quad + \begin{bmatrix} \overline{\mathbf{E}} & 0 & 0 & 0 & 0 & 0 \end{bmatrix}^T \mathbf{F}^T \begin{bmatrix} 0 & 0 & 0 & \overline{\mathbf{D}}^T & \mathbf{D}^T & 0 \end{bmatrix} \\ &\quad < 0. \end{aligned} \tag{28}$$

By Lemma 2, inequality (28) holds for any matrix $\mathbf{F}(k)$ satisfying $\mathbf{F}^T(k)\mathbf{F}(k) \leq \mu\mathbf{I}$, if and only if there exists a positive scalar $\varepsilon \geq \sqrt{\mu}$ such that

$$\begin{aligned} &\widehat{\mathbf{J}} + \varepsilon \begin{bmatrix} 0 & 0 & 0 & \overline{\mathbf{D}}^T & \mathbf{D}^T & 0 \end{bmatrix}^T \mathbf{F} \begin{bmatrix} 0 & 0 & 0 & \overline{\mathbf{D}}^T & \mathbf{D}^T & 0 \end{bmatrix} \\ &\quad + \varepsilon \begin{bmatrix} \overline{\mathbf{E}} & 0 & 0 & 0 & 0 & 0 \end{bmatrix}^T \begin{bmatrix} \overline{\mathbf{E}} & 0 & 0 & 0 & 0 & 0 \end{bmatrix} < 0. \end{aligned} \tag{29}$$

By Schur complement, inequality (29) is equivalent to (10). This completes the proof. □

It is noted that in the matrix inequality (10), the controller parameters $\mathbf{A}_c$, $\mathbf{B}_c$, and $\mathbf{C}_c$ are unknown and occur in nonlinear fashion; therefore, (10) is not an LMI problem. In the sequel, we will use a method of changing variables [21] to obtain an equivalent matrix inequality representation of the nonlinear matrix inequality (10), which enables us to use the CCL technique to design the output feedback controllers.

Now, we present a sufficient condition for the existence of the output feedback delay compensation controller of the form (3) for the NCS (4).

Theorem 4. *Consider the NCS (4) and the cost function $J(k)$. Suppose that for some prescribed matrices $\mathbf{S}_1 > 0$, $\mathbf{S}_2 > 0$; there exist scalars $\gamma(k) > 0$, $\varepsilon \geq \sqrt{\mu}$, $n \times n$ matrices $\mathbf{X} > 0$, $\mathbf{Y} > 0$, $\mathbf{Q} > 0$, and $\mathbf{R} > 0$, and matrices $\mathbf{M}_0 \in \mathfrak{R}^{n\times n}$, $\mathbf{M}_1 \in \mathfrak{R}^{n\times n}$, $\widehat{\mathbf{A}} \in \mathfrak{R}^{n\times n}$, $\widehat{\mathbf{B}} \in \mathfrak{R}^{n\times v}$, and $\widehat{\mathbf{C}} \in \mathfrak{R}^{l\times n}$ such that the following optimization problem is feasible at the initial time step $k = 0$:*

$$\text{Minimize} \quad \gamma(k), \tag{30}$$

$$\text{subject to} \quad \Lambda_1 \leq 0, \tag{31}$$

$$\Lambda_2 > 0, \tag{32}$$

and then the networked predictive control derived from the solutions to the above optimization problem robustly asymptotically stabilizes the system (1), and the cost function satisfies the bound

$$\max_{[\mathbf{A}(k+i),\mathbf{B}(k+i)],i\geq 0} J(k) \leq \gamma(k), \tag{33}$$

where

$$\Lambda_1 = \begin{bmatrix} -\gamma(k)\mathbf{I} & * & * & * & * \\ \Theta_1 & \Omega_1 & * & * & * \\ \Theta_2 & 0 & \Omega_2 & * & * \\ \Theta_3 & 0 & 0 & \Omega_3 & * \\ \Theta_4 & 0 & 0 & 0 & \Omega_4 \end{bmatrix},$$

$$\Lambda_2 = \begin{bmatrix} \Xi_1 & * & * & * & * & * & * & * & * \\ \mathbf{M}_2 & \mathbf{M}_c & * & * & * & * & * & * & * \\ 0 & 0 & \lambda\mathbf{I} & * & * & * & * & * & * \\ \Xi_2 & \Xi_6 & \Xi_7 & \Omega_5 & * & * & * & * & * \\ \Xi_3 & 0 & \mathbf{I} & 0 & \overline{\tau}^{-1}\mathbf{R}^{-1} & * & * & * & * \\ \mathbf{M}_3 & \mathbf{M}_1 & 0 & 0 & 0 & \overline{\tau}^{-1}\mathbf{R} & * & * & * \\ 0 & 0 & 0 & \Xi_8 & \mathbf{D}^T & 0 & \varepsilon^{-1}\mathbf{I} & * & * \\ \Xi_4 & 0 & 0 & 0 & 0 & 0 & 0 & \varepsilon^{-1}\mathbf{I} & * \\ \Xi_5 & 0 & 0 & 0 & 0 & 0 & 0 & 0 & \Xi_9 \end{bmatrix},$$

$$\Omega_1 = \begin{bmatrix} -\mathbf{C}\mathbf{Y}\mathbf{C}^T & * \\ -\mathbf{N}^T\mathbf{C}^T & -\mathbf{W} \end{bmatrix},$$

$$\Omega_2 = \mathrm{diag}\underbrace{\left\{d_c^{-1}\mathbf{Q}_c, \ldots, d_c^{-1}\mathbf{Q}_c\right\}}_{\underline{\tau}},$$

$$\Omega_3 = \mathrm{diag}\left\{d_1^{-1}\mathbf{Q}_c, \ldots, d_{\overline{\tau}-\underline{\tau}}^{-1}\mathbf{Q}_c\right\},$$

$$\Omega_4 = \mathrm{diag}\left\{\tau_1^{-1}\mathbf{R}_c, \ldots, \tau_{\overline{\tau}}^{-1}\mathbf{R}_c\right\},$$

$$\Omega_5 = \begin{bmatrix} \mathbf{X} & \mathbf{I} \\ \mathbf{I} & \mathbf{Y} \end{bmatrix},$$

$$\mathbf{Q}_c = \mathbf{C}\mathbf{Q}^{-1}\mathbf{C}^T,$$

$$d_i = d_c + i, \quad i = 1, \ldots, \overline{\tau} - \underline{\tau},$$

$$
\begin{aligned}
&\tau_i = -\overline{\tau} - 1 + i, \quad i = 1, \dots, \overline{\tau},\\
&\mathbf{R}_c = \mathbf{C}\mathbf{R}^{-1}\mathbf{C}^T,\\
&\mathbf{Y}_i = \mathbf{y}_{k-i+1|k-i+1} - \mathbf{y}_{k-i|k-i}, \quad i = 1, \dots, \overline{\tau},\\
&\Theta_1 = \begin{bmatrix}\mathbf{y}_{k|k}^T & \widehat{\mathbf{x}}_{k|k}^T\end{bmatrix}^T,\\
&\Theta_2 = \begin{bmatrix}\mathbf{y}_{k-1|k-1}^T & \cdots & \mathbf{y}_{k-\underline{\tau}|k-\underline{\tau}}^T\end{bmatrix}^T,\\
&\Theta_3 = \begin{bmatrix}\mathbf{y}_{k-\underline{\tau}-1|k-\underline{\tau}-1}^T & \cdots & \mathbf{y}_{k-\overline{\tau}|k-\overline{\tau}}^T\end{bmatrix}^T,\\
&\Theta_4 = \begin{bmatrix}\mathbf{Y}_1^T & \cdots & \mathbf{Y}_{\overline{\tau}}^T\end{bmatrix}^T,\\
&\Xi_1 = \begin{bmatrix}\mathbf{X}-\mathbf{L} & -\mathbf{Y}^{-1}+\mathbf{L}\\ -\mathbf{Y}^{-1}+\mathbf{L} & \mathbf{Y}^{-1}-\mathbf{L}\end{bmatrix},\\
&\Xi_2 = \begin{bmatrix}\mathbf{XA} & \mathbf{XA}+\widehat{\mathbf{A}}\\ \mathbf{A} & \mathbf{A}+\mathbf{B}\widehat{\mathbf{C}}\end{bmatrix},\\
&\Xi_3 = \begin{bmatrix}\mathbf{A}-\mathbf{I} & \mathbf{A}-\mathbf{I}+\mathbf{B}\widehat{\mathbf{C}}\end{bmatrix},\\
&\Xi_4 = \begin{bmatrix}\mathbf{E}_1 & \mathbf{E}_1+\mathbf{E}_2\widehat{\mathbf{C}}\end{bmatrix},\\
&\Xi_5 = \begin{bmatrix}0 & \widehat{\mathbf{C}}\\ 0 & \alpha\mathbf{H}_2\widehat{\mathbf{C}}\end{bmatrix},\\
&\Xi_6 = \begin{bmatrix}\mathbf{C}^T\widehat{\mathbf{B}}^T & 0\end{bmatrix}^T,\\
&\Xi_7 = \begin{bmatrix}\mathbf{X} & \mathbf{I}\end{bmatrix}^T,\\
&\Xi_8 = \begin{bmatrix}\mathbf{D}^T\mathbf{X} & \mathbf{D}^T\end{bmatrix},\\
&\Xi_9 = \operatorname{diag}\left\{\mathbf{S}_2^{-1}, \lambda^{-1}\mathbf{I}\right\},\\
&\mathbf{M}_2 = \begin{bmatrix}\mathbf{M}_1^T - \mathbf{M}_0 & \mathbf{M}_1^T - \mathbf{M}_0\end{bmatrix},\\
&\mathbf{M}_3 = \begin{bmatrix}\mathbf{M}_0 & \mathbf{M}_0\end{bmatrix},\\
&\mathbf{L} = -d_c\mathbf{Q} + \mathbf{S}_1 + \mathbf{M}_0 + \mathbf{M}_0^T + \lambda\alpha^2\mathbf{H}_1^T\mathbf{H}_1.
\end{aligned} \tag{34}
$$

Proof. First, partition $\mathbf{P}$ and its inverse as

$$\mathbf{P} = \begin{bmatrix}\mathbf{X} & \mathbf{M}\\ \mathbf{M}^T & \mathbf{Z}\end{bmatrix}, \qquad \mathbf{P}^{-1} = \begin{bmatrix}\mathbf{Y} & \mathbf{N}\\ \mathbf{N}^T & \mathbf{W}\end{bmatrix}, \tag{35}$$

where $\mathbf{X} > 0$ and $\mathbf{Y} > 0 \in \mathfrak{R}^{\mathbf{n}\times\mathbf{n}}$. Note the identity $\mathbf{P}^{-1}\mathbf{P} = \mathbf{I}$ gives

$$\mathbf{M}\mathbf{N}^T = \mathbf{I} - \mathbf{X}\mathbf{Y}. \tag{36}$$

Define

$$\mathbf{U}_1 = \begin{bmatrix}\mathbf{X} & \mathbf{I}\\ \mathbf{M}^T & 0\end{bmatrix}, \qquad \mathbf{U}_2 = \begin{bmatrix}\mathbf{I} & \mathbf{I}\\ 0 & \mathbf{N}^T\mathbf{Y}^{-1}\end{bmatrix}. \tag{37}$$

Then,

$$\mathbf{P}^{-1}\mathbf{U}_1 \operatorname{diag}\left\{\mathbf{I}, \mathbf{Y}^{-1}\right\} = \mathbf{U}_2, \qquad \mathbf{U}_1^T\mathbf{P}^{-1}\mathbf{U}_1 = \Omega_5. \tag{38}$$

Define the new controller variables as

$$
\begin{aligned}
&\widehat{\mathbf{A}} = \widehat{\mathbf{B}}\mathbf{C} + \mathbf{X}\mathbf{B}\widehat{\mathbf{C}} + \mathbf{M}\mathbf{A}_c\mathbf{N}^T\mathbf{Y}^{-1},\\
&\widehat{\mathbf{B}} = \mathbf{M}\mathbf{B}_c, \qquad \widehat{\mathbf{C}} = \mathbf{C}_c\mathbf{N}^T\mathbf{Y}^{-1}.
\end{aligned} \tag{39}
$$

Therefore, given $\mathbf{X} > 0$, $\mathbf{Y} > 0$, and invertible matrices $\mathbf{M}$ and $\mathbf{N}$, the controller matrices $\mathbf{A}_c$, $\mathbf{B}_c$, and $\mathbf{C}_c$ can be uniquely determined by $\widehat{\mathbf{A}}$, $\widehat{\mathbf{B}}$, and $\widehat{\mathbf{C}}$.

Pre- and postmultiply (10) by $\operatorname{diag}\{\mathbf{U}_2^T, \mathbf{I}, \mathbf{U}_1^T, \mathbf{I}, \mathbf{I}, \mathbf{I}, \mathbf{I}\}$ and by $\operatorname{diag}\{\mathbf{U}_2, \mathbf{I}, \mathbf{U}_1, \mathbf{I}, \mathbf{I}, \mathbf{I}, \mathbf{I}\}$, respectively, set $\mathbf{U}_2^T\mathbf{M}_a\mathbf{U}_2 = \Xi_1$, $\mathbf{M}_b^T\mathbf{U}_2 = \mathbf{M}_2$, $\mathbf{U}_1^T\overline{\mathbf{A}}\mathbf{U}_2 = \Xi_2$, $\overline{\mathbf{A}}_f\mathbf{U}_2 = \Xi_3$, $\widetilde{\mathbf{M}}_0\mathbf{U}_2 = \mathbf{M}_3$, $\overline{\mathbf{E}}\mathbf{U}_2 = \Xi_4$, $\mathbf{U}_1^T\overline{\mathbf{A}}_d = \Xi_6$, and $\overline{\mathbf{D}}^T\mathbf{U}_1 = \Xi_8$, and consider the change of controller variables (39) and Schur complement, and then (32) can be obtained.

By Theorem 3, the original min-max problem (6) can be redefined as the following optimization problem that minimizes an upper bound $\gamma(k) > 0$ on the worst value of the original cost function $J(k)$:

$$
\begin{aligned}
&\text{Minimize} \quad \gamma(k)\\
&\text{subject to} \quad \max_{[\mathbf{A}(k+i),\mathbf{B}(k+i)],i\geq 0} J(k) \leq \overline{V}(\overline{\mathbf{x}}_{k|k}) \leq \gamma(k).
\end{aligned} \tag{40}
$$

By Schur complement, $\overline{V}(\overline{\mathbf{x}}_{k|k}) \leq \gamma(k)$ is equivalent to the following matrix inequality:

$$\begin{bmatrix}
-\gamma(k)\mathbf{I} & * & * & * & *\\
\overline{\mathbf{x}}_{k|k} & -\mathbf{P}^{-1} & * & * & *\\
\widetilde{\Theta}_2 & 0 & \widetilde{\Omega}_2 & * & *\\
\widetilde{\Theta}_3 & 0 & 0 & \widetilde{\Omega}_3 & *\\
\widetilde{\Theta}_4 & 0 & 0 & 0 & \widetilde{\Omega}_4
\end{bmatrix} \leq 0, \tag{41}$$

where

$$
\begin{aligned}
&\widetilde{\Theta}_2 = \left[\mathbf{x}_{k-1|k-1}^T, \dots, \mathbf{x}_{k-\underline{\tau}|k-\underline{\tau}}^T\right]^T,\\
&\widetilde{\Theta}_3 = \left[\mathbf{x}_{k-\underline{\tau}-1|k-\underline{\tau}-1}^T, \dots, \mathbf{x}_{k-\overline{\tau}|k-\overline{\tau}}^T\right]^T,\\
&\widetilde{\Theta}_4 = \left[z_1^T, \dots, z_{\overline{\tau}}^T\right]^T,\\
&\mathbf{z}_i = \mathbf{x}_{k+1-i|k+1-i} - \mathbf{x}_{k-i|k-i}, \quad i = 1, \dots, \overline{\tau},\\
&\widetilde{\Omega}_2 = \operatorname{diag}\underbrace{\left\{d_c^{-1}\mathbf{Q}^{-1}, \dots, d_c^{-1}\mathbf{Q}^{-1}\right\}}_{\underline{\tau}},\\
&\widetilde{\Omega}_3 = \operatorname{diag}\left\{d_1^{-1}\mathbf{Q}^{-1}, \dots, d_{\overline{\tau}-\underline{\tau}}^{-1}\mathbf{Q}^{-1}\right\},\\
&\widetilde{\Omega}_4 = \operatorname{diag}\left\{\tau_1^{-1}\mathbf{R}^{-1}, \dots, \tau_{\overline{\tau}}^{-1}\mathbf{R}^{-1}\right\}.
\end{aligned} \tag{42}
$$

Define $\mathbf{K}_2 = \operatorname{diag}\{\mathbf{I}, [\mathbf{C} \quad \mathbf{I}], \mathbf{C}, \dots, \mathbf{C}\}$ and pre- and postmultiply (41) by $\mathbf{K}_2$ and $\mathbf{K}_2^T$, respectively, and it follows from (35) and $\mathbf{y}_{k|k} = \mathbf{C}\mathbf{x}_{k|k}$ that inequality (41) is equivalent to inequality (31). This completes the proof. □

Remark 5. Theorem 4 presents an optimization problem to construct the desired output feedback model predictive controllers. Note that the conditions in Theorem 4 are no more LMI conditions due to the terms $\mathbf{Y}$, $\mathbf{Y}^{-1}$, $\mathbf{Q}$, $\mathbf{Q}^{-1}$, $\mathbf{R}$, and $\mathbf{R}^{-1}$. As a result, we cannot find a minimum guaranteed cost by using convex optimization algorithms. However, by using a complementarity idea [18], we can cast the original nonconvex optimization problem to a nonlinear minimization problem involving LMI constraints and, by applying a related iterative algorithm, some suboptimal guaranteed costs can be obtained.

Replace the terms $\mathbf{Y}^{-1}$, $\mathbf{Q}^{-1}$, $\mathbf{R}^{-1}$, and ε^{-1} in Λ_1, Λ_2 by $\overline{\mathbf{Y}}$, $\overline{\mathbf{Q}}$, $\overline{\mathbf{R}}$, and $\overline{\varepsilon}$, respectively, and denote the obtained matrices by $\overline{\Lambda}_1$, $\overline{\Lambda}_2$, respectively. Let the cost bound $\gamma(k)$ be lower than some specific value $J^*(k)$, and then the nonlinear minimization problem involving LMI constraints can be formulated as follows:

$$\begin{aligned}
&\text{minimize} \quad \operatorname{Trace}\left(\mathbf{Y}\overline{\mathbf{Y}} + \mathbf{Q}\overline{\mathbf{Q}} + \overline{\mathbf{R}}\mathbf{R}\right), \\
&\text{subject to} \quad \overline{\Lambda}_1 \le 0, \qquad \overline{\Lambda}_2 > 0, \qquad \gamma(k) \le J^*(k), \\
&\qquad \begin{bmatrix} \mathbf{Y} & \mathbf{I} \\ \mathbf{I} & \overline{\mathbf{Y}} \end{bmatrix} \ge 0, \qquad \begin{bmatrix} \mathbf{Q} & \mathbf{I} \\ \mathbf{I} & \overline{\mathbf{Q}} \end{bmatrix} \ge 0, \qquad \begin{bmatrix} \overline{\mathbf{R}} & \mathbf{I} \\ \mathbf{I} & \mathbf{R} \end{bmatrix} \ge 0.
\end{aligned} \tag{43}$$

If the minimum of the above nonlinear minimization problem is 3, that is, $\operatorname{Trace}(\mathbf{YG} + \mathbf{QU} + \widetilde{\mathbf{R}}\mathbf{R}) = 3$, we can say from Theorem 4 that the closed-loop system (4) is asymptotically stable with guaranteed cost $\gamma(k)$. We propose an iterative algorithm shown in the following paragraph to solve the above nonlinear minimization problem. Since it is numerically very difficult in practice to obtain the optimal solution such that $\operatorname{Trace}(\mathbf{YG} + \mathbf{QU} + \widetilde{\mathbf{R}}\mathbf{R})$ is exactly equal to 3, we use (31) and (32) as a stopping criterion in the iterative algorithm, and, thus, only some suboptimal guaranteed costs can be obtained within a specified number of iterations.

Now, we summarize the proposed robust networked predictive control algorithm as follows (Figure 1).

(1) *Delay Evaluation*. Assuming that all clocks of the nodes in the NCS are synchronized and the message is time stamped, the delay τ^{sc} can be obtained easily. In general, the network-induced delays are time varying, but the approximate probability distributions are similar. Hence, we can evaluate τ_k^{sa} as follows:

$$\tau_k^{sa} = \tau_k^{sc} + \tau_k^{ca} = t_k^c - t_k^s + \frac{1}{\rho}\sum_{l=0}^{\rho-1}\left(t_{k-l}^c - t_{k-l}^s\right), \tag{44}$$

where t_k^c is the time when controller receives the data, t_k^s is the time when the sensor samples the data, and ρ is the length of the delay window. If the delay τ_k^{sa} is longer than one sampling period h, then it can be divided into two parts $\tau_k^{sa} = (\tau(k) - 1)h + \widehat{\tau}_k$, where $\tau(k)$ is an integer and $0 < \widehat{\tau}_k \le h$.

Remark 6. The main objective of the proposed networked predictive control algorithm is to provide the control strategy to compensate the time-varying delays in the case that τ_k^{sa} can be estimated and the effectiveness of the proposed control strategy depends on the exactness of the estimate

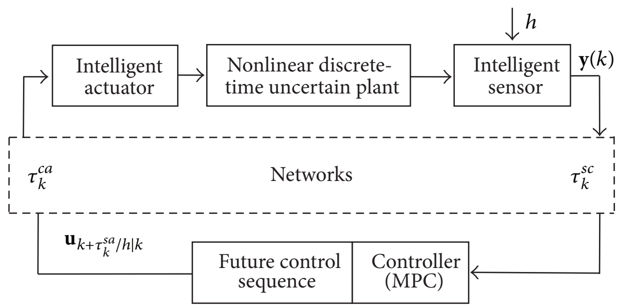

Figure 1: A robust networked predictive control system.

for τ_k^{sa}; that is, the more exact the estimate for τ_k^{sa} is, the more effective the proposed MPC algorithm will be. In this paper, a commonly used delay evaluation method is adopted just for reference, and, fortunately, a number of advanced delay evaluation methods have now been presented; see, for example, the master-slave clock synchronization technology [22], the Markov or Poisson process based evaluation method [23], and the virtual-queuing-based evaluation method [24]. Some better results can be obtained by applying these newly developed techniques. Using the proposed robust networked predictive control algorithm, the effect of the transmission lag of the manipulated variables can still be eliminated to some extent in the case that τ_k^{sa} cannot be exactly estimated.

(2) *The Iterative Algorithm*. At time step k, the nonlinear minimization problem is solved by using the iterative algorithm shown as follows to get a set of solutions $\widehat{\mathbf{A}}$, $\widehat{\mathbf{B}}$, $\widehat{\mathbf{C}}$, $\mathbf{X}$, $\mathbf{Y}$, $\mathbf{Q}$, $\overline{\mathbf{R}}$, and so forth and a suboptimal guaranteed cost $\gamma(k)$:

(a) choose a sufficiently large initial value of $J^*(k)$ such that LMIs in (43) are feasible;

(b) find feasible solutions $\mathbf{X}$, $\mathbf{Y}$, $\overline{\mathbf{Y}}$, $\mathbf{Q}$, $\overline{\mathbf{Q}}$, $\mathbf{R}$, $\overline{\mathbf{R}}$, $\widehat{\mathbf{A}}$, $\widehat{\mathbf{B}}$, $\widehat{\mathbf{C}}$, $\mathbf{M}_0$, $\mathbf{M}_1$, and $\overline{\varepsilon}$ to the LMI system in (43). Set $i = 0$;

(c) solve the optimization problem for the variables $\mathbf{Y}$, $\overline{\mathbf{Y}}$, $\mathbf{Q}$, $\overline{\mathbf{Q}}$, $\mathbf{R}$, and $\overline{\mathbf{R}}$;

$$\begin{aligned}
&\text{minimize} \quad \operatorname{Trace}\left(\mathbf{Y_i}\overline{\mathbf{Y}} + \overline{\mathbf{Y}}_\mathbf{i}\mathbf{Y} + \mathbf{R_i}\overline{\mathbf{R}} + \overline{\mathbf{R}}_\mathbf{i}\mathbf{R} + \mathbf{Q_i}\overline{\mathbf{Q}} + \overline{\mathbf{Q}}_\mathbf{i}\mathbf{Q}\right) \\
&\text{subject to} \quad (43);
\end{aligned} \tag{45}$$

(d) if conditions (31) and (32) are both satisfied within a specified number of iterations β, set $J^*(k) = J^*(k) - \Delta J^*(k)$ and return to step (b). Otherwise, if condition (31) or (32) is not satisfied, set $i = i + 1$, $\mathbf{Y}_{i+1} = \mathbf{Y}$, $\overline{\mathbf{Y}}_{i+1} = \overline{\mathbf{Y}}$, $\mathbf{Q}_{i+1} = \mathbf{Q}$, $\overline{\mathbf{Q}}_{i+1} = \overline{\mathbf{Q}}$, $\mathbf{R}_{i+1} = \mathbf{R}$, and $\overline{\mathbf{R}}_{i+1} = \overline{\mathbf{R}}$ and go to step (c). If there is no feasible solution to (31) or (32) when i has increased to β, then exit.

Remark 7. The CCL procedure is executed at each iterative step, so it will take some time to run the above algorithm. However, If a set of solutions $\widehat{\mathbf{A}}$, $\widehat{\mathbf{B}}$, $\widehat{\mathbf{C}}$, $\mathbf{X}$, $\mathbf{Y}$, $\mathbf{Q}$, and $\overline{\mathbf{R}}$ are obtained by using the iterative algorithm at the time step k, then, at the next time step $k + 1$, we can skip step (b) and use the solutions at the time step k to do step (c) directly.

By adopting the above procedures, the iterative algorithm with a faster converging rate can be obtained. Besides, the controller computational delays are trivial as compared with the network communication delays. Therefore, the proposed networked predictive control algorithm can be applied in an on-line fashion.

(3) *Calculation of the Controller Matrices*. Using the solutions obtained in step (2), the controller matrices $\mathbf{A}_c$, $\mathbf{B}_c$, and $\mathbf{C}_c$ can be uniquely determined as follows:

$$\begin{gathered}\mathbf{A}_c=\mathbf{M}^{-1}\left(\widehat{\mathbf{A}}-\mathbf{XA}-\widehat{\mathbf{B}}\mathbf{C}-\mathbf{XB}\widehat{\mathbf{C}}\right)\mathbf{YN}^{-T},\\ \mathbf{B}_c=\mathbf{M}^{-1}\widehat{\mathbf{B}},\qquad \mathbf{C}_c=\widehat{\mathbf{C}}\mathbf{YN}^{-T},\\ \mathbf{Y}=\overline{\mathbf{Y}}^{-1},\qquad \mathbf{M}=(\mathbf{I}-\mathbf{XY})\,\mathbf{N}^{-T}.\end{gathered}\tag{46}$$

(4) *Multistep Prediction and Delay Compensation*. The timing diagram of the NCS with network-induced delays is shown in Figure 3; it can be seen from Figure 3 that when the manipulated variable $\mathbf{u}(k)$ arrives at the actuator, the plant output has in fact changed from $\mathbf{y}(k)$ to $\mathbf{y}(k+\tau_k^{sa}/h)$ during data transmission in network. This situation can be viewed as the logging of the manipulated variable, which degrades the system performance and even causes the instability of the feedback control loop. The transmission lag of manipulated variable can be compensated through the method of multistep prediction. Firstly, since the old data $y(k+i-\tau(k))$, $i=0,\ldots,\tau(k)$ can be obtained at the instant $k+i$, the predicted value of the state of the output feedback controller $\widehat{\mathbf{x}}_{k+i+1|k}=\mathbf{A}_c\widehat{\mathbf{x}}_{k+i|k}+\mathbf{B}_c\mathbf{y}_{k+i-\tau(k)}$, $i=0,\ldots,\tau(k)$, and the predicted control inputs $\mathbf{u}_{k+i|k}=\mathbf{C}_c\widehat{x}_{k+i|k}$, $i=0,\ldots,1+\tau(k)$, can be calculated based on the MPC strategies. Then, we use the linear interpolation to calculate the predicted control inputs $\mathbf{u}_{k+\tau_k^{sa}/h|k}$, which is shown in Figure 2. Thus, $\mathbf{u}_{k+\tau_k^{sa}/h|k}$ can be obtained as follows:

$$\begin{aligned}\mathbf{u}_{k+\tau_k^{sa}/h|k}&=\mathbf{u}_{k+\tau(k)-1|k}\\&\quad+\left(\mathbf{u}_{k+\tau(k)|k}-\mathbf{u}_{k+\tau(k)-1|k}\right)*\left(1+\frac{\tau_k^{sa}}{h}-\tau(k)\right).\end{aligned}\tag{47}$$

Therefore, the actual plant input at time step k is $\mathbf{u}(k)=\mathbf{u}_{k+\tau_k^{sa}/h|k}$.

Remark 8. By multistep prediction, we can obtain the control input $\mathbf{u}_{k+\tau_k^{sa}/h|k}$, and it can be seen from Figure 3 that when the new manipulated variable $\mathbf{u}_{k+\tau_k^{sa}/h|k}$ arrives at the actuator, the plant output reaches $\mathbf{y}(k+\tau_k^{sa}/h)$ at the same time, so the effect of the transmission lag of the manipulated variable is eliminated and NCS can be controlled in time and effectively.

Remark 9. By using the multistep prediction and the linear interpolation method, the future control sequence can be obtained. It is assumed that a buffer is introduced at the actuator to store the future control sequence $\Pi_k=\{u_{k+\tau_k^{sa}/h|k}, u_{k+1+\tau_k^{sa}/h|k},\ldots,u_{k+\omega+\tau_k^{sa}/h|k}\}$, where the buffer size ω is set to be longer than the worst-case delay. It should be noted

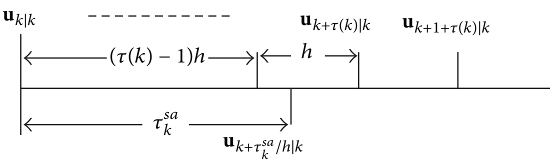

FIGURE 2: The timing diagram for multistep prediction.

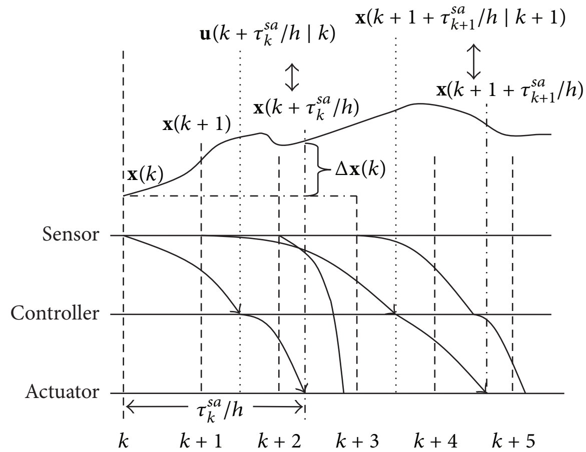

FIGURE 3: The timing diagram for sensors, controllers, and actuators in NCS.

that, with the multistep prediction and the actuator buffering method, we can treat the event of out-of-order data as well as the event of vacant sampling or packet losses. This is because, at a particular time instant, older data that arrive at the controller are used to replace data histories for use in prediction. On the other hand, older data that arrive at the actuator will be discarded if newer data are available. In the case that there is a packet loss, the corresponding control variables in the obtained future control sequence can also be chosen and implemented to eliminate the packet-loss effects. This is true as long as the sequential occurrences of out-of-order data, vacant sampling, or packet losses are within the worst-case delay.

(5) At the next time step, repeat steps (1)–(4) based on the measured output $\mathbf{y}(k)$ and the value $\widehat{\mathbf{x}}(k+1)$ of the controller state.

Remark 10. In the receding horizon framework, only the first computed control move $\mathbf{u}_{k|k}$ is implemented. At time step $k+1$, the optimization is solved again with new measurements from the plant. The purpose of taking measurements at each time step is to compensate for the unmeasured disturbances and model uncertainty. This is the main feature of the receding horizon control. Following a similar line as the proof of Lemma 6 in [25], we can conclude that the proposed networked predictive control algorithm is solvable at all time steps $k>0$ if (30) is solvable at time step $k=0$.

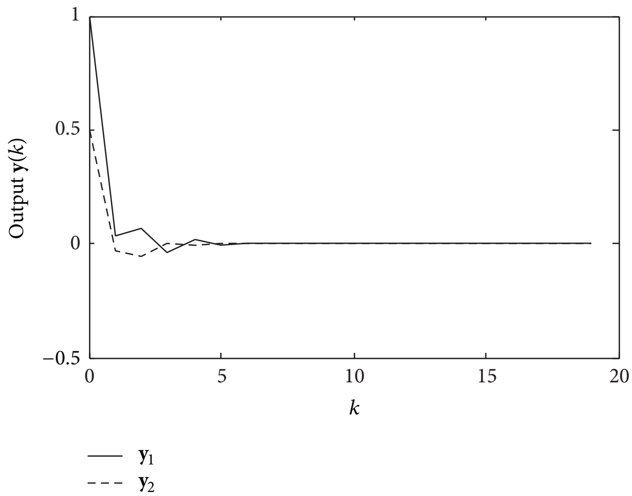

FIGURE 4: Output trajectories.

4. Illustrative Examples

In this section, an example is given to illustrate the effectiveness of the proposed robust networked model predictive controllers.

Example 11. Consider the uncertain nonlinear system (1) with the following system matrices:

$$\mathbf{A} = \begin{bmatrix} -0.3 & 0.53 \\ -0.28 & 0.4 \end{bmatrix}, \qquad \mathbf{B} = \begin{bmatrix} 0.25 \\ 1.4 \end{bmatrix},$$
$$\mathbf{C} = \begin{bmatrix} 1 & -1 \\ 0 & 0.5 \end{bmatrix}, \qquad \mathbf{D} = \begin{bmatrix} 0.2 \\ 0.12 \end{bmatrix},$$
$$\mathbf{H}_1 = \operatorname{diag}\{1, 1\}, \qquad \mathbf{E}_1 = \begin{bmatrix} 0.3 & -0.1 \end{bmatrix},$$
$$\mathbf{E}_2 = 0.7, \qquad \mathbf{F}(k) = \sin(k),$$
$$\mathbf{f} = \mathbf{x}(k)\sin\mathbf{u}(k), \qquad \mu = 1,$$
$$\alpha = 0.5, \qquad \mathbf{H}_2 = 1. \tag{48}$$

And the initial condition $\widehat{\mathbf{x}}(-i) = [2 \quad 1]^T$, $\mathbf{y}(-i) = [1 \quad 0.5]^T$, for $i = 0, 1, \ldots, \overline{\tau}$. The sampling time setup is chosen as $h = 20$ ms. We choose $\mathbf{S}_1 = \operatorname{diag}\{0.5, 0.5\}$, $\mathbf{S}_2 = 1$ in the cost function $J(k)$ defined in (4). Simulations are performed for the various values of $\tau(k)$ from 2 to 4.

We apply the proposed robust output feedback MPC algorithm to stabilize the NCS, and the simulation results are shown in Figures 4–7; Figure 4 shows the output trajectories of the NCS. Figure 5 shows the control signals. The time-varying delays are shown in Figure 6. The values of $\gamma(k)$ at each time step are shown in Figure 7. The figures illustrate that the designed control inputs lead to the stability of the NCS and guarantee an on-line suboptimal receding horizon guaranteed cost at each time step. Therefore, our method is effective.

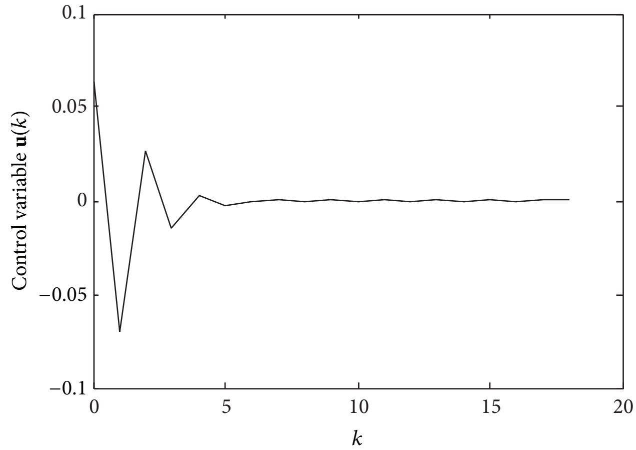

FIGURE 5: Control signals.

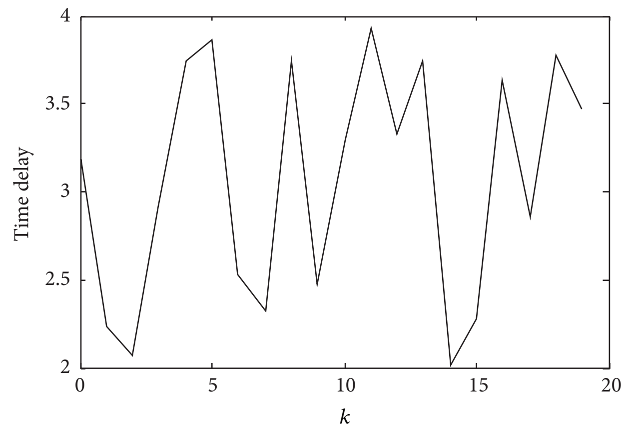

FIGURE 6: Time-varying delays.

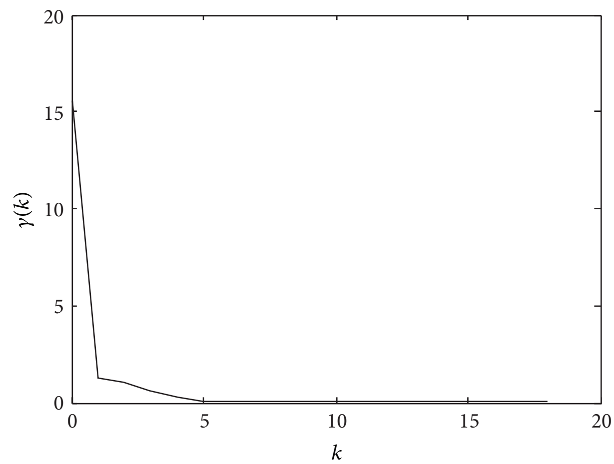

FIGURE 7: Guaranteed costs.

5. Conclusion

In this paper, we present a robust output feedback MPC method for the uncertain nonlinear discrete-time systems with time-varying network communication delays. The side-effect of the transmission lag of the manipulated variables is eliminated by using the method of delay evaluation and multistep prediction. By using the MPC strategies and the LMI techniques, a delay-dependent sufficient condition is derived for the existence of the dynamic output feedback controllers, and an on-line optimization algorithm is also presented to construct the desired controllers with a suboptimal guaranteed cost at each time step. Besides, it is not necessary to tune any parameter in the optimization algorithm. Therefore, it is quite suitable for practical applications.

Conflict of Interests

The authors declare that there is no conflict of interests regarding the publication of this paper.

Acknowledgments

This work is partially supported by the Environmental Projects of Zhejiang Province under Grant 2013A032, the Public Projects of Zhejiang Province under Grants 2014C33044 and 2012C32021, the Project of Education Department of Zhejiang Province under Grant Y201327680, and Research Center for Smart Agriculture and Forestry under Grant 2013ZHNL02.

References

[1] A. Bemporad, M. Heemels, and M. Johansson, *Networked Control Systems*, vol. 406 of *Lecture Notes in Control and Information Sciences*, Springer, London, UK, 2010.

[2] Y. Sun and N. H. El-Farra, "Quasi-decentralized model-based networked control of process systems," *Computers and Chemical Engineering*, vol. 32, no. 9, pp. 2016–2029, 2008.

[3] R. A. Gupta and M. Y. Chow, "Networked control system: overview and research trends," *IEEE Transactions on Industrial Electronics*, vol. 57, no. 7, pp. 2527–2535, 2010.

[4] D. Zhang, Q.-G. Wang, L. Yu, and H. Song, "Fuzzy-model-based fault detection for a class of nonlinear systems with networked measurements," *IEEE Transactions on Instrumentation and Measurement*, vol. 62, no. 12, pp. 3148–3159, 2013.

[5] D. Zhang, Q.-G. Wang, L. Yu, and Q.-K. Shao, "H_∞ filtering for networked systems with multiple time-varying transmissions and random packet dropouts," *IEEE Transactions on Industrial Informatics*, vol. 9, no. 3, pp. 1705–1716, 2013.

[6] Y. Zhang and H. Fang, "Stabilization of nonlinear networked systems with sensor random packet dropout and time-varying delay," *Applied Mathematical Modelling*, vol. 35, no. 5, pp. 2253–2264, 2011.

[7] M. C. F. Donkers, W. P. M. Heemels, D. Bernardini, A. Bemporad, and V. Shneer, "Stability analysis of stochastic networked control systems," *Automatica*, vol. 48, no. 5, pp. 917–925, 2012.

[8] N. W. Bauer, P. J. H. Maas, and W. P. M. Heemels, "Stability analysis of networked control systems: a sum of squares approach," *Automatica*, vol. 48, no. 8, pp. 1514–1524, 2012.

[9] W. J. Xu, Z. Zhou, and Q. Liu, "Hybrid one-way delay estimation for networked control system," *Advances in Engineering Software*, vol. 41, no. 5, pp. 705–711, 2010.

[10] H. Li, H. Yang, F. Sun, and Y. Xia, "A network-bound-dependent stabilization method of networked control systems," *Automatica*, vol. 49, no. 8, pp. 2561–2566, 2013.

[11] W. A. Zhang and L. Yu, "A robust control approach to stabilization of networked control systems with short time-varying delays," *Acta Automatica Sinica*, vol. 36, no. 1, pp. 87–91, 2010.

[12] G.-S. Tian, F. Xia, and Y.-C. Tian, "Predictive compensation for variable network delays and packet losses in networked control systems," *Computers and Chemical Engineering*, vol. 39, pp. 152–162, 2012.

[13] Z. H. Pang, G. P. Liu, D. H. Zhou, and M. Y. Chen, "Output tracking control for networked systems: a model-based prediction approach," *IEEE Transactions on Industrial Electronics*, vol. 61, no. 9, pp. 4867–4877, 2014.

[14] Y. Xia, W. Xie, B. Liu, and X. Wang, "Data-driven predictive control for networked control systems," *Information Sciences*, vol. 235, pp. 45–54, 2013.

[15] C. Tan and G. Liu, "Consensus of discrete-time linear networked multi-agent systems with communication delays," *IEEE Transactions on Automatic Control*, vol. 58, no. 11, pp. 2962–2968, 2013.

[16] G. Pin and T. Parisini, "Networked predictive control of uncertain constrained nonlinear systems: recursive feasibility and input-to-state stability analysis," *IEEE Transactions on Automatic Control*, vol. 56, no. 1, pp. 72–87, 2011.

[17] D. E. Quevedo and D. Nešić, "Robust stability of packetized predictive control of nonlinear systems with disturbances and Markovian packet losses," *Automatica*, vol. 48, no. 8, pp. 1803–1811, 2012.

[18] L. El Ghaoui, F. Oustry, and M. AitRami, "A cone complementarity linearization algorithm for static output-feedback and related problems," *IEEE Transactions on Automatic Control*, vol. 42, no. 8, pp. 1171–1176, 1997.

[19] D.-S. Kim, Y. S. Lee, W. H. Kwon, and H. S. Park, "Maximum allowable delay bounds of networked control systems," *Control Engineering Practice*, vol. 11, no. 11, pp. 1301–1313, 2003.

[20] L. Yu and F. Gao, "Optimal guaranteed cost control of discrete-time uncertain systems with both state and input delays," *Journal of the Franklin Institute*, vol. 338, no. 1, pp. 101–110, 2001.

[21] C. Scherer, P. Gahinet, and M. Chilali, "Multiobjective output-feedback control via LMI optimization," *IEEE Transactions on Automatic Control*, vol. 42, no. 7, pp. 896–911, 1997.

[22] W. Zhen, M. Xiang-Hua, and X. Jian-Ying, "A novel control scheme based on online delay evaluation for a class of networked control systems," in *Proceedings of the American Control Conference (ACC '03)*, pp. 4143–4148, June 2003.

[23] L. Zhang and F. Hua-Jing, "A novel controller design and evaluation for networked control systems with time-variant delays," *Journal of the Franklin Institute*, vol. 343, no. 2, pp. 161–167, 2006.

[24] B. Addad, S. Amari, and J.-J. Lesage, "A virtual-queuing-based algorithm for delay evaluation in networked control systems," *IEEE Transactions on Industrial Electronics*, vol. 58, no. 9, pp. 4471–4479, 2011.

[25] Y. Y. Cao and Z. L. Lin, "Min-max MPC algorithm for LPV systems subject to input saturation," *IET Control Theory & Applications*, vol. 152, pp. 266–272, 2005.

Hindawi Publishing Corporation
Mathematical Problems in Engineering
Volume 2015, Article ID 912535, 8 pages
http://dx.doi.org/10.1155/2015/912535

Research Article

Smart Demand Response Based on Smart Homes

Jingang Lai, Hong Zhou, Wenshan Hu, Dongguo Zhou, and Liang Zhong

Department of Automation, Wuhan University, Wuhan 430072, China

Correspondence should be addressed to Wenshan Hu; wenshan.hu@whu.edu.cn

Received 12 August 2014; Accepted 30 September 2014

Academic Editor: Yun-Bo Zhao

Smart homes (SHs) are crucial parts for demand response management (DRM) of smart grid (SG). The aim of SHs based demand response (DR) is to provide a flexible two-way energy feedback whilst (or shortly after) the consumption occurs. It can potentially persuade end-users to achieve energy saving and cooperate with the electricity producer or supplier to maintain balance between the electricity supply and demand through the method of peak shaving and valley filling. However, existing solutions are challenged by the lack of consideration between the wide application of fiber power cable to the home (FPCTTH) and related users' behaviors. Based on the new network infrastructure, the design and development of smart DR systems based on SHs are related with not only functionalities as security, convenience, and comfort, but also energy savings. A new multirouting protocol based on Kruskal's algorithm is designed for the reliability and safety of the SHs distribution network. The benefits of FPCTTH-based SHs are summarized at the end of the paper.

1. Introduction

The whole world including American, European, Chinese, Indian, and other major economics starts to pay more attention to DRM and implement strict policies in order to achieve energy saving and CO_2 reductions [1–4]. The pursuit of low-carbon economic and energy efficiency has strongly motivated the development of SG and energy management technologies [5, 6]. DR-based energy management which is able to improve energy efficiency and manageability of current power network is a crucial research topic of SGs. On the terminal user side, DR-based energy management systems, which are usually integrated with SHs systems, play an important role in the control and optimization of domestic energy consumption and enable increasing consumer participation [7–9]. Meanwhile, the energy network on SHs has received extensive attentions due to its flexible integration into people's daily lives, which could trigger significant commercial value to develop smart applications and corresponding services for ubiquitous homes [10]. These systems offer the end-users detailed information about their energy consumption patterns, which could potentially persuade them to adopt more energy efficient behaviors.

For many years, State Grid Corporation of China has been prompting the "strong smart grid" development strategy, whose main content is to build a modern power grid with ultrahigh voltage power transmission as the backbone, and the coordinated development of power grid at all levels, such as the features of information technology, automation, and interactions. In China, FPCTTH technologies are being widely used in the constructions of SG. The adoption of optical fibers provides strong communications capacities for the power cables. Apart from transmitting the control signals for the SG control, Power cables can also provide services for internet, telephones, and television to realize the "quadruple play." This paper concentrates on the issues with respect to the design and implementation of SHs based on FPCTTH, which are the key element for the DR of SG.

The ubiquitous SHs networks have gradually evolved into complex systems to deal with various tasks, such as security, environment control, health, and also energy management. To achieve the energy saving targets, the establishment of efficient two-way information exchanges between end-users and power utility is utterly important. In the near future, SHs will be expanded into large networks, called smart communities or smart cities, which provide potentially larger scale energy savings and other relevant power management services. However, without reliable information exchange channels, the smart appliances are not able to implement effective energy saving strategies regarding the official energy policies on SG, which could negatively affect the implementation of DR policies.

As a part of SG, SHs systems with the characters and functions of DRM have gained great attention from the State Grid Corporation of China. It has funded multiple projects on large-scale domestic FPCTTH energy monitoring, response and management. With adequate information provided for the users, rational analysis and feedback based on their energy costs can be made to persuade them to change behaviors towards more environmentally friendly and energy efficient patterns.

All the discussions in this paper are based on the FPCTTH with tree topology which have more than enough bandwidth capacities to offer various services, such as domestic energy monitoring, response, and management. In Section 2, some related works, such as the role of SHs in the DR programs and the optimization of energy networks, are introduced. The system architecture and relative technical issues on its implementation are discussed in Section 3. In Section 4, the details about how SHs based on FPCTTH play a more active role to offer relevant benefits to end-users are explained before the conclusions are made in Section 5.

2. Role of SHs in DRM

DRM employs the flexible control in reducing the electricity consumption and peak loads to seek a balance between supply and demand of electrical energy [11]. It can achieve better utilization of the available energy and more stable and effective operation of power industry. DR involves all conscious modifications of electricity usage patterns by end-users that are intended to change electricity time, instantaneous demand level, or total electricity consumption [12]. End-users are able to actively take part in the power market management via adjusting their power consumption patterns rather than passively receiving fixed electricity prices, which gives benefits to both the power utilities and end-users.

At present, the researches mainly focus on how to put forward the concrete programs on DR from the point of view of power generation business or management [13]. They mainly address the incentive-based programs such as direct control and market based demand bidding. However, how to actually implement these programs is not their primary consideration. With the fast development of SHs and FPCTTH, end-users are able to exchange information with their power producers through the information service platform. Through the reliable communication channels provided by the fiber power cables, DR policies can be easily implemented. As shown in Figure 1, the fiber power cables, which transmit both electricity and information, are able to form a closed loop between end-users and power grid enterprise.

The conventional methods to achieve DRM are price-based measures and incentive-based measures [10]. Price-based measures are based on dynamic pricing rates which fluctuate following the real-time costs of electricity. The final purpose is to keep the demand curve smooth by imposing high prices during peak periods and low prices during valley periods. The basic type of price-based programs is the time of use rates, which are the rates of electricity price per unit consumption that varies in different blocks of time. The rate design attempts to reflect the average cost of electricity during different periods [14]. During contingencies, critical peak pricing rates with a prespecified even higher price are imposed to the users [15, 16].

Incentive-based measures are composed of direct load control measures, interruptible/curtailable load measures, emergency DR measures, and so forth. End-users who agree to cooperate with DRM are rewarded with credits according to the amount of load reduction during critical conditions. However, as the price, power utilities may seek some kinds of direct control on the users electrical consumption. For example, in case of contingencies, they may require the authorities to shut down participants' non-time-critical equipment such as air conditioners or water heaters remotely [5].

In order to implement these measures, SHs systems are becoming the bridge between DRM and SG, since SHs systems are able to simultaneously and effectively communicate between the energy services and households. To achieve domestic energy saving, energy monitoring technologies that provide real-time feedback on energy consumption (e.g., time of use or real-time pricing) are being deployed worldwide. It can potentially reduce the energy usage by up to 15% [3]. Some well-known companies, including ABB, Honeywell, and Siemens, begin to focus on the energy management for smart electricity consumption. The analysis of electric energy data [17] gives the end-users the detailed information about the consumption. However, these studies are lacking the participation from the power industries. Although the domestic Haier's U-Home solutions have been put into application in several residential real estates [18], they are trying to derive information interpretability in the device layer of customers home. However, it requires dedicated communication link and home appliances and is subject to the operators' support of communications network [5, 19].

Although [20, 21] realize the intelligent management for the refrigerator and water heater, their DR systems are isolated from the latest SG development, without building AMI mesh networks [22] and popularizing the technology to the SHs. Power line communication has been used to transmit related data for SHs [23]; however, these wired systems have limitations on scalability and resiliency and are also lacking comprehensive security notion that satisfies the needs for security-critical SHs services. On the contrary, the implementation of ZigBee-based communication provides significant advantages comparing with conventional communication technologies [24], such as rapid deployment, low cost, flexibility, and aggregated intelligence through parallel processing. In [25, 26], the implementation of ZigBee-based communication in the demand side of SG is introduced.

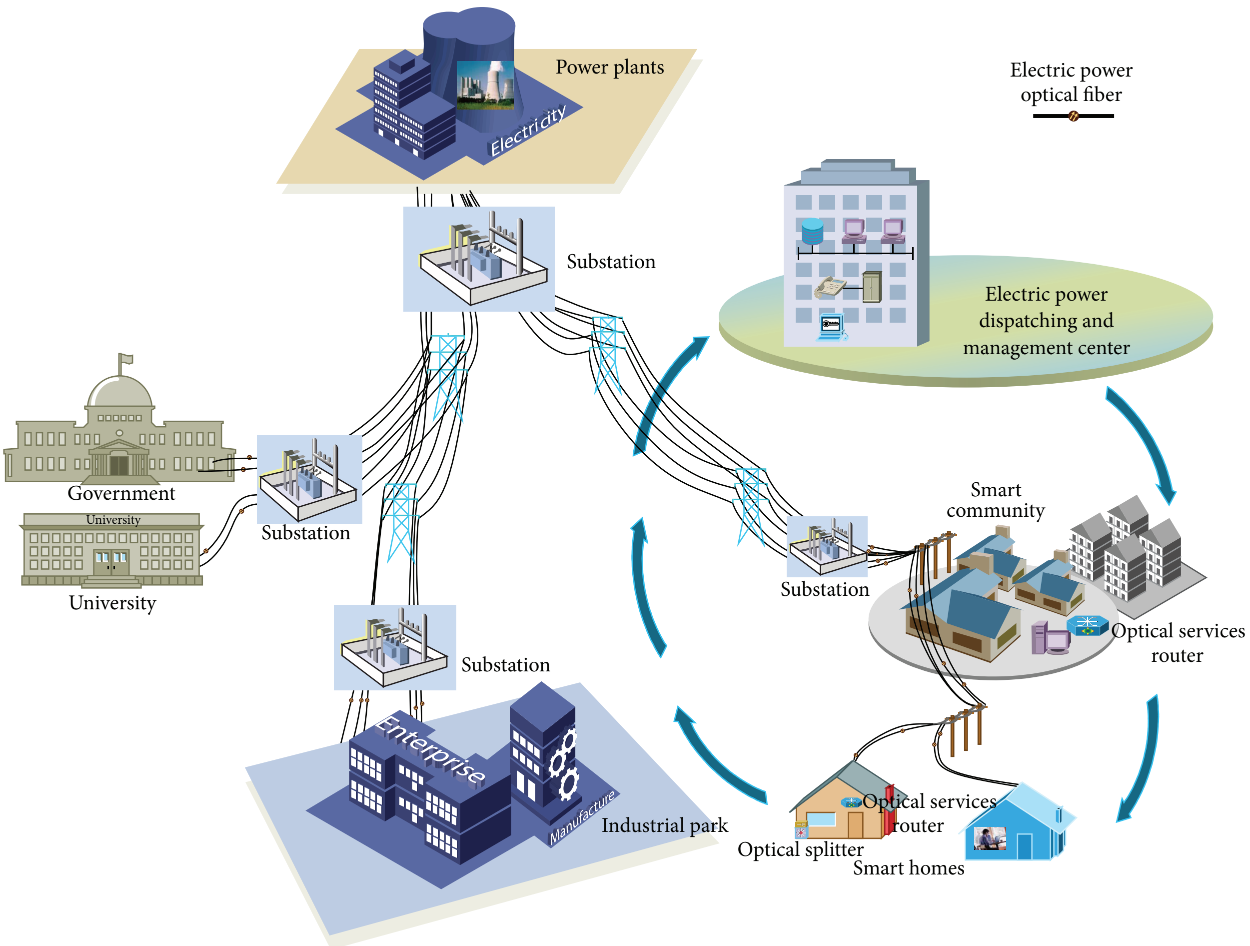

FIGURE 1: System architecture of the FPCTTH-based SG.

In [22, 27], SG network security issues in a wide forecasting volume and advanced measurement systems are discussed.

3. SHs System Architecture

SHs are able to potentially achieve energy savings and other energy-related services as long as effective two-way information exchange bridges between the world of energy service and the household world can be implemented. Due to the high communication capacity, FPCTTH can easily provide synchronous transmission of energy and massive information.

3.1. Overall Structure. The SHs network architecture proposed in the paper is as shown in Figure 2. This system is designed to coordinate and control the smart household appliances via "quadruple mode" based on FPCTTH with tree topology. The combination of distributed and centralized monitoring is carried out in the whole network architecture. In order to get the energy monitoring, demand side response, and management for SHs, the distributed monitoring mode is used not only to collect and analyze data with the help from higher layers or other distributed systems, but also to take the necessary decisions according to the calculation of local control, without any interventions from the control center. This system has a hierarchical network architecture as shown in Figure 2.

3.2. In-Home Control. The main element of in-home architectures is a ARM based smart terminal which is connected with all the indoor appliances, sensors, and actuators. A human-machine interface is provided for the users to manage all the home devices.

Figure 2 gives an overview of the proposed SHs system in the environment of smart community. The system is able to control various in-home appliances such as lamps, air conditioners, curtains, electric water heaters, and TVs. It can also be accessed using various internet terminals such as PC, tablets, and smart phones. Lots of sensors are deployed to measure the electricity consumption, indoor environment, security alarm, and so forth.

Further information about the detailed design and implementation of the FPCTTH-based SHs can be found in the early work [28]. The implementation in the laboratory environment is shown in Figure 3, where various components such as sensors and smart appliances are deployed.

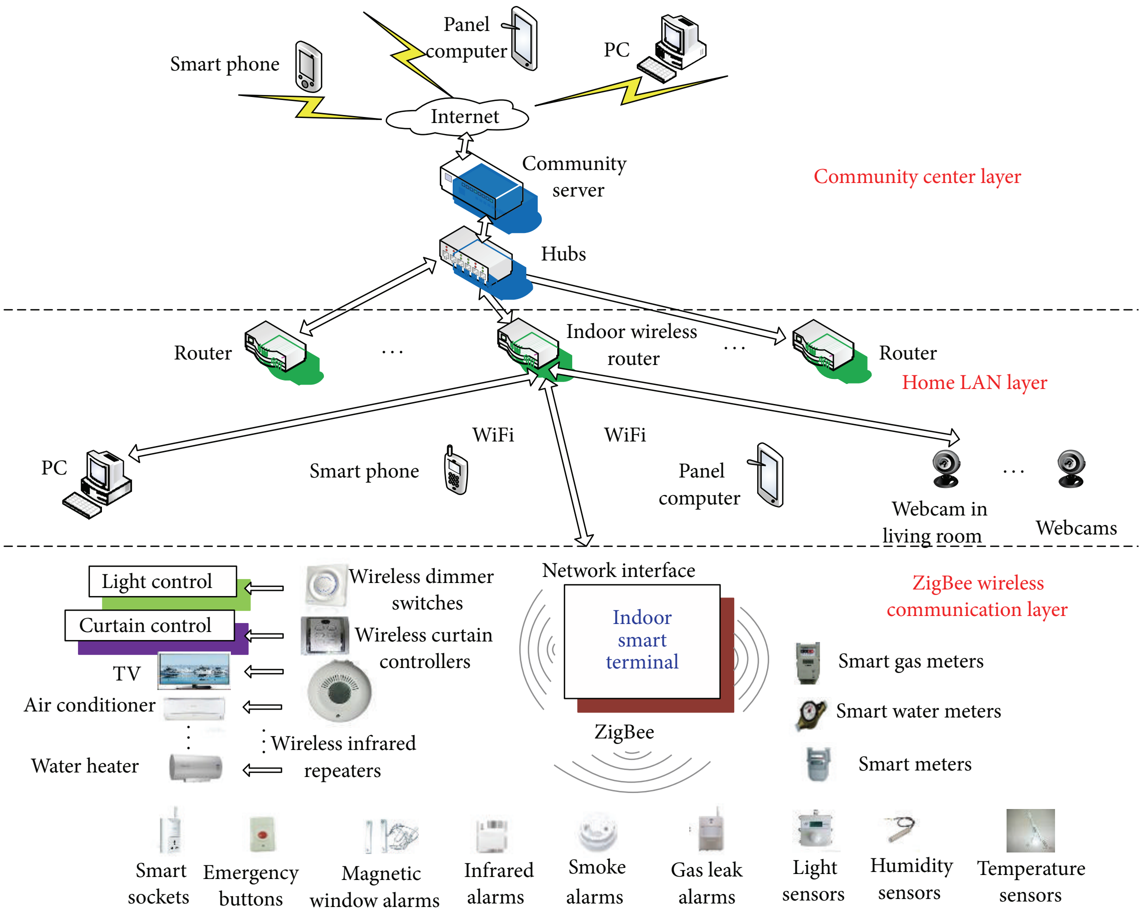

Figure 2: System architecture of the SHs.

They communicate with the indoor smart terminal via 2.5 GHz ZigBee transmitter in real time. The electricity consumption data such as power consumption, transient power, electricity consumption fare during on-peak periods and off-peak periods, and maximum current/power value are collected every ten seconds. These data can be exchanged between the power utilities and end-users through the FPCTTH-based communication channels.

3.3. System Network. The solution presented in this paper selects optical fiber composite low-voltage cable and ZigBee as primary communication technologies, also proposes an IP-based communication protocol between the indoor home smart terminals and the control center.

As the fiber power cable has big communication capacity, apart from transmitting power, it can also provide services for internet, telephone, and television to form the so-called "quadruple play technology" as shown in Figure 4. Using the "quadruple play technology", the internet, telephone, and television signals are transmitted through the fiber power cable. As it provides full solutions covering both power and communication services for end-users, theoretically other cabling towards the household is no longer necessary.

The proposed system supports the access from various smart terminals, such as PC, smart phones, and tablets. In the system network, there are in-home smart sensors, actuators, and controllers which support multiple communication technologies such as Ethernet, WiFi, and ZigBee. Ethernet acts as a bridge between Internet and smart terminals,so that the system can provide HTML web page browsing services. End-users can check their current home environment using the web browser anywhere, anytime. Since the wireless AP is also connected to the system, end-users can access the home HTTP server through laptops and PADs in the house. Itinerant users can access those home services via mobile devices.

In the home LAN layer, the quadruple signals are decoded into television signals, telephone signals, and Internet signals by an optical network unit. Inside the house, smart terminals are used to manage all of the household equipment, such as security sensors, smart meters, and smart sockets. Smart terminals communicate with the smart household devices via ZigBee-based wireless communication.

The pervasive ZigBee technology is adopted for in-home transmission of sensors/actuators due to very low battery consumption and also offering specific profiles for both the home automation and energy measurement. However, it can

Figure 3: SHs indoor physical map.

be a problem with tall buildings and with thick walls for ZigBee information transmission. It can be overcome owing to the inherent structure (mesh) of the wireless standard, where intermediate sensors/actuators operate as repeaters. Thus, it is necessary to create within each building an infrastructure with a number of distributed sensors/actuators in order to ensure proper connections and full coverage.

3.4. Multipath Routing Connection Protocol. In order to ensure a proper connection and full coverage, proper routing protocols are designed to manage the distributed sensors/actuators. Each sensor/actuator has multihop routing protocol to automatically establish the wireless network between smart nodes. Then, end-users or service-providers, at the house location, can utilize the messages directly as long as the same protocol is deployed for meter data transmission and home automation services. Nevertheless, conventional routing protocols are difficult to adapt with the characters of dynamic topology variations like the proposed SHs system like the proposed SHs system. Therefore, a new routing protocol is designed based on Kruskal's algorithm named multipath routing connection protocol (MPRCP) for the wireless networks on SHs. The formation of the network is based on the MPRCP value by means of measuring from the RF radio.

The specific operation mechanism is as follows. The communication network of a SH can be modeled by a digraph. The sensors/actuators are considered as the nodes of the communication digraph. The complex weighted graph is $\mathscr{G}(\mathscr{V}, \mathscr{E}, \mathscr{A})$ with node set $\mathscr{V} = \{1, 2, \ldots, n\}$, edge set $\mathscr{E}$, and symmetric edge weights $\mathscr{A}_{ij} = \mathscr{A}_{ji}$ involving link costs of time-delay, bandwidth, and traffic load for every branch $(i, j) \in \varepsilon$. The state of a node $\mathscr{V}_{ij}$ is defined as follows:

$$\mathscr{V}_{ij} = \begin{cases} 1, & \text{if there is the link from node } i \text{ to } j \text{ in solution,} \\ 0, & \text{otherwise.} \end{cases} \tag{1}$$

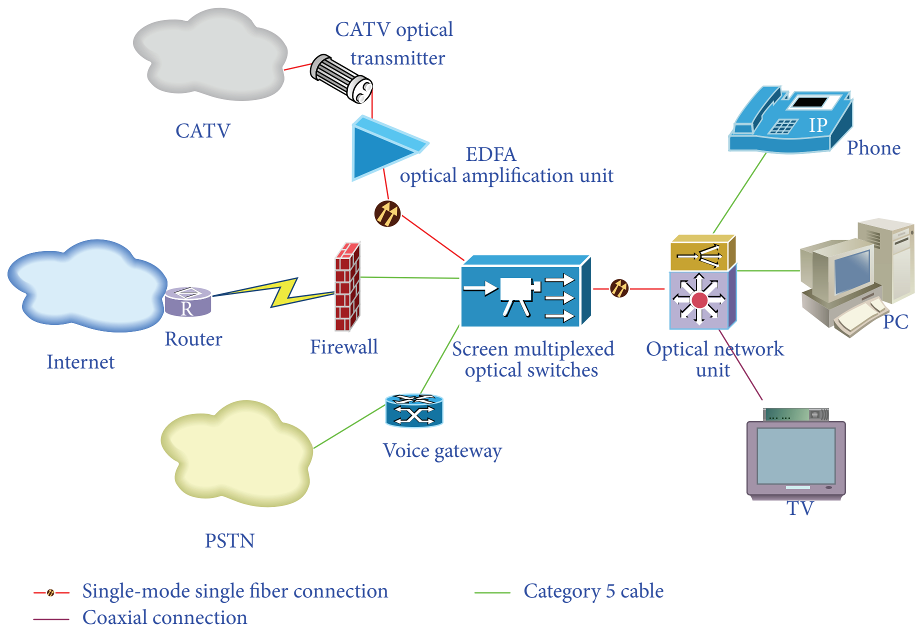

FIGURE 4: Quadruple play network structure.

A matrix $\mathscr{E} = [\mathscr{E}_{ij}]$ is defined for the link connection (or edge) as follows:

$$\mathscr{E}_{ij} = \begin{cases} 1, & \text{if there is the link from node } i \text{ to } j \\ 0, & \text{otherwise.} \end{cases} \quad (2)$$

If there is no link from node i to j, $\mathscr{A}_{ij}$ is set to a very large value so as to reject it from the routing path. P is the source node set, and Q is the destination node set. For multiple destinations problem, define $q \in \text{Q}$ as the set of destinations where $q_t \in \mathscr{V}$, $t = \{1, \ldots, n\} \in \mathscr{T}$. When P is nonempty and n is not yet spanning, we remove a node with minimum energy from P. If that node connects two different networks, then add it to the network, combining two networks into one network; otherwise, reject that node.

If an undirected routing regarding multiple destinations q is defined as follows [29]:

$$\text{Path}^{pq_t} = (p, \alpha, \beta, \ldots, q_1, \ldots, q_2, \ldots, i, q_t), \quad (3)$$

that is to say, the routing is $(p \rightarrow \alpha \rightarrow \beta \rightarrow \cdots \rightarrow q_1 \rightarrow \cdots \rightarrow q_2 \rightarrow \cdots \rightarrow i \rightarrow q_t)$, then the total cost $[\text{TotalCost}]_{pq_t}$ of this issue is turned into $[\text{TotalCost}]_{pq_t} = \mathscr{A}_{p\alpha}\mathscr{E}_{p\alpha} + \mathscr{A}_{\alpha\beta}\mathscr{E}_{\alpha\beta} + \cdots + \mathscr{A}_{ip_t}\mathscr{E}_{ip_t}$.

According to the above definitions, the problem of multiple destinations can describe the constrained combinatorial optimization issue; the expressions are as follows:

$$\text{Minimize} \quad \sum_{i=0}^{n-1}\sum_{j=0}^{n-1} \mathscr{A}_{ij}\mathscr{E}_{ij}, \quad (4)$$

for all $(p \rightarrow q_t)$

$$\text{Subject to} \quad \left(\sum_{\substack{j=0 \\ j \neq i}}^{n-1} \mathscr{A}_{ij} - \sum_{\substack{k=0 \\ k \neq i}}^{n-1} \mathscr{A}_{ki} \right) = \begin{cases} 1, & \text{if } i = p, \\ -1, & \text{if } i = q_t, \\ 0, & \text{otherwise.} \end{cases} \quad (5)$$

At the termination of the algorithm, the network has only one component and forms a minimum spanning network of the graph. It is shown that Kruskal's algorithm is run $0(n \log n)$ times or equivalently $0(n \log n)$ time, all with simple data structures. These running times are equivalent [25].

With the proposed tree topology MPRCP, each node only needs to communicate with its neighboring nodes intermittently to select the special node having the best MPRCP value even if their communication networks are local, while the data packet is put forward to the sink node. Meanwhile, the topology of routing path is dynamically adjusted because every node continuously monitors the neighbor information on the lists of MPRCP whenever exchanging information. The MAC protocol for shared media access is introduced, and the MPRCP value is provided by a special RF device with narrow band.

3.5. Home Security. In this section, the security issues of ZigBee-based wireless communication scheme for SHs are studied. All the data collected from the smart homes are related to the users daily lives. They could be of great privacy and should not be tapped during the communication. The completeness and precision of sensitive information must be protected against possible malicious attacks.

In the proposed SHs system, encryption security gateways are set up in the community layer to keep the sensitive

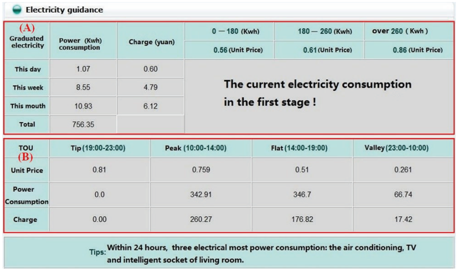

FIGURE 5: Snapshots of the dashboard pages on incentive-based demand response. Features are highlighted by red rectangles, graduate price on current energy consumption of each appliance using web technologies; (B) time of use (TOU) on current energy consumption of each appliance using web technologies.

FIGURE 6: Snapshots of electricity guidance using the third-party web or app technologies. Features are highlighted by red rectangles, including (A) navigation panel, (B) user info and network status, (C) news, (D) appliance control, (E) energy savings compared to historical usage and live energy usage, (F) monitoring alarms, (G) indoor environment, (H) video surveillance, and (I) three-meter information and history curve of current energy usage using web technologies.

information secure. The whole data encryption process for in-home security is divided into two stages: firstly, each sensor/actuator must be configured at the time of installation. Using this initial knowledge, each sensor/actuator is able to prove its identity and may dynamically join one or more secure communication relationships at the time of first running. Secondly, within such a secure relationship, the sensor/actuator is able to exchange data through a secured channel. Symmetric cryptographic algorithms are used to realize the objectives of a secured channel. A typical example could be the use of encryption algorithms like DES to guarantee data confidentiality and a MAC algorithm to guarantee data integrity.

4. Benefits of Smart Home

The SHs implement brings significant benefits to the electricity suppliers within a medium or short time. It supplies a more prompt and accurate billing information for the end-users and helps them to reduce the energy costs by adopting more energy efficient and environmentally friendly life styles. Nonetheless, a complete exploitation of DR in SG advantages can only be achieved when efficient FPCTTH-based communication channels between the energy services department and the household are established. The end-users also can enjoy lots of benefits as they have detailed information and more control about their electricity usage. Consider the following.

(1) From the aspect of consumption information and energy saving awareness for end-users, the proposed system lets end-users know their detailed consumption. Therefore, they are encouraged to change their behaviors to reduce the energy costs. Through the web-based interface as shown in Figures 5 and 6, end-users are able to intuitively see all kinds of home appliances, power consumption information, and the corresponding costs clearly.

(2) From the aspect of interactive services for DRM, the purpose of incentive DR policies is to make full use of mechanisms of the energy market and the differentiation on energy rate during the day to save the consumption costs for end-users. End-users are able to take these actions, such as the reduction of the power supply based on the information from the management platform (as shown in Figure 5) and the choice of usage hours at low price, to achieve energy saving. When end-users can easily see their consumption information, they would voluntarily perform relevant policies. Figure 6 shows incentive-based DR options including remote control of customer's electrical equipment for a short notice or the end-users reducing load during system contingencies in return for rate discounts.

5. Conclusion

In this paper, a novel DRM based on SHs and FPCTTH system has been introduced. The use of FPCTTH provides reliable communication channels for the interaction between electricity suppliers and end-users. The advantage of FPCTTH is that there is a considerable reduction of cabling and it can be achieved through a simple extension for the low-voltage lines of the previously installed network. The SHs system proposed in this paper has been implemented in the laboratories of State Grid Technology College in China. It is able to create an interactive environment for end-users to actually understand how the electricity is consumed and what is the real-time costs. With all the information which can be accessed through a web-based interface, the users can be encouraged to adjust their behaviors and consume less energy. ZigBee technologies are also used for the communications between the indoor smart terminal and various household smart appliances. In order to keep the radiabilities of the ZigBee communication for the SHs system, a new MPRCP based on Kruskal's algorithm is introduced in the paper.

Conflict of Interests

The authors declare that there is no conflict of interests regarding the publication of this paper.

Acknowledgments

This work was supported by National Key Technology Support Program of China under Grant 2013BAA01B01, by the National Natural Science Foundation of China under Grant 61374064, and by the Fundamental Research Funds for the Central Universities under Grant 2014208020201.

References

[1] S. M. Amin and B. F. Wollenberg, "Toward a smart grid: power delivery for the 21st century," *IEEE Power and Energy Magazine*, vol. 3, no. 5, pp. 34–41, 2005.

[2] H. Farhangi, "The path of the smart grid," *IEEE Power and Energy Magazine*, vol. 2, pp. 18–28, 2010.

[3] C.-C. Lin, C.-H. Yang, and J. Z. Shyua, "A comparison of innovation policy in the smart grid industry across the pacific: China and the USA," *Energy Policy*, vol. 57, pp. 119–132, 2013.

[4] Q. Liu, G. Cooper, N. Linge, H. Takruri, and R. Sowden, "DEHEMS: creating a digital environment for large-scale energy management at homes," *IEEE Transactions on Consumer Electronics*, vol. 59, no. 1, pp. 62–69, 2013.

[5] P. Palensky and D. Dietrich, "Demand side management: demand response, intelligent energy systems, and smart loads," *IEEE Transactions on Industrial Informatics*, vol. 7, no. 3, pp. 381–388, 2011.

[6] D. Dietrich, D. Bruckner, G. Zucker, and P. Palensky, "Communication and computation in buildings: a short introduction and overview," *IEEE Transactions on Industrial Electronics*, vol. 57, no. 11, pp. 3577–3584, 2010.

[7] F. Rahimi and A. Ipakchi, "Demand response as a market resource under the smart grid paradigm," *IEEE Transactions on Smart Grid*, vol. 1, no. 1, pp. 82–88, 2010.

[8] H. A. Aalami, M. P. Moghaddam, and G. R. Yousefi, "Demand response modeling considering interruptible/curtailable loads and capacity market programs," *Applied Energy*, vol. 87, no. 1, pp. 243–250, 2010.

[9] G. Strbac, "Demand side management: benefits and challenges," *Energy Policy*, vol. 36, no. 12, pp. 4419–4426, 2008.

[10] M. H. Albadi and E. F. El-Saadany, "A summary of demand response in electricity markets," *Electric Power Systems Research*, vol. 78, no. 11, pp. 1989–1996, 2008.

[11] US Department of Energy, "Benefits of demand response in electricity narkets and recommendations for achieving them," Report to the United States Congress, 2006, http://eetd.lbl.gov/.

[12] O. Sezgen, C. A. Goldman, and P. Krishnarao, "Option value of electricity demand response," *Energy*, vol. 32, no. 2, pp. 108–119, 2007.

[13] P. Jazayeri, A. Schellenberg, W. D. Rosehart et al., "A survey of load control programs for price and system stability," *IEEE Transactions on Power Systems*, vol. 20, no. 3, pp. 1504–1509, 2005.

[14] D. S. Kirschen, "Demand-side view of electricity markets," *IEEE Transactions on Power Systems*, vol. 18, no. 2, pp. 520–527, 2003.

[15] I. C. Paschalidis, B. Li, and M. C. Caramanis, "Demand-side management for regulation service provisioning through internal pricing," *IEEE Transactions on Power Systems*, vol. 27, no. 3, pp. 1531–1539, 2012.

[16] C.-L. Su and D. Kirschen, "Quantifying the effect of demand response on electricity markets," *IEEE Transactions on Power Systems*, vol. 24, no. 3, pp. 1199–1207, 2009.

[17] V. C. Gungor, D. Sahin, T. Kocak et al., "A Survey on smart grid potential applications and communication requirements," *IEEE Transactions on Industrial Informatics*, vol. 9, no. 1, pp. 28–42, 2013.

[18] L. J. Zhong, H. R. Su, and C. W. Feng, "Haier U-Home digital home system," *Digital Community and Smart Home*, vol. 7, pp. 21–24, 2007.

[19] M. A. Alahmad, P. G. Wheeler, A. Schwer, J. Eiden, and A. Brumbaugh, "A comparative study of three feedback devices for residential real-time energy monitoring," *IEEE Transactions on Industrial Electronics*, vol. 59, no. 4, pp. 2002–2013, 2012.

[20] A. Arteconi, N. J. Hewitt, and F. Polonara, "Domestic demand-side management (DSM): role of heat pumps and thermal energy storage (TES) systems," *Applied Thermal Engineering*, vol. 51, no. 1-2, pp. 155–165, 2013.

[21] M. A. Zehir and M. Bagriyanik, "Demand side management by controlling refrigerators and its effects on consumers," *Energy Conversion and Management*, vol. 64, pp. 238–244, 2012.

[22] H. Li, S. Gong, L. Lai, Z. Han, R. C. Qiu, and D. Yang, "Efficient and secure wireless communications for advanced metering infrastructure in smart grids," *IEEE Transactions on Smart Grid*, vol. 3, no. 3, pp. 1540–1551, 2012.

[23] J. Kim, D. Kim, K.-W. Lim, Y.-B. Ko, and S.-Y. Lee, "Improving the reliability of IEEE 802.11s Based wireless mesh networks for smart grid systems," *Journal of Communications and Networks*, vol. 14, no. 6, pp. 629–639, 2012.

[24] F. Benzi, N. Anglani, E. Bassi, and L. Frosini, "Electricity smart meters interfacing the households," *IEEE Transactions on Industrial Electronics*, vol. 58, no. 10, pp. 4487–4494, 2011.

[25] D.-M. Han and J.-H. Lim, "Design and implementation of smart home energy management systems based on ZigBee," *IEEE Transactions on Consumer Electronics*, vol. 56, no. 3, pp. 1417–1425, 2010.

[26] V. C. Gungor, B. Lu, and G. P. Hancke, "Opportunities and challenges of wireless sensor networks in smart grid," *IEEE Transactions on Industrial Electronics*, vol. 57, no. 10, pp. 3557–3564, 2010.

[27] W. Granzer, F. Praus, and W. Kastner, "Security in building automation systems," *IEEE Transactions on Industrial Electronics*, vol. 57, no. 11, pp. 3622–3630, 2010.

[28] H. Zhou, J. G. Lai, W. Hu, and Q. Deng, "Demand-side energy management: FTTH-based mode for smart homes," in *Proceedings of the American Control Conference (ACC '14)*, vol. 48, pp. 1704–1709, Portland, Ore, USA, June 2014.

[29] H. Chen and B. L. Sun, "Multicast routing optimization algorithm with bandwidth and delay constraints based on GA," *Journal of Communication and Computer*, vol. 2, no. 5, pp. 63–67, 2005.

Hindawi Publishing Corporation
Mathematical Problems in Engineering
Volume 2015, Article ID 812070, 9 pages
http://dx.doi.org/10.1155/2015/812070

Research Article

Stability and Time Delay Tolerance Analysis Approach for Networked Control Systems

Ashraf F. Khalil[1] and Jihong Wang[2]

[1] *Electrical and Electronic Engineering Department, University of Benghazi, Benghazi, Libya*
[2] *School of Engineering, University of Warwick, Coventry CV4 7AL, UK*

Correspondence should be addressed to Ashraf F. Khalil; ashraf.khalil@uob.edu.ly

Received 9 August 2014; Revised 27 October 2014; Accepted 29 October 2014

Academic Editor: Yun-Bo Zhao

Networked control system is a research area where the theory is behind practice. Closing the feedback loop through shared network induces time delay and some of the data could be lost. So the network induced time delay and data loss are inevitable in networked control Systems. The time delay may degrade the performance of control systems or even worse lead to system instability. Once the structure of a networked control system is confirmed, it is essential to identify the maximum time delay allowed for maintaining the system stability which, in turn, is also associated with the process of controller design. Some studies reported methods for estimating the maximum time delay allowed for maintaining system stability; however, most of the reported methods are normally overcomplicated for practical applications. A method based on the finite difference approximation is proposed in this paper for estimating the maximum time delay tolerance, which has a simple structure and is easy to apply.

1. Introduction

The key feature of networked control systems (NCSs) is that the information is exchanged through a network among control system components. So the network induced time delay is inevitable in NCSs. The time delay, either constant (up to jitter) or random, may degrade the performance of control systems and even destabilize the systems. NCSs can be defined as a control system where the control loop is closed through a real-time communication network [1]. The term networked control systems first appeared in Walsh's article in 1999 [2]. A typical organization of an NCS is shown in Figure 1. The reference input, plant output, and control input are exchanged through a real-time communication network. The main advantages of NCSs are modularity, simplified wiring, low cost, reduced weight, decentralization of control, integrated diagnosis, simple installation, quick and easy maintenance [3], and flexible expandability (easy to add/remove sensors, actuators, or controllers with low cost). NCSs are able to easily fuse global information to make intelligent decisions over large physical spaces which is important for many engineering systems such as the power system.

As the control loop is closed through a communication network the time delay and data dropout are unavoidable. Therefore networked control system can be regarded as a special case time delay system and many authors applied the time delay theorems to study NCSs [4]. Time delay, no doubt, increases complexity in analysis and design of NCSs. Conventional control theories built on a number of standing assumptions including synchronized control and nondelayed sensing and actuation must be reevaluated before they can be applied for NCSs [5].

The main goal of the most recent work is to reduce the conservativeness of the maximum time delay by using Lyapunov-Krasovskii functional with improved algorithms for solving the linear matrix inequalities (LMIs) set but with the expense of increasing complexity and computation time. Analytical and graphical methods have been studied in the literature (see, e.g., [6]). The stability criteria for NCSs based on Lyapunov-Krasovskii functional approach have been reported in [7–9]. In [7], a Lyapunov-Krasovskii function is used to derive a set of LMIs and the stability problem is generalized to a feasibility problem for the LMIs set. In many of the previously reported works, the controller is

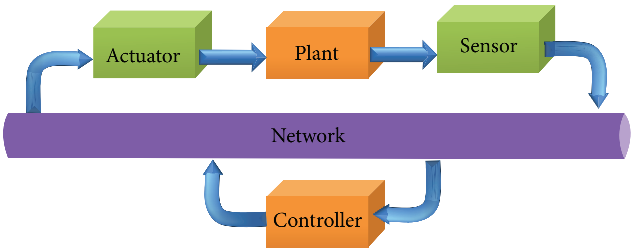

Figure 1: A typical networked control system.

designed in the absence of the time delay. In [10], an improved Lyapunov-Krasovskii function is used with triple integral terms. The LMI methods require the closed-loop system to be Hurwitz [8, 11, 12]. In [13], a modified cone complementary linearization algorithm based on the Lyapunov-Krasovskii approach is implemented. And the method reported in [14] is claimed to be less conservative and the computational complexity is reduced.

The authors in [15] derived an LMI-based method in the frequency domain, and then the LMI is transformed onto an equivalent nonfrequency domain LMI by applying Kalman-Yakubovich-Popov lemma. It has been reported in [16] that the ordinary Lyapunov stability analysis is linked by a suggested variable to state vectors through convolution and the stability analysis is simplified to only require solving a nonlinear algebraic matrix equation.

In [11], the hybrid system technique is used to derive a stability region. An upper bound is derived for time delay in an inequality form and the results are rather conservative. The hybrid system stability analysis technique has also been used in [17]. A simple analytical relation is derived between the sampling period, the time delay, and the controller gains. The same approach is used in [18] with more conservative stability region results. The model-based approach for deriving necessary and sufficient conditions for stability is presented in [19]. The stability criteria are derived in terms of the update time and the parameters of the model. The model-based approach is then extended to multiunits NCS in [20]. The optimal stochastic control was studied in [21] with a discrete-time system model where the random time delays are modeled using Markov chains and the controller uses the knowledge of the past state time delays by time stamping.

Most of the previously developed approaches require excessive load of computations, and also, for higher order systems, the load of computations will increase dramatically. In practice, engineers may find it difficult to apply those available methods in control system design because of the complexity of the methods and lack of guideline in linking between the design parameters and the system performance. Almost all the design procedures highly depend on the postdesign simulation to determine the design parameters. So there is a demand for a simple design approach with clear guidance for practical applications. In this paper, a new stability analysis and control design method is proposed, in which the design approach is simple and a clear design procedure is given.

The paper starts from the mathematical model of NCS and then the proposed method for estimating the maximum allowable delay bound is briefly described. A few examples are illustrated and the results are compared with those previously published in the literature. The cart and inverted pendulum problem is used to study the effect of the parameters on the maximum allowable delay bound.

2. Mathematical Analysis

Although the issues involved with time delays in control systems have been studied for a long time, it is difficult to find a method simple enough to be accepted by control system design engineers. It is found that the most previously reported methods rely on LMI techniques and they are generally too complicated for practical engineers to use and also involve heavy load of numerical calculations and computing time. The paper proposes a new method which has a simple structure and is used for estimating the maximum time delay allowed while the system stability can still be maintained. In most control systems the sampling time is preferred to be small [22]. The maximum allowable delay bound (MADB) can be defined as the maximum sampling period that guarantees the stability even with poor system performance. A continuous time-invariant linear system is shown in Figure 2 and given by

$$\begin{aligned} \dot{\mathbf{x}}(t) &= \mathbf{A}\mathbf{x}(t) + \mathbf{B}\mathbf{u}(t), \\ \mathbf{y}(t) &= \mathbf{C}\mathbf{x}(t) + \mathbf{D}\mathbf{u}(t), \end{aligned} \tag{1}$$

where $\mathbf{x}(t) \in \Re^n$ is the system state vector, $\mathbf{u}(t) \in \Re^m$ is the system control input, $\mathbf{y}(t) \in \Re^p$ is the system output, and $\mathbf{A} \in \Re^{n\times n}$, $\mathbf{B} \in \Re^{n\times m}$, $\mathbf{C} \in \Re^{p\times n}$, and $\mathbf{D} \in \Re^{p\times m}$ are constant matrices with appropriate sizes.

Suppose that the control signals are connected to the control plant through a kind of network, so the time delay is inevitable to be involved in the feedback loop. The state feedback is therefore can be written as

$$\mathbf{u}(t) = \mathbf{K}\mathbf{x}(t - \tau_{sc} - \tau_c - \tau_{ca}), \tag{2}$$

where τ_{sc} is the time delay between the sensor and the controller, τ_c is the time delay in the controller, and τ_{ca} is the time delay from the controller to the actuator. $\mathbf{K}$ represents the feedback control gains with appropriate size. From (2) the networked control system can be modeled where the time delay is lumped between the sensor and the controller as shown in Figure 3.

The time delay may be constant, variable, or even random. In NCSs, the time delay is composed of the time delay from sensors to controllers, time delay in the controller, and controllers to actuators time delay which is given by

$$\tau = \tau_{sc} + \tau_c + \tau_{ca}. \tag{3}$$

For a general formulation the packet dropouts can be incorporated in (3) as follows:

$$\tau = \tau_{sc} + \tau_c + \tau_{ca} + dh, \tag{4}$$

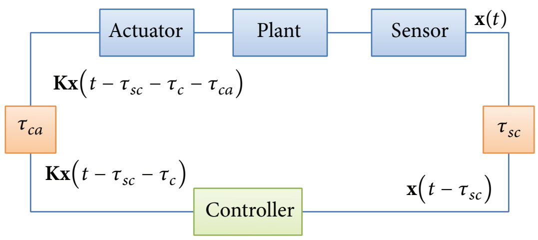

Figure 2: A networked control system with the time delay both from the sensor to the controller and from the controller to the actuator.

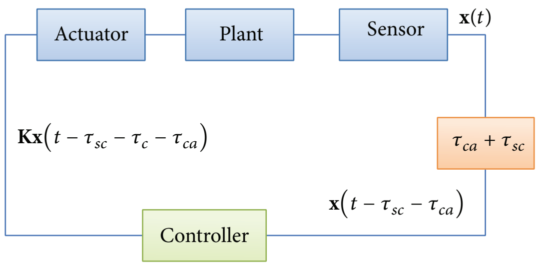

Figure 3: A simplified model of the networked control system.

where d is the number of dropouts and h the sampling period. And by (4) the data dropouts can be considered as a special case of time delay [23, 24]. It is supposed that the following hypotheses hold.

Hypothesis 1 (H.1). (i) The sensors are clock driven. (ii) The controllers and the actuators are event driven. (iii) The data are transmitted as a single packet. (iv) The old packets are discarded. (v) All the states are available for measurements and hence for transmission.

Hypothesis 2 (H.2). The time delay τ is small to be less than one unit of its measurement.

Definition 1 (D.1). For a function $f(t)$, the nth order reminder for its Taylor's series expansion is defined by

$$R_n(f(t),\tau)=\sum_{n}^{\infty}\frac{f^{(n)}(\xi)}{n!}\tau^n. \tag{5}$$

Applying the state feedback proposed in (2) to the system (1), we have

$$\dot{\mathbf{x}}(t)=\mathbf{Ax}(t)+\mathbf{BKx}(t-\tau). \tag{6}$$

From (6), the following can be derived:

$$\dot{\mathbf{x}}(t)=(\mathbf{A}+\mathbf{BK})\mathbf{x}(t)+\mathbf{BK}[\mathbf{x}(t-\tau)-\mathbf{x}(t)]. \tag{7}$$

Theorem 2. *Suppose that (H.1) and (H.2) hold. For system (1) with the feedback control of (2), the closed-loop system is globally asymptotically stable if $\lambda_i(\Psi)\in C^-$, for $i=1,2,\ldots,n$ and all the state variables' 2nd order reminders are small enough for the given value of τ, where $\mathbf{\Psi}$ is given by*

$$\mathbf{\Psi}=\left[(I+\tau\mathbf{BK})^{-1}(\mathbf{A}+\mathbf{BK})\right]. \tag{8}$$

Proof. The expression for $\mathbf{x}(t-\tau)$ can be obtained by Taylor expansion as

$$\mathbf{x}(t-\tau)=\sum_{n=0}^{\infty}(-1)^n\frac{\tau^n}{n!}\mathbf{x}^{(n)}(t), \tag{9}$$

where $\mathbf{x}^{(n)}(t)$ is the nth order derivative. The first order approximation of the delay term is given by

$$\begin{aligned}\mathbf{x}(t-\tau)&=\mathbf{x}(t)-\tau\dot{\mathbf{x}}(t)+\left(\frac{\tau^2}{2}\right)\ddot{\mathbf{x}}(t)+\mathbf{R}_3(\mathbf{x},\tau),\\ \mathbf{x}(t-\tau)&\approx\mathbf{x}(t)-\tau\dot{\mathbf{x}}(t)+\left(\frac{\tau^2}{2}\right)\ddot{\mathbf{x}}(t),\\ \mathbf{x}(t-\tau)&=\mathbf{x}(t)-\tau\dot{\mathbf{x}}(t)+\mathbf{R}_2(\mathbf{x},\tau).\end{aligned} \tag{10}$$

From (10) it can be seen that $\mathbf{R}_2(x,\tau)$ depends on the time delay, τ, and the higher order derivatives of $\mathbf{x}(t)$ which can be neglected if the time delay and the norm of $\mathbf{R}_2(x,\tau)$ are small. Then we have

$$\mathbf{x}(t-\tau)\approx\mathbf{x}(t)-\tau\dot{\mathbf{x}}(t). \tag{11}$$

The assumption in (11) can be used without significant error, and this can be true for the following reasons. Firstly, the time delay in a computer network is very small in order of milli- or microseconds and at the worst few tenths of the second. Secondly, in most of the real control system applications the linearized model is used and the higher order terms are already neglected. Additionally, the higher order derivatives will be multiplied by τ^n/n which is much more smaller than τ because $\tau\ll 1$. Substituting (11) into (7), the following can be derived:

$$\dot{\mathbf{x}}(t)\approx(\mathbf{A}+\mathbf{BK})\mathbf{x}(t)-\tau\mathbf{BK}\dot{\mathbf{x}}(t), \tag{12}$$

$$\dot{\mathbf{x}}(t)\approx\left[(\mathbf{I}+\tau\mathbf{BK})^{-1}(\mathbf{A}+\mathbf{BK})\right]\mathbf{x}(t), \tag{13}$$

$$\mathbf{\Psi}=\left[(\mathbf{I}+\tau\mathbf{BK})^{-1}(\mathbf{A}+\mathbf{BK})\right]. \tag{14}$$

The system (13) will be globally asymptotically stable if

$$\lambda_i(\mathbf{\Psi})\in C^-,\quad \text{for } i=1,2,\ldots,n. \tag{15}$$

□

Corollary 3. *Suppose (H.1) and (H.2) hold. For the control system (1) with the control law (2), the closed-loop system is globally asymptotically stable if*

$$\tau<\frac{1}{\|\mathbf{BK}\|}. \tag{16}$$

Proof. For system (1), suppose that the state feedback has been designed to ensure $\lambda(\mathbf{A}+\mathbf{BK})\in C^-$. Therefore, for a chosen positive definite matrix $\mathbf{P}=\mathbf{P}^T$, it will find a positive definite matrix $\mathbf{Q}=\mathbf{Q}^T$ to have

$$\mathbf{P}(\mathbf{A}+\mathbf{BK})+(\mathbf{A}+\mathbf{BK})^{\mathbf{T}}\mathbf{P}=-\mathbf{Q}. \tag{17}$$

Choose a Lyapunov functional candidate as

$$\mathbf{V}(x) = \mathbf{x}^{\mathbf{T}}\mathbf{P}\mathbf{x} > 0 \quad \forall \mathbf{x} \neq \mathbf{0}. \tag{18}$$

The objective for the next step is to find the range of τ that will ensure ($\dot{\mathrm{V}}(x) < 0\ \forall \mathbf{x} \neq \mathbf{0}$) [25–27]. Taking the derivative of (18),

$$\begin{aligned}
\dot{\mathbf{V}}(x) &= \dot{\mathbf{x}}^{\mathbf{T}}\mathbf{P}\mathbf{x} + \mathbf{x}^{\mathbf{T}}\mathbf{P}\dot{\mathbf{x}} \\
&\approx \mathbf{x}^{\mathbf{T}}\Big[(\mathbf{A}+\mathbf{BK})^{\mathbf{T}}\mathbf{P}\mathbf{P}^{-1}(\mathbf{I}+\tau\mathbf{BK})^{-\mathbf{T}}\mathbf{P} \\
&\qquad + \mathbf{P}(\mathbf{I}+\tau\mathbf{BK})^{-1}\mathbf{P}^{-1}\mathbf{P}(\mathbf{A}+\mathbf{BK})\Big]\mathbf{x} \\
&\quad - \mathbf{x}^{\mathbf{T}}\Big[\mathbf{P}(\mathbf{A}+\mathbf{BK}) + (\mathbf{A}+\mathbf{BK})^{\mathbf{T}}\mathbf{P}\Big]\mathbf{x} \\
&\quad + \mathbf{x}^{\mathbf{T}}\Big[\mathbf{P}(\mathbf{A}+\mathbf{BK}) + (\mathbf{A}+\mathbf{BK})^{\mathbf{T}}\mathbf{P}\Big]\mathbf{x} \\
&\approx \mathbf{x}^{\mathbf{T}}\Big[(\mathbf{A}+\mathbf{BK})^{\mathbf{T}}\mathbf{P}\mathbf{P}^{-1}(\mathbf{I}+\tau\mathbf{BK})^{-\mathbf{T}}\mathbf{P} \\
&\qquad - (\mathbf{A}+\mathbf{BK})^{\mathbf{T}}\mathbf{P} + \mathbf{P}(\mathbf{I}+\tau\mathbf{BK})^{-1}\mathbf{P}^{-1}\mathbf{P}(\mathbf{A}+\mathbf{BK}) \\
&\qquad - \mathbf{P}(\mathbf{A}+\mathbf{BK})\Big]\mathbf{x} - \mathbf{x}^{\mathbf{T}}\mathbf{Q}\mathbf{x}.
\end{aligned} \tag{19}$$

Rearranging the terms in the above equation, then

$$\begin{aligned}
\dot{\mathbf{V}}(\mathbf{x}) &\approx \mathbf{x}^{\mathbf{T}}\Big\{(\mathbf{A}+\mathbf{BK})^{\mathbf{T}}\mathbf{P}\Big[\mathbf{P}^{-1}(\mathbf{I}+\tau\mathbf{BK})^{-\mathbf{T}}\mathbf{P} - \mathbf{I}\Big] \\
&\qquad + \Big[\mathbf{P}(\mathbf{I}+\tau\mathbf{BK})^{-1}\mathbf{P}^{-1} - \mathbf{I}\Big]\mathbf{P}(\mathbf{A}+\mathbf{BK})\Big\}\mathbf{x} \\
&\quad - \mathbf{x}^{\mathbf{T}}\mathbf{Q}\mathbf{x}.
\end{aligned} \tag{20}$$

If $\mathbf{P}(\mathbf{I}+\tau\mathbf{BK})^{-1}\mathbf{P}^{-1} - \mathbf{I} = \mathbf{I}$ then (20) will become

$$\mathbf{x}^{\mathbf{T}}\Big[\mathbf{P}(\mathbf{A}+\mathbf{BK}) + (\mathbf{A}+\mathbf{BK})^{\mathbf{T}}\mathbf{P}\Big]\mathbf{x} - \mathbf{x}^{\mathbf{T}}\mathbf{Q}\mathbf{x} = 0. \tag{21}$$

Move the last term to the right hand side; the following will be derived:

$$\mathbf{x}^{\mathbf{T}}\Big[\mathbf{P}(\mathbf{A}+\mathbf{BK}) + (\mathbf{A}+\mathbf{BK})^{\mathbf{T}}\mathbf{P}\Big]\mathbf{x} = \mathbf{x}^{\mathbf{T}}\mathbf{Q}\mathbf{x}. \tag{22}$$

So $\|\mathbf{P}(\mathbf{A}+\mathbf{BK}) + (\mathbf{A}+\mathbf{BK})^{\mathbf{T}}\mathbf{P}\| \cdot \|\mathbf{x}\|^2 = \|\mathbf{Q}\| \cdot \|\mathbf{x}\|^2$.

Assuming that we can find a positive number to make the following hold:

$$\left\|\mathbf{P}(\mathbf{A}+\mathbf{BK}) + (\mathbf{A}+\mathbf{BK})^{\mathbf{T}}\mathbf{P}\right\| = 2\gamma\left\|(\mathbf{A}+\mathbf{BK})^{\mathbf{T}}\mathbf{P}\right\| = \|\mathbf{Q}\| \tag{23}$$

then γ can be considered as the norm of $\mathbf{P}^{-1}(\mathbf{I}+\tau\mathbf{BK})^{-1}\mathbf{P} - \mathbf{I}$. Therefore, we have

$$\begin{aligned}
&\mathbf{x}^{\mathbf{T}}\Big[(\mathbf{A}+\mathbf{BK})^{\mathbf{T}}\mathbf{P}\Big[\mathbf{P}^{-1}(\mathbf{I}+\tau\mathbf{BK})^{-\mathbf{T}}\mathbf{P} - \mathbf{I}\Big] \\
&\qquad + \Big[\mathbf{P}(\mathbf{I}+\tau\mathbf{BK})^{-1}\mathbf{P}^{-1} - \mathbf{I}\Big]\mathbf{P}(\mathbf{A}+\mathbf{BK})\Big]\mathbf{x} \\
&\quad \leq 2\left\|\Big(\mathbf{P}^{-1}(\mathbf{I}+\tau\mathbf{BK})^{-\mathbf{T}}\mathbf{P} - \mathbf{I}\Big)\mathbf{P}(\mathbf{A}+\mathbf{BK})\right\| \cdot \|\mathbf{x}\|^2.
\end{aligned} \tag{24}$$

Choose

$$\left\|\mathbf{P}^{-1}(\mathbf{I}+\tau\mathbf{BK})^{-1}\mathbf{P} - \mathbf{I}\right\| \leq 1. \tag{25}$$

Use Neumann series formula for the inverse of the sum of two matrices:

$$\begin{aligned}
&(\mathbf{I}+\tau\mathbf{BK})^{-1} \\
&\qquad = \mathbf{I} - \tau\mathbf{BK} + \tau^2(\mathbf{BK})^2 - \tau^3(\mathbf{BK})^3 + \cdots - .
\end{aligned} \tag{26}$$

For small time delays $\tau \ll 1$ (26) can be given as

$$(\mathbf{I}+\tau\mathbf{BK})^{-1} \approx \mathbf{I} - \tau\mathbf{BK}. \tag{27}$$

Applying (27) into (25) then we have

$$\begin{aligned}
&\left\|\mathbf{P}^{-1}(\mathbf{I}+\tau\mathbf{BK})^{-1}\mathbf{P} - \mathbf{I}\right\| \\
&\qquad \approx \left\|\mathbf{P}^{-1}(\mathbf{I}-\tau\mathbf{BK})\mathbf{P} - \mathbf{I}\right\| = \|\tau\mathbf{BK}\| < 1.
\end{aligned} \tag{28}$$

And finally we get

$$\tau < \frac{1}{\|\mathbf{BK}\|}. \tag{29}$$

That is, for any $\tau < 1/\|\mathbf{BK}\|$, $\dot{\mathrm{V}}(x) < 0$, the system will be globally asymptotically stable. □

Theorem 2 and Corollary 3 give us a simple tool in estimating the maximum allowable time delay for NCSs. Further analysis in the frequency domain is described below. Taking Laplace transform of (12), we have

$$\begin{aligned}
s\mathbf{X}(s) &= (\mathbf{A}+\mathbf{BK})\mathbf{X}(s) - \tau s\mathbf{BKX}(s), \\
[s\mathbf{I} - (\mathbf{A}+\mathbf{BK}) &+ \tau s\mathbf{BK}]\mathbf{X}(s) = 0.
\end{aligned} \tag{30}$$

The characteristics equation is defined as

$$[s\mathbf{I} - (\mathbf{A}+\mathbf{BK}) + \tau s\mathbf{BK}] = 0. \tag{31}$$

For a stable system the roots of the characteristics equation (31) must lie in the left hand side of the s-plane. From the characteristics equation, it is clear that the term $\tau s\mathbf{BK}$ influences the system performance and the stability as the term of $\tau s\mathbf{BK}$ may push the closed-loop system poles toward the right hand side of the s-plane.

As we have seen the system characteristic is determined by the term $\tau\mathbf{BK}\dot{\mathbf{x}}(t)$ in a certain level. This term can be regarded as a differentiator in the feedback loop, so it will introduce extra zeros to the closed-loop system and the time delay can be considered to have resulted in a variable gain to the feedback path. For more accurate estimation the second or third-order difference approximation can be used as follows:

$$\begin{aligned}
&\left[s\mathbf{I} - (\mathbf{A}+\mathbf{BK}) + \tau s\mathbf{BK} - \frac{\tau^2 s^2}{2}\mathbf{BK}\right] = 0, \\
&\left[s\mathbf{I} - (\mathbf{A}+\mathbf{BK}) + \tau s\mathbf{BK} - \frac{\tau^2 s^2}{2}\mathbf{BK} + \frac{\tau^3 s^3}{6}\mathbf{BK}\right] = 0.
\end{aligned} \tag{32}$$

In the following a simple corollary for estimating the MADB in single-input-single-output NCS will be derived.

Corollary 4. *Suppose that (H.1) and (H.2) hold. The system (2) with the controller (3) is asymptotically stable if*

$$\tau < \frac{1}{|\lambda_{\min}(\mathbf{BK})|}. \quad (33)$$

Proof. The main assumption is that the eigenvalues of the compensator, **BK**, are all negative, $s_1 < 0, \ldots, s_n < 0$, and are given by

$$\mathbf{BK} - s\mathbf{I}_{n\times n} = \begin{bmatrix} a_{11}-s & a_{12} & \cdots & a_{1n} \\ a_{21} & a_{22}-s & \cdots & a_{2n} \\ \vdots & \vdots & \ddots & \vdots \\ a_{n1} & a_{n2} & \cdots & a_{nn}-s \end{bmatrix}. \quad (34)$$

The characteristic equation is the determinant of (34). Assume that the eigenvalues are given by

$$\begin{gathered} s_1 = \alpha_1, \ldots, s_n = \alpha_n, \\ \alpha_1 < 0, \ldots, \alpha_n < 0. \end{gathered} \quad (35)$$

□

Preliminary 1 (inverse eigenvalues theorem [28]). Given a matrix **X** that is nonsingular, with eigenvalues $\lambda_1, \ldots, \lambda_n > 0$, $\lambda_1, \ldots, \lambda_n$ are eigenvalues of **X** if and only if $\lambda_1^{-1}, \ldots, \lambda_n^{-1}$ are eigenvalues of $\mathbf{X}^{-1}$.

The eigenvalues of $(\mathbf{I}_{n\times n} + \tau\mathbf{BK})$ are given by

$$\tau \cdot \mathbf{BK} + \mathbf{I}_{n\times n} - \lambda\mathbf{I}_{n\times n} = \begin{bmatrix} \tau a_{11}+1-\lambda & \tau a_{12} & \cdots & \tau a_{1n} \\ \tau a_{21} & \tau a_{22}+1-\lambda & \cdots & \tau a_{2n} \\ \vdots & \vdots & \ddots & \vdots \\ \tau a_{n1} & \tau a_{n2} & \cdots & \tau a_{nn}+1-\lambda \end{bmatrix}, \quad (36)$$

$$\Delta(\tau \cdot \mathbf{BK} + \mathbf{I}_{n\times n} - \lambda\mathbf{I}_{n\times n}) = \det\left(\begin{bmatrix} \tau a_{11}+1-\lambda & \tau a_{12} & \cdots & \tau a_{1n} \\ \tau a_{21} & \tau a_{22}+1-\lambda & \cdots & \tau a_{2n} \\ \vdots & \vdots & \ddots & \vdots \\ \tau a_{n1} & \tau a_{n2} & \cdots & \tau a_{nn}+1-\lambda \end{bmatrix}\right),$$

$$\Delta(\tau \cdot \mathbf{BK} + \mathbf{I}_{n\times n} - \lambda\mathbf{I}_{n\times n}) = \tau^n \det\left(\begin{bmatrix} a_{11}+\dfrac{1-\lambda}{\tau} & a_{12} & \cdots & a_{1n} \\ a_{21} & a_{22}+\dfrac{1-\lambda}{\tau} & \cdots & a_{2n} \\ \vdots & \vdots & \ddots & \vdots \\ a_{n1} & a_{n2} & \cdots & a_{nn}+\dfrac{1-\lambda}{\tau} \end{bmatrix}\right). \quad (37)$$

Replacing $(1-\lambda)/\tau$ by $-s$ in (37) we get

$$= \tau^n \det\left(\begin{bmatrix} a_{11}-s & a_{12} & \cdots & a_{1n} \\ a_{21} & a_{22}-s & \cdots & a_{2n} \\ \vdots & \vdots & \ddots & \vdots \\ a_{n1} & a_{n2} & \cdots & a_{nn}-s \end{bmatrix}\right) = 0. \quad (38)$$

Solving (38) the eigenvalues are given as

$$\begin{gathered} \frac{(\lambda_1 - 1)}{\tau} = \alpha_1, \ldots, \frac{(\lambda_n - 1)}{\tau} = \alpha_n, \\ \alpha_1 < 0, \ldots, \alpha_n < 0, \\ \lambda_1 = 1 + \tau\alpha_1, \ldots, \lambda_n = 1 + \tau\alpha_n, \\ \alpha_1 < 0, \ldots, \alpha_n < 0. \end{gathered} \quad (39)$$

If $\tau < 1/|\alpha_{\max}|$ then all the eigenvalues are positive and the system is asymptotically stable, and if $\tau > 1/|\alpha_{\max}|$ at least one of the eigenvalues will be negative then.

If $\tau < 1/|\lambda_{\min}(\mathbf{BK})|$ and (H.1) and (H.2) hold then the system is asymptotically stable.

Corollary 5. *Suppose that (H.1) and (H.2) hold. For system (1) with the control law (2), the closed-loop system is globally asymptotically stable if*

$$\tau < \frac{1}{abs(\mathbf{KB})} \quad (\textit{where abs is the absolute value}). \quad (40)$$

From Preliminary 1, the signs of the eigenvalues of $(\mathbf{I}_{n\times n} + \tau\mathbf{BK})^{-1}$ *and* $(\mathbf{I}_{n\times n} + \tau\mathbf{BK})$ *are the same. For a single-input-single-output control system the matrix* **BK** *can be written as*

$$\mathbf{BK} = \begin{bmatrix} b_1 \\ b_2 \\ \vdots \\ b_n \end{bmatrix} \begin{bmatrix} k_1 & k_2 & \cdots & k_n \end{bmatrix} = \begin{bmatrix} b_1k_1 & b_1k_2 & \cdots & b_1k_n \\ b_2k_1 & b_2k_2 & \cdots & b_2k_n \\ \vdots & \vdots & \ddots & \vdots \\ b_nk_1 & b_nk_2 & \cdots & b_nk_n \end{bmatrix}. \quad (41)$$

The interesting property of **BK** *is that it is singular. The eigenvalues of* **BK** *are given by*

$$\mathbf{BK} - \lambda\mathbf{I}_{n\times n} = \begin{bmatrix} b_1k_1-\lambda & b_1k_2 & \cdots & b_1k_n \\ b_2k_1 & b_2k_2-\lambda & \cdots & b_2k_n \\ \vdots & \vdots & \ddots & \vdots \\ b_nk_1 & b_nk_2 & \cdots & b_nk_n-\lambda \end{bmatrix}. \quad (42)$$

The characteristics equation of **BK** *is the determinant of (42) and is given by*

$$\begin{gathered} \lambda^2 - \mathrm{Tr}(\mathbf{BK})\lambda + \frac{1}{2}\left[\mathrm{Tr}\left(\mathbf{BK}^2\right) - \mathrm{Tr}(\mathbf{BK})^2\right] \\ \vdots \\ \lambda^n - \mathrm{Tr}(\mathbf{BK})\lambda^{n-1} + \frac{1}{2}\left[\mathrm{Tr}\left(\mathbf{BK}^2\right) - \mathrm{Tr}(\mathbf{BK})^2\right]\lambda^{n-2} \\ + \cdots + \frac{1}{2}\left[\mathrm{Tr}\left(\mathbf{BK}^2\right) - \mathrm{Tr}(\mathbf{BK})^2\right]. \end{gathered} \quad (43)$$

Because **BK** *is singular* $\det(\mathbf{BK}) = 0$ *and hence*

$$\begin{gathered} \det(\mathbf{BK}) = \frac{1}{2}\left[\mathrm{Tr}\left(\mathbf{BK}^2\right) - \mathrm{Tr}(\mathbf{BK})^2\right] = 0, \\ \mathrm{Tr}\left(\mathbf{BK}^2\right) = \mathrm{Tr}(\mathbf{BK})^2. \end{gathered} \quad (44)$$

Substituting (44) into (43), then (43) becomes

$$\begin{aligned}&\lambda^2 - \operatorname{Tr}(\mathbf{BK})\lambda \longrightarrow \lambda(\lambda - \operatorname{Tr}(\mathbf{BK}))\\ &\vdots\\ &(-1)^n\lambda^n - \operatorname{Tr}(\mathbf{BK})\lambda^{n-1} \longrightarrow (-1)^n\lambda^{n-1}(\lambda - \operatorname{Tr}(\mathbf{BK})).\end{aligned} \tag{45}$$

Finally the eigenvalues of **BK** *are*

$$\lambda_1,\ldots,\lambda_{n-1} = 0 \qquad \lambda_n = \operatorname{Tr}(\mathbf{BK}) < 0. \tag{46}$$

Equation (46) shows that the minimum eigenvalue of **BK** *equals* $\operatorname{Tr}(\mathbf{BK})$. *If the eigenvalues of* $(\mathbf{I}_{n\times n} + \tau\mathbf{BK})$ *are* $s_1,\ldots,s_n$, *then the eigenvalues of* $(\mathbf{I}_{n\times n} + \tau\mathbf{BK})^{-1}$ *are* $1/s_1,\ldots,1/s_n$. *The eigenvalues of* $(\mathbf{I}_{n\times n} + \tau\mathbf{BK})$ *are given by*

$$\begin{aligned}&\tau\cdot\mathbf{BK} + \mathbf{I}_{n\times n} - s\mathbf{I}_{n\times n}\\ &= \begin{bmatrix} \tau b_1k_1 + 1 - s & \tau b_1k_2 & \cdots & \tau b_1k_n\\ \tau b_2k_1 & \tau b_2k_2 + 1 - s & \cdots & \tau b_2k_n\\ \vdots & \vdots & \ddots & \vdots\\ \tau b_nk_1 & \tau b_nk_2 & \cdots & \tau b_nk_n + 1 - s\end{bmatrix}.\end{aligned} \tag{47}$$

By solving (47) it can be found that

$$\begin{aligned} s_1,\ldots,s_{n-1} &= 1,\\ s_n = 1 + \tau\cdot\operatorname{Tr}(\mathbf{BK}) &= 1 + \tau\cdot\lambda_{\max}(\mathbf{BK})\end{aligned} \tag{48}$$

if $\tau < 1/|\operatorname{Tr}(\mathbf{BK})| \rightarrow s_n > 0 \rightarrow s_1,\ldots,s_n > 0$.

For single-input-single-output NCS we have

$$\operatorname{abs}(\mathbf{KB}) = \operatorname{Tr}(\mathbf{BK}); \quad \text{then} \tag{49}$$

if $\tau < 1/|\mathbf{KB}|$ *and both (H.1) and (H.2) hold then the system is asymptotically stable.*

This inequality can be used as a simple and fast tool for estimating the MADB in NCS and involves only single calculation.

3. Stability Analysis Case Studies

In general, two approaches are applied to controller design for NCSs. The first approach is to design a controller without considering time delay and then to design a communication protocol that minimizes the effects caused by time delays. The second approach is to design the controller while taking the time delay and data dropouts into account [11, 29]. The proposed method in this paper is used to estimate the MADB for predesigned control system. In this section, a number of examples are studied to demonstrate the proposed method and compare its results with the previously published cases in the literature. In particular, the results derived using the method proposed in this paper have been compared with the results using the LMI method given in [7] and with the fourth-order Pade approximation. The fourth-order Pade approximation [6] is used for the delay term in the s-domain and is defined as

$$e^{-\tau s} \approx P_d(s) = \frac{N_d(s)}{D_d(s)} = \frac{\left(\sum_{k=0}^{n}(-1)^k c_k\tau^k s^k\right)}{\left(\sum_{k=0}^{n} c_k\tau^k s^k\right)}. \tag{50}$$

The coefficients are given by

$$c_k = \frac{((2n-k)!n!)}{(2n!k!(n-k)!)} \quad k = 0,1,\ldots,n \;\; (n = 4). \tag{51}$$

With the fourth-order Pade approximation, the truncation error in the time delay calculation is less than 0.0001. The LMI-based method which has been used for the comparisons is based on using Lyapunov-Krasovskii functional and can be summarized as follows.

Corollary 6 (see [7]). *For a given scalar* τ *and a matrix* **K**, *if there exist matrices* $\mathbf{P} > 0$, $\mathbf{T} > 0$, $\mathbf{N}_i$, *and* $\mathbf{M}_i$ $(i = 1,2,3)$ *of appropriate dimension such that*

$$\begin{bmatrix} \mathbf{M}_1 + \mathbf{M}_1^T - \mathbf{N}_1\mathbf{A} - \mathbf{A}^T\mathbf{N}_1^T & \mathbf{M}_2^T - \mathbf{M}_1 - \mathbf{A}^T\mathbf{N}_2^T - \mathbf{N}_1\mathbf{BK} & \mathbf{M}_3^T - \mathbf{A}^T\mathbf{N}_3^T + \mathbf{N}_1 + \mathbf{P} & \tau\mathbf{M}_1\\ * & -\mathbf{M}_2 - \mathbf{M}_2^T - \mathbf{N}_2\mathbf{BK} - (\mathbf{BK})^T\mathbf{N}_2^T & -\mathbf{M}_3^T + \mathbf{N}_2 - (\mathbf{BK})^T\mathbf{N}_3^T & \tau\mathbf{M}_2\\ * & * & \mathbf{N}_3 + \mathbf{N}_3^T + \tau\mathbf{T} & \tau\mathbf{M}_3\\ * & * & * & -\tau\mathbf{T}\end{bmatrix} < 0, \tag{52}$$

then the system (1)-(2) is exponentially asymptotically stable. With a given controller gain **K**, *solving the LMI in Corollary 6 using the LMI Matlab Toolbox the maximum time delay can be computed.*

Example 7. The system in this example is the most widely used example in the literature and is described by the following equation:

$$\dot{x}(t) = \begin{bmatrix} 0 & 1\\ 0 & -0.1\end{bmatrix}x(t) + \begin{bmatrix} 0\\ 0.1\end{bmatrix}u(t). \tag{53}$$

In previous reports [1, 7], the feedback control is chosen to be

$$u(t) = \begin{bmatrix} -3.75 & -11.5\end{bmatrix}x(t). \tag{54}$$

From Corollary 3, $1/\|\mathbf{BK}\| = 0.8695$, so the MADB is estimated to be 0.8695 s. Using Theorem 2 and Corollary 5 the MADB is 0.8695 s. The same result can be obtained using the LMI method as reported in [7, 23, 24, 30]. In [11, 17], the value reported for MADB is 4.5×10^{-4} s and in [22] it is 0.0538 s. In [29], the MADB is 0.785 s. It has been reported in [10], where an improved Lyapunov-Krasovskii approach has been used, that the MADB is 1.0551 s and also 1.05 s reported in [23] with improved algorithm for solving the LMI. In [1], the MADB is 1.0081 s. Using the proposed method with second order finite difference approximation we can obtain 1.13 s as the MADB. The system response with 0.8695 s time delay and $\mathbf{x}(0) = [0.1 \ \ 0]^{\mathrm{T}}$ is shown in Figure 4 which proves the system is stable with the estimated MADB.

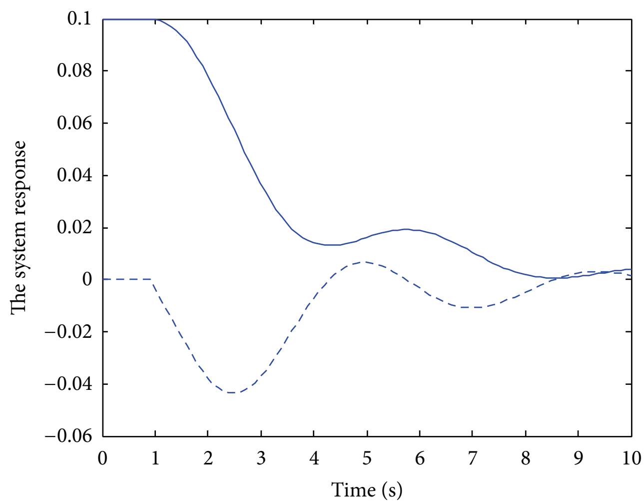

FIGURE 4: The response of the system in Example 7 with 0.8695 s delay.

Example 8 (see [31]). Consider

$$\dot{x}(t) = \begin{bmatrix} 0 & 1 & 0 \\ 0 & 0 & 1 \\ 0 & -2 & -3 \end{bmatrix} x(t) + \begin{bmatrix} 0 \\ 0 \\ 1 \end{bmatrix} u(t), \qquad (55)$$

$$u(t) = \begin{bmatrix} -160 & -54 & -11 \end{bmatrix} x(t).$$

For this third-order system both the LMI and our method give 0.0909 s as the MADB. Also with Corollary 5 the MADB is 0.0909 s.

Example 9 (see [31]). The last example is the fourth-order model of the inverted pendulum shown in Figure 5 which is in many papers reduced to a second order system in order to verify the stability of NCSs. The pendulum mass is denoted by m and the cart mass is M; the length of the pendulum rod is L. The open loop system is unstable. The states are defined as $x_1 = x$, $x_2 = \dot{x}$, $x_3 = \theta$, and $x_4 = \dot{\theta}$. The model is given by

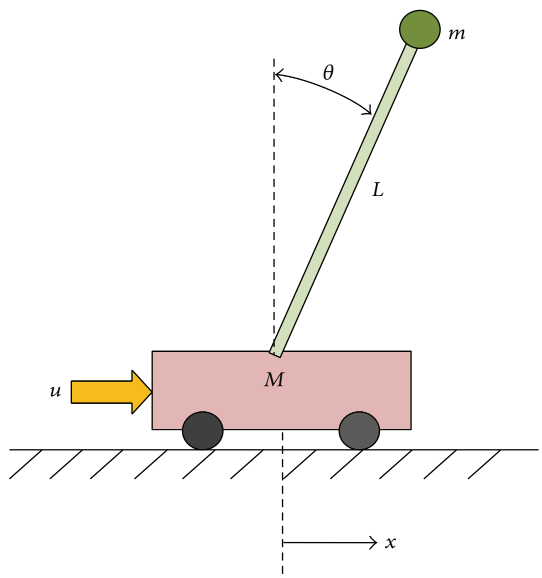

FIGURE 5: The inverted pendulum on a cart.

$$\dot{\mathbf{x}}(t) = \begin{bmatrix} 0 & 1 & 0 & 0 \\ 0 & 0 & \dfrac{-mg}{M} & 0 \\ 0 & 0 & 0 & 1 \\ 0 & 0 & \dfrac{(M+m)g}{ML} & 0 \end{bmatrix} \mathbf{x}(t) + \begin{bmatrix} 0 \\ \dfrac{1}{M} \\ 0 \\ \dfrac{-1}{ML} \end{bmatrix} u(t), \qquad (56)$$

$$\mathbf{y}(t) = \begin{bmatrix} x \\ \theta \end{bmatrix} = \begin{bmatrix} 1 & 0 & 0 & 0 \\ 0 & 0 & 1 & 0 \end{bmatrix} \mathbf{x}(t).$$

The parameters used are $M = 2$ kg, $m = 0.1$ kg, and $L = 0.5$ m. Then the linear model becomes

$$\dot{x}(t) = \begin{bmatrix} 0 & 1.000 & 0 & 0 \\ 20.601 & 0 & 0 & 0 \\ 0 & 0 & 0 & 1 \\ -0.4905 & 0 & 0 & 0 \end{bmatrix} x(t) + \begin{bmatrix} 0 \\ -1 \\ 0 \\ 0.5 \end{bmatrix} u(t). \qquad (57)$$

Using the LQR Matlab function with $\mathbf{Q} = \mathbf{I}$ and $\mathbf{R} = 1$, the controller is given by

$$\mathbf{K}_{\mathrm{LQR}} = \begin{bmatrix} 52.1238 & 11.5850 & 1.000 & 2.7252 \end{bmatrix}. \qquad (58)$$

Using the LMI method the MADB is 0.0978 s and our method gives 0.0978 s using Theorem 2 and Corollary 5. We noted that there is a good agreement between our method and the LMI method because τ is small enough to make the finite difference approximation hold. The system response with 0.0978 s time delay and with $x = 0$ and $\theta = 0.1$ is shown in Figure 6 which shows the system is stable. Many examples have been studied to compare the results obtained using the method proposed in this paper with the results obtained using the LMI method [7] and the fourth-order Pade approximation method. The calculation results are summarized in Table 1 along with the simulation based MADB.

Remarks. From Table 1, it can be seen that the proposed new method can give values of MADB similar to the values obtained using the LMI method and the other methods; however, the method proposed in this paper has a much

Table 1: The MADB (seconds) using the proposed method with 1st, 2nd, and 3rd order finite difference approximation for the delay term, the LMI method, the fourth-order Pade approximation method, and the simulation based method.

	The finite difference method			The LMI	Pade approximation	Simulation based
	1st order	2nd order	3rd order			
1	0.8695	0.8427	1.1321	0.8696	1.1672	1.180
2	0.1000	0.0995	0.1421	0.1000	0.1475	0.149
3	0.0100	0.0099	0.0149	0.0100	0.0156	0.0157
4	0.1428	0.1385	0.1808	0.1429	0.1855	0.1860
5	0.8217	0.8489	0.9085	0.8217	0.9091	0.9140
6	0.5000	0.4816	0.6303	0.5000	0.6474	0.6510
7	0.9940	0.9940	0.9960	0.9940	0.9960	0.9970
8	0.0856	0.0854	0.1192	0.0856	0.1230	0.1230
9	0.0906	0.0919	0.1251	0.0909	0.1284	0.1285
10	0.0416	0.0400	0.0496	0.0416	0.0505	0.0505

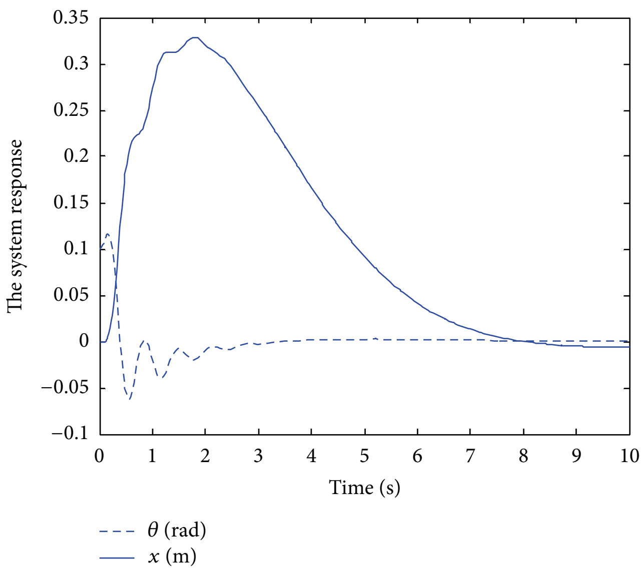

Figure 6: The response of the system in Example 9 with 0.0978 s delay.

simpler procedure, and it should have no difficulties for practical design engineers to accept this approach. Clearly, the MADB with the first-order finite difference approximation is comparable with the LMI method. Furthermore, we found good agreement between the third-order finite difference approximation and the fourth-order Pade approximation. The simulation based results for the MADB show that the estimated MADB through the proposed method sufficiently achieves the system stability. A simple controller design method has been developed by the authors based on the method presented in this paper. In the controller design method a stabilizing controller can be derived for a given network time delay. In all the case studies or examples, only linear system examples are given. The method is limited to linear systems only. The authors are now working on extending the methods to nonlinear systems, such as, multiconverter and inverter system and engine and electrical power generation systems [32, 33].

The application of the finite difference approximation for representing the time delay is not new but we found in this paper that using higher order approximations can sufficiently represent the time delay linear system. From Table 1 it can be concluded that using the first order approximation the estimated MADB is comparable with the other two methods. This is because the derivation of the linear model from the nonlinear model is based on neglecting the higher order derivative terms. In some cases we need to use the higher derivative terms for the time delay in order to achieve more accurate results for the MADB. The current research is to derive sufficient conditions for applying the method in order to find the tolerance of the estimated MADB.

4. Concluding Remarks

The main contribution of the paper is to have derived a new method for estimating the maximum time delay in NCSs. The most attractive feature of the new method is that it is a simple approach and easy to be applied, which can be easily interpreted to design engineers in industrial sectors. The results obtained in this method are compared with those obtained through the methods introduced in the literature. The method has demonstrated its merits in using less computation time due to its simple structure and giving less conservative results while showing good agreement with other methods. The method is limited to linear systems only and the work for extending the method for a class of nonlinear systems is on-going.

Conflict of Interests

The authors declare that there is no conflict of interests regarding the publication of this paper.

References

[1] X. Jiang, Q. L. Han, S. Liu, and A. Xue, "A new H_∞ stabilization criterion for networked control systems," *IEEE Transactions on Automatic Control*, vol. 53, no. 4, pp. 1025–1032, 2008.

[2] G. C. Walsh, H. Ye, and L. Bushnell, "Stability analysis of networked control systems," in *Proceedings of the American Control Conference (ACC '99)*, vol. 4, pp. 2876–2880, San Diego, Calif, USA, June 1999.

[3] G. C. Walsh, H. Ye, and L. G. Bushnell, "Stability analysis of networked control systems," *IEEE Transactions on Control Systems Technology*, vol. 10, no. 3, pp. 438–446, 2002.

[4] M. S. Mahmoud, *Robust Control and Filtering For Time Delay systems*, Marcel Dekker, New York, NY, USA, 2000.

[5] M. S. Mahmoud and A. Ismail, "Role of delays in networked control systems," in *Proceedings of the 10th IEEE International Conference on Electronics, Circuits and Systems (ICECS '03)*, vol. 1, pp. 40–43, December 2003.

[6] J. E. Marshall, H. Gorecki, A. Korytowski, and K. Walton, *Time-Delay Systems: Stability and Performance Criteria with Applications*, Ellis Horwood, 1992.

[7] D. Yue, Q.-L. Han, and C. Peng, "State feedback controller design of networked control systems," *IEEE Transactions on Circuits and Systems II: Express Briefs*, vol. 51, no. 11, pp. 640–644, 2004.

[8] P.-L. Liu, "Exponential stability for linear time-delay systems with delay dependence," *Journal of the Franklin Institute*, vol. 340, no. 6-7, pp. 481–488, 2003.

[9] B. Tang, G. P. Liu, and W. H. Gui, "Improvement of state feedback controller design for networked control systems," *IEEE Transactions on Circuits and Systems*, vol. 55, no. 5, pp. 464–468, 2008.

[10] J. Sun, G. Liu, and J. Chen, "State feedback stabilization of networked control systems," in *Proceedings of the 27th Chinese Control Conference (CCC '08)*, pp. 457–461, Kunming, China, July 2008.

[11] W. Zhang, M. S. Branicky, and S. M. Phillips, "Stability of networked control systems," *IEEE Control Systems Magazine*, vol. 21, no. 1, pp. 84–97, 2001.

[12] X. Li and C. E. de Souza, "Delay-dependent stability of linear time-delay systems: an LMI approach," *IEEE Transactions on Automatic Control*, vol. 42, no. 8, pp. 1144–1148, 1997.

[13] W. Min and H. Yong, "Improved stabilization method for networked control systems," in *Proceedings of the 26th Chinese Control Conference (CCC '07)*, pp. 544–548, Hunan, China, July 2007.

[14] X.-L. Zhu and G.-H. Yang, "New results on stability analysis of networked control systems," in *Proceedings of the American Control Conference*, pp. 3792–3797, Seattle, Wash, USA, June 2008.

[15] M. Jun and M. G. Safonov, "Stability analysis of a system with time-delay states," in *Proceeding of the American Control Conference*, Chicago, Ill, USA, June 2000.

[16] K. Kim, "A delay-dependent stability criterion in time delay system," *Journal of the Korean Society for Industrial and Applied Mathematics*, vol. 9, no. 2, pp. 1–11, 2005.

[17] M. S. Branicky, S. M. Phillips, and W. Zhang, "Stability of networked control systems: explicit analysis of delay," in *Proceedings of the American Control Conference*, pp. 2352–2357, Chicago, Ill, USA, June 2000.

[18] L. Xie, J.-M. Zhang, and S.-Q. Wang, "Stability analysis of networked control system," in *Proceedings of 1st International Conference on Machine Learning and Cybernetics*, pp. 757–759, Beijing, China, November 2002.

[19] A. Luis and P. J. Montestruque, "Model-based networked control systems- necessary and sufficient conditions for stability," in *Proceedings of the 10th Mediterranean Conference on Control and Automation*, pp. 1–58, Lisbon, Portugal, July 2002.

[20] Y. Sun and N. H. El-Farra, "Quasi-decentralized model-based networked control of process systems," *Computers & Chemical Engineering*, vol. 32, no. 9, pp. 2016–2029, 2008.

[21] J. Nilsson, *Real-time control systems with delays [Ph.D. thesis]*, Institute of Technology, Lund, Sweden, 1998.

[22] H. S. Park, Y. H. Kim, D.-S. Kim, and W. H. Kwon, "A scheduling method for network-based control systems," *IEEE Transactions on Control Systems Technology*, vol. 10, no. 3, pp. 318–330, 2002.

[23] Y. Zhang, Q. Zhong, and L. Wei, "Stability analysis of networked control systems with communication constraints," in *Proceedings of the Chinese Control and Decision Conference*, pp. 335–339, July 2008.

[24] Y. Zhang, Q. Zhong, and L. Wei, "Stability analysis of networked control systems with transmission delays," in *Proceedings of the Chinese Control and Decision Conference*, pp. 340–343, July 2008.

[25] J. Wang, Ü. Kotta, and J. Ke, "Tracking control of nonlinear pneumatic actuator systems using static state feedback linearisation of input/output map," *Proceedings of the Estonian Academy of Sciences: Physics, Mathematics*, vol. 56, no. 1, pp. 47–66, 2007.

[26] D. P. Goodall and J. Wang, "Stabilization of a class of uncertain nonlinear affine systems subject to control constraints," *International Journal of Robust and Nonlinear Control*, vol. 11, no. 9, pp. 797–818, 2001.

[27] J. Wang, J. Pu, P. R. Moore, and Z. Zhang, "Modelling study and servo-control of air motor systems," *International Journal of Control*, vol. 71, no. 3, pp. 459–476, 1998.

[28] C. D. Meyer, *Matrix Analysis and Applied Linear Algebra*, SIAM, 2000.

[29] F. Yang and H. Fang, "Control strategy design of networked control systems based on maximum allowable delay bounds," in *Proceedings of the IEEE International Conference on Control and Automation (ICCA '07)*, pp. 794–797, Guangzhou, China, June 2007.

[30] P. Naghshtabrizi, *Delay impulsive systems: a framework for modeling networked control systems [Ph.D. thesis]*, University of California, Los Angeles, Calif, USA, 2007.

[31] K. Ogata, *Modern Control Engineering*, Prentice Hall, New York, NY, USA, 3rd edition, 1997.

[32] J. L. Wei, J. Wang, and Q. H. Wu, "Development of a multi-segment coal mill model using an evolutionary computation technique," *IEEE Transactions on Energy Conversion*, vol. 22, no. 3, pp. 718–727, 2007.

[33] N. Jia, J. Wang, K. Nuttall et al., "HCCI engine modeling for real-time implementation and control development," *IEEE/ASME Transactions on Mechatronics*, vol. 12, no. 6, pp. 581–589, 2007.

Hindawi Publishing Corporation
Mathematical Problems in Engineering
Volume 2015, Article ID 148081, 10 pages
http://dx.doi.org/10.1155/2015/148081

Research Article

Multitarget Tracking with Spatial Nonmaximum Suppressed Sensor Selection

Liang Ma, Kai Xue, and Ping Wang

College of Mechanical and Electrical Engineering, Harbin Engineering University, Harbin, Heilongjiang, China

Correspondence should be addressed to Liang Ma; mllx01161110@hotmail.com

Received 12 August 2014; Revised 17 October 2014; Accepted 2 November 2014

Academic Editor: Xi-Ming Sun

Multitarget tracking is one of the most important applications of sensor networks, yet it is an extremely challenging problem since multisensor multitarget tracking itself is nontrivial and the difficulty is further compounded by sensor management. Recently, random finite set based Bayesian framework has opened doors for multitarget tracking with sensor management, which is modelled in the framework of partially observed Markov decision process (POMDP). However, sensor management posed as a POMDP is in essence a combinatorial optimization problem which is NP-hard and computationally unacceptable. In this paper, we propose a novel sensor selection method for multitarget tracking. We first present the sequential multi-Bernoulli filter as a centralized multisensor fusion scheme for multitarget tracking. In order to perform sensor selection, we define the hypothesis information gain (HIG) of a sensor to measure its information quantity when the sensor is selected alone. Then, we propose spatial nonmaximum suppression approach to select sensors with respect to their locations and HIGs. Two distinguished implementations have been provided using the greedy spatial nonmaximum suppression. Simulation results verify the effectiveness of proposed sensor selection approach for multitarget tracking.

1. Introduction

With recent advances in microelectromechanical systems, various kinds of sensors with strong communication ability and accurate data allocation have been manufactured at surprisingly low cost. Different applications of the sensor network have received increasing research interest, such as environmental monitoring, target tracking, and event detection [1, 2]. A static sensor network is a special type of sensor networks, which is composed of densely distributed sensors with fixed and known locations. In the static sensor network, sensor selection is of crucial importance for applications to fulfill a specific task in the optimal way, especially for multitarget tracking [3]. However, very little progress has been made in this area since multisensor multitarget tracking itself is nontrivial and the difficulty is further compounded by sensor selection [4].

In the literature, there are extensive studies on the sensor selection (also named as sensor management) problem for target tracking. For the single target tracking case, [5] adopted the decentralized posterior Cramr-Rao lower bound to measure tracking accuracy and used an iterative local search technique for sensor selection. [3] used convex relaxation for sensor selection and then adopted the sequential Kalman filter to track each target in a distributed manner. Recently, random finite set (RFS) based Bayesian framework has provided an elegant solution for multitarget tracking with sensor management using mathematical tools from the finite set statistics (FISST) [6]. In [4, 7], sensor management has been modelled by a partially observed Markov decision process (POMDP) given the multitarget state, which has been shown effective in single sensor control and single sensor selection [8, 9]. However, multisensor management modelled as a POMDP is in essence a combinatorial optimization problem which is NP-hard and computationally unacceptable for a sensor network.

This paper considers sensor selection problem for multitarget tracking from a new perspective: *which sensors should not be selected*. It is intuitive that we should only select informative sensors in use and ignore noninformative sensors in order to alleviate data transmission bandwidth in the sensor network. In this paper, we show that this perspective offers a better alternative to exploit the sensor selection problem which is effective and easy to implement. We first present a centralized multisensor fusion scheme in RFS based Bayesian framework for multitarget tracking and then propose the sequential multi-Bernoulli filter as a feasible approximation of multisensor multitarget state estimation. With respect to sensor selection, we define the *hypothesis information gain* (HIG) of a sensor to measure its information quantity when it is selected alone. Two types of HIG are presented using the Rényi divergence between the prior and posterior target density, respectively, for individual target state and multitarget state. Then, we propose the *spatial nonmaximum suppression* (SNMS) approach to suppress sensors with low HIG and subsequently select sensors with high HIG. Two sensor selection approaches via SNMS have been provided in the sequential Monte Carlo (SMC) implementation corresponding to two defined HIGs. Numerical simulations have verified the capability of the proposed sensor selection approach for multitarget tracking.

The reminder of this paper is organized as follows. Section 2 presents a general description of the sensor selection problem for multitarget tracking to lay a solid foundation. In Section 3, we illustrate the RFS based Bayesian framework, the Cardinality-Balanced multi-Bernoulli filter and then provide the sequential multi-Bernoulli filter as a centralized multisensor fusion scheme. The sensor selection approach via SNMS is discussed in Section 4. Section 5 provides numerical results, followed by the conclusions in Section 6.

2. Problem Formulation

Sensor selection for multitarget tracking entails a scenario where there are a large number of densely distributed sensors with fixed and known positions. Each sensor has limited field of view (FOV) but a relatively large communication range. The data allocated by each sensor are transmitted to a fusion center to perform centralized information fusion in order to track all targets in the surveillance area. Sensor selection is required to balance between tracking accuracy and the network workload which is highly dependent on the number of activated sensors. In this paper, we consider two-dimensional coordinate tracking as a particular interest that is demonstrated in Figure 1.

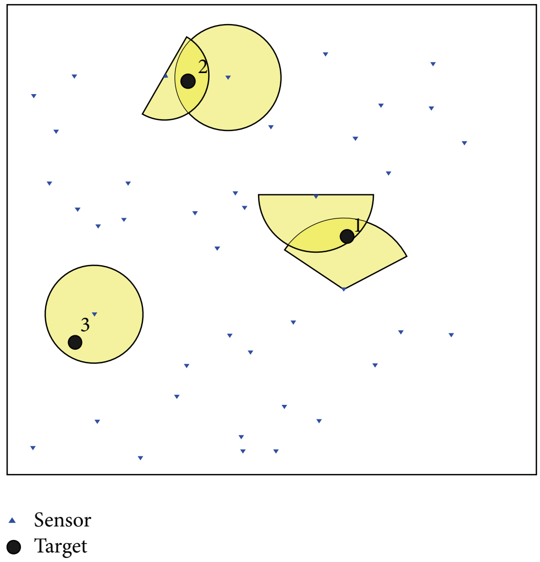

Figure 1: Multitarget tracking in a static sensor network. Yellow region is the FOV of a sensor. Only five of all sensors can detect targets. Target 1 and target 2 can be detected by two sensors, while target 3 is only detected by one sensor. The fusion center is not shown here but exists.

As illustrated in Figure 1, multitarget tracking in a sensor network requires multisensor fusion for multitarget state estimation and appropriate sensor selection approach to guarantee tracking accuracy with minimum number of activated sensors. Assume that target moves according to the nearly constant velocity model given by

$$\mathbf{x}_k = F\mathbf{x}_{k-1} + G\mathbf{v}_k, \quad (1)$$

where $\mathbf{x}_k = [p_{x,k}, v_{x,k}, p_{y,k}, v_{y,k}]^T$ and $p_{x,k}$, $p_{y,k}$ are planar position and $v_{x,k}$, $v_{y,k}$ are planar velocity, respectively, along x-, y-coordinate. Also $F = I_2 \otimes \left[\begin{smallmatrix} 1 & \Delta \\ 0 & 1 \end{smallmatrix}\right]$; $G = I_2 \otimes \left[\begin{smallmatrix} \Delta^2/2 \\ \Delta \end{smallmatrix}\right]$. I_2 is 2×2 identity matrix and $\otimes$ denotes Kronecker product. Δ is the sampling period, and $\mathbf{v}_k \sim \mathcal{N}(\mathbf{0}, Q_k)$ is a 2×1 i.i.d. Gaussian noise. Assume process noise is time invariant and identical for both $v_{x,k}$ and $v_{y,k}$; then $Q = \sigma_v^2 I_2$, where σ_v is the standard deviation.

The observation of sensor l originated from target with state $\mathbf{x}_k$ is a noisy vector $\mathbf{z}_k^l$, and the measurement model is given by

$$\mathbf{z}_k^l = h^l(\mathbf{x}_k) + w^l, \quad (2)$$

where w^l is zero mean Gaussian noise $\mathcal{N}(w^l; \mathbf{0}, R^l)$ and $h^l(\cdot)$ is dependent on the position of the lth sensor $\mathbf{s}_l = [x_l \;\, y_l]^T$ and the type of sensor l.

3. Bayesian Multitarget Filtering

This section provides the basic concepts and notations of RFS based Bayesian framework and presents the multisensor information fusion approach thereafter. Section 3.1 gives a general description of the RFS based multisensor multitarget Bayesian filtering. Due to the fact that the multisensor multitarget Bayesian filtering is intractable and computationally unacceptable, we provide the sequential multi-Bernoulli filter as a feasible approach. For clarity, we first introduce the multi-Bernoulli filter in Section 3.2 and then provide the SMC implementation of the sequential multi-Bernoulli filter in Section 3.3.

3.1. Multisensor Multitarget Bayesian Framework. Stochastic filtering in Bayesian framework has been developed for decades [10]. Under the assumption of linear model and Gaussian distribution, Kalman filter was first derived in [11] and has been widely used for target tracking since then. With respect to the multisource multitarget tracking case, RFS based Bayesian framework provides an elegant solution that outweighs the data association approach significantly.

A random finite set is a random variable that takes value as an unordered finite set. The randomness of an RFS refers to two aspects: the set cardinality (the number of elements in the set) is random; each element in the set is also a random variable. The probabilistic description of RFS has been studied regarding different types of probability distributions such as multi-Bernoulli (or Bernoulli) RFS, i.i.d. (short for independent identically distributed) cluster RFS, and Poisson RFS [12]. Let X_k and Z_k, respectively, denote the multitarget state set and the observation set of multiple sensors,

$$X_k = \left\{\mathbf{x}_{k,1}, \ldots, \mathbf{x}_{k,N_k}\right\},$$
$$Z_k = \left\{Z_k^1, \ldots, Z_k^m\right\}, \quad (3)$$

where m is the total number of sensors and $Z_k^l = \{\mathbf{z}_k^l, \ldots, \mathbf{z}_{k,M_{k,l}}^l\}$ for $l = 1, \ldots, m$. N_k is the time-varying cardinality of targets while $M_{k,l}$ is the cardinality of the measurement set generated by sensor l.

Using the RFS representation, the movement of multiobject can be described using two parts: an RFS for survival targets from previous time step S_k and an RFS for spontaneous birth targets at current time Γ_k. Thus, at time k we have the predicted RFS $X_k = S_k \cup \Gamma_k$. The RFS for measurements Z_k^l of sensor l can be represented as a union of two parts: target-generated measurements Θ_k^l and clutter K_k^l; thus, $Z_k^l = \Theta_k^l \cup K_k^l$.

Given any specific type of RFS, the Bayesian framework for optimal estimation via RFS is in the same form as the classical Bayesian filtering given as follows:

$$f_{k|k-1}(X \mid Z_{1:k-1}) = \int f_{k|k-1}(X \mid X') f_{k-1}(X' \mid Z_{1:k-1}) \delta X', \quad (4)$$

$$f_k(XZ_{1:k}) = \frac{f_k(Z_k X) f_{k|k-1}(XZ_{1:k-1})}{\int f_k(Z_k X) f_{k|k-1}(XZ_{1:k-1}) \delta X}, \quad (5)$$

which represent the prediction and update process of Bayesian recursion via set integrals, respectively. Notice that (4) and (5) are for multisensor multitarget Bayesian filtering and computationally intractable. Meanwhile, the single senor multitarget filtering version given in [13] is a particular case of it, from which the probability hypothesis density (PHD) [14], cardinalized PHD (CPHD) [15], and multi-Bernoulli filter [13] have been derived under different forms of RFS.

3.2. Cardinality-Balanced Multi-Bernoulli Filter. Here, we introduce the multi-Bernoulli RFS for multitarget state modelling, which offers a better alternative than the Poisson and i.i.d. cluster RFS in applications with highly nonlinear model and/or nonhomogeneous sensor type [13]. Assume the dimension of the target state is n; then the target state space is denoted by $\mathcal{X} \subseteq \mathbb{R}^n$. A multi-Bernoulli RFS X on $\mathcal{X}$ is a union of a fixed number of independent Bernoulli RFSs $X^{(j)}$ with existence probability $r^{(j)} \in (0, 1)$ and probability density $p^{(j)}$ (defined on $\mathcal{X}$), $j = 1, \ldots, M$; that is $X = \cup_{j=1}^M \{X^{(j)}\}$.

Use a Bernoulli set for modelling the state of a single target; then the multitarget state can be modeled as multi-Bernoulli RFS Ξ with probability density given in [13] as follows:

$$f(\{\mathbf{x}_1, \ldots, \mathbf{x}_n\}) = f(\emptyset) \cdot \sum_{(r^{(j)}, p^{(j)}) \in \Xi} \left(\prod_{i=1}^n \frac{r^{(j)} p^{(j)}(\mathbf{x}_i)}{1 - r^{(j)}} \right), \quad (6)$$

where $r^{(j)}$ and $p^{(j)}$, respectively, represent the existence probability and distribution of the jth target and $f(\emptyset) = \prod_{j=1}^M (1 - r^{(j)})$. It is clear that the multitarget density can be completely specified by multi-Bernoulli parameter set $\{(r^{(j)}, p^{(j)})\}_{j=1}^M$. Hence, let us denote the multitarget density at time k as $\pi_k = \{(r_k^{(j)}, p_k^{(j)})\}_{j=1}^{M_k}$ for short in the following content. In multi-Bernoulli filter, the probability hypothesis density (also known as the intensity function in [13, 16]), as the first-order moment, is propagated over time as approximations of the full posteriors $f(X \mid Z)$ [6]. In the following, we refer to "probability hypothesis density" as "density" for short. Let us denote the multitarget posterior density at time k using multi-Bernoulli parameters by $\pi_k = \{(r_k^{(j)}, p_k^{(j)})\}_{j=1}^{M_k}$ for short. The following gives the recursion of the Cardinality-Balanced multi-Bernoulli filter.

Prediction. At time k, if the posterior multitarget density is multi-Bernoulli given by $\pi_k = \{(r_k^{(j)}, p_k^{(j)})\}_{j=1}^{M_k}$ and the density of new births is also multi-Bernoulli $\pi_{\Gamma,k+1} = \{(r_{\Gamma,k+1}^{(j)}, p_{\Gamma,k+1}^{(j)})\}_{j=1}^{M_{\Gamma,k+1}}$, then the predicted density is given by

$$\pi_{k+1|k} = \left\{\left(r_{k+1|k}^{(j)}, p_{k+1|k}^{(j)}\right)\right\}_{j=1}^{M_k} \cup \left\{\left(r_{\Gamma,k+1}^{(j)}, p_{\Gamma,k+1}^{(j)}\right)\right\}_{j=1}^{M_{\Gamma,k+1}}, \quad (7)$$

where for survival targets

$$r_{k+1|k}^{(j)} = r_k^{(j)} \cdot \left\langle p_k^{(j)}, p_{S,k} \right\rangle,$$
$$p_{k+1|k}^{(j)}(\mathbf{x}) = \frac{\left\langle f_{k+1|k}(x \mid \cdot), p_k^{(j)} p_{S,k} \right\rangle}{\left\langle p_k^{(j)}, p_{S,k} \right\rangle}, \quad (8)$$

and, for new born targets, $r_{\Gamma,k+1}^{(j)}, p_{\Gamma,k+1}^{(j)}(\mathbf{x})$ are prior existence probability and distribution of birth model.

Update. At time $k+1$, if the predicted multitarget density is multi-Bernoulli $\pi_{k+1|k} = \{(r_{k+1|k}^{(j)}, p_{k+1|k}^{(j)})\}_{j=1}^{M_{k+1|k}}$, the output of corrector is composed of legacy tracks and measurement-updated tracks,

$$\pi_{k+1} = \left\{\left(r_{L,k+1}^{(j)}, p_{L,k+1}^{(j)}\right)\right\}_{j=1}^{M_{k+1|k}} \cup \left\{\left(r_{U,k+1}(\mathbf{z}), p_{U,k+1}(\cdot \mid \mathbf{z})\right)\right\}_{\mathbf{z} \in Z_k}, \quad (9)$$

Prediction:
Input: $\pi_k = \{r_k^{(j)}, p_k^{(j)}\}_{j=1}^{M_k}$
(1) **for** Survival targets: $j = 1, \dots, M_k$ **do**
(2) for $i = 1, \dots, L_k^{(j)}$, sample $x_{S,i,k+1|k}^{(j)}$, compute weight $\omega_{S,i,k+1|k}^{(j)}$ and normalization $\widetilde{\omega}_{S,i,k+1|k}^{(j)}$
(3) compute $r_{S,k+1|k}^{(j)}, p_{S,k+1|k}^{(j)}(\mathbf{x})$
(4) **end for**
(5) **for** newborn targets: $j = 1, \dots, M_{\Gamma,k+1}$ **do**
(6) for $i = 1, \dots, L_{\Gamma,k}^{(j)}$, sample $x_{\Gamma,i,k+1}^{(j)}$, compute weight $\omega_{\Gamma,i,k+1}^{(j)}$ and normalization $\widetilde{\omega}_{\Gamma,i,k+1}^{(j)}$
(7) compute $r_{\Gamma,k+1}^{(j)}, p_{\Gamma,k+1}^{(j)}(\mathbf{x})$
(8) **end for**
Output: $\pi_{k+1|k} = \{(r_{k+1|k}^{(j)}, p_{k+1|k}^{(j)})\}_{j=1}^{M_k} \cup \{(r_{\Gamma,k+1}^{(j)}, p_{\Gamma,k+1}^{(j)})\}_{j=1}^{M_{\Gamma,k+1}}$
Update:
Input: $\pi_{k+1|k} = \{r_{k+1|k}^{(j)}, p_{k+1|k}^{(j)}\}_{j=1}^{M_{k+1|k}}$, candidate sensors located at $\mathbf{s}_l$ with observation set Z_{k+1}^l $(l = 1, \dots, m')$
(1) **for** $l = 1, \dots, m'$ **do**
(2) **for** Legacy targets: $j = 1, \dots, M_{k+1|k}$ **do**
(3) compute $\omega_{L,i,k+1}^{(j),l}$ and normalization $\widetilde{\omega}_{L,i,k+1}^{(j),l}$, compute pseudo-likelihood $\varrho_{L,k+1}^{(j),l}$
(4) compute $r_{L,k+1}^{(j),l}, p_{L,k+1}^{(j),l}(\mathbf{x})$
(5) **end for**
(6) **for** $\mathbf{z} \in Z_{k+1}^l$ **do**
(7) **for** Measurement-updated targets: $j = 1, \dots, M_{k+1|k}$ **do**
(8) compute $\omega_{U,i,k+1}^{(j),l}(\mathbf{z})$ and normalization $\widetilde{\omega}_{U,i,k+1}^{(j),l}(\mathbf{z})$, compute pseudo-likelihood $\varrho_{U,k+1}^{(j),l}(\mathbf{z})$
(9) compute $r_{U,k+1}^{(j),l}(\mathbf{z}), p_{U,k+1}^{(j),l}(\mathbf{x}; \mathbf{z})$
(10) **end for**
(11) **end for**
(12) $\pi_{k+1|k} = \{(r_{L,k+1}^{(j),l}, p_{L,k+1}^{(j),l})\}_{j=1}^{M_{k+1|k}} \cup \{(r_{U,k+1}^{l}(\mathbf{z}), p_{U,k+1}^{l}(\cdot|\mathbf{z}))\}_{\mathbf{z}\in Z_{k+1}^l}$
(13) **end for**
Output: $\pi_{k+1} = \{(r_{L,k+1}^{(j),m'}, p_{L,k+1}^{(j),m'})\}_{j=1}^{M_{k+1|k}} \cup \{(r_{U,k+1}^{m'}(\mathbf{z}), p_{U,k+1}^{m'}(\cdot|\mathbf{z}))\}_{\mathbf{z}\in Z_{k+1}^{m'}}$

Algorithm 1: SMC sequential multisensor multi-Bernoulli filter.

where

$$r_{L,k+1}^{(j)} = r_{k+1|k}^{(j)} \frac{1 - \left\langle p_{k+1|k}^{(j)}, p_{D,k+1} \right\rangle}{1 - r_{k+1|k}^{(j)} \left\langle p_{k+1|k}^{(j)}, p_{D,k+1} \right\rangle},$$

$$p_{L,k+1}^{(j)}(\mathbf{x}) = p_{k+1|k}^{(j)}(\mathbf{x}) \frac{1 - p_{D,k+1}(\mathbf{x})}{1 - \left\langle p_{k+1|k}^{(j)}, p_{D,k+1} \right\rangle},$$

$$r_{U,k+1}(\mathbf{z}) = \left(\sum_{j=1}^{M_{k+1|k}} \frac{r_{k+1|k}^{(j)} \left(1 - r_{k+1|k}^{(j)}\right) \left\langle p_{k+1|k}^{(j)}, \psi_{k+1,\mathbf{z}} \right\rangle}{\left(1 - r_{k+1|k}^{(j)} \left\langle p_{k+1|k}^{(j)}, p_{D,k+1} \right\rangle\right)^2} \right) \times \left(\kappa_{k+1}(\mathbf{z}) + \sum_{j=1}^{M_{k+1|k}} \frac{r_{k+1|k}^{(j)} \left\langle p_{k+1|k}^{(j)}, \psi_{k+1,\mathbf{z}} \right\rangle}{1 - r_{k+1|k}^{(j)} \left\langle p_{k+1|k}^{(j)}, p_{D,k+1} \right\rangle} \right)^{-1},$$

$$p_{U,k+1}(\mathbf{z}) = \left(\sum_{j=1}^{M_{k+1|k}} \frac{r_{k+1|k}^{(j)}}{1 - r_{k+1|k}^{(j)}} p_{k+1|k}^{(j)}(\mathbf{x}) \psi_{k+1,\mathbf{z}}(\mathbf{x}) \right) \times \left(\sum_{j=1}^{M_{k+1|k}} \frac{r_{k+1|k}^{(j)}}{1 - r_{k+1|k}^{(j)}} \left\langle p_{k+1|k}^{(j)}, \psi_{k+1,\mathbf{z}} \right\rangle \right)^{-1},$$

$$\psi_{k+1,\mathbf{z}}(\mathbf{x}) = g_{k+1}(\mathbf{z}\mathbf{x}) \, p_{D,k+1}(\mathbf{x}). \tag{10}$$

p_S and p_D are probability of survival and detection for target. The inner product $\langle \cdot, \cdot \rangle$ is defined between two real valued functions β and γ by $\langle \beta, \gamma \rangle = \int \beta(x)\gamma(x)dx$. Note that without loss of generality we refer to the Cardinality-Balanced multi-Bernoulli filter as "multi-Bernoulli" filter for simplicity in this paper.

3.3. Sequential Multi-Bernoulli Filter. Sequential update has been widely used and verified to be a good approximation for information fusion of multiple sensors [3, 17]. Here, we introduce the sequential multi-Bernoulli filter in the SMC implementation which is proposed in [17].

Suppose that, at time k, the posterior multitarget density is given as $\{r_k^{(j)}, p_k^{(j)}\}_{j=1}^{M_k}$, and the distribution of each target is given by a set of weighted particles $p_k^{(j)}(\mathbf{x}) = \sum_{i=1}^{L_k^{(j)}} \omega_{i,k}^{(j)} \cdot \delta_{\mathbf{x}_{i,k}^{(j)}}(\mathbf{x})$. Then, the SMC implementation of the sequential multisensor multi-Bernoulli filter is provided in Algorithm 1. We refer the readers to subsection IV-A of [13] for detailed equations.

The superscript $(j), l$ in Algorithm 1 represents the predicted jth Bernoulli set updated with the lth sensor. To avoid the infinite growth of multi-Bernoulli set number, those with existence probability less than a predefined threshold (e.g., 0.001) are removed. Meanwhile, the particle number is limited between $L_{\min}$ and $L_{\max}$, in case that sampling is not enough or resampling reallocates too many particles. The number of particles for each Bernoulli set is proportional to each target existence $r_k^{(j)}$ during the resampling step. With a given existence threshold 0.75, those sets with $r_k^{(j)}$ over 0.75 are true tracks while the others are not.

4. Sensor Selection with Spatial Nonmaximum Suppression

In this section, we first illustrate the definition of hypothesis information gain in Section 4.1. Then, Section 4.2 provides the description of the spatial nonmaximum suppression. Then, we propose a greedy implementation of sensor selection in Section 4.3 given the proposed spatial nonmaximum suppression.

4.1. Hypothesis Information Gain. Before applying nonmaximum suppression, we need to define a proper measure of each sensor to determine whether the sensor is informative for target state estimation. Here, we first introduce the HIG for individual target and then give the HIG for multitarget directly. The HIG for individual target is defined with respect to target density, which is the product of existence probability and state distribution given in [6] as follows:

$$\pi_k^{(j)} = r_k^{(j)} \cdot p_k^{(j)}, \tag{11}$$

for Bernoulli set $\{r_k^{(j)}, p_k^{(j)}\}$. Notice that the density is the product of a scalar and a probability distribution. The Rényi divergence is adopted to measure the information gain between target prior and posterior distribution. Hence, the HIG of sensor l with respect to target j is defined as

$$\mathscr{H}_{k+1}^{(j),l} = \frac{r_{k+1}^{(j),l}}{r_{k+1|k}^{(j)}} \mathbf{E}\left[\mathscr{R}^l\left(p_{k+1}^{(j),l} \| p_{k+1|k}^{(j)}\right)\right], \tag{12}$$

where $\mathbf{E}[\cdot]$ is the expectation operator and $\mathscr{R}^l(p_{k+1}^{(j),l} \| p_{k+1|k}^{(j)})$ is the Rényi divergence between the prior and posterior distribution of target j denoted by $\mathscr{R}^{(j),l}$ for short. Given the Bayesian recursion, $\mathscr{R}^{(j),l}$ is given in [8] as follows:

$$\mathscr{R}^{(j),l} = \frac{1}{\alpha - 1} \log \frac{\int \left[g_{k+1}^l\left(\mathbf{z} \mid \mathbf{x}_{k+1}^{(j)}\right)\right]^\alpha p_{k+1|k}^{(j)}(\mathbf{x})\, d\mathbf{x}_{k+1}^{(j)}}{\left[p\left(\mathbf{z} \mid Z_k\right)\right]^\alpha}, \tag{13}$$

where $p(\mathbf{z} \mid Z_k) = \int g_{k+1}^l(\mathbf{z} \mid \mathbf{x}_{k+1}^{(j)}) p_{k+1|k}^{(j)}(\mathbf{x}) d\mathbf{x}_{k+1}^{(j)}$ and α is a parameter that determines how much we emphasize the tails of two distributions in the metric, and the Rényi divergence becomes the Kullback-Leibler discrimination and Hellinger affinity, respectively, when $\alpha \to 1$ and $\alpha = 0.5$ [18].

To compute (12), we only generate one future measurement $\mathbf{z}$ for sensor l based on the predicted state, assuming no clutter or unity detection rate as illustrated in [9]. Thus, $r_{k+1}^{(j),l} = r_{U,k+1}^{(j),l}(\mathbf{z})$ for unity detection rate. Assume that at time k the predicted multitarget density $\pi_{k+1|k} = \{r_{k+1|k}^{(j)}, p_{k+1|k}^{(j)}\}_{j=1}^{M_{k+1|k}}$ is given in SMC form where $p_{k+1|k}^{(j)}(\mathbf{x}) = \sum_{i=1}^{L_{k+1|k}^{(j)}} \omega_{i,k+1|k}^{(j)} \cdot \delta_{\mathbf{x}_{i,k+1|k}^{(j)}}(\mathbf{x})$; substitute SMC form of $p_{k+1|k}^{(j)}(\mathbf{x})$ into (13); then, we obtain

$$\mathscr{H}_{k+1}^{(j),l} = \frac{r_{U,k+1}^{(j),l}(\mathbf{z})}{(\alpha - 1)\, r_{k+1|k}^{(j)}} \times \log \frac{\sum_{i=1}^{L_{k+1|k}^{(j)}} \omega_{i,k+1|k}^{(j)} \left[g_{k+1}^l\left(\mathbf{z} \mid \mathbf{x}_{k+1}^{(j)}\right)\right]^\alpha}{\left[\sum_{i=1}^{L_{k+1|k}^{(j)}} \omega_{i,k+1|k}^{(j)} g_{k+1}^l\left(\mathbf{z}\mathbf{x}_{k+1}^{(j)}\right)\right]^\alpha}. \tag{14}$$

Notice that the HIG of sensor l described by (14) is defined for each individual target. Consequently, we also define another HIG of sensor l given by

$$\begin{aligned}\mathscr{H}_{k+1}^{l} &= \sum_{j=1}^{M_{k+1|k}} \mathscr{H}_{k+1}^{(j),l} \\ &= \sum_{j=1}^{M_{k+1|k}} \left[\frac{r_{U,k+1}^{(j),l}(\mathbf{z})}{(\alpha - 1)\, r_{k+1|k}^{(j)}} \times \log \frac{\sum_{i=1}^{L_{k+1|k}^{(j)}} \omega_{i,k+1|k}^{(j)} \left[g_{k+1}^l\left(\mathbf{z} \mid \mathbf{x}_{k+1}^{(j)}\right)\right]^\alpha}{\left[\sum_{i=1}^{L_{k+1|k}^{(j)}} \omega_{i,k+1|k}^{(j)} g_{k+1}^l\left(\mathbf{z} \mid \mathbf{x}_{k+1}^{(j)}\right)\right]^\alpha}\right],\end{aligned} \tag{15}$$

to capture the information gain of sensor l with regard to multitarget state. In this paper, we name $\mathscr{H}_{k+1}^{(j),l}$ in (14) as "individual HIG" and $\mathscr{H}_{k+1}^{l}$ in (15) as "sum HIG." The benefits of using the HIG is twofold: firstly, maximizing the measurement-updated existence probability tends to avoid losing targets; secondly, maximum Rényi divergence between the predicted and updated distribution obtains more information from future measurements and makes target state estimation more accurate.

4.2. Spatial Nonmaximum Suppression. Nonmaximum suppression (NMS) plays a very important role in computer vision field especially in the object detection process, which aims to pick real objects with local maxima and suppress those that are outliers. Nonmaximum suppression is first proposed in an edge detection context [19] and then widely used in many detectors, such as points [20, 21], edges [22], and objects [23, 24]. The original version of NMS is one-dimensional (1D) [19] and then extended to isotropic NMS to locate two-dimensional (2D) feature points from an image [20]. In this paper, we use the underlying rationale of the isotropic NMS and propose SNMS method in order to eliminate sensors with low HIG.

Since the SNMS method here is different from that in computer vision area, we first present a general description of the SNMS algorithm for spatially distributed valued-points.

Input: $\mathscr{V}_k^i, \mathbf{s}_i$ $(i = 1, \dots, n)$, suppression gate ϵ
$\mathcal{S}_k = \{\mathbf{s}_1, \dots, \mathbf{s}_n\}$
for $i = 1, \dots, n$ **do**
  for $j = 1, \dots, n$ **do**
    if $i \neq j$ and $\|\mathbf{s}_i - \mathbf{s}_j\| \leq \epsilon$ and $\mathscr{V}_k^j \geq \mathscr{V}_k^i$ **then**
      remove $\mathbf{s}_i$ from $\mathcal{S}_k$; continue;
    end if
  end for
end for
Output: $\mathcal{S}_k$

ALGORITHM 2: Spatial nonmaximum suppression (straightforward).

Input: $\mathscr{V}_k^i, \mathbf{s}_i$ $(l = 1, \dots, n)$, suppression gate ϵ
$\mathcal{S}_k = \{\mathbf{s}_1, \dots, \mathbf{s}_n\}$, $\mathcal{S}_k^{sclt} = \emptyset$
sort $\mathcal{S}_k$ given $\mathscr{V}_k^i$ in descending order
while $\mathcal{S}_k \neq \emptyset$ **do**
  take the first point $\mathbf{s}_{\text{first}}$ from $\mathcal{S}_k$
  for $i = 1, \dots, n$ **do**
    if $\|\mathbf{s}_i - \mathbf{s}_{\text{first}}\| \leq \epsilon$ **then**
      remove $\mathbf{s}_i$ from $\mathcal{S}_k$;
      $\mathcal{S}_k^{sclt} = \mathcal{S}_k^{sclt} \cup \{\mathbf{s}_{\text{first}}\}$
    end if
  end for
end while
Output: $\mathcal{S}_k^{sclt}$

ALGORITHM 3: Spatial nonmaximum suppression (greedy).

Input: $\pi_{k+1|k}, \mathbf{s}_l$ $(l = 1, \dots, m)$
for $j = 1, \dots, M_{k+1|k}$ **do**
  for $l = 1, \dots, m$ **do**
    predict $\mathbf{z} = \sum_{i=1}^{L_{k+1|k}^{(j)}} \omega_{i,k+1|k}^{(j)} h^l(\mathbf{x}_{i,k+1|k}^{(j)})$
    compute $\mathscr{H}_{k+1}^{(j),l}$ given by (14)
  end for
  greedy SNMS to obtain $\mathcal{S}_{k+1}^{(j)}$
end for
Output: $\mathcal{S}_{k+1} = unique(\cup_{j=1}^{M} \mathcal{S}_{k+1}^{(j)})$

ALGORITHM 4: Sensor selection I (individual HIG).

Input: $\pi_{k+1|k}, \mathbf{s}_l$ $(l = 1, \dots, m)$
for $j = 1, \dots, M_{k+1|k}$ **do**
  for $l = 1, \dots, m$ **do**
    predict $\mathbf{z} = \sum_{i=1}^{L_{k+1|k}^{(j)}} \omega_{i,k+1|k}^{(j)} h^l(\mathbf{x}_{i,k+1|k}^{(j)})$
    compute $\mathscr{H}_{k+1}^{(j),l}$ given by (14)
  end for
  compute $\mathscr{H}_{k+1}^{l}$ given by (15)
  greedy SNMS to obtain $\mathcal{S}_{k+1}$
end for
Output: $\mathcal{S}_{k+1}$

ALGORITHM 5: Sensor selection II (sum HIG).

At time k, assume that there are n valued-points with known positions $\mathbf{u}_i$ and values $\mathscr{V}_k^i$ for $i = 1, \dots, m$, given a predefined suppression gate ϵ; then, the ith point is suppressed if there is any point j that satisfies

$$\left\|\mathbf{u}_i - \mathbf{u}_j\right\| \leq \epsilon, \qquad \mathscr{V}_k^j \geq \mathscr{V}_k^i, \tag{16}$$

where $\|\cdot\|$ is the Euclidean distance between point i and point j. It is clear that the spatial nonmaximum suppression is trivial and easy to implement in a straightforward way. Algorithm 2 provides the straightforward implementation of proposed SNMS method. It is obvious that in each loop 3 comparisons are made. Hence, the computational complexity of the straightforward implementation is $\mathcal{O}(n)$ for the best case and $\mathcal{O}(n^2)$ for the worst case and $\mathcal{O}(n(n+1)/2)$ on average. This is because the inner loop in Algorithm 2 may stop at any i for $i = 1, \dots, n$ with equal probability $p(i) = 1/n$; thus, the expected number of comparisons $\mathbf{E}_{\text{cmp}}$ is

$$\mathbf{E}_{\text{cmp}} = 3 \times n \times \sum_{i=1}^{n} l \cdot \frac{1}{n} = \frac{3n(n+1)}{2}. \tag{17}$$

To reduce the computational cost when the number of valued-points is extremely large, we introduce the greedy implementation of SNMS by assuming suppressed points will no longer suppress other points. The greedy implementation has been proven to be as effective as the straightforward implementation and much more efficient in the literature [23, 24]. The greedy SMC implementation of SNMS is given in Algorithm 3. It is clear that the greedy implementation requires sorting the point first by its associated value, and this procedure can be achieved at $\mathcal{O}(n \log n)$ using proper sorting algorithm.

4.3. Implementation of SNMS Sensor Selection. Given the proposed SNMS above, the sensor selection via SNMS is direct given the location and HIG of each sensor. Assume the sensor network contains m candidate sensors with fixed and known position $\mathbf{s}_l$ $(l = 1, \dots, m)$, given the multitarget prediction $\pi_{k+1|k} = \{r_{k+1|k}^{(j)}, p_{k+1|k}^{(j)}\}_{j=1}^{M_{k+1|k}}$ at time $k+1$; we present the SMC implementation of sensor selection via SNMS in Algorithms 4 and 5, respectively, for individual HIG and sum HIG. In the following content, we refer to the sensor selection using individual HIG as "sensor selection I" and using sum HIG as "sensor selection II". The *unique*() function in Algorithm 4 eliminates repeatedly chosen sensor to ensure that each sensor will only be updated once in the sequential multi-Bernoulli filter.

In order to track targets accurately, we need to select sensors with higher HIG and eliminate those with lower HIG. The underlying rationale of SNMS sensor selection is that sensors with higher value of HIG are very likely to have some targets near them since each sensor has only limited FOV. Thus, sensors should be selected by seeking the local maxima given their spatial locations. A question may rise here: *why not use thresholding method to eliminate sensors with lower HIG*. Actually, the thresholding technique is inappropriate in this case for two reasons: firstly, it may *over select* sensors that observe the same targets; secondly, sensors that are not so informative but actually useful may be eliminated wrongly.

5. Simulation

In order to demonstrate the performance of proposed sensor selection approach for multitarget tracking, we present a planar multitarget tracking scenario in a static sensor network, in which 9×9 sensors were laid out uniformly over a square of size $[-1000\,\text{m}, 1000\,\text{m}] \times [-1000\,\text{m}, 1000\,\text{m}]$ divided into $200\,\text{m} \times 200\,\text{m}$ blocks. There are unknown and time-varying number of targets observed in clutter while range and bearing measurements from each sensor are available.

Targets can appear or disappear in the scene at any time, and survival probability $p_S = 0.95$ for each existing target. Newborn targets appear spontaneously according to $\gamma_k = 0.2\mathcal{N}(\cdot; \overline{\mathbf{x}}, Q)$. Each target moves according to the constant velocity model given by (1). Four targets are presented for tracking purpose as illustrated in Figure 2.

The tracker, composed of SNMS sensor selection and the sequential multi-Bernoulli filter, runs for 50 scans with sampling period $\Delta = 1\,\text{s}$. The standard derivation of process noise $\sigma_v = 1\,\text{m/s}$ for both $v_{x,k}$ and $v_{y,k}$. The $h^l(\mathbf{x}_k)$ of the measurement model described by (2) is given as

$$h^l(\mathbf{x}_k) = \begin{bmatrix} \|\mathbf{p}_k - \mathbf{s}_l\| \\ \arctan \dfrac{y_l - p_{y,k}}{x_l - p_{x,k}} \end{bmatrix}, \tag{18}$$

in which $\|\mathbf{p}_k - \mathbf{s}_l\| = \sqrt{(x_l - p_{x,k})^2 + (y_l - p_{y,k})^2}$. The covariance of measurement noise w_k^l for sensor l at time k is $R_k^l = \text{diag}([(\sigma_{r,k}^l)^2, (\sigma_{\phi,k}^l)^2])$, where

$$\begin{aligned} (\sigma_{r,k}^l)^2 &= \sigma_0 + \beta_r \|\mathbf{p}_k - \mathbf{s}_l\|^2, \\ (\sigma_{\phi,k}^l)^2 &= \sigma_1 + \beta_\phi \|\mathbf{p}_k - \mathbf{s}_l\|, \end{aligned} \tag{19}$$

with $\sigma_0 = 1\,\text{m}$, $\beta_r = 5 \times 10^{-5}\,\text{m}^{-1}$, $\sigma_1 = \pi/180\,\text{rad}$, $\beta_\phi = 10^{-5}\,\text{rad}\cdot\text{m}^{-1}$. The FOV of each sensor is $[-\pi/2, +\pi/2] \times [0, 500\,\text{m}]$ with clutter uniformly distributed over this interval. The clutter rate of each sensor is $\lambda_c = 5$ per scan. The probability of detection of sensor l is modelled by

$$p_D^l(\mathbf{x}_k) = \begin{cases} 0.99 & \|\mathbf{p}_k - \mathbf{s}_l\| \le R_1 \\ 0.99 - c\|\mathbf{p}_k - \mathbf{s}_l\| & R_1 < \|\mathbf{p}_k - \mathbf{s}_l\| \le R_2 \\ 0 & \|\mathbf{p}_k - \mathbf{s}_l\| > R_2, \end{cases} \tag{20}$$

with $R_1 = 200\,\text{m}$, $R_2 = 500\,\text{m}$, and $c = 5 \times 10^{-4}$.

Birth parameters for the sequential multi-Bernoulli filter are configured as $\overline{\mathbf{x}}_1 = [650\,\text{m}; -10\,\text{m/s}; 650\,\text{m}; -30\,\text{m/s}]^T$, $\overline{\mathbf{x}}_2 = [-300\,\text{m}; 15\,\text{m/s}; 300\,\text{m}; -15\,\text{m/s}]^T$, $\overline{\mathbf{x}}_3 = [-650\,\text{m}; 15\,\text{m/s}; -450\,\text{m}; 0]^T$, $\overline{\mathbf{x}}_4 = [-300\,\text{m}; 30\,\text{m/s}; 500\,\text{m}; -2\,\text{m/s}]^T$, respectively, for each target, and $Q = \text{diag}([(30\,\text{m}, 2\,\text{m/s}, 30\,\text{m}, 2\,\text{m/s}]^2)$ is identical for all four targets. $L_{\min} = 300$ and $L_{\max} = 1000$ are the minimum and maximum particle number of each Bernoulli set for track maintenance.

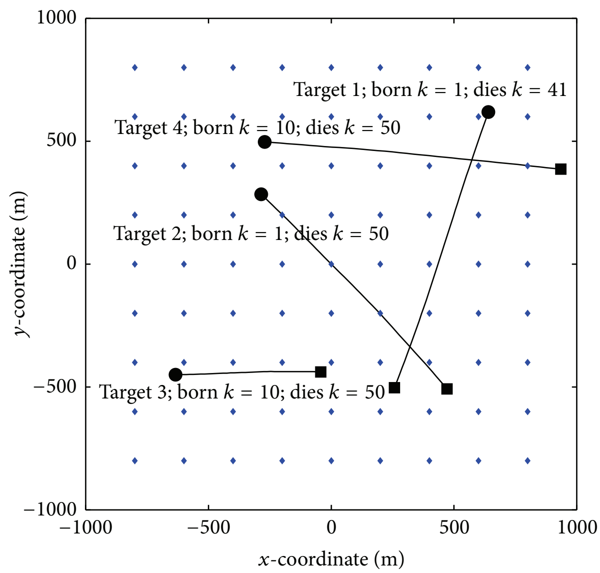

FIGURE 2: Target tracks. Start/stop positions for each track are shown with •/■. Blue dots are sensor locations.

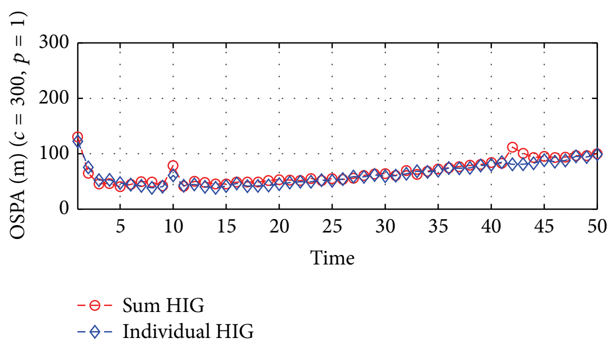

FIGURE 3: Comparison of OSPA distance.

We first compare the tracking performance, respectively, using sensor selection I and sensor selection II. The optimal subpattern assignment (OSPA) metric composed of location error and cardinality error is adopted for tracking performance evaluation [25]. Figure 3 shows the OSPA distance ($p = 1$, $c = 300\,\text{m}$) comparison from 500 Monte Carlo runs with SNMS gate $\epsilon = 500\,\text{m}$. It can be seen that there is only slight difference of the two selection approaches in tracking performance and either sensor selection approach can provide accurate target tracking. The difference occurs near time $k = 10$ and $k = 42$ when there are target births and deaths, and sensor selection using sum HIG has a relatively large error than that using individual HIG.

To further illustrate the SNMS sensor selection and multitarget tracking procedure, we take sensor selection II as an example and present three consecutive frames of one trial

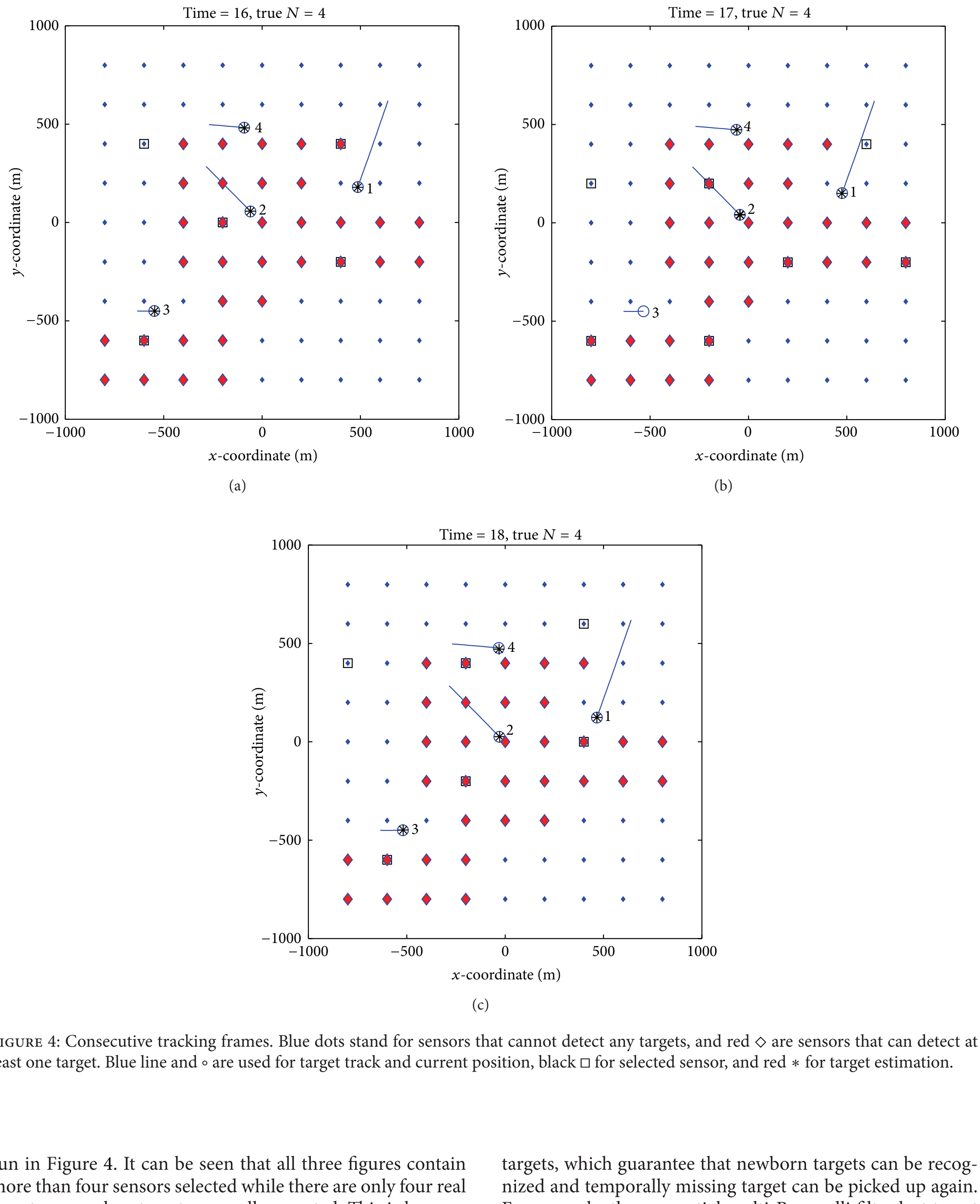

Figure 4: Consecutive tracking frames. Blue dots stand for sensors that cannot detect any targets, and red ◇ are sensors that can detect at least one target. Blue line and ∘ are used for target track and current position, black □ for selected sensor, and red ∗ for target estimation.

run in Figure 4. It can be seen that all three figures contain more than four sensors selected while there are only four real targets even when targets are well separated. This is because in the sequential multi-Bernoulli filter there are birth sets for new born targets and legacy sets for temporally undetected targets, and the SNMS sensor selection will treat all these sets as potential targets and compute the sensor HIG with respect to them. Thus, there are sensors selected to detect potential targets, which guarantee that newborn targets can be recognized and temporally missing target can be picked up again. For example, the sequential multi-Bernoulli filter lost target 3 in Figure 4(b) and picked it up right away in Figure 4(c). Trial runs of both selection approaches have been recorded in videos attached as supplement materials (see Supplementary Material available online at http://dx.doi.org/10.1155/2015/148081) for demonstration.

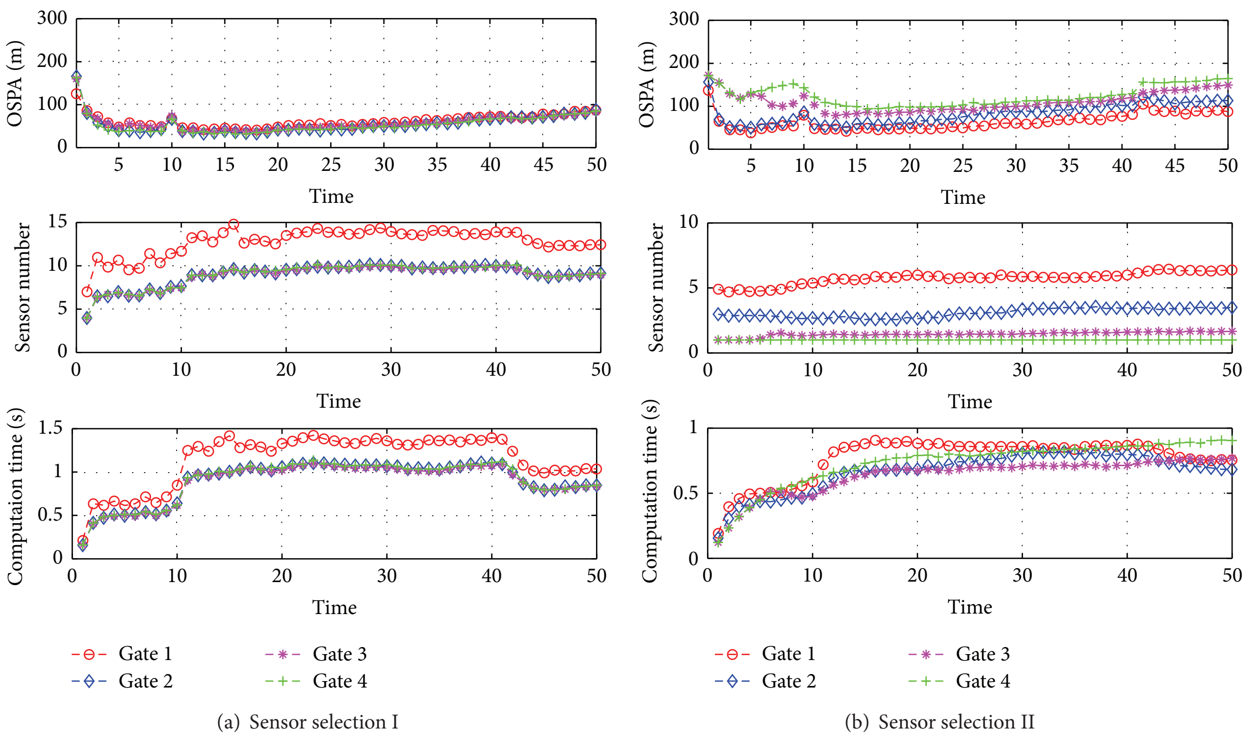

FIGURE 5: Comparison of different gates.

We also study the impact the SNMS gate ϵ has on the sensor selection procedure. We set four different SNMS gates $\epsilon_i = 500, 1000, 1500, \inf$ for $i = 1, 2, 3, 4$ and perform 500 Monte Carlo runs on each gate for the two selection methods. Figure 5 shows the simulation results of OSPA distance, average selected sensor number, and average computation time (algorithms are implemented in MATLAB 2012a on a PC with 8 GB RAM and Intel Core i7-4770k CPU). With respect to sensor selection I, it is clear in Figure 5(a) that the OSPA distance barely changes with the size of SNMS gate while the number of allocated sensors and computation time are big when $\epsilon_1 = 500$, which indicates that $\epsilon_1 = 500$ is too small to suppress less informative sensors. For sensor selection II in Figure 5(b), we can see that with bigger gate the OSPA distance increases and the number of selected sensors decreases to 1 (minimum). This is because there are chances of *oversuppression* when using sum HIG in SNMS sensor selection. Taking $\epsilon_4 = \inf$ as illustration, sensor selection II actually only picks one most informative sensor among the network and suppress all the other sensors, whereas the most informative sensor can barely detect all targets for a common case. Hence, bigger value of SNMS gate may cause *oversuppression* in sensor selection II and consequently lose targets. Nevertheless, the advantage of sensor selection II over sensor selection I lies in fewer selected sensors and less computation time given an appropriate SNMS gate.

To sum up, either of the proposed sensor selection approachs is shown effective and efficient in the simulations. Sensor selection with individual HIG will always provide satisfactory tracking performance while the number of selected sensors and computation time are relatively large. On the other hand, sensor selection with sum HIG may suffer from *oversuppression* with an inappropriately big SNMS gate but it is much more efficient and can be as effective as sensor selection I when using a proper SNMS gate.

6. Conclusion

In this paper, we propose a novel sensor selection method for multitarget tracking in the static sensor network. We provide the SMC implementation of the sequential multi-Bernoulli filter to perform multisensor fusion for multitarget tracking. With respect to sensor selection, we propose the SNMS sensor selection approach by considering the locations and HIGs of sensors and present the SMC implementation of two SNMS sensor selection approaches, respectively, using individual HIG and sum HIG. We thoroughly compare the performance of two sensor selection approaches and analyze the impact the SNMS gate has on either sensor selection approach in simulations. It is shown by the simulation results that either SNMS sensor selection approach is efficient and effective for multitarget tracking in sensor network.

Our future work is to consider more challenging measurement model, such as time-difference-of-arrival measurement or Doppler measurement, which is less informative than the bearing and range sensor used in the simulation. Besides, we will also analyze the proposed sensor selection method in the heterogeneous sensor network.

Conflict of Interests

The authors declare that there is no conflict of interests regarding the publication of this paper.

Acknowledgments

Liang Ma got financial support from the program of China Scholarships Council (no. 201206680025). This work is also sponsored by the Fundamental Research Funds for the Central Universities (HEUCF130703).

References

[1] J. Ferber, *Multi-Agent Systems: An Introduction to Distributed Artificial Intelligence*, vol. 1, Addison-Wesley, Reading, Mass, USA, 1999.

[2] J. Yick, B. Mukherjee, and D. Ghosal, "Wireless sensor network survey," *Computer Networks*, vol. 52, no. 12, pp. 2292–2330, 2008.

[3] Y. Fu, Q. Ling, and Z. Tian, "Distributed sensor allocation for multi-target tracking in wireless sensor networks," *IEEE Transactions on Aerospace and Electronic Systems*, vol. 48, no. 4, pp. 3538–3553, 2012.

[4] R. P. S. Mahler, "Global posterior densities for sensor management," in *Acquisition, Tracking and Pointing XII*, Proceedings of the SPIE, pp. 252–263, Orlando, Fla, USA, April 1998.

[5] R. Tharmarasa, T. Kirubarajan, A. Sinha, and T. Lang, "Decentralized sensor selection for large-scale multisensor-multitarget tracking," *IEEE Transactions on Aerospace and Electronic Systems*, vol. 47, no. 2, pp. 1307–1324, 2011.

[6] R. P. Mahler, *Statistical Multisource-Multitarget Information Fusion*, vol. 685, Artech House, Boston, Mass, USA, 2007.

[7] R. Mahler, "Multitarget sensor management of dispersed mobile sensors," in *Theory and Algorithm for Cooperative Systems*, Kluwer, Springer, 2005.

[8] B. Ristic and B.-N. Vo, "Sensor control for multi-object state-space estimation using random finite sets," *Automatica*, vol. 46, no. 11, pp. 1812–1818, 2010.

[9] H. G. Hoang and B.-T. Vo, "Sensor management for multi-target tracking via multi-Bernoulli filtering," *Automatica*, vol. 50, no. 4, pp. 1135–1142, 2014.

[10] A. H. Jazwinski, *Stochastic Processes and Filtering Theory*, Courier Dover Publications, 2007.

[11] R. E. Kalman, "A new approach to linear filtering and prediction problems," *Journal of Fluids Engineering*, vol. 82, no. 1, pp. 35–45, 1960.

[12] B. Ristic, B.-T. Vo, B.-N. Vo, and A. Farina, "A tutorial on Bernoulli filters: theory, implementation and applications," *IEEE Transactions on Signal Processing*, vol. 61, no. 13, pp. 3406–3430, 2013.

[13] B.-T. Vo, B.-N. Vo, and A. Cantoni, "The cardinality balanced multi-target multi-Bernoulli filter and its implementations," *IEEE Transactions on Signal Processing*, vol. 57, no. 2, pp. 409–423, 2009.

[14] R. P. S. Mahler, "Multitarget bayes filtering via first-order multitarget moments," *IEEE Transactions on Aerospace and Electronic Systems*, vol. 39, no. 4, pp. 1152–1178, 2003.

[15] R. Mahler, "PHD filters of higher order in target number," *IEEE Transactions on Aerospace and Electronic Systems*, vol. 43, no. 4, pp. 1523–1543, 2007.

[16] B.-N. Vo and W.-K. Ma, "The Gaussian mixture probability hypothesis density filter," *IEEE Transactions on Signal Processing*, vol. 54, no. 11, pp. 4091–4104, 2006.

[17] M. Liang, D. Y. Kim, and X. Kai, "Multi-bernoulli filter for target tracking with multi-static doppler only measurement," *Signal Processing*, vol. 108, pp. 102–110, 2015.

[18] A. O. Hero III, C. M. Kreucher, and D. Blatt, *Information Theoretic Approaches to Sensor Management*, Springer, New York, NY, USA, 2008.

[19] A. Rosenfeld and A. C. Kak, *Digital Picture Processing*, vol. 1, Elsevier, 2014.

[20] L. Kitchen and A. Rosenfeld, "Gray-level corner detection," *Pattern Recognition Letters*, vol. 1, no. 2, pp. 95–102, 1982.

[21] H. Bay, A. Ess, T. Tuytelaars, and L. Van Gool, "Speeded-up robust features (SURF)," *Computer Vision and Image Understanding*, vol. 110, no. 3, pp. 346–359, 2008.

[22] C. Harris and M. Stephens, "A combined corner and edge detector," in *Proceedings of the 4th Alvey Vision Conference*, vol. 15, p. 50, Manchester, UK, 1988.

[23] B. Alexe, T. Deselaers, and V. Ferrari, "What is an object?" in *Proceedings of the IEEE Computer Society Conference on Computer Vision and Pattern Recognition (CVPR '10)*, pp. 73–80, June 2010.

[24] P. Dollar, R. Appel, S. Belongie, and P. Perona, "Fast feature pyramids for object detection," *IEEE Transactions on Pattern Analysis and Machine Intelligence*, vol. 36, no. 8, pp. 1532–1545, 2014.

[25] D. Schuhmacher, B.-T. Vo, and B.-N. Vo, "A consistent metric for performance evaluation of multi-object filters," *IEEE Transactions on Signal Processing*, vol. 56, no. 8, pp. 3447–3457, 2008.

Hindawi Publishing Corporation
Mathematical Problems in Engineering
Volume 2015, Article ID 258189, 7 pages
http://dx.doi.org/10.1155/2015/258189

Research Article

Co-Design of Event Generator and Dynamic Output Feedback Controller for LTI Systems

Dan Ma,[1] Junxian Han,[1] Dali Zhang,[2] and Yanjun Liu[3]

[1] *State Key Laboratory of Synthetical Automation for Process Industries, College of Information Science and Engineering, Northeastern University, Shenyang 110819, China*
[2] *School of Aeronautics and Astronautics, Dalian University of Technology, Dalian 116024, China*
[3] *College of Science, Liaoning University of Technology, Jinzhou, Liaoning 121001, China*

Correspondence should be addressed to Dan Ma; madan@mail.neu.edu.cn

Received 8 July 2014; Revised 15 August 2014; Accepted 18 August 2014

Academic Editor: Xi-Ming Sun

This paper presents a co-design method of the event generator and the dynamic output feedback controller for a linear time-invariant (LIT) system. The event-triggered condition on the sensor-to-controller and the controller-to-actuator depends on the plant output and the controller output, respectively. A sufficient condition on the existence of the event generator and the dynamic output feedback controller is proposed and the co-design problem can be converted into the feasibility of linear matrix inequalities (LMIs). The LTI system is asymptotically stable under the proposed event-triggered controller and also reduces the computing resources with respect to the time-triggered one. In the end, a numerical example is given to illustrate the effectiveness of the proposed approach.

1. Introduction

With plenty of control applications on the digital platforms, event-triggered control becomes more and more popular due to its advantages on control systems with limited resources. For networked control systems, most literature focuses on the performance analysis of the system under the network bandwidth limitation; see [1–4]. However, less traffic requirement, better resource utilization, and better steady-state performance are all the significant factors. Compared with time-triggered control, event-triggered control has its advantages. In the traditional digital control techniques, the controller updates periodically. Analysis and synthesis of the system by using the periodic sampling is much easier than using the aperiodic sampling. However, the periodic sampling leads to a waste of computation and communication resources sometimes. From the resource allocation point of view, the event-triggered control was proposed; see the literature [5–7] and references therein. Event-triggered control is a control scheme in which the controller updates as long as the system state (or output) satisfies a well-designed condition. The condition is called event generator, which can maintain the necessary properties of the system, such as convergence and stability. By using event-triggered control, computation and communication resources will be utilized only when necessary. Therefore, the event-triggered mechanism is a kind of "on-demand" executive strategy and can guarantee the performance of the system as well.

Due to the advantage of reducing computation and communication resources, event-triggered control has been taken more and more into consideration. It is first presented by Dorf in [5]; several different event-triggered schemes are investigated for a variety of systems with control performances. In [6, 7], the authors experimentally demonstrate the saving resources of event-triggered control while simultaneously preserving the performance of the system. Event-triggered control for the first-order linear stochastic system forces the output variance to be considerably smaller with respect to periodic control [6]. A simple event-based PID controller is studied in [7], which contains a time-triggered event detector and an event-triggered PID controller. The PID controller cannot calculate the control signal unless the variable from the event detector has enough changes. An asynchronous emulation-based event-triggered feedback approach is taken into account in [8], where a directly digital design strategy is included. In [9], Tabuada proposes an event-triggered mechanism for nonlinear system to guarantee the asymptotical stability of the system and relax the traditional periodic execution requirements. The method proposed in [9] is extended to the exponential input-to-state stability (ISS) in [10]. In [11], Lunze and Lehmann propose a method on event-based state-feedback control for linear systems, with bounded disturbances, in which the sensitivity bound of the event generator can be chosen such that the event-triggered control system approximates the continuous state-feedback control loop.

However, not all of the system states can be directly measured in applications; the event-triggered control based on the system output (a part of the system state information) is much more practical; see, for example, [12–16]. Decentralized event-triggered mechanism is applied to the dynamic output feedback control system in [12]. For guaranteeing the L_∞ performance, the event generator is designed and the bound of interevent time is also provided. The optimal control problem under the event-triggered output feedback control is studied for discrete-time systems in [13] and an upper bound on the optimal cost is presented. The input-to-state stability under the self-triggered dynamic output feedback control is studied in [14], where a discrete-time observer is in cascade with a full state-feedback self-triggered controller. The designed event generator renders the ISS of the system with respect to exogenous disturbances. The result is extended to the decentralized event-triggered system in [15]. In [16], the event-triggered conditions are proposed for three kinds of event-triggered dynamic output feedback control architectures, in which a global lower bound on the inter-sample times is also provided to guarantee the asymptotic stability of the closed-loop system. However, most work in the literature focuses on designing the event generator, does not mention the continuous control algorithm. Most of them assume that the controller has been designed previously. But in fact, the event-triggered controller includes both the event generator and the controller. How to co-design the event generator and the controller simultaneously is much more challengeable. Li and Xu [17, 18] give us a co-design method for both discrete-time linear systems and LPV systems under the state feedback controller. While co-designing the event generator and the controller based on the system output is quite significant from the practical application point of view. To the best of the authors' knowledge, co-designing of event generator and the dynamic output feedback controller has not been investigated. Comparing to the static state feedback controller, the dynamic output feedback controller can often provide more adjustable parameters. It is a challenge to co-design the event generator and the dynamic output feedback controller as well.

The remainder of the paper is organized as follows. In Section 2, the necessary notations and preliminaries are provided. The problem statement of event-triggered dynamic output feedback control is presented in Section 3. Section 4 presents a sufficient condition on how to co-design the event generator and the dynamic output feedback controller, under which the linear system is asymptotically stable. Numerical simulation results are given in Section 5, which verify the effectiveness of the proposed methods. Finally, conclusions are included in Section 6.

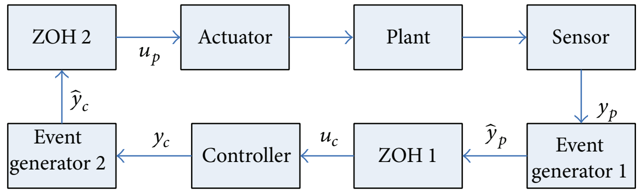

Figure 1: Event-triggered dynamic output feedback control loop.

2. Preliminaries

The notation $\|\cdot\|$ is used to denote the Euclidean norm. $X > 0$ ($X < 0$) represents that X is a positive (negative) definite matrix. X^T and X^{-1} denote the transpose and the inverse of matrix X. I represents the unit matrix with appropriate dimensions; $Z_0{}^+$ is the set of all nonnegative integers. For simplicity, the form $\left(\begin{smallmatrix} A & B \\ * & C \end{smallmatrix}\right)$ is equivalent to the symmetric matrix of the form $\left(\begin{smallmatrix} A & B \\ B^T & C \end{smallmatrix}\right)$. In what follows, if not explicitly stated, matrices are assumed to have compatible dimensions.

The following lemma will be used in the proof of the main result.

Lemma 1 (see [19]). *Consider a symmetric matrix* $S = \left[\begin{smallmatrix} S_{11} & S_{12} \\ S_{21} & S_{22} \end{smallmatrix}\right]$, *where* $S_{11} \in R^{r\times r}$, $S_{12} \in R^{r\times(n-r)}$, $S_{21} \in R^{(n-r)\times r}$, $S_{22} \in R^{(n-r)\times(n-r)}$. *Then* $S < 0$ *only if* $S_{11} < 0$ *and* $S_{22} - S_{12}^T S_{11}^{-1} S_{12} < 0$ *or equivalently,* $S_{22} < 0$ *and* $S_{11} - S_{12} S_{22}^{-1} S_{12}^T < 0$.

3. Problem Statement

A linear plant controlled by an event-triggered dynamic output feedback controller is shown in Figure 1. The event generator is an implementation of the event-triggered condition. We need to design an output-dependent event-triggered condition which can be used to decide when the measurement and the control law update. If the output signal y_p measured from the sensor satisfies the event-triggered condition 1, it will be sent to the controller through the zero-order-hold 1 (ZOH 1); otherwise it will not be sent. Similarly, if the output of the controller y_c satisfies the event-triggered condition 2, the output of the controller will be sent to the actuator through the ZOH 2; otherwise it does not transmit. Here we denote the triggered instant by $t_i, i \in Z_0^+$.

We consider a linear time-invariant plant given by

$$\begin{aligned} \dot{x}_p(t) &= A_p x_p(t) + B_p u_p(t), \quad x_p(0) = x_{p0}, \\ y_p(t) &= C_p x_p(t), \end{aligned} \tag{1}$$

where $x_p(t) \in R^n$ denotes the plant state; $x_p(0) = x_{p0}$ is the initial state of the plant; $u_p(t) \in R^m$ is the plant input;

$y_p(t) \in R^q$ is the output of the plant. A_p, B_p, and C_p are the known constant matrices with appropriate dimensions.

The plant is controlled by a dynamic output feedback controller given by

$$\dot{x}_c(t) = A_c x_c(t) + B_c u_c(t), \quad x_c(0) = x_{c0}, \quad y_c(t) = C_c x_c(t), \tag{2}$$

where $x_c(t) \in R^n$ denotes the controller state; $x_c(0) = x_{c0}$ is the initial state of the controller; $u_c(t) \in R^q$ is the controller input; $y_c(t) \in R^m$ is the output of the controller. A_c, B_c, and C_c are matrices appropriate dimensions, which will be designed in the following part.

Whether $y_p(t)$ and $y_c(t)$ are sent or not is up to the event generator conditions. That is to say, the controller cannot calculate the control signal unless y_p and y_c in the event generator have enough change. Since $t_i, i \in Z_0^+$ is the triggered instant, $y_p(t)$ and $y_c(t)$ are only sent at t_i; $\hat{y}_p(t)$ and $\hat{y}_c(t)$ update at the triggered instants. By using the zero-order holder, $\hat{y}_p(t)$ and $\hat{y}_c(t)$ maintain their values until the next triggered instant t_{i+1} arrives. Therefore, $u_p(t) = \hat{y}_c(t)$ and $u_c(t) = \hat{y}_p(t)$ can be expressed by

$$\begin{aligned} \hat{y}_c(t) &= y_c(t_i), \quad t \in [t_i, t_{i+1}), \\ \hat{y}_p(t) &= y_p(t_i), \quad t \in [t_i, t_{i+1}). \end{aligned} \tag{3}$$

Define the errors $e_p(t)$ and $e_c(t)$ as follows:

$$\begin{aligned} e_p(t) &= \hat{y}_p(t) - y_p(t), \\ e_c(t) &= \hat{y}_c(t) - y_c(t). \end{aligned} \tag{4}$$

Combining (1), (2), and (4), we have

$$\dot{x} = \begin{pmatrix} \dot{x}_p \\ \dot{x}_c \end{pmatrix} = \begin{pmatrix} A_p & B_p C_c \\ B_c C_p & A_c \end{pmatrix} \begin{pmatrix} x_p \\ x_c \end{pmatrix} + \begin{pmatrix} 0 & B_p \\ B_c & 0 \end{pmatrix} \begin{pmatrix} e_p(t) \\ e_c(t) \end{pmatrix}. \tag{5}$$

Thus the closed-loop system can be described by

$$\dot{x}(t) = \overline{A}x(t) + \overline{B}e(t), \tag{6}$$

where

$$\overline{A} = \begin{pmatrix} A_p & B_p C_c \\ B_c C_p & A_c \end{pmatrix}, \qquad \overline{B} = \begin{pmatrix} 0 & B_p \\ B_c & 0 \end{pmatrix},$$
$$e(t) = \begin{pmatrix} e_p(t) \\ e_c(t) \end{pmatrix}, \qquad x(t) = \begin{pmatrix} x_p(t) \\ x_c(t) \end{pmatrix}, \tag{7}$$
$$x_0 = \begin{pmatrix} x_{p0} \\ x_{c0} \end{pmatrix}.$$

We present the following event-triggered condition:

$$e_p^T e_p + e_c^T e_c \le \sigma_1 y_p^T y_p + \sigma_2 y_c^T y_c, \quad \sigma_1 > 0, \ \sigma_2 > 0 \tag{8}$$

which means $\hat{y}_p(t)$ is updated once if

$$\begin{aligned} & e_p^T(t) e_p(t) + e_c^T(t_i) e_c(t_i) \\ & \quad \le \sigma_1 y_p^T(t) y_p(t) + \sigma_2 y_c^T(t_i) y_c(t_i) \end{aligned} \tag{9}$$

is violated and $\hat{y}_c(t)$ is updated once if

$$\begin{aligned} & e_p^T(t_i) e_p(t_i) + e_c^T(t) e_c(t) \\ & \quad \le \sigma_1 y_p^T(t_i) y_p(t_i) + \sigma_2 y_c^T(t) y_c(t) \end{aligned} \tag{10}$$

is violated for $t \in [t_i, t_{i+1})$.

The objective of this paper is to co-design the dynamic output feedback controller (2) and the event generator satisfying condition (8) under which the closed-loop system (6) is asymptotically stable.

4. Main Results

In this section, we will give a sufficient condition on the existence of the event generator and the dynamic output feedback controller by using LIMs.

Theorem 2. *If there exist symmetric positive definite matrices $X \in R^{n\times n}$ and $Y \in R^{n\times n}$, matrices $V \in R^{r\times n}$ and $W \in R^{n\times m}$, and scalars $\delta_1 > 0$, $\delta_2 > 0$ satisfying the following LMIs*

$$\begin{bmatrix} YA_p^T + A_pY + V^TB_p^T + B_pV & YC_p^T & V^T & B_p \\ * & -\delta_1 I & 0 & 0 \\ * & * & -\delta_2 I & 0 \\ * & * & * & -I \end{bmatrix} < 0, \tag{11}$$

$$\begin{bmatrix} XA_p + A_p^TX + WC_p + C_p^TW^T & W & XB_p & C_p^T \\ * & -I & 0 & 0 \\ * & * & -I & 0 \\ * & * & * & -\delta_1 I \end{bmatrix} < 0, \tag{12}$$

then system (6) *under the dynamic output feedback controller* (2) *and the event-triggered condition* (8) *is asymptotically stable. The parameters of the controller are as follows:*

$$\begin{aligned} A_c &= -\left(Y - X^{-1}\right)\left(A_P + YA_p^TX + V^TB_p^TX + YC_P^TW^T \right. \\ &\quad \left. + B_pB_p^TX + \delta_1^{-1}YC_p^TC_p\right)^T Y^{-1}, \\ B_c &= \left(Y - X^{-1}\right)W, \\ C_c &= VY^{-1}, \end{aligned} \tag{13}$$

and the parameters of the event-triggered condition (8) *are* $\sigma_1 = \delta_1^{-1}$, $\sigma_2 = \delta_2^{-1}$.

Proof. Choosing a candidate Lyapunov function

$$V_x = x^T P x, \tag{14}$$

we have the following time derivative of V_x along with system (6):

$$\begin{aligned} \dot{V}_x &= 2x^T P\left(\overline{A}x + \overline{B}e\right) \\ &= x^T\left(P\overline{A} + \overline{A}^TP\right)x + 2x^TP\overline{B}e \\ &\le x^T\left(P\overline{A} + \overline{A}^TP + P\overline{B}\overline{B}^TP\right)x + e^Te. \end{aligned} \tag{15}$$

Letting $V = C_c Y$, and from (11), we use Lemma 1 three times and obtain

$$YA_p^T + A_p Y + Y^T C_c^T B_p^T + \delta_2^{-1} Y^T C_c^T C_c Y + \delta_1^{-1} Y C_p^T C_p Y + B_p C_c Y + B_p B_p^T < 0. \quad (16)$$

Similarly, letting $W = (Y^{-1} - X)B_c$ and applying the Schur lemma to LMI (12) three times, we get

$$XA_p + A_p^T X + \left(Y^{-1} - X\right) B_c C_p + C_p^T B_c^T \left(Y^{-1} - X\right)^T + XB_p B_p^T X + \delta_1^{-1} C_p^T C_p + \left(Y^{-1} - X\right) B_c B_c^T \left(Y^{-1} - X\right)^T < 0. \quad (17)$$

Considering

$$A_c = -\left(Y - X^{-1}\right)\left(A_P + YA_p^T X + V^T B_p^T X + YC_P^T W^T + B_p B_p^T X + \delta_1^{-1} Y C_p^T C_p\right)^T Y^{-1}, \quad (18)$$

we know that

$$YA_c^T \left(Y^{-1} - X\right)^T + A_P + YA_p^T X + YC_c^T B_p^T X + YC_P^T B_c^T \left(Y^{-1} - X\right)^T + B_p B_p^T X + \delta_1^{-1} Y C_P^T C_P = 0. \quad (19)$$

Combining (16), (17), and (19), we have

$$\begin{bmatrix} Q_1 & Q_2 \\ * & Q_3 \end{bmatrix} < 0, \quad (20)$$

where

$$\begin{aligned} Q_1 &= YA_p^T + A_p Y + Y^T C_c^T B_p^T + B_p C_c Y + B_p B_p^T + \delta_1^{-1} Y C_p^T C_p Y + \delta_2^{-1} Y^T C_c^T C_c Y, \\ Q_2 &= YA_c^T \left(Y^{-1} - X\right)^T + A_P + YA_p^T X + YC_c^T B_p^T X + YC_P^T B_c^T \left(Y^{-1} - X\right)^T + B_p B_p^T X + \delta_1^{-1} Y C_P^T C_P, \\ Q_3 &= XA_p + A_p^T X + \left(Y^{-1} - X\right) B_c C_p + C_p^T B_c^T \left(Y^{-1} - X\right)^T + XB_p B_p^T X + \delta_1^{-1} C_p^T C_p + \left(Y^{-1} - X\right) B_c B_c^T \left(Y^{-1} - X\right)^T. \end{aligned} \quad (21)$$

Furthermore, we have

$$\begin{bmatrix} Q_1 & Q_2 \\ * & Q_3 \end{bmatrix} = M_1 + M_2 + M_3 + M_4 < 0, \quad (22)$$

where

$$\begin{aligned} M_1 &= \begin{bmatrix} A_p Y + B_p C_c Y & A_p \\ XA_p Y + XB_p C_c Y + \left(Y^{-1} - X\right) B_c C_P Y + \left(Y^{-1} - X\right) A_c Y & XA_p + \left(Y^{-1} - X\right) B_c C_p \end{bmatrix}, \\ M_2 &= \begin{bmatrix} YA_p^T + Y^T C_c^T B_p^T & YA_p^T X + YC_c^T B_p^T X + YC_P^T B_c^T \left(Y^{-1} - X\right)^T + YA_c^T \left(Y^{-1} - X\right)^T \\ A_p^T & A_p^T X + C_p^T B_c^T \left(Y^{-1} - X\right)^T \end{bmatrix}, \\ M_3 &= \begin{bmatrix} B_p B_p^T & B_p B_p^T X \\ * & XB_p B_p^T X + \left(Y^{-1} - X\right) B_c B_c^T \left(Y^{-1} - X\right)^T \end{bmatrix}, \\ M_4 &= \begin{bmatrix} \delta_1^{-1} Y C_p^T C_p Y + \delta_2^{-1} Y^T C_c^T C_c Y & \delta_1^{-1} Y C_p^T C_p \\ * & \delta_1^{-1} C_p^T C_p \end{bmatrix}. \end{aligned} \quad (23)$$

Letting

$$H = \begin{bmatrix} 0 & I \\ Y^{-1} & -I \end{bmatrix}, \quad (24)$$

and premultiplying and postmultiplying LMI (22) by H and H^T, we obtain

$$HM_1 H^T + HM_2 H^T + HM_3 H^T + HM_4 H^T < 0. \quad (25)$$

Since

$$\begin{aligned}
HM_1H^T &= H\begin{bmatrix} A_pY + B_pC_cY & A_p \\ XA_pY + XB_pC_cY + \left(Y^{-1}-X\right)B_cC_PY + \left(Y^{-1}-X\right)A_cY & XA_p + \left(Y^{-1}-X\right)B_cC_p \end{bmatrix}H^T \\
&= H\begin{bmatrix} Y & Y \\ I & 0 \end{bmatrix}\begin{bmatrix} X & Y^{-1}-X \\ * & X-Y^{-1} \end{bmatrix}\begin{bmatrix} A_p & B_pC_c \\ B_cC_P & A_c \end{bmatrix}\begin{bmatrix} Y & I \\ Y & 0 \end{bmatrix}H^T \\
&= P\overline{A}, \\
HM_2H^T &= H\begin{bmatrix} YA_p^T + Y^TC_c^TB_p^T & YC_P^TB_c^T\left(Y^{-1}-X\right)^T + YA_c^T\left(Y^{-1}-X\right)^T + YA_p^TX + YC_c^TB_p^TX \\ A_p^T & A_p^TX + C_p^TB_c^T\left(Y^{-1}-X\right)^T \end{bmatrix}H^T \\
&= H\begin{bmatrix} Y & Y \\ I & 0 \end{bmatrix}\begin{bmatrix} A_p^T & C_P^TB_c^T \\ C_c^TB_p^T & A_c^T \end{bmatrix}\begin{bmatrix} X & Y^{-1}-X \\ * & X-Y^{-1} \end{bmatrix}\begin{bmatrix} Y & I \\ Y & 0 \end{bmatrix}H^T \\
&= \overline{A}^TP, \\
HM_3H^T &= H\begin{bmatrix} B_pB_p^T & B_pB_p^TX \\ * & XB_pB_p^TX + \left(Y^{-1}-X\right)B_cB_c^T\left(Y^{-1}-X\right)^T \end{bmatrix}H^T \\
&= H\begin{bmatrix} I & 0 \\ X & Y^{-1}-X \end{bmatrix}\begin{bmatrix} 0 & B_p \\ B_c & 0 \end{bmatrix}\begin{bmatrix} 0 & B_c^T \\ B_p^T & 0 \end{bmatrix}\begin{bmatrix} I & X \\ 0 & Y^{-1}-X \end{bmatrix}H^T \\
&= P\overline{B}\overline{B}^TP, \\
HM_4H^T &= H\begin{bmatrix} \delta_1^{-1}YC_p^TC_pY + \delta_2^{-1}Y^TC_c^TC_cY & \delta_1^{-1}YC_p^TC_p \\ * & \delta_1^{-1}C_p^TC_p \end{bmatrix}H^T \\
&= H\begin{bmatrix} Y & Y \\ I & 0 \end{bmatrix}\begin{bmatrix} \delta_1^{-1}C_p^TC_p & 0 \\ * & \delta_2^{-1}C_c^TC_c \end{bmatrix}\begin{bmatrix} Y & I \\ Y & 0 \end{bmatrix}H^T \\
&= \begin{bmatrix} \delta_1^{-1}C_p^TC_p & 0 \\ * & \delta_2^{-1}C_c^TC_c \end{bmatrix},
\end{aligned} \tag{26}$$

we know that LMI (25) is equivalent to the following inequality

$$P\overline{A} + \overline{A}^TP + P\overline{B}\overline{B}^TP + \begin{bmatrix} \delta_1^{-1}C_p^TC_p & 0 \\ * & \delta_2^{-1}C_c^TC_c \end{bmatrix} < 0, \tag{27}$$

which can be rewritten by

$$\begin{aligned} &x^T\left(P\overline{A} + \overline{A}^TP + P\overline{B}\overline{B}^TP\right)x \\ &\quad + x^T\begin{bmatrix} \delta_1^{-1}C_p^TC_p & 0 \\ * & \delta_2^{-1}C_c^TC_c \end{bmatrix}x < 0. \end{aligned} \tag{28}$$

Since

$$\begin{aligned} e^Te &= e_p^Te_p + e_c^Te_c \le \sigma_1y_p^Ty_p + \sigma_2y_c^Ty_c \\ &= x^T\begin{bmatrix} \sigma_1C_p^TC_p & 0 \\ 0 & \sigma_2C_c^TC_c \end{bmatrix}x \\ &= x^T\begin{bmatrix} \delta_1^{-1}C_p^TC_p & 0 \\ * & \delta_2^{-1}C_c^TC_c \end{bmatrix}x, \end{aligned} \tag{29}$$

then we obtain that

$$x^T\left(P\overline{A} + \overline{A}^TP + P\overline{B}\overline{B}^TP\right)x + e^Te < 0. \tag{30}$$

Combining (15) and (30), we have

$$\dot{V}_x < 0. \tag{31}$$

Hence, if LMIs (11) and (12) are satisfied, system (6) under the dynamic output feedback (2) with the matrices A_c, B_c, and C_c and event generator (8) with $\sigma_1 = \delta_1^{-1}$, $\sigma_2 = \delta_2^{-1}$ is asymptotically stable, where

$$A_c = -\left(Y - X^{-1}\right)\left(A_P + YA_p^T X + V^T B_p^T X + YC_P^T W^T + B_p B_p^T X + \delta_1^{-1} Y C_p^T C_p\right)^T Y^{-1},$$
$$B_c = \left(Y - X^{-1}\right) W,$$
$$C_c = VY^{-1}. \tag{32}$$

The proof is completed. □

Remark 3. Theorem 2 gives us a sufficient condition on how to co-design the event generator and the dynamic output feedback controller. Different from the co-design method in [16–18], this paper focuses on the dynamic output feedback. Moreover, the event-triggered condition in this paper also depends on the system output, which is much easier to realize with respect to the case depending on the system state.

Remark 4. For any given LTI model parameters A_p, B_p, C_p, we can calculate the inequalities (11) and (12) in Theorem 2. If the LMIs have feasible solutions X, Y, V, W, σ_1, σ_2, then we know system (6) is asymptotically stable. Furthermore, we obtain the parameters of the event generator and the controller. Therefore, the co-design problem is converted into the feasibility of LMIs, which is easy to be checked by using Matlab/LMI toolbox.

5. A Numerical Example

In this section, a numerical example is given to demonstrate the efficiency of the proposed method above. Consider the plant and its candidate dynamic output feedback controller as follows:

$$\dot{x}_p = \begin{bmatrix} 0 & 1 \\ 2 & -3 \end{bmatrix} x_p + \begin{bmatrix} 2.2 \\ 2.2 \end{bmatrix} u_p,$$
$$y_p = \begin{bmatrix} -1 & 4 \end{bmatrix} x_p,$$
$$\dot{x}_c(t) = A_c x_c(t) + B_c u_c(t),$$
$$y_c(t) = C_c x_c(t). \tag{33}$$

By solving the LMIs feasibility problem in Theorem 2, we have $X = \begin{bmatrix} 4.1064 & -4.4449 \\ -4.4449 & 5.4109 \end{bmatrix}$, $Y = \begin{bmatrix} 19.3972 & 4.3338 \\ 4.3338 & 4.2859 \end{bmatrix}$, $V = \begin{bmatrix} -9.1681 & -4.7274 \end{bmatrix}$ $W = \begin{bmatrix} -1.8795 \\ 0.7450 \end{bmatrix}$, $\delta_1 = 25.2983$, and $\delta_2 = 28.0767$ and then the parameters of the controller can be calculated as

$$A_c = \begin{bmatrix} 4.5499 & -18.8029 \\ 5.7729 & -19.7737 \end{bmatrix}, \qquad B_c = \begin{bmatrix} 4.2917 \\ 3.5312 \end{bmatrix},$$
$$C_c = \begin{bmatrix} -0.2922 & -0.8075 \end{bmatrix}. \tag{34}$$

From (8), we obtain that the event-triggered condition is

$$e_p^T e_p + e_c^T e_c \le 0.0395 y_p^T y_p + 0.0356 y_c^T y_c. \tag{35}$$

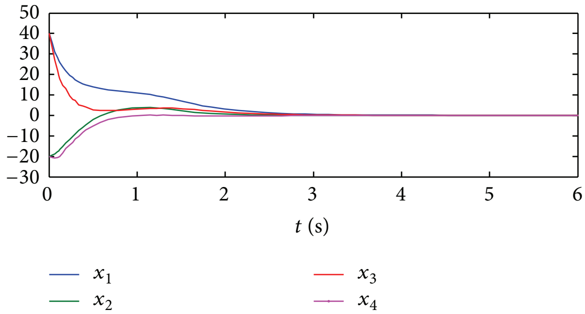

Figure 2: System state trajectories under the event-triggered dynamic output feedback controller.

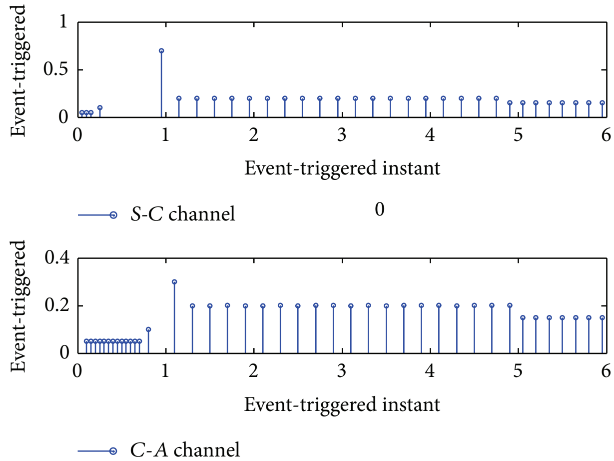

Figure 3: Event-triggered instant and event-triggered interval.

Given the initial state $x_0 = (40, -20, 40, -20)^T$, we have the trajectory of the closed-loop system shown in Figure 2. It can be seen that the system is asymptotically stable.

Setting the sampling step as 0.05 s, the effect of the event-triggered scheme from sensor to controller and from controller to actuator is shown in Figure 3, where the x-axis means the event-triggered instant and y-axis means the interval between the current event-triggered instant and the last event-triggered instant. After computation, the average sampling time from sensor to controller is 0.15 s, which is 3 times that of the sampling time of the system if there is no event-triggered scheme; the average sampling time from controller to actuator is 0.18 s, which is 3.6 times that of the sampling time of the system if there is no event-triggered scheme. Therefore, the simulation shows that the system resource utilization is greatly saved by using the event-triggered scheme and the unnecessary waste of system resources is reduced.

6. Conclusion

In this paper, we studied the asymptotical stabilization of linear systems based on the event-triggered dynamic output feedback control. We proposed an approach to co-design the event generator and the dynamic output feedback controller.

A sufficient condition was presented in terms of LMIs by using a quadratic Lyapunov function.

Conflict of Interests

The authors declare that there is no conflict of interests regarding the publication of this paper.

Acknowledgments

This work was supported by the National Natural Science Foundation of China under Grant 61233002 and the Fundamental Research Funds for the Central Universities under Grant N120404019.

References

[1] X.-M. Sun, G.-P. Liu, W. Wang, and D. Rees, "L2-gain of systems with input delays and controller temporary failure: zero-order hold model," *IEEE Transactions on Control Systems Technology*, vol. 19, no. 3, pp. 699–706, 2011.

[2] X. M. Sun, G. P. Liu, W. Wang, and D. Rees, "Stability analysis for networked control systems based on event-time-driven mode," *International Journal of Control*, vol. 82, no. 12, pp. 2260–2266, 2009.

[3] W. Zhang, M. S. Branicky, and S. M. Phillips, "Stability of networked control systems," *IEEE Control Systems Magazine*, vol. 21, no. 1, pp. 84–99, 2001.

[4] J. P. Hespanha, P. Naghshtabrizi, and Y. Xu, "A survey of recent results in networked control systems," *Proceedings of the IEEE*, vol. 95, no. 1, pp. 138–162, 2007.

[5] R. C. Dorf, M. Farren, and C. Phillips, "Adaptive sampling frequency for sampled-data control systems," *IRE Transactions on Automatic Control*, vol. 7, no. 1, pp. 38–47, 1962.

[6] K. J. Åström and B. Bo, "Comparison of periodic and event based sampling for first-order stochastic systems," in *Proceedings of the 14th IFAC World Congress*, Beijing, China, 1999.

[7] A. Karl-Erik, "A simple event-based PID controller," in *Proceedings of the 14th IFAC World Congress*, Beijing, China, 1999.

[8] E. Kofman and J. H. Braslavsky, "Level crossing sampling in feedback stabilization under data-rate constraints," in *Proceedings of the 45th IEEE Conference on Decision and Control (CDC '06)*, pp. 4423–4428, December 2006.

[9] P. Tabuada, "Event-triggered real-time scheduling of stabilizing control tasks," *IEEE Transactions on Automatic Control*, vol. 52, no. 9, pp. 1680–1685, 2007.

[10] J. Mazo, A. Anta, and P. Tabuada, "An ISS self-triggered implementation of linear controllers," *Automatica*, vol. 46, no. 8, pp. 1310–1314, 2010.

[11] J. Lunze and D. Lehmann, "A state-feedback approach to event-based control," *Automatica*, vol. 46, no. 1, pp. 211–215, 2010.

[12] M. C. F. Donkers and W. P. M. Heemels, "Output-based event-triggered control with guaranteed L_∞-gain and improved and decentralized event-triggering," *IEEE Transactions on Automatic Control*, vol. 57, no. 6, pp. 1362–1376, 2012.

[13] L. Li and M. Lemmon, "Event-triggered output feedback control of finite horizon discrete-time multi-dimensional linear processes," in *Proceedings of the 49th IEEE Conference on Decision and Control (CDC '10)*, pp. 3221–3226, Atlanta, Ga, USA, December 2010.

[14] J. Almeida, C. Silvestre, and A. M. Pascoal, "Observer based self-triggered control of linear plants with unknown disturbances," in *Proceedings of the American Control Conference (ACC '12)*, pp. 5688–5693, June 2012.

[15] P. Tallapragada and N. Chopra, "Event-triggered decentralized dynamic output feedback control for LTI systems," in *Proceedings of the 3rd IFAC Workshop on Distributed Estimation and Control in Networked Systems (NECSYS '12)*, vol. 3, pp. 31–36, September 2012.

[16] P. Tallapragada and N. Chopra, "Event-triggered dynamic output feedback control for LTI systems," in *Proceedings of the 51st IEEE Conference on Decision and Control (CDC '12)*, pp. 6597–6602, Maui, Hawaii, USA, December 2012.

[17] S. B. Li and B. G. Xu, "Co-design of event generator and controller for event-triggered control system," in *Proceedings of the 30th Chinese Control Conference (CCC '11)*, pp. 175–179, July 2011.

[18] S. B. Li and B. G. Xu, "Event-triggered control for discrete-time uncertain linear parameter-varying systems," in *Proceedings of the 32nd Chinese Control Conference*, Xi'an, China, July 2013.

[19] S. Boyd, L. El Ghaoui, and E. F. Balakrishnan, *Linear matrix inequalities in system and control theory*, vol. 15, SIAM, Philadelphia, Pa, USA, 1994.

Hindawi Publishing Corporation
Mathematical Problems in Engineering
Volume 2015, Article ID 608121, 11 pages
http://dx.doi.org/10.1155/2015/608121

Research Article

Energy Balanced Redeployment Algorithm for Heterogeneous Wireless Sensor Networks

Guang Ye, Baihai Zhang, Senchun Chai, and Lingguo Cui

School of Automation, Beijing Institute of Technology, Beijing 100081, China

Correspondence should be addressed to Senchun Chai; chaisc97@bit.edu.cn

Received 15 August 2014; Accepted 1 September 2014

Academic Editor: Yun-Bo Zhao

Wireless sensor networks (WSNs) have gained worldwide attention in recent years. Since WSNs can be conveniently deployed to monitor a given field of interest, they have been considered as a great long-term economic potential for military, environmental, and scientific applications and so forth. One of the most active areas of research in WSNs is the coverage which is one of the most essential functions to guarantee quality of service (QoS) in WSNs. However, less attention is paid on the heterogeneity of the node and the energy balance of the whole network during the redeployment process. In this work, the energy balanced problems in mobile heterogeneous WSNs redeployment have been analyzed. The virtual force algorithm with extended virtual force model is used to improve the QoS of the deployment. Furthermore energy model is added to enhance or limit the movement of the nodes so that the energy of nodes in the whole WSNs can be balanced and the lifetime of the networks can be prolonged. The simulation results verify the effectiveness of this proposed algorithm.

1. Introduction

WSNs consist of small-sized low cost sensor nodes which have several restrictions in energy supply, computing power, and bandwidth of the wireless communication [1]. The QoS of the network is highly related to the deployment performance of the nodes. However, in many working environments such as disaster areas, battlefields, and toxic gas regions, all sensor nodes are mainly deployed randomly by aircraft instead of human beings. In such case, the deployment result may not satisfy the requirement of the system. All the nodes may cluster in a small region or may even distribute sparsely without connectivity guarantee which would influence the QoS and reliability of the WSNs significantly.

Many researchers are currently engaged in coverage problem [2–4] and numerous algorithms are related to mobile WSNs.

Mobile WSNs are composed of a distributed collection of nodes, each of which has communication, sensing, computation, and locomotion capabilities. The mobility of sensor nodes allows more complex application scenarios. With locomotion capabilities, sensor nodes can adjust their positions after stochastic distribution; thus the whole networks could enhance the coverage performance and reach more precise placement. However, the movement of the node would expend the energy of the node. Some node may run out of power because of the long distance movement during redeployment.

Another actual problem in WSNs coverage is that the nodes in networks cannot be always the same in practice due to various reasons. The coverage analysis of heterogeneous WSNs is very useful for both academic and industrial fields. The concept of heterogeneous sensor network is proposed in [5]. The existence of heterogeneous WSNs is mainly due to the following aspects. (1) Nodes are different as physical devices, and the physical properties of the sensor node are very difficult to be completely homogenized. (2) The same type of sensor nodes may work differently due to work environment, regional terrain characteristics, and imbalanced workload or other reasons. All those could affect the behaviour of nodes in WSN.

In the literature, abundant work has been done in the redeployment of the mobile WSNs, and many effective algorithms have been put forward to obtain a required placement and improve the coverage rate. Pervious work on mobile WSNs redeployment algorithms can be classified into two main kinds: virtual force algorithms (VFA) and computational geometry-based approach. In VFA based algorithms [6], those models the mobile sensor nodes as electrons or molecules, and nodes move toward or away from each other by the virtual force (often related to the distance between nodes) or potential fields. However algorithms above do not consider some actuality problems such as connectivity maintenance and the energy cost [7]. References [8–10] are algorithms according to the computational geometry in which nodes update their positions to from a uniform Voronoi diagram or Delaunay triangulation. It can provide well performance but is hard to be used for the need of the global position information of the whole network which usually cannot be realized.

In this paper, the redeployment problem in mobile heterogeneous WSNs considering energy balanced is addressed. Delaunay triangulation is used in VFA to find the logic neighbors nodes in order to avoid nodes cluster in a small region. Furthermore according to the research fixed ideal distance is proposed to solve the serious coverage holes and redundant problem in traditional VFA. And the energy model of the nodes is proposed. In order to balance the energy of the whole networks, in this paper energy control function is added to the virtual force model.

Throughout the paper, it is assumed that the communication range is two times the sensing range. The rest of this paper is organized as follows. Section 2 gets over the past work that closely related to our work. Section 3 analyzes energy unbalanced problem in mobile WSNs redeployment and provides a solution. Section 4 gives the simulation results that illustrate the performance. Section 5 is the conclusion of the paper.

2. Related Works

The prior work on redeployment of mobile WSNs in recent years which closely related to this subject is summarized below.

The concept of redeployment of mobile WSNs is derived from dealing with coordination in behavior control of many robots teams [11, 12]. Gage [11] has classified the use of robot swarms to provide blanket, barrier, or sweep coverage of area. According to this classification, the redeployment problem studied in this paper focuses on the blanket coverage. Reference [12] considers multirobot exploration and mapping for larger teams and gives an evaluation of different strategies for coordinating the efforts of a robot team during an exploration mission in an unknown environment. In [13], a potential-field-based approach (PFBA) is presented to deploy sensor nodes in a target environment. In order to obtain a uniform deployment in an unknown enclosed area, control force defined as negative gradient of potential (NGOP) is employed. However, some crucial problems had not been considered such as connectivity maintenance and topology control. In [14], the author introduced the concept of virtual force algorithm (VFA) to the WSNs deployment. The VFA adopts the similar strategy as PFBA, by considering the virtual attractive and repulsive forces exerted on each node by neighbor nodes and obstacles. The VFA can significantly increase sensor coverage. These works only consider homogeneous sensing models. Based on works in [14], a distributed self-spreading algorithm is developed in [15]. The virtual force in (distributed self-spreading algorithm) DSSA is modeled as internuclear repulsion and attraction between molecules. Computational geometry such as Voronoi diagram and Delaunay triangulation is commonly used in redeployment of WSNs, and the vector-based algorithm (VEC), the Voronoi-based algorithm (VOR), and MiniMax are presented in [8]. The algorithms above use Voronoi diagrams to divide the coverage field into many small areas and enhance the covered area by pushing or pulling nodes according to virtual force. Computational geometry-based algorithms can solve the stacking problem. However the Voronoi diagram is a global structure; it means that the diagram can be obtained only if the global location information of all nodes in the WSNs is known.

3. Preliminaries

3.1. Network Model and Assumptions. In this paper we focus on the redeployment problem of heterogeneous WSNs in 2-dimensional plane. The position of node i is described as (x_i, y_i). The distance between node i and node j is defined as Euclidean distance d_{ij}. The initial deployment is a random deployment in unknown distribution. We assume that every node can learn its own position by GPS or other localization technologies. R_c is the communication range; if $d_{ij} \le R_c$, node i and node j are neighbor nodes. Nodes can receive and send message to their neighbors without losing data. Meanwhile, nodes can also get relative distances and orientations between them. Nodes are aware of their remaining energy and can share this information with their neighbors. R_s is the sensing range. The perceptual model C_{pi} is defined as follows (p is an arbitrary position in target area):

$$C_{pi} \begin{cases} 1, & d_{ip} < R_s \\ 0, & d_{ip} \ge R_s. \end{cases} \tag{1}$$

In general, R_c is larger than R_s.

All of the virtual physics algorithms for redeployment problem in WSNs are similar to the structure of virtual force, which include the ideas of potential field with circle packing that models the sensor node to be a particle in the potential field. And the potential field exerts forces on the nodes in its field. For a couple of neighbor nodes i and j, the potential function V_{ij} could be built. And the virtual force is shown as follows:

$$F_{ij} = -\nabla V_{ij}. \tag{2}$$

Nodes move toward the target area by the virtual forces. The force can be attractive force or repulsive force. Generally, there is an ideal distance D_{th}. If the distance between nodes i and j is less than D_{th}, repulsive force will act on nodes. Similarly, attractive force will act on nodes if the distance is larger than the ideal distance. The repulsive force is to insure the sensors are sparse enough without too much redundant area and the attractive force is to guarantee the coverage without coverage holes.

The control law for nodes is described in

$$\ddot{\mathbf{x}}_i = \sum_{j\in G_i} \mathbf{F}_{ij} - k_d\dot{\mathbf{x}}_i, \quad (3)$$

where $\ddot{\mathbf{x}}_i$ is the acceleration of the node, $\dot{\mathbf{x}}_i$ is the velocity of the node, k_d is damping coefficient, and G_i is the neighbors of node i.

In traditional VFA, the virtual force is defined as follows:

$$\mathbf{F}_{ij} = \begin{cases} \omega_A\left(d_{ij} - D_{th(i,j)}\right)\mathbf{u}_{ij}, & \text{if } d_{ij} > D_{th(i,j)} \\ \omega_R d_{ij}^{-1}\mathbf{u}_{ji}, & \text{if } d_{ij} < D_{th(i,j)} \\ 0, & \text{if } d_{ij} = D_{th(i,j)}, \end{cases} \quad (4)$$

where ω_A is the virtual force attractive coefficient, ω_R is the virtual force repulsive coefficient, d_{ij} is the Euclidean distance between node i and node j, and $\mathbf{u}_{ij}$ is the unit vector from node i to node j.

Nodes move to new positions according to (3). The total force F_i exerted on node i can be described as follows:

$$F_i = \sum_{j\in G_i} F_{ij}. \quad (5)$$

4. Energy Balanced Redeployment Algorithm for Heterogeneous WSNs

The extended virtual force algorithm is a redeployment algorithm with some novel features which can overcome the limitations of traditional VFA. In practical networks the sensing range R_s of nodes cannot be always the same due to various reasons; in that case coverage holes may appear which may influence the QoS of the WSNs seriously. Prior algorithm assumed that R_c is two times larger than R_s; however as a matter of fact R_c is much larger than R_s. High R_c may induce stacking problem in redeployment.

In order to solve the problem above, Energy Balanced Redeployment Algorithm (EBRA) is proposed.

Firstly we prove the stability of the algorithm.

4.1. Stability Analysis. The stability of the algorithm can be proved with Lyapunov stability theory.

Proof. Assume x_i is the position vector of node i. The control input of node i is the virtual force F_{ij} exerted on node i by its neighbor j. Then the virtual potential field can be known according to (2) and (5). The total force of the node i can be summarized as follows:

$$F_i = \sum_{j\in G_i} F_{ij} = \sum_{j\in G_i} -\nabla V_{ij}. \quad (6)$$

Then energy function $\mathbf{\Phi}$ which combines kinetic energy with potential energy is built as Lyapunov function:

$$\mathbf{\Phi} = \sum_{i=1}^{N}\frac{1}{2}\dot{x}_i^T\dot{x}_i + \frac{1}{2}\sum_{i=1}^{N}\sum_{j\in G_i} V_{ij}. \quad (7)$$

For the symmetry of V_{ij} and V_{ji}, $\dot{x}_i = -\dot{x}_j$ on the orientation from node i to node j. The time derivative V_{ij} is described as follows:

$$\begin{aligned} \frac{d}{dt}V_{ij} &= \frac{\partial V_{ij}}{\partial x_i}\cdot\frac{dx_i}{dt} + \frac{\partial V_{ij}}{\partial x_j}\cdot\frac{dx_j}{dt} \\ &= \nabla V_{ij}\cdot\dot{x}_i - \nabla V_{ij}\cdot\dot{x}_i \\ &= \nabla V_{ij}\cdot\left(\dot{x}_i - \dot{x}_j\right) \\ &= 2\nabla V_{ij}\cdot\dot{x}_i. \end{aligned} \quad (8)$$

The energy function $\mathbf{\Phi}$ can be simplified as follows:

$$\begin{aligned} \dot{\mathbf{\Phi}} &= \sum_{i=1}^{N}\frac{1}{2}\left(\dot{x}_i^T\dot{x}_i + \dot{x}_i^T\dot{x}_i\right) + \sum_{i=1}^{N}\sum_{j\in G_i}\nabla V_{ij}\dot{x}_i^T \\ &= \sum_{i=1}^{N}\dot{x}_i^T\left(\ddot{x}_i + \sum_{j\in G_i}\nabla V_{ij}\right). \end{aligned} \quad (9)$$

Combining (9) and (3), we get

$$\begin{aligned} \dot{\mathbf{\Phi}} &= \sum_{i=1}^{N}\dot{x}_i^T\left(\ddot{x}_i + \sum_{j\in G_i}\nabla V_{ij}\right) \\ &= \sum_{i=1}^{N}\dot{x}_i^T\left(\sum_{j\in G_i}F_{ij} - k_d\dot{x}_i + \sum_{j\in G_i}\nabla V_{ij}\right) \\ &= \sum_{i=1}^{N}\dot{x}_i^T\left(\sum_{j\in G_i} -\nabla V_{ij} - k_d\dot{x}_i + \sum_{j\in G_i}\nabla V_{ij}\right) \\ &= -k_d\sum_{i=1}^{N}\dot{x}_i^T\dot{x}_i, \end{aligned} \quad (10)$$

where k_d is the damping coefficient and $\dot{\mathbf{\Phi}}$ is seminegative definite. According to Lyapunov stability theory, the redeployment algorithm is asymptotically stable. □

4.2. Redeployment Algorithm for Heterogeneous WSNs. As exponential force model can achieve fast convergence, the force model is shown in (11) and Figure 1:

$$F_{ij}(d) = \begin{cases} \boldsymbol{\alpha}\left(d_{ij}^{-\beta} - D_{th}^{-\beta}\right)\mathbf{u}_{ij}, & \text{if } D_{th} < d_{ij} < R_c \\ 0, & \text{if } d_{ij} = D_{th} \\ \left|\boldsymbol{\alpha}\left(d_{ij}^{-\beta} - D_{th}^{-\beta}\right)\right|\mathbf{u}_{ij}, & \text{if } 0.5D_{th} < d_{ij} < D_{th} \\ 1\mathbf{u}_{ij} & \text{if } d_{ij} \le 0.5D_{th}, \end{cases} \quad (11)$$

where $\mathbf{u}_{ij}$ is the unit vector from node i to node j, $\boldsymbol{\alpha}$ and β are constants that may be changed in different situations, and D_{th} is the ideal distance.

In heterogeneous WSNs there is no ideal deployment to achieve, which is different from homogeneous WSNs, so a new balance point $D_{th(i,j)}$ and the new force field truncation coefficient which keeps the nodes from stacking should be

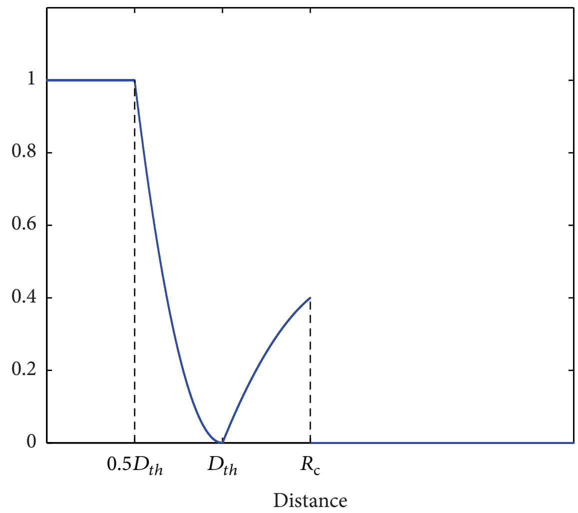

Figure 1: Virtual force model.

found. $D_{th(i,j)}$ in homogeneous WSNs is $\sqrt{3}R_s$. However, in heterogeneous WSNs every node has different R_s, so a new ideal distance for heterogeneous WSNs should be found.

Theorem 1. *As shown in Figure 2, there are three nodes i, j, and k with different sensing range.*

If $\sum\phi_{ijk} = \phi_{ij} + \phi_{ik} + \phi_{jk} > 2\pi$, there is a hole in coverage area; if $\sum\phi_{ijk} = \phi_{ij} + \phi_{ik} + \phi_{jk} < 2\pi$, redundant coverage exists in area; if $\sum\phi_{ijk} = \phi_{ij} + \phi_{ik} + \phi_{jk} = 2\pi$, neither coverage hole nor redundant coverage exists.

Assume the distance between node i and node j is $d_{ij} = \lambda(R_{si} + R_{sj})$, where λ is the distance coefficient. Then, if $\lambda = \sqrt{3}/2$, nodes cover the area without any hole.

Proof. Consider

$$\begin{aligned}\phi_{ij} &= \arccos\left(\frac{R_{si}^2 + R_{sj}^2 - d_{ij}^2}{2R_{si}R_{sj}}\right)\\ &= \arccos\left(\frac{R_{si}^2 + R_{sj}^2 - 0.75\left(R_{si} + R_{sj}\right)^2}{2R_{si}R_{sj}}\right)\\ &= \arccos\left(\frac{0.25R_{si}^2 + 0.25R_{sj}^2 - 1.5R_{si}R_{sj}}{2R_{si}R_{sj}}\right)\\ &= \arccos\left(\frac{0.25\left(R_{si} - R_{sj}\right)^2}{2R_{si}R_{sj}} - 0.5\right)\\ &\le \arccos(-0.5) = \frac{2}{3}\pi.\end{aligned} \tag{12}$$

Similarly $\phi_{ik} \le (2/3)\pi$ and $\phi_{jk} \le (2/3)\pi$, and sum them up.

Consider $\sum\phi_{ijk} = \phi_{ij} + \phi_{ik} + \phi_{jk} \le 2\pi$; that is, in heterogeneous sensor network, if we set $\lambda = \sqrt{3}/2$, we can get coverage results without holes.

From the above, $D_{th(i,j)} = (\sqrt{3}/2)(R_{si} + R_{sj})$.

In VFA for homogeneous WSNs, there is a force field truncation coefficient λ_2; generally $\lambda_2 = 1$ which equivalent reduce the value of R_c in order to avoid nodes stacking when the nodes have high R_c. However the connectivity of the networks cannot be ensured in the case of scatter initial deployment.

In this paper we employ Delaunay triangulation to solve the node gathering problem and on the other hand avoid affecting the connectivity of the networks.

Delaunay triangulation graph is composed of several disjoint triangles. The vertices of the triangle are sensor nodes. Delaunay figure is used as the logical topology of the network in the coverage control because it has no intersecting edge topology.

This paper uses Delaunay graph as the network topology where the balance point $D_{th(i,j)} = \sqrt{3}/2(R_{si} + R_{sj})$.

To make the algorithm as a distributed algorithm, every node uses its own local Delaunay triangulation graph. □

Definition 2. Every node and its neighbor nodes in its communication radius make up the Delaunay graph. This graph is the node's local Delaunay triangulation graph (Local DTG or LDTG). The LDTGs of all the nodes form Unit Delaunay Triangulation Graph (Unit DTG or UDTG). Obviously, UDTG is a subgraph of DTG.

To achieve better performance, another round of movement is employed; the proof is shown below.

Theorem 3. *If $D_{th(i,j)} = \sqrt{3}/2(R_{si} + R_{sj})$ in a Delaunay triangle, the increment of $\angle j_k i j_{k+1}$ causes monotone decrement of R_{si}.*

Proof. Consider

$$\begin{aligned}&\cos\angle j_k i j_{k+1}\\ &= \left(\left(\left(\frac{\sqrt{3}}{2}\right)\left(R_{si} + R_{sj}\right)\right)^2 + \left(\left(\frac{\sqrt{3}}{2}\right)\left(R_{si} + R_{s(j+1)}\right)\right)^2 - \left(\left(\frac{\sqrt{3}}{2}\right)\left(R_{sj} + R_{s(j+1)}\right)\right)^2\right)\\ &\quad\times\left(2\left(\left(\frac{\sqrt{3}}{2}\right)\left(R_{si} + R_{sj}\right)\left(\frac{\sqrt{3}}{2}\right)\left(R_{si} + R_{s(j+1)}\right)\right)\right)^{-1}\\ &= \frac{\left(R_{si} + R_{sj}\right)^2 + \left(R_{si} + R_{s(j+1)}\right)^2 - \left(R_{sj} + R_{s(j+1)}\right)^2}{2\left(R_{si} + R_{sj}\right)\left(R_{si} + R_{s(j+1)}\right)}.\end{aligned} \tag{13}$$

Assuming three circles are tangent to each other, $\cos\angle j_k i j_{k+1} = \sqrt{3}/2$ as shown in Figure 3.

It is clear that

$$\angle j_k i j_{k+1} = 2\arctan\left(\frac{R_{\mathrm{VL}}}{R_{si}}\right). \tag{14}$$

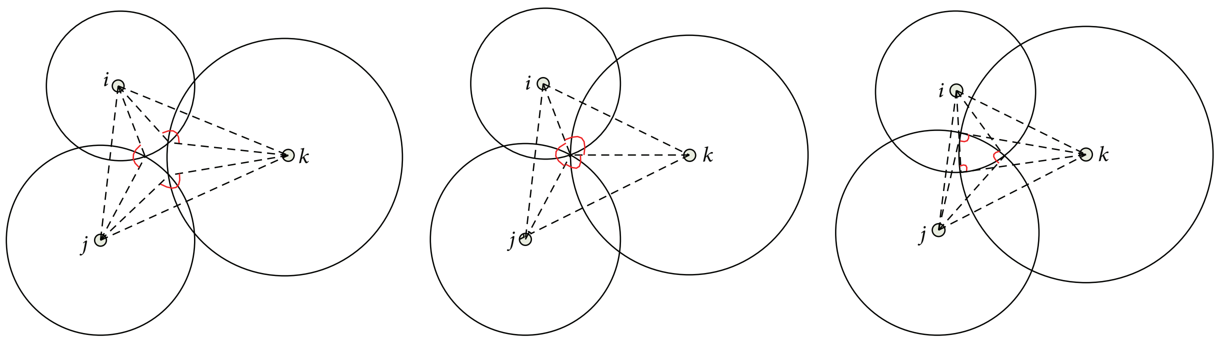

(a) $\sum \phi_{ijk} > 2\pi$ (b) $\sum \phi_{ijk} = 2\pi$ (c) $\sum \phi_{ijk} < 2\pi$

FIGURE 2: Localization effect in convex and concave holes.

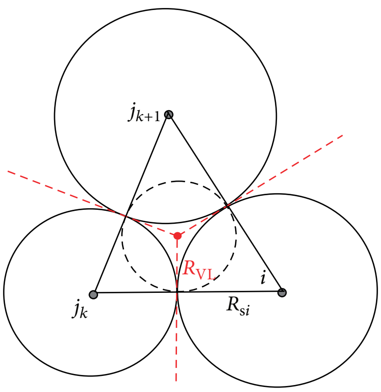

FIGURE 3: Delaunay triangle.

The area of the triangle can be described as follows:

$$S_{j_k i j_{k+1}} = 2 \times \frac{1}{2} R_{VL} R_{si} + 2 \times \frac{1}{2} R_{VL} R_{s j_k} + 2 \times \frac{1}{2} R_{VL} R_{s j_{k+1}} = R_{VL} \left(R_{si} + R_{s j_k} + R_{s j_{k+1}} \right). \quad (15)$$

Also the area of the triangle can be calculated by Heron's formula:

$$S_{j_k i j_{k+1}} = \sqrt{\left(R_{si} + R_{s j_k} + R_{s j_{k+1}} \right) \left(R_{si} R_{s j_k} R_{s j_{k+1}} \right)}. \quad (16)$$

Clearly from (14), (15), and (16),

$$\angle j_k i j_{k+1} = 2 \arctan \left(\sqrt{\frac{R_{s j_k} R_{s j_{k+1}}}{R_{si} \left(R_{si} + R_{s j_k} + R_{s j_{k+1}} \right)}} \right). \quad (17)$$

$\partial \angle j_k i j_{k+1} / \partial R_{si}$ is shown in

$$\begin{aligned} \frac{\partial \angle j_k i j_{k+1}}{\partial R_{si}} &= \frac{1}{1 + R_{s j_k} R_{s j_{k+1}} / R_{si} \left(R_{si} + R_{s j_k} + R_{s j_{k+1}} \right)} \\ &\quad \times \frac{1}{\sqrt{R_{s j_k} R_{s j_{k+1}} / R_{si} \left(R_{si} + R_{s j_k} + R_{s j_{k+1}} \right)}} \\ &\quad \times \left(- \frac{R_{s j_k} R_{s j_{k+1}}}{R_{si}{}^2 \left(R_{si} + R_{s j_k} + R_{s j_{k+1}} \right)} \right. \\ &\qquad \left. - \frac{R_{s j_k} R_{s j_{k+1}}}{R_{si} \left(R_{si} + R_{s j_k} + R_{s j_{k+1}} \right)^2} \right) < 0. \end{aligned} \quad (18)$$

Theorem 3 proves that the increment of $\angle j_k i j_{k+1}$ leads to the monotone decrement of R_{si} in Delaunay triangle. Therefore a node in each Delaunay triangle that meets the distance coefficient must be a determined value. But it is almost impossible to have all nodes meet the value at one time. So another step is used to improve the performance. □

As shown in Figure 2, if $\sum \phi_{ijk} = \phi_{ij} + \phi_{ik} + \phi_{jk} = 2\pi$, neither coverage holes nor coverage redundant exist. Then the main aim of the algorithm is to adjust the distance between the nodes according to the $\sum \phi_{ijk}$ in Delaunay triangle to approach 2π.

For node i shown in Figure 2(a),

$$\phi_{th(i,j_k)} = \phi_{ij_k} + \left(2\pi - \sum \phi_{ij_k j_{k+1}} \right) \frac{\phi_{ij_k}}{\sum \phi_{ij_k j_{k+1}}}. \quad (19)$$

The ideal distance between nodes can be described as follows:

$$D_{th(i,j_k)} = \left(R_{si}^2 + R_{s j_k}^2 - 2 R_{si} R_{s j_k} \cos \phi_{th(i,j_k)} \right). \quad (20)$$

// m: the number of the logic neighbors of node i
// Δt: the sampling time
Step 1. Find out logic neighbors node i in LDTG(i) of node i;
Step 2. For $1 \leq j \leq m$
Step 2.1. Set distance coefficient $\lambda = \sqrt{3}/2$
Step 2.2.
Calculate $\mathbf{F}_{ij}$ the virtual force between node i and its neighbor node j;
Step 3. Calculate the resultant virtual force;
Step 4. Calculate the accelerated speed a_i and speed v_i of node I and then move node i to new position;
Step 5. Update $t + \Delta t$;
Step 6. Go back to Step 1.
Step 7. Find out logic neighbors node i in LDTG(i) of node i;
Step 8. For $1 \leq j \leq m$
Step 8.1. Calculate the virtual force $\mathbf{F}_{ij}$ between node i and its logic neighbor j;
Step 9. Calculate the resultant virtual force;
Step 10. Calculate the accelerated speed a_i of node i and speed v_i, node i move to new position;
Step 11. Update to $t + \Delta t$
Step 12. Go back to Step 1.

Algorithm 1

Virtual force between nodes i and j is listed as follows:

$$F_{ij}(d) = \begin{cases} \boldsymbol{\alpha}\left(d_{ij}^{-\beta} - D_{th}^{-\beta}\right)\mathbf{u}_{ij}, & \text{if } D_{th(i,j)} < d_{ij} < R_c \\ 0, & \text{if } d_{ij} = D_{th(i,j)} \text{ or } E(i,j) \\ & \text{is the outside edge} \\ \left|\boldsymbol{\alpha}\left(d_{ij}^{-\beta} - D_{th}^{-\beta}\right)\right|\mathbf{u}_{ij}, & \text{if } 0.5D_{th(i,j)} < d_{ij} < D_{th(i,j)} \\ 1\mathbf{u}_{ij} & \text{if } d_{ij} \leq 0.5D_{th(i,j)}. \end{cases} \quad (21)$$

If $E(i, j)$ is the outside edge of the LDTG, the virtual force between nodes i and j is zero.

Then each node calculates its own resultant virtual force of its logic neighbors. Then it moves to the new position according to the motion dynamic model.

Furthermore, the algorithm above can be described in Algorithm 1.

4.3. Energy Balanced Revision. Actually the imbalanced energy cost of the network may cause some node to run out of energy in a short time. In this case the whole structure of the WSNs may change, the QoS of the network cannot be guaranteed, and the lifetime of the network may be greatly shortened. As analyzed above, in mobile WSNs we can prolong the lifetime of the whole network by balancing the energy cost of the nodes during the redeployment process. Minimum energy of node $\overline{E}_{\min}$ is to describe the minimum remaining energy of the nodes in the network.

Definition 4. $\overline{L_x}, \overline{L_{-x}}, \overline{L_y}$, and $\overline{L_{-y}}$ are the energy cost of the node when moving standard distance in each direction. Energy cost of node i is shown as follows:

$$\overline{L_i} = \sum_{\forall \text{dir}} \left|\overline{L_i} \times \overline{\text{dir}_i}\right|, \quad (22)$$

where $\overline{\text{dir}_i}$ is the distance that node i moves in each direction. $\overline{\text{EI}_i}$ is the initial energy of node i. $\overline{E_i}$ is the energy of the node i. Thus the lowest energy of the node $\overline{E}_{\min}$ is described as follows:

$$\overline{E}_{\min} = \text{Min}\left(\overline{\text{EI}_i} - \overline{L_i}\right). \quad (23)$$

In order to prolong the lifetime of the network, the algorithm should keep $\overline{E}_{\min}$ as large as possible.

Definition 5. Energy differential coefficient $\boldsymbol{\varphi}$ (see (24)) is used to describe the energy difference between two nodes:

$$\boldsymbol{\varphi}_{i,j} = \frac{\left|\overline{E_i} - \overline{E_j}\right|}{\text{Max}\left(\overline{E_i}, \overline{E_j}\right)}. \quad (24)$$

Obviously, $\boldsymbol{\varphi} \in [0, 1]$, and if $\boldsymbol{\varphi}$ approaches zero, more effort should be made to protect the nodes which have low energy to save their energy.

Definition 6. Node level $\boldsymbol{\gamma}$ shows the importance of the node. In practical application some key nodes are more important than other nodes. Those key nodes can influence the QoS of the whole network. Therefore the algorithm should give priority to economize the energy of those key nodes.

To balance the energy cost of the node energy control function (see (25)) is added to (21):

$$e\left(\varphi_{i,j}\right) = \begin{cases} \varepsilon & \left(\text{rand}[0,1] < \varphi_{i,j}\right) \\ 1 & \left(\text{rand}[0,1] \geq \varphi_{i,j}\right). \end{cases} \quad (25)$$

ε is the attenuation coefficient. Every time node i calculates the virtual force of its logic neighbor j, node i compares its energy with j and gets the energy differential coefficient $\varphi_{i,j}$, and then node i generates a random number $k \in [0, 1]$. If $k < \varphi_{i,j}$, the virtual force would be limited so that

// m: the number of the logic neighbors of node i
// Δt: the sampling time
Step 1. Find out logic neighbors node i in LDTG(i) of node i;
Step 2. For $1 \leq j \leq m$
Step 2.1. Set distance coefficient $\lambda = \sqrt{3}/2$
Step 2.2.
Calculate $\mathbf{F}_{ij}$ the virtual force between node i and its neighbor node j;
Step 2.3.
Compare the energy of node i and node j,
Step 2.4.
Calculate the energy differential coefficient φ to fix the Virtual force,
Step 3. Calculate the resultant virtual force;
Step 4. Calculate the accelerated speed a_i and speed v_i of node I and then move node i to new position;
Step 5. Update $t + \Delta t$;
Step 6. Go back to Step 1.
Step 7. Find out logic neighbors node i in LDTG(i) of node i;
Step 8. For $1 \leq j \leq m$
Step 8.1. Calculate the virtual force $\mathbf{F}_{ij}$ between node i and its logic neighbor j;
Step 9. Calculate the resultant virtual force considering node level γ;
Step 10. Calculate the accelerated speed a_i of node i and speed v_i, node i move to new position;
Step 11. Update to $t + \Delta t$
Step 12. Go back to Step 1.

Algorithm 2: EBRA.

the movement of the node i would be reduced and in that case node i may save its energy in this round.

Then the new virtual force between node i and node j is listed as follows:

$$\mathbf{F}_{\text{eb}}(i) = \sum_{j \in \text{LN}} e\left(\varphi_{i,j}\right) \cdot F_{ij}(d), \tag{26}$$

where LN is the set of logic neighbors of node i.

There are some key nodes in the networks, those nodes should always save energy no matter their neighbor's energy is low or not.

Node level control function is addressed in

$$\delta(\gamma) = (\gamma - \mu)^{-\sigma}, \tag{27}$$

where μ and σ are constants which can be adjusted according to different situations. And the final resultant virtual force $\mathbf{F}_i$ is described in

$$\mathbf{F}_i = \delta(\gamma) \sum_{j \in \text{LN}} e\left(\varphi_{i,j}\right) \cdot F_{ij}(d). \tag{28}$$

Then each node calculates its own resultant virtual force of its logic neighbors according to the distance and energy and node level. Then it moves to the new position according to the motion dynamic model.

EBRA can be described in Algorithm 2.

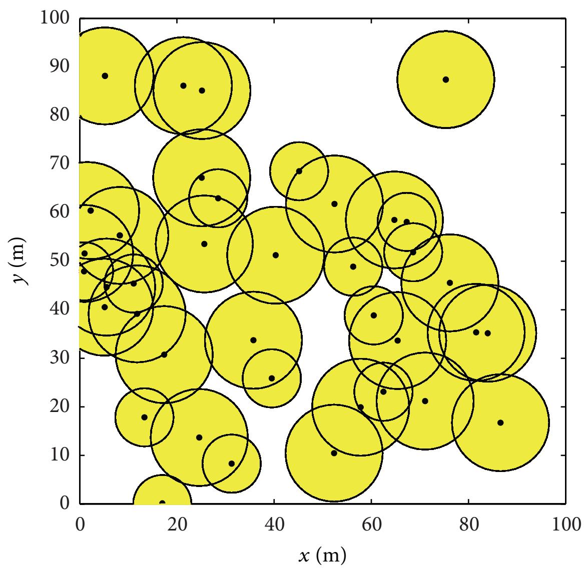

Figure 4: Scatter initial deployment.

4.4. Performance Evaluation

Coverage Rate. The coverage rate is a measure of the coverage quality for WSNs. It was originally introduced by Gage [11]. In the blanket coverage problem, coverage is defined by the ratio of the union of covered areas of each node to the complete area of interest. In this paper, the covered area of each node is defined as the circular area with sensing range R_s. The value of coverage rate C is as follows:

$$C = \frac{\bigcup_{i=1}^{n} A_i}{A}, \tag{29}$$

where A_i is the area covered by the node i, n is the total number of mobile sensor nodes, and A is the total area.

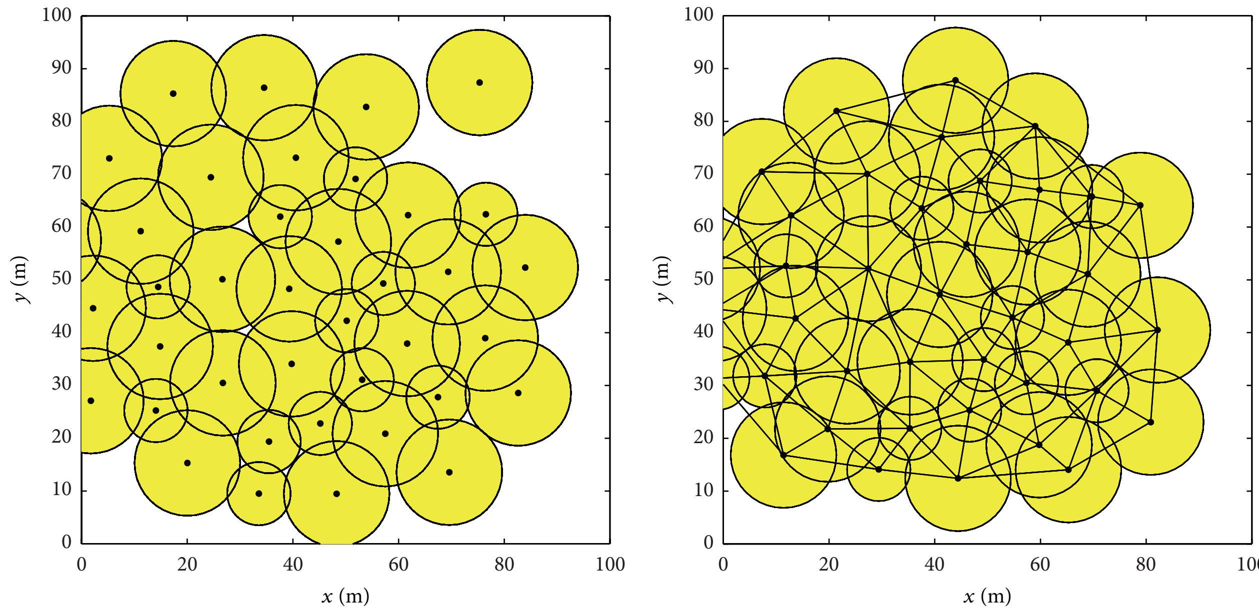

(a) Redeployment by VFA

(b) Redeployment by EBRA

FIGURE 5: Simulation result in scatter initial deployment.

Uniformity of Energy. In heterogeneous WSNs, the uniformity of energy can be measured by the average of the local standard deviation of the node energy

$$\sigma_E = \left(\frac{1}{n} \sum_{i=1}^{n} \left(E_i - \frac{1}{n} \sum_{j=1}^{n} E_i \right)^2 \right)^{1/2}. \quad (30)$$

Minimum Energy. $\overline{E}_{\min}$ stands for the minimum energy of all the nodes and is described in (23).

5. Numerical Simulation

In this section, we present the simulation results of EBRA.

In the simulation environment, 40 nodes are deployed randomly in a 100 m∗100 m square field. Communication range of all nodes is 30 m. The sensing range of 14 nodes is 10 m, and other nodes' sensing range is 8 m.

5.1. Performance of Energy Balanced Redeployment Algorithm. Firstly, simulation is done in scatter initial deployment. The scatter initial deployment is shown in Figure 4.

The redeployment results of VFA and EBRA in scatter initial deployment are shown in Figures 5(a) and 5(b).

It can be seen clearly from Figure 5 that EBRA shows the better result than VFA for guaranteeing the connectivity of the whole network. VFA employed force field truncation to avoid nodes stacking. $\lambda_2 = 1$ makes long-distance virtual force disappear. In EBRA use Delaunay triangulation to seek logic neighbor of nodes instead of real neighbor to settle the defects of VFA.

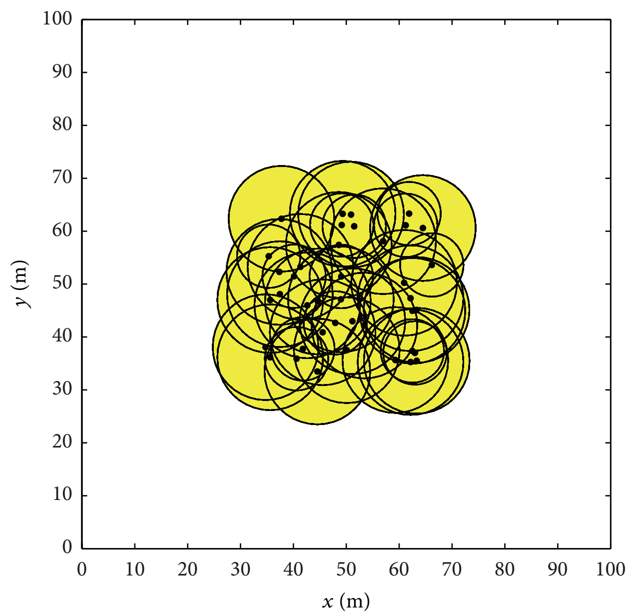

FIGURE 6: Concentrated initial deployment.

Then simulation is done in concentrated initial deployment. The concentrated initial deployment is shown in Figure 6.

The redeployment results of VFA and EBRA in concentrated initial deployment are shown in Figures 7(a) and 7(b).

It can be seen clearly from Figure 7(a). Compared with Figure 7(b), less holes and redundant coverage exist in the deployment result. In VFA, ideal distance coefficient is settled, and neighbor nodes cannot reach the ideal distance

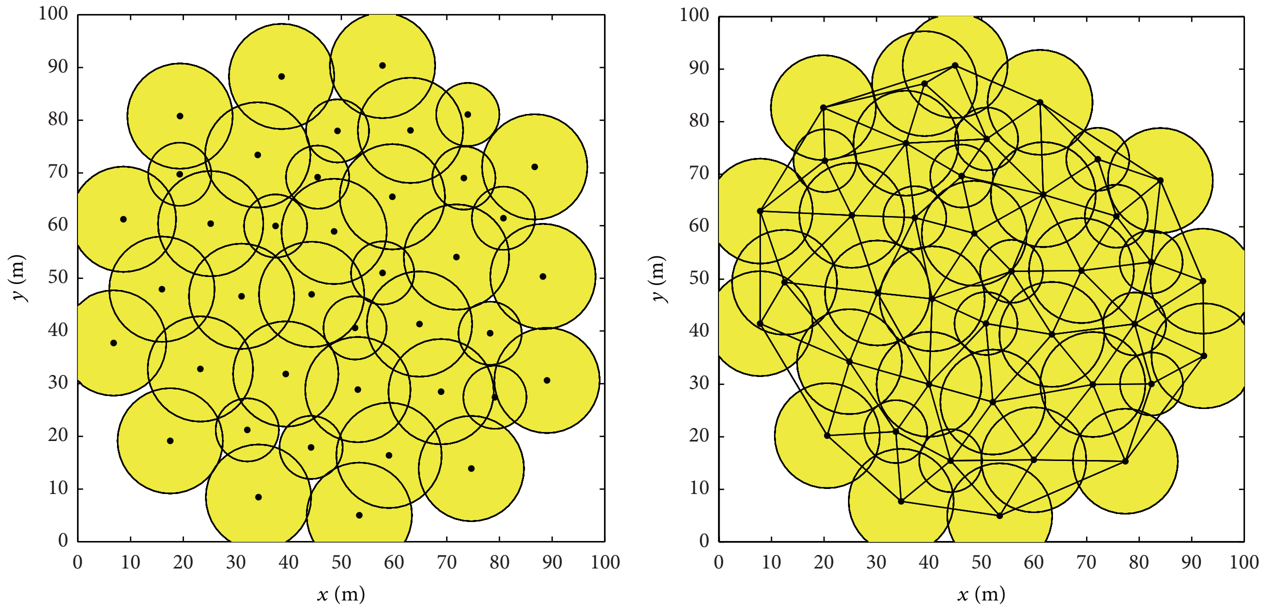

(a) Redeployment by VFA

(b) Redeployment by EBRA

FIGURE 7: Simulation result in concentrated initial deployment.

coefficient at same time. To improve the performance of the algorithm, another round of movement begins with modified ideal distance coefficient. Due to the modified ideal distance coefficient, the virtual forces between nodes change causing two scenarios. In area with redundant coverage virtual force makes the nodes move away from each other and in area with holes virtual force makes nodes get closer to each other.

The above experiments have been carried out for 100 times, and the simulation results are illustrated below.

Figure 8 shows the k-coverage rates of VFA and EBRA with the initial deployment as shown in Figure 6.

It can be seen clearly that EBRA can achieve better deployment than VFA, because it has less redundant coverage, and holes.

Figure 9 shows the minimum energy of all the nodes in mobile WSNs. Compared with traditional VFA, the minimum energy value of nodes reduces more slowly, and at step 100, both algorithms meet the ending condition, and EBRA saves more energy for the mobile WSNs which means the mobile WSNs employed EBRA can provide longer service time and better QoS.

Figure 10 shows the uniformity of energy of the whole networks. The uniformity of energy of EBRA is lower than traditional VFA which means the energy in EBRA is more uniform distribution which provides better robustness for the whole system.

Figure 11 shows the energy cost of the key nodes with and without energy protecting. Simulations are done in same initial deployment. Firstly a random node is selected as a key node whose energy cost will be recoded. Secondly, the node which has been selected changes its node level and then recodes the energy cost. It can be seen clearly from Figure 11 that EBRA saves the energy for the key nodes.

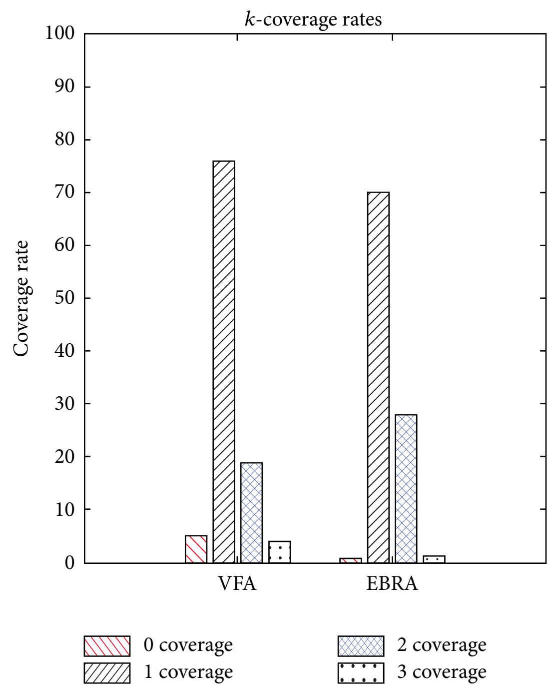

FIGURE 8: k-coverage rates of the final deployment.

6. Conclusion

In this paper, we analyze the coverage problem in heterogeneous WSNs. We argue the energy unbalanced, coverage holes, and redundant coverage problems that appear when traditional VFA algorithms are used in heterogeneous WSNs.

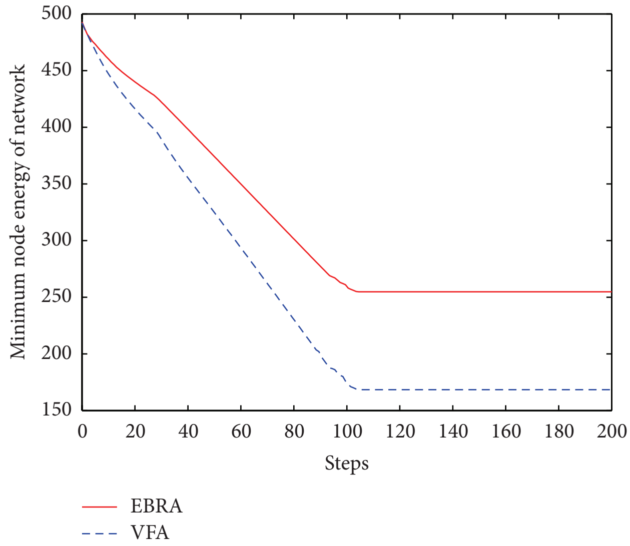

FIGURE 9: Minimum energy of node.

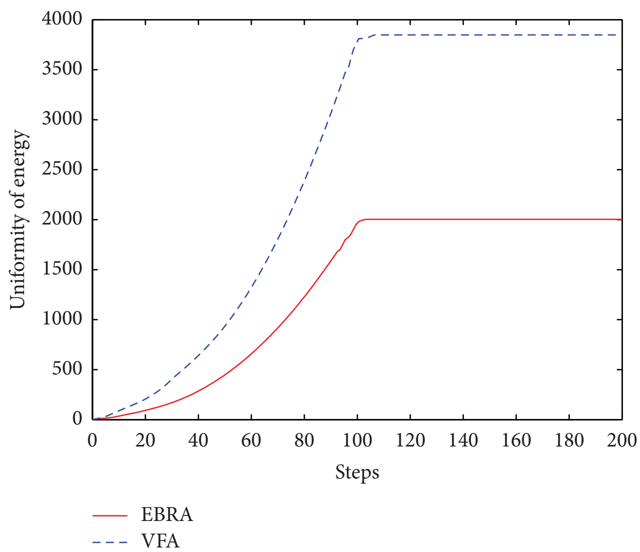

FIGURE 10: Uniformity of energy.

In order to solve these problems, EBRA which can be applied for heterogeneous WSNs in any initial deployment is proposed. Furthermore, it provides better performance than VFA. Moreover the energy cost of the nodes in the network has been balanced to prolong the lifetime and enhance the QoS of the WSNs (heterogeneous WSNs).

Compared with VFA, EBRA saves almost about 20% energy for key nodes and reduces the energy waste of network. Moreover EBRA provides better coverage performance (larger coverage area, less redundant, and holes). All the above insure that EBRA is more suitable in redeployment heterogeneous WSNs for its longer lifetime, better coverage performance, and higher QoS. Future work involves studying k-coverage requirement of heterogeneous WSNs.

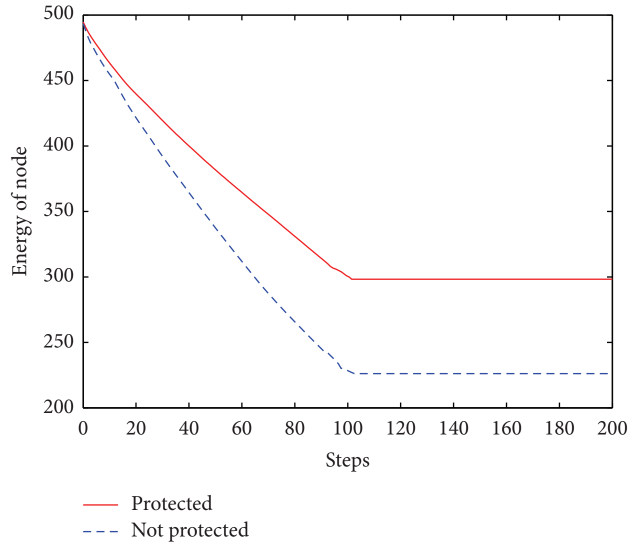

FIGURE 11: Energy cost of the key nodes with and without energy protecting.

Conflict of Interests

The authors declare that there is no conflict of interests regarding the publication of this paper.

Acknowledgments

This work was supported by National Defense Advanced Research Project of China (Grants nos. 104080 and 40405020401), National Natural Science Foundation of Youth Science Fund (no. 61203144 and no. 61104086), and Research Fund for the Doctoral Program of Higher Education of China (no. 20121101110032).

References

[1] L. Krishnamurthy, R. Adler, P. Buonadonna, J. Chhabra, M. Flanigan, and N. Kushalnagar, "Design and deployment of industrial sensor networks: experiences from a semiconductor plant and the North Sea," in *Proceedings of the 3rd ACM International Conference on Embedded Networked Sensor Systems (SenSys '05)*, pp. 64–75, Association for Computing Machinery, San Diego, Calif, USA, November 2005.

[2] S. Meguerdichian, F. Koushanfar, M. Potkonjak, and M. B. Srivastava, "Coverage problems in wireless ad-hoc sensor networks," in *Proceedings of the 20th Annual Joint Conference of the IEEE Computer and Communications Societies*, pp. 1380–1387, IEEE, Piscataway, NJ, USA, April 2001.

[3] K. Derr and M. Manic, "Extended virtual spring mesh (EVSM): the distributed self-organizing mobile ad hoc network for area exploration," *IEEE Transactions on Industrial Electronics*, vol. 58, no. 12, pp. 5424–5437, 2011.

[4] R. S. Chang and S. H. Wang, "Self-deployment by density control in sensor networks," *IEEE Transactions on Vehicular Technology*, vol. 57, no. 3, pp. 1745–1755, 2008.

[5] E. J. Duarte-Melo and M. Liu, "Analysis of energy consumption and lifetime of heterogeneous wireless sensor networks," in

Proceedings of the IEEE Global Telecommunications Conference (GLOBECOM '02), pp. 21–25, Institute of Electrical and Electronics Engineers, Taipei, Taiwan, November 2002.

[6] N. Heo and P. K. Varshney, "Energy-efficient deployment of intelligent mobile sensor networks," *IEEE Transactions on Systems, Man, and Cybernetics Part A:Systems and Humans*, vol. 35, no. 1, pp. 78–92, 2005.

[7] M.-L. Lam and Y.-H. Liu, "ISOGRID: an efficient algorithm for coverage enhancement in mobile sensor networks," in *Proceedings of the IEEE/RSJ International Conference on Intelligent Robots and Systems (IROS '06)*, pp. 1458–1463, Piscataway, NJ, USA, October 2006.

[8] G. Wang, G. Cao, and T. L. Porta, "Movement-assisted sensor deployment," in *Proceedings of the 23rd Annual Joint Conference of the IEEE Computer and Communications Societies (INFOCOM '04)*, vol. 4, pp. 2469–2479, March 2004.

[9] C. H. Wu, K. C. Lee, and Y. C. Chung, "A Delaunay Triangulation based method for wireless sensor network deployment," *Computer Communications*, vol. 30, no. 14-15, pp. 2744–2752, 2007.

[10] W. Li, Y. I. Kamil, and A. Manikas, "Wireless array based sensor relocation in mobile sensor networks," in *Proceedings of the ACM International Wireless Communications and Mobile Computing Conference (IWCMC '09)*, Association for Computing Machinery, pp. 832–838, Leipzig, Germany, June 2009.

[11] D. W. Gage, "Development and command-control tools for many-robot systems," in *Microrobotics and Micromechanical Systems*, vol. 25, pp. 121–129, Society of Photo-Optical Instrumentation Engineers, Philadelphia, Pa, USA, 1995.

[12] C. Nieto-Granda, J. G. Rogers, and H. I. Christensen, *Coordination Strategies for Multi-Robot Exploration and Mapping*, Sage, Thousand Oaks, Calif, USA, 4th edition, 2014.

[13] X. Wang and S. Wang, "Hierarchical deployment optimization for wireless sensor networks," *IEEE Transactions on Mobile Computing*, vol. 10, no. 7, pp. 1028–1041, 2011.

[14] Y. Zou and K. Chakrabarty, "Sensor deployment and target localization based on virtual forces," in *Proceedings of the 22nd Annual Joint Conference of the IEEE Computer and Communications Societies (IEEE INFOCOM '03)*, pp. 1293–1303, Institute of Electrical and Electronics Engineers, San Francisco, Calif, USA, March 2003.

[15] H. Nojeong and P. K. Varshney, "A distributed self spreading algorithm for mobile wireless sensor networks," in *Proceedings of the IEEE Wireless Communications and Networking Conference (WCNC '03)*, vol. 3, pp. 1597–1602, 2003.

Hindawi Publishing Corporation
Mathematical Problems in Engineering
Volume 2015, Article ID 505941, 8 pages
http://dx.doi.org/10.1155/2015/505941

Research Article

Matrix-Type Network DEA Model with Its Application Based on Input-Output Tables

Yun Cheng[1] and Huan-Li Gao[2]

[1] *School of Mechanical, Electrical & Information Engineering, Shandong University at Weihai, Weihai 264209, China*
[2] *School of Automation Science and Engineering, South China University of Technology, Guangzhou, China*

Correspondence should be addressed to Yun Cheng; chy81@wh.sdu.edu.cn

Received 6 August 2014; Revised 25 November 2014; Accepted 1 December 2014

Academic Editor: Jinhui Zhang

The matrix-type network data envelopment analysis (DEA) model is established for evaluating the relative performance of the matrix-type structure. The existence of solution and property of the new model is given. The equivalence of DEA efficiency and Pareto solutions of corresponding objective programming problem is proved. Using data in input-output tables, the new model is tested and the results show that the new model can be feasible in evaluating the relative performance of the matrix-type structure.

1. Introduction

In the process of enterprise, logistics, and supply chain management, we tend to analyze complex systems such as supply chain systems based on life cycle assessment (LCA), input-output systems, and others. The structure of the systems can be shown in Figure 1 and the efficiency scores of these systems are often required to be evaluated for the need of management decision making.

The generally accepted method for evaluating the relative performance of a set of comparable decision making units (DMUs) is data envelopment analysis (DEA). The first DEA model was introduced in 1978 [1] and several classic DEA models have been proposed over the past thirty years [2–5]. In recent years, DEA models were applied to evaluate the efficiency scores of complex systems and the concept of network DEA was put forward. The first network DEA model was introduced in 2000 [6], and then different models were put forward according to different system structure. The representative work includes models for series systems [5, 7–14], models for the parallel system [15–20], and model for complex system containing multiple subsystems introduced by Amatatsu and Ueda [21], Wang et al. [22], and Zhao et al. [23]. However, the models above cannot efficiently evaluate the efficiency score of the system shown in Figure 1.

In the following sections, a new model for evaluating the efficiency score of the system shown in Figure 1 is presented. As the model can be transformed into the linear programming problem, the existence of solution and property of the new model will be given. Computational experiments will be also presented to study the performances of the proposed model.

2. Network DEA Model for Matrix-Type Organizations

In the system shown in Figure 1, each subsystem has its own external inputs and external outputs, produces goods for other subsystems, and receives goods from other subsystems simultaneously. We refer to this type of system as a matrix-type system. Because of the complex internal structure, the relative performance of the system cannot be evaluated by the models mentioned above.

Consider the subsystem s_l $(l = 1, 2, \dots, n)$ of $\mathbf{DMU}_j$ $(j = 1, 2, \dots, m)$ shown in Figure 2. Here, x_j^l, y_j^l $(l = 1, 2, \dots, n; j = 1, 2, \dots, m)$, respectively, represent the external inputs and outputs for the subsystem s_l $(l = 1, 2, \dots, n)$ of $\mathbf{DMU}_j$ $(j = 1, 2, \dots, m)$; $z_j^{(k,l)}$ $(k = 1, 2, \dots, m, k \neq l)$ represent the internal inputs from other subsystems; and $z_j^{(l,k)}$

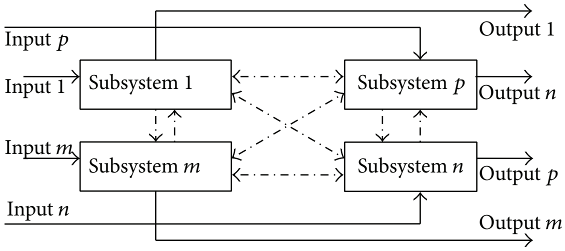

Figure 1: Matrix-type structure.

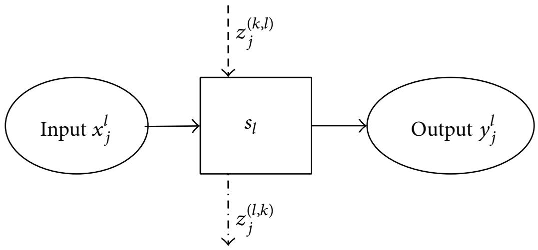

Figure 2: Subsystem s_l of $\mathbf{DMU}_j$.

$(k = 1, 2, \ldots, m,\ k \neq l)$ represent the internal outputs to other subsystems.

Let $x_0^l = x_{j_0}^l$, $y_0^l = y_{j_0}^l$, $z_0^{(k,l)} = z_{j_0}^{(k,l)}$, and $z_0^{(l,k)} = z_{j_0}^{(l,k)}$ $(l = 1, 2, \ldots, n;\ k = 1, 2, \ldots, n)$; the efficiency score of subsystem s_l $(l = 1, 2, \ldots, n)$ in $\mathbf{DMU}_{j_0}$ $(j_0 \in \{1, 2, \ldots, n\})$ can be gotten through the following model:

$$\begin{aligned}
\max \quad & \Psi_l = \frac{u_l y_0^l + \sum_{k=1,\, k\neq l}^{m} \xi_{lk} z_0^{(l,k)}}{v_l x_0^l + \sum_{k=1,\, k\neq l}^{m} \varsigma_{kl} z_0^{(k,l)}} \\
\text{s.t.} \quad & \frac{u_l y_j^l + \sum_{k=1,\, k\neq l}^{m} \xi_{lk} z_j^{(l,k)}}{v_l x_j^l + \sum_{k=1,\, k\neq l}^{m} \varsigma_{kl} z_j^{(k,l)}} \leq 1, \quad j = 1, 2, \ldots, m, \\
& u_l, v_l, \xi_{lk}, \varsigma_{kl} \geq 0, \quad k = 1, 2, \ldots, m,\ k \neq l,
\end{aligned} \tag{1}$$

where v_l, ς_{kl} represent the measure of the inputs and u_l, ξ_{lk} represent the measure of the outputs. The optimal values of these parameters can be obtained by the optimization problem (1).

Considering the relationship among the inputs and outputs of subsystems in matrix-type structure, we can get the flow balance as follows:

$$\sum_{k=1,\, k\neq l}^{m} \varsigma_{kl} z_j^{(k,l)} = \sum_{k=1,\, k\neq l}^{m} \xi_{kl} z_j^{(k,l)}. \tag{2}$$

Then the model in (1) can be rewritten to the following form:

$$\begin{aligned}
\max \quad & \Psi^l = \frac{u_l y_0^l + \sum_{k=1,\, k\neq l}^{m} \xi_{lk} z_0^{(l,k)}}{v_l x_0^l + \sum_{k=1,\, k\neq l}^{m} \xi_{kl} z_0^{(k,l)}} \\
\text{s.t.} \quad & \frac{u_l y_j^l + \sum_{k=1,\, k\neq l}^{m} \xi_{lk} z_j^{(l,k)}}{v_l x_j^l + \sum_{k=1,\, k\neq l}^{m} \xi_{kl} z_j^{(k,l)}} \leq 1, \quad j = 1, 2, \ldots, n, \\
& u_l, v_l, \xi_{lk} \geq 0, \quad k = 1, 2, \ldots, m,\ k \neq l.
\end{aligned} \tag{3}$$

According to the properties of CCR model [1], we can get $\Psi^{l^*} \leq 1$ which is the optimal value of subsystem s_l $(l = 1, 2, \ldots, n)$ and the following definition can be made.

Definition 1. If $\Psi^{l^*} = 1$ and $\mu_l^*, \omega_l^* > 0$ $(k = 1, 2, \ldots, m,\ k \neq l)$ in model (3), the subsystem s_l $(l = 1, 2, \ldots, n)$ of $\mathbf{DMU}_{j_0}$ $(j_0 \in \{1, 2, \ldots, n\})$ is DEA efficient.

Furthermore, the efficiency score of $\mathbf{DMU}_{j_0}$ can be obtained through averaging the efficiency score of each subsystem s_l $(l = 1, 2, \ldots, n)$ with certain weight [17], which is the proportion of all inputs of subsystem s_l $(l = 1, 2, \ldots, n)$ which accounted for the entire inputs of the system. Then the efficiency score of $\mathbf{DMU}_{j_0}$ $(j_0 \in \{1, 2, \ldots, n\})$ can be evaluated by the following model:

$$\begin{aligned}
\max \quad & \Phi = \sum_{l=1}^{m} \alpha_l \Psi^l \\
\text{s.t.} \quad & \frac{u_l y_j^l + \sum_{k=1,\, k\neq l}^{m} \xi_{lk} z_j^{(l,k)}}{v_l x_j^l + \sum_{k=1,\, k\neq l}^{m} \xi_{kl} z_j^{(k,l)}} \leq 1, \\
& j = 1, 2, \ldots, n; \quad l = 1, 2, \ldots, m, \\
& u_l, v_l, \xi_{lk} \geq 0, \quad l = 1, 2, \ldots, m;\ k = 1, 2, \ldots, m,\ k \neq l.
\end{aligned} \tag{4}$$

Here, $\alpha_l = (v_l x_0^l + \sum_{k=1,\, k\neq l}^{m} \xi_{kl} z_0^{(k,l)}) / \sum_{l=1}^{m} (v_l x_0^l + \sum_{k=1,\, k\neq l}^{m} \xi_{kl} z_0^{(k,l)})$ represents the percentage of the subsystems' inputs in the total inputs.

Then we can get

$$\begin{aligned}
\sum_{l=1}^{m} \alpha_l \Psi^l &= \sum_{l=1}^{m} \frac{v_l x_0^l + \sum_{k=1,\, k\neq l}^{m} \xi_{kl} z_0^{(k,l)}}{\sum_{l=1}^{m} \left(v_l x_0^l + \sum_{k=1,\, k\neq l}^{m} \xi_{kl} z_0^{(k,l)} \right)} \\
&\quad * \frac{u_l y_0^l + \sum_{k=1,\, k\neq l}^{m} \xi_{lk} z_0^{(l,k)}}{v_l x_0^l + \sum_{k=1,\, k\neq l}^{m} \xi_{kl} z_0^{(k,l)}} \\
&= \frac{\sum_{l=1}^{m} \left(u_l y_0^l + \sum_{k=1,\, k\neq l}^{m} \xi_{lk} z_0^{(l,k)} \right)}{\sum_{l=1}^{m} \left(v_l x_0^l + \sum_{k=1,\, k\neq l}^{m} \xi_{kl} z_0^{(k,l)} \right)};
\end{aligned} \tag{5}$$

model (4) can be rewritten as

$$\begin{aligned}\max\quad & \Phi=\sum_{l=1}^{m}\alpha_l\Psi^l=\frac{\sum_{l=1}^{m}\left(u_l y_0^l+\sum_{k=1,k\neq l}^{m}\xi_{lk}z_0^{(l,k)}\right)}{\sum_{l=1}^{m}\left(v_l x_0^l+\sum_{k=1,k\neq l}^{m}\xi_{kl}z_0^{(k,l)}\right)}\\ \text{s.t.}\quad & \frac{u_l y_j^l+\sum_{k=1,k\neq l}^{m}\xi_{lk}z_j^{(l,k)}}{v_l x_j^l+\sum_{k=1,k\neq l}^{m}\xi_{kl}z_j^{(k,l)}}\le 1,\\ & j=1,2,\ldots,n;\quad l=1,2,\ldots,m,\\ & u_l,v_l,\xi_{lk}\ge 0,\quad l=1,2,\ldots,m;\ k=1,2,\ldots,m,\ k\neq l.\end{aligned}\tag{6}$$

To reduce model (6) to an ordinary linear programming problem, we rescale all data by means of the following formula:

$$\begin{aligned}& t=\frac{1}{\sum_{l=1}^{m}\left(v_l x_0^l+\sum_{k=1,k\neq l}^{m}\xi_{kl}z_0^{(k,l)}\right)},\\ & \mu_l=tu_l,\qquad \omega_l=tv_l,\qquad \eta_{lk}=t\xi_{lk},\\ & (l,k=1,2,\ldots,n).\end{aligned}\tag{7}$$

Using these rescaled data in model (6), we obtain

$$\begin{aligned}\max\quad & \Phi=\sum_{l=1}^{m}\left(\mu_l y_0^l+\sum_{k=1,k\neq l}^{m}\eta_{lk}z_0^{(l,k)}\right)\\ \text{s.t.}\quad & \sum_{l=1}^{m}\left(\omega_l x_0^l+\sum_{k=1,k\neq l}^{m}\eta_{kl}z_0^{(k,l)}\right)=1,\\ & \mu_l y_j^l+\sum_{k=1,k\neq l}^{m}\eta_{lk}z_j^{(l,k)}\le\omega_l x_j^l+\sum_{k=1,k\neq l}^{m}\eta_{kl}z_j^{(k,l)},\\ & j=1,2,\ldots,n;\quad l=1,2,\ldots,m,\\ & \mu_l,\omega_l,\eta_{lk}\ge 0,\quad l=1,2,\ldots,m;\ k=1,2,\ldots,m,\ k\neq l.\end{aligned}\tag{8}$$

Obviously, the optimal objective values of both model (6) and model (8) are equal.

The dual problem of model (8) can be expressed as

$$\begin{aligned}\min\quad & \theta\\ \text{s.t.}\quad & \sum_{j=1}^{n}x_j^l\lambda_j^l\le\theta x_0^l,\quad l=1,2,\ldots,m,\\ & \sum_{j=1}^{n}y_j^l\lambda_j^l\ge y_0^l,\quad l=1,2,\ldots,m,\\ & \sum_{j=1}^{n}z_j^{(k,l)}\lambda_j^l-\sum_{j=1}^{n}z_j^{(k,l)}\lambda_j^k\le\theta z_0^{(k,l)}-z_0^{(k,l)},\\ & l=1,2,\ldots,m,\quad k=1,2,\ldots,m,\quad k\neq l,\\ & \lambda_j^l\ge 0,\quad l=1,2,\ldots,m,\ j=1,2,\ldots,n.\end{aligned}\tag{9}$$

3. Property of New Model

Theorem 2. *The optimal solution of model (8) exists and the optimal objective values $\Phi^*\le 1$.*

Proof. See the Appendix. □

Definition 3. The $\mathbf{DMU}_{j_0}$ $(j_0\in\{1,2,\ldots,n\})$ is DEA efficient if the optimal objective value of model (8) is 1 and $\mu_l^*,\omega_l^*>0$, $l=1,2,\ldots,m$.

According to the duality theorem and elastic theorem of linear programming, we can get the following.

Definition 4. The $\mathbf{DMU}_{j_0}$ $(j_0\in\{1,2,\ldots,n\})$ is DEA efficient if the optimal solutions of model (9) which can be represented as θ^*, λ_j^{l*} $(j=1,2,\ldots,n; l=1,2,\ldots,m)$ meet

$$\theta^*=1,\qquad \sum_{j=1}^{n}x_j^l\lambda_j^{l*}=\theta^* x_0^l,\qquad \sum_{j=1}^{n}y_j^l\lambda_j^{l*}=y_0^l,\qquad l=1,2,\ldots,m.\tag{10}$$

Theorem 5. *The $\mathbf{DMU}_{j_0}$ $(j_0\in\{1,2,\ldots,n\})$ is DEA efficient if and only if all subsystems of the $\mathbf{DMU}_{j_0}$ are DEA efficient.*

Proof. See the Appendix. □

4. Equivalence of DEA Efficiency and Pareto Solution

Consider the following multiple objective programming problems:

$$\begin{aligned}\min\quad & F(\mathbf{X},\mathbf{Y})=(\mathbf{X},-\mathbf{Y})\\ & =\left(x^1,x^2,\ldots,x^m;-y^1,-y^2,\ldots,-y^m\right)^T\\ \text{s.t.}\quad & (\mathbf{X},\mathbf{Y})\in T.\end{aligned}\tag{11}$$

Here,

$$T=\left\{(\mathbf{X},\mathbf{Y})\mid\sum_{j=1}^{n}x_j^l\lambda_j^l\le x^l,\ \sum_{j=1}^{n}y_j^l\lambda_j^l\ge y^l,\ \sum_{j=1}^{n}z_j^{(k,l)}\lambda_j^l\le\sum_{j=1}^{n}z_j^{(k,l)}\lambda_j^k,\ l=1,2,\ldots,m;\ k=1,2,\ldots,m,\ k\neq l\right\}\tag{12}$$

is the production possibility set of the matrix-type DEA model.

Definition 6. Let $(\mathbf{X}^*,\mathbf{Y}^*)\in T$ and if there does not exist $(\mathbf{X},\mathbf{Y})\in T$ which makes $F(\mathbf{X},\mathbf{Y})\le F(\mathbf{X}^*,\mathbf{Y}^*)$, $(\mathbf{X}^*,\mathbf{Y}^*)$ is defined as the Pareto solution of model (11).

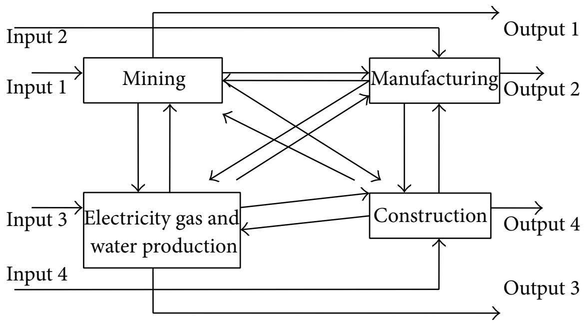

FIGURE 3: The construction of the second industry.

Lemma 7. *If* $(\mathbf{X_0}, \mathbf{Y_0})$ *is the optimal solution of* $\min_{(\mathbf{X},\mathbf{Y})\in T}(\boldsymbol{\omega}^{\mathbf{0T}}\mathbf{X} - \boldsymbol{\mu}^{\mathbf{0T}}\mathbf{Y})$ *and* $(\boldsymbol{\omega}^{\mathbf{0T}}, \boldsymbol{\mu}^{\mathbf{0T}}) > \mathbf{0}$, $(\mathbf{X_0}, \mathbf{Y_0})$ *is the Pareto solution of model (11).*

Proof. See the Appendix. □

Theorem 8. *The* $\mathbf{DMU}_{j_0}$ $(j_0 \in \{1, 2, \ldots, n\})$ *is DEA efficient if and only if* $(\mathbf{X_0}, \mathbf{Y_0})$ *is the Pareto solution of model (11).*

Proof. See the Appendix. □

5. Analysis of Efficiencies of the Second Industry of 27 Provinces in China Based on Input-Output Tables

Input-output tables are fundamental statistical data in economic, social, and environmental issues. Chiang et al. applied black box DEA programs to input-output tables [24]. Jiang et al. analyzed the national economy efficiency through input-output tables with the DEA method [25] and Amatatsu and Ueda applied the new SBM model to input-output tables of 47 prefectures in Japan and assessed the industrial efficiencies of them [21].

In this part, we apply the matrix model to input-output tables. We consider the efficiency scores of the second industry of 27 provinces in China in 2007. Referring to the statistics specification of the National Bureau of China, there are four sectors in the second industry including mining, manufacturing, electricity gas and water production, and construction. Taking Shanxi for example, the data of four sectors input-output table can be listed in Table 1.

The construction of the second industry can be shown in Figure 3. Conventional DEA models construction as a "black box" as shown in Figure 4.

From Figure 3, we can see that the efficiency scores of the second industry of these provinces can be calculated by the matrix-type model. Using model (8), the efficiency scores of the 27 provinces in China can be shown in Table 2. Then, each sector's scores can be obtain by the formula

$$\Phi_l = \mu_l^* y_0^l + \sum_{k=1,\,k\neq l}^{m} \eta_{lk}^* z_0^{(l,k)}, \tag{13}$$

and the scores are also shown in Table 2.

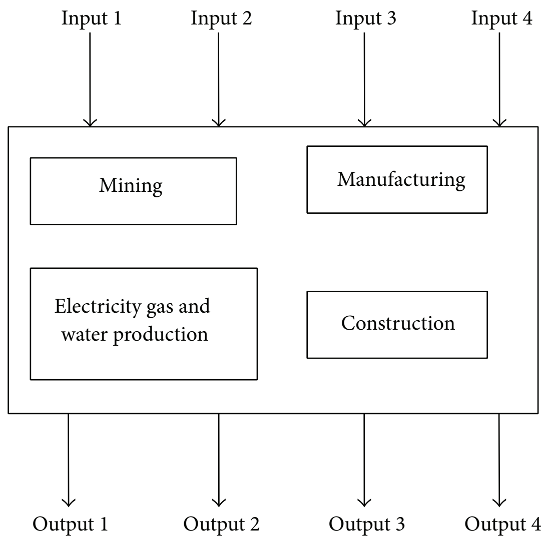

FIGURE 4: The traditional "black model."

It can be seen that the efficiency scores obtained from the matrix-type model are not accurate for ignoring the internal inputs and outputs among the subsystems. There are five DMUs' efficiency scores which are equal to 1 in black model and only the efficiency scores of Henan province are equal to 1 in our new model.

The new model can not only calculate the more accurate efficiency scores of the DMUs but also give the efficiency score of each subsystem which provides detailed information for the decision makers. As Hebei, the efficiency score got by black model is 0.386. Analyzing the efficiency score got by matrix model, not all the sectors are inefficient. The mining and the electricity gas and water production are both DEA efficient, and the low efficiency score is because of the manufacture and constructor.

6. Conclusions

This paper has established a matrix-type DEA model for matrix-type organization and proved the existence of solution. Also, the property of the new model and the equivalence of DEA efficiency and Pareto solutions of corresponding objective programming problem are given. Then the new model has been applied to the input-output tables and got the meaningful conclusions.

A point that should be stressed is that the new model considers the internal linking activities, and the influence of the interaction of the subsystems on the whole efficiency score is represented. Based on model (8), the relative performance of each subsystem can be evaluated. In contrast to the black model, the new model gives more accurate result.

Finally, in addition to input-output tables, cycle industry is also typical matrix-type organization, such as cycle automobile industry which includes production, marketing, repair and recovery, the four sectors are influenced each other. We will give special discussion on the efficiency of this kind of industry in the further study.

Table 1: Example of four sectors of Shanxi's I-O table (unit: billion).

	Mining	Manufacturing	Electricity gas and water production	Construction	Output
Mining	3.68	65.26	11.41	20.2	96.72
Manufacturing	20.9	209.6	3.94	82.2	572.3
Electricity gas and water production	5.49	20.4	8.72	1.85	25.3
Construction	0.18	0.24	0.023	0	293.79
Input	132.4	55.7	24.3	57.3	

Table 2: Efficiency scores obtained from the "black model" and new model.

$\mathbf{DMU}_j$	Black box model	Matrix model Subsystem			
		Primary	Secondary	Tertiary	Quaternary
Anhui	0.26	0.584	0.683	0.518	0.629
Beijing	0.156	0.586	0.604	1	0.025
Chongqing	0.507	0.446	0.634	0.789	0.498
Fujian	0.328	0.456	0.402	0.266	0.674
Gansu	0.143	0.543	0.558	0.171	0.833
Guangdong	0.576	0.655	1	0.301	0.249
Guangxi	0.161	0.535	0.485	0.368	0.762
Guizhou	0.141	0.636	0.482	0.503	0.819
Hainan	1	0.603	0.211	1	0.887
Heilongjiang	1	0.706	0.88	0.904	0.325
Henan	1	1	1	1	1
Hubei	0.313	0.596	1	0.478	1
Hunan	0.089	0.482	0.66	0.188	0.562
Inner Mongolia	0.268	0.439	0.423	0.268	0.496
Jiangsu	0.274	0.732	0.975	0.557	1
Jiangxi	0.32	0.5	0.669	0.915	0.63
Jilin	0.222	0.435	0.514	0.552	1
Liaoning	0.19	0.46	0.405	0.387	0.509
Ningxia	1	0.822	0.871	0.012	0.067
Shaanxi	0.512	0.566	0.976	0.64	0.478
Shandong	0.174	0.61	0.186	0.546	1
Shanxi	1	0.716	0.594	0.934	0.456
Tianjin	0.399	0.476	0.266	0.426	0.585
Xinjiang	0.612	0.447	0.282	0.578	0.372
Yunnan	0.334	0.511	0.619	0.573	0.579
Zhejiang	0.241	0.528	0.93	0.174	0.755

Appendix

Proof of Theorem 2. Let $\overline{\theta} = 1$, $\overline{\lambda}_j^l = \{0, j \neq j_0; 1, j = j_0\}$, $l = 1, 2, \ldots, m$; it is easy to see that $\overline{\theta}_l, \overline{\lambda}_j^l$, $l = 1, 2, \ldots, m$, $j = 1, 2, \ldots, n$, is the feasible solutions of model (9). Referring to the linear programming optimal solution existence theorem, we can know that the optimal solutions of model (9) and model (8) exist. Denote by

$$\begin{aligned}&\omega_1^*, \ldots, \omega_m^*, \mu_1^*, \ldots, \mu_m^*, \eta_{21}^*, \eta_{31}^*, \ldots, \eta_{m1}^*,\\ &\eta_{12}^*, \eta_{32}^*, \ldots, \eta_{m2}^*, \ldots, \eta_{1m}^*, \eta_{2m}^*, \ldots, \eta_{m-1,m}^*\end{aligned} \tag{A.1}$$

the optimal solutions of model (8); we then obtain

$$-\omega_l^* x_0^l + \mu_l^* y_0^l - \sum_{k=1,\, k\neq l}^{m} \eta_{kl}^* z_0^{(k,l)} + \sum_{k=1,\, k\neq l}^{m} \eta_{lk}^* z_0^{(l,k)} \leq 0, \quad l = 1, 2, \ldots, m, \tag{A.2}$$

$$\sum_{l=1}^{m} \left(\omega_l^* x_0^l + \sum_{k=1,\, k\neq l}^{m} \eta_{kl}^* z_0^{(k,l)} \right) = 1. \tag{A.3}$$

From (A.2), we can get

$$\sum_{l=1}^{m}\left(-\omega_l^* x_0^l + \mu_l^* y_0^l - \sum_{k=1,\,k\neq l}^{m} \eta_{kl}^* z_0^{(k,l)} + \sum_{k=1,\,k\neq l}^{m} \eta_{lk}^* z_0^{(l,k)}\right) \leq 0. \tag{A.4}$$

Considering (A.3) and $\sum_{l=1}^{m}\sum_{k=1,k\neq l}^{m}\eta_{kl}^* z_0^{(k,l)} = \sum_{l=1}^{m}\sum_{k=1,k\neq l}^{m}\eta_{lk}^* z_0^{(l,k)}$, (A.4) can be rewritten as

$$1 - \sum_{l=1}^{m}\sum_{k=1,\,k\neq l}^{m} \eta_{kl}^* z_0^{(k,l)} + \sum_{l=1}^{m} \mu_l^* y_0^l \leq 0. \tag{A.5}$$

Then $\Phi^* = \sum_{l=1}^{m}(\mu_l^* y_0^l + \sum_{k=1,k\neq l}^{m}\eta_{lk}^* z_0^{(l,k)}) \leq 1$; the theorem is confirmed. □

Proof of Theorem 5.

Sufficiency. If the subsystems of the $\mathbf{DMU}_{j_0}$ are all DEA efficient, there exist the optimal solutions $u_l^* > 0, v_l^* > 0, \xi_{kl}^* \geq 0$ $(k = 1,2,\ldots,m, k \neq l)$ which make $\Psi^{l*} = 1$ $(l = 1,2,\ldots,m)$ for model (3). Considering the constraint conditions in model (3) and model (4), we can know that $u_l^* > 0, v_l^* > 0, \xi_{kl}^* \geq 0$ $(k = 1,2,\ldots,m, k \neq l)$ are also the feasible solutions of model (4). According to those feasible solutions, the value of model (4) is $\Phi^* = \sum_{l=1}^{m}\alpha_l \Psi^{l*} = \sum_{l=1}^{m}\alpha_l = 1$.

Combined with Theorem 2, $\Phi^* = 1$ is the optimal solutions of model (4) and is also the optimal solutions of model (8); then the $\mathbf{DMU}_{j_0}$ $(j_0 \in \{1,2,\ldots,n\})$ is DEA efficient.

Necessity. If the $\mathbf{DMU}_{j_0}$ $(j_0 \in \{1,2,\ldots,n\})$ is DEA efficient, the optimal solutions $u_l^* > 0, v_l^* > 0, \xi_{kl}^* \geq 0, l = 1,2,\ldots,m, k = 1,2,\ldots,m, k \neq l$, of model (4) exist which make $\Phi^* = \sum_{l=1}^{m}\alpha_l \widehat{\Psi}^{l*} = 1$.

According to $\sum_{l=1}^{m}\alpha_l = 1$ and $\widehat{\Psi}^{l*} \leq 1, l = 1,2,\ldots,m$, we can get $\widehat{\Psi}^{l*} = 1, l = 1,2,\ldots,m$. Considering the constraint conditions in model (3) and model (4), we know that $u_l^* > 0, v_l^* > 0, \xi_{kl}^* \geq 0, k = 1,2,\ldots,m, k \neq l$, are the feasible solutions of model (3) when $l = 1,2,\ldots,m$, respectively. Then there are $\Psi^{l*} = \widehat{\Psi}^{l*} = 1, l = 1,2,\ldots,m$, and the subsystems of the $\mathbf{DMU}_{j_0}$ $(j_0 \in \{1,2,\ldots,n\})$ are all DEA efficient. □

Proof of Lemma 7. If $(\mathbf{X_0},\mathbf{Y_0})$ is not the Pareto solution of model (11), then there exists $(\widehat{\mathbf{X}},\widehat{\mathbf{Y}}) \in T$ which makes $\begin{pmatrix}\widehat{\mathbf{X}}\\ -\widehat{\mathbf{Y}}\end{pmatrix} \leq \begin{pmatrix}\mathbf{X_0}\\ -\mathbf{Y_0}\end{pmatrix}$. Let $(\boldsymbol{\omega}^{\mathbf{0T}},\boldsymbol{\mu}^{\mathbf{0T}}) > \mathbf{0}$; we have

$$\left(\boldsymbol{\omega}^{\mathbf{0T}},\boldsymbol{\mu}^{\mathbf{0T}}\right)\left[\begin{pmatrix}\widehat{\mathbf{X}}\\ -\widehat{\mathbf{Y}}\end{pmatrix} - \begin{pmatrix}\mathbf{X_0}\\ -\mathbf{Y_0}\end{pmatrix}\right] \leq 0. \tag{A.6}$$

Then $\boldsymbol{\omega}^{\mathbf{0T}}\widehat{\mathbf{X}} - \boldsymbol{\mu}^{\mathbf{0T}}\widehat{\mathbf{Y}} \leq \boldsymbol{\omega}^{\mathbf{0T}}\mathbf{X_0} - \boldsymbol{\mu}^{\mathbf{0T}}\mathbf{Y}_0$, which is contrary to the hypothesis that $(\mathbf{X_0},\mathbf{Y_0})$ is the optimal solution of $\min_{(X,Y)\in T}(\boldsymbol{\omega}^{\mathbf{0T}}\mathbf{X} - \boldsymbol{\mu}^{\mathbf{0T}}\mathbf{Y})$. □

Proof of Theorem 8.

Sufficiency. If the $\mathbf{DMU}_{j_0}$ is DEA efficient, the optimal solutions of model (8) exist which are denoted by $\omega_l^* > 0$, $\mu_l^* > 0, \eta_{kl}^* \geq 0$ $(k = 1,2,\ldots,m, k \neq l)$ and the corresponding optimal value is $\Phi^* = 1$. Then,

$$\sum_{l=1}^{m}\left(\mu_l^* y_0^l + \sum_{k=1,\,k\neq l}^{m}\eta_{lk}^* z_0^{(l,k)}\right) = 1, \tag{A.7}$$

$$\sum_{l=1}^{m}\left(\omega_l^* x_0^l + \sum_{k=1,\,k\neq l}^{m}\eta_{kl}^* z_0^{(k,l)}\right) = 1, \tag{A.8}$$

$$\begin{gathered} -\omega_l^* x_j^l + \mu_l^* y_j^l - \sum_{k=1,\,k\neq l}^{m}\eta_{kl}^* z_j^{(k,l)} + \sum_{k=1,\,k\neq l}^{m}\eta_{lk}^* z_j^{(l,k)} \leq 0, \\ l = 1,2,\ldots,m; \quad j = 1,2,\ldots,n. \end{gathered} \tag{A.9}$$

Let $\beta_j^l \geq 0$, $j = 1,2,\ldots,n$, $l = 1,2,\ldots,m$, and

$$\begin{gathered} \sum_{j=1}^{n} z_j^{(k,l)}\beta_j^l \leq \sum_{j=1}^{n} z_j^{(k,l)}\beta_j^k, \\ l = 1,2,\ldots,m; \quad k = 1,2,\ldots,m, \quad k \neq l. \end{gathered} \tag{A.10}$$

We can rewrite (A.9) as

$$\begin{aligned} \sum_{j=1}^{n}\sum_{l=1}^{m}\Bigg(&-\omega_l^* x_j^l\beta_j^l + \mu_l^* y_j^l\beta_j^l - \sum_{k=1,\,k\neq l}^{m}\eta_{kl}^* z_j^{(k,l)}\beta_j^l \\ &+ \sum_{k=1,\,k\neq l}^{m}\eta_{lk}^* z_j^{(l,k)}\beta_j^l\Bigg) \leq 0. \end{aligned} \tag{A.11}$$

Arranging (A.11) and considering

$$\begin{aligned} &\sum_{j=1}^{n}\sum_{l=1}^{m}\left(-\sum_{k=1,\,k\neq l}^{m}\eta_{kl}^* z_j^{(k,l)}\beta_j^l + \sum_{k=1,\,k\neq l}^{m}\eta_{lk}^* z_j^{(l,k)}\beta_j^l\right) \\ &\quad = \sum_{j=1}^{n}\left(-\sum_{l=1}^{m}\sum_{k=1,\,k\neq l}^{m}\eta_{kl}^* z_j^{(k,l)}\beta_j^l + \sum_{l=1}^{m}\sum_{k=1,\,k\neq l}^{m}\eta_{lk}^* z_j^{(l,k)}\beta_j^l\right) \\ &\quad = \sum_{j=1}^{n}\left(\sum_{l=1}^{m}\sum_{k=1,\,k\neq l}^{m}\eta_{kl}^* z_j^{(k,l)}\left(-\beta_j^l + \beta_j^k\right)\right) \geq 0, \end{aligned} \tag{A.12}$$

we can get $\sum_{j=1}^{n}\sum_{l=1}^{m}(-\omega_l^* x_j^l\beta_j^l + \mu_l^* y_j^l\beta_j^l) \leq 0$.

Applying (A.7) and equation $\sum_{l=1}^{m}\sum_{k=1,k\neq l}^{m}\eta_{lk}^* z_0^{(l,k)} = \sum_{l=1}^{m}\sum_{k=1,k\neq l}^{m}\eta_{kl}^* z_0^{(k,l)}$ to (A.4), the equality $-\sum_{l=1}^{m}\omega_l^* x_0^l + \sum_{l=1}^{m}\mu_l^* y_0^l = 0$ is gotten.

That is,

$$\sum_{j=1}^{n}\sum_{l=1}^{m}\left(\omega_l^* x_j^l\beta_j^l - \mu_l^* y_j^l\beta_j^l\right) \geq \sum_{l=1}^{m}\omega_l^* x_0^l - \sum_{l=1}^{m}\mu_l^* y_0^l. \tag{A.13}$$

So, $\forall(\mathbf{X},\mathbf{Y}) \in T$ we can get

$$\begin{aligned} \boldsymbol{\omega}^{*T}X - \boldsymbol{\mu}^{*T}Y &\geq \boldsymbol{\omega}^{*T}\sum_{j=1}^{n} x_j^l\lambda_j^l - \boldsymbol{\mu}^{*T}\sum_{j=1}^{n} y_j^l\lambda_j^l \\ &\geq \boldsymbol{\omega}^{*T}X_0 - \boldsymbol{\mu}^{*T}Y_0, \end{aligned} \tag{A.14}$$

where $\boldsymbol{\omega}^* = (\omega_1^*, \omega_2^*, \ldots, \omega_m^*)^T > 0$; $\boldsymbol{\mu}^* = (\mu_1^*, \mu_2^*, \ldots, \mu_m^*)^T > 0$. Then $(\mathbf{X_0}, \mathbf{Y_0})$ is the optimal solution of

$$\begin{aligned} \min \quad & \boldsymbol{\omega}^{*\mathbf{T}}\mathbf{X} - \boldsymbol{\mu}^{*\mathbf{T}}\mathbf{Y} \\ \text{s.t.} \quad & (\mathbf{X}, \mathbf{Y}) \in T. \end{aligned} \tag{A.15}$$

According to Lemma 7, $(\mathbf{X_0}, \mathbf{Y_0})$ is also the Pareto solution of model (11).

Necessity. We suppose $(\mathbf{X_0}, \mathbf{Y_0})$ is the Pareto solution of model (11) and the $\mathbf{DMU}_{j_0}$ is not DEA efficient. The following situations can be gotten as follows.

(a) The optimal solution of model (9) is less than 1; that is, $\theta^* < 1$.

(b) The optimal solution of model (9) is 1 and there exists at least 1 serial number i which belongs to the array $\{1, 2, \ldots, m\}$ and $\sum_{j=1}^n x_j^i \lambda_j^{i*} < \theta^* x_0^i$.

(c) The optimal solution of model (9) is 1 and there exists at least 1 serial number i which belongs to the array $\{1, 2, \ldots, m\}$ and $\sum_{j=1}^n y_j^i \lambda_j^{i*} > y_0^i$.

Now, we make the proof, respectively, according to the situations above.

(a) Let $\widehat{x}_0^l = \theta^* x_0^l < x_0^l$, $\widehat{\mathbf{X}}_\mathbf{0} = \{\widehat{x}_0^1, \ldots, \widehat{x}_0^l, \ldots \widehat{x}_0^n\}$; then $\widehat{\mathbf{X}}_\mathbf{0} < \mathbf{X_0}$. Considering the constraint conditions in model (9), we can get

$$\begin{gathered} \sum_{j=1}^n x_j^l \lambda_j^{*l} \le \theta^* x_0^l = \widehat{x}_0^l, \quad l = 1, 2, \ldots m, \\ \sum_{j=1}^n y_j^l \lambda_j^{l*} \ge y_0^l, \quad l = 1, 2, \ldots m, \\ \sum_{j=1}^n z_j^{(k,l)} \lambda_j^{l*} - \sum_{j=1}^n z_j^{(k,l)} \lambda_j^{k*} \le \theta^* z_0^{(k,l)} - z_0^{(k,l)} \le 0, \\ l = 1, 2, \ldots, m, \quad k = 1, 2, \ldots, m, \quad k \ne l. \end{gathered} \tag{A.16}$$

Then $(\widehat{\mathbf{X}}_\mathbf{0}, \mathbf{Y_0})$ is the feasible solution of model (11) and $\begin{pmatrix} \widehat{\mathbf{X}}_\mathbf{0} \\ -\mathbf{Y_0} \end{pmatrix} \le \begin{pmatrix} \mathbf{X_0} \\ -\mathbf{Y_0} \end{pmatrix}$. The conclusion is contrary to the hypothesis before.

(b) There exists $s > 0$ and $\sum_{j=1}^n x_j^i \lambda_j^{i*} + s = x_0^i$. Let $\widehat{x}_0^i = x_0^i - s < x_0^l$ and $\widehat{\mathbf{X}}_\mathbf{0} = \{x_0^1, \ldots, \widehat{x}_0^i, \ldots x_0^n\}$; then we have $\widehat{\mathbf{X}}_\mathbf{0} \le \mathbf{X_0}$. Considering the constraint conditions in model (9), we can get

$$\begin{gathered} \sum_{j=1}^n x_j^l \lambda_j^{*l} \le \theta^* x_0^l = x_0^l, \quad l = 1, 2, \ldots, m, \; l \ne i, \\ \sum_{j=1}^n x_j^i \lambda_j^{*i} = \widehat{x}_0^i, \\ \sum_{j=1}^n y_j^l \lambda_j^{l*} \ge y_0^l, \quad l = 1, 2, \ldots, m, \\ \sum_{j=1}^n z_j^{(k,l)} \lambda_j^{l*} - \sum_{j=1}^n z_j^{(k,l)} \lambda_j^{k*} \le \theta^* z_0^{(k,l)} - z_0^{(k,l)} \le 0, \\ l = 1, 2, \ldots, m, \quad k = 1, 2, \ldots, m, \quad k \ne l. \end{gathered} \tag{A.17}$$

Then $(\widehat{\mathbf{X}}_\mathbf{0}, \mathbf{Y_0})$ is the feasible solution of model (9) and $\begin{pmatrix} \widehat{\mathbf{X}}_\mathbf{0} \\ -\mathbf{Y_0} \end{pmatrix} \le \begin{pmatrix} \mathbf{X_0} \\ -\mathbf{Y_0} \end{pmatrix}$. The conclusion is contrary to the hypothesis before.

(c) There exists $s > 0$ and $\sum_{j=1}^n y_j^i \lambda_j^{i*} - s = y_0^i$. Let $\widehat{y}_0^i = y_0^i + s > y_0^i$ and $\widehat{\mathbf{Y}}_\mathbf{0} = \{y_0^1, \ldots, \widehat{y}_0^i, \ldots, y_0^n\}$; then we have $\widehat{\mathbf{Y}}_\mathbf{0} \ge \mathbf{Y_0}$. Considering the constraint conditions in model (9), we can get

$$\begin{gathered} \sum_{j=1}^n x_j^l \lambda_j^{*l} \le \theta^* x_0^l = x_0^l, \quad l = 1, 2, \ldots, m, \\ \sum_{j=1}^n y_j^l \lambda_j^{l*} \ge y_0^l, \quad l = 1, 2, \ldots, m, \; l \ne i, \\ \sum_{j=1}^n y_j^i \lambda_j^{i*} = \widehat{y}_0^i, \quad l = 1, 2, \ldots, m, \\ \sum_{j=1}^n z_j^{(k,l)} \lambda_j^{l*} - \sum_{j=1}^n z_j^{(k,l)} \lambda_j^{k*} \le \theta^* z_0^{(k,l)} - z_0^{(k,l)} \le 0, \\ l = 1, 2, \ldots, m, \quad k = 1, 2, \ldots, m, \quad k \ne l. \end{gathered} \tag{A.18}$$

$(\mathbf{X_0}, \widehat{\mathbf{Y}}_\mathbf{0})$ is the feasible solution of model (11) and $\begin{pmatrix} \mathbf{X_0} \\ -\widehat{\mathbf{Y}}_\mathbf{0} \end{pmatrix} \le \begin{pmatrix} \mathbf{X_0} \\ -\mathbf{Y_0} \end{pmatrix}$. The conclusion is contrary to the hypothesis before.

Then the hypothesis is not set up, and if $(\mathbf{X_0}, \mathbf{Y_0})$ is the Pareto solution of model (11), the $\mathbf{DMU}_{j_0}$ $(j_0 \in \{1, 2, \ldots n\})$ is DEA efficient. □

Conflict of Interests

The authors declare that there is no conflict of interests regarding the publication of this paper.

References

[1] A. Charnes, W. W. Cooper, and E. Rhodes, "Measuring the efficiency of decision making units," *European Journal of Operational Research*, vol. 2, no. 6, pp. 429–444, 1978.

[2] A. Charnes, W. W. Cooper, B. Golany, L. Seiford, and J. Stutz, "Foundations of data envelopment analysis for Pareto-Koopmans efficient empirical production functions," *Journal of Econometrics*, vol. 30, no. 1-2, pp. 91–107, 1985.

[3] A. Charnes, W. Cooper, and Q. L. Wei, "A semi-infinite multicriteria programming approach to Data Envelopment Analysis," *Management Science*, vol. 9, pp. 1078–1092, 1984.

[4] J. K. Sengupta, "A fuzzy systems approach in data envelopment analysis," *Computers & Mathematics with Applications*, vol. 24, no. 8-9, pp. 259–266, 1992.

[5] T. R. Sexton and H. F. Lewis, "Two-stage DEA: an application to major league baseball," *Journal of Productivity Analysis*, vol. 19, no. 2-3, pp. 227–249, 2003.

[6] R. Färe and S. Grosskopf, "Network DEA," *Socio-Economic Planning Sciences*, vol. 34, no. 1, pp. 35–49, 2000.

[7] P.-C. Chen, C.-C. Chang, M.-M. Yu, and S.-H. Hsu, "Performance measurement for incineration plants using multi-activity network data envelopment analysis: the case of Taiwan," *Journal of Environmental Management*, vol. 93, no. 1, pp. 95–103, 2012.

[8] Y. Chen, L. Liang, F. Yang, and J. Zhu, "Evaluation of information technology investment: a data envelopment analysis approach," *Computers and Operations Research*, vol. 33, no. 5, pp. 1368–1379, 2006.

[9] Y. Chen, L. Liang, and J. Zhu, "Equivalence in two-stage DEA approaches," *European Journal of Operational Research*, vol. 193, no. 2, pp. 600–604, 2009.

[10] H. Fukuyama and W. L. Weber, "A slacks-based inefficiency measure for a two-stage system with bad outputs," *Omega*, vol. 38, no. 5, pp. 398–409, 2010.

[11] C. Kao and S.-N. Hwang, "Efficiency decomposition in two-stage data envelopment analysis: an application to non-life insurance companies in Taiwan," *European Journal of Operational Research*, vol. 185, no. 1, pp. 418–429, 2008.

[12] C. Kao, "Efficiency decomposition for general multi-stage systems in data envelopment analysis," *European Journal of Operational Research*, vol. 232, no. 1, pp. 117–124, 2014.

[13] L. Liang, Z.-Q. Li, W. D. Cook, and J. Zhu, "Data envelopment analysis efficiency in two-stage networks with feedback," *IIE Transactions*, vol. 43, no. 5, pp. 309–322, 2011.

[14] Q. L. Wei and T.-S. Chang, "Optimal system design series-network DEA models," *Journal of the Operational Research Society*, vol. 62, no. 6, pp. 1109–1119, 2011.

[15] G. Bi, J. Ding, Y. Luo, and L. Liang, "Resource allocation and target setting for parallel production system based on DEA," *Applied Mathematical Modelling*, vol. 35, no. 9, pp. 4270–4280, 2011.

[16] R. Y. Duan, P. Tian, and W. P. Zhang, "DEA models with independent subsystems and their application," *Journal of Industrial Engineering/Engineering Management*, vol. 20, no. 1, pp. 27–31, 2006.

[17] C. Kao, "Efficiency measurement for parallel production systems," *European Journal of Operational Research*, vol. 196, no. 3, pp. 1107–1112, 2009.

[18] C. Kao and P.-H. Lin, "Qualitative factors in data envelopment analysis: a fuzzy number approach," *European Journal of Operational Research*, vol. 211, no. 3, pp. 586–593, 2011.

[19] N. Rogge and S. de Jaeger, "Evaluating the efficiency of municipalities in collecting and processing municipal solid waste: a shared input DEA-model," *Waste Management*, vol. 32, no. 10, pp. 1968–1978, 2012.

[20] Y. S. Yang, B. J. Ma, and M. Koike, "Efficiency-measuring DEA model for production syst em with k independent subsystems," *Journal of the Operations Research Society of Japan*, vol. 43, no. 3, pp. 343–354, 2000.

[21] H. Amatatsu and T. Ueda, "Input-output tables and network DEA: efficiencies of the 47 prefectures of Japan," in *Proceedings of the DEA Symposium*, Report, Osaka University, 2009.

[22] C.-H. Wang, Y.-H. Lu, and C.-W. Huang, "R&D, productivity, and market value: an empirical study from high-technology firms," *Omega*, vol. 41, no. 1, pp. 143–155, 2013.

[23] Y. Zhao, K. Triantis, P. Murray-Tuite, and P. Edara, "Performance measurement of a transportation network with a downtown space reservation system: a network-DEA approach," *Transportation Research Part E: Logistics and Transportation Review*, vol. 47, no. 6, pp. 1140–1159, 2011.

[24] Y.-H. Chiang, E. W.-L. Cheng, and B.-S. Tang, "Examining repercussions of consumptions and inputs placed on the construction sector by use of I-O tables and DEA," *Building and Environment*, vol. 41, no. 1, pp. 1–11, 2006.

[25] B. Jiang, S. Liu, and Q. Wang, "Integration of DEA with input-output tables for national economy efficiency analysis," *International Journal of Services*, vol. 1, pp. 88–97, 2006.

Hindawi Publishing Corporation
Mathematical Problems in Engineering
Volume 2015, Article ID 549347, 9 pages
http://dx.doi.org/10.1155/2015/549347

Research Article

Guaranteed Cost Fault-Tolerant Control for Networked Control Systems with Sensor Faults

Qixin Zhu,[1,2] Kaihong Lu,[2] Guangming Xie,[3] and Yonghong Zhu[4]

[1] *School of Mechanical Engineering, Suzhou University of Science and Technology, Suzhou 215009, China*
[2] *School of Electronical and Electronic Engineering, East China Jiaotong University, Nanchang 330013, China*
[3] *Department of Mechanics and Engineering Science, Peking University, Beijing 100871, China*
[4] *School of Mechanical and Electronic Engineering, Jingdezhen Ceramic Institute, Jingdezhen 333001, China*

Correspondence should be addressed to Qixin Zhu; bob21cn@163.com

Received 7 June 2014; Accepted 17 November 2014

Academic Editor: Jinhui Zhang

For the large scale and complicated structure of networked control systems, time-varying sensor faults could inevitably occur when the system works in a poor environment. Guaranteed cost fault-tolerant controller for the new networked control systems with time-varying sensor faults is designed in this paper. Based on time delay of the network transmission environment, the networked control systems with sensor faults are modeled as a discrete-time system with uncertain parameters. And the model of networked control systems is related to the boundary values of the sensor faults. Moreover, using Lyapunov stability theory and linear matrix inequalities (LMI) approach, the guaranteed cost fault-tolerant controller is verified to render such networked control systems asymptotically stable. Finally, simulations are included to demonstrate the theoretical results.

1. Introduction

Feedback control systems wherein the control loops are closed through a real-time network are called networked control systems (NCS) [1]. Due to their suitable and flexible structure, NCS is frequently encountered in practice for such fields as information technology, life science, and aeronautical and space technologies. However, there exist not only induced delay, data packet loss, and sequence disordering in NCS, but also actuators or sensors faults, which could cause negative impact on the performance of the system and even lead to system instability. Recently, the fault-tolerant control of NCS has become a new popular issue in the control field [2–9].

A fault-tolerant control algorithm for networked control systems is proposed based on Lyapunov stability theorem by Zheng and Fang [2]. Qu et al. have devised a fault-tolerant robust control for a class of nonlinear uncertain systems with possible sensor faults considered and developed a robust measure to identify the stability- and performance-vulnerable failures [3]. The faults of each sensor or actuator were taken as occurring randomly by Tian et al. [5], and their failure rates are governed by two sets of unrelated random variables satisfying certain probabilistic distribution. A sufficient condition is given by Zhang et al. [7], which could guarantee the stability of NCS with sensor failures or actuator failures and guarantee robustness to parameter uncertainties, but the issue of guaranteed cost is not discussed. A robust fault-tolerant control based on the integrity control theory when actuator faults occur is discussed by Zhang et al. [9]. Wang et al. [10] investigated the issue of integrity against actuator faults for NCS under variable-period sampling, in which the existence conditions of guaranteed cost faults-tolerant control law are testified in terms of Lyapunov stability theory, but not referring to the effects of uncertain parameters.

Almost all literatures above consider the faults in some special cases. However, in practical application, because of large scale and complicated structure of NCS, the faults could vary from time to time when the system works in a poor environment. It is of great importance to explore a reasonable control method to guarantee the performance of NCS when

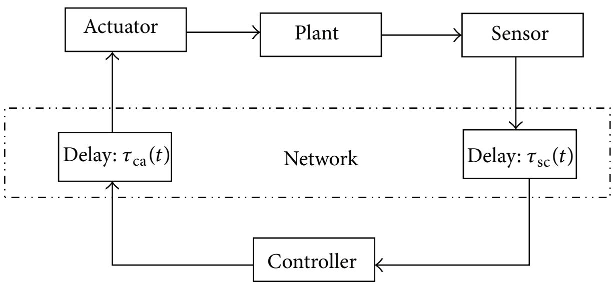

Figure 1: The structure of networked control systems.

time-varying faults occur. This motivates us to conduct the research work.

Based on the network transmission environment and sampling theory, the networked control systems are firstly modeled as a discrete-time closed-loop system by considering the time-varying transmission delay and sensor faults simultaneously. The model of NCS is related to the boundary values of the sensor faults. Using Lyapunov stability theory, a sufficient condition is given, which can render the closed-loop NCS asymptotically stable and can guarantee it to meet the requirements of performance indicator (the upper bound of cost function). Based on LMI, the method of designing guaranteed cost fault-tolerant controller of NCS with time-varying faults is proposed in this paper.

2. Modeling of Networked Control Systems with Sensor Faults

A typical structure of NCS is shown in Figure 1.

In Figure 1, τ_{sc} represents the transmission delay from sensor to the controller, while τ_{ca} represents that from controller to the actuator. When the controller is static, the induced-delay time of system can be lumped as $\tau = \tau_{\mathrm{sc}} + \tau_{\mathrm{ca}}$.

A linear control plant is described by state equation as follows:

$$\begin{aligned} \dot{x}(t) &= A_o x(t) + B_o u(t) \\ y(t) &= C_o x(t) + D_o u(t), \end{aligned} \tag{1}$$

where $x \in R^n$, $u \in R^m$, and $y \in R^r$ represent state, input, and output vectors separately, while A_o, B_o, C_o, and D_o are matrices with appropriate dimensions.

In order to facilitate the model, some rational assumptions for networked control systems are introduced as follows.

(A1) Single data package is transmitted. The packet loss and sequence disorder are not taken into consideration during the transmission process.

(A2) Uncertain time delay exists during the data transmission process. But time delay is bounded, and the maximum time delay does not exceed one sampling period; namely, $\tau \in [0, T]$, where T is the sampling period.

(A3) Sensor is clock driving; controller and actuator are all event driving.

Based on the above assumptions (see Figure 2), within a sampling period, the system input is not a constant value but is a piecewise constant. In a cycle, system input can be described as

$$u(t) = \begin{cases} u(k-1), & t_k < t \le t_k + \tau_k \\ u(k), & t_k + \tau_k < t \le t_k + T, \end{cases} \tag{2}$$

where t_k is the kth cycle sampling time and τ_k is the kth cycle delay.

The discrete-time model of system (1) can be obtained as follows:

$$\begin{aligned} x(k+1) &= Ax(k) + B_1(\tau_k) u(k) + B_2(\tau_k) u(k-1) \\ &= Ax(k) + B_1(\tau_k) u(k) + (B - B_1(\tau_k)) u(k-1), \end{aligned} \tag{3}$$

where $A = e^{A_o T}$, $B_1(\tau_k) = \int_0^{T-\tau_k} e^{A_o t} B_o\,dt$, $B_2(\tau_k) = \int_{T-\tau_k}^{T} e^{A_o t} B_o\,dt$, and $B = \int_0^T e^{A_o t} B_o\,dt$.

Moreover, according to the Jordan canonical form, matrix A_0 can be described as follows:

$$A_0 = \Lambda \operatorname{diag}\left(0_{p_1 \times p_1}, \widehat{J}_{p_2 \times p_2}, \check{J}_{p_3 \times p_3}\right) \Lambda^{-1}, \tag{4}$$

where $0 \le p_i \le n$ $(i = 1, 2, 3)$, $p_1 + p_2 + p_3 = n$; $\widehat{J}$ is Jordan block that is a diagonal matrix consisting of the different eigenvalues with a total of p_2, denoted by $\lambda_1, \lambda_2, \ldots, \lambda_{p_2}$, while $\check{J}$ is Jordan block for the repeated eigenvalues with a total of p_3, denoted by λ_0; matrix Λ is the transformational matrix of Jordan canonical form for matrix A_0.

Correspondingly, the matrix B_1 with the variable τ_k can be equivalently calculated as

$$\begin{aligned} B_1(\tau_k) = \Lambda \operatorname{diag}\Bigg(& T_s - \tau_k, \ldots, T_s - \tau_k, \frac{e^{\lambda_1 (T_s - \tau_k)} - 1}{\lambda_1}, \\ & \ldots, \frac{e^{\lambda_{p_2} (T_s - \tau_k)} - 1}{\lambda_{p_2}}, J \Bigg) \Lambda^{-1} B_0, \end{aligned} \tag{5}$$

where

$$J = \begin{bmatrix} \dfrac{e^{\lambda_0 (T_s - \tau_k)} - 1}{\lambda_0} & \displaystyle\int_0^{T_s - \tau_k} t e^{\lambda_0}\,dt & \cdots & \dfrac{\int_0^{T_s - \tau_k} t e^{\lambda_0}\,dt}{(p_3 - 1)!} \\ 0 & \dfrac{e^{\lambda_0 (T_s - \tau_k)} - 1}{\lambda_0} & \cdots & \dfrac{\int_0^{T_s - \tau_k} t e^{\lambda_0}\,dt}{(p_3 - 2)!} \\ \vdots & \vdots & \ddots & \vdots \\ 0 & 0 & \cdots & \dfrac{e^{\lambda_0 (T_s - \tau_k)} - 1}{\lambda_0} \end{bmatrix}_{p_3 \times p_3}. \tag{6}$$

Here a set of real numbers which are not equal to zero are denoted by $\alpha, \alpha_1, \alpha_2, \ldots, \alpha_{p_2}, \alpha_0$.

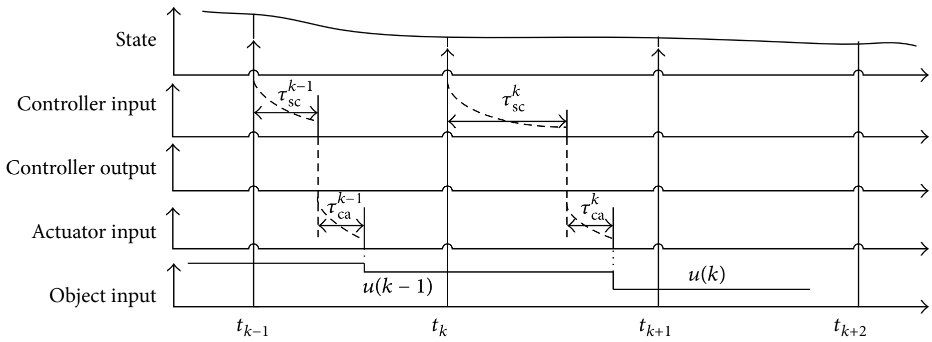

Figure 2: Timing diagram of signals transmitting in NCS.

And we define

$$E = \Lambda^{-1} B_0$$

$$F(\tau_k) = \operatorname{diag}\left(\frac{T_s - \tau_k}{\alpha}, \dots, \frac{T_s - \tau_k}{\alpha}, \frac{e^{\lambda_1 (T_s - \tau_k)} - 1}{\alpha_1 \lambda_1}, \dots, \frac{e^{\lambda_{p_2} (T_s - \tau_k)} - 1}{\alpha_{p_2} \lambda_{p_2}}, \frac{J}{\alpha_0}\right). \quad (7)$$

From (7), we know appropriate values of $\alpha, \alpha_1, \alpha_2, \dots, \alpha_{p_2}, \alpha_0$ always can be chosen to satisfy $F^T(\tau_k)F(\tau_k) \le I^{n\times n}$.

Comparing equality (7) with equality (5), we only need to define $D = \Lambda \operatorname{diag}(\alpha, \alpha_1, \alpha_2, \dots, \alpha_{p_2}, \alpha_0)$; the matrix $B_1(\tau_k)$ can be expressed as

$$B_1(\tau_k) = DF(\tau_k)E. \quad (8)$$

Submitting equality (8) into equality (3), the following model can be obtained:

$$x(k+1) = Ax(k) + DF(\tau_k)Eu(k) + (B - DF(\tau_k)E)u(k-1). \quad (9)$$

Assume that the system is fully measurable; state feedback is introduced as follows:

$$u(k) = Kx(k). \quad (10)$$

Considering the sensor faults that may occur, the controller is expanded as

$$u^F(k) = KG(k)x(k), \quad (11)$$

where $u^F(k) = [u_1^F(k), u_2^F(k), \dots, u_m^F(k)]^T$ represents faulty signal. $G(k) = \operatorname{diag}(g_1(k), g_2(k), \dots, g_m(k))$; $g_i = 0$ represents the fact that sensor i faults occur; $g_i = 1$ represents the fact that sensor i is normal; $0 \le g_i \le 1$ represents the fact that partial faults occur at sensor i. When $G = I$, it represents the fact that all sensors are normal. The situation that all actuators' failure occurs at the same time is not taken into consideration here.

Moreover, the boundaries of faults usually can be measured in the practical work. The following definition is presented.

Definition 1. The upper bound of fault matrices is defined as follows:

$$G_u = \operatorname{diag}(g_{u1}, g_{u2}, \dots, g_{un}), \quad 1 \ge g_{ui} > 0, \quad (12)$$

while the lower bound of fault matrices is defined as follows:

$$G_l = \operatorname{diag}(g_{l1}, g_{l2}, \dots, g_{ln}), \quad 1 > g_{li} \ge 0. \quad (13)$$

That is to say, $G(k) \in [G_l, G_u]$, which is time-varying. The mean value of matrices in Definition 1 can also be obtained as

$$G_0 = \operatorname{diag}(g_{01}, g_{02}, \dots, g_{0n}), \qquad g_{0i} = \frac{g_{ui} + g_{li}}{2}; \quad (14)$$

furthermore, the following matrices are introduced:

$$L(k) = \operatorname{diag}(l_1(k), l_2(k), \dots, l_n(k)), \qquad l_i(k) = \frac{g_i(k) - g_{0i}}{g_{0i}}. \quad (15)$$

Obviously, we have

$$-1 \le \frac{g_{li} - g_{0i}}{g_{0i}} \le l_i(k) = \frac{g_i(k) - g_{0i}}{g_{0i}} \le \frac{g_{ui} - g_{0i}}{g_{0i}} = \frac{g_{ui} - g_{li}}{g_{ui} + g_{li}} \le 1. \quad (16)$$

Based on (16), we have $-I_{n\times n} \le L(k) \le I_{n\times n}$. Based on (16), the following can be obtained:

$$g_i = g_{0i}(1 + l_i), \quad i = 1, 2, \dots n; \qquad \text{Naturally, we have } G = G_0(I + L). \quad (17)$$

The model of closed-loop systems with sensor faults can be obtained as

$$x(k+1) = Ax(k) + DF(\tau_k)EKG_0(I + L(k))x(k) + (B - DF(\tau_k)E)KG_0(I + L(k-1))x(k-1). \quad (18)$$

Remark 2. The NCS with time-varying delay and sensor faults is modeled as a closed-loop system (18) with the uncertain parameter $F(\tau_k)$ and time-varying parameter $L(k)$; unlike the previous models as [5], this model is related to the boundary values of the faults G_u and G_l. Moreover, according to the expression of matrix G_0, we undoubtedly know it is invertible.

3. The Design of Guaranteed Cost Fault-Tolerant Control

For the system model (18) established above, the cost function is given as follows:

$$J_\infty = \sum_{k=0}^{\infty} \left\{ x^T(k) Q x(k) + \left[K G_0 (I+L) x(k) \right]^T \times R K G_0 (I+L) x(k) \right\}, \tag{19}$$

where Q and R are symmetric positive definite matrices.

To analyze the stability of the system expediently, the following lemmas are introduced.

Lemma 3 (Schur complement). *For a symmetric matrix* $S = \begin{bmatrix} S_{11} & S_{12} \\ S_{21} & S_{22} \end{bmatrix}$, *where* $S_{11} = S_{11}^T$, $S_{12}^T = S_{21}$, *and* $S_{22} = S_{22}^T$, *the following three conditions are equivalent:*

(1) $S < 0$;

(2) $S_{11} < 0$, $S_{22} - S_{12}^T S_{11}^{-1} S_{12} < 0$;

(3) $S_{22} < 0$, $S_{11} - S_{12} S_{22}^{-1} S_{12}^T < 0$.

Lemma 4 (see [11]). *For any matrices* W, M, N, *or* $F(t)$ *with* $F^T F \le I$ *and any scalar* $\varepsilon > 0$, *the following inequality holds.* $W + MF(t)N + N^T F^T(t) M^T \le W + \varepsilon M M^T + \varepsilon^{-1} N^T N$.

Theorem 5. *Given symmetric positive definite matrices* Q, R *and gain matrix* K, *if symmetric positive definite matrices* P *and* S *exist, as well as a scalar* $\varepsilon > 0$, *satisfying*

$$\begin{bmatrix} \varepsilon D D^T - P^{-1} & A & B K G_0 (I+L) & 0 \\ * & -P + S + \left(K G_0 (I+L) \right)^T R L K G_0 (I+L) + Q & 0 & \left(E K G_0 (I+L) \right)^T \\ * & * & -S & \left(-E K G_0 (I+L) \right)^T \\ * & * & * & -\varepsilon I \end{bmatrix} < 0, \tag{20}$$

then the NCS (18) is asymptotically stable, where $*$ *represents the symmetry blocks of matrix.*

Proof. Consider the following Lyapunov function:

$$V(k) = x^T(k) P x(k) + x^T(k-1) S x(k-1). \tag{21}$$

For the convenience of writing, we denote $L = L(k)$ in the following expressions. Based on (18) conducting subtraction calculation can be obtained

$$\begin{aligned} \Delta V(k) &= v(k+1) - v(k) \\ &= x^T(k+1) P x(k+1) + x^T(k) S x(k) \\ &\quad - x^T(k) P x(k) - x^T(k-1) S x(k-1) \\ &= \left[A x(k) + D F E K G_0 (I+L) x(k) \right. \\ &\quad \left. + (B - DFE) K G_0 (I+L) x(k-1) \right]^T \\ &\quad \times P \left[A x(k) + D F E K G_0 (I+L) x(k) \right. \\ &\quad \left. + (B - DFE) K G_0 (I+L) x(k-1) \right] \\ &\quad + x^T(k) S x(k) - x^T(k) P x(k) \\ &\quad - x^T(k-1) S x(k-1) \\ &= \begin{bmatrix} x(k) \\ x(k-1) \end{bmatrix}^T \begin{bmatrix} \Gamma^T P \Gamma - P + S & \Gamma^T P \Omega \\ * & \Omega^T P \Omega - S \end{bmatrix} \\ &\quad \times \begin{bmatrix} x(k) \\ x(k-1) \end{bmatrix}, \end{aligned} \tag{22}$$

where $\Gamma = A + D F E K G_0 (I+L)$ and $\Omega = B K G_0 (I+L) - D F E K G_0 (I+L)$.

System (18) is asymptotically stable, only if it satisfies $\Delta V < 0$. It is equivalent to

$$\begin{bmatrix} \Gamma^T P \Gamma - P + S & \Gamma^T P \Omega \\ * & \Omega^T P \Omega - S \end{bmatrix} < 0. \tag{23}$$

Now, take the following inequality into consideration:

$$\begin{bmatrix} \Gamma^T P \Gamma - P + S + Q + \left(K G_0 (I+L) \right)^T R K G_0 (I+L) & \Gamma^T P \Omega \\ * & \Omega^T P \Omega - S \end{bmatrix} < 0. \tag{24}$$

Inequality (24) is equivalent to

$$\begin{bmatrix} \Gamma^T P\Gamma - P + S & \Gamma^T P\Omega \\ * & \Omega^T P\Omega - S \end{bmatrix} + \begin{bmatrix} Q + (KG_0(I+L))^T RLKG_0(I+L) & 0 \\ 0 & 0 \end{bmatrix} < 0. \tag{25}$$

Q and R are symmetric positive definite matrices; therefore, inequality (24) is a sufficient condition of inequality (23). Inequality (24) can be expressed as follows:

$$\begin{bmatrix} -P + S + Q + (KG_0(I+L))^T RKG_0(I+L) & 0 \\ * & -S \end{bmatrix} + \begin{bmatrix} \Gamma^T \\ \Omega^T \end{bmatrix} P \begin{bmatrix} \Gamma & \Omega \end{bmatrix} < 0. \tag{26}$$

From Lemma 3, it follows that

$$\begin{bmatrix} -P^{-1} & \Gamma & \Omega \\ * & -P + S + Q + (KG_0(I+L))^T RKG_0(I+L) & 0 \\ * & * & -S \end{bmatrix} < 0. \tag{27}$$

Inequality (27) can be rewritten as

$$\begin{bmatrix} -P^{-1} & A & BKG_0(I+L) \\ * & -P + S + Q + (KG_0(I+L))^T RKG_0(I+L) & 0 \\ * & * & -S \end{bmatrix} + \begin{bmatrix} D \\ 0 \\ 0 \end{bmatrix} F \begin{bmatrix} 0 & EKG_0(I+L) & -EKG_0(I+L) \end{bmatrix} + \begin{bmatrix} 0 & EKG_0(I+L) & -EKG_0(I+L) \end{bmatrix}^T F^T \begin{bmatrix} D \\ 0 \\ 0 \end{bmatrix}^T < 0. \tag{28}$$

From Lemma 4, the sufficient condition of inequality (28) follows that

$$\begin{bmatrix} -P^{-1} & A & BKG_0(I+L) \\ * & -P + S + Q + (KG_0(I+L))^T RKG_0(I+L) & 0 \\ * & * & -S \end{bmatrix} + \varepsilon^{-1} \begin{bmatrix} 0 \\ (EKG_0(I+L))^T \\ (-EKG_0(I+L))^T \end{bmatrix} \begin{bmatrix} 0 \\ (EKG_0(I+L))^T \\ (-EKG_0(I+L))^T \end{bmatrix}^T + \varepsilon \begin{bmatrix} D \\ 0 \\ 0 \end{bmatrix} \begin{bmatrix} D^T & 0 & 0 \end{bmatrix} < 0. \tag{29}$$

Therefore, inequality (29) is a sufficient condition of inequality (23). That is to say, if inequality (29) exists, NCS (18) is asymptotically stable. From Lemma 3, the inequality above is equivalent to inequality (20). This completes the proof. □

Theorem 6. *If the conditions of Theorem 5 are satisfied, for all allowable uncertainties of system (18), its cost function is defined as (19) satisfying*

$$J_\infty \le J_0 = x^T(0) Px(0) + x^T(-1) Sx(-1). \tag{30}$$

Proof. If inequality (20) exists, inequality (25) must exist.

Pre- and postmultiplying (25) by $\begin{bmatrix} x(k) \\ x(k-1) \end{bmatrix}^T$ and by $\begin{bmatrix} x(k) \\ x(k-1) \end{bmatrix}$ separately, it follows that

$$\begin{aligned} &\begin{bmatrix} x(k) \\ x(k-1) \end{bmatrix}^T \begin{bmatrix} \Gamma^T P\Gamma - P + S & \Gamma^T P\Omega \\ * & \Omega^T P\Omega - S \end{bmatrix} \begin{bmatrix} x(k) \\ x(k-1) \end{bmatrix} \\ &\le \begin{bmatrix} x(k) \\ x(k-1) \end{bmatrix}^T \begin{bmatrix} -Q - (KG_0(I+L))^T RKG_0(I+L) & 0 \\ 0 & 0 \end{bmatrix} \times \begin{bmatrix} x(k) \\ x(k-1) \end{bmatrix} \\ &= x^T(k) \left(-Q - (KG_0(I+L))^T RKG_0(I+L) \right) x(k). \end{aligned} \tag{31}$$

Therefore,

$$\begin{aligned} J_\infty &\le -\sum_{k=0}^{\infty} \Delta V(k) = V(0) - \lim_{k\to\infty} V(k) \\ &= x^T(0) P x(0) + x^T(-1) S x(-1) - \lim_{k\to\infty} V(k). \end{aligned} \tag{32}$$

According to Theorem 5, system (18) is asymptotically stable. Therefore, $\lim_{k\to\infty} x(k) = \lim_{k\to\infty} x(k-1) = 0$. Logically, there must exist $\lim_{k\to\infty} V(k) = 0$. Inserting it into (32), inequality (30) can be obtained. □

Theorem 7. *Given symmetric positive definite matrices Q and R, as well as a set of constants σ_1 and σ_2, if symmetric positive definite matrices X, Y and matrix W exist, as well as scalar $\varepsilon > 0$, satisfying the following LMI:*

$$\begin{bmatrix} -Q^{-1} & 0 & 0 & 0 & 0 & 0 & 0 & X & 0 & 0 \\ * & -\sigma_1 I & 0 & 0 & 0 & 0 & 0 & X & 0 & 0 \\ * & * & -\sigma_2 I & 0 & 0 & 0 & 0 & 0 & X & 0 \\ * & * & * & -\sigma_1 X & 0 & W^T & 0 & 0 & 0 & (EW)^T \\ * & * & * & * & -\sigma_2 X & 0 & (BW)^T & 0 & 0 & (-EW)^T \\ * & * & * & * & * & -R^{-1} & 0 & W & 0 & 0 \\ * & * & * & * & * & * & \varepsilon DD^T - X & A & BW & 0 \\ * & * & * & * & * & * & * & -X+Y & 0 & (EW)^T \\ * & * & * & * & * & * & * & * & -Y & (-EW)^T \\ * & * & * & * & * & * & * & * & * & -\varepsilon I \end{bmatrix} < 0, \tag{33}$$

then the NCS (18) is asymptotically stable with control gain $K = WX^{-1}G_0^{-1}$, and for all allowable uncertainties of system, its performance indicator defined as (19) satisfies inequality (30).

Proof. If inequality (20) exists, Theorems 5 and 6 must exist. Inequality (20) is equivalent to

$$\begin{bmatrix} \varepsilon DD^T - P^{-1} & A & BKG_0(I+L) & 0 \\ * & -P+S+Q & 0 & \left(EKG_0(I+L)\right)^T \\ * & * & -S & -\left(EKG_0(I+L)\right)^T \\ * & * & * & -\varepsilon I \end{bmatrix} + \begin{bmatrix} 0 \\ \left(KG_0(I+L)\right)^T \\ 0 \\ 0 \end{bmatrix} R \begin{bmatrix} 0 & KG_0(I+L) & 0 & 0 \end{bmatrix} < 0. \tag{34}$$

From Lemma 3, it follows that

$$\begin{bmatrix} -R^{-1} & 0 & KG_0(I+L) & 0 & 0 \\ * & \varepsilon DD^T - P^{-1} & A & BKG_0(I+L) & 0 \\ * & * & -P+S+Q & 0 & \left(EKG_0(I+L)\right)^T \\ * & * & * & -P & \left(-EKG_0(I+L)\right)^T \\ * & * & * & * & -\varepsilon I \end{bmatrix} < 0. \tag{35}$$

Inequality (35) can be rewritten as

$$\Phi + \Xi_1 L\widehat{I}_1 + \Xi_2 L\widehat{I}_2 + \left(\Xi_1 L\widehat{I}_1\right)^T + \left(\Xi_2 L\widehat{I}_2\right)^T < 0, \quad (36)$$

where

$$\Phi = \begin{bmatrix} -R^{-1} & 0 & KG_0 & 0 & 0 \\ * & \varepsilon DD^T - P^{-1} & A & BKG_0 & 0 \\ * & * & -P+S+Q & 0 & \left(EKG_0\right)^T \\ * & * & * & -P & \left(-EKG_0\right)^T \\ * & * & * & * & -\varepsilon I \end{bmatrix} < 0,$$

$$\Xi_1 = \begin{bmatrix} KG_0 \\ 0 \\ 0 \\ 0 \\ EKG_0 \end{bmatrix}, \quad \widehat{I}_1 = \begin{bmatrix} 0 \\ 0 \\ I \\ 0 \\ 0 \end{bmatrix}^T, \quad \Xi_2 = \begin{bmatrix} 0 \\ BKG_0 \\ 0 \\ 0 \\ -EKG_0 \end{bmatrix}, \quad \widehat{I}_1 = \begin{bmatrix} 0 \\ 0 \\ 0 \\ I \\ 0 \end{bmatrix}^T. \quad (37)$$

Using Lemma 4, it can be obtained that

$$\Phi + \sigma_1^{-1}\Xi_1\Xi_1^{\ T} + \sigma_1\widehat{I}_1^T\widehat{I}_1 + \sigma_2^{-1}\Xi_2\Xi_2^{\ T} + \sigma_2\widehat{I}_2^T\widehat{I}_2 < 0. \quad (38)$$

Using Lemma 3 repeatedly, the following inequality can be obtained:

$$\begin{bmatrix} -Q^{-1} & 0 & 0 & 0 & 0 & 0 & 0 & I & 0 & 0 \\ * & -\sigma_1^{-1}I & 0 & 0 & 0 & 0 & 0 & I & 0 & 0 \\ * & * & -\sigma_2^{-1}I & 0 & 0 & 0 & 0 & 0 & I & 0 \\ * & * & * & -\sigma_1 I & 0 & \left(KG_0\right)^T & 0 & 0 & 0 & \left(EKG_0\right)^T \\ * & * & * & * & -\sigma_2 I & 0 & \left(BKG_0\right)^T & 0 & 0 & \left(-EKG_0\right)^T \\ * & * & * & * & * & -R^{-1} & 0 & KG_0 & 0 & 0 \\ * & * & * & * & * & * & \varepsilon DD^T - P^{-1} & A & BKG_0 & 0 \\ * & * & * & * & * & * & * & -P+S & 0 & \left(EKG_0\right)^T \\ * & * & * & * & * & * & * & * & -S & \left(-EKG_0\right)^T \\ * & * & * & * & * & * & * & * & * & -\varepsilon I \end{bmatrix} < 0. \quad (39)$$

Pre- and postmultiplying (39) by block-diag$(I, \sigma_1 I, \sigma_2 I, P^{-1}, P^{-1}, I, I, P^{-1}, P^{-1}, I)$ and then letting $X = P^{-1}$, $W = KG_0P^{-1} = KG_0X$, $Y = P^{-1}SP^{-1}$, inequality (33) can be obtained. Because G_0 is invertible, K can be obtained by calculating $K = WX^{-1}G_0^{\ -1}$. This completes the proof. □

4. Simulations

Consider the model of inverted pendulum device as follows:

$$\dot{x}(t) = \begin{bmatrix} -0.5 & -0.51 & 0 & 0 \\ 0 & -1.3 & 0 & 0 \\ 0.1 & 0.2 & -0.3 & 0 \\ 0 & 0 & 0 & 0.3 \end{bmatrix} x(t) + \begin{bmatrix} 0.1 \\ 1 \\ 0.5 \\ 1.2 \end{bmatrix} u(t). \quad (40)$$

Consider the sampling period $T = 0.1$ s; the network induced time delay satisfies $\tau_k < T$ and is time-varying. We choose the parameters as $\alpha_1 = 1.3$, $\alpha_2 = 1.8$, $\alpha_3 = -1.1$, and $\alpha_4 = 1.5$. Computing (5)–(8), we have

$$D = \begin{bmatrix} 0 & 1.61 & -0.5772 & 0 \\ 0 & 0 & -0.9054 & 0 \\ 1.3 & -0.805 & 0.2388 & 0 \\ 0 & 0 & 0 & 0 \end{bmatrix}, \qquad E = \begin{bmatrix} 0.495 \\ -0.6009 \\ 1.2149 \\ 1.2 \end{bmatrix}, \quad (41)$$

$$F(\tau_k) = \operatorname{diag}\left(\frac{e^{-0.3(0.1-\tau_k)} - 1}{-0.39}, \frac{e^{-0.5(0.1-\tau_k)} - 1}{-0.9}, \frac{e^{-1.3(0.1-\tau_k)} - 1}{1.43}, \frac{e^{0.3(0.1-\tau_k)} - 1}{0.45}\right). \quad (42)$$

Obviously, $F^T(\tau_k)F(\tau_k) < I$ is satisfied.

Table 1: The boundaries of sensor faults.

	Upper bound	Lower bound	Mean value
Sensor faults matrix G	$\begin{bmatrix} 0.9 & 0 & 0 & 0 \\ 0 & 0.9 & 0 & 0 \\ 0 & 0 & 0.86 & 0 \\ 0 & 0 & 0 & 0.78 \end{bmatrix}$	$\begin{bmatrix} 0.1 & 0 & 0 & 0 \\ 0 & 0.2 & 0 & 0 \\ 0 & 0 & 0.12 & 0 \\ 0 & 0 & 0 & 0.2 \end{bmatrix}$	$\begin{bmatrix} 0.5 & 0 & 0 & 0 \\ 0 & 0.55 & 0 & 0 \\ 0 & 0 & 0.49 & 0 \\ 0 & 0 & 0 & 0.49 \end{bmatrix}$

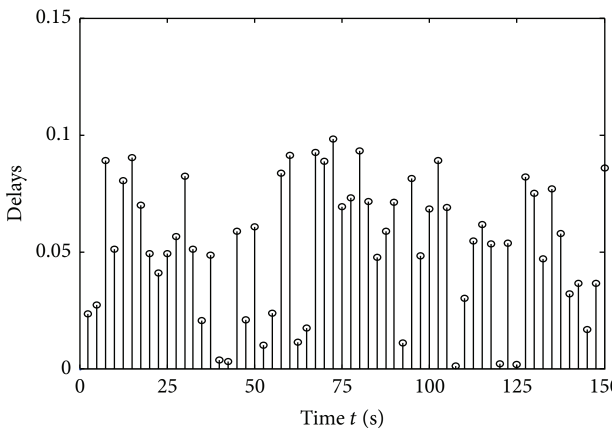

Figure 3: The distribution of delays in NCS.

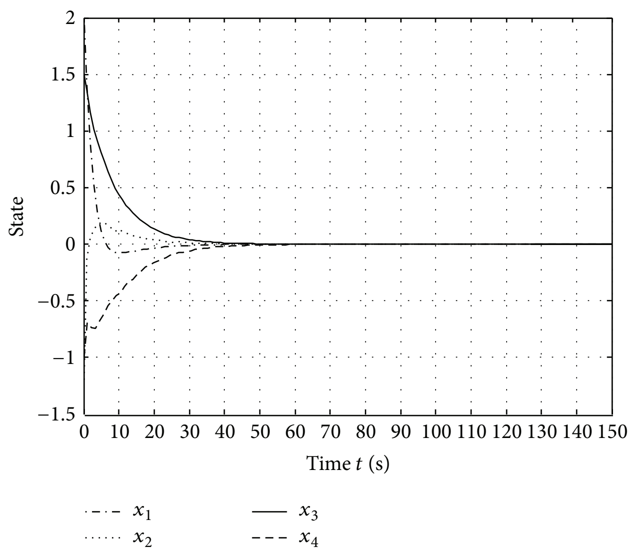

Figure 4: State response of NCS without sensor faults.

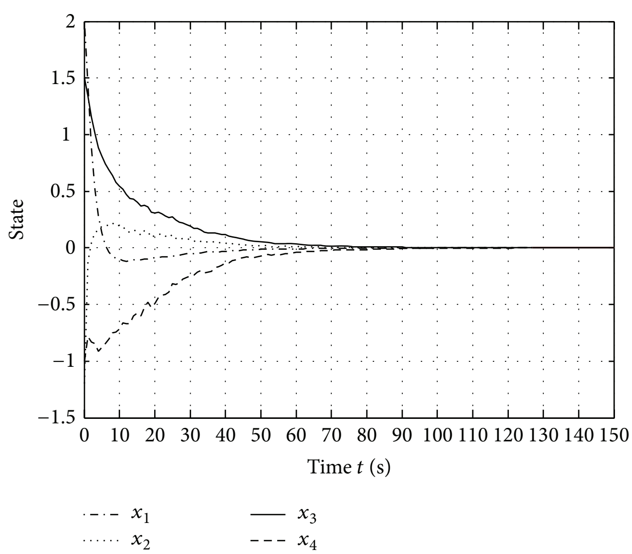

Figure 5: State response of NCS with time-varying sensor faults.

And the following parameters are given:

$$Q = \begin{bmatrix} 50 & 0 & 0 & 0 \\ 0 & 80 & 0 & 0 \\ 0 & 0 & 130 & 0 \\ 0 & 0 & 0 & 220 \end{bmatrix}, \quad R = 1800, \ \sigma_1 = \sigma_2 = 10^9. \tag{43}$$

Considering the sensor faults that may occur, the boundaries of faults are given in Table 1.

By making use of LMI toolbox in MATLAB to solve the linear matrix inequality (33), guaranteed cost fault-tolerant controller parameters of NCS can be obtained:

$$K = WX^{-1}G_0^{-1} = \begin{bmatrix} -0.0756 & -1.03 & -0.7531 & -1.9025 \end{bmatrix}. \tag{44}$$

It assumes the initial state of the system is $x(0) = x(-1) = [2 \ \ -1.2 \ \ 1.5 \ \ -1]^T$; the comprehensive performance indicator can be obtained $J_0 = 16.3685$. The time-varying transmission delays produced in network are shown in Figure 3. When all sensors are normal, namely, $G = I$, the state responses of NCS are shown in Figure 4, from which we know the system gets steady at 40 s. When sensor faults vary in the scope of boundary values in Table 1, the state responses of NCS are shown in Figure 5, from which we can see the transition time of state response obviously becomes longer than that in Figure 4 because of the effects of time-varying sensor faults, but the system is still asymptotically stable and gets steady at 80 s. So, the performance of NCS can be well maintained by the guaranteed cost fault-tolerant controller, which demonstrates the effectiveness and feasibility of the approach proposed in this paper.

5. Conclusions

When time-varying sensor faults occur, guaranteed cost fault-tolerant control problem of networked control systems is studied in this paper. Using Lyapunov stability theory and linear matrix inequality (LMI) approach, a sufficient condition is given, which can render the closed-loop NCS with sensor faults asymptotically stable and can guarantee it to meet the requirements of performance indicator. And based on LMI, the method of designing guaranteed cost fault-tolerant controller is proposed. Moreover, the feasibility and effectiveness of this method have been demonstrated by a simulation example. The next research task will be analyzing the time-varying actuator faults to improve the performance of NCS further.

Conflict of Interests

The authors declare that there is no conflict of interests regarding the publication of this paper.

Acknowledgments

This work was partly supported by the National Nature Science Foundation of China (61164014, 51375323) and Qing Lan Project of Jiangsu Province, China.

References

[1] J. K. Yook, D. M. Tilbury, and N. R. Soparkar, "Trading computation for bandwidth: reducing communication in distributed control systems using state estimators," *IEEE Transactions on Control Systems Technology*, vol. 10, no. 4, pp. 503–518, 2002.

[2] Y. Zheng and H. J. Fang, "Robust fault tolerant control of networked control system with time-varying delays," *Journal of Xi'an Jiaotong University*, vol. 38, no. 8, pp. 804–807, 2004.

[3] Z. Qu, C. M. Ihlefeld, Y. Jin, and A. Saengdeejing, "Robust fault-tolerant self-recovering control of nonlinear uncertain systems," *Automatica*, vol. 39, no. 10, pp. 1763–1771, 2003.

[4] C. Peng, T. C. Yang, and E. G. Tian, "Robust fault-tolerant control of networked control systems with stochastic actuator failure," *IET Control Theory & Applications*, vol. 4, no. 12, pp. 3003–3011, 2010.

[5] E. Tian, D. Yue, and C. Peng, "Brief Paper: reliable control for networked control systems with probabilistic sensors and actuators faults," *IET Control Theory and Applications*, vol. 4, no. 8, pp. 1478–1488, 2010.

[6] Y. Zhang and J. Jiang, "Bibliographical review on reconfigurable fault-tolerant control systems," *Annual Reviews in Control*, vol. 32, no. 2, pp. 229–252, 2008.

[7] J.-H. Zhang, J.-L. Li, and Y. Chen, "Robust fault tolerant control for a kind of uncertain networked control system," *Journal of Kunming University of Science and Technology*, vol. 37, no. 1, pp. 36–40, 2012 (Chinese).

[8] Q. Zhu, K. Lu, and Y. Zhu, "Robust guaranteed cost control for networked control system with actuator failure," *International Journal of Applied Mathematics & Statistics*, vol. 50, no. 20, pp. 55–68, 2013.

[9] W. Zhang, M. S. Branicky, and S. M. Phillips, "Stability of networked control systems," *IEEE Control Systems Magazine*, vol. 21, no. 1, pp. 84–99, 2001.

[10] Y. Wang, L. Xie, and C. E. de Souza, "Robust control of a class of uncertain nonlinear systems," *Systems & Control Letters*, vol. 19, no. 2, pp. 139–149, 1992.

[11] X. Y. Luo, M. J. Shang, C. L. Chen, and X. P. Guan, "Guaranteed cost active fault-tolerant control of networked control system with packet dropout and transmission delay," *International Journal of Automation and Computing*, vol. 7, no. 4, pp. 509–515, 2010.

Hindawi Publishing Corporation
Mathematical Problems in Engineering
Volume 2015, Article ID 545827, 8 pages
http://dx.doi.org/10.1155/2015/545827

Research Article

Pinning Synchronization of Switched Complex Dynamical Networks

Liming Du,[1,2] Feng Qiao,[2] and Fengying Wang[2]

[1] *State Key Laboratory of Synthetical Automation for Process Industries, College of Information Science & Engineering, Northeastern University, Shenyang 110819, China*
[2] *Faculty of Information & Control Engineering, Shenyang Jianzhu University, Shenyang 110168, China*

Correspondence should be addressed to Liming Du; duliming_666@163.com

Received 15 August 2014; Revised 8 October 2014; Accepted 28 October 2014

Academic Editor: Xi-Ming Sun

Network topology and node dynamics play a key role in forming synchronization of complex networks. Unfortunately there is no effective synchronization criterion for pinning synchronization of complex dynamical networks with switching topology. In this paper, pinning synchronization of complex dynamical networks with switching topology is studied. Two basic problems are considered: one is pinning synchronization of switched complex networks under arbitrary switching; the other is pinning synchronization of switched complex networks by design of switching when synchronization cannot achieved by using any individual connection topology alone. For the two problems, common Lyapunov function method and single Lyapunov function method are used respectively, some global synchronization criteria are proposed and the designed switching law is given. Finally, simulation results verify the validity of the results.

1. Introduction

A complex dynamical network is a set of coupled nodes interconnected by edges, in which each node is a dynamical system [1, 2]. Undoubtedly, many systems in nature can be described by models of complex networks, such as ecological networks, power grids, wireless communication networks, and World Wide Web. Over the last decade, the analysis and control of dynamical networks have become research focus in many fields, such as mathematics, physics, biology, and engineering.

Synchronization, the most important collective behavior of complex dynamical networks, has received much of the focus [3–5]. The synchronization of complex dynamical networks has been extensively investigated and many synchronization criteria for complex networks have been proposed, such as the master stability function based criteria [6], Lyapunov function based criteria [7, 8], and graph stability method based criteria [9].

As we know now, some complex network can be synchronized by itself, but the general case is that the whole network cannot synchronize by itself; from the perspective of control theory, designing controllers is an effective method, and one natural idea is to assign controllers to all nodes of the controlled complex dynamical network [10–12].

However, complex networks in the real world normally have a large number of nodes. Therefore, it is usually difficult to control a complex network by adding the controllers to all nodes. To reduce the number of the controllers, a natural approach is to control a complex network by pinning part of nodes. This idea is actually adding the controllers to a small fraction of network nodes to achieve synchronization of the whole complex networks. In [13], Grigoriev et al. investigated the pinning control of spatiotemporal chaos. Subsequently, Parekh et al. studied the local and global control in coupled map lattices [14]. In [15, 16], Wang and Chen considered the problem of pinning a complex dynamical network to its equilibrium, and both specific and random pinning strategies were proposed. In [17], the controllability of a coupled complex network via pinning has been studied by means of a Master Stability Function approach. In [18], Chen et al. pointed out that a general complex network can be pinned by a single controller if the coupling strength is large enough. A network under a typical framework can realize synchronization subject to any linear feedback pinning scheme and the relationship between coupling strength and the number of pinning nodes for a general complex dynamical network through adaptive pinning [19, 20].

Note that most investigations about synchronization of complex networks under pinning control are with the constant connection topology. Actually, constant connection is only a special case. It is well known that the interaction of two different nodes in the real world networks always evolves with time continuously, and the interaction between different nodes may change abruptly at some time instants, which results in switching topology, such as mobile agents [21] and power grids [22].

The switched system theory provides an effective tool for studying complex networks with switching topology [23]. By using the common Lyapunov function method, the synchronization problem for complex dynamical networks with switching topology has been studied in [24]. In [25], the synchronization of switched complex dynamical networks was discussed from the view point of switched systems, under the assumptions that all the connection outer matrices are simultaneous triangularization, and several synchronization criteria have been established by means of constructing a common Lyapunov function and single Lyapunov and multiple Lyapunov functions, respectively. In [26], the synchronization problem was studied with switched coupling using the average dwell time method. A synchronization criterion for dynamical networks with nonidentical nodes and switching topology was given in [27]. However, to our knowledge, so far, none of the results of pinning synchronization of complex networks with switching topology have been reported. Motivated by the above discussions, in this paper, the pinning synchronization of complex dynamical networks is investigated with switching topology. First, we study the problem of pinning synchronization of switched complex network under arbitrary switching. Second, when pinning synchronization is impossible for each individual connection topology, the problem of synchronization via the design of switching signal of pregiven connection topology is studied. By using common Lyapunov function method and single Lyapunov function method, respectively, we design controllers and the switching laws to ensure the pinning synchronization. Without assuming that the coupling matrix is symmetric, we give some criteria for the global pinning synchronization of complex networks with switching topology.

The remainder of the paper is organized as follows. Some preliminaries are described in Section 2. Pinning synchronization criteria for arbitrary switching are derived in Section 3. In Section 4, pinning synchronization via design of switching is studied. In Section 5, several numerical examples are given. Conclusions are drawn in Section 6.

2. Preliminaries

Now consider a switched complex dynamical network with N identical nodes; the mathematics model of the system can be described as follows:

$$\dot{x}_i = f(x_i) + c\sum_{j=1}^{N} a_{ij}^{\sigma(t)}\Gamma x_j, \quad i = 1, 2, \ldots, N, \tag{1}$$

where $x_i = (x_{i1}, x_{i2}, \ldots, x_{in})^T \in R^n$ is the state vector of the ith node, Γ is the inner-coupling matrix between two connected nodes, f is a continuously differentiable vector function, c is the coupling strength, $\sigma : [0, \infty) \rightarrow M = \{1, 2, \ldots, m\}$, for each $k \in M$, $A_k = \{a_{ij}^k\} \in R^{N\times N}$ is the outer-coupling matrix, assume $a_{ii}^k = \sum_{j=1, j\neq i}^{N} a_{ij}^k$, and let $s(t)$ be a solution of each isolated node; that is, $\dot{s}(t) = f(s(t))$.

Normally, a complex dynamical network has a large number of nodes, so it is difficult to add the controllers to all nodes. By pinning control methods, the controllers are to be added to part of nodes, and the other nodes need not be controlled; without loss of generality, let the first l nodes be controlled; then (1) can be expressed as

$$\begin{aligned} \dot{x}_i &= f(x_i) + c\sum_{j=1}^{N} a_{ij}^{\sigma(t)}\Gamma x_j + u_i^{\sigma(t)}, \quad i = 1, 2, \ldots, l, \\ \dot{x}_i &= f(x_i) + c\sum_{j=1}^{N} a_{ij}^{\sigma(t)}\Gamma x_j, \quad i = l+1, l+2, \ldots, N, \end{aligned} \tag{2}$$

where u_i^k are the given controller, which can be described as

$$u_i^k = -cq_i^k\Gamma(x_i - s), \quad i = 1, 2, \ldots, l, \; q_i^k > 0. \tag{3}$$

It is easy to see that the systems (2) are pinned to synchronization if $\lim_{t\rightarrow\infty}\|x_i(t) - s(t)\| = 0$. Next, define $e_i = x_i - s$; then the error system can be described as

$$\begin{aligned} \dot{e}_i &= f(x_i) - f(s) + c\sum_{j=1}^{N} a_{ij}^{\sigma(t)}\Gamma e_j - cq_i^{\sigma(t)}\Gamma e_i, \quad i = 1, 2, \ldots, l, \\ \dot{e}_i &= f(x_i) - f(s) + c\sum_{j=1}^{N} a_{ij}^{\sigma(t)}\Gamma e_j, \quad i = l+1, l+2, \ldots, N, \end{aligned} \tag{4}$$

and it should be noted that only the first l nodes have controllers, so the last term of the second line of (4) is zero. Now, the synchronization problem of system (2) turns into the stability of system (4); throughout this paper, we need the following assumption.

Assumption 1. Assume that there is a positive defined matrix P and a constant matrix K, such that f satisfies the following inequality:

$$(x - y)^T P(f(x) - f(y)) \leq (x - y)^T K\Gamma(x - y), \quad \forall x, y \in R^n. \tag{5}$$

Note that Assumption 1 is very mild; many systems satisfy this condition, such as Lorenz system, Liu system, and Chen system. In the following section, we will investigate the problems of pinning synchronization by common Lyapunov function method and single Lyapunov function method, respectively.

3. Arbitrary Switching

In this section, we study the pinning synchronization of complex dynamical networks under arbitrary switching topology. A network with switching topology may not realize synchronization by pinning controller, even if pinning synchronization is achieved by using each individual connection topology alone. Therefore, seeking for pinning synchronization criteria for arbitrary switching topology is not trivial. By using common Lyapunov function method, a criterion is derived to ensure the global synchronization under arbitrary switching.

Theorem 2. *Suppose that Assumption 1 holds, the pinning controlled complex dynamical system in (2) achieves global synchronization under arbitrary switching if there exist a positive definite matrix P such that the condition*

$$I_N \otimes K\Gamma + c\left(A_k - Q_k\right) \otimes P\Gamma < 0, \quad k = 1, 2, \ldots, m, \tag{6}$$

holds, where $\otimes$ *is Kronecker product,* I_N *is an N-dimensional identity matrix, and* $Q_k = \operatorname{diag}\{q_1^k, q_2^k, \ldots, q_l^k, 0, \ldots, 0\} \in R^{N\times N}$.

Proof. Construct the common Lyapunov function as the form of

$$V(t) = \frac{1}{2}\sum_{i=1}^{N} e_i^T P e_i. \tag{7}$$

The derivative of $V(t)$ along the trajectories of each subsystem of (4) gives

$$\begin{aligned}
\dot{V}(t) &= \sum_{i=1}^{N} e_i^T P \dot{e}_i \\
&= \sum_{i=1}^{N} e_i^T P \left[f(x_i) - f(s) + c\sum_{j=1}^{N} a_{ij}^k \Gamma e_i \right] - c\sum_{i=1}^{l} q_i^k e_i^T P\Gamma e_i \\
&\le \sum_{i=1}^{N} e_i^T \left[K\Gamma e_i + cP\sum_{j=1}^{N} a_{ij}^k \Gamma e_i \right] - c\sum_{i=1}^{l} q_i^k e_i^T P\Gamma e_i \\
&= e^T \left[I_N \otimes K\Gamma + c\left(I_N \otimes P\right)\left(A_k \otimes \Gamma\right) - c\left(Q_k \otimes P\Gamma\right)\right] e \\
&= e^T \left[I_N \otimes K\Gamma + c\left(A_k \otimes P\Gamma\right) - c\left(Q_k \otimes P\Gamma\right)\right] e,
\end{aligned} \tag{8}$$

where $e = (e_1^T, e_2^T, \ldots, e_N^T)^T$. From (6), it is easy to see that

$$\dot{V}(t) < 0, \tag{9}$$

the switched complex network in (2) achieves global synchronization with the pinning controller (3) under arbitrary switching, which completes the proof. □

Remark 3. For the special case is that $P = I$ and let the network has only one connection topology; then the synchronization condition (6) degenerates into

$$I_N \otimes K\Gamma + c\left(A - Q\right) \otimes \Gamma < 0, \tag{10}$$

which is expressed in [20].

Remark 4. If Γ is a positive definite matrix and P is replaced with I, then the conditions (6) in Theorem 2 can be simplified as

$$\theta I_N + c\left(A_k - Q_k\right) < 0, \quad k = 1, 2, \ldots, m, \tag{11}$$

where $\theta = \|K\|$.

4. Switching Design

In this section, we will study the case that none of subnetworks can bring pinning synchronization if each individual connection topology is put in use alone. So pinning synchronization of switched networks under arbitrary switching is impossible to be achieved for this case. But pinning synchronization may still be achieved by switching between connection topologies, so we discuss how to realize synchronization by the suitable design of switching ruler between connection topologies and give a convex combination based method.

Let $\overline{A} = \sum_{k=1}^{m} \varepsilon_k A_k$ with $\varepsilon_k \ge 0$ and $\sum_{k=1}^{m} \varepsilon_k = 1$; then the convex combination of system (2) and the convex combination of error system (3) can be described as

$$\begin{aligned}
\dot{x}_i &= f(x_i) + c\sum_{j=1}^{N} \overline{a}_{ij}\Gamma x_j + \overline{u}_i, \quad i = 1, 2, \ldots, l, \\
\dot{x}_i &= f(x_i) + c\sum_{j=1}^{N} \overline{a}_{ij}\Gamma x_j, \quad i = l+1, l+2, \ldots, N,
\end{aligned} \tag{12}$$

$$\begin{aligned}
\dot{e}_i &= f(x_i) - f(s) + c\sum_{j=1}^{N} \overline{a}_{ij}\Gamma e_j - c\overline{q}_i\Gamma e_i, \quad i = 1, 2, \ldots, l, \\
\dot{e}_i &= f(x_i) - f(s) + c\sum_{j=1}^{N} \overline{a}_{ij}\Gamma e_j, \quad i = l+1, l+2, \ldots, N,
\end{aligned} \tag{13}$$

where $\overline{a}_{ij} = \sum_{k=1}^{m} \varepsilon_k a_{ij}$, $\overline{u}_i = \sum_{k=1}^{m} \varepsilon_k u_i$, $\overline{q}_i = \sum_{k=1}^{m} \varepsilon_k q_i$, and $\sum_{k=1}^{m} \varepsilon_k = 1$.

Theorem 5. *Suppose that Assumption 1 holds, and there exist a positive definite matrix P, and some convex combination coefficients* ε_i*, which satisfies the following condition:*

$$\begin{aligned}
&I_N \otimes K\Gamma + c\sum_{k=1}^{m} \varepsilon_k \left(A_k - Q_k\right) \otimes P\Gamma < 0, \\
&k = 1, 2, \ldots, m, \quad \sum_{k=1}^{m} \varepsilon_k = 1,
\end{aligned} \tag{14}$$

where $\otimes$ *is Kronecker product,* I_N *is an N-dimensional identity matrix, and* $Q_k = \mathrm{diag}\{q_1^k, q_2^k, \ldots, q_l^k, 0, \ldots, 0\} \in R^{N\times N}$*; then the controlled complex dynamical system in (13) achieves global pinning synchronization under the following switching laws:*

$$\begin{aligned} \sigma(t) &= i \quad if\ \sigma(t^-) = i,\ e \in \Omega_i(t), \\ \sigma(t) &= j \quad if\ \sigma(t^-) = i,\ e \in \partial\Omega_i(t) \cap \Omega_j(t), \end{aligned} \tag{15}$$

with

$$\begin{aligned} &\Omega_i(t) \\ &\quad = \{e \mid e^T [I_N \otimes K\Gamma + c(A_i \otimes P\Gamma) - c(Q_i \otimes P\Gamma)] e < 0\}, \\ &\Omega_j(t) \\ &\quad = \{e \mid e^T [I_N \otimes K\Gamma + c(A_j \otimes P\Gamma) - c(Q_j \otimes P\Gamma)] e < 0\}, \\ &\partial\Omega_i(t) \\ &\quad = \{e \mid e^T [I_N \otimes K\Gamma + c(A_i \otimes P\Gamma) - c(Q_i \otimes P\Gamma)] e = 0\}, \end{aligned} \tag{16}$$

where $i, j \in \{1, 2, \ldots, m\}$.

Proof. Construct the Lyapunov function as the form of

$$V(t) = \frac{1}{2}\sum_{i=1}^{N} e_i^T P e_i. \tag{17}$$

The derivative of $V(t)$ along the trajectories of system (12) gives

$$\begin{aligned} \dot V(t) &= \sum_{i=1}^{N} e_i^T P \dot e_i \\ &= \sum_{i=1}^{N} e_i^T P \left[f(x_i) - f(s) + c\sum_{j=1}^{N} \overline{a}_{ij}\Gamma e_i \right] - c\sum_{i=1}^{l} \overline{q}_i e_i^T P\Gamma e_i \\ &\le \sum_{i=1}^{N} e_i^T \left[K\Gamma e_i + cP\sum_{j=1}^{N} \overline{a}_{ij}\Gamma e_i \right] - c\sum_{i=1}^{l} \overline{q}_i e_i^T P\Gamma e_i \\ &= e^T \left[I_N \otimes K\Gamma + c(I_N \otimes P)(\overline{A} \otimes \Gamma) - c(\overline{Q} \otimes P\Gamma) \right] e \\ &= e^T \left[I_N \otimes K\Gamma + c(\overline{A} \otimes P\Gamma) - c(\overline{Q} \otimes P\Gamma) \right] e, \end{aligned} \tag{18}$$

where $e = (e_1^T, e_2^T, \ldots, e_N^T)^T$, $\overline{A} = \sum_{k=1}^m \varepsilon_k A_k$, and $\overline{Q} = \sum_{k=1}^m \varepsilon_k Q_k$. If the condition in (14) is satisfied, then the sets $\Omega_i(t)$ in (16) will make a partition of R^{Nn} by the convex combination technique [23]; that is, $\cup_{i=1}^m \Omega_i = R^{Nn}$. According to the switching laws (16), if the kth subsystem is activated, then the kth subsystem is described as

$$\begin{aligned} \dot e_i &= f(x_i) - f(s) + c\sum_{j=1}^{N} a_{ij}^k \Gamma x_j - c q_i^k \Gamma e_i, \quad i = 1, 2, \ldots, l, \\ \dot e_i &= f(x_i) - f(s) + c\sum_{j=1}^{N} a_{ij}^k \Gamma x_j, \quad i = l+1, l+2, \ldots, N. \end{aligned} \tag{19}$$

The derivative of $V(t)$ along the trajectories of system (19) is

$$\begin{aligned} \dot V(t) &= \sum_{i=1}^{N} e_i^T P \dot e_i \\ &= \sum_{i=1}^{N} e_i^T P \left[f(x_i) - f(s) + c\sum_{j=1}^{N} a_{ij}^k \Gamma e_i \right] - c\sum_{i=1}^{l} q_i^k e_i^T P\Gamma e_i \\ &\le \sum_{i=1}^{N} e_i^T \left[K\Gamma e_i + cP\sum_{j=1}^{N} a_{ij}^k \Gamma e_i \right] - c\sum_{i=1}^{l} q_i^k e_i^T P\Gamma e_i \\ &= e^T \left[I_N \otimes K\Gamma + c(I_N \otimes P)(A_k \otimes \Gamma) - c(Q_k \otimes P\Gamma) \right] e \\ &= e^T \left[I_N \otimes K\Gamma + c(A_k \otimes P\Gamma) - c(Q_k \otimes P\Gamma) \right] e < 0. \end{aligned} \tag{20}$$

From single Lyapunov function method [23], the complex networks in (2) achieve global pinning synchronization under the switching law (15), which completes the proof. □

Remark 6. Similar to Remark 4, if Γ is a positive definite matrix and P is replaced with I, then the conditions (14) in Theorem 5 can be simplified as

$$\theta I_N + c\sum_{k=1}^{m} \varepsilon_k (A_k - Q_k) < 0, \quad \sum_{k=1}^{m} \varepsilon_k = 1, \tag{21}$$

where $\theta = \|K\|$.

Remark 7. Although (7) and (17) are the same expression, these equations have different meanings. Equation (7) has been used as common Lyapunov function, which needs $\dot V(t) < 0$ for all the subnetworks. It means that each pinning controlled subnetwork can achieve synchronization. However, (17) has been used as single Lyapunov function, compared with common Lyapunov function; it only needs $\dot V(t) < 0$ for the time period when the subnetwork is activated; it is easy to see that single Lyapunov function method can deal with more general case of switched complex networks.

Remark 8. Compared with [25], there are three distinct features. First of all, we investigated the pinning synchronization problems of switched complex networks, including pinning controller and switching laws design, however, [25] only considering the synchronization problems of complex networks from the switched system point of view, and it does not deal with the design of controller. So far, no synchronization criteria have been reported for dynamical networks with switching topology via pinning controller, so the research topic is significant. Secondly, the assumptions in the two papers are different. The results of [25] are under the assumptions that all the connection outer matrices are simultaneous triangularization, and these assumptions are not easily satisfied. Compared with it, this paper does not need these assumptions. Therefore, the results of this paper cover more general cases of the dynamical networks in the real world. Thirdly, compared with [25], the result of this paper is more simpler and is easy to be verified, which is conducive to engineering applications.

5. Examples

In this section, two simple examples are used to explain the effectiveness of the proposed network synchronization criteria.

Example 1. Consider the network

$$\begin{aligned} \dot{x}_i &= f(x_i) + c\sum_{j=1}^{N} a_{ij}^k \Gamma x_j + u_i^k, \quad i = 1, 2, \ldots, l, \ k = 1, 2 \\ \dot{x}_i &= f(x_i) + c\sum_{j=1}^{N} a_{ij}^k \Gamma x_j, \quad i = l+1, l+2, \ldots, N, \ k = 1, 2, \end{aligned} \tag{22}$$

where

$$f(x_i) = \begin{cases} \dot{x}_{i1} = 10(x_{i2} - x_{i1}), \\ \dot{x}_{i2} = 40x_{i1} - 25x_{i1}x_{i3}, \\ \dot{x}_{i3} = -x_{i3} + 4x_{i1}^2. \end{cases} \tag{23}$$

Let $T = \mathrm{diag}(1, 2, 1)$, $c = 6$; herein we assume that the network structure of (21) obeys the scale-free distribution of the BA model [27]; the first subsystem's parameters are given by $N = 30$, $m_0 = m = 3$, and the second subsystem's parameters are given by $N = 30$, $m_0 = m = 5$, and, without loss of generality, the pinning controllers are added to the first node. Let $q_1^1 = q_1^2 = 20$; the conditions of Theorem 2 are satisfied. The states of error e_i $(i = 1, 2, \ldots, 30)$ are illustrated in Figures 1, 2, and 3 with switching signal in Figure 4, which show that the controlled network is globally asymptotically stable under arbitrary switching by the pinning controller (3).

Example 2. Let f and Γ be the same as (21), and the pinning controllers are added to the first node. The outer-coupling matrices A_1 and A_2 are pregiven; let $q_1^1 = q_1^2 = 90$; then the states of error e_i $(i = 1, 2, \ldots, 30)$ are illustrated in Figures 5, 6, 7, 8, 9, and 10.

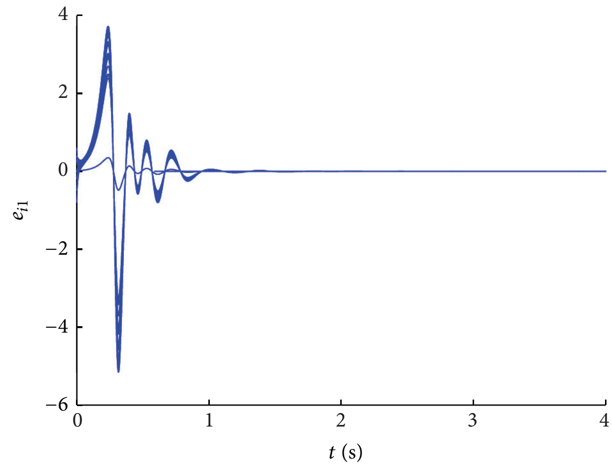

FIGURE 1: The synchronization errors e_{i1} of complex dynamical system (22).

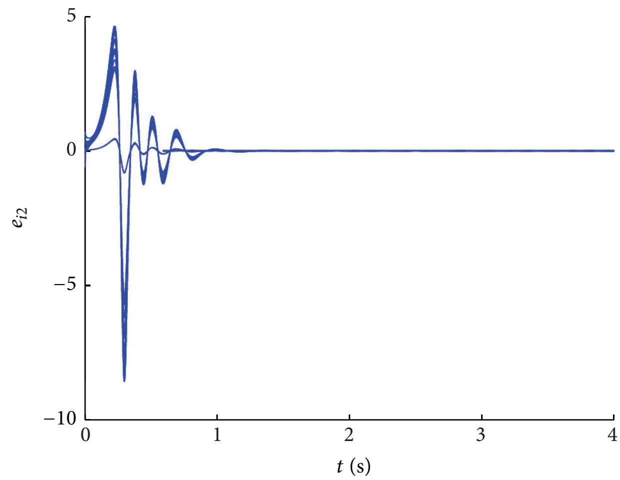

FIGURE 2: The synchronization errors e_{i2} of complex dynamical system (22).

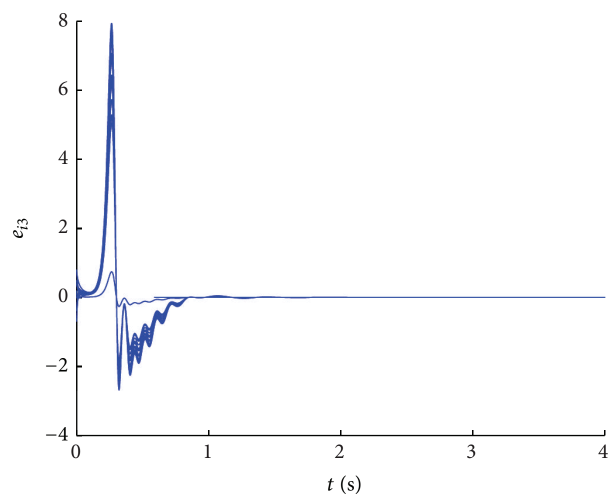

FIGURE 3: The synchronization errors e_{i3} of complex dynamical system (22).

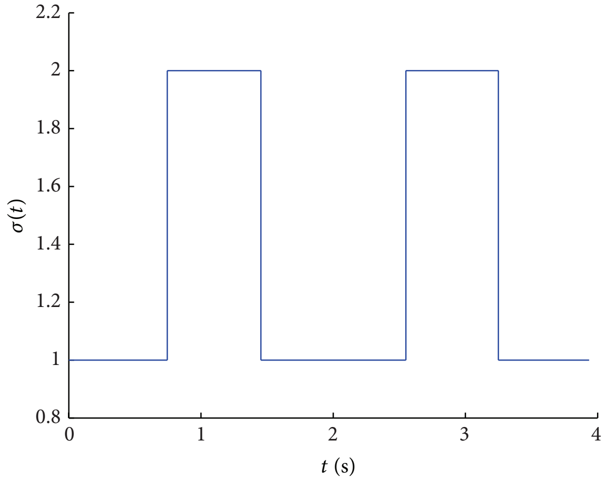

FIGURE 4: The switching signal of system (22).

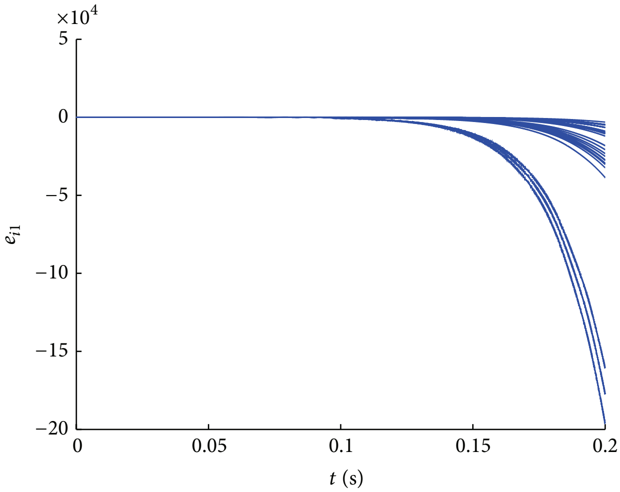

FIGURE 5: The synchronization errors e_{i1} of the subnetwork 1 of Example 2.

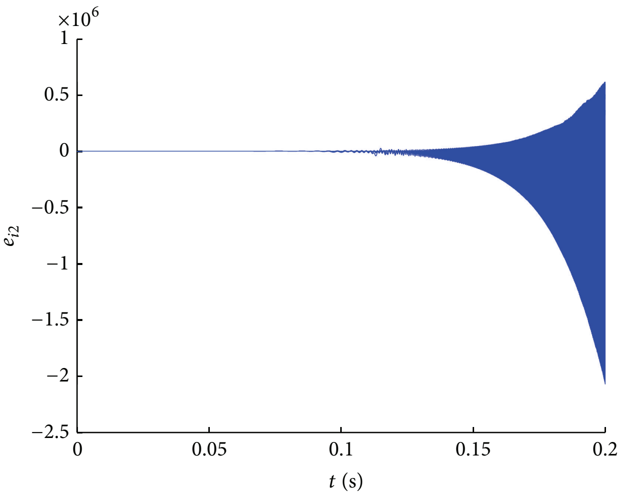

FIGURE 6: The synchronization errors e_{i2} of the subnetwork 1 of Example 2.

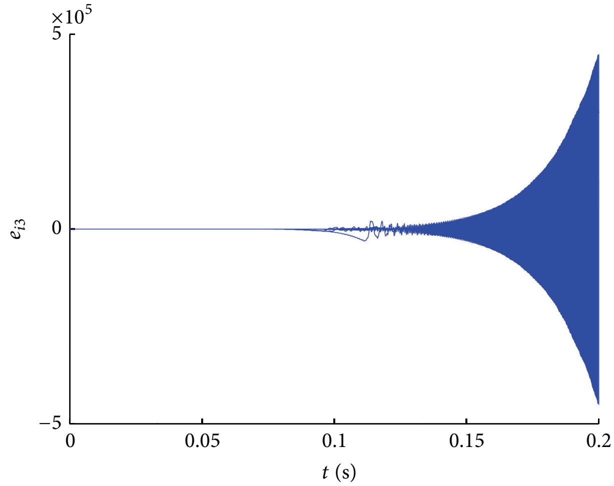

FIGURE 7: The synchronization errors e_{i3} of the subnetwork 1 in Example 2.

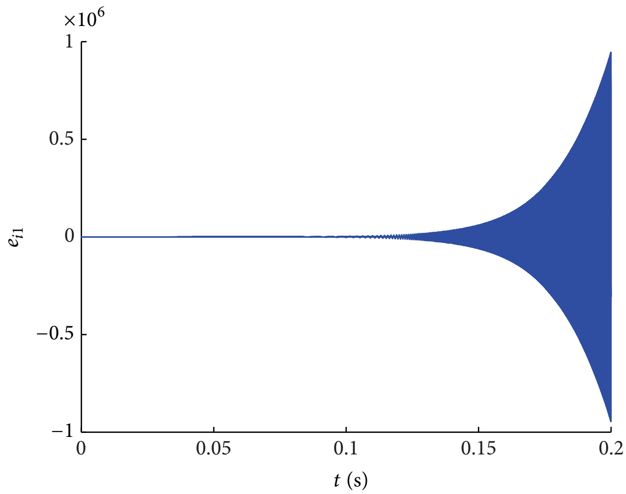

FIGURE 8: The synchronization errors e_{i1} of the subnetwork 2 of Example 2.

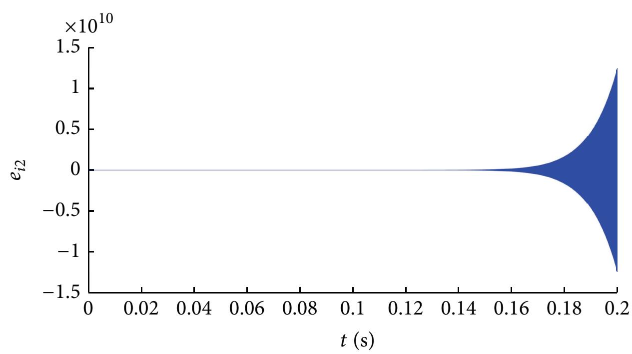

FIGURE 9: The synchronization errors e_{i2} of the subnetwork 2 of Example 2.

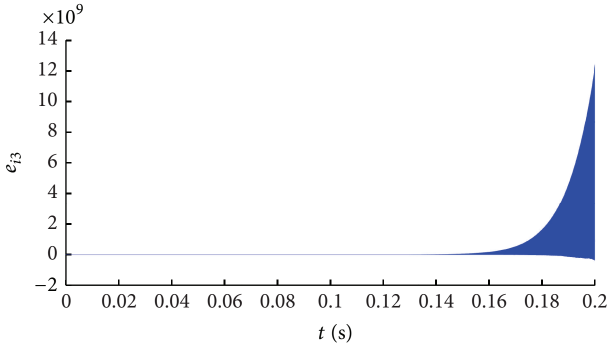

Figure 10: The synchronization errors e_{i3} of the subnetwork 2 of Example 2.

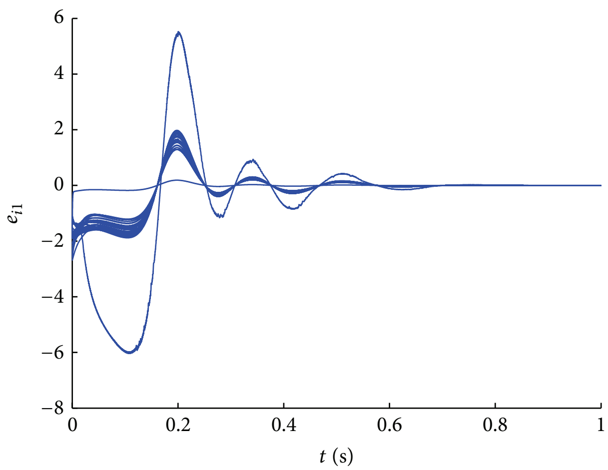

Figure 11: The synchronization errors e_{i1} of the switched networks in Example 2.

From Figures 5 to 10, it is easy to see that two pinning controlled subnetworks cannot achieve synchronization. Applying Theorem 5, we can get synchronization via the designed switching law:

$$\sigma(t) = \begin{cases} 1, & \text{if } e^T\left[\theta I_{30}\otimes\Gamma + c\left(A_1\otimes P\Gamma\right) - c\left(Q_1\otimes P\Gamma\right)\right]e \le 0, \\ 2, & \text{if } e^T\left[\theta I_{30}\otimes\Gamma + c\left(A_2\otimes P\Gamma\right) - c\left(Q_2\otimes P\Gamma\right)\right]e \le 0. \end{cases} \tag{24}$$

The simulations are shown in Figures 11, 12, 13, and 14.

Form Figures 11 to 13, it is easy to see that the states of error systems are very large at the initial time, but after a while, it converges to zero quickly, so the switched complex networks achieved synchronization under the designed switching laws, which verify the validity of Theorem 5. In Figure 14, the value of $\sigma(t)$ denotes the activated subsystem; it means that if $\sigma(t) = 1$, the first subnetwork is activated, and if $\sigma(t) = 2$, the second subnetwork is activated.

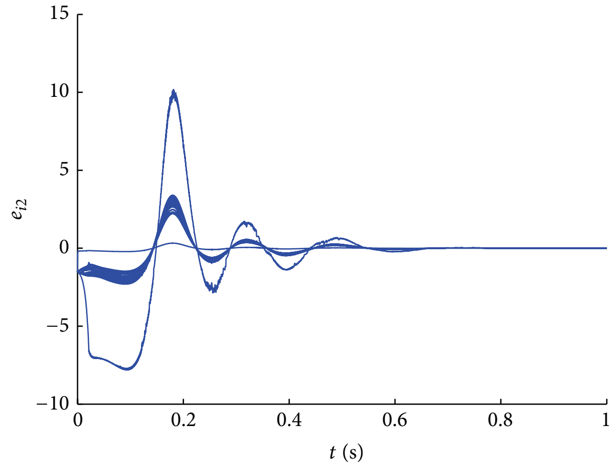

Figure 12: The synchronization errors e_{i2} of the switched networks in Example 2.

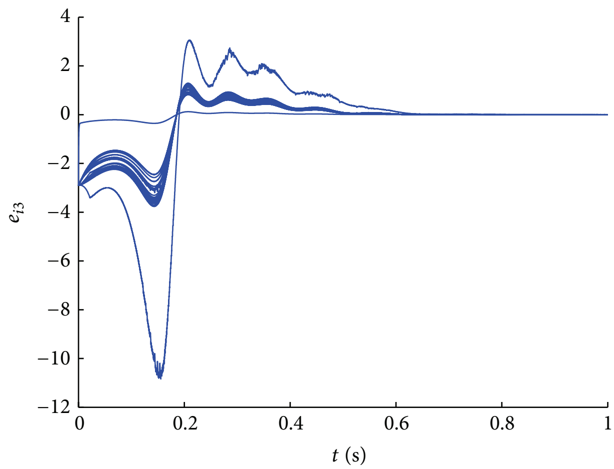

Figure 13: The synchronization errors e_{i3} of the switched networks in Example 2.

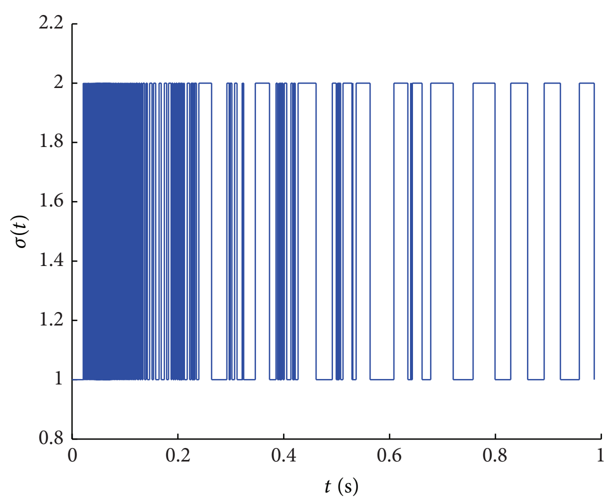

Figure 14: Switching signal of Example 2.

6. Conclusion

The pining synchronization problem of a complex network with switching topology is investigated in this paper. Employing common Lyapunov function method and single Lyapunov function method, some criteria are given to ensure the controlled complex networks achieve global pinning synchronization under arbitrary switching and some designed switching law, respectively. The criteria are simple and easy to verified, but this paper only discussed the pinning synchronization problem of switched dynamical networks by common Lyapunov function and single Lyapunov function method. How to solve this problem by multiple Lyapunov function method is a challenging problem which deserves future study.

Conflict of Interests

The authors declare that there is no conflict of interests regarding the publication of this paper.

Acknowledgments

This project was supported by the National Natural Science Foundation of China (Grant no. 61272253) and the Programs Foundation of Technology Bureau of Shenyang (Grant no. F12-277-1-08).

References

[1] D. J. Watts and S. H. Strogatz, "Collective dynamics of "small-world" networks," *Nature*, vol. 393, no. 6684, pp. 440–442, 1998.

[2] S. Boccaletti, V. Latora, Y. Moreno, M. Chavez, and D.-U. Hwang, "Complex networks: structure and dynamics," *Physics Reports*, vol. 424, no. 4-5, pp. 175–308, 2006.

[3] S. H. Strogatz, "Exploring complex networks," *Nature*, vol. 410, no. 6825, pp. 268–276, 2001.

[4] J. Lü and G. Chen, "A brief overview of some recent advances in complex dynamical networks control and synchronization," in *Proceedings of the IEEE International Symposium on Circuits and Systems (ISCAS '08)*, pp. 2518–2521, Seattle, Wash, USA, May 2008.

[5] A. Arenas, A. Díaz-Guilera, J. Kurths, Y. Moreno, and C. Zhou, "Synchronization in complex networks," *Physics Reports A*, vol. 469, no. 3, pp. 93–153, 2008.

[6] L. M. Pecora and T. L. Carroll, "Master stability functions for synchronized coupled systems," *Physical Review Letters*, vol. 80, no. 10, pp. 2109–2112, 1998.

[7] J. Lu and D. W. C. Ho, "Local and global synchronization in general complex dynamical networks with delay coupling," *Chaos, Solitons and Fractals*, vol. 37, no. 5, pp. 1497–1510, 2008.

[8] L. Guo, X.-H. Nian, and H. Pan, "Synchronization criteria for general coupling complex networks with time varying delay," *Control Theory and Applications*, vol. 28, no. 1, pp. 73–78, 2011.

[9] V. N. Belykh, I. V. Belykh, and M. Hasler, "Connection graph stability method for synchronized coupled chaotic systems," *Physica D: Nonlinear Phenomena*, vol. 195, no. 1-2, pp. 159–187, 2004.

[10] B. Liu, X. Liu, G. Chen, and H. Wang, "Robust impulsive synchronization of uncertain dynamical networks," *IEEE Transactions on Circuits and Systems. I. Regular Papers*, vol. 52, no. 7, pp. 1431–1441, 2005.

[11] J. Zhou, J. Lu, and J. Lü, "Adaptive synchronization of an uncertain complex dynamical network," *IEEE Transactions on Automatic Control*, vol. 51, no. 4, pp. 652–656, 2006.

[12] W. W. Yu and J. D. Cao, "Adaptive synchronization and lag synchronization of uncertain dynamical system with time delay based on parameter identification," *Physica A*, vol. 375, no. 2, pp. 467–482, 2007.

[13] R. O. Grigoriev, M. C. Cross, and H. G. Schuster, "Pinning control of spatiotemporal chaos," *Physical Review Letters*, vol. 79, no. 15, pp. 2795–2798, 1997.

[14] N. Parekh, S. Parthasarathy, and S. Sinha, "Global and local control of spatiotemporal chaos in coupled map lattices," *Physical Review Letters*, vol. 81, no. 7, pp. 1401–1404, 1998.

[15] X. F. Wang and G. Chen, "Pinning control of scale-free dynamical networks," *Physica A: Statistical Mechanics and Its Applications*, vol. 310, no. 3-4, pp. 521–531, 2002.

[16] X. Li, X. Wang, and G. Chen, "Pinning a complex dynamical network to its equilibrium," *IEEE Transactions on Circuits and Systems I: Regular Papers*, vol. 51, no. 10, pp. 2074–2087, 2004.

[17] F. Sorrentino, M. di Bernardo, F. Garofalo, and G. Chen, "Controllability of complex networks via pinning," *Physical Review E*, vol. 75, no. 4, Article ID 046103, 6 pages, 2007.

[18] T. Chen, X. Liu, and W. Lu, "Pinning complex networks by a single controller," *IEEE Transactions on Circuits and Systems I*, vol. 54, no. 6, pp. 1317–1326, 2007.

[19] W. Yu, G. Chen, and J. Lü, "On pinning synchronization of complex dynamical networks," *Automatica*, vol. 45, no. 2, pp. 429–435, 2009.

[20] J. Zhou, J.-A. Lu, and J. Lü, "Pinning adaptive synchronization of a general complex dynamical network," *Automatica*, vol. 44, no. 4, pp. 996–1003, 2008.

[21] F. Xiao and L. Wang, "State consensus for multi-agent systems with switching topologies and time-varying delays," *International Journal of Control*, vol. 79, no. 10, pp. 1277–1284, 2006.

[22] D. J. Hill and G. Chen, "Power systems as dynamic networks," in *Proceedings of the IEEE International Symposium on Circuits and Systems*, pp. 722–725, May 2006.

[23] D. Liberzon, *Switching in Systems and Control*, Birkhäuser, Boston, Mass, USA, 2003.

[24] J. Yao, D. J. Hill, Z.-H. Guan, and H. O. Wang, "Synchronization of complex dynamical networks with switching topology via adaptive control," in *Proceedings of the 45th IEEE Conference on Decision and Control (CDC '06)*, pp. 2819–2824, December 2006.

[25] J. Zhao, D. J. Hill, and T. Liu, "Synchronization of complex dynamical networks with switching topology: a switched system point of view," *Automatica*, vol. 45, no. 11, pp. 2502–2511, 2009.

[26] K. Sehjeong and J. H. David, "Synchronization of a complex network with switched coupling," in *Proceedings of the 17th World Congress the International Federation of Automatic Control*, pp. 1559–1564, 2008.

[27] L. M. Du and J. Zhao, "A synchronization criterion for dynamical networks with non-identical nodes and switching topology," *Control Theory and Applications*, vol. 30, no. 5, pp. 649–655, 2013.

Hindawi Publishing Corporation
Mathematical Problems in Engineering
Volume 2015, Article ID 189013, 8 pages
http://dx.doi.org/10.1155/2015/189013

Research Article

The Design of Robust Controller for Networked Control System with Time Delay

Zhongda Lu,[1,2] Lijing Wang,[2] Fengbin Zhang,[1] and Fengxia Xu[2]

[1] *College of Computer Science & Technology, Harbin University of Science & Technology, Harbin 150080, China*
[2] *School of Computer and Control Engineering, Qiqihar University, Qiqihar, Heilongjiang 161000, China*

Correspondence should be addressed to Zhongda Lu; lu_zhongda@163.com

Received 13 August 2014; Revised 5 November 2014; Accepted 17 November 2014

Academic Editor: Jinhui Zhang

This paper considers the stability and H_∞ control problem of networked control systems with time delay. Taking into account the influence of network with delay, unknown input disturbance, and uncertainties of the system modeling, meanwhile we establish a precise, closed-loop model for networked control systems with time delay. By selecting a proper Lyapunov-Krasovskii function and using Lyapunov theorem, a sufficient condition for stability of the system in the form of LMI is demonstrated, corresponding controller parameters are acquired, and the convergence of the control algorithm is proved. The simulation example shows that the construction of the network robust control system with time delay indeed improves the stability performance of the system, which indicates the effectiveness of the design.

1. Introduction

With the continuous development of science and technology, the structure of the control system is getting more and more complex, and spatial distribution is becoming wider. In the meanwhile, the requirements of system control performance also increasingly have improved. Networked control system arises at the historic moment. Networked control system is a feedback control system composed of the sharing of communication network, which consists of sensors, controllers, and plants which are often connected over a network medium [1]. Compared with traditional feedback control systems, where these components are usually connected via point-to-point cables, the introduction of communication network media brings great advantages, such as low cost, reduced weight and power requirements, simple installation and maintenance, and higher reliability [2]. Therefore, networked control systems are widely applied to industrial system and have received more and more attention. However, the intervention of the network, because of connection interruption and network congestion, makes the system produce time delay. Considering the characteristics of networked control system, time delay can be divided into input delay, output delay, state time delay, and uncertain time delay. According to inherent features of delay, it can be divided into inherent delay, stochastic time delay, uncertainty time delay, and so forth. These delays are time varying in nature, and their presence in a system has an adverse impact not only on system performance but also on its stability [3, 4]. Reducing the influence of the system time delay to improve the controlling precision of the system has high practical value. Therefore, the problems of time delay have received more and more attention and have become more and more popular in many practical applications in recent years. At the same time the limitation of network bandwidth and the collision of date transmission cause the phenomenon of packet dropout and cause the data to be out of order [5].

At present, research issues of NCS are concentrated on the influence of the control quality of network induced delay and data packet dropout [6–9]. In the literature [10], the method of setting a cache in the receiving end was raised by Luck and Ray. On the assumption that the maximum transmission delay in the network is known, all the uncertain time delay was defined into the maximum transmission, because of the artificial extending of the transmission time. In 1998, stochastic optimal control method was used to convert the problem of the random network delay into linear quadratic gauss problem by Nilsson, who considered that the network time delay is less than the sampling period. In the literature [11–13], by using random delay control method and the theory of stochastic control. In the research on the performance of networked control systems, the method can ensure stability of statistical significance. But the precondition is that the network delay must obey a certain distribution. This is difficult to achieve in practical engineering. In the literature [14], the H_∞ control problem was addressed for a class of networked control systems with induced delays and packet dropouts. The NCS was modeled as a switched system with four subsystems via system states augmentation. By using the notion of time-window packet dropout rate and the average dwell time method, we have achieved sufficient condition of system stability, applied the linear matrix inequality technique and the cone complementarity linearization algorithm, and completed the controller design. At the same time, LMI and interior-point method used for solving the convex optimization problem are proposed, to provide an effective tool for analyzing and solving control problems. Using LMI method, the controller can be designed without adjusting parameters, and can be obtained delay related conclusion with less conservativeness. Compared with the solution of the Riccati equation, LMI toolbox of MATLAB can be used for all variables directly. It brings great convenience for design [15–18]. On the other hand, in the networked control system, consider network induced delay generally and ignore the inherent delay in the system. Time delay system is an infinite dimensional system. Processing method for time delay at this stage includes Smith predictor method. By establishing the model, by implementation of compensating with the aid of the model, transfer the time delay to the outside of the closed loop, to achieve the purpose of treatment delays and improve the performance of system [19]. Proportional integral controller and the first differential control are a traditional control method. There are still many missing, such as slow response speed, low control precision, and cannot fully ensure meet the requirements of high performance of complex system [20]. Internal model control, its main idea is to make the dynamic type of inverse phase approximation between controller and system model. The main research method is to transfer time delay control system to a nondelay system by using the Lyapunov functional analysis.

For networked control systems research, this study is more focused on solving the problem of network induced delay and data packet dropout, ignoring the inherent delay of the system. However, the inherent time delay is also a widespread phenomenon of networked control systems. In this paper, being aimed at the networked control systems with time delay, considering the network induced delay, unknown input disturbance, and uncertainties of the system modeling, we establish a precise system model and research on robust control method to design the controller for networked control system.

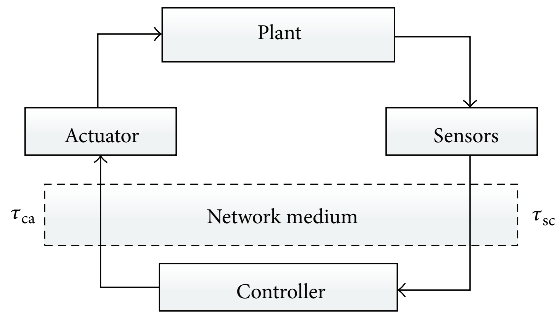

Figure 1: Networked control system model.

2. System Description and Preliminaries

Consider a typical NCS, as shown in Figure 1, controller, sensor, and actuator; these components are often connected over network media. Define the transmission delays as τ_k; τ_{sc} is the delay from the sensor to the controller, τ_{ca} is the delay from the controller to the actuator, and τ_c is the delay for calculation.

Consider the following networked control system with time delay given by

$$\begin{aligned}\dot{x}(t) &= Ax(t) + A_d x(t - d(t)) + Bu(t),\\ y(t) &= Cx(t),\\ z(t) &= Cx(t) + C_d x(t - d(t)) + Du(t),\end{aligned} \tag{1}$$

where $x(t) \in R^n$, $x(t - d(t)) \in R^n$, $u(t) \in R^m$, and $\omega(t) \in R^l$ are the system state vector, the system delay state vector, control input vector, and disturbance input vector, respectively; they belong to $L_2[0\ \ \infty)$, $z(t) \in R^p$ is the output vector control, and $\varphi(t)$ is continuous-time initial function defined on $[-\tau\ \ 0]$. $A \in R^{nn}$, $B \in R^{nm}$, $B_\omega \in R^{nl}$, $C \in R^{pn}$, and $D \in R^{pm}$ are some constant matrix of appropriate dimensions. The state delay of system is $d(t)$ that meets $0 \le d(t) \le \tau$, $\dot{d}(t) \le \rho \le 1$.

Consider the influence of uncertainties from modeling inaccuracies and noise disturbance. A model for time delay networked control systems is described by

$$\begin{aligned}\dot{x}(t) &= [A + \Delta A(t)]\, x(t) + [A_d + \Delta A_d(t)]\, x(t - d(t))\\ &\quad + [B + \Delta B(t)]\, u(t) + [B_\omega + \Delta B_\omega(t)]\, \omega(t),\\ y(t) &= Cx(t),\\ z(t) &= Cx(t) + C_d x(t - d(t)) + Du(t).\end{aligned} \tag{2}$$

The problem of stability and H_∞ stabilization of systems with time-varying delay using static state feedback control law have received considerable attention in recent times [21–23]. Suppose the control law for (1) is $u(t) = Kx(t)$, and when the network transmission delay is small, the actual value transmitted from sensor to actuator decides that the controller acts on this moment of the current value of the object. When the network transmission delay is large, the controller acts on the current object value, depending on the latest value of retainer. At the same time, considering the influence of bounded uncertainties of time delay, in Figure 1, the state feedback controller can be described as

$$u(t) = K_1(t - d(t)) + K_2 x(t - \tau), \tag{3}$$

where $\tau = d(t) + \tau_k$; put (3) into (2) as

$$\begin{aligned}
&\dot{x}(t) \\
&\quad = [A + \Delta A(t)] x(t) + [A_d + \Delta A_d(t) + BK_1 + \Delta BK_1] \\
&\qquad \times x(t - d(t)) + (B + \Delta B) K_2 x(t - \tau) \\
&\qquad + [B_\omega + \Delta B_\omega(t)] \omega(t), \\
&z(t) \\
&\quad = Cx(t) + (C_d + DK_1) x(t - d(t)) + DK_2 x(t - \tau), \\
&\qquad\qquad x(t) = \phi(t), \quad t \in [-\tau, 0],
\end{aligned} \tag{4}$$

where $\Delta A(t)$, $\Delta A_d(t)$, $\Delta B(t)$, and $\Delta B_\omega(t)$ are known, real time-varying matrices of appropriate dimensions representing time-varying parametric perturbations; they are assumed to have the following form:

$$\begin{aligned}
&[\Delta A(t) \;\; \Delta A_d(t) \;\; \Delta B(t) \;\; \Delta B_\omega(t)] \\
&\quad = EF(t)[D_x \;\; D_d \;\; D_u \;\; D_\omega],
\end{aligned} \tag{5}$$

where E, D_x, D_d, D_u, and D_ω are constant matrices of appropriate dimensions and $F(t)$ is an unknown time-varying matrix, which is Lebesgue measurable in t and satisfies $F^T(t)F(t) \le I, \forall \ge 0$.

3. Performance Analysis and Robust Controller Design

Theorem 1. *For a given scalar $\gamma > 0$, there exist real symmetric matrices P, Q, R, matrices K_1, K_2, and scalars $\varepsilon_1 > 0$, $\varepsilon_2 > 0$, $\varepsilon_3 > 0$, $\varepsilon_4 > 0$, $\varepsilon_5 > 0$ which satisfy the following inequality:*

$$\begin{bmatrix}
S & PA_d + PBK_1 & PBK_2 & PB_\omega & C^T & D_x^T & 0 & 0 \\
* & -R + \varepsilon_4^{-1} K_1^T D_u^T & 0 & 0 & C_d^T + K_1^T D^T & 0 & D_d^T & 0 \\
* & * & -Q & 0 & K_2^T D^T & 0 & 0 & K_2^T D_u^T \\
* & * & * & -\gamma I + \varepsilon_5^{-1} D_\omega^T D_\omega & 0 & 0 & 0 & 0 \\
* & * & * & * & -I & 0 & 0 & 0 \\
* & * & * & * & * & -\varepsilon_1^{-1} I & 0 & 0 \\
* & * & * & * & * & * & -\varepsilon_2^{-1} I & 0 \\
* & * & * & * & * & * & * & -\varepsilon_3^{-1} I
\end{bmatrix} < 0, \tag{6}$$

where $S = A^T P + PA + \varepsilon_1 PEE^T P + \varepsilon_2 PEE^T P + \varepsilon_3 PEE^T P + \varepsilon_4 PEE^T P + \varepsilon_5 PEE^T P + R + Q$. Then the NCS like (4) marches the control law shown in (3) and the system is asymptotically stable with an H_∞ norm bound γ. Obtained controller K_1, K_2 is state feedback suboptimal H_∞ controller.

Proof. Consider the following Lyapunov-Krasovskii functional:

$$\begin{aligned}
V(x_t, \omega_t, t) = x^T(t) Px(t) + \int_{t-d(t)}^{t} x^T(s) Rx(s)\, ds \\
+ \int_{t-\tau}^{t} x^T(s) Qx(s)\, ds,
\end{aligned} \tag{7}$$

where P, R, and Q are positive definite matrices. The time derivative of the LK functional along the trajectory of (7) is given by

$$\begin{aligned}
\dot{V}(x_t, \omega_t, t) = \dot{x}^T(t) Px(t) + x^T(t) P\dot{x}(t) + x^T(t) Rx(t) \\
- x^T(t - d) Rx(t - d) + x^T(t) Qx(t) \\
- x^T(t - \tau) Qx(t - \tau)
\end{aligned} \tag{8}$$

without considering the interference factors $\omega(t) = 0$, so

$$\begin{aligned}
&\dot{V}(x_t, \omega_t, t) \\
&\quad = x^T(t) A^T Px(t) + x^T(t) PAx(t) \\
&\qquad + x^T(t) D_x^T F^T x(t) E^T Px(t) + x^T(t) Rx(t) \\
&\qquad + x^T(t) Qx(t) \\
&\qquad + x^T(t) PEF(t) D_x x(t) + x^T(t - d) A_d^T Px(t) \\
&\qquad + x^T(t) PA_d x(t - d) + x^T(t - d) D_d^T F^T(t) E^T Px(t) \\
&\qquad + x^T(t) PEF(t) D_d x(t - d) + x^T(t - \tau) K_2^T B^T Px(t)
\end{aligned}$$

$$
\begin{aligned}
&+ x^T(t) PBK_2 x(t-\tau) - x^T(t-d) R x(t-d) \\
&+ x^T(t) PEF(t) D_u K_2 x(t-\tau) \\
&+ x^T(t-\tau) K_2^T D_u^T F^T(t) E^T P x(t) - x^T(t-\tau) \\
&\times Q x(t-\tau) \\
&+ x^T(t-d) K_1^T B^T P x(t) + x^T(t) PBK_1 x(t-d) \\
&+ x^T(t) PEF(t) D_u K_1 x(t-d) \\
&+ x^T(t-d) K_1^T D_u^T F^T(t) E^T P x(t).
\end{aligned} \tag{9}
$$

Change (9) to get (10) as follows:

$$
\begin{aligned}
&\dot{V}(x_t, \omega_t, t) \\
&\quad \le x^T(t) \left[A^T P + PA + \varepsilon_1^{-1} D_x^T D_x + \varepsilon_1 PEE^T P \right. \\
&\qquad + \varepsilon_2 PEE^T P + \varepsilon_2^{-1} K_1^T D_u^T K_1 + \varepsilon_3 PEE^T P \\
&\qquad \left. + \varepsilon_4 PEE^T P + \varepsilon_5 PEE^T P + R + Q \right] \\
&\quad \times x(t) + x^T(t) \left[PA_d + PBK_1 \right] x(t-d) + x^T(t-d) \\
&\quad \times \left[\varepsilon_2^{-1} D_d^T D_d + \varepsilon_5^{-1} K_1^T D_u^T D_u K_1 - R \right] x(t-d) \\
&\quad + x^T(t) PBK_2 x(t-\tau) + x^T(t-d) \left[A_d^T P + K_1^T B^T P \right] \\
&\quad \times x(t) + x^T(t-\tau) K_2^T B^T P x(t) + x^T(t-\tau) \\
&\quad \times \left[\varepsilon_3^{-1} K_2^T D_u^T D_u K_2 - Q \right] x(t-\tau).
\end{aligned} \tag{10}
$$

Consider reduction for the following form:

$$\dot{V}(x_t, \omega_t, t) = \xi^T(t) \Sigma \xi(t). \tag{11}$$

Define

$$
\xi(t) = \begin{bmatrix} x(t) \\ x(t-d(t)) \\ x(t-\tau) \end{bmatrix}, \qquad
\Sigma = \begin{bmatrix} S_0 & PA_d + PBK_1 & PBK_2 \\ A_d^T P + K_1^T B^T P & \varepsilon_2^{-1} D_d^T D_d + \varepsilon_4^{-1} K_1^T D_u^T D_u K_1 - R & 0 \\ K_2^T B^T P & 0 & \varepsilon_3^{-1} K_2^T D_u^T D_u K_2 - Q \end{bmatrix}, \tag{12}
$$

where $S_0 = A^T P + PA + \varepsilon_1 PEE^T P + \varepsilon_2 PEE^T P + \varepsilon_3 PEE^T P + \varepsilon_5 PEE^T P + R + Q$. □

When $\Sigma < 0$, we have $\dot{V}(x_t, \omega_t, t) < 0$. The system is robust quadratic stability at this time. Considering the interference factors $\omega(t)$, we will have

$$
\begin{aligned}
&\omega^T(t) \overline{B} P(x) + x^T(t) P \overline{B} \omega(t) \\
&\quad = \omega^T(t) B_\omega^T P x(t) + \omega^T(t) D_\omega^T F^T E P x(t) + x^T(t) PB_\omega \omega(t) \\
&\qquad + x^T(t) PEF(t) D_\omega \omega(t) \\
&\quad \le \omega^T(t) B_\omega^T P x(t) + x^T(t) PB_\omega \omega(t) + x^T(t) \varepsilon_5 PEE^T P x(t) \\
&\qquad + \omega^T(t) \varepsilon_5^{-1} D_\omega^T D_\omega \omega(t).
\end{aligned} \tag{13}
$$

Now, for a prescribed scalar $\gamma > 0$, we define a performance index J as follows:

$$\dot{V}(x_t, \omega_t, t) + z^T(t) z(t) - \gamma \omega^T(t) \omega(t) < 0. \tag{14}$$

Then

$$\xi_1^{\ T}(t) \Sigma_1 \xi_1(t) + z^T(t) z(t) < 0. \tag{15}$$

Define

$$
\begin{gathered}
\xi_1(t) = \begin{bmatrix} x(t) \\ x(t-d(t)) \\ x(t-\tau) \\ \omega(t) \end{bmatrix}, \\
\Sigma_1 = \begin{bmatrix} S_1 & PA_d + PBK_1 & PBK_2 & PB_\omega \\ A_d^T P + K_1^T B^T P & \varepsilon_2^{-1} D_d^T D_d + \varepsilon_4^{-1} K_1^T D_u^T D_u K_1 - R & 0 & 0 \\ K_2^T B^T P & 0 & \varepsilon_3^{-1} K_2^T D_u^T D_u K_2 - Q & 0 \\ B_\omega^T P & 0 & 0 & -\gamma I + \varepsilon_5^{-1} D_\omega^T D_\omega \end{bmatrix},
\end{gathered} \tag{16}
$$

where $S_1 = A^T P + PA + \varepsilon_1 PEE^T P + \varepsilon_2 PEE^T P + \varepsilon_3 PEE^T P + \varepsilon_4 PEE^T P + \varepsilon_5 PEE^T P + R + Q$ as

$$\xi_1^T(t)\Sigma_1\xi_1(t) + \begin{bmatrix} C^T \\ C_d^T + K_1^T D^T \\ K_2^T D^T \\ 0 \end{bmatrix} \begin{bmatrix} C & C_d + DK_1 & DK_2 & 0 \end{bmatrix} < 0. \tag{17}$$

Now, for any $x(t)$, $x(t-d)$, $x(t-\tau)$, and $\omega(t)$ the following holds good:

$$\begin{bmatrix} x(t) \\ x(t-d(t)) \\ x(t-\tau) \\ \omega(t) \end{bmatrix}^T \begin{bmatrix} S_1 & PA_d + PBK_1 & PBK_2 & PB_\omega \\ A_d^T P + K_1^T B^T P & \varepsilon_2^{-1} D_d^T D_d + \varepsilon_4^{-1} K_1^T D_u^T D_u K_1 - R & 0 & 0 \\ K_2^T B^T P & 0 & \varepsilon_3^{-1} K_2^T D_u^T D_u K_2 - Q & 0 \\ B_\omega^T P & 0 & 0 & -\gamma I + \varepsilon_5^{-1} D_\omega^T D_\omega \end{bmatrix} \begin{bmatrix} x(t) \\ x(t-d(t)) \\ x(t-\tau) \\ \omega(t) \end{bmatrix}$$
$$+ \begin{bmatrix} x(t) \\ x(t-d(t)) \\ x(t-\tau) \\ \omega(t) \end{bmatrix}^T \begin{bmatrix} C^T \\ C_d^T + K_1^T D^T \\ K_2^T D^T \\ 0 \end{bmatrix} \begin{bmatrix} C & C_d + DK_1 & DK_2 & 0 \end{bmatrix} \begin{bmatrix} x(t) \\ x(t-d(t)) \\ x(t-\tau) \\ \omega(t) \end{bmatrix} < 0. \tag{18}$$

According to the Schur complement lemma, we have

$$\Sigma_2 = \begin{bmatrix} S_1 & PA_d + PBK_1 & PBK_2 & PB_\omega & C^T \\ A_d^T P + K_1^T B^T P & \varepsilon_2^{-1} D_d^T D_d + \varepsilon_4^{-1} K_1^T D_u^T D_u K_1 - R & 0 & 0 & C_d^T + K_1^T D^T \\ K_2^T B^T P & 0 & \varepsilon_3^{-1} K_2^T D_u^T D_u K_2 - Q & 0 & K_2^T D^T \\ B_\omega^T P & 0 & 0 & -\gamma I + \varepsilon_5^{-1} D_\omega^T D_\omega & 0 \\ C & C_d + DK_1 & DK_2 & 0 & -I \end{bmatrix} < 0. \tag{19}$$

Get (19) linear transformation into (6).

The system like (4) is robust asymptotically stable for any $x(t) \in L_2[0\ \ \infty)$, $\omega(t) \in L_2[0\ \ \infty)$, $x(t-d(t)) \in L_2[0\ \ \infty)$, and the system state variables march $\lim_{t\to\infty} x(t) = 0$, $\lim_{t\to\infty} x(t-d) = 0$, and $V(x_0, \omega_0, 0) = 0$, and to make $J = \int_0^\infty [z^T(t)z(t) + \gamma\omega^T(t)\omega(t)]\,dt$ for any $\omega(t) \in L_2[0\ \ \infty)$, we will have

$$J \le \int_0^\infty \left[z^T(t)\,z(t) - \gamma\omega^T(t)\,\omega(t) + \dot{V}(x_t, \omega_t, t)\right] dt < 0. \tag{20}$$

From the formula, $\|z(t)\|_2 \le \gamma\|\omega(t)\|_2$ can be obtained. So, the system shown in (4) is asymptotically stable with an H_∞ norm bound γ. By applying successively Schur complement to (19), we deduce the LMIs stated in Theorem 1.

Theorem 2. *For a given scalar $\gamma > 0$, there exist real symmetric matrices X, matrices Y_1, and scalars $\varepsilon_1 > 0$, $\varepsilon_2 > 0$, $\varepsilon_3 > 0$, which satisfy the following inequality:*

$$\begin{bmatrix} S & A_d + BY_1 & BK_2 & B_\omega & XC^T & XD_x^T & 0 & 0 \\ * & -R + \varepsilon_4^{-1} Y_1^T D_u^T & 0 & 0 & C_d^T + Y_1^T D^T & 0 & D_d^T & 0 \\ * & * & -Q & 0 & K_2^T D^T & 0 & 0 & K_2^T D_u^T \\ * & * & * & -\gamma I + \varepsilon_5^{-1} D_\omega^T D_\omega & 0 & 0 & 0 & 0 \\ * & * & * & * & -I & 0 & 0 & 0 \\ * & * & * & * & * & -\varepsilon_1^{-1} I & 0 & 0 \\ * & * & * & * & * & * & -\varepsilon_2^{-1} I & 0 \\ * & * & * & * & * & * & * & -\varepsilon_3^{-1} I \end{bmatrix} < 0, \tag{21}$$

where $S = AX + XA^T + \varepsilon_1 EE^T + \varepsilon_2 EE^T + \varepsilon_3 EE^T + \varepsilon_4 EE^T + \varepsilon_5 EE^T + R + Q$. The system like (4) under the action of the control law $u(t) = K_1 x(t - d(t)) + K_2 x(t - \tau)$ is asymptotically stable with an H_∞ norm bound γ.

Proof. Put (6) the linear, at both sides, respectively, by $\delta = \operatorname{diag}\{P^{-1}, I, I, I, I, I, I, I\}$, and by $X = P^{-1}$, $Y_1 = K_1 X$ we can get

$$\begin{bmatrix} S & A_d + BK_1 & BK_2 & B_\omega & XC^T & XD_x^T & 0 & 0 \\ * & -R + \varepsilon_4^{-1} K_1^T D_u^T & 0 & 0 & C_d^T + K_1^T D^T & 0 & D_d^T & 0 \\ * & * & -Q & 0 & K_2^T D^T & 0 & 0 & K_2^T D_u^T \\ * & * & * & -\gamma I + \varepsilon_5^{-1} D_\omega^T D_\omega & 0 & 0 & 0 & 0 \\ * & * & * & * & -I & 0 & 0 & 0 \\ * & * & * & * & * & -\varepsilon_1^{-1} I & 0 & 0 \\ * & * & * & * & * & * & -\varepsilon_2^{-1} I & 0 \\ * & * & * & * & * & * & * & -\varepsilon_3^{-1} I \end{bmatrix} < 0. \tag{22}$$

Based on linear matrix inequality can be obtained K_1, K_2. Get the parameters of the corresponding memory state feedback controller. If considering state delay does not contain uncertainties, order $A_d = 0$. □

4. Numerical Example

Consider the actual system with the following parameters:

$$\begin{gathered} A = \begin{bmatrix} -0.9489 & -0.2387 \\ -0.238 & -0.7536 \end{bmatrix}, \qquad A_d = \begin{bmatrix} -0.01 & 0.02 \\ -0.03 & -0.01 \end{bmatrix}, \\ B = \begin{bmatrix} -0.3 \\ 0.1 \end{bmatrix}, \qquad B_\omega = \begin{bmatrix} -0.05 \\ 0.01 \end{bmatrix}, \\ C = \begin{bmatrix} 1.63 & 0 \end{bmatrix}, \qquad Cd = \begin{bmatrix} 0.292 & 0 \end{bmatrix}, \qquad D = 1, \\ I = \begin{bmatrix} 1 & 0 \\ 0 & 1 \end{bmatrix}, \qquad E = \begin{bmatrix} 0.004 & -0.003 \\ 0 & -0.004 \end{bmatrix}, \qquad \gamma = 1, \\ Dx = \begin{bmatrix} 0.06 & -0.02 \\ 0.05 & -0.06 \end{bmatrix}, \qquad Du = \begin{bmatrix} 0.01 \\ 0.02 \end{bmatrix}, \\ D\omega = \begin{bmatrix} 0.01 \\ -0.01 \end{bmatrix}, \qquad Dd = \begin{bmatrix} 0.04 & 0.1 \\ 0.05 & -0.04 \end{bmatrix}. \end{gathered} \tag{23}$$

Using LMI toolbox solving controller, we will have

$$K_1 = \begin{bmatrix} 18.1515 & 14.5412 \end{bmatrix}, \qquad K_2 = \begin{bmatrix} -1.02653 & 0.0064 \end{bmatrix}. \tag{24}$$

A general model for continuous system is $\dot{x}(t) = Ax(t) + Bu(t)$, $z(t) = Cx(t) + Du(t)$. Taking step signal introducing the system, the output curve of the system is shown in Figure 2.

Considering the influence of bounded inherent time delay in networked control system, the output curve is shown in Figure 3. Further, network system existence of bounded fixed time delay, network with delay, and outside disturbance, obtaining output curve, is shown in Figure 4. In order to improve the system performance index, overcome the influence of system from time delay, external disturbance, the modeling error, and the uncertainty factors. By adding a control law of memory $u(t) = K_1 x(t - d) + K_2 x(t - \tau)$, the output response curve is shown in Figure 5.

With reference to Figure 3, when the networked control system with system delay and steady-state error increases, the adjustment time increases. Description that the inherent delay has a great impact on the system. In Figure 4, the system is affected by the inherent time delay, outside disturbance, and

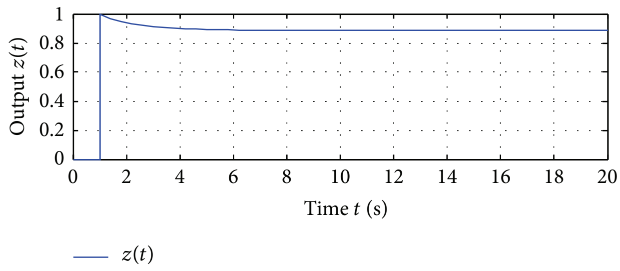

Figure 2: The ideal output response curve of the system.

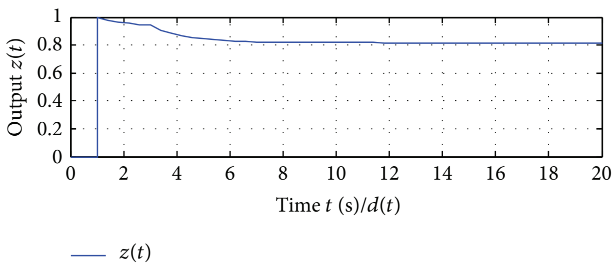

Figure 3: Output curve of the system with inherent time delay.

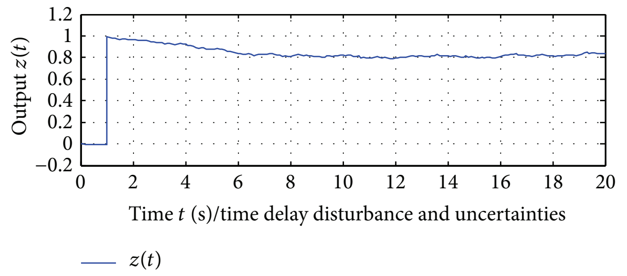

Figure 4: The actual output response curve.

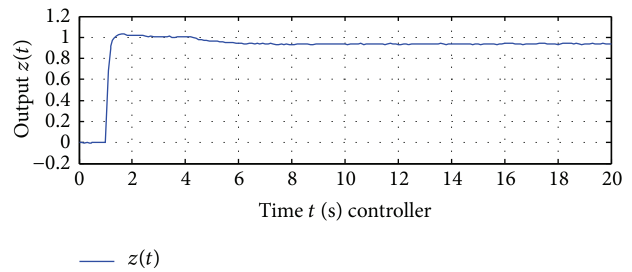

Figure 5: The system output response curve under the action of the controller.

uncertainties. System performance is further deteriorated. From Figure 5, the system output response curve is under the action of the state feedback controller approaching the system ideal output curve. The system can be restored to the stable equilibrium point in a short time. Steady-state error decreases obviously.

5. Conclusion

In the networked control system, delay is universal. In this paper, the research object is the networked control systems with bounded time delay. Considering the influence of network induced delay, unknown input disturbance, and uncertainty of the system modeling, we establish the appropriate system model. The convergence of control algorithm has been proved via the selection of Lyapunov-Krasovskii function. Sufficient conditions for the robust stability of the system are given in the form of LMI. The design method of the controller is given. The simulation example shows that the designed networked control system with bounded time delays reduces the system steady-state error and improves the performance of the system. The problem of networked control systems with bounded inherent time delay has been solved. An effective solution has been proposed, which has certain practical value.

Conflict of Interests

The authors declare that there is no conflict of interests regarding the publication of this paper.

Acknowledgment

This work is partially supported by the project of Scientific Research Foundation for the Returned Overseas Chinese Scholars, Ministry of Education of China.

References

[1] J. P. Hespanha, P. Naghshtabrizi, and Y. Xu, "A survey of recent results in networked control systems," *Proceedings of the IEEE*, vol. 95, no. 1, pp. 138–162, 2007.

[2] H. Ishii and B. A. Francis, *Limited Data Rate in Control Systems with Networks*, Lecture Notes in Control and Information Sciences, Springer, 2002.

[3] Y. Q. Xia, M. Y. Fu, and B. Liu, "Design and performance analysis of networked control systems with random delay," *Journal of Systems Engineering and Electronics*, vol. 20, no. 4, pp. 807–822, 2009.

[4] A. K. Sharma and G. Ray, "Robust controller with state-parameter estimation for uncertain networked control system," *IET Control Theory & Applications*, vol. 6, no. 18, pp. 2775–2784, 2012.

[5] Y. L. Wang and G. H. Yang, "H_∞ control of networked control systems with time delay and packet disordering," *IET Control Theory & Applications*, vol. 1, no. 5, pp. 1344–1354, 2007.

[6] X.-M. Tang and B.-C. Ding, "Design of networked control systems with bounded arbitrary time delays," *International Journal of Automation and Computing*, vol. 9, no. 2, pp. 182–190, 2012.

[7] M. B. G. Cloosterman, N. van de Wouw, W. P. M. H. Heemels, and H. Nijmeijer, "Stability of networked control systems with uncertain time-varying delays," *IEEE Transactions on Automatic Control*, vol. 54, no. 7, pp. 1575–1580, 2009.

[8] K. You and L. Xie, "Survey of recent progress in networked control systems," *Acta Automatica Sinica*, vol. 39, no. 2, pp. 101–117, 2013.

[9] S. Chae, D. Huang, and S. K. Nguang, "Robust partially mode delay dependent H_∞ control of discrete-time networked control systems," *International Journal of Systems Science: Principles and Applications of Systems and Integration*, vol. 43, no. 9, pp. 1764–1773, 2012.

[10] R. Luck and A. Ray, "An observer-based compensator for distributed delays," *Automatica*, vol. 26, no. 5, pp. 903–908, 1990.

[11] F.-L. Lian, J. Moyne, and D. Tilbury, "Network design consideration for distributed control systems," *IEEE Transactions on Control Systems Technology*, vol. 10, no. 2, p. 297, 2002.

[12] S. Hu and Q. Zhu, "Stochastic optimal control and analysis of stability of networked control systems with long delay," *Automatica*, vol. 39, no. 11, pp. 1877–1884, 2003.

[13] J. Nilsson, *Real-Time Control Systems with Delays*, Lund Institute of Technology, Lund, Sweden, 1998.

[14] L. Wei, W. Qing, and D. Chaoyang, "Robust H_∞ control of networked control systems with short delays and packet dropouts," *Journal of Northeastern University*, vol. 6, no. 35, pp. 774–779, 2014.

[15] F. Yang, Z. Wang, Y. S. Hung, and M. Gani, "H_∞ control for networked systems with random communication delays," *IEEE Transactions on Automatic Control*, vol. 51, no. 3, pp. 511–518, 2006.

[16] Y. Wang and Z. Sun, "H_∞ control of networked control systems via lmi approach," *International Journal of Innovative Computing, Information and Control*, vol. 3, no. 2, pp. 343–352, 2007.

[17] S. Chae, D. Huang, and S. K. Nguang, "Robust partially mode delay dependent H_∞ control of discrete-time networked control systems," *International Journal of Systems Science*, vol. 43, no. 9, pp. 1764–1773, 2012.

[18] M. Yu, L. Wang, and T. Chu, "An LMI approach to networked control systems with data packet dropout and transmission delays," in *Proceedings of the 43rd IEEE Conference on Decision and Control (CDC '04)*, vol. 4, pp. 3545–3550, Nassau, Bahamas, 2004.

[19] E. Fridman and U. Shaked, "A new H_∞ filter design for linear time delay systems," *Browse Journals & Magazines*, vol. 8, no. 7, pp. 2839–2843, 2002.

[20] G. J. Silva, A. Datta, and S. P. Bhattacharyya, "PI stabilization of first-order systems with time delay," *Automatica*, vol. 37, no. 12, pp. 2025–2031, 2001.

[21] C. E. de Souza and X. Li, "Delay-dependent robust H_∞ control of uncertain linear state-delayed systems," *Automatica*, vol. 35, no. 7, pp. 1313–1321, 1999.

[22] H. Gao and C. Wang, "Comments and further results on a descriptor system approach to H_∞ control of linear time-delay systems," *Automatic Control*, vol. 48, no. 3, pp. 520–525, 2003.

[23] E. Fridman and U. Shaked, "Delay-dependent stability and H_∞ control: constant and time-varying delays," *International Journal of Control*, vol. 76, no. 1, pp. 48–60, 2003.

Hindawi Publishing Corporation
Mathematical Problems in Engineering
Volume 2015, Article ID 596916, 11 pages
http://dx.doi.org/10.1155/2015/596916

Research Article

Dynamic Quantized Predictive Control for Systems with Time-Varying Delay and Packet Loss in the Forward Channel

Mu Li,[1,2] Lihua Dou,[1,2] Jian Sun,[1,2] and Di Wang[1,2]

[1] *School of Automation, Beijing Institute of Technology, Beijing 100081, China*
[2] *Key Laboratory of Intelligent Control and Decision of Complex Systems, Beijing Institute of Technology, Beijing 100081, China*

Correspondence should be addressed to Jian Sun; sunjian@bit.edu.cn

Received 15 August 2014; Accepted 20 October 2014

Academic Editor: Yun-Bo Zhao

Stability and design of a dynamic quantized predictive control system with time-varying delay and packet loss are studied. For the system with time-varying delay and packet loss in the forward channel, a dynamic quantizer that can minimize the quantized output error is designed and a networked quantized predictive control (NQPC) strategy is proposed to compensate for the delay and packet loss. Stability of the NQPC system is then analyzed and a sufficient stability condition is derived and presented in the form of matrix inequality. Finally, both simulation and experimental results are given to demonstrate the effectiveness of the proposed approach.

1. Introduction

In past decades, networked control systems (NCSs) have been widely studied, whose data are transmitted by networks with finite capacity. Different from traditional control systems, there exist many inevitable problems such as network induced delays and packet losses in networked control systems. To overcome such difficulties, some effective methods have been proposed, among which a representative one is the networked predictive control (NPC) method [1–5].

For example, predictive control system design with time-varying delay in the feedback channel was considered in [1], where sufficient conditions for stability of the closed-loop NCS were given. Meanwhile, NPC systems with delays both in forward and feedback channel were investigated in [2, 3]. The implementation of NPC scheme was addressed in [4], where both simulation and practical implementation were carried out. In [5] an event-driven predictive controller was designed and a practical example was presented to confirm the effectiveness of the NPC method.

For control systems that use networks for communication, data quantization is an important problem which should be taken into consideration. Strictly speaking, all networked control systems are quantized control systems, because data quantization is inevitable before transmission.

There are generally two representative quantizers for quantization: the static quantizer and the dynamic quantizer. In [6–8], a static logarithmic quantizer was studied, where stabilization of discrete-time systems was investigated. In [9, 10], stabilization of systems using finite data rates was analyzed, and it was proved that the finite horizon coder is actually a quantizer. In [11, 12], analysis of systems with a quantized feedback was considered by investigating quantizer complexity versus system performance. In [13, 14], the coarsest logarithmic quantizer design and stabilization of quantized system with packet loss were analyzed. Compared with the static quantizer, dynamic quantizer has been an important topic in last several years. In [15, 16], a novel dynamic quantizer with a scaling factor was proposed, and asymptotic stability was studied using the "zooming" approach. In [17], an optimal dynamic quantizer was investigated, which can minimize the output error between the quantized system and the unquantized system.

For the studies mentioned above, quantization has not been considered for NPC systems that is able to compensate time-varying delay and packet loss. Meanwhile, active

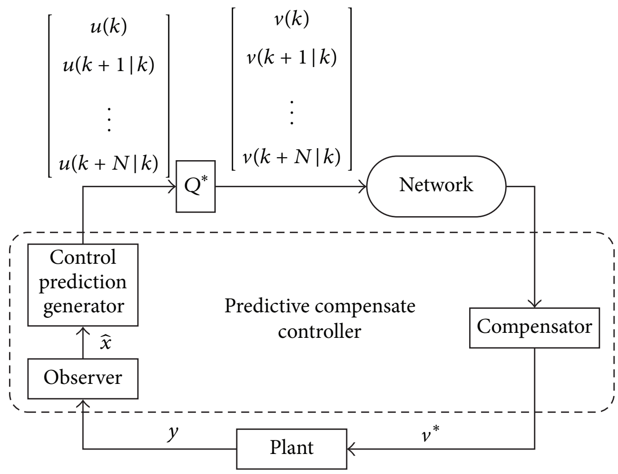

FIGURE 1: Dynamic quantized predictive control system.

compensation of networked delay and packet loss has not been studied for quantized systems before. For these reasons, in this paper, a synthesis method of NQPC system is given. Both time-varying delay and packet loss are compensated using the predictive control method. An improved dynamic quantizer that can minimize the quantized error in the input-output relation is designed for the NQPC system. The closed-loop system is then lifted to a switched system [18–21] and a sufficient condition for stability is given.

The whole paper is organized as follows. Section 2 describes the NQPC system with time-varying delay and packet loss. Section 3 studies the predictive compensation strategy. Section 4 designs a dynamic quantizer that can minimize the maximum output error of the system. Section 5 analyzes stability of the NQPC system. Section 6 gives both simulation and experimental results to indicate that our control strategy is effective and Section 7 concludes the paper.

2. NQPC System Description

The networked quantized predictive control (NQPC) system with time-varying delay in the forward channel as shown in Figure 1 is studied in this paper. The key idea of NQPC is that all the possible future control inputs are quantized and packed into a single packet before being transmitted through the network. Then the compensator chooses an appropriate quantized control input from the received packet and applies it to the plant.

The discrete-time system studied in this paper is described by

$$P : \begin{cases} x(k+1) = Ax(k) + Bv^*(k) \\ y(k) = Cx(k), \end{cases} \tag{1}$$

where $x \in \mathbf{R}^n$, $v^* \in \mathbf{R}^l$, and $y \in \mathbf{R}^p$ are state vector, control input, and system output, respectively. $A \in \mathbf{R}^{n\times n}$, $B \in \mathbf{R}^{n\times l}$, and $C \in \mathbf{R}^{p\times n}$ are system matrices. The initial state is $x_0 \in \mathbf{R}^n$.

The dynamic quantizer Q^* $(i = 0, 1, 2, \dots, N)$ is given by

$$Q^* : \begin{cases} \xi(k+1) \\ \quad = \mathscr{A}\xi(k) + \mathscr{B}(v(k) - u(k)) \\ \xi(k+2 \mid k) \\ \quad = \mathscr{A}\xi(k+1 \mid k) \\ \qquad + \mathscr{B}(v(k+1 \mid k) - u(k+1 \mid k)) \\ \quad \vdots \\ \xi(k+N+1 \mid k) \\ \quad = \mathscr{A}\xi(k+N \mid k) \\ \qquad + \mathscr{B}(v(k+N \mid k) - u(k+N \mid k)) \\ v(k) = q_\mu(\mathscr{C}\xi(k) + u(k)) \\ v(k+1 \mid k) = q_\mu(\mathscr{C}\xi(k+1 \mid k) + u(k+1 \mid k)) \\ \quad \vdots \\ v(k+N \mid k) \\ \quad = q_\mu(\mathscr{C}\xi(k+N \mid k) + u(k+N \mid k)), \end{cases} \tag{2}$$

where $\xi(k+1) = \xi(k+1 \mid k)$, $\xi \in \mathbf{R}^n$, $u^* \in \mathbf{R}^l$, and $v \in \mathbf{V}^l$ are the state, input, and output of Q_i^* ($\mathbf{V} \subset \mathbf{R}$ are quantization sets of Q_i^*) and $\mathscr{A}$, $\mathscr{B}$, and $\mathscr{C}$ are system matrices that will be designed in Section 4. Set the initial states $\xi(0) = 0$ and $v(k) = 0$ when $u(k) = 0$.

The static part q_μ of (2) can be obtained as [15]

$$q_\mu(x) = \begin{cases} \mu(k)M, & \text{if } \dfrac{x}{\mu(k)} > M - \dfrac{\Delta}{2} \\ -\mu(k)M, & \text{if } \dfrac{x}{\mu(k)} \le -M + \dfrac{\Delta}{2} \\ \left\lfloor \dfrac{x}{\Delta\mu(k)} + \dfrac{1}{2} \right\rfloor \Delta\mu(k), & \text{if } \dfrac{|x|}{\mu(k)} \le M - \dfrac{\Delta}{2}, \end{cases} \tag{3}$$

where Δ is its sensitivity and M is the saturation value. We use $\lfloor a \rfloor$ to represent the biggest integer that satisfies $\lfloor a \rfloor \le a$ in our paper. $\mu(k)$ is the scaling factor that is monotonically nonincreasing, which will be considered later in our paper.

Moreover, the following assumptions are made in this paper.

Assumption 1. Consider $l = p$ (the dimensions of v and y are the same) and the matrix CB is nonsingular.

Assumption 2. (A, B) is controllable and (A, C) is observable.

Assumption 3. The delay in the forward channel satisfies $0 \le d(k) \le d_m$.

Assumption 4. The maximum consecutive number of packet loss in the forward channel is p_m.

3. The Predictive Compensation Strategy

To compensate time-varying delay and packet loss in our system, we introduce the predictive compensate controlstrategy

[1, 2] in our paper, which is composed of an observer, a prediction generator, and a delay compensator. The idea of our NQPC method is that all the possible future control inputs are quantized and packed into a packet before transmission, and then the compensator chooses an appropriate control input from the received packet and applies it to the plant.

Firstly a state observer can be given as

$$\begin{aligned}\hat{x}(k+1 \mid k) &= A\hat{x}(k \mid k-1) + Bu(k) \\ &\quad + L\left[y(k) - C\hat{x}(k \mid k-1)\right],\end{aligned} \tag{4}$$

where $\hat{x}(k+1 \mid k) \in \mathbf{R}^n$ is the one step state prediction, $u(k)$ is the input, and L is the system matrix.

For the quantized predictive control system, it is clear that the length of predictive sequence must be equal to or bigger than upper bound of the total network induced delay and packet loss. Therefore, we have integer N satisfying $N \geq d_m + p_m$ which means the prediction is able to compensate for delay and pack loss in the forward channel and N is the length of the predictive sequence.

Based on (4) and the output data up to k, state predictive sequence from instant $k+1$ to $k+N$ can be constructed as

$$\begin{aligned}\hat{x}(k+1 \mid k) &= A\hat{x}(k \mid k-1) + Bu(k) \\ &\quad + L\left[y(k) - C\hat{x}(k \mid k-1)\right] \\ \hat{x}(k+2 \mid k) &= A\hat{x}(k+1 \mid k) + Bu(k+1 \mid k) \\ \hat{x}(k+3 \mid k) &= A\hat{x}(k+2 \mid k) + Bu(k+2 \mid k) \\ &\vdots \\ \hat{x}(k+N \mid k) &= A\hat{x}(k+N-1 \mid k) + Bu(k+N-1 \mid k)\end{aligned} \tag{5}$$

with

$$u(k+i \mid k) = K\hat{x}(k+i \mid k), \tag{6}$$

where, $i = \{1, 2, \ldots, N\}$, $K \in \mathbf{R}^{l\times n}$ is the state feedback gain, and the way we choose K is the same as that of traditional control systems.

This results in

$$\begin{aligned}&\hat{x}(k+i \mid k) \\ &\quad = (A+BK)^{i-1}\hat{x}(k+1 \mid k) \\ &\quad = (A+BK)^{i-1}\left[(A+BK-LC)\hat{x}(k \mid k-1) + LCx(k)\right],\end{aligned} \tag{7}$$

where $i = \{1, 2, \ldots, N\}$.

In this paper, output of the control prediction generator at instant k can be given as

$$\left[u(k)^T \;\; u(k+1 \mid k)^T \;\; u(k+2 \mid k)^T \;\; \cdots \;\; u(k+N \mid k)^T\right]^T. \tag{8}$$

Remark 5. It is clear in (8) that output sequence length of the control prediction generator is $N+1$, which means that the sequence is composed of two parts: the real-time control part $u(k)$ and the predictive control part $[u(k+1 \mid k)^T \;\; u(k+2 \mid k)^T \;\; \cdots \;\; u(k+N \mid k)^T]^T$. When a control output is transmitted without suffering delay or packet loss, the real-time control part $u(k)$ will be used for control. When delay or packet loss occurs during transmission, the predictive control part will be used for control.

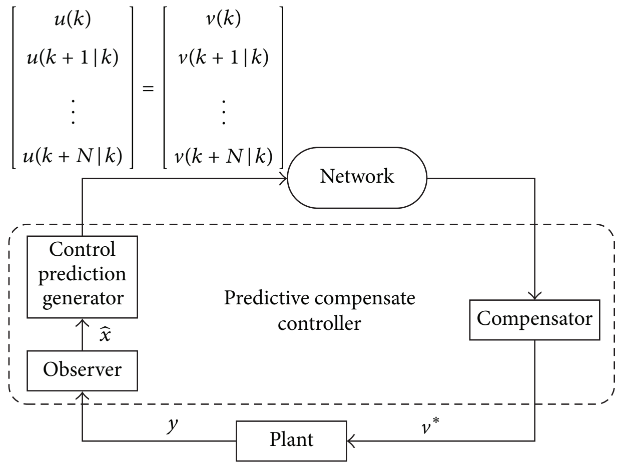

Figure 2: Unquantized predictive control system.

Output of the dynamic quantizer Q^* at instant k is a sequence

$$\begin{aligned}v(k) &= q_\mu\left(\mathscr{C}\xi(k) + u(k)\right) \\ v(k+1 \mid k) &= q_\mu\left(\mathscr{C}\xi(k+1 \mid k) + u(k+1 \mid k)\right) \\ &\vdots \\ v(k+N \mid k) &= q_\mu\left(\mathscr{C}\xi(k+N \mid k) + u(k+N \mid k)\right),\end{aligned} \tag{9}$$

where $v(k+i \mid k)$ $(i = \{0, 1, 2, \ldots, N\})$ is the quantized output signal obtained by quantizer Q^*.

In this paper both packet loss and time-varying delay are considered as delay. Define a bounded random scalar $0 \leq \tau(k) \leq d_m + p_m$. As is depicted in Figure 1, since the quantizer output $v(k)$ is transmitted through the network with delay and packet loss, let $v(k-\tau(k))$ denote the delayed quantizer output received by the compensator at instant k.

For the system considered in this paper, since more than one predictive sequence may arrive at the compensator side at the same time, assume that only the newest predictive sequence is used at each instant.

Then output of the delay compensator at instant k can be obtained as

$$\begin{aligned}v^*(k) &= v(k \mid k-\tau(k)) \\ &= q_\mu\left[\mathscr{C}\xi(k \mid k-\tau(k)) + u(k \mid k-\tau(k))\right].\end{aligned} \tag{10}$$

4. Design of a Dynamic Quantizer

In this section, parameters of the dynamic quantizer (2) are designed.

The system in Figure 2 is an unquantized nominal system, where the initial state, plant, controller, predictive strategy, delay, and packet losses process of that system are same as those in the quantized system in Figure 1.

Definition 6. Define the maximum output error between the two systems as

$$\mathrm{Er}\left(Q^{*}\right)=\max_{k\in\mathbf{Z}_{+}}\left\|y\left(k,x_{0}\right)-y^{*}\left(k,x_{0}\right)\right\|, \tag{11}$$

where for instance k, $y(k)$ is output of the NQPC system in Figure 1 and $y^{*}(k)$ is output of the nominal system in Figure 2 and the initial state is $x(0)=x_0$.

Remark 7. $\mathrm{Er}(Q^{*})$ in (11) represent the output difference between the NQPC system and its nominal system. The upper bound of $\mathrm{Er}(Q^{*})$ is minimized through parameters redesigning of (2), which is an optimal approximation of the nominal system in the sense of input-output relation.

Through parameters redesigning, a dynamic quantizer for our NQPC system can be given according to the following theorem.

Theorem 8. *The dynamic quantizer of the NQPC system that is able to minimize the quantized error can be given as*

$$Q^{*}:\begin{cases}\xi(k+1)=A\xi(k)B(v(k)-u(k))\\ \xi(k+2\mid k)\\ \quad=A\xi(k+1\mid k)\\ \qquad+B(v(k+1\mid k)-u(k+1\mid k))\\ \quad\vdots\\ \xi(k+N+1\mid k)\\ \quad=A\xi(k+N\mid k)\\ \qquad+B(v(k+N\mid k)-u(k+N\mid k))\\ v(k)=q_{\mu}\left(C_{Q}\xi(k)+u(k)\right)\\ v(k+1\mid k)=q_{\mu}\left(C_{Q}\xi(k+1\mid k)+u(k+1\mid k)\right)\\ \quad\vdots\\ v(k+N\mid k)\\ \quad=q_{\mu}\left(C_{Q}\xi(k+N\mid k)+u(k+N\mid k)\right)\end{cases} \tag{12}$$

and the upper bound of the maximum output error can be minimized by

$$Er\left(Q^{*}\right)\leq\|CB\|\frac{\Delta\mu(0)}{2}, \tag{13}$$

where $C_{Q}=-(CB)^{-1}CA$.

Proof. For the NQPC system described in previous section, from (1), (2), (6), and (9) we have the following equations:

$$\begin{aligned}u(k)&=u(k\mid k-\tau(k))\\ &=K(A+BK)^{\tau(k)-1}[(A+BK-LC)\hat{x}\\ &\qquad\times(k-\tau(k)\mid k-\tau(k)-1)\\ &\qquad+LCx(k-\tau(k))],\\ x(k+1)&=Ax(k)+Bv^{*}(k)\\ &=Ax(k)+B\mathscr{C}\xi(k\mid k-\tau(k))+B\omega(k)\\ &\quad+Bu(k\mid k-\tau(k))\\ &=Ax(k)+B\mathscr{C}\xi(k\mid k-\tau(k))+B\omega(k)\\ &\quad+BK(A+BK)^{\tau(k)-1}\\ &\quad\times[(A+BK-LC)\hat{x}(k-\tau(k)\mid k-\tau(k)-1)\\ &\qquad+LCx(k-\tau(k))],\\ \hat{x}(k+1\mid k)&=A\hat{x}(k\mid k-1)+Bu(k)\\ &\quad+L\left[y(k)-C\hat{x}(k\mid k-1)\right]\\ &=(A+BK-LC)\hat{x}(k\mid k-1)+LCx(k),\\ \xi(k+1)&=\mathscr{A}\xi(k)+\mathscr{B}(v(k)-u(k))\\ &=(\mathscr{A}+\mathscr{B}\mathscr{C})\xi(k)+\mathscr{B}\omega(k)\\ \xi(k+1\mid k)&=(\mathscr{A}+\mathscr{B}\mathscr{C})\xi(k)+\mathscr{B}\omega(k)\\ \xi(k+1\mid k-1)&=(\mathscr{A}+\mathscr{B}\mathscr{C})\xi(k\mid k-1)+\mathscr{B}\omega(k),\\ &\vdots\\ \xi(k+1\mid k-N+1)&\\ &=(\mathscr{A}+\mathscr{B}\mathscr{C})\xi(k\mid k-N+1)+\mathscr{B}\omega(k),\end{aligned} \tag{14}$$

where $\omega(k)=q_{\mu}(\mathscr{C}\xi(k\mid\cdot)+u(k))-(\mathscr{C}\xi(k\mid\cdot)+u(k))$. □

Letting $S=(A+BK)$,

$$\begin{aligned}&z(k)\\ &=\Big[\,x(k)^{T}\;\;x(k-1)^{T}\;\cdots\;x(k-N)^{T}\;\;\hat{x}(k\mid k-1)^{T}\;\;\hat{x}(k-1\mid k-2)^{T}\;\cdots\;\hat{x}(k-N\mid k-N-1)^{T}\\ &\qquad u(k-1)^{T}\;\;u(k-2)^{T}\;\cdots\;u(k-N)^{T}\;\;\xi(k)^{T}\,\xi(k-1)^{T}\;\cdots\;\xi(k-N)^{T}\;\;\xi(k\mid k-1)^{T}\\ &\qquad \xi(k-1\mid k-2)^{T}\;\cdots\;\xi(k-N+1\mid k-N)^{T}\;\;\xi(k\mid k-2)^{T}\;\;\xi(k-1\mid k-3)^{T}\;\cdots\;\xi(k-N+2\mid k-N)^{T}\\ &\qquad\cdots\;\;\xi(k\mid k-N)^{T}\,\Big]^{T},\end{aligned}$$

$$\overline{B}=\left[B^{T}\;\;0^{T}_{l\times[n(2N+1)+lN]}\;\;\mathscr{B}^{T}\;\;0^{T}_{l\times nN}\;\;\mathscr{B}^{T}\;\;0^{T}_{l\times n(N-1)}\;\cdots\;\mathscr{B}^{T}\right]^{T},$$

$$\overline{C}=\left[C\;\;0_{p\times[n(3N+2+N(N+1)/2)+lN]}\right],$$

$$\Xi_{\sigma(k)}=\begin{bmatrix}\prod_{11} & \prod_{12} & 0 & \prod_{14}\\ \prod_{21} & \prod_{22} & 0 & 0\\ \prod_{31} & \prod_{32} & \prod_{33} & 0\\ 0 & 0 & 0 & \prod_{44}\end{bmatrix},$$

$$\prod_{11}=\begin{bmatrix} A & 0_{n\times n(\tau(k)-1)} & BKS^{\tau(k)-1}LC & 0_{n\times n(N-\tau(k))}\\ I_{nN\times nN} & 0_{nN\times n} & & \end{bmatrix},$$

$$\prod_{12}=\begin{bmatrix} 0_{n\times n\tau(k)} & BKS^{\tau(k)-1}\left(A+BK-LC\right) & 0_{n\times n(N-\tau(k))}\\ 0_{nN\times n(N+1)} & & \end{bmatrix},$$

$$\prod_{14}=\begin{bmatrix} 0_{n\times n[(\tau(k)+1)N-\tau(k)(\tau(k)-1)/2]} & \mathscr{B}\mathscr{C} & 0_{n\times n(N(N+1)/2-\tau(k)N+\tau(k)(\tau(k)-1)/2-1)}\\ 0_{nN\times n(N(N+1)/2)} & & \end{bmatrix},$$

$$\prod_{21}=\begin{bmatrix} LC & 0_{n\times nN}\\ 0_{nN\times n(N+1)} & \end{bmatrix},$$

$$\prod_{22}=\begin{bmatrix} A-LC & 0_{n\times n(\tau(k)-1)} & BKS^{\tau(k)-1}\left(A-LC\right) & 0_{n\times n(N-\tau(k))}\\ I_{nN\times nN} & 0_{nN\times n} & & \end{bmatrix},$$

$$\prod_{31}=\begin{bmatrix} 0_{l\times n\tau(k)} & KS^{\tau(k)-1}LC & 0_{l\times n(N-\tau(k))}\\ 0_{l(N-1)\times n(N+1)} & & \end{bmatrix},$$

$$\prod_{32}=\begin{bmatrix} 0_{l\times n\tau(k)} & KS^{\tau(k)-1}\left(A+BK-LC\right) & 0_{l\times n(N-\tau(k))}\\ 0_{l(N-1)\times n(N+1)} & & \end{bmatrix},$$

$$\prod_{33}=\begin{bmatrix} 0_{l\times lN} & \\ I_{l(N-1)\times l(N-1)} & 0_{l(N-1)\times l}\end{bmatrix},$$

$$\prod_{44}=\left[\begin{array}{cccccc}
\mathscr{A}+\mathscr{B}\mathscr{C} & \multicolumn{5}{c}{\overbrace{0_{n\times n} \qquad\qquad\qquad \cdots \qquad 0_{n\times n}}^{\frac{N(N+3)}{2}}}\\
I_{nN\times nN} & 0_{nN\times n} & & & \cdots & 0_{nN\times n}\\
\mathscr{A}+\mathscr{B}\mathscr{C} & 0_{n\times n} & & & \cdots & 0_{n\times n}\\
0_{n(N-1)\times n} & I_{n(N-1)\times n(N-1)} & 0_{n(N-1)\times n} & & \cdots & 0_{n(N-1)\times n}\\
0_{n\times n} & \mathscr{A}+\mathscr{B}\mathscr{C} & 0_{n\times n} & & \cdots & 0_{n\times n}\\
0_{n(N-2)\times n} & 0_{n(N-2)\times n} & I_{n(N-2)\times n(N-2)} & 0_{n(N-2)\times n} & \cdots & 0_{n(N-2)\times n}\\
\vdots & & \ddots & & & \\
0_{n\times n} & \cdots & 0_{n\times n} & \mathscr{A}+\mathscr{B}\mathscr{C} & & 0_{n\times nN}\\
0_{n\times n} & \cdots & 0_{n\times n} & 0_{n\times n} & & I_{nN\times nN}\\
0_{n\times n} & \cdots & 0_{n\times n} & 0_{n\times n} & & \mathscr{A}+\mathscr{B}\mathscr{C}
\end{array}\right].
\tag{15}$$

Then the NQPC system can be written as the following switched system:

$$z(k+1) = \Xi_{\sigma(k)} z(k) + \overline{B}\omega(k)$$
$$y(k) = \overline{C} z(k), \tag{16}$$

where the state matrix $\Xi_{\sigma(k)}$ switches in the set of possible matrices $\{\Xi_0 \ \cdots \ \Xi_N\}$ according to the parameter $\sigma(k)$ called the switching function, which takes value from the finite index set $\mathbf{F} = \{0, 1, 2, \ldots, N\}$.

Moreover, the nominal system in Figure 2 is given as

$$\xi(k+1) = \Phi_{\sigma(k)}\xi(k)$$
$$y^*(k) = \widehat{C}\xi(k), \tag{17}$$

where

$$\begin{gathered}\xi_k = \left[\, x(k)^T \ \ x(k-1)^T \ \cdots \ x(k-N)^T \ \ \widehat{x}(k \mid k-1)^T \right. \\ \widehat{x}(k-1 \mid k-2)^T \ \cdots \ \widehat{x}(k-N \mid k-N-1)^T \\ \left. u(k-1)^T \ \ u(k-2)^T \ \cdots \ u(k-N)^T \,\right]^T, \\ \Phi_{\sigma(k)} = \begin{bmatrix} \prod_{11} & \prod_{12} & 0 \\ \prod_{21} & \prod_{22} & 0 \\ \prod_{31} & \prod_{32} & \prod_{33} \end{bmatrix}, \qquad \widehat{C} = \left[C \ \ 0_{p\times n(3N+1)}\right].\end{gathered} \tag{18}$$

Therefore, difference between $y^*(S, x_0)$ and $y(S, x_0)$ ($S \in \mathbf{Z}_+$) is

$$\begin{aligned} &y^*(S, x_0) - y(S, x_0) \\ &\quad = \widehat{C}\Phi_{\sigma(k)}^S \begin{bmatrix} x_0 \\ 0_{n(4N+2)\times 1} \end{bmatrix} - \overline{C}\Xi_{\sigma(k)}^S \begin{bmatrix} x_0 \\ 0_{n(3N+1)\times 1} \end{bmatrix} \\ &\qquad - \overline{C}\sum_{l=0}^{S-1} \Xi_{\sigma(k)}^{(S-1)-l}\overline{B}\omega(l) \\ &\quad = -\overline{C}\sum_{l=0}^{S-1} \Xi_{\sigma(k)}^{(S-1)-l}\overline{B}\omega(l). \end{aligned} \tag{19}$$

It is clear that

$$\begin{aligned} \left\| y^*(S, x_0) - y(S, x_0) \right\| &\le \left\| \sum_{l=0}^{S-1} \overline{C}\Xi_{\sigma(k)}^{(S-1)-l}\overline{B} \right\| \frac{\Delta\mu(0)}{2} \\ &= \left\| CB + \sum_{l=1}^{S-1} \overline{C}\Xi_{\sigma(k)}^{(S-1)-l}\overline{B} \right\| \frac{\Delta\mu(0)}{2}. \end{aligned} \tag{20}$$

Moreover, when $\mathscr{A} = A$, $\mathscr{B} = B$, and $\mathscr{C} = C_Q$, we can get $\overline{C}\Xi_{\sigma(k)}^{(S-1)-l}\overline{B} = 0$ ($l = 1, 2, \ldots, \infty$), which means that the latter part of (20) is minimized, and therefore it can be given that

$$\mathrm{Er}(Q^*) \le \|CB\| \frac{\Delta\mu(0)}{2}. \tag{21}$$

As a result, upper bound of the maximum output error $\mathrm{Er}(Q^*)$ between the NQPC system and its nominal system is minimized, the dynamic quantizer is given in (12), and the smallest upper bound of $\mathrm{Er}(Q^*)$ is obtained in (21).

Remark 9. In this paper the dynamic quantizer (12) is different from that in [17]. Since the scaling quantizer q_μ (3) is used for dynamic quantization instead of traditionally static quantizer in [17], improved dynamic quantizers are obtained for our system, which can finally eliminate the quantized error by adjusting the parameter $\mu(k)$. The adjustment procedure of $\mu(k)$ will be considered in the proof of Theorem 11.

5. Stability Analysis

In this section, a sufficient condition for stability is obtained for the NQPC system, and the way dynamic quantizer works is explained.

Firstly, we have the following lemma.

Lemma 10. *System state $z(k)$ that starts from region R_1 described in (30) will enter region R_{i+1} in $i\pi$ steps, where R_{i+1} can be given by*

$$R_{i+1} = \left\{ z(k) : z^T(k) P z(k) \le \mu(k)^2 \frac{M^2}{\|\mathcal{F}\|^2} \lambda_{\min}(P) \right\}. \tag{22}$$

Proof of Lemma 10 is in the appendix, and $R_1, \pi, \mu(k)$, and $\mathcal{F}$ are defined in the proof of Theorem 11.

Then, main result of our paper is presented by the following theorem.

Theorem 11. *For NQPC system (16) with time-varying delay and packet loss in the forward channel, it is asymptotically stable if there exist $P = P^T > 0$ and $\alpha > 0$ satisfying that*

$$(1+\alpha)\,\Xi_i^T P \Xi_i - P < 0, \tag{23}$$

where $i = \{0, 1, 2, \ldots, N\}$.

Proof. Firstly, let $V(k) = z^T(k) P z(k)$, where $P \in \mathbf{R}^{[n(3N+3+N(N+1)/2)+lN]\times[n(3N+3+N(N+1)/2)+lN]}$ is a positive definite matrix, and $\Delta V(k)$ can be obtained as

$$\begin{aligned} \Delta V(k) &= V(k+1) - V(k) \\ &= z^T(k+1) P z(k+1) - z^T(k) P z(k) \\ &= z^T(k)\left(\Xi_{\sigma(k)}^T P \Xi_{\sigma(k)} - P\right) z(k) \\ &\quad + 2z^T(k)\,\Xi_{\sigma(k)}^T P\overline{B}\omega(k) + \omega^T(k)\,\overline{B}^T P\overline{B}\omega(k) \\ &\le z^T(k)\left[(1+\alpha)\,\Xi_{\sigma(k)}^T P \Xi_{\sigma(k)} - P\right] z(k) \\ &\quad + \left(1+\alpha^{-1}\right)\omega^T(k) P\omega(k) \\ &\le -\left[\lambda_{\min}(D_i)\,|z(k)|^2 + \left(1+\alpha^{-1}\right)\left\|\overline{B}^T P\overline{B}\right\| \Delta^2\mu^2(k)\right] \\ &\le -\left[\lambda_{\min}(D)\,|z(k)|^2 + \left(1+\alpha^{-1}\right)\left\|\overline{B}^T P\overline{B}\right\| \Delta^2\mu^2(k)\right], \end{aligned} \tag{24}$$

where α is a positive scalar, $D_i = -[(1+\alpha)\Xi_i^T P \Xi_i - P]$ is assumed to satisfy $D_i > 0$ for $i = \{0, 1, 2, \ldots, (N_1+1)(N_2+1)-1\}$, and $\lambda_{\min}(D) = \min[\lambda_{\min}(D_i)]$, where $\lambda_{\min}(D_i)$ denotes the smallest eigenvalue of D_i.

It is clear that $\Delta V(k) < 0$ when Theorem 11 is satisfied, and the state of (16) outside the region

$$H = \{z(k) : |z(k)| \leq \Theta\Delta\mu(k)\} \tag{25}$$

will ultimately converge to H, where $\Theta = \sqrt{(1+\alpha^{-1})\|\overline{B}^T P\overline{B}\|/\lambda_{\min}(D)}$.

To ensure asymptotic stability of the system (16) inside region H, the "zoom" method proposed in [15, 16] is used for the following proof.

The zooming-in stage is as follows.

Rewrite $\omega(k)$ as $\omega(k) = q_\mu(\digamma z(k)) - \digamma z(k)$, where

$$\digamma = \begin{bmatrix} K & 0_{p\times n(3N+1+\tau(k)(N+1)-\tau(k)(\tau(k)-1)/2)} & C_Q & 0_{p\times n(N(N+3)/2-\tau(k)(N+1)-\tau(k)(\tau(k)-1)/2)} \end{bmatrix}. \tag{26}$$

Let $\mu(k) = \beta^k$, where β is a given constant satisfying $\beta < 1$. Then $\mu(k)$ can be initialized as

$$\mu(0) = \|A\|^\gamma, \tag{27}$$

where $\gamma = \min\{k \geq 1 : \|q_\mu(\digamma z(k)/\mu(k))\| \leq M\sqrt{\lambda_{\min}(P)/\lambda_{\max}(P)} - \Delta/2\}$.

It follows that

$$\left\|\frac{\digamma z(k)}{\mu(0)}\right\| \leq \left\|q_\mu\left(\frac{\digamma z(k)}{\mu(0)}\right)\right\| + \frac{\Delta}{2} \leq M\sqrt{\frac{\lambda_{\min}(P)}{\lambda_{\max}(P)}}. \tag{28}$$

Then we can obtain that

$$|z_k| \leq \frac{M\mu(0)}{\|\digamma\|}\sqrt{\frac{\lambda_{\min}(P)}{\lambda_{\max}(P)}}. \tag{29}$$

Therefore, we can get that the initial state $z(0)$ belongs to the region

$$R_1 = \left\{z(k) : z^T(k)Pz(k) \leq \frac{M^2}{\|\digamma\|^2}\mu^2(0)\lambda_{\min}(P)\right\}. \tag{30}$$

Define the scaling factor χ as

$$\chi = \sqrt{\frac{\lambda_{\max}(P)}{\lambda_{\min}(P)}}\sqrt{\Theta^2+\varepsilon}\|\digamma\|\Delta M^{-1}, \tag{31}$$

where $\varepsilon > 0$ is a fixed constant. Choose M, Δ in (31) to ensure $\chi < 1$, and it is clear that $R_1 \supset H$, and $z(k)$ will never leave R_1.

The zooming-out stage is as follows. Define

$$\begin{gathered}\widehat{\pi} = \frac{M^2\lambda_{\min}(P)}{\|\digamma\|^2\lambda_{\min}(D)\Delta^2\varepsilon} - \frac{\Theta^2\lambda_{\max}(P)}{\lambda_{\min}(D)\varepsilon},\\ \mu(k) = \chi^{\lfloor k/\pi\rfloor}\mu(0),\end{gathered} \tag{32}$$

where $k \geq 0$ and $\pi = \lfloor\widehat{\pi}\rfloor$, and it is clear that $\widehat{\pi} > 0$ as $\chi < 1$.

From Lemma 10, we can obtain that the system state $z(k)$ belongs to R_2 for $k \geq \pi$

$$R_2 = \left\{z(k) : z^T(k)Pz(k) \leq (\chi\mu(0))^2\frac{M^2}{\|\digamma\|^2}\lambda_{\min}(P)\right\}, \tag{33}$$

where $\mu(k) = \chi\mu(0)$ for $k \geq \pi$.

It is clear that the radius of region R_2 becomes smaller than R_1, which means that the state of the system converges after π steps from the initial state.

Similarly, we have the system state $z(k)$ belonging to R_{i+1} for $k \geq i\pi$

$$R_{i+1} = \left\{z(k) : z^T(k)Pz(k) \leq (\chi^i\mu(0))^2\frac{M^2}{\|\digamma\|^2}\lambda_{\min}(P)\right\}, \tag{34}$$

where $\mu(k) = \chi^i\mu(0)$ for $k \geq \pi$.

As a result, it can be obtained that $\mu(k) \to 0$ when $k \to \infty$ and $\lim_{k\to\infty}|z(k)| = 0$ as the radius of R_n $(n \to \infty)$ goes to 0, and then the proof of Theorem 11 is completed. □

6. Simulation and Practical Examples

In this section, both simulation and practical examples are given to illustrate the advantages of the proposed method.

6.1. Simulation Example. Consider the discrete-time plant described by

$$\begin{gathered}A = \begin{bmatrix} 0.9994 & 0.0096 \\ -0.1125 & 0.9154 \end{bmatrix}, \qquad B = \begin{bmatrix} 4.8563\times 10^{-5} \\ 0.0096 \end{bmatrix},\\ C = \begin{bmatrix} 17630 & 11840 \end{bmatrix}\end{gathered} \tag{35}$$

which is controlled over the network, and matrices A, B, and C are obtained through system identification of the DC motor with sampling period 10 ms. Set $N = 9$, which means that the maximum delay in the forward channel is 90 ms. The networked delay in our simulation is shown in Figure 3.

Choose K and L to be

$$\begin{gathered}K = \begin{bmatrix} -6.75 & -4.784 \end{bmatrix},\\ L = \begin{bmatrix} 1.763\times 10^{-6} & 1.184\times 10^{-6} \end{bmatrix}.\end{gathered} \tag{36}$$

There exist positive scalars $\alpha = 0.01$, positive definite matrix P, and quantizer parameters $\Delta = 0.05$, $M = 6$ satisfying Theorem 8.

Let $\Omega = 0.8$, $\tau = 80$, and give a step input to the plant at $t = 1$ s. Then simulation results of the system can be shown in Figure 4, where the proposed quantized predictive control method is compared with six other methods: the predictive

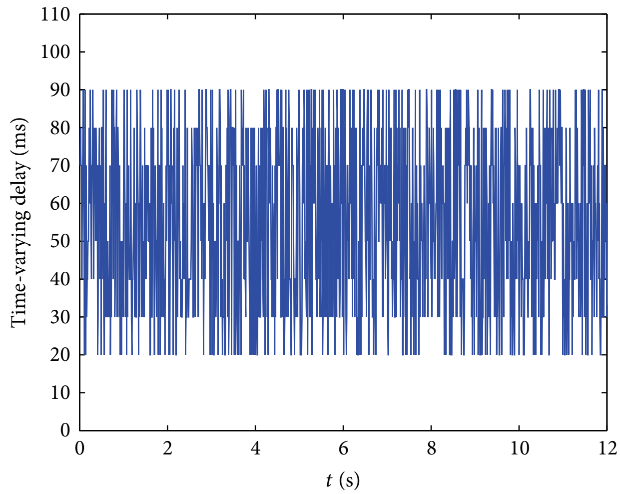

FIGURE 3: Networked delay in simulation.

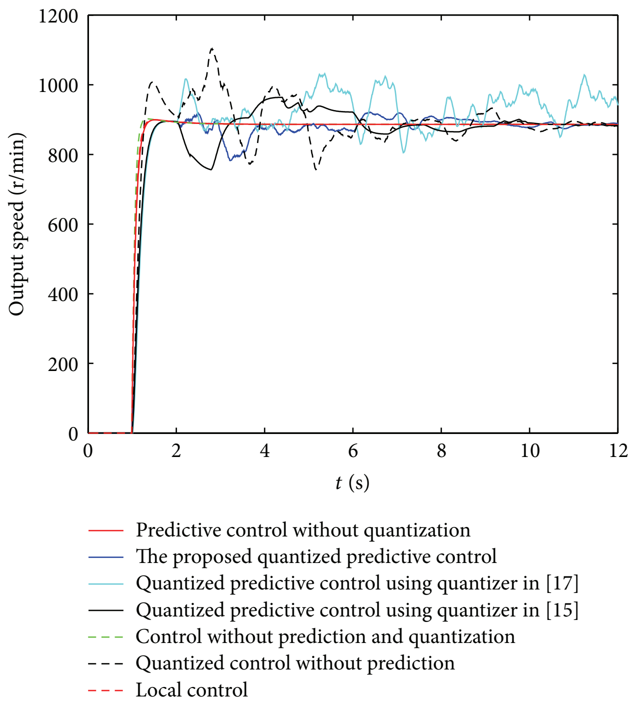

FIGURE 4: Outputs of the system in simulation.

method without quantization, the predictive method using quantizer in [17], the predictive method using quantizer in [15], networked method without prediction and quantization, the proposed quantized method without prediction, and local method. It is clear in Figure 4 that proposed quantized predictive control method is better than other quantized predictive control methods and is more similar to local control, which means that the proposed method is able to compensate the networked delay well.

6.2. Experimental Example. A test rig was built in our lab to test the proposed method, whose experimental diagram is given in Figure 5. Signals were sent from the control box (Figure 8) to the actuator with the help of the trans-

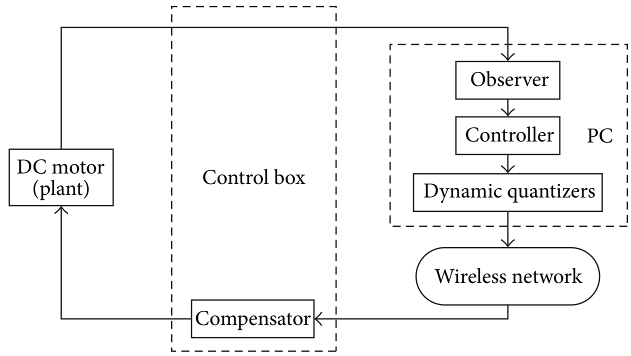

FIGURE 5: Experimental diagram.

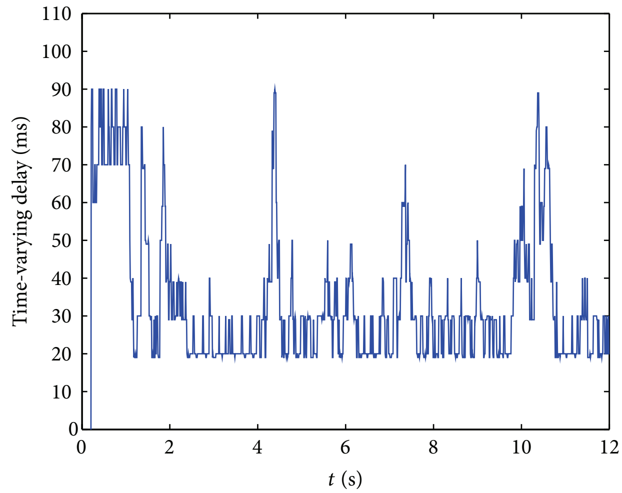

FIGURE 6: Networked delay in experiment.

mission board (Figure 9). The control box's IP address is 192.168.100.20, and the computer's IP address is 192.168.100.21. They communicate with each other by Wi-Fi IEEE 802.11b.

In our test rig, a DC motor (Figure 10) with sampling period 10 ms is controlled, which can be given by (35). Matrices K, L, P, and α and quantizer parameters Δ, M, Ω, and τ are the same as those in simulation example section.

To illustrate the effectiveness of the proposed method, seven cases are studied. Firstly, predictive control without quantization is studied. Then the proposed quantized predictive control method is studied, where networked delay varies between 0 s and 0.18 s as shown in Figure 6. Compared with the proposed method, quantized predictive control methods using quantizer in [15, 17] are studied. Meanwhile, networked control without prediction, quantized control without prediction, and local control are studied. Results of the experiments are given in Figure 7, and it is clear that proposed method performs well and its output of DC motor is very close to that of the local control method.

7. Conclusion

The design and stability of networked quantized predictive control systems where time-varying delay and packet loss

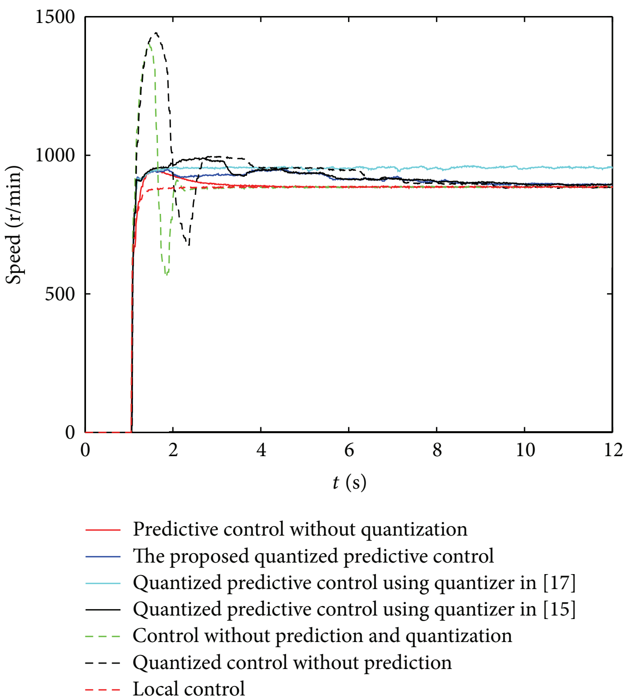

FIGURE 7: Outputs of the system in experiment.

FIGURE 8: The control box.

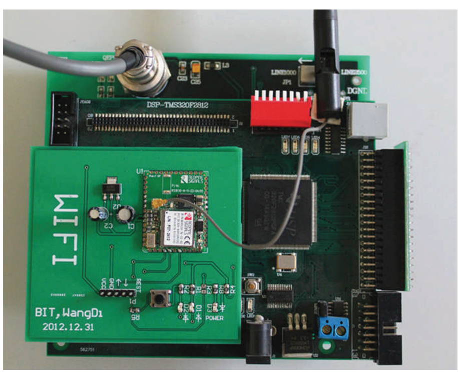

FIGURE 9: The transmission board.

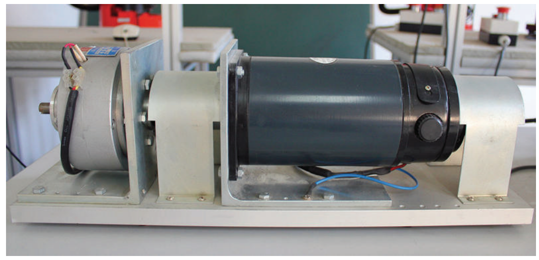

FIGURE 10: The DC motor.

occur in the forward channel have been investigated in this paper. Based on predictive control method, a model that considers delay, packet loss, and optimal quantization has been analyzed. By redesigning the original dynamic quantizer, a dynamic quantizer that can minimize output error of our system is obtained. The stability problem of the given NQPC system has been transformed into stability of a switched system, and a sufficient condition has been presented. Finally, effectiveness of our method has been shown by both simulation and experimental examples.

Appendix

Proof of Lemma 10. Assume the system state at instant π satisfying that

$$z^T(\pi) Pz(\pi) \leq \Delta^2\mu^2(0)\left(\Theta^2+\varepsilon\right)\lambda_{\max}(P). \tag{A.1}$$

If inequality (A.1) is not true, then we have

$$z^T(\pi) Pz(\pi) > \Delta^2\mu^2(0)\left(\Theta^2+\varepsilon\right)\lambda_{\max}(P) \tag{A.2}$$

which means that $|z(\pi)|^2 > \Delta^2\mu^2(0)(\Theta^2+\varepsilon)$ for all $k \in [0,\pi]$.

From (30) and (A.2) we can obtain that

$$\begin{aligned} & z^T(\pi) Pz(\pi) - z^T(0) Pz(0) \\ & \quad \geq \Delta^2\mu^2(0)\left(\Theta^2+\varepsilon\right)\lambda_{\max}(P) - \frac{M^2}{\|F\|^2}\mu^2(0)\lambda_{\min}(P) \\ & \quad = \lambda_{\max}(P)\Theta^2\Delta^2\mu^2(0) - \frac{M^2}{\|F\|^2}\mu^2(0)\lambda_{\min}(P). \end{aligned} \tag{A.3}$$

Nevertheless, from (24), (A.1), and $\chi < 1$, the following inequality can be obtained:

$$\begin{aligned} & \Delta V(\pi-1) \\ & \quad = z^T(\pi) Pz(\pi) - z^T(\pi-1) Pz(\pi-1) \\ & \quad \leq -\lambda_{\min}(D)|z(\pi-1)|^2 + \lambda_{\min}(D)\Theta^2\Delta^2\mu^2(0) \\ & \quad < -\lambda_{\min}(D)\Delta^2\mu^2(0)\varepsilon. \end{aligned} \tag{A.4}$$

Similarly, it can be obtained that

$$\begin{aligned}
&\Delta V(\pi - j) \\
&\quad = z^T(\pi - j + 1) P z(\pi - j + 1) - z^T(\pi - j) P z(\pi - j) \\
&\quad \leq -\lambda_{\min}(D) |z(\pi - j)|^2 + \lambda_{\min}(D) \Theta^2 \Delta^2 \mu^2(0) \\
&\quad < -\lambda_{\min}(D) \Delta^2 \mu^2(0) \varepsilon,
\end{aligned} \tag{A.5}$$

where $j = \{1, 2, 3, \ldots, \pi\}$.

Then we have

$$\begin{aligned}
&z^T(\pi) P z(\pi) - z^T(0) P z(0) \\
&\quad < -\lambda_{\min}(D) \Delta^2 \mu^2(0) \varepsilon\pi \\
&\quad \leq -\lambda_{\min}(D) \Delta^2 \mu^2(0) \varepsilon\widehat{\pi} \\
&\quad = \lambda_{\max}(P) \Theta^2 \Delta^2 \mu^2(0) - \frac{M^2}{\|F\|^2} \mu^2(0) \lambda_{\min}(P).
\end{aligned} \tag{A.6}$$

As there is a contradiction between (A.3) and (A.6), validity of (A.1) has been proved.

Based on (A.1) and $\chi < 1$, it follows that

$$\begin{aligned}
&z^T(\pi) P z(\pi) \\
&\quad \leq \Delta^2 \mu^2(0) \left(\Theta^2 + \varepsilon\right) \lambda_{\max}(P) \\
&\quad < (\chi\mu(0))^2 \frac{M^2}{\|F\|^2} \lambda_{\min}(P).
\end{aligned} \tag{A.7}$$

Thus, $z(\pi)$ belongs to

$$R_2 = \left\{ z(k) : z^T(k) P z(k) \leq (\chi\mu(0))^2 \frac{M^2}{\|F\|^2} \lambda_{\min}(P) \right\}. \tag{A.8}$$

For $\pi \leq k \leq 2\pi$, a similar result can be obtained as

$$z^T(2\pi) P z(2\pi) \leq \left(\chi^2 \mu(0)\right)^2 \frac{M^2}{\|F\|^2} \lambda_{\min}(P). \tag{A.9}$$

Moreover, for $(i-1)\pi \leq k \leq i\pi$, it can be obtained that

$$z^T(i\pi) P z(i\pi) \leq \left(\chi^i \mu(0)\right)^2 \frac{M^2}{\|F\|^2} \lambda_{\min}(P), \tag{A.10}$$

which means that the scaling factor $\mu(k)$ is narrowed every π steps. That is, $z(i\pi)$ belongs to

$$R_{i+1} = \left\{ z(k) : z^T(k) P z(k) \leq \left(\chi^i \mu(0)\right)^2 \frac{M^2}{\|F\|^2} \lambda_{\min}(P) \right\}. \tag{A.11}$$

The proof of Lemma 10 is completed. □

Conflict of Interests

The authors declare that there is no conflict of interests regarding the publication of this paper.

Acknowledgments

This work was supported in part by the Natural Science Foundation of China under Grant no. 61104097, Foundation for Innovative Research Groups of the National Natural Science Foundation of China under Grant no. 61321002, Projects of Major International (Regional) Joint Research Program NSFC under Grant no. 61120106010, Research Fund for the Doctoral Program of Higher Education of China 20111101120027, and Program for New Century Excellent Talents in University under Grant no. NCET-13-0045.

References

[1] G.-P. Liu, Y. Xia, D. Rees, and W. Hu, "Design and stability criteria of networked predictive control systems with random network delay in the feedback channel," *IEEE Transactions on Systems, Man and Cybernetics Part C: Applications and Reviews*, vol. 37, no. 2, pp. 173–184, 2007.

[2] G.-P. Liu, Y. Xia, J. Chen, D. Rees, and W. Hu, "Networked predictive control of systems with random network delays in both forward and feedback channels," *IEEE Transactions on Industrial Electronics*, vol. 54, no. 3, pp. 1282–1297, 2007.

[3] Y.-B. Zhao, G. P. Liu, and D. Rees, "Improved predictive control approach to networked control systems," *IET Control Theory & Applications*, vol. 2, no. 8, pp. 675–681, 2008.

[4] S. Chai, G.-P. Liu, D. Rees, and Y. Xia, "Design and practical implementation of internet-based predictive control of a servo system," *IEEE Transactions on Control Systems Technology*, vol. 16, no. 1, pp. 158–168, 2008.

[5] W. Hu, G. Liu, and D. Rees, "Event-driven networked predictive control," *IEEE Transactions on Industrial Electronics*, vol. 54, no. 3, pp. 1603–1613, 2007.

[6] N. Elia and S. K. Mitter, "Stabilization of linear systems with limited information," *IEEE Transactions on Automatic Control*, vol. 46, no. 9, pp. 1384–1400, 2001.

[7] M. Fu and L. Xie, "The sector bound approach to quantized feedback control," *IEEE Transactions on Automatic Control*, vol. 50, no. 11, pp. 1698–1711, 2005.

[8] H. Haimovich, M. M. Seron, and G. C. Goodwin, "Geometric characterization of multivariable quadratically stabilizing quantizers," *International Journal of Control*, vol. 79, no. 8, pp. 845–857, 2006.

[9] G. N. Nair and R. J. Evans, "Stabilization with data-rate-limited feedback: tightest attainable bounds," *Systems & Control Letters*, vol. 41, no. 1, pp. 49–56, 2000.

[10] G. N. Nair and R. J. Evans, "Stabilizability of stochastic linear systems with finite feedback data rates," *SIAM Journal on Control and Optimization*, vol. 43, no. 2, pp. 413–436, 2004.

[11] F. Fagnani and S. Zampieri, "Stability analysis and synthesis for scalar linear systems with a quantized feedback," *IEEE Transactions on Automatic Control*, vol. 48, no. 9, pp. 1569–1584, 2003.

[12] F. Fagnani and S. Zampieri, "Quantized stabilization of linear systems: complexity versus performance," *IEEE Transactions on Automatic Control*, vol. 49, no. 9, pp. 1534–1548, 2004.

[13] H. Hoshina, K. Tsumura, and H. Ishii, "The coarsest logarithmic quantizers for stabilization of linear systems with packet losses," in *Proceedings of the 46th IEEE Conference on Decision and Control (CDC'07)*, pp. 2235–2240, December 2007.

[14] K. Tsumura, H. Ishii, and H. Hoshina, "Tradeoffs between quantization and packet loss in networked control of linear systems," *Automatica*, vol. 45, no. 12, pp. 2963–2970, 2009.

[15] R. W. Brockett and D. Liberzon, "Quantized feedback stabilization of linear systems," *IEEE Transactions on Automatic Control*, vol. 45, no. 7, pp. 1279–1289, 2000.

[16] D. Liberzon, "Hybrid feedback stabilization of systems with quantized signals," *Automatica*, vol. 39, no. 9, pp. 1543–1554, 2003.

[17] S. Azuma and T. Sugie, "Optimal dynamic quantizers for discrete-valued input control," *Automatica*, vol. 44, no. 2, pp. 396–406, 2008.

[18] Z. Sun and S. S. Ge, "Analysis and synthesis of switched linear control systems," *Automatica*, vol. 41, no. 2, pp. 181–195, 2005.

[19] J. Sun and J. Chen, "A note on stability and stabilization of discrete-time systems with time-varying delay," in *Proceedings of the 31st Chinese Control Conference (CCC '12)*, pp. 1430–1434, IEEE, Hefei, China, July 2012.

[20] Y. Xia, G. P. Liu, P. Shi, D. Rees, and E. J. Thomas, "New stability and stabilization conditions for systems with time-delay," *International Journal of Systems Science*, vol. 38, no. 1, pp. 17–24, 2007.

[21] M. B. Cloosterman, L. Hetel, N. van de Wouw, W. P. Heemels, J. Daafouz, and H. Nijmeijer, "Controller synthesis for networked control systems," *Automatica*, vol. 46, no. 10, pp. 1584–1594, 2010.

Hindawi Publishing Corporation
Mathematical Problems in Engineering
Volume 2015, Article ID 639793, 9 pages
http://dx.doi.org/10.1155/2015/639793

Review Article

Networked Control Systems: The Communication Basics and Control Methodologies

Yun-Bo Zhao,[1] Xi-Ming Sun,[2] Jinhui Zhang,[3] and Peng Shi[4,5]

[1] *Department of Automation, Zhejiang University of Technology, Hangzhou 310023, China*
[2] *Research Center of Information and Control, Dalian University of Technology, Dalian 116024, China*
[3] *College of Information Science and Technology, Beijing University of Chemical Technology, Beijing 100029, China*
[4] *College of Automation, Harbin Engineering University, Harbin, Heilongjiang 150001, China*
[5] *School of Electrical and Electronic Engineering, University of Adelaide, Adelaide, SA 5005, Australia*

Correspondence should be addressed to Yun-Bo Zhao; yunbo.zhao@imperial.ac.uk

Received 11 December 2014; Accepted 23 February 2015

Academic Editor: Bo Shen

As an emerging research field, networked control systems have shown the increasing importance and attracted more and more attention in the recent years. The integration of control and communication in networked control systems has made the design and analysis of such systems a great theoretical challenge for conventional control theory. Such an integration also makes the implementation of networked control systems a necessary intermediate step towards the final convergence of control, communication, and computation. We here introduce the basics of networked control systems and then describe the state-of-the-art research in this field. We hope such a brief tutorial can be useful to inspire further development of networked control systems in both theory and potential applications.

1. Introduction

"Networked control systems" (NCSs) are the name of a general class of control systems where "the control loop is closed via a serial communication network" [1]. Interest in such a system configuration can date back to as early as 1980s, when the so-called "Integrated Communication and Control Networks" attracted much attention from the control community [2]. From that time on, other aliases, such as "Network-Based Control Systems" and "Control over (through) Networks," have also been used to describe similar, if not the same, system configuration as NCSs but are seldom used today.

As indicated by its name, the most distinct feature of NCSs is the use of communication networks in the control loop [3, 4]. Earlier days have witnessed the use of the control-oriented communication networks, such as the Control Area Network and DeviceNet, as the first choice of the communication networks in NCSs; the fast development of the communication technology as well as the increasing needs of large scale systems has now made the Internet an overwhelmingly attracting alternative. The Internet offers us the capability of building a large control system at much lower cost and easier maintenances, with also more flexible reconfiguration. Built on such fundamental theoretical advances in NCSs, we have seen various innovations, such as the smart home, smart transportation, remote surgery, and Internet of Things, in recent years [5–8].

The advantages brought by NCSs however do not come at no cost. A fundamental basis of conventional control systems is that the data exchanges among the control components are lossless. In NCSs, the data have to be transmitted through the communication network, and the nature of the Internet and other variations of data networks means that perfect data exchanges among the control components are essentially unavailable. The imperfect data translation in NCSs thus introduces the so-called communication constraints to the control system, which include, for example, the network-induced delay (the delays occurred in transmitting the sensing and control data),

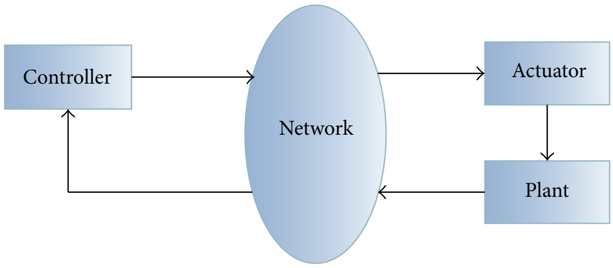

Figure 1: Networked control systems in the direct structure.

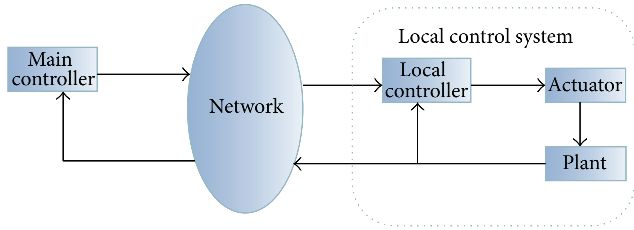

Figure 2: Networked control systems in the hierarchical structure.

the data packet dropout (the data packet may be missing during transmission), and the time synchronization issue (different control components may work on different clocks) [9]. These communication constraints can greatly degrade the system performance or even destabilize the system at certain conditions, while simple extensions of conventional control approaches cannot be obtained directly in a networked control environment [10–16]. These difficulties thus pose great challenges for the control and communication communities and considerable works have been done for a better understanding and design of such systems at the boundary of control theory and communication technology [17–19].

Here, we provide a brief tutorial on NCSs. This consists of two parts. We first give an extensive introduction of the communication networks in NCSs, including its basic characteristics and more importantly its interactions with the control system. Note that we focus on data networks such as the Internet but not the control-oriented networks, simply because of the increasing use and more complicated communication features of the former. We then survey the state-of-the-art research on NCSs, from mainly the control perspective with also an emphasis on the codesign approach which integrates both control and communication. This tutorial is not necessarily thorough or comprehensive. Rather, our main purpose is to introduce to the new researchers the basics of NCSs. By attracting more and more young researchers to this field, we believe that the glorious future that NCSs have promised will become true very soon.

For simplicity in this tutorial, we focus on a simpler structure of NCSs. In fact, from a general perspective of system structure, NCSs may contain two different structures [20]: the "direct structure" (Figure 1) and the "hierarchical structure" (Figure 2). The latter is different from the former as a local controller is present and the communication network is used to close the loop between the main controller and the local system. This structural distinction may have some theoretical as well as practical values; the latter, however, may be regarded as a hierarchical combination of the direct structured NCS and a conventional local control system and therefore it is not absolutely necessary to investigate the hierarchical structure as a brand new type of NCSs. In fact, most available works on NCSs to date have focused on the direct structure, which is also the main focus of this brief tutorial.

2. The Basics of Networked Control Systems

This section introduces the basics of NCSs, where an emphasis is made on the differences between NCSs and conventional control systems, that is, the distinct and unique characteristics of NCSs that are brought by the inserted communication network.

2.1. Network Topology. In the presence of the communication network in the NCSs, the conventional control components include the sensor, the controller, and the actuator work as network nodes from the perspective of network topology. From this perspective, two issues need to be addressed as follows.

2.1.1. Time-Synchronization. The control components need to be time synchronized to act properly. This is a fundamental basis of conventional control systems but is usually missing in NCSs due to the use of the distributed communication networks [21]. Under certain conditions, time-synchronization in NCSs may not be a necessary condition if the network-induced delay in the backward channel is not required for the calculation of the control signals and/or the network-induced delay in the forward channel is not required for the implementation of the control actions. In some other cases, as discussed in [22, 23], time-synchronization together with the use of time stamps in NCSs can offer an advantage over conventional time delay systems since the backward channel delay is known by the controller and the forward channel delay (round trip delay as well) is known by the actuator. This advantage can then be used to derive a better control structure for NCSs as done in [22, 24].

2.1.2. Drive Mechanism. The sensor and the actuator can be driven either by time or event. The difference between the two drive mechanisms lies in the trigger method that initiates the control components. For the time-driven mechanism, the control components are trigged to work at regular intervals, while for the event-driven mechanism the control components are only trigged by predefined "events." From a broad perspective, time-driven mechanism can be regarded as a special case of event-driven mechanism, when the trigger events for the latter are chosen as the time. Therefore, it is no wonder why the event-driven mechanisms are more sophisticated and may require ancillary devices to work.

The sensor is usually time driven, while the controller and the actuator can either be time driven or event driven. For

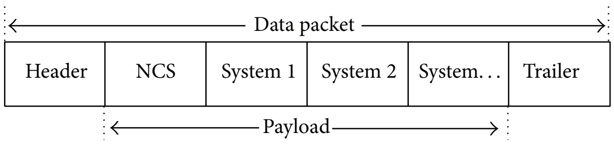

FIGURE 3: The typical data packet structure where NCS is sharing the data packet with other applications.

more information on the drive mechanism for the control components, the reader is referred to [25] and the references therein. It is worth mentioning though that, with different drive mechanisms, different system models for NCSs are obtained and event-driven control components generally lead to a better system performance.

2.2. Packet-Based Data Transmission. The data in NCSs is encoded in the data packets and then transmitted through the communication network. A typical data packet is shown in Figure 3. Packet-based transmission is one of the most important characteristics of NCSs which distinguishes it from conventional control systems [26–28]. This characteristic can mean that the perfect data transmission as assumed in conventional control systems is absent in NCSs, posing the most challenging aspect in NCSs. The communication constraints caused by the packet-based transmission in NCSs include the network-induced delay, data packet dropout, and data packet disorder, which are detailed in what follows.

2.2.1. Network-Induced Delay. The transmission time for the data packets introduces network-induced delays to NCSs, which are well known to degrade the performance of the control systems.

There are two types of network-induced delays according to where they occur.

(i) τ_{sc} is network-induced delay from the sensor to the controller, that is, backward channel delay.

(ii) τ_{ca} is network-induced delay from the controller to the actuator, that is, forward channel delay.

The two types of network-induced delays may have different characteristics [29]. In most cases, however, these delays are not treated separately and only the round trip delay is of interest [4, 30–32].

According to the types of the communication networks being used in NCSs, the characteristics of the network-induced delay vary as follows [20, 33, 34].

(i) Cyclic service networks (e.g., Toking-Ring and Toking-Bus) are bounded delays which can be regarded as constant for most occasions.

(ii) Random access networks (e.g., Ethernet and CAN) are random and unbounded delays.

(iii) Priority order networks (e.g., DeviceNet) are bounded delays for the data packets with higher priority and unbounded delays for those with lower priority.

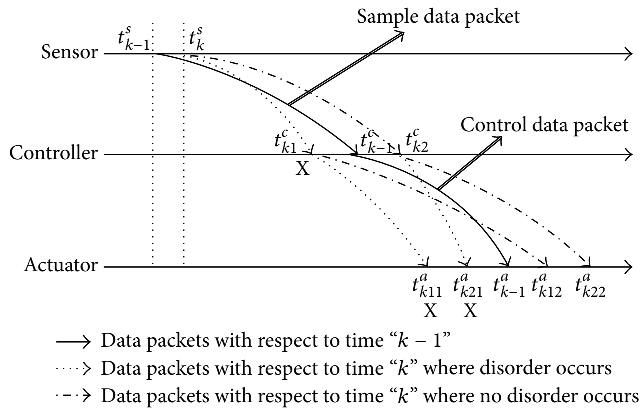

FIGURE 4: Data packet disorder in NCSs.

Network-induced delay is one of the most important characteristics of NCSs which has been widely addressed in the literature to date; see, for example, [4, 30, 32, 35–48].

2.2.2. Data Packet Dropout. Data transmission error in communication networks is inevitable, which in the case of NCSs then produces a situation called "data packet dropout." Data packet dropout can occur either in the backward or forward channel, and it makes either the sensing data or the control signals unavailable to NCSs, thus significantly degrading the performance of NCSs.

In communication networks, two different strategies are applied when a data packet is lost, that is, either to send the packet again or simply discard it. Using the terms from communication networks, these two strategies are called transmission control protocol (TCP) and user datagram protocol (UDP), respectively [21]. It is readily seen that, with TCP, all the data packets will be received successfully, although it may take a considerably long time for some data packets, while, with UDP, some data packets will be lost forever.

As far as NCSs are concerned, UDP is used in most applications due to the real-time requirement and the robustness of control systems. As a result, the effect of data packet dropout in NCSs has to be explicitly considered, as done in, for example, [49–54].

2.2.3. Data Packet Disorder. In most communication networks, different data packets suffer different delays, which then produces a situation where a data packet sent earlier may arrive at the destination later or vice versa; see Figure 4. This phenomenon is referred to as data packet disorder. The existence of data packet disorder can mean that a newly arrived control signal in NCSs may not be the latest, which never occurs in conventional control systems. The control performance will be inevitably degraded if the control algorithm has not taken explicit consideration of the disordered data. Some preliminary works have been done, usually using an active compensation scheme [55–57].

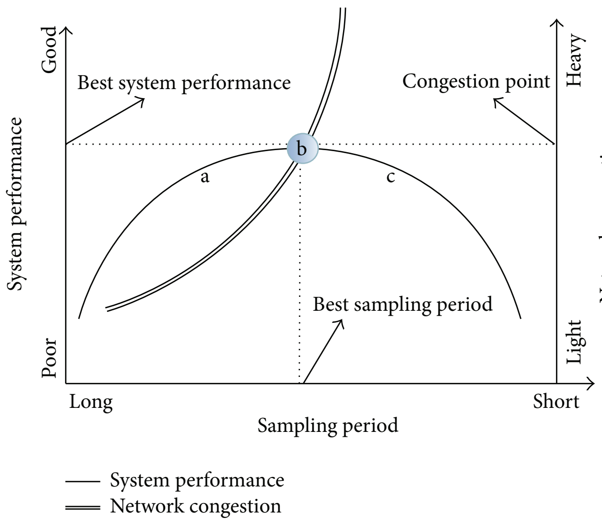

FIGURE 5: Relationship between the sampling period, network loads, and system performance in NCSs.

2.2.4. Single and Multipacket. When the sensing data and the control signals are sent via data packets of the network, another situation occurs: in a case where, for example, multiple sensors are used and distributed geographically in NCSs and thus they send their sensing data separately to the controller over the network, the controller may have to wait for the arrival of all the sensing data packets before it is able to calculate the control actions, and if only one sensing data packet is lost, all the other sensing data packets have to be discarded due to incompleteness. We call this situation the "multipacket" transmission of the data in NCSs.

Another situation in NCSs is where the sensing data or the control signals of multiple steps are sent via a single data packet over the network, since the packet size used in NCSs can be very large compared with the data size required to encode a single step of sensing data or control signal. This "single packet" transmission of the data in NCSs is the fundamental basis of the so-called packet-based control approach [24].

2.3. Limited Network Resources. The limitation of the network resources in NCSs is primarily caused by the limited bandwidth of the communication network, which results in the following three situations in NCSs that are distinct from conventional control systems.

2.3.1. Sampling Period, Network Loads, and System Performance. NCSs are a special class of sampled data systems due to the digital transmission of the data in communication networks. However, in NCSs, the limited bandwidth of the network produces a situation where, a smaller sampling period may not result in a better system performance which is normally true for sampled data systems [58].

This situation happens because, with a too small sampling period, too much sensing data will be produced, thus overloading the network and causing congestion, which will result

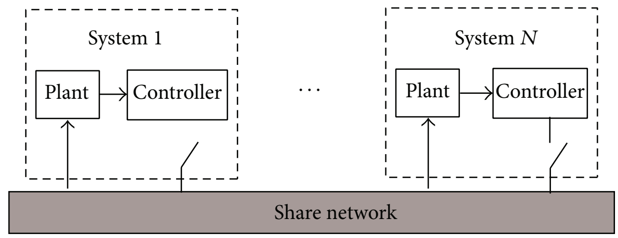

FIGURE 6: Multiple NCSs can share the communication network.

in more data packet dropouts and longer delays, and then degrading the system performance. The relationship between the sampling period, network loads, and system performance in NCSs is illustrated in Figure 5. For example, when the sampling period decreases from the value corresponding to points "a" to "b," the system performance is getting better as in conventional sampled data systems since the network congestion does not appear until point "b"; however, the system performance is likely to deteriorate due to the network congestion when the sampling period is getting even smaller from the value corresponding to points "b" to "c." Therefore, the relationship shown in Figure 5 implies that there is a trade-off between the period of sampling of the plant data and the system performance in NCSs; that is, in NCSs, an optimal sampling period exists which offers the best system performance (point "b" in Figure 5).

2.3.2. Quantization. Due to the use of data networks with limited bandwidth, signal quantization is inevitable in NCSs, which has a significant impact on the system performance. Quantization in the meantime is also a potential method to reduce the bandwidth usage which enables it to be an effective tool to avoid the network congestion in NCSs and thus improve the system performance of NCSs. For more information on the quantization effects in NCSs, the reader is referred to [59–64] and the references therein.

2.3.3. Network Access Constraint and Scheduling. As shown in Figure 3, an NCS may use only part of the payload and share the data packet with other applications. In particular, in Figure 6, the other applications can also be NCSs, meaning that multiple NCSs share the same communication network. In such a case, the limited bandwidth of the network means that subsystems may not be able to access the network resources at all times due to resource competition. A scheduling algorithm is therefore needed to schedule the timeline of when and how long a specific subsystem can occupy the network resource. At the same time, under the satisfactory control performance constraint, the less bandwidth an NCS uses, the better it does to other applications.

3. The Research on Networked Control Systems

In this section, we briefly survey the state-of-the-art research on NCSs. This consists of two parts, categorized according to the methodologies used in these research; that is, the first category is dominated by the use of the control theory, while the second one adopts a codesign strategy by combining control and communication together.

3.1. Control-Centred Research on NCSs. Since the renewed interest in NCSs [1], the research on NCSs has been primarily done within the control theory community [20].

From the control theory community, one is concerned with the theoretical analysis of the control performance of NCSs where the network in NCSs is modeled by predetermined parameters to the control system. In this type of research, the communication characteristics of NCSs, for example, the network-induced delay, can be formulated and incorporated into the system as some parameters, thereby yielding a conventional control system for further analysis and design. This type of research simplifies the modeling and analysis of NCSs, enabling all existing control methods to be readily applied to NCSs. Hence, such a research strategy has been dominating the research field for a significant period [20, 65].

Since the communication characteristics are assumed to be given parameters, the design of NCSs then faces great conservativeness. Most works can only focus on the extension of existing control approaches to NCSs without full use of the communication characteristics of NCSs. This then ignores the possibility of optimizing the system performance by making efficient use of the network characteristics [66–69].

The conventional control approaches and theories that have been applied to NCSs are briefly surveyed as follows.

(i) Time Delay Systems. As far as the network-induced delay is concerned, it is natural to model NCSs as a special class of time delay systems. This research method covers a vast range of research on NCSs; see, for example, [39, 41, 70–77] and the survey in [4, 20, 78].

An interesting issue here is to determine the maximum allowable delay bound (MADB) of NCSs, which is the upper bound of the transfer interval that ensures the stability or other performance objectives of NCSs [79]. The determination of MADB is important in theory and can also play a guiding role for practical applications. One can refer to the survey paper in [36] for more information on this issue.

(ii) Stochastic Control. As mentioned above, the communication constraints in NCSs are stochastic in nature, thus enabling the application of conventional stochastic control approaches to NCSs. An early study can be found in [29], where the characteristics of the network-induced delay were explicitly formulated and preliminary stochastic stability criteria of NCSs were obtained; [35] extended the work in [2] to a stochastic optimal control framework and gave the stochastic optimal state feedback and output feedback controllers, respectively; in [42], the sufficient and necessary conditions of the stochastic stability of NCSs were obtained based on the Markov jump system framework. For further information, the reader is referred to the survey in [9].

(iii) Optimal Control. As a very successful idea both in theory and practical applications, optimal control has also found its position in NCSs. Undoubtedly, conventional optimal control approaches can be used in the networked control environment to design the controller for NCSs; see, for example, [48, 50, 51, 80–82]; and, as a special class of optimal control approaches, model predictive control (MPC or receding horizon control (RHC)) seems to be more suitable for the networked control environment and "a major extension required to apply model predictive control in networked environments would be the distributed solution of the underlying optimization problem" [27]. Examples of the application of MPC to NCSs can be seen, for example, in [23, 44, 83–86].

(iv) Switched System Theory. Another important tool in the study on NCSs is switched system theory, which is typically used by modelling different network conditions in NCSs as different system modes. This approach can readily deal with network-induced delay as well as data packet dropout in NCSs, and the limitation of the approach is caused mainly by how well we understand the properties of the changes of the network conditions, which is generally difficult. For the research in this area, the reader is referred to [72, 75, 87–93] and the references therein.

3.2. Codesign for NCSs. As has been pointed out earlier, it is the communication network which replaces the direct connections among the control components in conventional control systems that makes NCSs distinct. Therefore, the so-called codesign approach to NCSs, an approach that integrates both control and communication, has been an emerging trend in recent years. The communication constraints are no longer assumed as predetermined parameters but act as designable factors, and by the efficient use of these factors a better performance can be expected [23, 26, 67, 68, 85, 94–97]. We give two examples of the codesign approach to NCSs.

(i) Packet-Based Control Approach. As discussed in Section 2.2, the packet-based transmission is one of the most distinct characteristics of NCSs. This characteristic can be used to derive a codesign control structure for NCSs, called the packet-based control framework, as done in [23, 24, 98–100]. The packet-based control approach has its origin in [44, 97], where, with the use of generalized predictive control method, the packet-based structure of the data transmission was efficiently used to actively compensate for the communication constraints in NCSs.

(ii) Control and Scheduling Codesign. In NCSs, a situation may occur where multiple control components share a network with limited bandwidth. In such a situation, network resource scheduling among the control components is necessary; see Section 2.3.3. As far as the scheduling algorithms are concerned, [1] proposed a dynamic scheduling algorithm called "try-once-discard" (TOD) which allocates the network resources in a way that the node with the greatest error in the last reported period has access to the network resource.

Reference [101] proposed a Lyapunov uniformly globally asymptotically stable (UGAS) protocol based on TOD, which is further improved in [102]. In [103], the authors used the technique of "communication sequence" (see also [104]) to deal with the network access constraint for such a system configuration and modeled the subsystems as switched systems with two modes "open loop" and "closed loop" which switch according to whether the current subsystem has access to the medium or not. In [105], the authors considered a special case of the configuration shown in Figure 6 where the channel from controller to actuator is linked directly, and the rate monotonic scheduling algorithm is applied to schedule the transmissions of the sensing data of the subsystems.

4. Conclusions

Despite all the achievements that have been made for networked control systems in the past decades, more efforts are still needed in the future. Most of these ongoing researches adopt the codesign methodology, and the collaborations between the control and communication as well as computation communities are desirable.

These collaborations will then reveal the values of networked control systems in broader perspectives, by looking into its close relationship with other systems such as the Internet of Things, cyber-physical systems, and multiagent systems. All these together then bring us the promising future of the networked intelligent automation.

Conflict of Interests

The authors declare that there is no conflict of interests regarding the publication of this paper.

Acknowledgments

This work was supported in part by the National Natural Science Foundation of China under Grants 61304048, 61174058, and 61473024, the Australian Research Council under Grant DP140102180 and Grant LP140100471, and the 111 Project under Grant B12018.

References

[1] G. C. Walsh, O. Beldiman, and L. Bushnell, "Asymptotic behavior of networked control systems," in *Proceedings of the IEEE International Conference on Control Applications*, vol. 2, pp. 1448–1453, Kohala Coast, Hawaii, August 1999.

[2] Y. Halevi and A. Ray, "Integrated communication and control systems. Part 1. Analysis," *Journal of Dynamic Systems, Measurement and Control, Transactions of the ASME*, vol. 110, no. 4, pp. 367–373, 1988.

[3] R. A. Gupta and M.-Y. Chow, "Networked control system: overview and research trends," *IEEE Transactions on Industrial Electronics*, vol. 57, no. 7, pp. 2527–2535, 2010.

[4] J. P. Hespanha, P. Naghshtabrizi, and Y. Xu, "A survey of recent results in networked control systems," *Proceedings of the IEEE*, vol. 95, no. 1, pp. 138–172, 2007.

[5] V. C. Gungor and G. P. Hancke, "Industrial wireless sensor networks: challenges, design principles, and technical approaches," *IEEE Transactions on Industrial Electronics*, vol. 56, no. 10, pp. 4258–4265, 2009.

[6] M. Kranz, P. Holleis, and A. Schmidt, "Embedded interaction: interacting with the internet of things," *IEEE Internet Computing*, vol. 14, no. 2, pp. 46–53, 2010.

[7] F. Mattern and C. Floerkemeier, "From the internet of computers to the internet of things," in *From Active Data Management to Event-Based Systems and More*, K. Sachs, I. Petrov, and P. Guerrero, Eds., vol. 6462 of *Lecture Notes in Computer Science*, pp. 242–259, Springer, Berlin, Germany, 2010.

[8] J. Davis, T. Edgar, J. Porter, J. Bernaden, and M. Sarli, "Smart manufacturing, manufacturing intelligence and demand-dynamic performance," *Computers and Chemical Engineering*, vol. 47, pp. 145–156, 2012.

[9] P. Antsaklis and J. Baillieul, "Special issue on technology of networked control systems," *Proceedings of the IEEE*, vol. 95, no. 1, pp. 5–8, 2007.

[10] M. S. Mahmoud and M. Sabih, "Experimental investigations for distributed networked control systems," *IEEE Systems Journal*, vol. 8, no. 3, pp. 717–725, 2014.

[11] M. Nagahara, D. E. Quevedo, and J. Ostergaard, "Sparse packetized predictive control for networked control over erasure channels," *IEEE Transactions on Automatic Control*, vol. 59, no. 7, pp. 1899–1905, 2014.

[12] B. Xue, N. Li, S. Li, and Q. Zhu, "Moving horizon scheduling for networked control systems with communication constraints," *IEEE Transactions on Industrial Electronics*, vol. 60, no. 8, pp. 3318–3327, 2013.

[13] R. Postoyan and D. Nesic, "A framework for the observer design for networked control systems," *IEEE Transactions on Automatic Control*, vol. 57, no. 5, pp. 1309–1314, 2012.

[14] J.-N. Li, Y.-J. Pan, H.-Y. Su, and C.-L. Wen, "Stochastic reliable control of a class of networked control systems with actuator faults and input saturation," *International Journal of Control, Automation and Systems*, vol. 12, no. 3, pp. 564–571, 2014.

[15] M. Pajic, S. Sundaram, G. J. Pappas, and R. Mangharam, "The wireless control network: a new approach for control over networks," *IEEE Transactions on Automatic Control*, vol. 56, no. 10, pp. 2305–2318, 2011.

[16] N. S. Mkondweni and R. Tzoneva, "LabNS2—co-simulation, co-emulation, and real-time control toolkit for investigation of network induced time delays and packet loss in networked control systems," *International Journal of Innovative Computing, Information and Control*, vol. 10, no. 1, pp. 1–18, 2014.

[17] K. Y. You and L. H. Xie, "Survey of recent progress in studying networked control systems," *Acta Automatica Sinica*, vol. 39, no. 2, pp. 101–118, 2013.

[18] L. Zhang, H. Gao, and O. Kaynak, "Network-induced constraints in networked control systems: a survey," *IEEE Transactions on Industrial Informatics*, vol. 9, no. 1, pp. 403–416, 2013.

[19] Y. Ge, L. Tian, and Z. Liu, "Survey on the stability of networked control systems," *Journal of Control Theory and Applications*, vol. 5, no. 4, pp. 374–379, 2007.

[20] Y. Tipsuwan and M.-Y. Chow, "Control methodologies in networked control systems," *Control Engineering Practice*, vol. 11, no. 10, pp. 1099–1111, 2003.

[21] W. Stallings, *Data and Computer Communications*, Prentice Hall, Englewood Cliffs, NJ, USA, 6th edition, 2000.

[22] W. Zhang, M. S. Branicky, and S. M. Phillips, "Stability of networked control systems," *IEEE Control Systems Magazine*, vol. 21, no. 1, pp. 84–99, 2001.

[23] Y.-B. Zhao, G. P. Liu, and D. Rees, "Integrated predictive control and scheduling co-design for networked control systems," *IET Control Theory & Applications*, vol. 2, no. 1, pp. 7–15, 2008.

[24] Y.-B. Zhao, G.-P. Liu, and D. Rees, "Design of a packet-based control framework for networked control systems," *IEEE Transactions on Control Systems Technology*, vol. 17, no. 4, pp. 859–865, 2009.

[25] W. Hu, G. Liu, and D. Rees, "Event-driven networked predictive control," *IEEE Transactions on Industrial Electronics*, vol. 54, no. 3, pp. 1603–1613, 2007.

[26] J. Baillieul and P. J. Antsaklis, "Control and communication challenges in networked real-time systems," *Proceedings of the IEEE*, vol. 95, no. 1, pp. 9–28, 2007.

[27] R. M. Murray, Ed., *Control in an Information-Rich World: Report of the Panel on Future Directions in Control, Dynamics, and Systems*, Society for Industrial and Applied Mathematics, 2003.

[28] R. M. Murray, K. J. Astrom, S. P. Boyd, R. W. Brockett, and G. Stein, "Future directions in control in an information-rich world," *IEEE Control Systems Magazine*, vol. 23, no. 2, pp. 20–33, 2003.

[29] J. Nilsson, B. Bernhardsson, and B. Wittenmark, "Stochastic analysis and control of real-time systems with random time delays," *Automatica*, vol. 34, no. 1, pp. 57–64, 1998.

[30] L.-S. Hu, T. Bai, P. Shi, and Z. Wu, "Sampled-data control of networked linear control systems," *Automatica*, vol. 43, no. 5, pp. 903–911, 2007.

[31] Y. Fan, Z.-P. Jiang, and H. Zhang, "Network flow control under capacity constraints: a case study," *Systems & Control Letters*, vol. 55, no. 8, pp. 681–688, 2006.

[32] F. Yang, Z. Wang, Y. S. Hung, and M. Gani, "H_∞ control for networked systems with random communication delays," *IEEE Transactions on Automatic Control*, vol. 51, no. 3, pp. 511–518, 2006.

[33] F.-L. Lian, *Analysis, design, modeling, and control of networked control systems [Ph.D. dissertation]*, University of Michigan, Ann Arbor, Mich, USA, 2001.

[34] F.-L. Lian, J. R. Moyne, and D. M. Tilbury, "Performance evaluation of control networks: Ethernet, ControlNet, and DeviceNet," *IEEE Control Systems Magazine*, vol. 21, no. 1, pp. 66–83, 2001.

[35] S. Hu and Q. Zhu, "Stochastic optimal control and analysis of stability of networked control systems with long delay," *Automatica*, vol. 39, no. 11, pp. 1877–1884, 2003.

[36] D.-S. Kim, Y. S. Lee, W. H. Kwon, and H. S. Park, "Maximum allowable delay bounds of networked control systems," *Control Engineering Practice*, vol. 11, no. 11, pp. 1301–1313, 2003.

[37] F.-L. Lian, J. Moyne, and D. Tilbury, "Modelling and optimal controller design of networked control systems with multiple delays," *International Journal of Control*, vol. 76, no. 6, pp. 591–606, 2003.

[38] L. A. Montestruque and P. J. Antsaklis, "On the model-based control of networked systems," *Automatica*, vol. 39, no. 10, pp. 1837–1843, 2003.

[39] D. Yue, Q.-L. Han, and C. Peng, "State feedback controller design of networked control systems," *IEEE Transactions on Circuits and Systems II: Express Briefs*, vol. 51, no. 11, pp. 640–644, 2004.

[40] A. Sala, "Computer control under time-varying sampling period: an LMI gridding approach," *Automatica*, vol. 41, no. 12, pp. 2077–2082, 2005.

[41] D. Yue and Q.-L. Han, "Delayed feedback control of uncertain systems with time-varying input delay," *Automatica*, vol. 41, no. 2, pp. 233–240, 2005.

[42] L. Zhang, Y. Shi, T. Chen, and B. Huang, "A new method for stabilization of networked control systems with random delays," *IEEE Transactions on Automatic Control*, vol. 50, no. 8, pp. 1177–1181, 2005.

[43] X. Fan and M. Arcak, "Delay robustness of a class of nonlinear systems and applications to communication networks," *IEEE Transactions on Automatic Control*, vol. 51, no. 1, pp. 139–144, 2006.

[44] G. P. Liu, J. X. Mu, D. Rees, and S. C. Chai, "Design and stability analysis of networked control systems with random communication time delay using the modified MPC," *International Journal of Control*, vol. 79, no. 4, pp. 288–297, 2006.

[45] X. Liu and J. Shen, "Stability theory of hybrid dynamical systems with time delay," *IEEE Transactions on Automatic Control*, vol. 51, no. 4, pp. 620–625, 2006.

[46] P. L. Tang and C. W. de Silva, "Compensation for transmission delays in an ethernet-based control network using variable-horizon predictive control," *IEEE Transactions on Control Systems Technology*, vol. 14, no. 4, pp. 707–718, 2006.

[47] M. García-Rivera and A. Barreiro, "Analysis of networked control systems with drops and variable delays," *Automatica*, vol. 43, no. 12, pp. 2054–2059, 2007.

[48] L. Schenato, B. Sinopoli, M. Franceschetti, K. Poolla, and S. S. Sastry, "Foundations of control and estimation over lossy networks," *Proceedings of the IEEE*, vol. 95, no. 1, pp. 163–187, 2007.

[49] B. Azimi-Sadjadi, "Stability of networked control systems in the presence of packet," in *Proceedings of the 42nd IEEE Conference on Decision and Control*, vol. 1, pp. 676–681, December 2003.

[50] D. Georgiev and D. M. Tilbury, "Packet-based control: the H2-optimal solution," *Automatica*, vol. 42, no. 1, pp. 137–144, 2006.

[51] O. C. Imer, S. Yuksel, and T. Basar, "Optimal control of LTI systems over unreliable communication links," *Automatica*, vol. 42, no. 9, pp. 1429–1439, 2006.

[52] S. Hu and W.-Y. Yan, "Stability robustness of networked control systems with respect to packet loss," *Automatica*, vol. 43, no. 7, pp. 1243–1248, 2007.

[53] J. Xiong and J. Lam, "Stabilization of linear systems over networks with bounded packet loss," *Automatica*, vol. 43, no. 1, pp. 80–87, 2007.

[54] S. Sun, "Linear optimal state and input estimators for networked control systems with multiple packet dropouts," *International Journal of Innovative Computing, Information and Control*, vol. 8, no. 10, pp. 7289–7305, 2012.

[55] Y.-L. Wang and G.-H. Yang, "H_∞ control of networked control systems with time delay and packet disordering," *IET Control Theory & Applications*, vol. 1, no. 5, pp. 1344–1354, 2007.

[56] Y.-B. Zhao, J. Kim, G.-P. Liu, and D. Rees, "Compensation and stochastic modeling of discrete-time networked control systems with data packet disorder," *International Journal of Control, Automation and Systems*, vol. 10, no. 5, pp. 1055–1063, 2012.

[57] Y.-B. Zhao, G.-P. Liu, and D. Rees, "Actively compensating for data packet disorder in networked control systems," *IEEE Transactions on Circuits and Systems II: Express Briefs*, vol. 57, no. 11, pp. 913–917, 2010.

[58] H. Zhang, G. Hui, and Y. Wang, “Stabilization of networked control systems with piecewise constant generalized sampled-data hold function,” *International Journal of Innovative Computing, Information and Control*, vol. 9, no. 3, pp. 1159–1170, 2013.

[59] N. Elia and S. K. Mitter, “Stabilization of linear systems with limited information,” *IEEE Transactions on Automatic Control*, vol. 46, no. 9, pp. 1384–1400, 2001.

[60] D. Liberzon, “Quantization, time delays, and nonlinear stabilization,” *IEEE Transactions on Automatic Control*, vol. 51, no. 7, pp. 1190–1195, 2006.

[61] C. Peng and Y.-C. Tian, “Networked H_∞ control of linear systems with state quantization,” *Information Sciences*, vol. 177, no. 24, pp. 5763–5774, 2007.

[62] E. Tian, D. Yue, and X. Zhao, “Quantised control design for networked control systems,” *IET Control Theory and Applications*, vol. 1, no. 6, pp. 1693–1699, 2007.

[63] R. Lu, F. Wu, and A. Xue, “Networked control with reset quantized state based on bernoulli processing,” *IEEE Transactions on Industrial Electronics*, vol. 61, no. 9, pp. 4838–4846, 2014.

[64] R. Lu, H. Li, A. Xue, J. Zheng, and Q. She, “Quantized H_∞ filtering for different communication channels,” *Circuits, Systems, and Signal Processing*, vol. 31, no. 2, pp. 501–519, 2012.

[65] J.-P. Richard, “Time-delay systems: an overview of some recent advances and open problems,” *Automatica*, vol. 39, no. 10, pp. 1667–1694, 2003.

[66] L. Zhang, *Access scheduling and controller design in networked control systems [Ph.D. dissertation]*, University of Maryland, College Park, Md, USA, 2005.

[67] G. C. Goodwin, D. E. Quevedo, and E. I. Silva, “Architectures and coder design for networked control systems,” *Automatica*, vol. 44, no. 1, pp. 248–257, 2008.

[68] J. Colandairaj, G. W. Irwin, and W. G. Scanlon, “Wireless networked control systems with QoS-based sampling,” *IET Control Theory and Applications*, vol. 1, no. 1, pp. 430–438, 2007.

[69] G.-P. Liu, Y. Xia, D. Rees, and W. Hu, “Design and stability criteria of networked predictive control systems with random network delay in the feedback channel,” *IEEE Transactions on Systems, Man and Cybernetics Part C: Applications and Reviews*, vol. 37, no. 2, pp. 173–184, 2007.

[70] F. Mazenc and S.-I. Niculescu, “Lyapunov stability analysis for nonlinear delay systems,” *Systems & Control Letters*, vol. 42, no. 4, pp. 245–251, 2001.

[71] H.-J. Hoo, H.-S. Ryu, K.-S. Yoo, and O.-K. Kwon, “Compensation of networked control systems using LMI-based delay-dependent optimization method,” in *Proceedings of the 41st SICE Annual Conference (SICE ’02)*, vol. 1, pp. 364–369, August 2002.

[72] H. Lin, G. Zhai, and P. J. Antsaklis, “Robust stability and disturbance attenuation analysis of a class of networked control systems,” in *Proceedings of the 42nd IEEE Conference Decision and Control*, vol. 2, pp. 1182–1187, Maui, Hawaii, USA, December 2003.

[73] J. K. C. So, *Delay modeling and controller design for networked control systems [Ph.D. dissertation]*, University of Toronto, Toronto, Canada, 2003.

[74] Z.-H. Guan, W.-H. Chen, and J. Xu, “Delay-dependent stability and stabilizability of uncertain jump bilinear stochastic systems with mode-dependent time-delays,” *International Journal of Systems Science*, vol. 36, no. 5, pp. 275–285, 2005.

[75] J. Wu, F.-Q. Deng, and J.-G. Gao, “Modeling and stabilty of long random delay networked control systems,” in *Proceedings of the 4th International Conference on Machine Learning and Cybernetics (ICMLC ’05)*, pp. 947–952, Guangzhou, China, August 2005.

[76] L. Zhang and F. Hua-Jing, “A novel controller design and evaluation for networked control systems with time-variant delays,” *Journal of the Franklin Institute*, vol. 343, no. 2, pp. 161–167, 2006.

[77] H. Gao and T. Chen, “New results on stability of discrete-time systems with time-varying state delay,” *IEEE Transactions on Automatic Control*, vol. 52, no. 2, pp. 328–334, 2007.

[78] P. Antsaklis and J. Baillieul, “Guest editorial special issue on networked control systems,” *IEEE Transactions on Automatic Control*, vol. 49, no. 9, pp. 1421–1423, 2004.

[79] M. S. Branicky, S. M. Phillips, and W. Zhang, “Stability of networked control systems: explicit analysis of delay,” in *Proceedings of the American Control Conference*, vol. 4, pp. 2352–2357, Chicago, Ill, USA, June 2000.

[80] P. Seiler and R. Sengupta, “An H_∞ approach to networked control,” *Institute of Electrical and Electronics Engineers. Transactions on Automatic Control*, vol. 50, no. 3, pp. 356–364, 2005.

[81] M. Basin and J. Rodriguez-Gonzalez, “Optimal control for linear systems with multiple time delays in control input,” *IEEE Transactions on Automatic Control*, vol. 51, no. 1, pp. 91–97, 2006.

[82] M. Sahebsara, T. Chen, and S. L. Shah, “Optimal H_∞ filtering in networked control systems with multiple packet dropouts,” *Systems & Control Letters*, vol. 57, no. 9, pp. 696–702, 2008.

[83] G. C. Goodwin, H. Haimovich, D. E. Quevedo, and J. S. Welsh, “A moving horizon approach to networked control system design,” *IEEE Transactions on Automatic Control*, vol. 49, no. 9, pp. 1427–1445, 2004.

[84] Y.-B. Zhao, G.-P. Liu, and D. Rees, “Networked predictive control systems based on the hammerstein model,” *IEEE Transactions on Circuits and Systems II: Express Briefs*, vol. 55, no. 5, pp. 469–473, 2008.

[85] Y.-B. Zhao, G.-P. Liu, and D. Rees, “A predictive control-based approach to networked hammerstein systems: design and stability analysis,” *IEEE Transactions on Systems, Man, and Cybernetics, Part B: Cybernetics*, vol. 38, no. 3, pp. 700–708, 2008.

[86] Y.-B. Zhao, G.-P. Liu, and D. Rees, “A predictive control based approach to networked wiener systems,” *International Journal of Innovative Computing, Information and Control*, vol. 4, no. 11, pp. 2793–2802, 2008.

[87] N. H. El-Farra and P. D. Christofides, “Coordinating feedback and switching for control of hybrid nonlinear processes,” *AIChE Journal*, vol. 49, no. 8, pp. 2079–2098, 2003.

[88] P. V. Zhivoglyadov and R. H. Middleton, “Networked control design for linear systems,” *Automatica*, vol. 39, no. 4, pp. 743–750, 2003.

[89] Z.-H. Guan, D. J. Hill, and X. Shen, “On hybrid impulsive and switching systems and application to nonlinear control,” *IEEE Transactions on Automatic Control*, vol. 50, no. 7, pp. 1058–1062, 2005.

[90] P. A. Kawka and A. G. Alleyne, “Stability and feedback control of wireless networked systems,” in *Proceedings of the American Control Conference (ACC ’05)*, vol. 4, pp. 2953–2959, Portland, Ore, USA, June 2005.

[91] M. Yu, L. Wang, and G. Xie, “A switched system approach to stabilization of networked control systems,” *Journal of Control Theory and Applications*, vol. 4, no. 1, pp. 86–95, 2006.

[92] Y. Xia, G. P. Liu, P. Shi, D. Rees, and E. J. C. Thomas, "New stability and stabilization conditions for systems with time-delay," *International Journal of Systems Science*, vol. 38, no. 1, pp. 17–24, 2007.

[93] X.-M. Sun, D. Wu, G.-P. Liu, and W. Wang, "Input-to-state stability for networked predictive control with random delays in both feedback and forward channels," *IEEE Transactions on Industrial Electronics*, vol. 61, no. 7, pp. 3519–3526, 2014.

[94] M. S. Branicky, V. Liberatore, and S. M. Phillips, "Networked control system co-simulation for co-design," in *Proceedings of the American Control Conference*, vol. 4, pp. 3341–3346, 2003.

[95] J. R. Hartman, *Networked control system co-simulation for code-sign: theory and experiments [Ph.D. dissertation]*, Department of Electrical Engineering and Computer Science, Case Western Reserve University, Cleveland, Ohio, USA, 2004.

[96] M. E. M. Ben Gaid, A. Çela, and Y. Hamam, "Optimal integrated control and scheduling of networked control systems with communication constraints: Application to a car suspension system," *IEEE Transactions on Control Systems Technology*, vol. 14, no. 4, pp. 776–787, 2006.

[97] G.-P. Liu, Y. Xia, J. Chen, D. Rees, and W. Hu, "Networked predictive control of systems with random network delays in both forward and feedback channels," *IEEE Transactions on Industrial Electronics*, vol. 54, no. 3, pp. 1282–1297, 2007.

[98] Y.-B. Zhao, G.-P. Liu, and D. Rees, "Design and stability analysis of packet-based networked control systems in continuous time," in *Proceedings of the IEEE International Conference on Systems, Man and Cybernetics (SMC '08)*, pp. 3206–3210, Singapore, October 2008.

[99] Y.-B. Zhao, G.-P. Liu, and D. Rees, "Packet-based deadband control for internet-based networked control systems," *IEEE Transactions on Control Systems Technology*, vol. 18, no. 5, pp. 1057–1067, 2010.

[100] Y.-B. Zhao, J. Kim, and G.-P. Liu, "Error bounded sensing for packet-based networked control systems," *IEEE Transactions on Industrial Electronics*, vol. 58, no. 5, pp. 1980–1989, 2011.

[101] D. Nešić and A. R. Teel, "Input-to-state stability of networked control systems," *Automatica*, vol. 40, no. 12, pp. 2121–2128, 2004.

[102] M. Tabbara, D. Nešić, and A. Teel, "Stability of wireless and wireline networked control systems," *IEEE Transactions on Automatic Control*, vol. 52, no. 9, pp. 1615–1630, 2007.

[103] D. Hristu-Varsakelis and P. R. Kumar, "Interrupt-based feedback control over a shared communication medium," in *Proceedings of the 41st IEEE Conference on Decision & Control*, vol. 3, pp. 3223–3228, December 2002.

[104] R. Brockett, "Stabilization of motor networks," in *Proceedings of the 34th IEEE Conference on Decision and Control*, vol. 2, pp. 1484–1488, December 1995.

[105] M. S. Branicky, S. M. Phillips, and W. Zhang, "Scheduling and feedback co-design for networked control systems," in *Proceedings of the 41st IEEE Conference on Decision and Control*, vol. 2, pp. 1211–1217, Las Vegas, Nev, USA, December 2002.

Hindawi Publishing Corporation
Mathematical Problems in Engineering
Volume 2015, Article ID 354292, 12 pages
http://dx.doi.org/10.1155/2015/354292

Research Article

Cognitive Self-Scheduled Mechanism for Access Control in Noisy Vehicular Ad Hoc Networks

Mario Manzano,[1] Felipe Espinosa,[1] Ángel M. Bravo-Santos,[2] and Alfredo Gardel-Vicente[1]

[1] *Electronics Department, Polytechnic School, University of Alcala, Campus Universitario s/n, 28871 Alcalá de Henares, Spain*
[2] *Signal and Communications Theory Department, Higher Polytechnic School, Carlos III University, Avenida de la Universidad 30, 28911 Leganes, Spain*

Correspondence should be addressed to Felipe Espinosa; espinosa@depeca.uah.es

Received 15 August 2014; Accepted 17 November 2014

Academic Editor: Jinhui Zhang

Within the challenging environment of intelligent transportation systems (ITS), networked control systems such as platooning guidance of autonomous vehicles require innovative mechanisms to provide real-time communications. Although several proposals are currently under discussion, the design of a rapid, efficient, flexible, and reliable medium access control mechanism which meets the specific constraints of such real-time communications applications remains unsolved in this highly dynamic environment. However, cognitive radio (CR) combines the capacity to sense the radio spectrum with the flexibility to adapt to transmission parameters in order to maximize system performance and has thus become an effective approach for the design of dynamic spectrum access (DSA) mechanisms. This paper presents the enhanced noncooperative cognitive division multiple access (ENCCMA) proposal combining time division multiple access (TDMA) and frequency division multiple access (FDMA) schemes with CR techniques to obtain a mechanism fulfilling the requirements of real-time communications. The analysis presented here considers the IEEE WAVE and 802.11p as reference standards; however, the proposed medium access control (MAC) mechanism can be adapted to operate on the physical layer of different standards. The mechanism also offers the advantage of avoiding signaling, thus enhancing system autonomy as well as behavior in adverse scenarios.

1. Introduction

The scientific community has shown an increasing interest in intelligent transportation systems (ITS) over the last few years. Early attempts to apply information technologies to road transport systems yielded various approaches, such as digital short range communications (DSRC) [1] in the USA. Later, with the goal of establishing a universal framework, several international bodies launched their proposals to support future intelligent transport system applications [2]. These agencies include an industrial consortium, the car to car communication consortium (C2C-CC) [3], the international organization for standardization (ISO), which has developed the communications access for land mobiles (CALM) initiative, the CVIS (cooperative vehicle infrastructure systems) project [4, 5], and the IEEE, which has developed the wireless access for the vehicular environment (WAVE) protocol suite [6] and the 802.11p specification [7], which is considered the most acceptable proposal of all these frameworks.

More recently, several technology companies, research centers, and leading vehicle manufacturers have been developing a number of alternatives in order to offer vehicles with different automatic driving levels [8–10]. Several research bodies and technology companies have demonstrated their proposals, including VisLab [11], IAI-CSIC, which has developed the AUTOPIA project [12], Google [13], and Bosch [14]. Consequently, ITS are considered a very important source of innovative ideas, projects, and applications, for example, those related to platooning guidance [15, 16] or others related to more typical situations in ITS [17, 18].

One of the most interesting challenges in regard to these systems is to develop a universal wireless communication system which provides the communication capacity required by the vast majority of possible applications envisaged for this field. Such is the aim of the IEEE standard known as WAVE [6], which includes the 802.11p specification [7], a new member of the extensive IEEE 802.11 family. The design of this new specification is based on the great advantages of the other protocols in the 802.11 family but also includes particular modifications to improve its adaptation to vehicle surroundings [6, 7].

The IEEE 802.11p medium access control protocol incorporates the carrier sensing multiple access/collision avoidance (CSMA/CA) mechanism contained in the b and g specifications widely used to gain access to networks and the Internet. In order to improve system performance, enhanced distributed channel access (EDCA), an update in the IEEE 802.11a specification, has been included to provide quality of service [19]. However, not all ITS applications have the same communication requirements. Furthermore, some traffic safety applications require real-time communication with high reliability, meaning that packets must be successfully delivered before a certain deadline [20–23]. To meet a real-time deadline, timely and predictable access to the channel is paramount; however, the medium access method used in IEEE 802.11p does not guarantee channel access before a finite deadline [21–23].

Several techniques within the cognitive radio (CR) paradigm [24–26] have recently been developed related to spectrum exploration [27–29] and dynamic spectrum access [30–32]. These techniques can be applied to the design of medium access control mechanisms in the quest for solutions offering a better performance than the conventional proposals.

This paper outlines the enhanced noncooperative cognitive multiple access (ENCCMA) proposal, which has evolved from the noncooperative cognitive time division multiple access (NCC-TDMA) proposal [20, 33]. Dynamic spectrum access (DSA) and spectrum exploration techniques are used in order to expand the mechanism's capacities and improve its performance by applying a combination of both time division multiple access (TDMA) and frequency division multiple access (FDMA) schemes. The rest of the paper is organized as follows. Section 2 gives a detailed description of the problem. Section 3 presents an analysis of recent papers on cognitive radio. Section 4 provides a description of the model of the system analyzed. The ENCCMA proposal is described in detail in Section 5, while the simulation results and conclusions are given in Sections 6 and 7, respectively.

2. Real-Time Communication in ITS

The physical layer and MAC sublayer of the WAVE standard developed by the IEEE to meet ITS requirements are described in the IEEE 802.11p specification [7].

Various attempts have been made in the design of the WAVE medium access control sublayer to simplify the connection and information exchange operations in local area wireless networks and to provide effective use of ad hoc communication among vehicles [6]. Consequently, a new communication mode, the WAVE mode, has been included in the specification. This mode does not require prior network authentication and connection, which therefore reduces the time and signaling required for a node to send information to network members.

However, as with the rest of the IEEE 802.11 family, the IEEE 802.11p uses CSMA/CA as a medium access control (MAC) mechanism. In addition, IEEE 802.11p also includes enhanced distributed channel access (EDCA) in order to improve the performance of this mechanism in ITS scenarios [19]. This mechanism was already included in the IEEE 802.11e amendment to improve quality of service by classifying traffic according to four different priorities. Therefore, the resulting medium access control mechanism is contention-based, rather than deterministic, since it cannot guarantee medium access within a bounded time [21], and thus the improvement provided by EDCA does not ensure deterministic access delay. EDCA performance depends on the level of priority assigned to messages exchanged within the system [19, 34], and the existence of a large number of high priority messages will reduce effectiveness. Because of this nondeterministic nature of the IEEE 802.11p, it is not suitable for traffic safety applications where low-delay, reliable, real-time communication is required.

There are several published solutions that attempt to improve the properties of the IEEE 802.11p medium access control mechanism and satisfy the specific functions required by ITS applications. These are classified as contention-based and schedule-based protocols [35]. Schedule-based dynamic schemes are suitable for networks in which the topology or members are variable. In these cases, access schedules are continuously calculated to reflect network changes. Self-organized dynamic access is more suited to the special characteristics of vehicular environments [20]. In this case, allocation becomes the responsibility of the system users themselves. Consequently, the medium access control mechanism can contend with high levels of user mobility and inherent network topology variations in ITS.

Another possible classification for MAC mechanisms in the field of ITS can be made between proposals for a final specific application in the system versus fully generic solutions whose operation is not restricted to a certain type of application. There are several proposals for application-based MACs, such as position-based MACs which leverage the need to disseminate the current position, speed, and direction of vehicles in the context of ITS. The self-organizing time division multiple access (STDMA) mechanism [21] is an illustrative example of this type of proposal, which requires the transmission of protocol signaling in order to allow users to generate access planning.

This paper presents a generic, self-organized, and scheduled medium access control mechanism. This proposal provides the deterministic features required by real-time communications in the ITS field. Moreover, it can be adapted to any application and act as a single MAC or as a complementary MAC for the solution.

3. Cognitive Radio

This section describes how cognitive radio has become an important source of new techniques frequently used to design medium access control mechanisms. Several proposals in this field have recently leveraged both spectrum sensing and dynamic spectrum access, including the present ENCCMA proposal.

3.1. Cognitive Radio Properties. Cognitive radio [24–26] is an intelligent wireless communication system that is aware of its environment and uses understanding-by-building methodology to learn from the environment and adapt to statistical variations in the input stimuli by effecting the corresponding changes in determined real-time parameters. The twofold aim of CR, to obtain a highly reliable and efficient communication system, constitutes a perfect match with ITS requirements.

The core of the cognitive network is the cognitive cycle [36], which consists of six processes: observe, orient, plan, decide, act, and learn. A cognitive network achieves network-level cognition by integrating the cognitive cycle across layers in the protocol stack and through the network nodes. Such cognitive nodes require an architecture that supports observation of the state of the network, collective reasoning to achieve end-to-end network goals, learning from past actions, and reconfiguration of cognitive nodes based on collective decisions.

One of the main ideas that CR exploits is observation of spectrum use in order to take advantage of free spectrum zones (spectrum holes) at any given moment. Searching for these holes and using them constitute one of the main objectives of CR [37]. Consequently, CR systems have receptors observing the medium (spectrum sensing) [27] and detecting occupancy by any kind of signal.

The result of this spectrum occupancy observation leads to one of the greatest challenges of CR-based systems: the design of dynamic spectrum access techniques. These techniques are designed according to the level of cooperation among users and range from noncooperative distributed schemes to completely centralized ones.

3.2. Spectrum Sensing and Dynamic Spectrum Sensing. In a previous paper presenting the NCC-TDMA proposal [20, 33], the concepts of CR were applied in terms of spectrum sensing, learning, and system adaptability to the radio environment.

Observation of medium occupancy is one of the most important capabilities of CR, as this enables detection of underutilized spectrum holes which can therefore be used for transmissions by secondary users. This feature of CR is associated with spectrum sensing and DSA techniques, with the latter being defined as a method to adapt to the use of spectrum resources to the present situation and user requirements [30]. Both of them now constitute one of the main pillars in the design of medium access mechanisms, as can be seen in [27, 31].

One example of a medium access control mechanism using these techniques is cognitive MAC for VANET (CMV) [38]. In this paper, the spectrum sensing techniques described in [28] are applied over the channel distribution described in the WAVE standard.

3.3. Multichannel in WAVE. Following the guidelines established in DSRC [1], the WAVE standard includes a multichannel operation based on seven different channels: six of them are called service channels (SCH) [34, 39], while the seventh is the control channel (CCH) [6]. Although the EDCA strategy is applied to each of these channels, the control one is responsible for critical messages, or, in terms of ITS, real-time communications. Moreover, the possibility is provided of using a higher transmission power for the control channel in order to improve the likelihood of successfully carrying out a transmission on that channel. In summary, the capacity of WAVE to support real-time communications can be measured by the operation of the protocol on the control channel.

3.4. Learning and Adaptability. The NCC-TDMA proposal leverages the concept of learning and adaptability through the *estimation allocation vector* (EAV). This tool enables each user to associate each transmission slot to a value of the estimated probability of finding that slot free for transmission. The values of this vector are updated in accordance with the result of the previous transmission attempt using the algorithm described in [20]. This same idea is applied in the CMV mechanism [38]. Unlike the generic approach employed in NCC-TDMA, CMV specifically executes the mechanism over the WAVE channel scheme using a tool named *spectrum status table* (SST), which stores the status of the spectrum sensed near the device. By storing this information, each user can adapt to any environment condition, at least to those registered in the SST in the case of CMV [38] or in the EAV in the case of NCC-TDMA.

The advantages of this mechanism are taken to a higher level in the proposal described in the present paper. The ENCCMA exploits this functionality and enhances it in two ways:

(i) by maintaining a generic approach that is not restricted to the division of channels included in WAVE but is rather applied to a division of both frequency channels and time slots using a combination of TDMA and FDMA and the *estimation allocation vector* (EAV) thus becomes the *estimation allocation matrix* (EAM);

(ii) by improving the accuracy of the information stored for each user through the inclusion of a secondary updating mechanism that decreases the time required for the information stored in the EAM to accurately reflect spectrum occupancy conditions at any given time.

The next section describes the model of the system designed, analyzed, and simulated in order to develop the ENCCMA proposal described in detail in Section 5.

4. System Model

The starting point for an analysis of the ENCCMA proposal is platooning guidance of autonomous vehicles. In this collaborative transport scenario, vehicles are grouped into convoys, and each convoy is headed by a leader vehicle which transmits the route information to the rest of the convoy members (followers). Control of each follower requires knowledge of the motion state of the preceding unit, and the dissemination of this information is critical because loss of these messages could jeopardize the stability of the convoy chain [15]. In addition, other maneuvers can produce variations in spectrum occupancy, such as vehicles joining or leaving the convoy. In summary, it is a system in which users must convey critical information within a specified maximum deadline and the system itself must cope with a variable number of users as well as different interfering signals due to the existence of other convoys or other services sharing the medium.

4.1. Scenario. To simplify the experiments, the special conditions of start, stop, line change, and the generation of reference paths for the convoy on a real map are not discussed here. Thus, the convoy can be considered as a group of freely flowing vehicles on an unbounded map. It is assumed that the vehicles are traveling in convoy and can separate from it (leaving the communication system) in the same way that other vehicles can join it as new users.

Trajectory control and tracking tasks require cooperation among users. However, from the point of view of the communication system and CR, the system is not cooperative because the messages exchanged among users only contain application information which is not related to management of the medium access control mechanism. There is no need for signaling among users as the vehicles never send information about the transmission region they are using. This feature renders users completely autonomous from the communication point of view.

4.2. Channel. According to the definition of WAVE, the shared medium should be divided in accordance with the channel scheme included in the specification [6]. As a result, only the seven specified channels may be applied, ignoring the specific use defined in the standard for each channel. It should be noted that, for the simulation experiments conducted, the shared medium was divided into channels in a generic way in order to avoid the temporary restriction imposed by the WAVE specification. The main requirement of real-time applications in ITS is that the exchange of messages must be made within a critical time limit T_c. The shared medium is divided according to this limit in order to conform to the TDMA-FDMA frame. Both time slot duration and channel frequency range are determined by the needs of the application.

In addition, the following is assumed.

(a) During each transmission, it is possible to transmit all the information needed by each user to fulfill the system requirements.

(b) Once the medium has been accessed, there are no external interferences in the communication process.

4.3. Communication. To perform the envisaged functions of the new proposal, it is assumed that all users rely on a communication system capable of observing the medium (spectrum sensing) in the same way as the systems described in [27–29], which is equipped with an auxiliary device providing time synchronization [27]. Given both these capabilities, the end users will be able to manage their communications themselves in a decentralized and autonomous way without the need to receive information from any other user in the system (signaling).

4.4. Key Aspects. In summary, the following aspects characterize the model of the communication system under study.

(i) The shared medium is exploited using a combination of TDMA and FDMA schemes. The main frame lasts T_c and is divided into r time slots. Each time slot is also divided into f frequency channels.

(ii) Thus, a total number of rf transmission regions are established for the system users in a *multiframe*.

(iii) Each participant must transmit his data within the time limit T_c. Thus, it is necessary and sufficient to access the medium in one transmission region.

(iv) Once a participant has accessed the medium during the period of transmission in the selected region, it will be considered that the transmission has been carried out correctly.

(v) Vehicles are equipped with a spectrum sensing communication system which provides each user with spectrum occupancy knowledge.

(vi) Vehicles are equipped with time devices to provide *multiframe* synchronization.

(vii) For the medium access control mechanism, there is no cooperation among users. They neither exchange signaling nor have explicit knowledge of transmission regions used by the remaining users.

5. The ENCCMA Proposal

The enhanced noncooperative cognitive medium access (ENCCMA) proposal represents a development of the NCC-TDMA mechanism which improves the latter's efficiency by guaranteeing a bounded medium access delay to ITS applications which require real-time communications.

The original proposal consisted of a TDMA-based medium access control mechanism. Each user stored information about the occupancy estimation of each slot by applying CR techniques. This information was then used to select the best slot to perform the information transmission required by the application. Subsequently, that information was updated depending on the result of each of these transmissions by applying a bonuses-and-penalties algorithm. This was a nondeterministic mechanism that enabled each user to learn and adapt to rapid changes in VANET environments.

The ENCCMA mechanism has been designed in response to the need for an improvement in the application of DSA and CR techniques to enhance the performance of the original proposal.

5.1. Increasing System Capacity. As with other existing alternatives [38], including WAVE itself [6], the ENCCMA proposal incorporates a multichannel operation. Following the principle of neutrality and generality of the mechanism, it is not applied in a fixed frequency division scheme. Rather, the mechanism has been designed bearing in mind that the availability of spectrum and channels can be freely set. Therefore, the shared medium is not only divided into time slots, as in the NCC-TDMA, but an FDMA scheme is also implemented in each time slot. Thus, the medium is operated using a combination of TDMA and FDMA schemes, resulting in transmission regions defined by time slots and frequency channels which notably increase the maximum number of users that can interact in a given application. The granularity of these divisions is not restricted by the mechanism but rather the requirements of the application determine the medium division scheme.

The tool used by the NCC-TDMA mechanism to store the estimated spectrum occupancy information was a vector whose elements represented the estimated occupancy information for each user and time slot. In the ENCCMA proposal and with the emergence of multichannel operations, this vector has evolved into a matrix, the *estimation allocation matrix* (EAM), in which each user can store his information about the estimated occupancy of each transmission region. As with the NCC-TDMA, it is necessary to organize the access to the *multiframe* transmission regions according to the possibility of finding these regions occupied by other system users. Consequently, the use of transmission schemes operates as shown in the example illustrated in Figure 3. It should be noted that this operation is performed while maintaining the constraint of avoiding signal transmission, rendering each user completely autonomous in the system.

5.2. Improving Spectrum Sensing. The ENCCMA strategy provides a substantial improvement in spectrum scan capabilities compared to the original NCC-TDMA proposal. The estimated occupancy information stored in the EAM changes as a result of accessing the medium to perform the transmission required by the application. In addition, it also changes by means of a complementary exploration mechanism, the aim of which is to increase the accuracy of the stored information within the shortest possible time. Therefore, users can select the best transmission region in each iteration. However, this additional exploration is not free in terms of the efficiency pursued by CR. Therefore, the ENCCMA strategy establishes a cost function in order to determine the optimal number of regions to be explored in each iteration. This cost function can be adapted to the needs of each application or system by modifying the parameters shown in Table 1.

5.3. Performance Index. A performance index has been designed with the aim of increasing the adaptability, learning, and efficiency of the system. It describes the exploration cost in the system and it allows the algorithm to determine the optimum number of regions to inspect in each iteration.

Table 1: Parameters used to obtain the cost function curve of Figure 1.

Parameter	Value
Total number of available transmission regions	100
Number of previous iterations (N value in (5))	20
Number of regions explored in previous iterations	50
Unit cost of scan	From 0.5 to 2
s	10
α	0.9
d_s	10
w	0.7

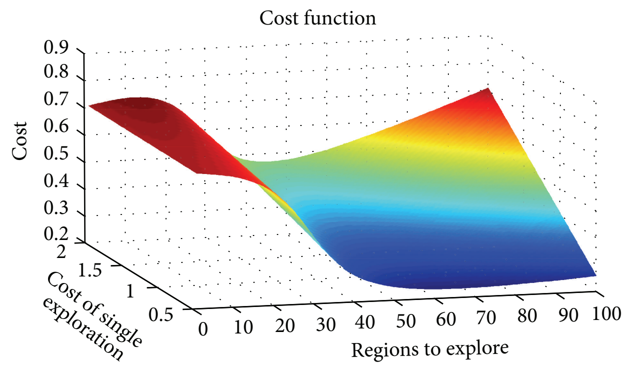

Figure 1: Cost function: cost of exploration versus regions to explore.

To take into account all the elements of the system, in the design process the following considerations have been made.

(1) Resources Consumption versus Spectrum Occupancy Knowledge. Two main terms determine the algorithm decision: the cost of exploring the regions and the current knowledge of the spectrum occupancy. It is necessary to maintain a compromise solution between the algorithm performance (always exploring everything in the ideal case) and the minimum consumption situation (not to explore any extra region).

The parameter W was included to balance the relative importance of each term in the performance index evaluation:

$$C = W \cdot E + (1 - W) \cdot R, \tag{1}$$

where:

(i) C is cost function or performance index,

(ii) W is weight parameter, aimed to balance the importance of the two main terms in the performance index; $W \in (0, 1)$,

(iii) E is parameter related to the current spectrum occupancy knowledge, and

(iv) R is parameter related to the cost of exploration.

(2) Parameter Related to the Cost of Exploration. The definition of the term R implies, on one hand, a relation between

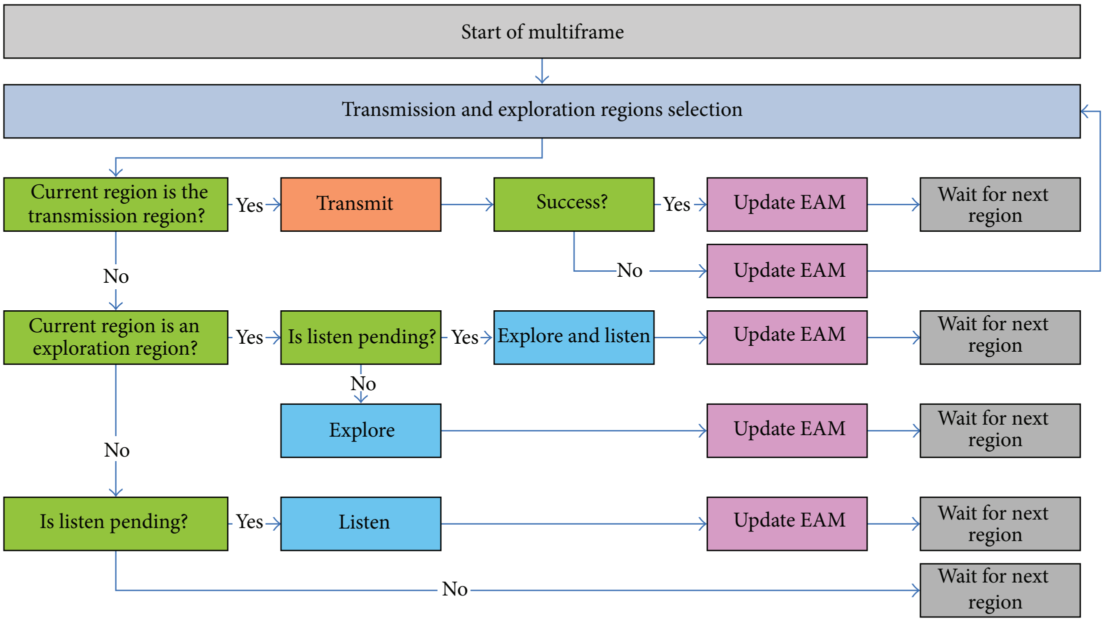

Figure 2: ENCCMA algorithm flowchart.

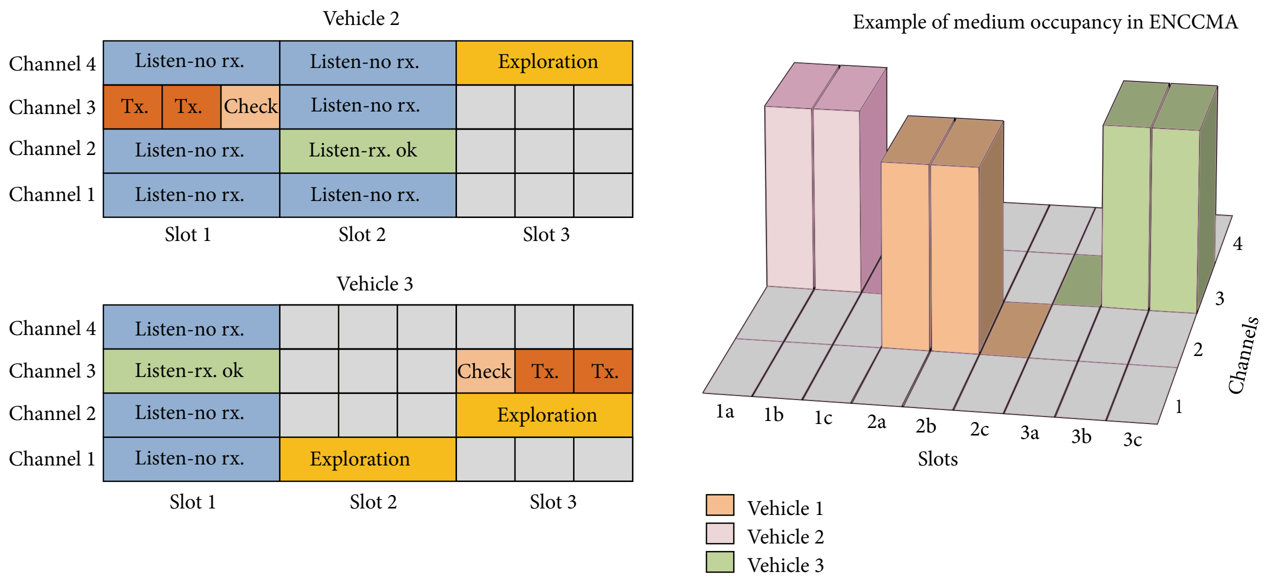

Figure 3: Application of TDMA-FDMA *multiframe* and transmission schemes in ENCCMA to an example of two followers and a leader formation. Three time slots and four frequency channels are available for the MAC mechanism.

the number of regions to explore in the iteration and the total number of regions and, on the other hand, the cost of exploration of a single region which is a term defined by the hardware characteristic of the system. The number of regions to explore is the value that the algorithm has to determine by minimizing the cost function. Therefore,

$$R = \frac{X}{T} R_c, \tag{2}$$

where

(i) X is number of regions to explore,

(ii) T is total number of regions, and

(iii) R_c is exploration cost of a single region.

(3) Parameter Related to the Spectrum Occupancy Knowledge. The parameter E is defined from a curve obtained from a set of configuration parameters and a variable related to the knowledge of the historical spectrum occupancy. If the information about spectrum occupancy is recent, the number of regions to explore can be reduced. However, if the information was obtained many iterations ago, the number

of explorations must be increased. The configuration parameters s and d are considered for allowing the adaptation of the performance index to different scenarios. The parameter s is simply a slope modifier that can be used to soften the curve variation near the minimum. On the other hand, the parameter d contains the information about the exploration in previous iterations. Other variables have been included in the definition of E in order to constrain its value in the range $(0, 1)$. The resulting expression for E is

$$E = 1 - \left(\frac{1}{\pi} a \tan\left(\frac{d - T + 2X}{2s}\right) + a \tan\left(\frac{T - d}{2s}\right)\right), \quad (3)$$

where $s \in (1, 30)$ and d includes the information about the exploration history.

The term d represents a measure of the previous knowledge about the spectrum occupancy. It depends on the total number of regions T, a configuration parameter d_s, and the factor h which contains the information about the previous iterations:

$$d = d_s T h. \quad (4)$$

The factor h is evaluated as a sum of N values that represent the number of explorations X_n performed at iteration n, normalized by the total number of regions T, and weighted by an exponential function with an adjusting parameter α ($\alpha \in (0, 1)$), as shown in the following equation:

$$h = \sum_{n=1}^{n=N} \frac{X_n}{T} e^{\alpha(n-N)}. \quad (5)$$

According to this definition, the number of regions explored in a recent iteration will be more relevant for h than the number of regions explored in a previous iteration. Therefore, a higher value of h will determine a lower value of the number of regions to explore. In the same way, the higher the value of the parameter α is, the lower the value of h is. It means that if in the previous iterations there were not a large number of explorations, in the current iteration the vehicle needs to perform a lot of them to reach a certain level of spectrum occupancy knowledge.

The performance index C is completely defined by expressions (1) to (5). The algorithm determines the number X of regions to explore in each iteration by obtaining the minimum C value.

In Table 1, the values of parameters used to obtain the cost function plotted in Figure 1 are shown. The same values are used in the simulations performed in Section 6.

As the parameter d is related to the exploration history and depends on the number of regions explored in each iteration, the resultant performance index is time dependent and therefore the algorithm has to find the minimum value of the curve in each iteration.

5.4. The ENCCMA Algorithm. The ENCCMA algorithm manages the actions of each user in each iteration. Basically, it determines the transmission region and the exploration regions (number and identification). It also updates the EAM with the information obtained from the explorations. The following actions can be performed by each user when accessing the medium: *transmit*, *listen*, and *explore and listen*. The *transmit* action is performed in the transmission region determined by the algorithm for that purpose. The *listen* action is performed in order to receive the information transmitted by the other system users. Besides receiving information provided by other users, the *explore and listen* action senses the medium in the regions identified by the algorithm for this purpose without interfering with any other potential users transmitting in the same regions. Figure 2 presents a flowchart of the ENCCMA algorithm.

5.5. Transmission Schemes. According to the ENCCMA transmission mechanism, each transmission region is divided into three time intervals and each user makes use of them in a different way. If the selected region is the same as the one in the previous iteration, the *listen* + *transmission* scheme is applied. First, the user transmits the required information and listens during the third interval of the region to check for the presence of any interference. If the selected region is different from the one selected in the previous iteration, the user senses the medium to check the availability of this region. If it is free, the user transmits its information; otherwise, the user has to reexecute the algorithm to check another region.

An example of the application of different transmission schemes can be seen in Figure 3, where a convoy of three units exchanges motion information to guarantee the stable movement of the formation. The medium access control mechanism considers three time slots and four frequency channels.

5.6. Estimation Allocation Matrix Update. The EAM is the tool that enables each user to determine the present status of the medium. In the ENCCMA, the EAM is rapidly updated via the auxiliary scanning process. Before transmission, each element of the matrix represents an estimate of finding the associated transmission region unoccupied. Each scan of the available transmission regions provides occupancy information which is used by the algorithm to apply bonuses if the region is found to be free or penalties if it is found to be busy. Thus, a penalty is applied to a matrix element associated with an occupied region, in order to lower its possibilities of being selected as a transmission region by the algorithm. In contrast, a bonus is applied to a matrix element associated with a region found to be unoccupied in each iteration, facilitating its selection as transmission region for the user in future iterations. A detailed definition of the bonuses and penalties used for the EAM update can be found in [20, 33]. A user who has successfully transmitted, after applying bonuses, remains in the *listen* state until the next frame; otherwise, a new iteration is triggered.

5.7. Summary of Main Features. Summing up, the main aspects of the ENCCMA proposal are as follows.

(i) It represents a natural evolution of the NCC-TDMA strategy described in [20].

(ii) Improvements have been made in two main areas:

(a) leverage of multichannel capacity, increasing the system's capacity by using a combination of TDMA and FDMA schemes;

(b) leverage of new CR techniques in the field of spectrum sensing [27] and dynamic spectrum access [30]. Consequently, this new proposal senses medium status (spectrum occupancy) and reflects potential environment variations in VANET scenarios more rapidly. It allows each user to select the best region to transmit in each iteration.

(iii) These original restrictions have also been considered.

(a) The resultant MAC must meet the real-time communications requirements of VANET scenarios.

(b) The use of signaling must be avoided in order to maintain the complete autonomy of each system user. Each user must be able to perform any application function by transmitting the required information without the need to receive any signaling information from any other user or central station.

(iv) A generic approach has been employed in the design of the ENCCMA.

(a) The protocol can be used as the main medium access control mechanism or as a complementary one.

(b) The new multichannel capacity can be freely adapted to any spectrum division scheme, including the IEEE 802.11p multichannel scheme or any other multichannel configurations.

(v) Various aspects of the cost function defined for the complementary exploration function can be configured:

(a) depending on the cost of a single operation of spectrum sensing in terms of energy efficiency;

(b) the balance between historical exploration values and immediate ones.

6. Results

To evaluate the performance of the ENCCMA, a specific tool called SIMITS was implemented using NET C# (available in [40]). This tool starts from a scenario that matches the characteristics described in Section 4 and allows the user to select the following main aspects: number of users, time as well as frequency divisions, and medium access control mechanisms, including Slotted-Aloha [41], RR-ALOHA [42], and the ENCCMA proposal presented here. Slotted-Aloha is one of the most widely studied protocols in the literature. This generic MAC mechanism is not oriented to the application and does not use signaling. RR-ALOHA is based on Slotted-Aloha but includes a signaling mechanism to render the mechanism self-scheduled.

Section 3 made a reference to the cognitive MAC for VANET (CMV). However, the SIMITS tool does not include this alternative among its available protocols because it is a specific mechanism for the spectrum division given in IEEE 802.11p. This means that it is not possible to perform a simulation using CMV over a generic medium scheme without modifying its performance. It should be noted that both Slotted-Aloha and RR-ALOHA are proposals which start from a TDMA scheme. However, SIMITS is capable of simulating environments with combined TDMA and FDMA schemes for these access mechanisms without taking into account the considerations of a real implementation of these protocols over any kind of combined TDMA and FDMA schemes. This is also the reason why all the selected mechanisms are generic and not application oriented. This means that every MAC selectable by the simulator can operate over any kind of access (TDMA, FDMA, or combinations of TDMA and FDMA). In the case of the previously described protocol (CMV), this is not possible because its nature is strictly associated with the WAVE spectrum division scheme.

In addition, this tool is capable of simulating channel occupancy by means of interfering signals. Therefore, scenarios with very dense spectrum occupancy have been tested, revealing some interesting conclusions about mechanism performance in such types of situation, as can be seen in Section 6.2.

6.1. Throughput Comparison in Nominal Scenario. The software tool calculates the performance of the medium access control mechanism in terms of throughput as follows:

$$
\begin{aligned}
\text{simulated\_time} &= \text{simulated\_time\_slots} \cdot \text{time\_per\_slot} \\
\text{bytes\_sent} &= \text{successful\_transmissions} \cdot \text{message\_size} \\
\text{bytes\_sent\_per\_user} &= \frac{\text{bytes\_sent}}{\text{number\_of\_users}} \\
\text{total\_throughput} &= \frac{\text{bytes\_sent} \cdot 8}{\text{simulated\_time}} \\
\text{throughput\_per\_channel} &= \frac{\text{total\_throughput}}{\text{number\_of\_frequency\_channels}},
\end{aligned}
\tag{6}
$$

where message size is calculated according to the encoding for each modulation type [7], as shown in Table 2.

In the case of RR-ALOHA, it is necessary to take into account the extra size of the message related to the signaling required for the protocol [42]. Consequently, to calculate the throughput when using RR-ALOHA, an extrasized user message is added according to

$$\text{rr\_aloha\_user\_data\_size} = \text{user\_data} + 2 * \text{number\_of\_users}. \tag{7}$$

Table 2: Coding rates used for each modulation in IEEE 802.11p.

Modulation	Coding rate	Transfer rate
BPSK	1/2	3 Mbps
BPSK	3/4	4.5 Mbps
QPSK	1/2	6 Mbps
QPSK	3/4	9 Mbps
16-QAM	1/2	12 Mbps
16-QAM	3/4	18 Mbps
64-QAM	2/3	24 Mbps
64-QAM	3/4	27 Mbps

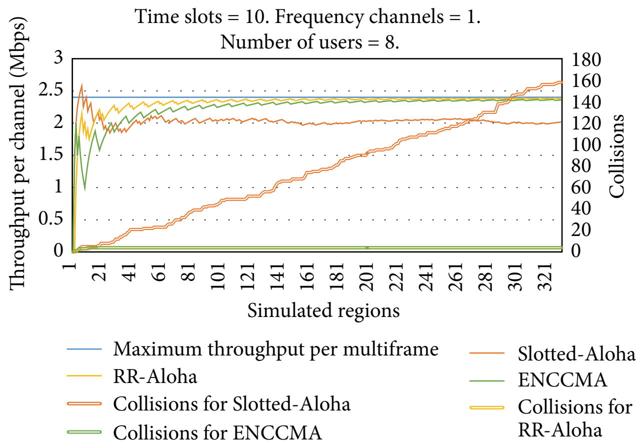

Figure 4: Throughput comparison of several MAC mechanisms in an ideal small scenario.

Figure 4 shows the simulation results for a small scenario in ideal conditions (no interferences), where all the mechanisms tended to reach the maximum throughput per user and per frequency channel. As can be seen, both the ENCCMA and RR-ALOHA were capable of reaching an equilibrium situation and avoiding the occurrence of collisions. However, this was not the case of Slotted-Aloha, where collisions occurred throughout the simulation experiment.

The results shown in Figure 5 were obtained using the same conditions as in the previous experiment but with a shared medium divided into a combined TDMA and FDMA scheme and modifying the protocol behavior of S-Aloha and RR-ALOHA to allow frequency channels. It can be seen that the performance of the tested mechanisms was quite similar to that obtained with the basic scenario, which only considered time division. As expected, Slotted-ALOHA offered a lower throughput since vehicles using this mechanism collided when trying to communicate.

6.2. Throughput Comparison in a High Interference Scenario. Simulation results were also obtained for the scenario described in the previous section but considering the existence of multiple interfering signals so that the remaining available transmission regions were equal to the number of users. Each vehicle had to use one of these remaining free regions to transmit without interfering with other vehicles

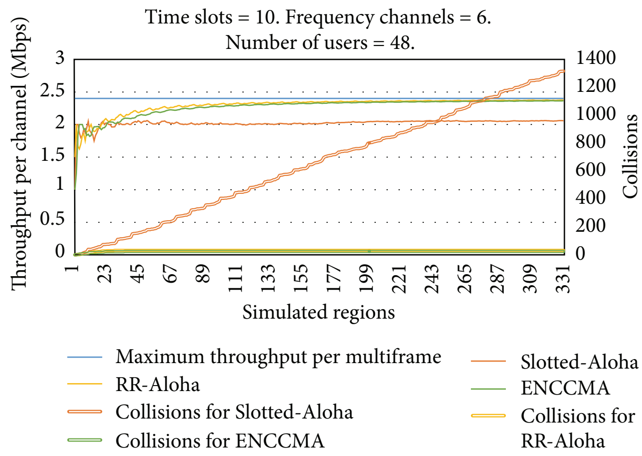

Figure 5: Throughput comparison of several MAC mechanisms in an ideal large scenario.

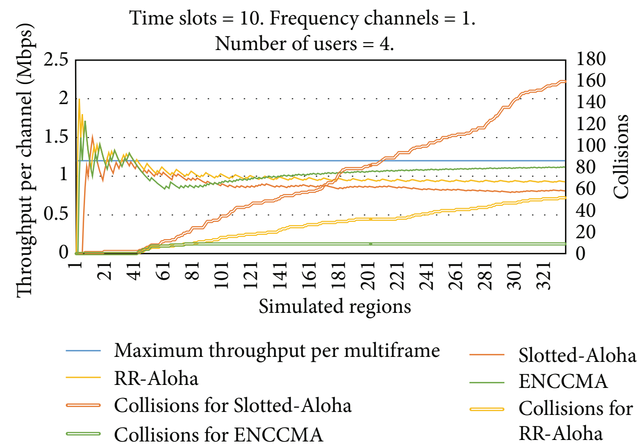

Figure 6: Throughput comparison in high interference small scenario.

or with the external signals purposely generated in the experiment. This situation illustrates the capacity of the mechanisms to adapt to changes in the environment and also highlights the capabilities and performance of each evaluated mechanism in similar situations of high interference scenarios.

As can be seen in Figure 6, only the ENCCMA mechanism was capable of recovering equilibrium in the system. In the equilibrium situation, all the users were able to carry out transmission of the information required by the application. In the case of RR-ALOHA, the throughput curve did not reach the downward trend of Slotted-Aloha, but the mechanism was nevertheless still unable to return to the equilibrium situation. For the platooning guidance of autonomous vehicles, only the ENCCMA mechanism could ensure convoy stability. Thus, in order to ensure convoy stability, the system parameters must be configured to maintain the maximum communication time among vehicles lower than the maximum time to reach equilibrium by the medium access control mechanism. It should be noted that the case

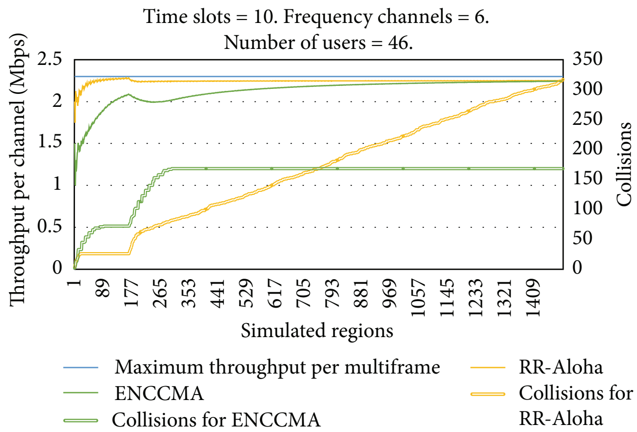

Figure 7: Throughput comparison in high interference large scenario.

under study is a difficult communication scenario due to the presence of multiple interfering signals, which requires the mechanism to work at maximum capacity. In this situation, the mechanism can still reach the equilibrium, but the system is brought to its capacity limit. The same conditions were also applied to a more complex scenario with an increased number of users over a combined TDMA-FDMA scheme, and the simulation results are shown in Figure 7.

The Slotted-Aloha mechanism values have obviously been removed from Figure 7. The behavior of this mechanism was worse than the other two alternatives analyzed, as can be seen in the previous experiments. The RR-ALOHA mechanism reached initial equilibrium faster, due to the benefits that this protocol obtains from using signaling. In this initial stage, the ENCCMA had not yet acquired any knowledge about spectrum occupancy, and thus it required more iterations than RR-ALOHA to reach equilibrium. Given that the medium was divided into 10 time slots and 6 frequency channels in the test scenario, the *multiframe* system consisted of 60 transmission regions, so that the ENCCMA mechanism reached equilibrium in the second *multiframe*. Typical values for the specific case of platooning guidance of autonomous vehicles could be about 100 ms. The interferences were introduced into the system around the simulation of transmission region number 180. At this point, both mechanisms had to begin adapting to the shared medium changes in order to recover an equilibrium situation, as required in ITS applications.

The RR-ALOHA mechanism was unable to achieve equilibrium, as indicated by the indefinite increase in the number of collisions. The throughput curve corresponding to this mechanism continued to grow slightly since some users managed to find a transmission region to transmit without collision. However, other users tried to transmit in busy regions, generating collisions and indicating that the mechanism was not able to recover an equilibrium situation.

The ENCCMA mechanism recovered the equilibrium situation following exploration of around 300 regions after two *multiframes*. This would be around 200 ms, considering typical values in platooning guidance. Although the drop in initial performance of the ENCCMA was more noticeable than in the case of the RR-ALOHA mechanism, it was actually able to recover the equilibrium situation in the worst case scenario. This thus allowed the ITS application to meet the special real-time communication requirements.

7. Conclusions

This paper describes an enhanced medium access mechanism which has evolved from the proposal made by the same authors described in [20, 33]. The aim of the current proposal is to improve the capacity and efficiency of the system by fulfilling real-time communication requirements in environments such as VANET in ITS. In a scenario involving platooning guidance of autonomous vehicles, the loss of critical information endangers the global stability of the convoy formation. This ITS application, in which it is essential to meet real-time requirements, is a clear example of the application of networked control systems to smart transportation.

The ENCCMA proposal can be considered an alternative mechanism for medium access control in VANET applications that require real-time communication. It provides full autonomy to the vehicle in terms of communications as it does not require signaling for operation. In addition, it can be applied to a system as the sole medium access control mechanism or as a complementary one (e.g., as a CSMA/CA complement). Furthermore, it is completely generic and therefore not application oriented. This means that it is not necessary for an application requiring ITS communication among vehicles to meet any special precondition in order to use the mechanism, unlike the case of other proposals such as the STDMA [21], which works better for position dissemination applications. Moreover, it can operate multiple schemes of shared medium division: TDMA, FDMA, or combination of both. It is neither restricted to a particular spectrum division in order to share access among users (as is the case of CMV [38]). Lastly, it is based on the principles of CR (learning and adaptability) and leverages recently developed spectrum sensing and DSA techniques. As a result, it is capable of adapting to rapid changes in medium occupancy either by system users or by external interfering signals.

The global result is a dynamic and autonomous mechanism that takes advantage of medium observation to determine the best transmission region for use each time, and which continuously learns and adapts to environment changes. For guidance of autonomous vehicles in convoy, medium access control is of vital relevance in split and merge maneuvers. In these cases, the medium access control mechanism must deal with new vehicles joining the convoy while maintaining satisfactory transmission for member vehicles. Lastly, although the present version of the mechanism requires time synchronization between system users, a possible future area of research would be to incorporate sufficient complexity into the mechanism to avoid this need.

Conflict of Interests

The authors declare that there is no conflict of interests regarding the publication of this paper.

Acknowledgments

This work has been funded by the Spanish Ministry of Economy and Competitiveness through the ALCOR project (ref. DPI2013-47347-C2-1-R) and by the University of Alcala through the MACRE project (CCG2013/EXP-001).

References

[1] Y. L. Morgan, "Notes on DSRC & WAVE standards suite: its architecture, design, and characteristics," *IEEE Communications Surveys and Tutorials*, vol. 12, no. 4, pp. 504–518, 2010.

[2] S. A. Mohammad, A. Rasheed, and A. Qayyum, "VANET architectures and protocols stacks: a survey," in *Communication Technologies for Vehicles*, vol. 6596 of *Lecture Notes in Computer Science*, pp. 95–105, Springer, 2011.

[3] CAR 2 CAR Communication Consortium Manifesto, 2007, http://elib.dlr.de/48380/1/C2C-CC_manifesto_v1.1.pdf.

[4] T. Ernst, V. Nebehaj, and R. Søråsen, "CVIS: CALM proof of concept preliminary results," in *Proceedings of the 9th International Conference on Intelligent Transport Systems Telecommunications (ITST '09)*, pp. 80–85, October 2009.

[5] http://www.cvisproject.org/.

[6] D. Jiang and L. Delgrossi, "EEE 802.11p: towards an international standard for wireless access in vehicular environments," in *Proceedings of the 67th IEEE Vehicular Technology Conference (VTC '08)*, pp. 2036–2040, May 2008.

[7] IEEE 802.11p, "Standard for Information technology—Telecommunications and information exchange between systems—Local and metropolitan area networks—Specific requirements. Part 11: Wireless LAN Medium Access Control (MAC) and Physical Layer (PHY) Specifications. Amendment 6: Wireless Access in Vehicular Environment".

[8] J. Funke, P. Theodosis, R. Hindiyeh, G. Stanek, K. Kritatakirana, and C. Gerdes, "Up to the limits: autonomous Audi TTS," in *Proceedings of the Intelligent Vehicles Symposium*, Alcalá de Henares, Spain, June 2012.

[9] http://www.toyota-europe.com/about/news_and_events/editorial/autonomous-driving.tmex.

[10] https://www.media.volvocars.com/global/en-gb/media/pressreleases/136182/volvo-car-group-initiates-world-unique-swedish-pilot-project-with-self-driving-cars-on-public-roads.

[11] A. Broggi, P. Medici, E. Cardarelli, P. Cerri, A. Giacomazzo, and N. Finardi, "Development of the control system for the VisLab intercontinental autonomous challenge," in *Proceedings of the 13th International IEEE Conference on Intelligent Transportation Systems (ITSC '10)*, pp. 635–640, Madeira Island, Portugal, September 2010.

[12] E. Onieva, J. Alonso, J. Pérez, V. Milanés, and T. de Pedro, "Autonomous car fuzzy control modeled by iterative genetic algorithms," in *Proceedings of the IEEE International Conference on Fuzzy Systems (FUZZ-IEEE '09)*, pp. 1615–1620, Jeju Island, Republic of Korea, August 2009.

[13] http://www.google.com/about/careers/lifeatgoogle/self-driving-car-test-steve-mahan.html.

[14] J. Levinson, J. Askeland, J. Becker et al., "Towards fully autonomous driving: systems and algorithms," in *Proceedings of the IEEE Intelligent Vehicles Symposium (IV '11)*, pp. 163–168, June 2011.

[15] C. Santos, F. Espinosa, D. Pizarro, F. Valdés, E. Santiso, and I. Díaz, "Fuzzy decentralized control for guidance of a convoy of robots in non-linear trajectories," in *Proceedings of the IEEE International Conference on Emerging Technologies and Factory Automation (ETFA '10)*, pp. 1–8, Bilbao, Spain, September 2010.

[16] M. Gerla, E.-K. Lee, G. Pau, and U. Lee, "Internet of vehicles: from intelligent grid to autonomous cars and vehicular clouds," in *Proceedings of the IEEE World Forum on Internet of Things (WF-IoT '14)*, pp. 241–246, March 2014.

[17] M.-W. Li, T.-H. Wu, W.-Y. Lin, K.-C. Lan, C.-M. Chou, and C.-H. Hsu, "On the feasibility of using 802.11p for communication of electronic toll collection systems," *ISRN Communication and Networking*, vol. 2011, Article ID 723814, 11 pages, 2011.

[18] V. Milanés, J. Villagrá, J. Godoy, J. Simó, J. Pérez, and E. Onieva, "An intelligent V2I-based traffic management system," *IEEE Transactions on Intelligent Transportation Systems*, vol. 13, no. 1, pp. 49–58, 2012.

[19] S. Sehrawat, R. P. Bora, and D. Harihar, "Performance analysis of QoS supported by Enhanced Distributed Channel Access (EDCA) mechanism in IEEE 802.11e," *IAENG International Journal of Computer Science*, vol. 33, no. 1, 2007.

[20] M. Manzano, F. Espinosa, Á. M. Bravo-Santos, E. Santiso, I. Bravo, and D. Garcia, "Dynamic cognitive self-organized TDMA for medium access control in real-time vehicle to vehicle communications," *Mathematical Problems in Engineering*, vol. 2013, Article ID 574528, 13 pages, 2013.

[21] K. Bilstrup, E. Uhlemann, E. G. Ström, and U. Bilstrup, "On the ability of the 802.11p MAC method and STDMA to support real-time vehicle-to-vehicle communication," *EURASIP Journal on Wireless Communications and Networking*, vol. 2009, Article ID 902414, pp. 1687–1472, 2009.

[22] K. Bilstrup, E. Uhlemann, E. G. Ström, and U. Bilstrup, "Evaluation of the IEEE 802.11p MAC method for vehicle-to-vehicle communication," in *Proceedings of the IEEE 68th Vehicular Technology Conference (VTC '08)*, pp. 1–5, Calgary, Canada, September 2008.

[23] K. Sjöberg-Bilstrup, E. Uhlemann, and E. G. Ström, "Scalability issues of the MAC methods STDMA and CSMA of IEEE 802.11p when used in VANETs," in *Proceedings of the IEEE International Conference on Communications Workshops (ICC '10)*, pp. 1–5, Capetown, South Africa, May 2010.

[24] S. Haykin, "Cognitive radio: brain-empowered wireless communications," *IEEE Journal on Selected Areas in Communications*, vol. 23, no. 2, pp. 201–220, 2005.

[25] J. Mitola, *Cognitive Radio Architecture: The Engineering Foundations of Radio XML*, John Wiley & Sons, 2006.

[26] E. Hossain and V. K. Bhargava, *Cognitive Wireless Communication Networks*, Springer, 2007.

[27] D. Cabric, S. M. Mishra, and R. W. Brodersen, "Implementation issues in spectrum sensing for cognitive radios," in *Proceedings of the Conference Record of the 38th Asilomar Conference on Signals, Systems and Computers*, pp. 772–776, November 2004.

[28] T. A. Weiss and F. K. Jondral, "Spectrum pooling: an innovative strategy for the enhancement of spectrum efficiency," *IEEE Communications Magazine*, vol. 42, no. 3, pp. S8–S14, 2004.

[29] Z. Yan, Z. Ma, H. Cao, G. Li, and W. Wang, "Spectrum sensing, access and coexistence testbed for cognitive radio using USRP," in *Proceedings of the 4th IEEE International Conference on Circuits and Systems for Communications (ICCSC '08)*, pp. 270–274, May 2008.

[30] E. Hossain, D. Niyato, and Z. Han, *Dynamic Spectrum Access and Management in Cognitive Radio Networks*, Cambridge University Press, Cambridge, UK, 2009.

[31] Y. Yuan, P. Bahl, R. Chandra, T. Moscibroda, and Y. Wu, "Allocating dynamic time-spectrum blocks in cognitive radio networks," in *Proceedings of the 8th ACM International Symposium on Mobile Ad Hoc Networking and Computing (MobiHoc '07)*, pp. 130–139, Montreal, Canada, September 2007.

[32] M. Parsapoor and U. Bilstrup, "Imperialist competitive algorithm for DSA in cognitive radio networks," in *Proceedings of the 8th International Conference on Wireless Communications, Networking and Mobile Computing (WiCOM '12)*, pp. 1–4, IEEE, Shanghai, China, September 2012.

[33] M. Manzano, F. Espinosa, Á. M. Bravo, D. García, A. Gardel, and I. Bravo, "Medium access control based on a non cooperative cognitive radio for platooning communications," in *Proceedings of the IEEE Intelligent Vehicles Symposium (IV '12)*, pp. 408–413, June 2012.

[34] S. Eichler, "Performance evaluation of the IEEE 802.11p WAVE communication standard," in *Proceedings of the 66th IEEE Vehicular Technology Conference (VTC '07)*, pp. 2199–2203, October 2007.

[35] S. Kumar, V. S. Raghavan, and J. Deng, "Medium access control protocols for ad hoc wireless networks: a survey," *Ad Hoc Networks*, vol. 4, no. 3, pp. 326–358, 2006.

[36] J. Mitola III and G. Q. Maguire Jr., "Cognitive radio: making software radios more personal," *IEEE Personal Communications*, vol. 6, no. 4, pp. 13–18, 1999.

[37] M. di Felice, K. R. Chowdhury, and L. Bononi, "Analyzing the potential of cooperative cognitive radio technology on inter-vehicle communication," in *Proceedings of the IFIP Wireless Days (WD '10)*, October 2010.

[38] S.-E. Chung, J. Yoo, and C.-K. Kim, "A cognitive MAC for VANET based on the WAVE systems," in *Proceedings of the 11th International Conference on (ICACT '09)*, pp. 41–46, Dublin, Ireland, February 2009.

[39] S. Gräfling, P. Mähönen, and J. Riihijärvi, "Performance evaluation of IEEE 1609 WAVE and IEEE 802.11p for vehicular communications," in *Proceedings of the 2nd International Conference on Ubiquitous and Future Networks (ICUFN '10)*, pp. 344–348, June 2010.

[40] http://www.geintra-uah.org/idi/sofware-abierto/sofware-abierto.

[41] L. Roberts, "Aloha packet system with and without slots and capture," *ACM SIGCOMM Computer Communication Review*, vol. 5, no. 2, pp. 28–42, 1975.

[42] F. Borgonovo, A. Capone, M. Cesana, and L. Fratta, *RR-ALOHA, a Reliable R-ALOHA Broadcast Channel for Ad-Hoc Inter-Vehicle Communication Networks*, Dipart Elettronica e Informazione, Politec di Milano, 2002, ftp://ftp.dei.polimi.it/outgoing/Flaminio.Borgonovo/PUBBC/2002medhoc.pdf.

Hindawi Publishing Corporation
Mathematical Problems in Engineering
Volume 2015, Article ID 264514, 8 pages
http://dx.doi.org/10.1155/2015/264514

Research Article

Banknote Validation through an Embedded RFID Chip and an NFC-Enabled Smartphone

Mohamed Hamdy Eldefrawy and Muhammad Khurram Khan

Center of Excellence in Information Assurance, King Saud University, P.O. Box 92144, Riyadh 11653, Saudi Arabia

Correspondence should be addressed to Mohamed Hamdy Eldefrawy; meldefrawy@ksu.edu.sa

Received 14 August 2014; Accepted 17 November 2014

Academic Editor: Jinhui Zhang

With the new, state-of-the-art printing devices and equipment, there has been rapid growth in the counterfeiting of banknotes. Traditional security features on banknotes are easy targets for counterfeiters, and they can easily imitate the original banknotes with fake ones. Conventional methods for validating currency require specialized devices for the authentication of banknotes. However, cost and lack of mobility of sophisticated banknote validation devices are big problems for general consumers. Modern digital solutions are attempting to complement the traditional security features through embedding radio frequency identification (RFID) chips in the banknotes, for example, Euro currency. Unfortunately, the requirement of specialized RFID readers for banknote validation impedes their widespread proliferation among consumers. To overcome this problem, a new method of banknote validation using an RFID chip and an NFC-enabled smartphone is presented. The consumer sends a banknote validation request to the Monetary Agency ($\mathscr{MA}$) using her or his smartphone and an Internet connection. The $\mathscr{MA}$ replies by sending a random challenge to the consumer's smartphone. The RFID chip in the banknote receives the challenge, via the NFC, and calculates an equivalent response to the $\mathscr{MA}$'s challenge. If any of the messages are incorrect, authentication is denied. By the proposed method, consumers can easily and instantly check the originality of currency notes with the $\mathscr{MA}$ using their smartphones and an Internet connection. The proposed system is less expensive, computationally, than regular methods and preserves the privacy of people who carry banknotes.

1. Introduction

Counterfeiting money has become an enormous problem around the world. Traditional security features on banknotes, for example, holograms, are easily prone to counterfeiting. Existing techniques do not provide realistic solutions because of complexity of the sophisticated devices that are used for banknote validation. Recently, RFID chips have been used on banknotes to complement the existing security features printed on the banknotes. The new digital solutions embed the banknote's serial number in the attached RFID chips. Robust solutions require appending cryptographic methods to stop forgery and counterfeiting. RFID devices have been experimentally assessed and tested as a means for confronting the problem of counterfeit currency notes.

RFID systems are comprised of RF tags and RF tag readers. RFID tags are small, wireless microchips that are used to spot their attached targets. RFID tags generally can be classified into two categories; that is, (1) RFID tags with a power source are delivered dynamically to a reader and identified as "active tags" and (2) powerless devices, which are prompted by a reader, are identified as "passive tags" [1–3]. The reader is a machine that identifies and retrieves the RFID information from the card [4, 5]. The reader challenges the tag by generating a radio frequency wave, and the tag answers the reader with an equivalent response [6]. The reader delivers the tag's answers to a final host (server). The server obtains the tag's record and recovers the tag's complete information from its response. Near-field communication (NFC) is an emerging area of communication for connecting RFID tags; hence NFC standards are based on existing RFID standards, including ISO/IEC 14443. [7]. The NFC protocol establishes a radio communication channel with NFC-enabled devices by putting them in close proximity, normally no more than a few centimeters. With the improvement of computing and digital printing technology, the counterfeit industry recently has grown exponentially. An accepted counterfeiting technique is digital printing using computer scanners and high-resolution printers. Although banknotes already contain security attributes, such as holograms, foil lines, special threads, microprinting, special inks, and watermarks [6], additional protection is required. The aim of this paper is to offer a comprehensive solution against the use of counterfeit banknotes using RFID chips embedded in currency notes. The proposed technique will allow individuals to verify banknotes using a portable token (e.g., their smartphones) without going to a facility or making personal or direct contact with an agency. In the proposed system, the consumer does not need to have specialized RFID readers; rather he or she can use an NFC-enabled smartphone for this purpose. The capability of using smartphones for detecting counterfeit money will, in turn, lead to their widespread use for this purpose by consumers. It will influence wide-ranging consumers to validate their currency by their smartphones extensively without the need for any complicated currency validation tools. The proposed protocol provides a set of required security features, and it guarantees low communication and computational costs in terms of number of communications required between the reader-tag and the mathematical operations, respectively. The analysis shows that the proposed protocol achieved the required performance goal and the security goal. The rest of the paper is organized as follows. Section 2 discusses the related work, Section 3 illustrates the security requirements, Section 4 proposes our currency validation protocol, Section 5 analyzes the security attributes and evaluates performance, and Section 6 presents our conclusions.

2. Related Work

Several research scientists have attempted to develop secure communication protocols for detecting counterfeit money using lightweight RFIDs. RFIDs facilitate non-line-of-sight and very rapid examining of unique IDs. It allows practical handling of unique identifiers in open-loop supply chains. Generally, identifiers can be symbolized in barcodes or holograms as well, but a line-of-sight communication would be required, and they must be read one by one in a very exhaustive process. RFID chips can obtain a single factory programmed ID that is locked after writing, making it unchangeable. The number of chips is limited and requires trusted chip authorities who do not produce duplicate IDs. They should be made in a random distribution instead of used sequential numbers inside a certain number-space, making it essentially impervious to unauthorized disclosures of the legal ID. Preventing counterfeiting by tracking and tracing possessions across the supply chain utilizes central or connected databases by detecting any abnormal trace patterns of RFID tags. There are two fundamental categories of RFID authentication schemes, that is, the use of digital signature-based protocols and challenge-response protocols. However, in the challenge-response authentication, we could have a mutual authentication with a symmetric scheme as well as a one-sided authentication with an asymmetric scheme. To prevent counterfeiting, the authenticity of the service distributed is verified alongside the delivery chain and possibly at the end-users as well. However, many checkpoints are not online. Also, public key cryptography offers different options between complexity on the tag and complexity in the infrastructure. Therefore public key cryptography is an attractive alternative to symmetric key systems, in particular for open and offline systems. However, cryptographic tags have cost and performance limitations due to their additional hardware and the processing time required. The following subsection illustrates some of the schemes that have been presented and their weaknesses. Hash-based access control (HAC), proposed by Weis et al. [5, 8], uses a one-way hashing to latch the RFID tags. A latched tag uses a hash of a random key to be its meta-ID. When latched, a tag reacts to every inquiry by its fixed meta-ID. HAC is vulnerable to location tracking attacks because the meta-ID is stationary at any time when a tag is needed. Randomized access control (RAC) stops this tracking vulnerability, but it is susceptible to tag impersonation attacks since a captured tag's answer can be repeated. In addition, it does not grant backward untraceability since the tag's ID is stationary. Lane et al. disclosed a method and apparatus for authenticating currency wherein the currency contains a foundation, such as paper, and an implanted RFID transponder [9]. An implanted RFID transponder or electronic watermark could include several sequencing levels of electronic passwords, which could be used to defend the host currency from any illegal alteration. In addition, such smart RFID tags may, *outstandingly*, classify an original certificate and its related information. The validating organization can use a public/private electronic product code (EPC) database as a facility to authenticate documents by the authenticating agency. The smart EPC could be used as an anticounterfeit system to facilitate a third party's request in order to offer services, profits, or monetary payments to validate documents and stop the counterfeiting of money.

Pareskevakos presented a system and method for currency authentication [10]. In Pareskevakos's system, the currency is authenticated by evaluating the classifying information taken from the banknote itself, such as the note's correlated serial number, to identify information in a directory related to invalid currency, such as fake currency. If the extorted classifying information matches information on the directory, the note is considered original. Optical character recognition could be used to extract the classifying information.

Ohkubo et al. presented an inexpensive hash chain method to revise the tag's secret data and grant forward security [11, 12]. It was intended to classify a communication party while guaranteeing privacy. However, it is susceptible to replay attacks [9], and, consequently, it allows an intruder to masquerade as a tag without any knowledge of the hidden information on the tag.

Henrici and Müller (HM) proposed a one-way hash function to countermeasure tag-tracing violations by enhancing the privacy of the location. The tag answers a reader's inquiry with double hashes and renews its saved values after a legal validation. This proposition still allows an amount of tag tracing because a tag replies with the identical answer before its legitimate validation. In addition, forward security cannot be guaranteed since an intruder can analyze prior sessions' tag identifiers from the tag's present identifier with the random number of the server.

In 2007, a mutual authentication protocol for RFID was researched by Chien and Chen [13]. A challenge-response technique was presented to stop replay attacks. The server record contains images of previous and fresh tag keys to prevent denial-of-service attacks. The authentication key and the access-key are renewed cooperatively subsequent to a valid authentication to give backward untraceability. However, the system authorizes backward and forward traceability, since an intruder who exposes a tag could recognize a tag's earlier exchanges from the prior communications and can examine the tag's upcoming dealings. Furthermore, an intruder can impersonate an authorized server to a tag by obtaining the tag's private values.

Duc et al. demonstrated a synchronized connection method for the RFID tag of the EPCGlobal-Class-1-Gen-2 [14]. It considers a pseudo-random number producer and a CRC check. It is not able to counter replay attacks prior to the subsequently valid authentication. Critically, a DoS attack can get a server and a tag out of synchronization [15]. It cannot present backward intractability if the fixed EPC and the access-key PIN are disclosed [13].

Song and Mitchell presented a scheme by utilizing the challenge-response approach to avoid tag impersonation attacks and replay attacks [5]. It uses random challenge values to give unpredictable tag responses. To circumvent denial-of-service attacks in case of a lack of synchronization in the shared private updating, the back-end server saves the updated values with their earlier values for the next validations. If the validation and authentication process is successful, subsequently, the tag and the server will update their common private values using swapped random numbers, thereby achieving untraceability. A main attribute of the algorithm is that a random number produced by a tag acts as a short-term private value for the tag. An alternative attribute is that a tag only requires saving identification, which is a cryptohash function of a bit-string allocated to the tag. The scheme was intended to decrease the use of complicated cryptographic functions and to replace them with straightforward functions, such as bit-wise exclusive-or and left and right shift registers to join data sequences. Security threats to RFID protocols also are discussed in [5, 11, 16–18], and the use of RFID μ-chips for detecting counterfeit money is discussed in [18–25].

2.1. RFID μ-Chip. Improvement of low-cost RFIDs was initiated in 1998 as an authentication enclosure integrated circuit to help avert the counterfeiting of currency [26]. Each μ-chip IC has a 128-bit, exclusive identifier that is configurationally part of the chip. The μ-chips function at an operating frequency of 2.45 GHz. The normal time for the exchange of messages to and from the reader and the μ-chip is about 20 ms [15]. Maximum reading distance between the reader and the tag is about 30 cm in the free space. With an area of $0.4\,\mathrm{mm}^2$, μ-chips can be implanted in the currency and transmit defined information over a low-range space. Also, the fabrication of chips per silicon wafer is roughly twice that of the typical $0.7\,\mathrm{mm}^2$ RFID chips. The smaller chip is called the powder large-scale integrated (LSI) chip, which also saves a 128-bit identification.

Table 1: Banknote data storage format in Juels and Pappu's scheme.

RFID	
Cell γ ispublicly readable and keyed-writable	Cell δ is keyed-readable and keyed-writable
$C = \mathrm{Enc}(PK_L, \sum \| S, r)$	r
Optical	
S	$\sum = \mathrm{Sign}(SK_B, S\|\mathrm{den})$

Powder LSI chips contain basically the identical constituents as the μ-chip, but they are cuddled into minor pieces. A main reason for the added efficiency was the use of what is named "90-nanometer silicon-on-insulator" (SOI) expertise. SOI allows processors to execute better and use less power than those formed by traditional methods as it separates transistors with an insulator. The insulator decreases the absorption of electrical energy into the surrounding medium and maintains the transistors separated which stops interference between transistors and lets them be grouped more closely together, making the chip smaller in size [27].

2.2. Juels and Pappu's Scheme. In [25], Juels and Pappu proposed a scheme that allows the verification of banknotes, which allows a law enforcement agency $\mathscr{L}$ to legally track interesting banknotes. They identified four entities that are involved in treating banknotes; that is, (1) a central bank that is authorized to produce and issue banknotes is denoted by $\mathscr{B}$, (2) a law enforcement agency that is able to trace the flow of banknotes is denoted by $\mathscr{L}$, (3) the merchant is denoted by $\mathscr{M}$, and (4) the consumer is denoted by $\mathscr{C}$. $\mathscr{B}$ creates the banknotes and has a signing key pair (SK_B, PK_B) for $\mathrm{Sign}(\cdot)$. $\mathscr{L}$ is the banknote tracing agency, and it has an encryption key pair (SK_L, PK_L) for $\mathrm{Enc}(\cdot)$. $\mathscr{M}$ checks the received banknotes in a trade and has the responsibility of notifying $\mathscr{L}$ when a forgery is detected. The Juels-Pappu banknote protection scheme (RBPS) uses RFID μ-chips (tags) to prevent counterfeiting the banknote. They used two data sources on the currency, that is, the visual or ocular data issued on the currency, for example, the PDF417 2D bar code, and the digital data saved on an RFID tag with keyed-reading and keyed-writing abilities. Table 1 presents two data sources on currency (a bill).

The serial number and the value of a banknote are denoted by S and den, respectively. Juels-Pappu RBPS involves the following procedure.

(1) Banknote Creation

$\mathscr{B}$ calculates $\sum_i = \mathrm{Sign}(SK_B, S_i\|\mathrm{den}_i)$ and prints the serial number S_i and the signature $\sum_i$ on a banknote.

$\mathscr{B}$ picks a random value r and puts it in the δ-cell.

$\mathscr{B}$ does $\text{Enc}(PK_L, \sum_i \| S_i, r_i)$ in the γ-cell.

$\mathscr{B}$ evaluates the key $D_i = h(\sum_i)$ for a banknote.

$\mathscr{B}$ adjusts the reading/writing facilities as below: the γ-cell ispublicly readable and writable with a D_i as an access-key; the δ-cell is readable/writable with an access-key D_i.

(2) Banknote Verification

$\mathscr{M}$ examines the optical region to get S_i and $\sum_i$ and then calculates an access-key $D_i = h(\sum_i)$.

$\mathscr{M}$ reads C_i from the γ-cell and reads r with a key from the δ-cell.

$\mathscr{M}$ validates $C_i \stackrel{?}{=} \text{Enc}(PK_L, \sum_i \| S_i, r_i)$.

(3) Banknote Anonymity

$\mathscr{M}$ selects r' in a random way and keyed-writes it into the δ-cell.

$\mathscr{M}$ computes $C = \text{Enc}(PK_L, \sum_i \| S_i, r')$ and keyed-writes it into the γ-cell.

(4) Banknote Tracking

$\mathscr{L}$ gets C_i from the γ-cell.

$\mathscr{L}$ does $C = \text{Dec}(SK_L, C_i)$ to get $(\sum_i \| S_i)$.

$\mathscr{L}$ validates a signature $(S_i \| \text{den}_i) \stackrel{?}{=} \text{Veri}(PK_B \| \sum_i)$ to obtain the serial number S_i for tracking.

Unless all of these steps in currency validation and banknote anonymity are successful, the merchant must inform $\mathscr{L}$. Juels-Pappu RBPS is vulnerable to data recovery, the cookies threat, access-key tracking, denial-of-service attack, and cipher-text tracking, as shown in [7].

3. Security Requirements

In this section, a number of advantageous security attributes as well as security threats to RFID protocols are discussed [5, 11, 16–18].

3.1. Nonrepudiation. Typically, "nonrepudiation" refers to the capability of ensuring that a communication party cannot deny the authenticity of the receipt security credentials that have been originated by the main server. Consequently, the RFID tags are not able to deny what they receive from the server.

3.2. Freshness. Encryption materials must be fresh and different from the reprocessing of previous keying material.

3.3. Known-Key Security. A protocol output should come with an exclusive shared secret. If a shared secret is compromised, it should have no effect on the other shared secrets.

3.4. Server Impersonation. An opponent, with knowledge of a tag internal condition, is able to masquerade as a legitimate server to the tag.

3.5. Timeliness. The process has to be accomplished in a planned amount of time and message exchange should be in a limited session.

3.6. Monitoring. Administration deals with keeping track of banknotes in exchange.

3.7. Replay Attack. In such an attack, the intruder reprocesses exchanged messages from prior communication sessions to perform the replay attack.

4. Currency Validation Protocol

RFID μ-chips have had a significant impact on security, especially in the detection of counterfeit currency [18–25]. However, those systems do not provide a high confidence level in terms of security and accuracy. The RFID μ-chip holds a 128-bit storage, including the note's serial number, which cannot be easily duplicated. However, there is concern that success in duplication of a serial number will lead to mass counterfeiting and failure to detect counterfeit notes. In the proposed work, an NFC-enabled smartphone was used to verify the authenticity of a banknote with high confidence in the accuracy. A key element of the present technique is the step of requiring the μ-chip on the banknote to do a calculation in response to a challenge that includes a random question.

4.1. Notation. We used the coming notation in the illustration of the protocol.

$\mathscr{U}$: regular consumer (user);

$\mathscr{MA}$: *Monetary Agency;*

$h(\cdot)$: public cryptographic one-way hash function;

$h_A(\cdot)$: first hash function;

$h_B(\cdot)$: second hash function;

s_i: banknote i serial number;

sd_i: seed initial value for banknote i;

$sd_i(t)$: seed number t for the tth authentication (current seed) for banknote i;

AC_i: authentication counter for banknote i;

(x_t, y_t): nested hashing progress, random challenge, values for tth authentication;

$h_B^{y_t}(h_A^{x_t}(sd_i(t)))$: hashing the current seed number t by $h_A(\cdot)$ for x_t times followed by an $h_B(\cdot)$ hashing for y_t times;

$\|$: concatenation operation.

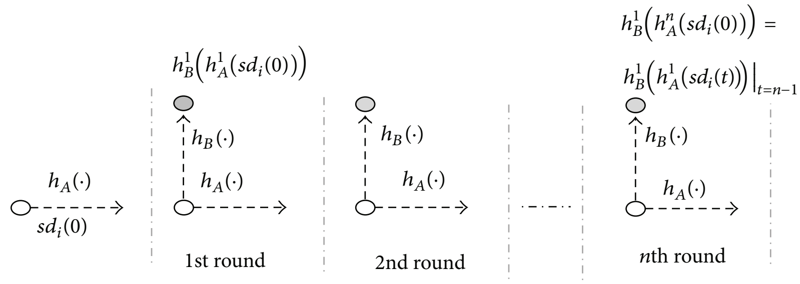

FIGURE 1: Challenge-response internal function based on two different types of hashes.

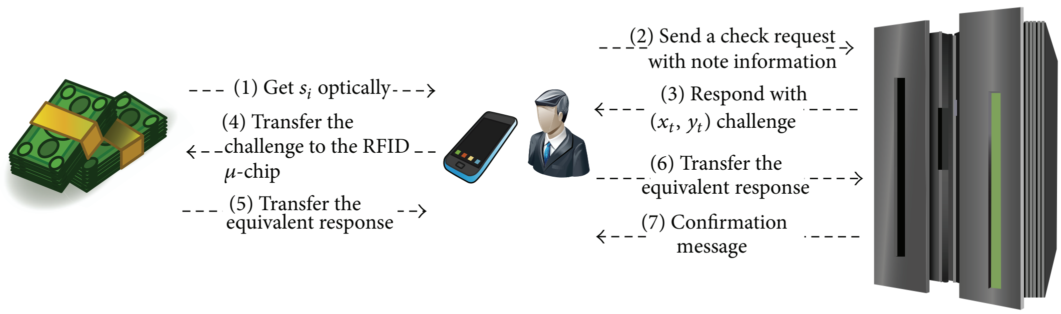

FIGURE 2: Framework and operations of the proposed scheme.

4.2. Description of the Protocol. The aim of the proposed scheme is to use a zero-knowledge proof instead of using public key cryptography. Two dissimilar hashes, $h_A(\cdot)$ and $h_B(\cdot)$, were included to satisfy the algorithm's challenge-response function [24], as depicted in Figure 1.

We integrated two dissimilar one-way hashes, $h_A(\cdot)$ and $h_B(\cdot)$, to preset our algorithm challenge-response function [10], as shown in Figure 1. Hence, $\mathscr{MA}$ sends refreshed challenge indexes (x_t, y_t) to $\mathscr{U}$ for the tth authentication. Then, $\mathscr{U}$ prompts those indexes to her or his token to be transferred to the μ-chip using RFID communication. The μ-chip responds with the corresponding response to the user's smartphone over the RFID channel. The smartphone transfers the μ-chip's response to $\mathscr{MA}$ for validation. With the result of the validation, the server confirms the validity of the banknote. Both $\mathscr{U}$ and $\mathscr{MA}$ have the same initial seed value.

4.3. Currency Creation. (1) As shown in Table 2, $\mathscr{MA}$ embeds the two RFID μ-chips (i.e., γ and δ chips) [25, 28] in the currency that contains a tamperproof primary value (the bill seed) sd_i and issues the serial number on the banknote.

(2) The validation counting value for each note is kept in the issuer/authenticator's server $\mathscr{MA}$.

(3) The issuer/authenticator's server $\mathscr{MA}$ does not need to indicate the bill's serial number.

(4) The issuer/authenticator's server $\mathscr{MA}$ ensures that the γ-cell is unreadable and self-writable and that the δ-cell is openly readable and only writable by γ.

4.4. Currency Validation. (1) When an individual consumer or $\mathscr{U}$ receives a banknote and wishes to check its validity, $\mathscr{U}$ uses the NFC smartphone to read the information on μ-chip

TABLE 2: Banknote data storage format in the proposed scheme.

RFID	
Cell γ is unreadable and self-writable	Cell δ is publicly readable/only writable by γ
$sd_i(t)$	$h_B^{y_t}(h_A^{x_t}(sd_i(t)))$
Optical	
S	

message number 1 and to automatically send a request to the issuer/authenticator's server message, that is, number 2. The message communication is shown in Figure 2.

(2) Then the issuer/authenticator's server $\mathscr{MA}$ verifies the value and serial number and, upon correction of values, it corresponds with a random challenge (x_t, y_t) for the next authentication round $(t+1)$th message number 3 that requires a calculation by the RFID μ-chip embedded in the banknote. This calculation is done by hashing $(sd_i(t))$ by $h_A(\cdot)$ x_t times to get $(sd_i(t+1)) = (h_A^{x_t}(sd_i(t)))$ and define it for the current seed and afterwards hash this current seed by $h_B(\cdot) y_t$ times to get $h_B^{y_t}(h_A^{x_t}(sd_i(t)))$ to be transferred to δ-cell, $(\gamma) \rightarrow (\delta)$, which is publicly readable. This challenge is sent to the smartphone and transferred to the banknote's μ-chip, as shown in Figure 2, message number 4.

(3) The server $\mathscr{MA}$ receives and digests the response for the $(t+1)$th authentication in step message number 5 and message number 6. If $\mathscr{MA}$ receives the correct response, it sends a confirmation or authentication through message number 7.

4.5. Currency Secrecy. The knowledge of δ which obtains $h_B^{y_t}(h_A^{x_t}(sd_i(t)))$, which is openly readable, cannot reveal any

Table 3: Comparison of the presented scheme and related schemes in terms of computational costs.

		DPLK [14]	CC [13]	SM [5]	Proposed
$\mathscr{TAG}$	Operations	$4F$	$4F$	$3F$	$(x_t + y_t) F = 2F\|_{x_t=y_t=1}$
$\mathscr{MA}$	Operations	$(k+3) F$	$(k+3) F$	$(k+1) F$	$(x_t + y_t) F = 2F\|_{x_t=y_t=1}$

F: a computationally complex function (such as a CRC or a hash function).
k: an integer that satisfies $1 \leq k \leq 2N$.
N: the number of tags.

information about the banknote. In each authentication session, the equivalent reply value must be distorted.

4.6. Currency Tracing. The proposed scheme allows standard and nonspecialist consumers to identify fake banknotes by using their smartphones. Individual consumers can report fake banknotes to the administration $\mathscr{MA}$. Consequentially, the capability of identifying fake currency is fully achieved.

5. Security, Performance Analysis, and Comparison

The algorithm we presented can obstruct the off-line guessing attack; thus it leads to strong answers, anchored in strong hash functions. The prevention of counterfeiting comes by detecting and eliminating banknote forgeries and the production of fake bills over a random generation of serial numbers. In the following subsections, a security analysis of the proposed scheme is illustrated [29, 30].

5.1. Nonrepudiation Attack. To circumvent the nonrepudiation attack, the authentication parties $\mathscr{U}$ and $\mathscr{MA}$ must update their shared secret value, $(sd_i(t+1)) = (h_A^{x_t}(sd_i(t)))$, one time per round. Consequently, the client updating will be used as the host's next verifier, and vice versa, so that any unauthorized modification of the exchanged vectors will be detected by the authentication party.

5.2. Freshness. The authentication credentials should be fresh; that is, material that has been used should not be reused. This is to be done by maintaining the randomization of the generated challenges and, consequently, the equivalent response.

5.3. Known-Key Security. The proposed protocol grants security against the known key. That is why each run of the protocol between authentication parties $\mathscr{U}$ and $\mathscr{MA}$ should make an exclusive shared key, which relies on random challenges. Even if an adversary has discovered some other earlier keys, he or she cannot guess a future key. Therefore, the protocol attains its goal against the adversary.

5.4. Server Impersonation. An opponent could demand a certain tag to renew its common secrets. The tag and the genuine server could then be unsynchronized with authentication counter AC_i and incapable of successful communication.

5.5. Timeliness. In the proposed protocol, we tried to decrease the number of swapped messages between authentication parties and the direct message exchange in real-time. In addition, the size of the messages was short.

5.6. Monitoring and Tracking. The trusted authority (i.e., issuer/authenticator's server $\mathscr{MA}$) has the full keying resources and sequentially achieves admittance to those associated keys, such that key-escrow is fully achieved. Thus, nonspecialist consumers have the ability to detect counterfeiting easily. Then the tracking capability is implicitly and completely achieved.

5.7. Preplay Attack. To avoid this attack, shared secrets should be revealed only to tags and the server. Also, challenge-response authentication addresses this threat.

5.8. Replay Attack. Gaining of unauthorized access by replaying reusable passwords is restricted by encoding passwords, which are used only once.

5.9. Forgery Attack. The algorithm we used has a high forgery-attack confrontation. The data recovery attack is banned provided that the second hash function $h_B(\cdot)$ is unbroken, and $h_B(\cdot)$ will not help a counterfeiter recover any information required to make a counterfeit copy with a certain serial number. However, in case of the failure of $h_B(\cdot)$ and obtaining the required information by the forger to generate multiple copies of given banknote with a serial number, $\mathscr{MA}$ will achieve a lack of synchronization with its counter AC_i.

5.10. Recovery Attack. As has been illustrated previously, the recovery attack cannot be executed in the survival of $h_B(\cdot)$, which is the blockade for any intruder who is attempting to acquire any hidden information. Also, it is important to note that no access-key is needed for hiding information. Table 3 [5] demonstrates a judgment between the presented algorithm and contemporary algorithms considering the number of operations required by each communication party.

6. Conclusions

In this paper, the currency counterfeiting problem has been addressed. Schemes for protecting electronic cash must include cryptomethods to deal with forgery and counterfeiting problems. A new banknote validation technique has been presented which is based on the use of an RFID μ-chip and an

NFC-enabled smartphone. A banknote is issued with a value, a serial number, and a secret seed message that is also saved on the $\mathscr{MA}$. A tamperproof RFID μ-chip is embedded in the currency note and includes the value, serial number, and secret message that is used for validation. The smartphone reads the information on the chip and requests the $\mathscr{MA}$ to validate the note. The $\mathscr{MA}$ transmits a challenge through an Internet connection and the μ-chip calculates an equivalent answer that is sent to the $\mathscr{MA}$. An approval or disapproval is then sent to the smartphone.

This possibility of using these devices to detect counterfeit money results in the extensive deployment of this technology among regular and nonspecialist end-users. It will encourage the general public to check for counterfeit money using smartphones without the need for any sophisticated and expensive optical devices. The presented validation technique satisfies the security requirements for banknote counterfeit detection. It has been compared with some related schemes with regard to computational efficiency and performance analysis. The comparisons showed that the proposed scheme is more efficient and effective than existing schemes.

Conflict of Interests

The authors declare that there is no conflict of interests regarding the publication of this paper.

References

[1] Y.-J. Huang, W.-C. Lin, and H.-L. Li, "Efficient implementation of RFID mutual authentication protocol," *IEEE Transactions on Industrial Electronics*, vol. 59, no. 12, pp. 4784–4791, 2012.

[2] Y. J. Huang, C. C. Yuan, M. K. Chen, W. C. Lin, and H. C. Teng, "Hardware implementation of RFID mutual authentication protocol," *IEEE Transactions on Industrial Electronics*, vol. 57, no. 5, pp. 1573–1582, 2010.

[3] M. H. Eldefrawy and M. K. Khan, "Detecting counterfeit-money using RFID-enabled mobile devices," in *Proceedings of the 7th International Conference for Internet Technology and Secured Transactions*, 2012.

[4] B. Glover and H. Bhatt, *RFID Essentials: O'Reilly Media*, Incorporated, 2006.

[5] B. Song and C. J. Mitchell, "RFID authentication protocol for low-cost tags," in *Proceedings of the 1st ACM Conference on Wireless Network Security (WiSec '08)*, pp. 140–147, April 2008.

[6] F. Thornton, B. Haines, A. M. Das, H. Bhargava, A. Campbell, and J. Kleinschmidt, *RFID Security*, Syngress Media Incorporated, 2006.

[7] L. Francis, G. Hancke, K. Mayes, and K. Markantonakis, "Practical NFC peer-to-peer relay attack using mobile phones," in *Proceedings of the 6th International Workshop on Radio Frequency Identification: Security and Privacy Issues (RFIDSec '10)*, pp. 35–49, 2010.

[8] S. Weis, S. Sarma, R. Rivest, and D. Engels, "Security and privacy aspects of low-cost radio frequency identification systems," in *Security in Pervasive Computing*, pp. 50–59, 2004.

[9] K. Lane, W. Lane, and R. Stewart, "Hierarchical electronic watermarks and method of use," US7221258, 2007.

[10] T. G. Pareskevakos, "System and method for intelligent currency validation," US Patent no. US7724938, 2010.

[11] S. Cai, Y. Li, T. Li, and R. H. Deng, "Attacks and improvements to an RFID mutual authentication protocol and its extensions," in *Proceedings of the 2nd ACM Conference on Wireless Network Security (WiSec '09)*, pp. 51–58, March 2009.

[12] M. Ohkubo, K. Suzuki, and S. Kinoshita, "Cryptographic approach to "privacy-friendly" tags," in *Proceedings of the RFID Privacy Workshop*, 2003.

[13] H.-Y. Chien and C.-H. Chen, "Mutual authentication protocol for RFID conforming to EPC Class 1 Generation 2 standards," *Computer Standards & Interfaces*, vol. 29, no. 2, pp. 254–259, 2007.

[14] D. N. Duc, H. Lee, and K. Kim, "Enhancing security of EPCglobal Gen-2 RFID against traceability and cloning," White Paper, Auto-ID Labs Information and Communication University, 2006.

[15] D. Henrici and P. Müller, "Hash-based enhancement of location privacy for radio-frequency identification devices using varying identifiers," in *Proceedings of the 2nd IEEE Annual Conference on Pervasive Computing and Communications, Workshops (PerCom '04)*, pp. 149–153, March 2004.

[16] S. Karthikeyan and M. Nesterenko, "RFID security without extensive cryptography," in *Proceedings of the ACM Workshop on Security of Ad Hoc and Sensor Networks (SASN '05)*, pp. 63–67, November 2005.

[17] T. Van Deursen and S. Radomirović, "Security of an RFID protocol for supply chains," in *Proceedings of the IEEE International Conference on e-Business Engineering (ICEBE '08)*, pp. 568–573, Xi'an, China, October 2008.

[18] P. Rizomiliotis, E. Rekleitis, and S. Gritzalis, "Security analysis of the Song-Mitchell authentication protocol for low-cost RFID tags," *IEEE Communications Letters*, vol. 13, no. 4, pp. 274–276, 2009.

[19] C.-L. Chen, Y.-Y. Chen, Y.-C. Huang, C.-S. Liu, C.-I. Lin, and T.-F. Shih, "Anti-counterfeit ownership transfer protocol for low cost RFID system," *WSEAS Transactions on Computers*, vol. 7, no. 8, pp. 1149–1158, 2008.

[20] I. Vajda and L. Buttyán, "Lightweight authentication protocols for low-cost RFID tags," in *Proceedings of the 2nd Workshop on Security in Ubiquitous Computing (Ubicomp '03)*, 2003.

[21] M. O. Lehtonen, F. Michahelles, and E. Fleisch, "Trust and security in RFID-based product authentication systems," *IEEE Systems Journal*, vol. 1, pp. 129–144, 2007.

[22] D. Huang and H. Kapoor, "Towards lightweight secure communication protocols for passive RFIDs," in *Proceedings of the 6th Annual IEEE Communications Society Conference on Sensor, Mesh and Ad Hoc Communications and Networks (SECON '09)*, pp. 1–9, IEEE, Rome, Italy, June 2009.

[23] P. Najera, J. Lopez, and R. Roman, "Real-time location and inpatient care systems based on passive RFID," *Journal of Network and Computer Applications*, vol. 34, no. 3, pp. 980–989, 2011.

[24] S. K. Kwok, J. S. L. Ting, A. H. C. Tsang, W. B. Lee, and B. C. F. Cheung, "Design and development of a mobile EPC-RFID-based self-validation system (MESS) for product authentication," *Computers in Industry*, vol. 61, no. 7, pp. 624–635, 2010.

[25] A. Juels and R. Pappu, "Squealing Euros: privacy protection in RFID-enabled banknotes," in *Computer Aided Verification*, pp. 103–121, 2003.

[26] G. Andrechak and R. A. Wiens, *Hitachi μ-chip RFID Technology Compatible with Gamma Sterilization*, 2008.

[27] T. Hornyak, "RFID powder," *Scientific American*, vol. 298, no. 2, pp. 68–71, 2008.

[28] C.-N. Yang, J.-R. Chen, C.-Y. Chiu, G.-C. Wu, and C.-C. Wu, "Enhancing privacy and security in RFID-enabled banknotes," in *Proceedings of the IEEE International Symposium on Parallel and Distributed Processing with Applications (ISPA '09)*, pp. 439–444, August 2009.

[29] M. H. Eldefrawy, M. K. Khan, K. Alghathbar, T.-H. Kim, and H. Elkamchouchi, "Mobile one-time passwords: two-factor authentication using mobile phones," *Security and Communication Networks*, vol. 5, no. 5, pp. 508–516, 2012.

[30] M. H. Eldefrawy, M. K. Khan, and K. Alghathbar, "One-time password system with infinite nested Hash chains," in *Security Technology, Disaster Recovery and Business Continuity*, vol. 122 of *Communications in Computer and Information Science*, pp. 161–170, Springer, Berlin, Germany, 2010.

Hindawi Publishing Corporation
Mathematical Problems in Engineering
Volume 2014, Article ID 235804, 11 pages
http://dx.doi.org/10.1155/2014/235804

Research Article

Robust H_∞ Fuzzy Control for Nonlinear Discrete-Time Stochastic Systems with Markovian Jump and Parametric Uncertainties

Huiying Sun and Long Yan

College of Electrical Engineering and Automation, Shandong University of Science and Technology, Qingdao 266590, China

Correspondence should be addressed to Huiying Sun; sunhying@gmail.com

Received 4 May 2014; Revised 2 August 2014; Accepted 3 August 2014; Published 18 August 2014

Academic Editor: Peng Shi

The paper mainly investigates the H_∞ fuzzy control problem for a class of nonlinear discrete-time stochastic systems with Markovian jump and parametric uncertainties. The class of systems is modeled by a state space Takagi-Sugeno (T-S) fuzzy model that has linear nominal parts and norm-bounded parameter uncertainties in the state and output equations. An H_∞ control design method is developed by using the Lyapunov function. The decoupling technique makes the Lyapunov matrices and the system matrices separated, which makes the control design feasible. Then, some strict linear matrix inequalities are derived on robust H_∞ norm conditions in which both robust stability and H_∞ performance are required to be achieved. Finally, a computer-simulated truck-trailer example is given to verify the feasibility and effectiveness of the proposed design method.

1. Introduction

Over the past decade, there has been a rapidly growing interest in control and filtering of nonlinear systems, and there have been many successful applications [1–4]. In [1], based on the sum of squares approach, sufficient conditions for the existence of a nonlinear state feedback controller for polynomial discrete-time systems are given in terms of solvability of polynomial matrix inequalities. Reference [3] presents a stochastic distribution control algorithm; an optimal control law is then obtained using the penalty function method. Despite the success, it has become evident that many basic issues remain to be addressed. In particular, the control technique based on the so-called Takagi-Sugeno (T-S) fuzzy model [5] has attracted a great deal of attention (see [6–12]). This is because it is regarded as a powerful solution to bridging the gap between the fruitful linear control and the fuzzy logic control targeting complex nonlinear systems. The common practice of the technique is as follows. First, the nonlinear plant is represented by the T-S fuzzy model. This fuzzy model is described by a set of fuzzy IF-THEN rules which correspond to local linear input-output relations of the system, respectively. The overall model of the system is achieved by fuzzy "blending" of these fuzzy models. Then, based on this fuzzy model, a control design is carried out based on the fuzzy models via the so-called parallel distributed compensation (PDC) scheme. The idea is that a linear feedback control is designed for each local linear model. The resulting overall controller, which is, in general, nonlinear, is again a fuzzy blending of each individual linear controller. Their works introduce the model-based analysis methods into fuzzy logic control.

In recent years, the stability issue and robust performance of T-S fuzzy control systems have been discussed in an extensive literature. Since the pioneering work on the so-called H_∞ optimal control theory, there has been a dramatic progress in the H_∞ control theory. Recently, the problem of nonlinear H_∞ control was intensively studied (see [5, 7, 8, 13]). The design of H_∞ controller for fuzzy dynamic systems was presented in the paper [5]. Reference [4] introduces a new class of discrete-time networked nonlinear systems with mixed random delays and packet dropouts, and sufficient conditions for the existence of an admissible filter are established, which ensure the asymptotical stability as well as a prescribed H_∞ performance. The authors in [13] analyzed the H_∞ control design problem systematically for a class of nonlinear stochastic active fault-tolerant control systems with Markovian parameters. H_∞ controller design which was considered in [7] noted that most of the aforementioned research efforts focused on the use of single quadratic Lyapunov function, which tended to give more conservative conditions. This is because with the use of parameter-dependent or basis-dependent Lyapunov function less conservative control results can be obtained than with the use of single Lyapunov quadratic function. More recently, there were many results on stability analysis and control synthesis of discrete-time uncertain systems based on parameter-dependent Lyapunov functions [9] or basis-dependent Lyapunov function (see [8, 14]). It is shown that with the use of Lyapunov function well-pleasing control results can be obtained.

In practice, a lot of physical systems have variable structures subject to random changes. These changes may result from abrupt phenomena such as random failures and repairs of the components, changes in the interconnections of subsystems, and sudden environment changes. The so-called Markovian jump systems (MJSS) are special class of hybrid systems. As one of the most basic dynamics models, Markov jump nonlinear system can be used to represent these random failure processes in manufacturing and some investment portfolio models. In the MJSS, the random jumps in system parameters are governed by a Markov process which takes values in a finite set. The class of systems may represent a large variety of processes including those in the production systems, fault-tolerant systems, communication systems, and economic systems [15]. In the past two decades, many important issues of MJSS were researched extensively, such as the controllability and observability [16], stability and stabilization (see [17–22]), H_2 [23] and H_∞ performance [24–27], and robustness [28, 29]. To the best of our knowledge, despite these efforts, very few results are available for the control design for nonlinear MJSS. In this study, a mode-dependent control design is proposed to achieve robust stability of uncertain discrete-time nonlinear MJSS via fuzzy control.

In the paper, robust H_∞ control is investigated for nonlinear discrete-time stochastic MJSS with parametric uncertainties. Under our proposed fuzzy rules, the nonlinear discrete-time stochastic MJSS could be translated into a class of equivalent T-S fuzzy models with parametric uncertainties. The uncertainty could be translated into a linear fractional form, which includes the norm-bounded uncertainty as a special case and can describe a kind of rational nonlinearities. With the PDC scheme, the control law is designed to make the closed-loop system with H_∞ norm bound γ stable. Besides, some matrix variables and the Lyapunov function for robust stabilization with l_2-norm bound for the fuzzy discrete-time stochastic MJSS are given. It is shown that the solution of the control design problem can be obtained by solving a class of LMIs.

The paper is organized as follows. Section 2 discusses the T-S fuzzy models. And definitions and preliminary results are given for uncertain nonlinear discrete-time MJSS. Section 3 gives the analysis results of robust stability with H_∞ performance, and the results are employed in the following to develop an H_∞ control design. In Section 4, a numerical simulation example is proposed to illustrate the effectiveness of the approach. Finally, the paper is concluded in Section 5.

For convenience, the following basic notations are adopted throughout the paper. $\mathscr{R}^n$ denotes the n-dimensional real space, and $\mathscr{R}^{n\times m}$ denotes the set of all real $n\times m$ matrices. U' indicates the transpose of matrix U and $U \geq 0$ ($U > 0$) represents a nonnegative definite (positive definite) matrix. Similarly, $U \leq 0$ ($U < 0$) represents a nonpositive definite matrix (negative definite). $l_2[0,\infty)$ refers to the space of square summable infinite vector sequences. $\|\cdot\|_2$ stands for the usual $l_2[0,\infty)$ norm. $E(\cdot)$ represents the mathematical expectation.

2. Problem Formulation and Preliminaries

Consider the following nonlinear MJSS:

$$\begin{aligned} x(k+1) &= f(x(k),\theta_k) + g(x(k),\theta_k)u(k) \\ &\quad + k(x(k),\theta_k)v(k) + l(x(k),\theta_k)w(k), \\ y(k) &= m(x(k),\theta_k) + t(x(k),\theta_k)u(k) \\ &\quad + n(x(k),\theta_k)v(k). \end{aligned} \tag{1}$$

Assume that $f(x(k),\theta_k)$, $g(x(k),\theta_k)$, $k(x(k),\theta_k)$, $l(x(k),\theta_k)$, $m(x(k),\theta_k)$, $t(x(k),\theta_k)$, and $n(x(k),\theta_k)$ are Borel measurable on $\mathscr{R}^n$. And $x(k) \in \mathscr{R}^n$ is the system state, $u(k) \in \mathscr{R}^m$ and $v(k) \in \mathscr{R}^p$ represent the system control inputs and disturbance signal, and $y(k) \in \mathscr{R}^q$ is system output. $w(k)$ is a sequence of real random variables defined on a complete probability space $(\Omega,\mathscr{F}_k,P)$, which is wide sense stationary, second-order processes with $E[w(k)] = 0$ and $E[w(i)w(j)] = \delta_{ij}$, where δ_{ij} refers to a Kronecker function; that is, $\delta_{ij} = 1$ if $i = j$ and $\delta_{ij} = 0$ if $i \neq j$. $\{\theta_k; k \geq 0\}$ is a measurable Markov chain taking values in a finite set $\mathscr{X} = \{1,2,\ldots,N\}$, with transition probability matrix $\mathbb{P} = [p_{\alpha\beta}]$, where

$$p_{\alpha\beta} := P(\theta_{k+1} = \beta \mid \theta_k = \alpha), \quad \forall\alpha,\beta \in \mathscr{X},\ k \geq 0. \tag{2}$$

The paper considers the nonlinear discrete-time MJSS which can be described by the following T-S fuzzy model with uncertainties.

Rule i. If $z_1(k)$ is F_1^i, $z_2(k)$ is $F_2^i,\ldots,$ and $z_n(k)$ is F_n^i, then

$$\begin{aligned} x(k+1) &= \mathscr{A}\mathscr{A}_{i,\theta_k}x(k) + \mathscr{B}_{i,\theta_k}u(k) + \mathscr{C}_{i,\theta_k}v(k) \\ &\quad + \mathscr{D}_{i,\theta_k}x(k)w(k), \\ y(k) &= \mathscr{M}_{i,\theta_k}x(k) + \mathscr{T}_{i,\theta_k}u(k) + \mathscr{N}_{i,\theta_k}v(k). \end{aligned} \tag{3}$$

The F_j^i are fuzzy sets; r is the number of IF-THEN rules. Moreover, $\mathscr{A}_{i,\theta_k}$, $\mathscr{B}_{i,\theta_k}$, $\mathscr{C}_{i,\theta_k}$, $\mathscr{D}_{i,\theta_k}$, $\mathscr{M}_{i,\theta_k}$, $\mathscr{T}_{i,\theta_k}$, and $\mathscr{N}_{i,\theta_k}$ are system matrices with parametric uncertainties. Besides, $z_1(k), z_2(k),\ldots,z_n(k)$ are the premise variables of the fuzzy modes and they are the functions of state variables.

Following the PDC scheme, we consider a state feedback fuzzy controller which shares the same structure of the above T-S fuzzy system, as follows.

Rule j. IF $z_1(k)$ is F_1^j, $z_2(k)$ is $F_2^j, \ldots,$ and $z_n(k)$ is F_n^j, then

$$u(k) = K_{j,\theta_k} x(k), \tag{4}$$

where K_{j,θ_k} are the local feedback gain matrices.

And the fuzzy basis functions are given by

$$h_i[z(k)] = \frac{\prod_{j=1}^{n} \mu_{ij}[z_j(k)]}{\sum_{l=1}^{r} \prod_{j=1}^{n} \mu_{ij}[z_j(k)]}, \quad i = 1, 2, \ldots, r, \tag{5}$$

where $\mu_{ij}[z_j(k)]$ is the grade of membership of $z_j(k)$ in F_j^i. By definition, the fuzzy basis functions satisfy

$$\begin{gathered} h_i[z(k)] \geq 0, \quad i = 1, 2, \ldots, r, \\ \sum_{i=1}^{r} h_i[z(k)] = 1. \end{gathered} \tag{6}$$

A more compact presentation of the discrete-time T-S fuzzy model is given by

$$\begin{aligned} x(k+1) &= \sum_{i=1}^{r} h_i(z(k)) \left(\mathscr{A}_{i,\theta_k} x(k) + \mathscr{B}_{i,\theta_k} u(k) + \mathscr{C}_{i,\theta_k} v(k) \right. \\ &\qquad \left. + \mathscr{D}_{i,\theta_k} x(k) w(k) \right), \end{aligned} \tag{7}$$

$$\begin{aligned} y(k) &= \sum_{i=1}^{r} h_i(z(k)) \\ &\quad \times \left(\mathscr{M}_{i,\theta_k} x(k) + \mathscr{T}_{i,\theta_k} u(k) + \mathscr{N}_{i,\theta_k} v(k) \right), \end{aligned} \tag{8}$$

where

$$\begin{aligned} \mathscr{A}_{i,\theta_k} &= A_{i,\theta_k} + \Delta A_{i,\theta_k}, \\ \mathscr{B}_{i,\theta_k} &= B_{i,\theta_k} + \Delta B_{i,\theta_k}, \\ \mathscr{C}_{i,\theta_k} &= C_{i,\theta_k} + \Delta C_{i,\theta_k}, \\ \mathscr{D}_{i,\theta_k} &= D_{i,\theta_k}, \\ \mathscr{M}_{i,\theta_k} &= M_{i,\theta_k} + \Delta M_{i,\theta_k}, \\ \mathscr{T}_{i,\theta_k} &= T_{i,\theta_k} + \Delta T_{i,\theta_k}, \\ \mathscr{N}_{i,\theta_k} &= N_{i,\theta_k} + \Delta N_{i,\theta_k}. \end{aligned} \tag{9}$$

And $A_{i,\theta_k}, B_{i,\theta_k}, C_{i,\theta_k}, D_{i,\theta_k}, M_{i,\theta_k}, T_{i,\theta_k}$, and N_{i,θ_k} are assumed to be deterministic matrices with appropriate dimension; $\Delta A_{i,\theta_k}, \Delta B_{i,\theta_k}, \Delta C_{i,\theta_k}, \Delta M_{i,\theta_k}, \Delta T_{i,\theta_k}$, and $\Delta N_{i,\theta_k}$ are unknown matrices which represent the time-varying parameter uncertainties and are assumed to be of the form

$$\begin{gathered} \begin{bmatrix} \Delta A_{i,\theta_k} & \Delta B_{i,\theta_k} & \Delta C_{i,\theta_k} \\ \Delta M_{i,\theta_k} & \Delta T_{i,\theta_k} & \Delta N_{i,\theta_k} \end{bmatrix} = \begin{bmatrix} E_{1i} \\ E_{2i} \end{bmatrix} \Delta \begin{bmatrix} H_{1i} & H_{2i} & H_{3i} \end{bmatrix}, \\ \Delta = \left[I - F_{i,\theta_k} J \right]^{-1} F_{i,\theta_k}, \end{gathered} \tag{10}$$

where $E_{1i}, H_{1i}, E_{2i}, H_{2i}, H_{3i}$, and J are known real constant matrices with appropriate dimension and unknown nonlinear time-varying matrix $F_{i,\theta_k} \in \mathscr{R}^{m \times n}$ satisfying $F_{i,\theta_k} F'_{i,\theta_k} \leq I$. To guarantee that the matrix $I - F_{i,\theta_k} J$ is invertible for all admissible F_{i,θ_k}, it is necessary that $I - JJ' > 0$.

The following definition and lemmas will be used later.

Definition 1. The discrete-time unforced uncertain fuzzy system is said to be robust stable with H_∞ norm bound γ if it is stable with H_∞ norm bound γ for all uncertainly admissible F_{i,θ_k}. For a given control law (4) and a prescribed level of disturbance attenuation $\gamma > 0$ to be achieved, the discrete-time fuzzy system (3) is said to be stabilizable with H_∞ norm bound γ if for all $v(k) \in l_2[0, \infty)$, $v(k) \neq 0$, the closed-loop system (7)-(8) is asymptotically stable and the response $\{y(k)\}$ of the system under the zero initial condition ($x(0) = x_0 = 0$) satisfies

$$\|y(k)\|_2 < \gamma \|v(k)\|_2. \tag{11}$$

Lemma 2. *It is supposed that* $u(k) = 0$, $v(k) = 0$, *and* $\Delta = 0$, *so the discrete-time MJSS becomes*

$$x(k+1) = \sum_{i=1}^{r} h_i(z(k)) \left(A_{i,\theta_k} x(k) + D_{i,\theta_k} x(k) w(k) \right). \tag{12}$$

The system (12) *is globally asymptotically stable if there exists a symmetric piecewise matrix* $P_{i,\theta_k} > 0$ *such that*

$$A'_{i,\theta_k} \widetilde{P}_{j,\theta_k} A_{i,\theta_k} + D'_{i,\theta_k} \widetilde{P}_{j,\theta_k} D_{i,\theta_k} - P_{i,\theta_k} < 0, \tag{13}$$

where $\widetilde{P}_{j,\theta_k} = P_{j,\theta_{k+1}} = \sum_{\theta_k=1}^{N} p_{\theta_k \theta_{k+1}} P_{i,\theta_k}$.

Lemma 3. *Given a matrix* A_{i,θ_k}, D_{i,θ_k}, *suppose* $P_{i,\theta_k} > 0$, $\widetilde{P}_{j,\theta_k} > 0$, $P_{l,\theta_k} > 0$. *If*

$$\begin{gathered} A'_{i,\theta_k} \widetilde{P}_{j,\theta_k} A_{i,\theta_k} + D'_{i,\theta_k} \widetilde{P}_{j,\theta_k} D_{i,\theta_k} - P_{i,\theta_k} < 0, \\ A'_{l,\theta_k} \widetilde{P}_{j,\theta_k} A_{l,\theta_k} + D'_{l,\theta_k} \widetilde{P}_{j,\theta_k} D_{l,\theta_k} - P_{l,\theta_k} < 0, \end{gathered} \tag{14}$$

then

$$\begin{gathered} A'_{i,\theta_k} \widetilde{P}_{j,\theta_k} A_{l,\theta_k} + A'_{l,\theta_k} \widetilde{P}_{j,\theta_k} A_{i,\theta_k} + D'_{i,\theta_k} \widetilde{P}_{j,\theta_k} D_{l,\theta_k} \\ + D'_{l,\theta_k} \widetilde{P}_{j,\theta_k} D_{i,\theta_k} - P_{i,\theta_k} - P_{l,\theta_k} < 0. \end{gathered} \tag{15}$$

Proof. It is noted that

$$\begin{aligned} \widetilde{P}_{j,\theta_k} > 0 \Longrightarrow & \left(A_{i,\theta_k} - A_{l,\theta_k} \right)' \widetilde{P}_{j,\theta_k} \left(A_{i,\theta_k} - A_{l,\theta_k} \right) \\ & + \left(D_{i,\theta_k} - D_{l,\theta_k} \right)' \widetilde{P}_{j,\theta_k} \left(D_{i,\theta_k} - D_{l,\theta_k} \right) \geq 0, \end{aligned} \tag{16}$$

which gives

$$A'_{i,\theta_k}\widetilde{P}_{j,\theta_k}A_{l,\theta_k}+A'_{l,\theta_k}\widetilde{P}_{j,\theta_k}A_{i,\theta_k}+D'_{i,\theta_k}\widetilde{P}_{j,\theta_k}D_{l,\theta_k}+D'_{l,\theta_k}\widetilde{P}_{j,\theta_k}D_{i,\theta_k}\le A'_{i,\theta_k}\widetilde{P}_{j,\theta_k}A_{i,\theta_k}+A'_{l,\theta_k}\widetilde{P}_{j,\theta_k}A_{l,\theta_k}+D'_{i,\theta_k}\widetilde{P}_{j,\theta_k}D_{i,\theta_k}+D'_{l,\theta_k}\widetilde{P}_{j,\theta_k}D_{l,\theta_k}. \tag{17}$$

Therefore, the result of Lemma 3 can be easily proven. □

Lemma 4 (see [14]). *Suppose* Δ *is given by* (10). *With matrices* $M = M'$, S, *and* N *with appropriate dimension, the inequality*

$$M + S\Delta N + N'\Delta' S' < 0 \tag{18}$$

holds for all F_{i,θ_k} *such that* $F_{i,\theta_k}F'_{i,\theta_k}\le I$, *if and only if, for some* $\delta=\epsilon^2>0$,

$$\begin{bmatrix}\delta M & S & \delta N' \\ S' & -I & J' \\ \delta N & J & -I\end{bmatrix}<0. \tag{19}$$

3. Robust Stability and H_∞ Performance Analysis

In this section, the stability and H_∞ performance for the nominal fuzzy system will be analyzed. Under control law (4), the closed-loop fuzzy system becomes

$$x(k+1)=\sum_{i=1}^{r}h_i(z(k))\left[\left(\mathscr{A}_{i,\theta_k}+\mathscr{B}_{i,\theta_k}K_{j,\theta_k}\right)x(k)+\mathscr{C}_{i,\theta_k}v(k)+\mathscr{D}_{i,\theta_k}x(k)w(k)\right], \tag{20}$$

$$y(k)=\sum_{i=1}^{r}h_i(z(k))\times\left[\left(\mathscr{M}_{i,\theta_k}+\mathscr{T}_{i,\theta_k}K_{j,\theta_k}\right)x(k)+\mathscr{N}_{i,\theta_k}v(k)\right]. \tag{21}$$

When $\Delta=0$, the nominal closed-loop system becomes

$$x(k+1)=\sum_{i=1}^{r}\sum_{j=1}^{r}h_i(z(k))h_j(z(k))\times\left(A_{ij,\theta_k}x(k)+C_{i,\theta_k}v(k)+D_{i,\theta_k}x(k)w(k)\right), \tag{22}$$

$$y(k)=\sum_{i=1}^{r}\sum_{j=1}^{r}h_i(z(k))h_j(z(k))\times\left(M_{ij,\theta_k}x(k)+N_{i,\theta_k}v(k)\right), \tag{23}$$

where

$$A_{ij,\theta_k}=A_{i,\theta_k}+B_{i,\theta_k}K_{j,\theta_k},\qquad M_{ij,\theta_k}=M_{i,\theta_k}+T_{i,\theta_k}K_{j,\theta_k}. \tag{24}$$

Theorem 5. *The nominal closed-loop fuzzy system* (22) *is stable with* H_∞ *norm bound* γ; *that is,* $\|y(k)\|_2<\gamma\|v(k)\|_2$ *for all nonzero* $v(k)\in l_2[0,\infty)$ *under the zero initial condition, if there exists matrices* $\{P_{i,\theta_k}>0\}_{i=1}^{r}$ *for all* $i,j,l\in\{1,2,\dots,r\}$ *such that*

$$\begin{bmatrix}\Phi & \Gamma \\ \Lambda & \Psi\end{bmatrix}<0, \tag{25}$$

where

$$\widetilde{P}_{l,\theta_k}=\sum_{\theta_k=1}^{N}p_{\theta_k\theta_{k+1}}P_{i,\theta_k},$$
$$\Phi=A'_{ij,\theta_k}\widetilde{P}_{l,\theta_k}A_{ij,\theta_k}+D'_{i,\theta_k}\widetilde{P}_{l,\theta_k}D_{i,\theta_k}+M'_{ij,\theta_k}M_{ij,\theta_k}-P_{i,\theta_k},$$
$$\Gamma=A'_{ij,\theta_k}\widetilde{P}_{l,\theta_k}C_{i,\theta_k}+M'_{ij,\theta_k}N_{i,\theta_k},$$
$$\Lambda=C'_{i,\theta_k}\widetilde{P}_{l,\theta_k}A_{ij,\theta_k}+N'_{i,\theta_k}M_{ij,\theta_k},$$
$$\Psi=C'_{i,\theta_k}\widetilde{P}_{l,\theta_k}C_{i,\theta_k}+N'_{i,\theta_k}N_{i,\theta_k}-\gamma^2 I. \tag{26}$$

Proof. Obviously, inequality (25) implies the following inequality:

$$A'_{ij,\theta_k}\widetilde{P}_{l,\theta_k}A_{ij,\theta_k}+D'_{i,\theta_k}\widetilde{P}_{l,\theta_k}D_{i,\theta_k}-P_{i,\theta_k}<0. \tag{27}$$

It can be checked from the result of Lemma 3 that for all $i,j,l,p,q\in\{1,2,\dots,r\}$,

$$A'_{ip,\theta_k}\widetilde{P}_{j,\theta_k}A_{lq,\theta_k}+A'_{lq,\theta_k}\widetilde{P}_{j,\theta_k}A_{ip,\theta_k}+D'_{i,\theta_k}\widetilde{P}_{j,\theta_k}D_{l,\theta_k}+D'_{l,\theta_k}\widetilde{P}_{j,\theta_k}D_{i,\theta_k}-P_{i,\theta_k}-P_{l,\theta_k}<0. \tag{28}$$

When $i=l$, the inequality (28) becomes

$$A'_{ip,\theta_k}\widetilde{P}_{j,\theta_k}A_{iq,\theta_k}+A'_{iq,\theta_k}\widetilde{P}_{j,\theta_k}A_{ip,\theta_k}+2D'_{i,\theta_k}\widetilde{P}_{j,\theta_k}D_{i,\theta_k}-2P_{i,\theta_k}<0. \tag{29}$$

Let

$$V\left(x(k),\theta_k\right)=x'(k)\left[\sum_{i=1}^{r}h_i(z(k))P_{i,\theta_k}\right]x(k). \tag{30}$$

When $v(k)=0$, the system (22) becomes

$$x(k+1)=\sum_{i=1}^{r}\sum_{j=1}^{r}h_i(z(k))h_j(z(k))\times\left(A_{ij,\theta_k}x(k)+D_{i,\theta_k}x(k)w(k)\right). \tag{31}$$

In what follows, we will drop the argument of $h_i(z(k))$ for clarity. By some algebraic manipulation, with $h_j^+ = h_j(z(k+1))$, the difference of Lyapunov function $V(x(k),\theta_k)$ given by $\Delta V(x(k),\theta_k) = V(x(k+1),\theta_{k+1}) - V(x(k),\theta_k)$ along the solution of system (31) is

$$\begin{aligned}
&E\left[\Delta V\left(x(k),\theta_k\right)\big|_{(31)}\right] \\
&\quad = E\left[V\left(x(k+1),\theta_{k+1}\right) - V\left(x(k),\theta_k\right)\right] \\
&\quad = E\left\{x'(k+1)\left[\sum_{j=1}^{r} h_j(z(k))P_{j,\theta_{k+1}}\right]x(k+1)\right. \\
&\qquad \left. -x'(k)\left[\sum_{i=1}^{r} h_i(z(k))P_{i,\theta_k}\right]x(k)\right\} \\
&\quad = x'(k)\left[\sum_{j=1}^{r} h_j^+ \sum_{i=1}^{r}\sum_{l=1}^{r}\sum_{p=1}^{r}\sum_{q=1}^{r} h_i h_l h_p h_q\right. \\
&\qquad \times\left(A'_{ip,\theta_k}\widetilde{P}_{j,\theta_k}A_{lq,\theta_k}\right. \\
&\qquad \left.\left. +D'_{i,\theta_k}\widetilde{P}_{j,\theta_k}D_{l,\theta_k} - P_{i,\theta_k}\right)\right]x(k) \\
&\quad = x'(k) \\
&\qquad \times\left\{\sum_{j=1}^{r} h_j^+\left[\sum_{i=1}^{r}\sum_{p=1}^{r} h_i^2 h_p^2\right.\right. \\
&\qquad \times\left(A'_{ip,\theta_k}\widetilde{P}_{j,\theta_k}A_{ip,\theta_k}\right. \\
&\qquad \left. +D'_{i,\theta_k}\widetilde{P}_{j,\theta_k}D_{i,\theta_k} - P_{i,\theta_k}\right) \\
&\qquad + \sum_{i=1}^{r}\sum_{l>i}\sum_{p=1}^{r}\sum_{q=1}^{r} h_i h_l h_p h_q \\
&\qquad \times\left(A'_{ip,\theta_k}\widetilde{P}_{j,\theta_k}A_{lq,\theta_k}\right. \\
&\qquad + A'_{lq,\theta_k}\widetilde{P}_{j,\theta_k}A_{ip,\theta_k} + D'_{i,\theta_k}\widetilde{P}_{j,\theta_k}D_{l,\theta_k} \\
&\qquad \left. +D'_{l,\theta_k}\widetilde{P}_{j,\theta_k}D_{i,\theta_k} - P_{i,\theta_k} - P_{l,\theta_k}\right) \\
&\qquad + \sum_{i=1}^{r}\sum_{p=1}^{r}\sum_{q>p}^{r} h_i^2 h_p h_q \\
&\qquad \times\left(A'_{iq,\theta_k}\widetilde{P}_{j,\theta_k}A_{iq,\theta_k}\right. \\
&\qquad + A'_{iq,\theta_k}\widetilde{P}_{j,\theta_k}A_{ip,\theta_k} \\
&\qquad \left.\left.\left. +2D'_{i,\theta_k}\widetilde{P}_{j,\theta_k}D_{i,\theta_k} - 2P_{i,\theta_k}\right)\right]\right\}x(k),
\end{aligned} \tag{32}$$

where

$$\widetilde{P}_{j,\theta_k} = P_{j,\theta_{k+1}} = \sum_{\theta_k=1}^{N} p_{\theta_k\theta_{k+1}} P_{i,\theta_k}. \tag{33}$$

It follows from (13), (28), and (29) that

$$\Delta V\left(x(k),\theta_k\right)\big|_{(31)} < 0, \tag{34}$$

which proves the stability of system (31).

It follows from (25) that for all $i, j, l \in \{1, 2, \ldots, r\}$ exists

$$\begin{aligned}
&\begin{bmatrix} A_{ij,\theta_k} & C_{i,\theta_k} \\ M_{ij,\theta_k} & N_{i,\theta_k} \end{bmatrix}' \begin{bmatrix} \widetilde{P}_{l,\theta_k} & 0 \\ 0 & I \end{bmatrix} \begin{bmatrix} A_{ij,\theta_k} & C_{i,\theta_k} \\ M_{ij,\theta_k} & N_{i,\theta_k} \end{bmatrix} \\
&\quad - \begin{bmatrix} P_{i,\theta_k} - D'_{i,\theta_k}\widetilde{P}_{l,\theta_k}D_{i,\theta_k} & 0 \\ 0 & \gamma^2 I \end{bmatrix} < 0.
\end{aligned} \tag{35}$$

Let

$$J_N = \sum_{k=0}^{N-1} E\left[y'(k)\,y(k) - \gamma^2 v'(k)\,v(k)\right]. \tag{36}$$

For zero initial condition $x(0) = x_0 = 0$, one has

$$\begin{aligned}
\sum_{k=0}^{N-1} E\left[\Delta V\left(x(k),\theta_k\right)\big|_{(22)}\right] &= V\left(x(N),\theta_N\right) - V\left(x(0),\theta_0\right) \\
&= V\left(x(N),\theta_N\right).
\end{aligned} \tag{37}$$

Therefore,

$$\begin{aligned}
J_N &= \sum_{k=0}^{N-1} E\left[y'(k)\,y(k) - \gamma^2 v'(k)\,v(k)\right] \\
&= \sum_{k=0}^{N-1} E\left[y(k)'y(k) - \gamma^2 v'(k)\,v(k) + \Delta V\left(x(k),\theta_k\right)\big|_{(22)}\right] \\
&\quad - V\left(x(N),\theta_N\right),
\end{aligned} \tag{38}$$

where $\Delta V(x(k),\theta_k)|_{(22)}$ defines the difference of $V(x(k),\theta_k)$ along system (22). It is noted that, with $\zeta(k)$ defined by

$$\zeta(k) = \begin{bmatrix} x(k) \\ v(k) \end{bmatrix}, \tag{39}$$

we have

$$E\left[y'(k)\,y(k)-\gamma^2 v'(k)\,v(k)\right]$$
$$=\zeta'(k)\times\left\{\sum_{i=1}^{r}\sum_{p=1}^{r}\sum_{l=1}^{r}\sum_{q=1}^{r}h_ih_ph_lh_q\times\left(\begin{bmatrix}M'_{ip,\theta_k}\\ N'_{i,\theta_k}\end{bmatrix}\begin{bmatrix}M_{lq,\theta_k} & N_{l,\theta_k}\end{bmatrix}-\begin{bmatrix}0 & 0\\ 0 & \gamma^2 I\end{bmatrix}\right)\right\}\zeta(k),$$

$$E\left[\Delta V\left(x(k),\theta_k\right)\big|_{(22)}\right]$$
$$=\zeta'(k)\times\left\{\sum_{i=1}^{r}\sum_{p=1}^{r}\sum_{j=1}^{r}\sum_{l=1}^{r}\sum_{q=1}^{r}h_ih_j^+h_ph_lh_q\times\left(\begin{bmatrix}A'_{ip,\theta_k}\\ C'_{i,\theta_k}\end{bmatrix}\widetilde{P}_{j,\theta_k}\begin{bmatrix}A_{lq,\theta_k} & C_{l,\theta_k}\end{bmatrix}-\begin{bmatrix}P_{i,\theta_k}-D'_{i,\theta_k}\widetilde{P}_{j,\theta_k}D_{l,\theta_k} & 0\\ 0 & 0\end{bmatrix}\right)\right\}\zeta(k). \tag{40}$$

Then, it is obtained that

$$J_N\le\sum_{k=0}^{N-1}\zeta'(k)\times\left\{\sum_{j=1}^{r}h_j^+\sum_{i=1}^{r}\sum_{p=1}^{r}\sum_{l=1}^{r}\sum_{q=1}^{r}h_ih_ph_lh_q\times\left(\begin{bmatrix}M'_{ip,\theta_k}\\ N'_{i,\theta_k}\end{bmatrix}\begin{bmatrix}M_{lq,\theta_k} & N_{l,\theta_k}\end{bmatrix}+\begin{bmatrix}A'_{ip,\theta_k}\\ C'_{i,\theta_k}\end{bmatrix}\widetilde{P}_{j,\theta_k}\begin{bmatrix}A_{lq,\theta_k} & C_{l,\theta_k}\end{bmatrix}-\begin{bmatrix}P_{i,\theta_k}-D'_{i,\theta_k}\widetilde{P}_{j,\theta_k}D_{l,\theta_k} & 0\\ 0 & \gamma^2 I\end{bmatrix}\right)\right\}\zeta(k)$$
$$=\sum_{k=0}^{N-1}\zeta'(k)\times\left\{\sum_{j=1}^{r}h_j^+\sum_{i=1}^{r}\sum_{p=1}^{r}\sum_{l=1}^{r}\sum_{q=1}^{r}h_ih_ph_lh_q\times\left(\begin{bmatrix}A_{ip,\theta_k} & C_{i,\theta_k}\\ M_{ip,\theta_k} & N_{i,\theta_k}\end{bmatrix}'\begin{bmatrix}\widetilde{P}_{j,\theta_k} & 0\\ 0 & I\end{bmatrix}\begin{bmatrix}A_{lq,\theta_k} & C_{l,\theta_k}\\ M_{lq,\theta_k} & N_{l,\theta_k}\end{bmatrix}-\begin{bmatrix}P_{i,\theta_k}-D'_{i,\theta_k}\widetilde{P}_{j,\theta_k}D_{l,\theta_k} & 0\\ 0 & \gamma^2 I\end{bmatrix}\right)\right\}\zeta(k), \tag{41}$$

which can be rewritten as

$$J_N\le\sum_{k=0}^{N-1}\zeta'(k)\times\left\{\sum_{j=1}^{r}h_j^+\sum_{i=1}^{r}\sum_{p=1}^{r}h_i^2h_p^2\times\left(\begin{bmatrix}A_{ip,\theta_k} & C_{i,\theta_k}\\ M_{ip,\theta_k} & N_{i,\theta_k}\end{bmatrix}'\times\begin{bmatrix}\widetilde{P}_{j,\theta_k} & 0\\ 0 & I\end{bmatrix}\begin{bmatrix}A_{ip,\theta_k} & C_{i,\theta_k}\\ M_{ip,\theta_k} & N_{i,\theta_k}\end{bmatrix}-\begin{bmatrix}P_{i,\theta_k}-D'_{i,\theta_k}\widetilde{P}_{j,\theta_k}D_{i,\theta_k} & 0\\ 0 & \gamma^2 I\end{bmatrix}\right)\right\}\zeta(k)$$
$$+\sum_{k=0}^{N-1}\zeta'(k)\times\left\{\sum_{j=1}^{r}h_j^+\sum_{i=1}^{r}\sum_{p=1}^{r}\sum_{l>i}^{r}\sum_{q=1}^{r}h_ih_ph_lh_q\times\left(\begin{bmatrix}A_{ip,\theta_k} & C_{i,\theta_k}\\ M_{ip,\theta_k} & N_{i,\theta_k}\end{bmatrix}'\begin{bmatrix}\widetilde{P}_{j,\theta_k} & 0\\ 0 & I\end{bmatrix}\times\begin{bmatrix}A_{lq,\theta_k} & C_{l,\theta_k}\\ M_{lq,\theta_k} & N_{l,\theta_k}\end{bmatrix}-\begin{bmatrix}P_{i,\theta_k}-D'_{i,\theta_k}\widetilde{P}_{j,\theta_k}D_{l,\theta_k} & 0\\ 0 & \gamma^2 I\end{bmatrix}+\begin{bmatrix}A_{lq,\theta_k} & C_{l,\theta_k}\\ M_{lq,\theta_k} & N_{l,\theta_k}\end{bmatrix}'\times\begin{bmatrix}\widetilde{P}_{j,\theta_k} & 0\\ 0 & I\end{bmatrix}\begin{bmatrix}A_{ip,\theta_k} & C_{i,\theta_k}\\ M_{ip,\theta_k} & N_{i,\theta_k}\end{bmatrix}-\begin{bmatrix}P_{l,\theta_k}-D'_{l,\theta_k}\widetilde{P}_{j,\theta_k}D_{i,\theta_k} & 0\\ 0 & \gamma^2 I\end{bmatrix}\right)\right\}\zeta(k)$$
$$+\sum_{k=0}^{N-1}\zeta'(k)\times\left\{\sum_{j=1}^{r}h_j^+\sum_{i=1}^{r}\sum_{p=1}^{r}\sum_{q>p}^{r}h_i^2h_ph_q\times\left(\begin{bmatrix}A_{ip,\theta_k} & C_{i,\theta_k}\\ M_{ip,\theta_k} & N_{i,\theta_k}\end{bmatrix}'\times\begin{bmatrix}\widetilde{P}_{j,\theta_k} & 0\\ 0 & I\end{bmatrix}\begin{bmatrix}A_{iq,\theta_k} & C_{i,\theta_k}\\ M_{iq,\theta_k} & N_{i,\theta_k}\end{bmatrix}\right.\right.$$

$$+\begin{bmatrix} A_{iq,\theta_k} & C_{i,\theta_k} \\ M_{iq,\theta_k} & N_{i,\theta_k} \end{bmatrix}'$$

$$\times \begin{bmatrix} \widetilde{P}_{j,\theta_k} & 0 \\ 0 & I \end{bmatrix} \begin{bmatrix} A_{ip,\theta_k} & C_{i,\theta_k} \\ M_{ip,\theta_k} & N_{i,\theta_k} \end{bmatrix}$$

$$\left. -2\begin{bmatrix} P_{i,\theta_k} - D'_{i,\theta_k}\widetilde{P}_{j,\theta_k}D_{i,\theta_k} & 0 \\ 0 & \gamma^2 I \end{bmatrix} \Big) \right\} \zeta(k). \tag{42}$$

By following similar line as in the proof of (34) it can be checked that, for any N, $J_N < 0$, which gives for any nonzero $v(k) \in l_2[0,\infty)$, $y(k) \in l_2[0,\infty)$, and $\|y(k)\|_2 < \gamma\|v(k)\|_2$. □

Theorem 6. *For the nominal fuzzy system* (20)*, there exists a state feedback fuzzy control law* (4) *such that the closed-loop system is stable with H_∞ norm bound γ, if there exist matrices $\{X_{i,\theta_k} > 0\}_{i=1}^r$, $\{\Omega_{i,\theta_k}\}_{i=1}^r$, and $\{Y_{i,\theta_k}\}_{i=1}^r$, $i, j, l \in \{1,2,\ldots,r\}$ satisfying the following LMIs:*

$$\begin{bmatrix} X_{i,\theta_k} - \left(\Omega_{j,\theta_k} + \Omega'_{j,\theta_k}\right) & * & * & * \\ 0 & -\gamma^2 I & * & * \\ A_{i,\theta_k}\Omega_{j,\theta_k} + B_{i,\theta_k}Y_{j,\theta_k} & C_{i,\theta_k} & -X_{l,\theta_k} & * \\ M_{i,\theta_k}\Omega_{j,\theta_k} + T_{i,\theta_k}Y_{j,\theta_k} & N_{i,\theta_k} & 0 & -I \end{bmatrix} < 0, \tag{43}$$

where $*$ represents the transposed matrices that are readily inferred by symmetry for all i and j except the pairs (i, j) such that $h_i(z(k))h_j(z(k)) = 0$, for all k. A robust stabilizing controller gain can be given by

$$K_{j,\theta_k} = Y_{j,\theta_k}\Omega^{-1}_{j,\theta_k}. \tag{44}$$

Proof. By using (24) and (44), (43) becomes

$$\begin{bmatrix} X_{i,\theta_k} - \left(\Omega_{j,\theta_k} + \Omega'_{j,\theta_k}\right) & * & * & * \\ 0 & -\gamma^2 I & * & * \\ A_{ij,\theta_k}\Omega_{j,\theta_k} & C_{i,\theta_k} & -X_{l,\theta_k} & * \\ M_{ij,\theta_k}\Omega_{j,\theta_k} & N_{i,\theta_k} & 0 & -I \end{bmatrix} < 0, \tag{45}$$

which gives $0 < X_{i,\theta_k} < \Omega_{j,\theta_k} + \Omega'_{j,\theta_k}$. $(X_{i,\theta_k} - \Omega_{j,\theta_k})'X^{-1}_{i,\theta_k}(X_{i,\theta_k} - \Omega_{j,\theta_k}) \geq 0$ implies that $\Omega'_{j,\theta_k}X^{-1}_{i,\theta_k}\Omega_{j,\theta_k} \geq \Omega_{j,\theta_k} + \Omega'_{j,\theta_k} - X_{i,\theta_k}$ yielding

$$\begin{bmatrix} -\Omega'_{j,\theta_k}X^{-1}_{i,\theta_k}\Omega_{j,\theta_k} & * & * & * \\ 0 & -\gamma^2 I & * & * \\ A_{ij,\theta_k}\Omega_{j,\theta_k} & C_{i,\theta_k} & -X_{l,\theta_k} & * \\ M_{ij,\theta_k}\Omega_{j,\theta_k} & N_{i,\theta_k} & 0 & -I \end{bmatrix} < 0. \tag{46}$$

Note that Ω_{j,θ_k} is invertible. Premultiplying $\mathrm{diag}(\Omega'_{j,\theta_k}, I, I, I)^{-1}$ and postmultiplying $\mathrm{diag}(\Omega^{-1}_{j,\theta_k}, I, I, I)$ to (46) give

$$\begin{bmatrix} -X^{-1}_{i,\theta_k} & * & * & * \\ 0 & -\gamma^2 I & * & * \\ A_{ij,\theta_k} & C_{i,\theta_k} & -X_{l,\theta_k} & * \\ M_{ij,\theta_k} & N_{i,\theta_k} & 0 & -I \end{bmatrix} < 0. \tag{47}$$

Set $X^{-1}_{i,\theta_k} = P_{i,\theta_k} - D'_{i,\theta_k}\widetilde{P}_{l,\theta_k}D_{i,\theta_k}$ and $X^{-1}_{l,\theta_k} = \widetilde{P}_{l,\theta_k}$; there is

$$\begin{bmatrix} -\left(P_{i,\theta_k} - D'_{i,\theta_k}\widetilde{P}_{l,\theta_k}D_{i,\theta_k}\right) & * & * & * \\ 0 & -\gamma^2 I & * & * \\ A_{ij,\theta_k} & C_{i,\theta_k} & -\widetilde{P}^{-1}_{l,\theta_k} & * \\ M_{ij,\theta_k} & N_{i,\theta_k} & 0 & -I \end{bmatrix} < 0. \tag{48}$$

It follows from Schur complement equivalence that

$$\begin{aligned} &\begin{bmatrix} A_{ij,\theta_k} & C_{i,\theta_k} \\ M_{ij,\theta_k} & N_{i,\theta_k} \end{bmatrix}' \begin{bmatrix} \widetilde{P}_{l,\theta_k} & 0 \\ 0 & I \end{bmatrix} \begin{bmatrix} A_{ij,\theta_k} & C_{i,\theta_k} \\ M_{ij,\theta_k} & N_{i,\theta_k} \end{bmatrix} \\ &\quad - \begin{bmatrix} P_{i,\theta_k} - D'_{i,\theta_k}\widetilde{P}_{l,\theta_k}D_{i,\theta_k} & 0 \\ 0 & \gamma^2 I \end{bmatrix} < 0. \end{aligned} \tag{49}$$

The result then follows from Theorem 5. □

Theorem 7. *For the uncertain discrete-time MJSS* (7)*, there exists a state feedback fuzzy control law* (4) *such that the closed-loop system is stable with H_∞ norm bound γ, if there exist matrices $\{X_{i,\theta_k} > 0\}_{i=1}^r$, $\{\Omega_{i,\theta_k}\}_{i=1}^r$, and $\{Y_{i,\theta_k}\}_{i=1}^r$, $i, j, l \in \{1,2,\ldots,r\}$ satisfying the following LMIs:*

$$\begin{bmatrix} X_{i,\theta_k} - \left(\Omega_{j,\theta_k} + \Omega'_{j,\theta_k}\right) & * & * & * & * & * \\ 0 & -\epsilon\gamma^2 I & * & * & * & * \\ A_{i,\theta_k}\Omega_{j,\theta_k} + B_{i,\theta_k}Y_{j,\theta_k} & \epsilon C_{i,\theta_k} & -X_{l,\theta_k} & * & * & * \\ M_{i,\theta_k}\Omega_{j,\theta_k} + T_{i,\theta_k}Y_{j,\theta_k} & \epsilon N_{i,\theta_k} & 0 & -\epsilon I & * & * \\ 0 & 0 & E'_{1i} & E'_{2i} & -I & * \\ H'_{1i}\Omega_{j,\theta_k} + H'_{2i}Y_{j,\theta_k} & \epsilon H_{3i} & 0 & 0 & J & -I \end{bmatrix} < 0, \tag{50}$$

where $*$ represents the transposed matrices that are readily inferred by symmetry for all i and j except the pairs (i, j) such that $h_i(z(k))h_j(z(k)) = 0$, for all k. A robust stabilizing controller gain can be given by

$$K_{j,\theta_k} = Y_{j,\theta_k}\Omega^{-1}_{j,\theta_k}. \tag{51}$$

Proof. By using Lemma 4, it can be checked that the feasibility of inequality (50) is equivalent to

$$\begin{bmatrix} \widehat{X}_{i,\theta_k} - \left(\widehat{\Omega}_{j,\theta_k} + \widehat{\Omega}'_{j,\theta_k}\right) & * & * & * \\ 0 & -\gamma^2 I & * & * \\ \mathscr{A}_{i,\theta_k}\widehat{\Omega}_{j,\theta_k} + \mathscr{B}_{i,\theta_k}\widehat{Y}_{j,\theta_k} & \mathscr{C}_{i,\theta_k} & -\widehat{X}_{l,\theta_k} & * \\ \mathscr{M}_{i,\theta_k}\widehat{\Omega}_{j,\theta_k} + \mathscr{T}_{i,\theta_k}\widehat{Y}_{j,\theta_k} & \mathscr{N}_{i,\theta_k} & 0 & -I \end{bmatrix} < 0, \tag{52}$$

where

$$\widehat{X}_{i,\theta_k} = \epsilon^{-1}X_{i,\theta_k}, \qquad \widehat{\Omega}_{j,\theta_k} = \epsilon^{-1}\Omega_{j,\theta_k}, \qquad \widehat{Y}_{j,\theta_k} = \epsilon^{-1}Y_{j,\theta_k}. \tag{53}$$

It follows from (51)–(53) that

$$\begin{bmatrix} \widehat{X}_{i,\theta_k} - \left(\widehat{\Omega}_{j,\theta_k} + \widehat{\Omega}'_{j,\theta_k}\right) & * & * & * \\ 0 & -\gamma^2 I & * & * \\ \left(\mathscr{A}_{i,\theta_k} + \mathscr{B}_{i,\theta_k}K_{j,\theta_k}\right)\widehat{\Omega}_{j,\theta_k} & \mathscr{C}_{i,\theta_k} & -\widehat{X}_{l,\theta_k} & * \\ \left(\mathscr{M}_{i,\theta_k} + \mathscr{T}_{i,\theta_k}K_{j,\theta_k}\right)\widehat{\Omega}_{j,\theta_k} & \mathscr{N}_{i,\theta_k} & 0 & -I \end{bmatrix} < 0, \tag{54}$$

which implies that the closed-loop system (20) and (21) is robustly stable with H_∞ norm bound γ by Theorem 6. □

Corollary 8. *Consider the nominal unforced system*

$$x(k+1)=\sum_{i=1}^{r}h_i(z(k))\times\left(A_{i,\theta_k}x(k)+C_{i,\theta_k}v(k)+D_{i,\theta_k}x(k)w(k)\right),$$
$$y(k)=\sum_{i=1}^{r}h_i(z(k))\left(M_{i,\theta_k}x(k)+N_{i,\theta_k}v(k)\right). \tag{55}$$

The nominal unforced fuzzy system is stable with H_∞ norm bound γ; that is, $\|y(k)\|_2<\gamma\|v(k)\|_2$ for all nonzero $v(k)\in l_2[0,\infty)$ under the zero initial condition, if there exist matrices $\{P_{i,\theta_k}>0\}_{i=1}^{r}$, for all $i,j\in\{1,2,\dots,r\}$ such that

$$\begin{bmatrix}A_{i,\theta_k} & C_{i,\theta_k}\\ M_{i,\theta_k} & N_{i,\theta_k}\end{bmatrix}'\begin{bmatrix}\widetilde{P}_{j,\theta_k} & 0\\ 0 & I\end{bmatrix}\begin{bmatrix}A_{i,\theta_k} & C_{i,\theta_k}\\ M_{i,\theta_k} & N_{i,\theta_k}\end{bmatrix}-\begin{bmatrix}P_{i,\theta_k}-D'_{i,\theta_k}\widetilde{P}_{j,\theta_k}D_{i,\theta_k} & 0\\ 0 & \gamma^2I\end{bmatrix}<0, \tag{56}$$

where $\widetilde{P}_{j,\theta_k}=\sum_{\theta_k=1}^{N}p_{\theta_k\theta_{k+1}}P_{i,\theta_k}$.

Corollary 9. *The nominal unforced fuzzy system* (55) *is stable with H_∞ norm bound γ, if there exist matrices $\{X_{i,\theta_k}>0\}_{i=1}^{r}$, $\{\Omega_{i,\theta_k}\}_{i=1}^{r}$, $i,j\in\{1,2,\dots,r\}$ satisfying the following LMIs:*

$$\begin{bmatrix}X_{i,\theta_k}-\left(\Omega_{j,\theta_k}+\Omega'_{j,\theta_k}\right) & * & * & *\\ 0 & -\gamma^2I & * & *\\ A_{i,\theta_k}\Omega_{j,\theta_k} & C_{i,\theta_k} & -X_{j,\theta_k} & *\\ M_{i,\theta_k}\Omega_{j,\theta_k} & N_{i,\theta_k} & 0 & -I\end{bmatrix}<0. \tag{57}$$

Corollary 10. *When $u(k)=0$, the unforced system* (7) *and* (8) *is robustly stable with H_∞ norm bound γ, if there exist matrices $\{X_{i,\theta_k}>0\}_{i=1}^{r}$ and $\epsilon>0$, $i,j\in\{1,2,\dots,r\}$ satisfying the following LMIs:*

$$\begin{bmatrix}-X_{i,\theta_k} & * & * & * & * & *\\ 0 & -\epsilon\gamma^2I & * & * & * & *\\ A_{i,\theta_k}X_{i,\theta_k} & \epsilon C_{i,\theta_k} & -X_{j,\theta_k} & * & * & *\\ M_{i,\theta_k}X_{i,\theta_k} & \epsilon N_{i,\theta_k} & 0 & -\epsilon I & * & *\\ 0 & 0 & E'_{1i} & E'_{2i} & -I & *\\ H'_{1i}X_{i,\theta_k} & \epsilon H_{3i} & 0 & 0 & J & -I\end{bmatrix}<0. \tag{58}$$

4. Numerical Simulation Example

In this section, to illustrate the proposed new H_∞ fuzzy control method, the backing-up control of a computer-simulated truck-trailer is considered [30]. For example, the truck-trailer model is given by

$$x_1(k+1)=\left(1-\frac{vt}{L}\right)x_1(k)+\delta\frac{vt}{\ell}u(k), \tag{59}$$

$$x_2(k+1)=x_2(k)+\frac{vt}{L}x_1(k), \tag{60}$$

$$x_3(k+1)=x_3(k)+vt\sin\left(x_2(k)+\frac{vt}{2L}x_1(k)\right), \tag{61}$$

where $x_1(k)$ is the angle difference between truck and trailer, $x_2(k)$ is the angle of trailer, and $x_3(k)$ is the vertical position of rear end of trailer. The parameter $\delta\in[0,1]$ is used to describe the actuator failure, where $\delta=1$ implies no failure, $\delta=0$ implies a total failure, and $0<\delta<1$ implies a partial failure. It is assumed that there is no actuator failure. Equations (59) and (60) are linear, but (61) is nonlinear. The model parameters are given as $L=5.5$, $\ell=2.8$, $v=-1.0$, $t=2.0$, and $\delta=0$.

The transition probability matrix that relates the three operation modes is given as follows:

$$\mathbb{P}=\begin{bmatrix}0.48 & 0.29 & 0.23\\ 0.6 & 0.1 & 0.3\\ 0.1 & 0.65 & 0.25\end{bmatrix}. \tag{62}$$

As in [30], we set $\omega=0.01/\pi$ and the nonlinear term $\sin(z(k))$ as

$$\sin(z(k))=h_1(z(k))z(k)+h_2(z(k))\omega z(k), \tag{63}$$

where $h_1(z(k)),h_2(z(k))\in[0,1]$, and $h_1(z(k))+h_2(z(k))=1$. By solving the equations, it can be seen that the membership functions $h_1(z(k))$, $h_2(z(k))$ have the following relations. When $z(k)$ is about 0 rad, $h_1(z(k))=1$, $h_2(z(k))=0$, and when $z(k)$ is about $\pm\pi$ rad, $h_1(z(k))=0$, $h_2(z(k))=1$. Then the following fuzzy models can be used to design the fuzzy controller for the uncertain nonlinear MJSS.

Rule 1. If $z(k)=x_2(k)+(vt/2L)x_1(k)$ is about 0 rad, then

$$x(k+1)=\left(A_{1,\theta_k}+\Delta A_{1,\theta_k}\right)x(k)+\left(B_{1,\theta_k}+\Delta B_{1,\theta_k}\right)u(k)+\left(C_{1,\theta_k}+\Delta C_{1,\theta_k}\right)v(k)+D_{1,\theta_k}x_1(k)w(k). \tag{64}$$

Rule 2. If $z(k)=x_2(k)+(vt/2L)x_1(k)$ is about $\pm\pi$ rad, then

$$x(k+1)=\left(A_{2,\theta_k}+\Delta A_{2,\theta_k}\right)x(k)+\left(B_{2,\theta_k}+\Delta B_{2,\theta_k}\right)u(k)+\left(C_{2,\theta_k}+\Delta C_{2,\theta_k}\right)v(k)+D_{2,\theta_k}(k)w(k), \tag{65}$$

where

$$A_{1,\theta_k}=\begin{bmatrix}1-\dfrac{vt}{L} & 0 & 0\\ \dfrac{vt}{L} & 1 & 0\\ \dfrac{v^2t^2}{2L} & vt & 1\end{bmatrix},$$

$$A_{2,\theta_k}=\begin{bmatrix}1-\dfrac{vt}{L} & 0 & 0\\ \dfrac{vt}{L} & 1 & 0\\ \dfrac{\omega v^2t^2}{2L} & \omega vt & 1\end{bmatrix},$$

$$B_{1,\theta_k} = B_{2,\theta_k} = \left[\frac{vt}{L} \ \ 0 \ \ 0\right]',$$

$$C_{1,\theta_k} = C_{2,\theta_k} = \left[-0.1 \ \ 0.2 \ \ 0.15\right]',$$

$$D_{1,\theta_k} = D_{2,\theta_k} = \begin{bmatrix} 0.1 & 0 & 0 \\ 0 & 0.01 & 0 \\ 0 & 0 & 0 \end{bmatrix}. \tag{66}$$

In the above uncertain fuzzy models, the uncertainty to describe the modeling error is assumed to be in the following form:

$$\begin{gathered} \Delta A_{1,\theta_k} = E_{11}\Delta H_{11}, \qquad \Delta B_{1,\theta_k} = E_{11}\Delta H_{21}, \\ \Delta C_{1,\theta_k} = E_{11}\Delta H_{31}, \\ \Delta A_{2,\theta_k} = E_{12}\Delta H_{12}, \qquad \Delta B_{2,\theta_k} = E_{12}\Delta H_{22}, \\ \Delta C_{2,\theta_k} = E_{12}\Delta H_{32}, \end{gathered} \tag{67}$$

where

$$\begin{gathered} E_{11} = E_{12} = \begin{bmatrix} 0.06 & 0 & 0 \\ 0 & 0.06 & 0 \\ 0 & 0 & 0.06 \end{bmatrix}, \\ E_{21} = E_{22} = \begin{bmatrix} 0.1 & 0 & 0 \\ 0 & 0.1 & 0 \\ 0 & 0 & 0.1 \end{bmatrix}, \\ H_{11} = H_{12} = \begin{bmatrix} 0.3 & 0 & 0 \\ 0 & 0.3 & 0 \\ 0 & 0 & 0.3 \end{bmatrix}, \\ H_{21} = H_{22} = 0, \qquad H_{31} = H_{32} = \begin{bmatrix} 0 \\ 0 \\ 0 \end{bmatrix}. \end{gathered} \tag{68}$$

We choose the following matrices for the uncertain discrete-time MJSS:

$$\begin{gathered} M_{1,\theta_k} = M_{2,\theta_k} = \begin{bmatrix} 0.1 & 0 & 0 \\ 0 & 0.1 & 0 \\ 0 & 0 & 0.3 \end{bmatrix}, \\ N_{1,\theta_k} = N_{2,\theta_k} = \left[0.5 \ \ 0 \ \ 0\right]', \\ T_{1,\theta_k} = T_{2,\theta_k} = \left[0.5 \ \ 0 \ \ 0\right]', \\ J = \begin{bmatrix} 0 & 0 & 0 \\ 0 & 0 & 0 \\ 0 & 0 & 0 \end{bmatrix}. \end{gathered} \tag{69}$$

We set $i = 1$, $j = 1$, $l = 1$, $\theta_k = 1$ and $i = 2$, $j = 2$, $l = 2$, $\theta_k = 2$, respectively. Based on Theorem 7 and using LMI control toolbox in Matlab to solve LMIs (50), we can obtain the feasible set of solutions as follows:

$$\begin{gathered} X_{1,1} = \begin{bmatrix} 0.2389 & 0.1410 & 0.1770 \\ 0.1410 & 0.1387 & 0.3577 \\ 0.1770 & 0.3577 & 1.9030 \end{bmatrix}, \\ \Omega_{1,1} = \begin{bmatrix} 0.3259 & 0.1769 & 0.2347 \\ 0.1768 & 0.1730 & 0.4467 \\ 0.2286 & 0.4594 & 2.3108 \end{bmatrix}, \\ X_{2,2} = \begin{bmatrix} 0.2725 & 0.2913 & -0.0027 \\ 0.2913 & 0.8440 & 0.0210 \\ -0.0027 & 0.0210 & 0.0402 \end{bmatrix}, \\ \Omega_{2,2} = \begin{bmatrix} 0.3559 & 0.2937 & -0.0047 \\ 0.2937 & 0.9264 & 0.0186 \\ -0.0047 & 0.0186 & 0.0370 \end{bmatrix}, \\ Y_{1,1} = \left[0.8566 \ \ 0.2418 \ \ 0.0753\right], \\ Y_{2,2} = \left[0.8592 \ \ 0.2091 \ \ -0.0203\right]. \end{gathered} \tag{70}$$

By (51), there are the local state feedback gains given by

$$\begin{gathered} K_{1,1} = \left[5.0451 \ \ -5.1128 \ \ 0.5086\right], \\ K_{2,2} = \left[3.0255 \ \ -0.7375 \ \ 0.2056\right]. \end{gathered} \tag{71}$$

Then, we can get

$$\begin{gathered} P_{1,1} = \begin{bmatrix} 11.7492 & -15.7505 & 2.0651 \\ -15.7505 & 37.4327 & -4.7133 \\ 2.0651 & -4.7133 & 1.4101 \end{bmatrix}, \\ P_{2,2} = \begin{bmatrix} 107.2937 & -35.1096 & 10.0427 \\ -35.1096 & 29.0490 & -8.5669 \\ 10.0427 & -8.5669 & 3.3892 \end{bmatrix}. \end{gathered} \tag{72}$$

It can be found that the LMIs of Theorem 7 have some feasible solution for the uncertain discrete-time MJSS. Setting $\epsilon = 1$, $\gamma = 2.6$, the aforementioned simulation results are obtained. Employing the feedback gains K, the fuzzy controller can be obtained by (4). By using Theorem 7, with the fuzzy control applied, if the LMIs in (50) and (25) have a positive-definite solution for K_{j,θ_k} and P_{i,θ_k}, respectively, then the system (7) and (8) driven by the designed fuzzy controller is stable with satisfying the H_∞ performance constraint.

5. Conclusions

In the paper, the robust H_∞ control has been discussed for a class of nonlinear discrete-time stochastic MJSS. First, a new LMI characterization of stability with H_∞ norm bound for uncertain discrete-time stochastic MJSS has been given. Moreover, sufficient conditions on robust stabilization and H_∞ performance analysis and control have been presented on LMIs. Furthermore, there are some corollaries of the stability, and the nominal unforced system has been given. Finally, a numerical simulation example has been presented to show the effectiveness.

Conflict of Interests

The authors declare that there is no conflict of interests regarding the publication of this paper.

Acknowledgments

The work is supported by the National Natural Science Foundation of China (no. 61304080 and no. 61174078), a Project of Shandong Province Higher Educational Science and Technology Program (no. J12LN14), the Research Fund for the Taishan Scholar Project of Shandong Province of China, and the State Key Laboratory of Alternate Electrical Power System with Renewable Energy Sources (no. LAPS13018).

References

[1] S. Saat, D. Huang, and S. K. Nguang, "Robust state feedback control of uncertain polynomial discrete-time systems: an integral action approach," *International Journal of Innovative Computing, Information and Control*, vol. 9, no. 3, pp. 1233–1244, 2013.

[2] R. N. Yang, P. Shi, G. P. Liu, and H. J. Gao, "Network-based feedback control for systems with mixed delays based on quantization and dropout compensation," *Automatica*, vol. 47, no. 12, pp. 2805–2809, 2011.

[3] J. H. Zhang, M. F. Ren, Y. Tian, G. L. Hou, and F. Fang, "Constrained stochastic distribution control for nonlinear stochastic systems with non-Gaussian noises," *International Journal of Innovative Computing, Information and Control*, vol. 9, no. 4, pp. 1759–1767, 2013.

[4] R. Yang, P. Shi, and G. Liu, "Filtering for discrete-time networked nonlinear systems with mixed random delays and packet dropouts," *IEEE Transactions on Automatic Control*, vol. 56, no. 11, pp. 2655–2660, 2011.

[5] S. G. Cao, N. W. Rees, and G. Feng, "H_∞ control of uncertain dynamical fuzzy discrete-time systems," *IEEE Transactions on Systems, Man, and Cybernetics*, vol. 31, no. 5, pp. 802–812, 2001.

[6] X. J. Su, P. Shi, L. G. Wu, and S. K. Nguang, "Induced l_2 filtering of fuzzy stochastic systems with time-varying delays," *IEEE Transactions on Cybernetics*, vol. 43, no. 4, pp. 1251–1264, 2013.

[7] Y. Y. Cao and P. M. Frank, "Robust H_∞ disturbance attenuation for a class of uncertain discrete-time fuzzy systems," *IEEE Transactions on Fuzzy Systems*, vol. 8, no. 4, pp. 406–415, 2000.

[8] D. J. Choi and P. Park, "H_∞ state-feedback controller design for discrete-time fuzzy systems using fuzzy weighting-dependent lyapunov functions," *IEEE Transactions on Fuzzy Systems*, vol. 11, no. 2, pp. 271–278, 2003.

[9] G. Feng, "Stability analysis of piecewise discrete-time linear systems," *IEEE Transactions on Automatic Control*, vol. 47, no. 7, pp. 1108–1112, 2002.

[10] G. Feng and J. Ma, "Quadratic stabilization of uncertain discrete-time fuzzy dynamic systems," *IEEE Transactions on Circuits and Systems I: Fundamental Theory and Applications*, vol. 48, no. 11, pp. 1337–1343, 2001.

[11] R. Qi, L. Zhu, and B. Jiang, "Fault-tolerant reconfigurable control for MIMO systems using online fuzzy identification," *International Journal of Innovative Computing, Information and Control*, vol. 9, no. 10, pp. 3915–3928, 2013.

[12] X. J. Su, L. G. Wu, and P. Shi, "Sensor networks with random link failures: distributed filtering for T-S fuzzy systems," *IEEE Transactions on Industrial Informatics*, vol. 9, no. 3, pp. 1739–1750, 2013.

[13] Z. Lin, Y. Lin, and W. H. Zhang, "H_∞ stabilisation of nonlinear stochastic active fault-tolerant control systems: fuzzy-interpolation approach," *IET Control Theory &; Applications*, vol. 4, no. 10, pp. 2003–2017, 2010.

[14] S. Zhou, G. Feng, J. Lam, and S. Xu, "Robust H_∞ control for discrete-time fuzzy systems via basis-dependent Lyapunov functions," *Information Sciences*, vol. 174, no. 3-4, pp. 197–217, 2005.

[15] M. Mariton, *Jump Linear Systems in Automatic Control*, Marcel Dekker, New York, NY, USA, 1990.

[16] Y. D. Ji and H. J. Chizeck, "Controllability, observability and discrete-time Markovian jump linear quadratic control," *International Journal of Control*, vol. 48, no. 2, pp. 481–498, 1988.

[17] O. L. V. Costa and M. D. Fragoso, "Stability results for discrete-time linear systems with Markovian jumping parameters," *Journal of Mathematical Analysis and Applications*, vol. 179, no. 1, pp. 154–178, 1993.

[18] W. H. Zhang and B. S. Chen, "On stabilizability and exact observability of stochastic systems with their applications," *Automatica*, vol. 40, no. 1, pp. 87–94, 2004.

[19] Y. G. Fang and K. A. Loparo, "Stabilization of continuous-time jump linear systems," *IEEE Transactions on Automatic Control*, vol. 47, no. 10, pp. 1590–1603, 2002.

[20] X. Feng, K. A. Loparo, Y. Ji, and H. J. Chizeck, "Stochastic stability properties of jump linear systems," *IEEE Transactions on Automatic Control*, vol. 37, no. 1, pp. 38–53, 1992.

[21] L. Arnold, W. Kliemann, and E. Oelijeklaus, "Lyapunov exponents of linear stochastic systems," in *Lyapunov Exponents*, vol. 1186 of *Lecture Notes in Mathematics*, pp. 85–125, Springer, Berlin, Germany, 1986.

[22] O. L. V. Costa, J. B. R. do Val, and J. C. Geromel, "A convex programming approach to H_2-control of discrete-time Markovian jump linear systems," *International Journal of Control*, vol. 66, no. 4, pp. 557–580, 1997.

[23] H. Sun, L. Jiang, and W. Zhang, "Feedback control on nash equilibrium for discrete-time stochastic systems with markovian jumps: finite-horizon case," *International Journal of Control, Automation and Systems*, vol. 10, no. 5, pp. 940–946, 2012.

[24] O. L. V. Costa and R. P. Marques, "Mixed H_2/H_∞control of discrete-time Markovian jump linear systems," *IEEE Transactions on Automatic Control*, vol. 43, no. 1, pp. 95–100, 1998.

[25] D. Hinrichsen and A. J. Pritchard, "Stochastic H_∞," *SIAM Journal on Control and Optimization*, vol. 36, no. 5, pp. 1504–1538, 1998.

[26] W. Zhang and B. Chen, "State feedback H_∞ control for a class of nonlinear stochastic systems," *SIAM Journal on Control and Optimization*, vol. 44, no. 6, pp. 1973–1991, 2006.

[27] E. Boukas and P. Shi, "Stochastic stability and guaranteed cost control of discrete-time uncertain systems with Markovian jumping parameters," *International Journal of Robust and Nonlinear Control*, vol. 8, no. 13, pp. 1155–1167, 1998.

[28] T. Takagi and M. Sugeno, "Fuzzy identification of systems and its applications to modeling and control," *IEEE Transactions on Systems, Man and Cybernetics*, vol. 15, no. 1, pp. 116–132, 1985.

[29] H. J. Lee, J. B. Park, and G. Chen, “Robust fuzzy control of nonlinear systems with parametric uncertainties,” *IEEE Transactions on Fuzzy Systems*, vol. 9, no. 2, pp. 369–379, 2001.

[30] K. Tanaka and M. Sano, “Robust stabilization problem of fuzzy control systems and its application to backing up control of a truck-trailer,” *IEEE Transactions on Fuzzy Systems*, vol. 2, no. 2, pp. 119–134, 1994.

Hindawi Publishing Corporation
Mathematical Problems in Engineering
Volume 2014, Article ID 121636, 8 pages
http://dx.doi.org/10.1155/2014/121636

Research Article

Distributed Fault Estimation of Nonlinear Networked Systems: Application to Robotic Manipulator

Juntong Chen,[1,2] Rongyao Ling,[1] Hongjie Ni,[1] and Dan Zhang[1]

[1] *Department of Automation, Zhejiang University of Technology, Hangzhou 310032, China*
[2] *School of Automation and Electrical and Engineering, Zhejiang University of Science and Technology, Hangzhou 310032, China*

Correspondence should be addressed to Dan Zhang; jason_zhang19850626@hotmail.com

Received 10 June 2014; Accepted 15 July 2014; Published 12 August 2014

Academic Editor: Yun-Bo Zhao

This paper is concerned with the distributed fault estimation for a class of nonlinear networked systems, where the T-S fuzzy model is utilized to approximate the nonlinear plant and the whole fault estimation task is operated by a wireless sensor network. Due to the limited power in sensors, signal is quantized before transmission. Based on the Lyapunov stability theory and the robust control approach, a sufficient condition is obtained such that the estimation error system is asymptotic stable with a prescribed H_∞ performance level. Finally, a case study on the actuator fault estimation of robotic manipulator is given to show the effectiveness of the proposed design.

1. Introduction

Fault detection and isolation (FDI) and fault tolerant control (FTC) have received considerable attention in the past two decades due to the increasing demand for higher performance, higher safety, and reliability standards in engineering. Till now, many effective FDI methods have been proposed including the model-based fault detection approach [1], parity relations approach [2], the Kalman filter-based approach [3], and so on. Based on the FDI information, the controller is reconstructed to compensate the fault, which can guarantee the stability of systems and also some certain performance [4, 5]. For example, the authors in [6] proposed a methodology for detection and accommodation of actuator faults for a class of multi-input-multi-output (MIMO) stochastic systems. Firstly, a new real-time fault estimation module that estimates the actuator effectiveness was developed. Then, the output of the nominal controller is reconfigured to compensate for the loss of actuator effectiveness in the system. Simulation results of a helicopter in vertical plane were finally presented to demonstrate the performance of the proposed fault-tolerant control scheme. In [7], the authors studied the problem of robust fault estimation (FE) observer design for discrete-time Takagi-Sugeno (T-S) fuzzy systems via piecewise Lyapunov functions. Both the full-order FE observer (FFEO) and the reduced-order FE observer (RFEO) were presented. They showed that the optimal fault estimator can be determined by solving a set of linear matrix inequalities. It should be noted that all the above fault estimators are designed in a centralized way, and such a framework may have low reliability; for example, the estimation task may fail once the estimator has unrecoverable fault.

With the development of wireless sensor networks (WSNs), distributed estimation has received much attention in the last decade. Compared with the centralized filtering systems, the distributed filtering one has more redundancies, and thus it has higher reliability. Once some sensors have unrecoverable fault, other sensors can also provide the estimation signal. For example, a distributed Kalman filtering algorithm has been introduced in [8] that allows the nodes of a sensor network to track the average of n sensor measurements using an average consensus based distributed filter. In the scenario that the priori information on the external noises is not precisely known, the authors in [9] proposed an average H_∞ performance and the distributed observer design has been presented such that the prescribed estimation performance is guaranteed in the H_∞ sense. Recently, the distributed filtering for a class of sensor networks with switching topology is investigated in our earlier work [10]. Based on the switched system approach, we showed that the sensor working mode can be regulated to save energy. Recent advancement on the distributed filtering in sensor networks is referred to [8–10].

It is worth pointing out that the above distributed filtering results only focused on the state estimation problem. However, certain faults may occur in practical systems as we have mentioned above. In particular, in today's industrial systems, actuator fault may occur due to the increasing complexity of systems. Then, a natural problem is how to estimate the fault in a distributed way? To the best of the author's knowledge, such a challenging work has not been investigated yet. In this paper, we are concerned with the distributed fault estimation for a class of nonlinear systems. Two fundamental difficulties are identified as follows: (1) in the sensor-network-based distributed fault estimation systems, the first difficulty is how to prolong the lifetime of the networks as the sensor power is usually limited and it is impossible to be replaced when deployed in a large geometric area. (2) For a sensor network, each filter is designed based on the local information and the information from its neighboring ones, so the second difficulty is how to handle the complicated couplings between one sensor and its neighboring sensors in the presence of multiple quantization errors.

To handle the above challenges, attention of this paper is focused on designing a set of distributed fault estimators such that the estimation error system is asymptotically stable and achieves a prescribed H_∞ performance. Firstly, the Kronecker product is introduced to help solve the complex coupling of sensors in network. Then, signal quantization technique is utilized to reduce the transmitted packet size and thus save the transmission power. Based on the robust control technique and the Lyapunov stability theory, a new sufficient condition is obtained for the solvability of the considered estimation problem. Finally, a case study of robotic manipulator is given to show the effectiveness of the proposed design.

Notation. Some definitions for the notation used throughout the paper are given as follows. A superscript T stands for matrix transposition and superscript -1 stands for the inverse of a matrix; $\mathbb{R}^n$ denotes the n-dimensional Euclidean space and $\|\cdot\|$ denotes the Euclidean norm; $l_2[0,\infty)$ denotes the space of square-integrable vector functions over $[0,\infty)$ and the symbol $\otimes$ denotes the Kronecker product; I and 0 represent the identity matrix and zero matrix with appropriate dimensions; e_n represents an n-dimensional column vector with all the entries being identity.

2. Problem Formulation

The sensor network is deployed to monitor the plant, where there is no centralized fusion center in the network, and every sensor in the network acts also as an estimator.

Standard definitions for the sensor networks are now given as follows. Let the topology of a given sensor network be represented by a direct graph $\pi(k) = (\vartheta, \chi, A)$ of order n with the set of sensors $\vartheta = \{1, 2, \dots, n\}$, set of edges $\chi \subseteq \vartheta \times \vartheta$, and a weighted adjacency matrix $A = [a_{ij}]$ with nonnegative adjacency elements a_{ij}. An edge of π is denoted by (i, j). The adjacency elements associated with the edges of the graph are $a_{ij} = 1$, $(i, j) \in \vartheta$, if sensor i receives information from sensor j, whereas $a_{ij} = 0$, if sensor i can not receive information from sensor j. Moreover, we assume $a_{ii} = 1$ for all $i \in \vartheta$. The set of neighbors of node $i \in \vartheta$ plus the node itself are denoted by $N_i = \{j \in \delta : (i, j) \in \vartheta\}$. $A = [a_{ij}]$ is a square matrix representing the topology of the sensor network.

In this paper, the nonlinear plant is described by the following T-S model.

Plant Rule i. IF $\phi_1(k)$ is ψ_{i1} and $\phi_2(k)$ is ψ_{i2} and $\cdots$ and $\phi_t(k)$ is ψ_{it}, THEN

$$\begin{aligned} x(k+1) &= A_i x(k) + B_i u(k) + D_i w(k) + E_i f(k) \\ y_p(k) &= C_{pi} x(k) + D_{pi} w(k), \quad i = 1, 2, \dots, r, \end{aligned} \tag{1}$$

where $\phi(k) = [\phi_1(k), \phi_2(k), \dots, \phi_t(k)]$ is the premise variable vector, ψ_{ij} is the fuzzy set, and r is the number of IF-THEN rules. $x(t) \in \mathbb{R}^x$ is the state variable, $u(k) \in \mathbb{R}^u$ is the input, $w(k) \in \mathbb{R}^w$ is the unknown disturbance belonging to $l_2[0,\infty)$, $f(k) \in \mathbb{R}^f$ is the fault vector, $y_p(k) \in \mathbb{R}^{y_p}$ $(p = 1, 2, \dots, n)$ is the output measured by the pth fault estimator, and A_i, B_i, D_i, E_i, C_{pi}, D_{pi} are all known real matrices with appropriate dimensions.

Remark 1. It should be pointed out that the T-S fuzzy model (1) can only approximate the smooth nonlinear control systems, but not all the nonlinear control systems. Our attention in this paper is to design the fault estimator for such a class of nonlinear systems described by the T-S fuzzy model. We will show in the simulation part that such a T-S fuzzy system can be used to model the nonlinear robotic manipulator.

By using a center-average defuzzifier, product fuzzy inference, and a singleton fuzzifier, the overall fuzzy system is inferred as

$$\begin{aligned} x(k+1) &= \sum_{i=1}^{r} h_i(\phi(k)) \\ &\quad \times \left[A_i x(k) + B_i u(k) + D_i w(k) + E_i f(k)\right] \\ y_p(k) &= \sum_{i=1}^{r} h_i(\phi(k)) \left[C_{pi} x(k) + D_{pi} w(k)\right], \end{aligned} \tag{2}$$

where $h_i(\phi(k)) = \pi_i(\phi(k)) / \sum_{i=1}^{r} \pi_i(\phi(k))$ and $\pi_i(\phi(k)) = \prod_{j=1}^{p} \psi_{ij}(\phi_j(k))$, with $\psi_{ij}(\phi_j(k))$ representing the grade of membership of $\phi_j(k)$ in ψ_{ij}. Usually, it is assumed that $\pi_i((\phi(k))) \geq 0$ and $\sum_{i=1}^{r} \pi_i(\phi(k)) > 0$ for all $\phi(k)$.

For system (2), the following distributed fault estimator form is constructed.

Plant Rule i. IF $\phi_1(k)$ is ψ_{i1} and $\phi_2(k)$ is ψ_{i2} and $\cdots$ and $\phi_t(k)$ is ψ_{it}, THEN

$$\begin{aligned}\hat{x}_p(k+1) &= A_i x_p(k) + B_i u(k) \\ &\quad + E_i \hat{f}_p(k) - \sum_{q=1}^{n} a_{pq} H_{pq}^i Q_q\left(\hat{y}_q(k) - y_q(k)\right), \\ \hat{y}_p(k) &= C_{pi}\hat{x}_p(k), \\ \hat{f}_p(k+1) &= \hat{f}_p(k) - \sum_{q=1}^{n} a_{pq} K_{pq}^i Q_q\left(\hat{y}_q(k) - y_q(k)\right),\end{aligned} \tag{3}$$

where $\hat{x}_p \in \mathbb{R}^x$ is the estimator state vector, $\hat{y}_p(k) \in \mathbb{R}^{y_p}(p = 1, 2, \ldots, n)$ is the estimator output, and $\hat{f}_p(k) \in \mathbb{R}^f$ is an estimate of $f(k)$; H_{pq}^i and K_{pq}^i are the estimator gain matrices to be designed. $Q_q(\cdot)$ represents the quantizer in pth estimator with the quantization density $0 < \rho_p < 1$ and the set of quantization levels are described as

$$\begin{gathered}U_j = \left\{\pm u_i^j : u_{i+1}^j = \rho_j u_i^j, i = 1, 2, 3 \cdots\right\} \cup \left\{\pm u_0^j\right\} \cup \{0\} \\ 0 < \rho_j < 1,\ u_0^j > 0.\end{gathered} \tag{4}$$

Its quantization is described by

$$Q_q(\sigma) = \left[Q_q(\sigma_1)\ \ Q_q(\sigma_2)\ \ \cdots\ \ Q_q(\sigma_N)\right]^{\mathrm{T}}. \tag{5}$$

Here, $\sigma = [\sigma_1, \sigma_2, \ldots, \sigma_N]$ is the input vector; the quantized output $Q_q(\sigma_k)$ is given by the following piecewise function

$$Q_q(\sigma_k) = \begin{cases}\rho_q^i u_0^q, & \text{if } \dfrac{u_i^q}{1+\delta_q} < \sigma_k \le \dfrac{u_i^q}{1-\delta_q},\ \sigma_k > 0 \\ 0, & \text{if } \sigma_k = 0 \\ -Q_q(-\sigma_k), & \text{if } \sigma_k < 0,\end{cases} \tag{6}$$

where $\delta_q = (1-\rho_q)/(1+\rho_q)$ is the maximum error coefficient of quantizer $Q_q(\cdot)$. In this paper, the quantization error is defined as

$$e_{Q_q} = Q_q(\sigma_k) - \sigma_k = \Delta_q \sigma_k, \quad \Delta_q \in \left[-\delta_q, \delta_q\right]. \tag{7}$$

Let $\Delta f(k) = f(k+1) - f(k)$, and let the tracking errors of x and f be

$$\begin{aligned}e_{x_p}(k) &= \hat{x}_p(k) - x(k), \\ e_{f_p}(k) &= \hat{f}_p(k) - f(k).\end{aligned} \tag{8}$$

Then, based on (1) and (3), the error dynamics can be derived as

$$\begin{aligned}e_{x_p}(k+1) &= \sum_{i=1}^{r}\sum_{j=1}^{r} h_i(\phi(k))\, h_j(\phi(k)) \\ &\quad \times \Bigg[A_i e_{x_p}(k) + E_i e_{f_p}(k) \\ &\quad - \sum_{q=1}^{n} a_{pq} H_{pq}^i \left(I + \overline{\Delta}_q(k)\right) \\ &\quad \times \left(C_{qj} e_{x_p}(k) - D_{qj} w(k)\right) - D_i w(k)\Bigg]\end{aligned} \tag{9}$$

$$\begin{aligned}e_{f_p}(k+1) &= \sum_{i=1}^{r}\sum_{j=1}^{r} h_i(\phi(k))\, h_j(\phi(k)) \\ &\quad \times \Bigg[e_{f_p}(k) - \Delta f(k) \\ &\quad - \sum_{q=1}^{n} a_{pq} K_{pq}^i \left(I + \overline{\Delta}_q(k)\right) \\ &\quad \times \left(C_{qj} e_{x_p}(k) - D_{qj} w(k)\right)\Bigg],\end{aligned} \tag{10}$$

where $\overline{\Delta}_q(k) = \operatorname{diag}\{\Delta_{q1}(k), \Delta_{q2}(k), \ldots, \Delta_{qy}(k)\}$, and $\Delta_{qi} \in [-\delta_q, \delta_q]$, $i = 1, 2, \ldots, y$.

Let

$$\begin{gathered}\bar{e}_x(k) = \left[e_{x_1}^{\mathrm{T}}(k)\ \cdots\ e_{x_n}^{\mathrm{T}}(k)\right]^{\mathrm{T}}, \qquad \overline{A}_i = I_n \otimes A_i, \\ \bar{e}_f(k) = \left[e_{f_1}^{\mathrm{T}}(k)\ \cdots\ e_{f_n}^{\mathrm{T}}(k)\right]^{\mathrm{T}}, \qquad \overline{E}_i = I_n \otimes E_i, \\ \overline{C}_i = \operatorname{diag}\{C_{1i}, C_{2i} \cdots C_{ni}\}, \\ \overline{D}_i = \left[D_{1i}^{\mathrm{T}}\ \cdots\ D_{ni}^{\mathrm{T}}\right]^{\mathrm{T}}, \qquad \widetilde{D}_i = e_n \otimes D_i, \\ \Delta(k) = \operatorname{diag}\left\{\overline{\Delta}_1(k), \overline{\Delta}_2(k) \cdots \overline{\Delta}_n(k)\right\}, \\ \overline{H}_i = \begin{bmatrix} a_{11}H_{11}^i & \cdots & a_{1n}H_{1n}^i \\ \vdots & \ddots & \vdots \\ a_{n1}H_{n1}^i & \cdots & a_{nn}H_{nn}^i \end{bmatrix}, \\ \overline{K}_i = \begin{bmatrix} a_{11}K_{11}^i & \cdots & a_{1n}K_{1n}^i \\ \vdots & \ddots & \vdots \\ a_{n1}K_{n1}^i & \cdots & a_{nn}K_{nn}^i \end{bmatrix}.\end{gathered} \tag{11}$$

By defining $h_i^k = h_i(\phi(k))$, $\bar{e}(k) = \left[\bar{e}_x^{\mathrm{T}}(k)\ \ \bar{e}_f^{\mathrm{T}}(k)\right]^{\mathrm{T}}$, $v(k) = \left[w^{\mathrm{T}}(k)\ \ \Delta f^{\mathrm{T}}(k)\right]^{\mathrm{T}}$, combining (9) and (10), the following augmented estimation error system is obtained:

$$\begin{aligned} \bar{e}(k+1) &= \sum_{i=1}^{r}\sum_{j=1}^{r} h_i^k h_j^k \left[\overline{M}_{ij}\bar{e}(k) + \overline{N}_{ij}v(k)\right], \\ z(k) &= L\bar{e}(k), \end{aligned} \tag{12}$$

where

$$\begin{aligned} \overline{M}_{ij} &= \begin{bmatrix} \overline{A}_i - \overline{H}_i (I+\Delta(k))\overline{C}_j & \overline{E}_i \\ -\overline{K}_i (I+\Delta(k))\overline{C}_j & I \end{bmatrix}, \\ \overline{N}_{ij} &= \begin{bmatrix} \overline{H}_i (I+\Delta(k))\overline{D}_j - \widetilde{D}_i & 0 \\ \overline{K}_i (I+\Delta(k))\overline{D}_j & e_n \otimes I \end{bmatrix}, \\ L &= \begin{bmatrix} 0 & I \end{bmatrix}. \end{aligned} \tag{13}$$

The objective of this paper is to design the robust distributed fault estimator in the form of (3) such that the estimation error system (12) is asymptotic stable and achieves an H_∞ performance. To be more specific, the estimation requirements are expressed as follows.

(1) The augmented estimation error system in (12) with $v(k) \equiv 0$ is asymptotically stable.

(2) For any nonzero external disturbance $v(k) \in l_2[0,\infty)$, its effect on the estimation error $e_{f_p}(k)$ is attenuated below a desired level $\gamma > 0$. More specifically, it is required that

$$\sum_{k=0}^{\infty} \frac{1}{n}\|z(k)\|^2 \le \gamma^2 \sum_{k=0}^{\infty}\|v(k)\|^2. \tag{14}$$

The estimation error system (12) is said to be asymptotically stable with an average H_∞ performance γ if the aforementioned requirements are met.

Remark 2. In this paper, our attention is focused on estimating the fault signal in the presence of unknown disturbance. Hence, we choose $L = [\,0\ \ I\,]$. It is interesting to see that when we choose L as an identity matrix, both state and fault signals can be estimated such that the estimation error system is asymptotic stable and achieves a prescribed H_∞ performance level.

The following lemmas are introduced before further proceeding.

Lemma 3 (see [11]). *For given matrices of appropriate dimensions Σ_1, Σ_2, and Σ_3 with Σ_1 satisfying $\Sigma_1 = \Sigma_1^T$, then*

$$\Sigma_1 + \Sigma_2\Delta\Sigma_3 + \Sigma_3^T\Delta^T\Sigma_2^T < 0 \tag{15}$$

holds for all $\Delta^T\Delta \le I$ if and only if there exists a scalar $\varepsilon > 0$ such that

$$\Sigma_1 + \varepsilon\Sigma_2\Sigma_2^T + \varepsilon^{-1}\Sigma_3^T\Sigma_3 < 0. \tag{16}$$

Lemma 4 (see [12]). *For matrices A, $Q = Q^T$, and $P > 0$ the following matrix inequality*

$$A^T P A - Q < 0 \tag{17}$$

holds if and only if there exists a matrix T of appropriate dimensions such that

$$\begin{bmatrix} -Q & A^T T \\ * & P - T - T^T \end{bmatrix} < 0. \tag{18}$$

3. Main Results

In this section, we aim to solve the distributed fault estimation problem. Some theorems are derived that the estimation error system (12) is asymptotic stable and achieves an H_∞ performance. Theorem 5 guarantees that the estimation error system (12) is asymptotic stable with an H_∞ performance $\gamma > 0$, and the specific design method for distributed fault estimator is proposed in Theorem 7.

Theorem 5. *For a given system* (3) *and a scalar $\gamma > 0$, the estimation error system* (12) *is asymptotic stable with an H_∞ performance $\gamma > 0$ if there exist symmetric positive matrices P and a scalar $\varepsilon > 0$, the following inequalities*

$$\begin{bmatrix} -P & 0 & \widehat{M}_{ij}^T & L^T & \varepsilon\widehat{C}_j^T\Delta & 0 \\ * & -\gamma^2 I & \widehat{N}_{ij}^T & 0 & \varepsilon\widehat{D}_j^T\Delta & 0 \\ * & * & -P^{-1} & 0 & 0 & F_i \\ * & * & * & -nI & 0 & 0 \\ * & * & * & * & -\varepsilon I & 0 \\ * & * & * & * & * & -\varepsilon I \end{bmatrix} < 0 \tag{19}$$

hold for all $i, j = 1, 2, \ldots, r$, where

$$\begin{aligned} \widehat{M}_{ij} &= \begin{bmatrix} \overline{A}_i - \overline{H}_i\overline{C}_j & \overline{E}_i \\ -\overline{K}_i\overline{C}_j & I \end{bmatrix}, \qquad \widehat{C}_j = \begin{bmatrix} -\overline{C}_j & 0 \end{bmatrix}, \\ \widehat{N}_{ij} &= \begin{bmatrix} \overline{H}_i\overline{D}_j - \widetilde{D}_i & 0 \\ \overline{K}_i\overline{D}_j & e_n \otimes I \end{bmatrix}, \qquad \widehat{D}_j = \begin{bmatrix} \overline{D}_j & 0 \end{bmatrix}, \\ F_i &= \begin{bmatrix} \overline{H}_i^{\,T} & \overline{K}_i^{\,T} \end{bmatrix}^T, \qquad \Delta = \operatorname{diag}\left\{\delta_1 I_y, \delta_2 I_y, \ldots, \delta_n I_y\right\}. \end{aligned} \tag{20}$$

Proof. We first consider the asymptotic stability of the augmented estimation error system (12) with $v(k) \equiv 0$. Construct the following Lyapunov function:

$$V(k) = \bar{e}^{\mathrm{T}}(k) P \bar{e}(k); \tag{21}$$

then the dynamics of $V(k)$ is given by

$$\begin{aligned} \Delta V(k) &\triangleq V(k+1) - V(k) \\ &= \sum_{i=1}^{r}\sum_{j=1}^{r} h_i^k h_j^k \left[\bar{e}^{\mathrm{T}}(k+1) P\bar{e}(k+1) - \bar{e}^{\mathrm{T}}(k) P\bar{e}(k)\right] \\ &= \sum_{i=1}^{r}\sum_{j=1}^{r} h_i^k h_j^k \left[\bar{e}^{\mathrm{T}}(k)\left(\overline{M}_{ij}^{\mathrm{T}} P \overline{M}_{ij} - P\right)\bar{e}(k)\right], \end{aligned} \tag{22}$$

where $\overline{M}_{ij} = M_i + F_i\widehat{C}_j + F_i\Delta(k)\widehat{C}_j$ and $M_i = \begin{bmatrix} \overline{A}_i & \overline{E}_i \\ 0 & I \end{bmatrix}$, $N_i = \begin{bmatrix} -\overline{D}_i & 0 \\ 0 & e_n \otimes I \end{bmatrix}$. It can be obtained that $\Delta V(k) = \sum_{i=1}^{r}\sum_{j=1}^{r} h_i^k h_j^k [\Omega_{ij}]$, where $\Omega_{ij} = \Omega_{1i} + \Omega_{2j}\Delta(k)\Omega_{3i} + \Omega_{3i}^{\mathrm{T}}\Delta^{\mathrm{T}}(k)\Omega_{2j}^{\mathrm{T}}$, $\Omega_{1i} = \begin{bmatrix} -P & \widehat{M}_i^{\mathrm{T}} \\ * & -P^{-1} \end{bmatrix}$, $\Omega_{2j} = \begin{bmatrix} \widehat{C}_j & 0 \end{bmatrix}^{\mathrm{T}}$, $\Omega_{3i} = \begin{bmatrix} 0 & F_i^{\mathrm{T}} \end{bmatrix}$.

Notice that $(\Delta(k)\Delta^{-1})^{\mathrm{T}}\Delta(k)\Delta^{-1} \leq I$; by using Lemma 3 and Schur complement, it can be seen that $\Omega_{ij} < 0$ is equivalent to

$$\begin{bmatrix} -P & \widehat{M}_{ij}^{\mathrm{T}} & \varepsilon\widehat{C}_j^{\mathrm{T}}\Delta & 0 \\ * & -P^{-1} & 0 & F_i \\ * & * & -\varepsilon I & 0 \\ * & * & * & -\varepsilon I \end{bmatrix} < 0, \quad i, j = 1, 2, \ldots, r. \tag{23}$$

It is noted that (23) holds if (19) holds; hence we have $\Delta V(k) < 0$, indicating that the estimation error system (12) is asymptotic stable.

We then consider the H_∞ performance of the estimation error system (12). Define

$$J \triangleq \sum_{k=0}^{\infty}\left[\frac{1}{n}z^{\mathrm{T}}(k)\,z(k) - \gamma^2 v^{\mathrm{T}}(k)\,v(k)\right]. \tag{24}$$

Denote $\eta(k) = \begin{bmatrix} \overline{e}^{\mathrm{T}}(k) & v^{\mathrm{T}}(k) \end{bmatrix}^{\mathrm{T}}$; then it can be obtained under the zero initial conditions that

$$\begin{aligned} J &\leq \sum_{k=0}^{\infty}\left[\frac{1}{n}z^{\mathrm{T}}(k)\,z(k) - \gamma^2 v^{\mathrm{T}}(k)\,v(k) + \Delta V\right] \\ &= \sum_{k=0}^{\infty}\sum_{i=1}^{r}\sum_{j=1}^{r} h_i^k h_j^k\left[\eta^{\mathrm{T}}(k)\,\Theta_{ij}\eta(k)\right], \end{aligned} \tag{25}$$

where $\Theta_{ij} = \Theta_{1i} + \Theta_{2j}\Delta(k)\Theta_{3i} + \Theta_{3i}^{\mathrm{T}}\Delta^{\mathrm{T}}(k)\Theta_{2j}^{\mathrm{T}}$ with

$$\begin{aligned} \Theta_{1j} &= \begin{bmatrix} \widehat{C}_j & \widehat{D}_j & 0 & 0 \end{bmatrix}^{\mathrm{T}}, \\ \Theta_{2i} &= \begin{bmatrix} 0 & 0 & F_i^{\mathrm{T}} & 0 \end{bmatrix}, \\ \Theta_{3i} &= \begin{bmatrix} -P & 0 & \widehat{M}_i^{\mathrm{T}} & L^{\mathrm{T}} \\ * & -\gamma^2 I & \widehat{N}_i^{\mathrm{T}} & 0 \\ * & * & -P^{-1} & 0 \\ * & * & * & -nI \end{bmatrix}. \end{aligned} \tag{26}$$

Based on Lemma 3 and Schur complement, it can be derived from (19) that $\Theta_{ij} < 0$. Thus $J < 0$ and the estimation error system (12) is asymptotic stable with an H_∞ performance $\gamma > 0$. The proof is completed. □

Remark 6. In Theorem 5, it is difficult to determine the estimator gains due to the nonlinear term in (19). Toward this end, based on Theorem 5, Theorem 7 is proposed to determine the estimator gains.

Theorem 7. *For a given system* (3) *and a scalar $\gamma > 0$, the estimation error system* (12) *is asymptotic stable with an average H_∞ performance $\gamma > 0$ if there exist symmetric positive matrices P, a matrix T, and a scalar $\varepsilon > 0$; the following inequalities*

$$\begin{bmatrix} -P & 0 & M_i^T T + \widehat{C}_j^T\overline{F}_i^T & L^T & \varepsilon\widehat{C}_j^T\Delta & 0 \\ * & -\gamma^2 I & N_i^T T + \widehat{D}_j^T\overline{F}_i^T & 0 & \varepsilon\widehat{D}_j^T\Delta & 0 \\ * & * & P - T - T^T & 0 & 0 & \overline{F}_i \\ * & * & * & -nI & 0 & 0 \\ * & * & * & * & -\varepsilon I & 0 \\ * & * & * & * & * & -\varepsilon I \end{bmatrix} < 0 \tag{27}$$

hold for all $i, j = 1, 2, \ldots, r$. Meanwhile, the estimator gains can be determined as

$$F_i = T^{-T}\overline{F}_i. \tag{28}$$

Proof. Based on Lemma 4 and Schur complement, it is easy to derive from (27) that (29) holds. Denote $\overline{T} = \mathrm{diag}\{I, I, T^{-\mathrm{T}}, I, I, I\}$; premultiplying (28) by $\overline{T}$ and postmultiplying (29) by $\overline{T}^{\mathrm{T}}$ simultaneously, (18) is obtained, which ends the proof. Consider

$$\begin{bmatrix} -P & 0 & M_i^{\mathrm{T}} T + \widehat{C}_j^{\mathrm{T}}\overline{F}_i^{\mathrm{T}} & L^{\mathrm{T}} & \varepsilon\widehat{C}_j^{\mathrm{T}}\Delta & 0 \\ * & -\gamma^2 I & N_i^{\mathrm{T}} T + \widehat{D}_j^{\mathrm{T}}\overline{F}_i^{\mathrm{T}} & 0 & \varepsilon\widehat{D}_j^{\mathrm{T}}\Delta & 0 \\ * & * & TP^{-1}T^{\mathrm{T}} & 0 & 0 & \overline{F}_i \\ * & * & * & -nI & 0 & 0 \\ * & * & * & * & -\varepsilon I & 0 \\ * & * & * & * & * & -\varepsilon I \end{bmatrix} < 0. \tag{29}$$

□

Remark 8. Optimal solutions for the problem of distributed fault estimation can be obtained by solving the following optimization problem:

$$\begin{aligned} &\min \ \gamma^2 \\ &\text{s.t.} \ \ (27). \end{aligned} \tag{30}$$

The estimator gains can be determined through (28).

4. Illustrative Example

In this section, a simulation example is presented to illustrate the effectiveness of the proposed design methods. Consider a single-link rigid robot that is connected through a revolute joint to the basement and whose plane of motion is vertical. The motion equation of this mechanical system is given by [13, 14]

$$J\ddot{\vartheta} = -\left(0.5mgl + Mgl\right)\sin(\vartheta) + u, \tag{31}$$

where ϑ denotes the joint rotation angle in radians, $m = 1.5$ kg is the mass of the load, $M = 3$ kg is the mass of the rigid link, $g = 9.8\,\mathrm{m/s^2}$ is the gravity constant, $l = 0.5$ m is the length of the robot link, $J = 0.875\,\mathrm{kg\cdot m^2}$ is the moment of inertia, and u is the control torque applied at the joint in Nm. $\vartheta = 0$ denotes the lowest vertical equilibrium position.

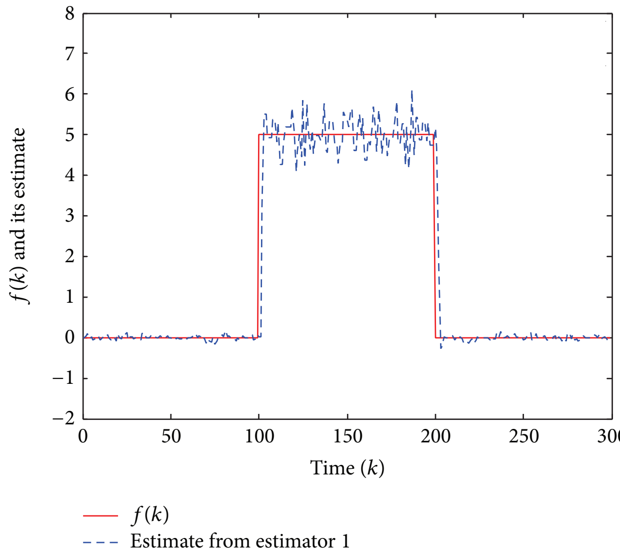

FIGURE 1: $f(k)$ and its estimate $f_1(k)$.

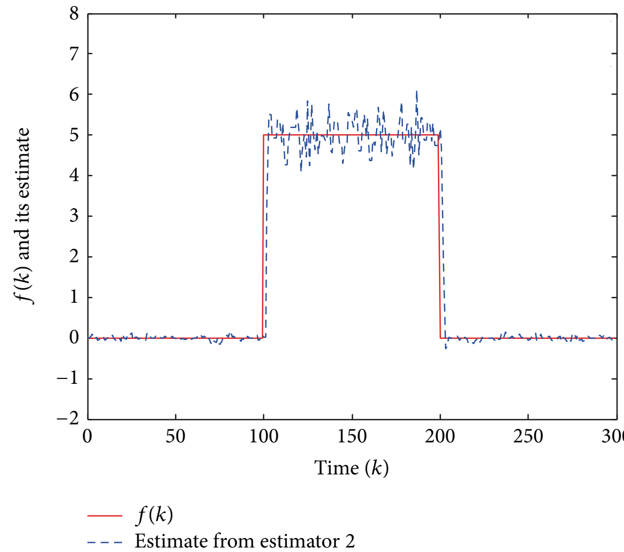

FIGURE 2: $f(k)$ and its estimate $f_2(k)$.

By applying the approach in [13], a T-S fuzzy model is constructed for system (31) as follows:

$$\begin{gathered}\text{Plant rule 1: IF } x_1 \text{ is about } 0, \text{THEN} \\ \dot{x} = A_{1c}x + B_1 u + w \\ \text{Plant rule 2: IF } x_1 \text{ is about } \Pi, \text{ THEN} \\ \dot{x} = A_{2c}x + B_2 u + w,\end{gathered} \tag{32}$$

where $x = \begin{bmatrix} \vartheta \\ \dot{\vartheta} \end{bmatrix}$, $A_{1c} = \begin{bmatrix} 0 & 1 \\ -(0.5mgl+Mgl)/J & 0 \end{bmatrix}$, $A_{2c} = \begin{bmatrix} 0 & 1 \\ -2(0.5mgl+Mgl)/\pi J & 0 \end{bmatrix}$, and $B_{1c} = B_{2c} = \begin{bmatrix} 0 \\ 1/J \end{bmatrix}$.

The fuzzy membership functions are set as $h_1(x_1) = (0.5\pi - |x_1|)/0.5\pi$ and $h_2(x_1) = 1 - h_1(x_1)$. By using the controller gain $K_1 = [10.5000 \ \ -5.1057]$, $K_2 = [3.8800 \ \ -5.0628]$, with a sampling time $T_s = 0.5$ s, the discrete-time model for system (32) is obtained as

$$\begin{gathered}\text{Plant rule 1: IF } x_1(k) \text{ is about } 0, \text{THEN} \\ x(k+1) = A_1 x(k) + B_1 w(k) \\ \text{Plant rule 2: IF } x_1(k) \text{ is about } \Pi, \text{THEN} \\ x(k+1) = A_2 x(k) + B_2 w(k),\end{gathered} \tag{33}$$

where

$$\begin{gathered}A_1 = \begin{bmatrix} 0.5508 & 0.1139 \\ -1.0252 & -0.1139 \end{bmatrix}, \qquad B_1 = \begin{bmatrix} 0.0570 \\ 0.1302 \end{bmatrix}, \\ A_2 = \begin{bmatrix} 0.5515 & 0.1149 \\ -1.0270 & -0.1136 \end{bmatrix}, \qquad B_2 = \begin{bmatrix} 0.0574 \\ 0.1314 \end{bmatrix}.\end{gathered} \tag{34}$$

In this example, we consider the actuator fault problem, and we aim to estimate the fault in a distributed framework. Hence, $E_i = B_i$ and $f(k)$ is estimated by two distributed estimators, with $C_{pi} = [1 \ \ 0]$, $(p, i = 1, 2)$, $D_{11} = 0.1$, $D_{12} = 0.1$, $D_{21} = 0.3$, and $D_{22} = 0.3$. In order to achieve a better estimation performance, these two estimators share their measurements to each other. This is reasonable as two sensors may be enough to monitor the robotic manipulator and the sensors are usually deployed in the working area of this manipulator such that they can communicate with each other. By choosing $\rho_1 = 0.9$, $\rho_2 = 0.7$, solving the optimization problem (30), the minimized value for H_∞ performance is obtained as $\gamma^* = 3.2053$ and the corresponding filter parameter matrices are given as follows:

$$\begin{gathered}\overline{H}_1 = \begin{bmatrix} 1.3854 & -0.1770 \\ 0.4810 & 0.2116 \\ 1.3770 & -0.1739 \\ 0.4969 & 0.2057 \end{bmatrix}, \\ \overline{H}_2 = \begin{bmatrix} 1.3907 & -0.1772 \\ 0.4937 & 0.2117 \\ 1.3825 & -0.1741 \\ 0.5095 & 0.2059 \end{bmatrix}, \\ \overline{K}_1 = \begin{bmatrix} 14.7365 & -3.3897 \\ 14.7365 & -3.3897 \end{bmatrix}, \\ \overline{K}_2 = \begin{bmatrix} 14.7305 & -3.3878 \\ 14.7305 & -3.3878 \end{bmatrix}.\end{gathered} \tag{35}$$

For simulation, the disturbance $w(k)$ is randomly varying in $[-0.5, 0.5]$ and $f(k)$ is chosen as

$$f(k) = \begin{cases} 0 & 0 \le k < 100; \ \ 200 \le k < 300 \\ 5 & 100 \le k < 200; \ \ 300 \le k < 400. \end{cases} \tag{36}$$

Simulation results are depicted as follows. The state trajectories of $f(k)$ as well as its estimates $f_1(k)$ and $f_2(k)$ are shown in Figures 1 and 2, respectively. It follows from

Table 1: Relation between the estimation performance and the quantization density.

ρ_1	0.9	0.9	0.9	0.9	0.9
ρ_2	0.9	0.8	0.7	0.6	0.5
γ^*	3.1971	3.2053	3.2231	3.2587	3.3578

Figures 1 and 2 that the two sensors have the same estimation performance due the the consensus based estimation technique. Hence, once one sensor has temporary failure such that it cannot provide the estimation signal, we can also have the fault estimation signal from the other sensor. The relation between the quantization density and the estimation performance is given in Table 1. It is seen that the estimation performance becomes worse when the quantization density is small; however more energy may be saved as less information is transmitted.

5. Conclusions

We have investigated the distributed fault estimation for a class of nonlinear systems, where the nonlinear plant is approximated by a T-S fuzzy model. Due to the limited power in sensors, signal quantization technique has been utilized to save sensor power. Based on the Lyapunov stability theory and the robust control approach, a sufficient condition is obtained such that the estimation error system is asymptotic stable with a prescribed H_∞ performance level. Finally, a case study on the fault estimation of actuator fault in the robotic manipulator is given to show the effectiveness of the proposed design. Some other future works, for example, the distributed fault estimation, with various networked issues will be considered [15–18]. In addition, in order to reduce the energy consumption of network, stochastic transmission protocol may be employed [19]. In this scenario, how to design the distributed fault estimator deserves further study.

Conflict of Interests

The authors declare that there is no conflict of interests regarding the publication of this paper.

Acknowledgments

This work was supported by the Zhejiang Provincial Natural Science Foundation of China (no. LQ14F030002) and also by the National Key Technology R&D Program (no. 2012BAH38F01-02).

References

[1] R. J. Patton and J. Chen, "Robust fault detection using eigenstructure assignment: a tutorial consideration and some new results," in *Proceedings of the 30th IEEE Conference on Decision and Control*, pp. 2242–2247, Brighton, UK, December 1991.

[2] R. J. Patton and J. Chen, "Review of parity space approaches to fault diagnosis for aerospace systems," *Journal of Guidance, Control, and Dynamics*, vol. 17, no. 2, pp. 278–285, 1994.

[3] R. K. Mehra and J. Peschon, "An innovations approach to fault detection and diagnosis in dynamic systems," *Automatica*, vol. 7, no. 5, pp. 637–640, 1971.

[4] I. Hwang, S. Kim, Y. Kim, and C. E. Seah, "A survey of fault detection, isolation, and reconfiguration methods," *IEEE Transactions on Control Systems Technology*, vol. 18, no. 3, pp. 636–653, 2010.

[5] S. X. Ding, *Model-Based Fault Diagnosis Techniques: Design Schemes, Algorithms, and Tools*, Springer, Berlin, Germany, 2008.

[6] B. Jiang and F. N. Chowdhury, "Fault estimation and accommodation for linear MIMO discrete-time systems," *IEEE Transactions on Control Systems Technology*, vol. 13, no. 3, pp. 493–499, 2005.

[7] K. Zhang, B. Jiang, and P. Shi, "Fault estimation observer design for discrete-time takagi-sugeno fuzzy systems based on piecewise lyapunov functions," *IEEE Transactions on Fuzzy Systems*, vol. 20, no. 1, pp. 192–200, 2012.

[8] R. Olfati-Saber and J. S. Shamma, "Consensus filters for sensor networks and distributed sensor fusion," in *Proceedings of the 44th IEEE Conference on Decision and Control, and the European Control Conference (CDC-ECC '05)*, pp. 6698–6703, Seville, Spain, December 2005.

[9] B. Shen, Z. Wang, and Y. S. Hung, "Distributed H_∞-consensus filtering in sensor networks with multiple missing measurements: the finite-horizon case," *Automatica*, vol. 46, no. 10, pp. 1682–1688, 2010.

[10] D. Zhang, L. Yu, H. Song, and Q.-G. Wang, "Distributed H_∞ filtering for sensor networks with switching topology," *International Journal of Systems Science*, vol. 44, no. 11, pp. 2104–2118, 2013.

[11] M. Fu and L. Xie, "The sector bound approach to quantized feedback control," *IEEE Transactions on Automatic Control*, vol. 50, no. 11, pp. 1698–1711, 2005.

[12] J. C. Geromel, M. C. de Oliveira, and J. Bernussou, "Robust filtering of discrete-time linear systems with parameter dependent Lyapunov functions," *SIAM Journal on Control and Optimization*, vol. 41, no. 3, pp. 700–711, 2002.

[13] Y. J. Pan, H. J. Marquez, and T. Chen, "Sampled-data iterative learning control for a class of nonlinear networked control systems," in *Proceedings of the American Control Conference*, vol. 1–12, pp. 3494–3499, June 2006.

[14] H. Zhang, J. Yang, and C. Y. Su, "T-S fuzzy-model-based robust H_∞ design for networked control systems with uncertainties," *IEEE Transactions on Industrial Informatics*, vol. 3, no. 4, pp. 289–301, 2007.

[15] H. Shen, S. Xu, J. Lu, and J. Zhou, "Passivity-based control for uncertain stochastic jumping systems with mode-dependent round-trip time delays," *Journal of the Franklin Institute*, vol. 349, no. 5, pp. 1665–1680, 2012.

[16] H. Shen, J. H. Park, L. X. Zhang, and Z. G. Wu, "Robust extended dissipative control for sampled-data Markov jump systems," *International Journal of Control*, vol. 87, no. 8, pp. 1549–1564, 2014.

[17] Z. G. Wu, P. Shi, H. Su, and J. Chu, "Asynchronous l_2-l_∞ filtering for discrete-time stochastic Markov jump systems with

randomly occurred sensor nonlinearities," *Automatica*, vol. 50, no. 1, pp. 180–186, 2014.

[18] Y. Tang, H. Gao, and J. Kurths, "Distributed robust synchronization of dynamical networks with stochastic coupling," *IEEE Transactions on Circuits and Systems I: Regular Papers*, vol. 61, no. 5, pp. 1508–1519, 2014.

[19] C. Zhang, G. Feng, J. Qiu, and W.-A. Zhang, "T—S fuzzy-model-based piecewise H_∞ output feedback controller design for networked nonlinear systems with medium access constraint," *Fuzzy Sets and Systems*, vol. 248, pp. 86–105, 2014.

Hindawi Publishing Corporation
Mathematical Problems in Engineering
Volume 2014, Article ID 257079, 10 pages
http://dx.doi.org/10.1155/2014/257079

Research Article

Joint Design of Control and Power Efficiency in Wireless Networked Control System

Yan Wang and Zhicheng Ji

Department of IoT Engineering, Jiangnan University, Wuxi 214122, China

Correspondence should be addressed to Yan Wang; violetwang0929@gmail.com

Received 29 April 2014; Accepted 10 July 2014; Published 6 August 2014

Academic Editor: Xi-Ming Sun

This paper presents a joint design method for wireless networked control system (WNCS) to balance both the demands of network service and the control performance. Since the problems of power consumption, communication reliability, and system stability exist simultaneously and interdependently in WNCS, most of the achieved results in the wireless network and wired networked control system cannot be used directly. To coordinate the three problems, sampling period is found to be the linking bridge. An adaptive sampling power efficiency algorithm is proposed to manage the power consumption such that it can meet the demands of network life span. The sampling period is designed to update periodically on the constraints of network schedulability and system stability. The convergence of the power efficiency algorithm is further proved. The sampling period is no longer a fixed value, however; thus, increasing the difficulty in modeling and controlling such a complicated time-varying system remains. In this work, a switched control system scheme is applied to model such a WNCS, and the effect of network-induced delay is considered. Switched feedback controllers are introduced to stabilize the WNCS, and some considerations on stability condition and the bounds of the update circle for renewing sampling period are discussed. A numerical example shows the effectiveness of the proposed method.

1. Introduction

Wireless networked control systems are composed of distributed fields and plant devices (sensors, actuators, and controllers) interconnected via a wireless network [1]. The sensors, controllers, and actuators exchange information with one another through the wireless network. Sensors collect the status or outputs of plants at every sampling instant, packet the data with time-stamp, and then send the information to each corresponding controller via the wireless network. Controllers then compute the control variables as soon as they receive the newest data from their plants. After that, the control variables are sent to their corresponding actuators. Plants will not update their status until they receive the newest command from controllers. Wireless capabilities clearly provide opportunities to be more inventive in system organization [2]. The use of wireless network offers several advantages compared with a conventional wired networked control system in terms of cost, maintenance, scalability, and implementation flexibility. However, wireless nodes also have obvious weak points such as reliability and availability, particularly the power consumption. Power efficiency technologies are important research areas in wireless network applications.

Most studies on WNCS analyze the effects of the wireless medium on overall closed-loop control systems in [3–11]. The first critical analysis on the use of wireless control is performed by Kumar in [3]. Kumar explores the impact of different protocol layers, from routing to physical, on control performance. In [4], Liu and Goldsmith analyzed the performance of a control system in terms of variation in data rate, error correcting codes, and different maximum bounds in the number of retransmissions. They also studied the impact of IEEE 802.11b medium access control. In [5], Colandairaj et al. discuss the impact of data flow on the stability of a closed-loop wireless network control system based on IEEE 802.11. Sampling rate adaption is proposed as a codesign solution to enhance control and wireless network performance. Different from our work in this paper, the purpose of adapting the sampling rate is to optimize bandwidth utilization not to save power. A robust and dynamic cross-layer communication architecture for wireless networked control system is presented in [6] by Israr et al. The protocol stack for WNCS comprises five layers. Each layer contributes to the overall goal of reliable, power-efficient communication. However, the control performance is not taken into account in their work.

A number of studies related to power efficiency in wireless sensor networks (WSNs) and wireless networks have also been conducted in [12–18]. Current power efficiency research always falls into two categories: one is reducing the power consumption of each single node in the network and the other is balancing the power consumption of all the nodes in network. In [12], Colandairaj et al. present a dynamic power control strategy to minimize the communication power consumption of nodes by varying the transmission rate. A protocol intending to balance power consumption from the remaining battery power of the node-based routing policy is proposed by Liang and Yang in [13]. The nodes with greater remaining power are allocated with more communication tasks. In [15], Kim et al. propose a lifetime-based routing strategy in which the survival time is estimated according to the residual power and current ratio of power consumption. The path with the longest node survival time is selected for data transmission.

Recently, limited studies in [19–21] are conducted on effective power saving strategies that specifically target at WNCS. Fischione et al. [20] propose a trade-off between wireless output power related to reliability and power consumption, where a physical characteristic model revealed quantitative relations with communication outage probability. They also focus on the lower layer optimal protocol design by considering the application layer requirements. Lino [21] discusses the optimal sleep mode control of wireless network nodes and proposes a trade-off method between control performance and power consumption. An optimal control strategy is applied to optimize the control period. In [22], event-predictive control for power saving of wireless networked control system is discussed. The key idea is to save power by maximizing the control interval with constrains of appropriate control performance. The proposed control method is rather complicated and requires online optimization mixed integer programming, which reduces the practicability. Thus, a simpler trade-off method for WNCS is required.

Power consumption, communication reliability, and system stability exist simultaneously and react with one another in wireless networked control systems. Supposed that the three factors are interdependent, most results achieved in wireless network power management and wired networked control systems cannot be directly applied to WNCS. Thus, the motivation of this paper is to find a bridge which can link the three factors and make a balance among these factors through the bridge parameter, such that the overall satisfactory performance can be achieved. Fortunately, the sampling period of sensor node is found to be the bridge parameter. From this point, a joint design method of adaptive sampling power efficiency algorithm and coordinated control method are discussed in this paper. An updating rule of sampling period is presented to satisfy the demands of wireless life span under constrains of network schedulability and control system stability. Convergence of the power efficiency algorithm is further proved. Subsequently, the control system is a varying-period system since the sampling periods of sensors are time-varying. It is then modeled as a class of switched control system with two types of behavior in each update period. The switched control law is applied to stabilize the control system and stability conditions are discussed. Also, the choosing rule of update period is given.

The remaining sections are organized as follows. Section 2 is the problem formulation. Section 3 presents the adaptive power efficiency algorithm. Section 4 discusses the coordinated wireless networked control system modeling and design method. Numerical simulation is given in Section 5. Section 6 is the conclusion of this paper.

2. Problem Formulation

2.1. Description of WNCSs. Consider the wireless networked control systems shown in Figure 1. There are three kinds of node in the system. Power consumption varies for the different kinds of node.

Besides, some necessary assumptions are made in this paper as the follows.

Assumption 1. The power of sensor and actuator nodes is supplied by battery while the power of controller is supplied by base station.

Assumption 2. The sensor and the actuator are clock driven while the controller is event driven. The sampling data is packed in one packet for transmission with time stamp.

Assumption 3. There exists transmission delay in the control loop, and it is assumed to be less than one sampling period.

2.2. Analysis of Power Consumption in WNCSs. Sensor power is consumed by three processes: data sampling, sample data reading by the ADC, and data transfer. The power consumption of the controller node is also consumed by three processes: receiving data, calculating control variables, and sending data packet. The power of the actuator is consumed by two processes: receiving data and D/A conversion. The power consumption of different tasks is shown in Table 1 (see in [6]).

From the table, we get the following two conclusions:

(1) when the sensor transfers the same amount of data as the actuator receives, it will consume 2.5 times more power than the actuator will consume.

(2) data transfer consumes over 90% of the total sensor power consumption.

Given that the power required by control nodes can be supplied by the base station in most situations, the power required by the sensor nodes and actuators can be provided by batteries. Thus, sensors utilize the maximum amount

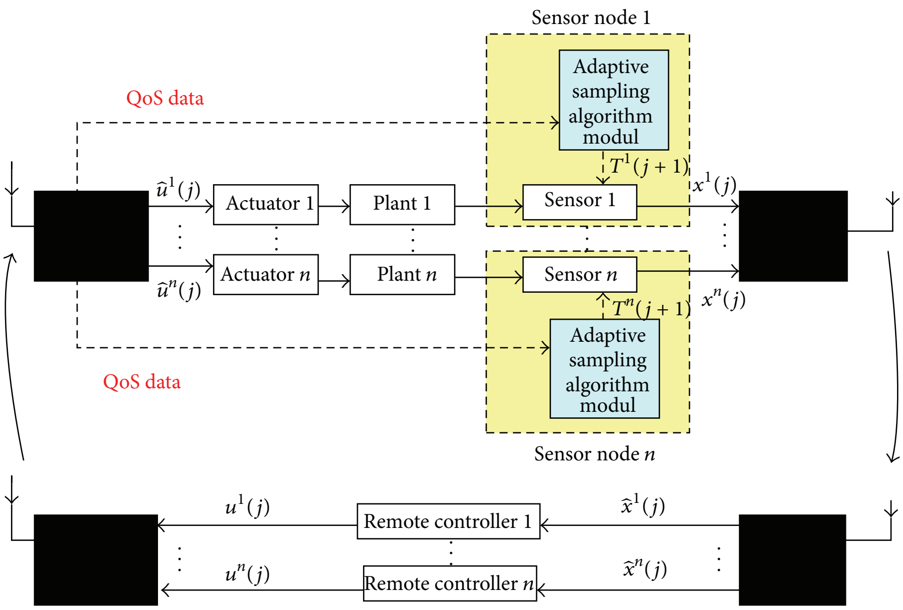

FIGURE 1: Structure of wireless networked control systems.

TABLE 1: Power consumption of different tasks.

Task	Energy consumption (nAh)
Receive data	8
Transfer data	20
Read data	0.011
Sample data	1.08

of power consumption in WNCS. Managing the power consumption of sensors is the key to prolonging the survival time of the wireless network. A direct and effective method is to reduce as much of the transmission consumption as possible by properly adjusting the amount of sample data. This principle is the basis of our power control algorithm.

In wireless networks, the average power consumption of sending a packet can be described as [3]

$$\overline{E} = b \times \text{packet\_size} + c, \tag{1}$$

where b is the coefficient of power consumption and c is the fixed power consumption of the node sending a data packet. According to Assumptions 1 and 2, a sensor node sends a packet to the corresponding controller at every sampling time. Given the lack of packet retransmission, the survival time of the sensor can be described as

$$L = \sum_{i=1}^{\text{sum}} \left(t\left(i\right) - t\left(i-1\right)\right), \tag{2}$$

where L is the survival time of the sensor node, sum is the maximum number of packets sent by the sensor given an initial power, sum $= \lfloor E_{\text{init}}/\overline{E} \rfloor$, $\lfloor x \rfloor$ is the integral part of x, E_{init} is the given initial power of the sensor, $t(i)$, $i \in \{1, 2, \ldots, \text{sum}\}$ is the time that the sensor node sends the ith data packet, and $t(0)$ is the initial time.

Survival time is dependent on transfer intervals. It can be prolonged by increasing the transfer intervals. Based on this premise as well as on the knowledge of the relationship between sampling period and control performance, we can cooperatively design the control and the network performances by adaptively adjusting the sampling period with a proper rule.

3. Adaptive Sampling Power Efficiency Algorithm

3.1. Update Rule of Sampling Period. For the consideration of simplicity and generality, we choose one of the control loops in the WNCS to describe the power control algorithm. Let $T^{\min}$ be the lower bound of the sampling period to guarantee the schedulability of the network and let $T^{\max}$ be the upper bound of the sampling period to ensure system stability. Supposing that there are M candidate sampling periods for choosing in the allowable range between the maximum and minimum bounds, $T_l \in [T^{\min}, T^{\max}]$, $l = 1, 2, \ldots, M$. Furthermore, an update period T_M, $T_M > T^{\max}$ is designed for the sampling period renewal. The sampling period is renewed at each update instant as follows:

$$\begin{aligned} T\left(j+1\right) &= T\left(j\right) + \Delta T\left(j+1\right) \\ \Delta T\left(j+1\right) &= -\operatorname{sgn}\left(\widehat{L}\left(j\right) - L_e\right) \cdot \frac{S\left(T^{\max} - T^{\min}\right)}{M-1}, \end{aligned} \tag{3}$$

where

$$S = \min\left\{\left\lfloor 2(M-1)\left|\widehat{L}(j)-L_e\right| \times\left(\left(\frac{E_{\text{init}}}{\overline{E}}-\sum_{l=1}^{M}k_l(j)\frac{T_M}{T_l}-\frac{T_M}{T_j}\right) \times\left(T^{\max}-T^{\min}\right)\right)^{-1}\right\rfloor, M-1\right\}; \tag{4}$$

L_e is the demand of sensor survival time; $T(j)$ is the value of the sampling period in the jth updating interval; $\operatorname{sgn}(x)$ is the signal of scalar x; $\lfloor x\rfloor$ is the integral part of scalar x; $k_l(j)$ is the number of updating intervals in which the sampling period is T_l during the previous j updates; $\widehat{L}(j)$ is the current predicted survival time of sensor node calculated by the following formula:

$$\widehat{L}(j) = jT_M + \frac{E_{\text{rem}}(j)}{\overline{E}} \times T(j); \tag{5}$$

$E_{\text{rem}}(j)$ is the current remaining power at the updating instant jT_M.

3.2. Convergence of Power Efficiency Algorithm

Theorem 1. *For the WNCS described in Figure 1, considering the update rule of adaptive sampling period* (3), *if the minimum sampling period satisfies*

$$T^{\min} > \frac{L_e}{sum}, \tag{6}$$

then the actual survival time of sensor node will reach its expected value L_e through the proposed rule of sampling period update.

Proof. According to Formula (1), we have

$$\widehat{L}(j+1) = (j+1)T_M + \frac{E_{\text{rem}}(j+1)}{\overline{E}} \times T(j+1). \tag{7}$$

The remaining power relationship at the two adjacent updating instants is given by

$$E_{\text{rem}}(j+1) = E_{\text{rem}}(j) - \frac{T_M}{T(j)} \times \overline{E}. \tag{8}$$

We assume that the sensor node has sampled the plant with the sampling period T_l for $k_l(j)$ times from the initial to the current time instant. The remaining power can be calculated based on the initial power and consumed power:

$$E_{\text{rem}}(j) = E_{\text{init}} - \sum_{l=1}^{M}k_l(j)\frac{T_M\overline{E}}{T_l}. \tag{9}$$

Power control error is defined as $e(j) = \widehat{L}(j) - L_e$. According to formulas (7), (8), and (9), the dynamics of the error can be described as

$$e(j+1) = e(j) + K(j)\Delta T(j+1), \tag{10}$$

where $K(j)$ is defined as $K(j) = \text{sum} - \sum_{l=1}^{M}k_l(j)(T_M/T_l) - (T_M/T(j))$. At the current time instant, $K(j)$ is a known variable.

The following Lyapunov function is introduced to prove convergence of the adaptive sampling power efficiency algorithm:

$$V(j) = \frac{1}{2}e^2(j). \tag{11}$$

Considering Formula (10), it follows that

$$\begin{aligned}\Delta V(j) &= V(j+1) - V(j)\\ &= K(j)\Delta T(j+1)e(j) + \frac{1}{2}K^2(j)\Delta T^2(j+1).\end{aligned} \tag{12}$$

With formula (3), we obtain

$$\begin{aligned}&\left.\begin{array}{l} e(j)>0,\ \ \Delta T(j+1)<0\\ e(j)<0,\ \ \Delta T(j+1)>0\end{array}\right\} \Longrightarrow \Delta T(j+1)e(j)<0,\\ &\left|\Delta T(j+1)\right|\left|e(j)\right| > \frac{1}{2}K(j)\Delta T^2(j+1).\end{aligned} \tag{13}$$

From inequalities (13), it can be concluded that $\Delta V(j) < 0$. Furthermore, to guarantee that the minimum survival time can reach the expected value, the minimum sampling period is bounded by $T^{\min} \geq L_e/\text{sum}$. Consequently, the error system is stable, and the survival time can converge to the expected value if the conditions in Theorem 1 are satisfied. □

Remark 2 (prediction of survival time). The actual survival time is unavailable at the current instant because the power consumption is time varying. However, it can be predicted by the known information of the remaining power and sampling period at the current instant. Formula (5) provides the prediction and indicates that the survival time of the node will be $\widehat{L}(j)$ if the sensor node maintains the sampling period $T(j)$ as unchanged from the current instant $t = jT_M$. The prediction of the survival time serves as a substitute for real survival time and is used to calculate the new sampling period.

Remark 3 (lower bound of sampling period). Taking IEEE 802.11b as an example, the lower bound of the sampling period of sensor $T^{\min}$ can be determined by the following formula:

$$T^{\min} = \max\left\{\frac{L_e}{\text{sum}}, \frac{S_{\text{mc}} \times 2 \times N}{Q}\right\}, \tag{14}$$

where $(S_{mc} \times 2 \times N)/Q$, is the allowable minimum sampling period when the wireless network can be schedulable (see in [6]), and

$$Q = \frac{S_{mc}}{T_{\text{DIFS}} + (CW_{\min} \times T_{\text{SIFS}}/2) + T_{\text{frame}} + T_{\text{SIFS}} + T_{\text{ACK}}} \quad (15)$$

$$\begin{aligned} T_{\text{frame}} &= \frac{S_{\text{PHY}}}{R_l} + \frac{S_{\text{MAC}} + S_{mc}}{R_t}, \\ T_{\text{frame}} &= \frac{S_{\text{PHY}}}{R_l} + \frac{S_{\text{MAC}} + S_{mc}}{R_t}. \end{aligned} \quad (16)$$

R_t is the transmission rate, R_l is the legacy transmission rate, S_{mc} is the measurement-control data size, S_{PHY} is the size of control frame in physical layer, and S_{MAC} is the data size of ACK and is a confirmed sign in the header of TCP data packet that confirms the received TCP message. T_{SIFS} is the shortest time period of the 802.11b protocol for the interval of frames requiring immediate response. T_{DIFS} is the time segment for the interval of the time frame of the distributed coordination function for sending in IEEE 802.11b. T_{PIFS} is the time segment for the interval of the time frame of the centralized coordination function for sending, which satisfies

$$T_{\text{PIFS}} = T_{\text{DIFS}} - T_{\text{slot}}, \quad T_{\text{slot}} = T_{\text{PIFS}} - T_{\text{SIFS}}. \quad (17)$$

CW is the contention window. Wireless network parameters under the 802.11b direct sequence spread spectrum are shown in Table 2.

Remark 4 (upper bound of sampling period). For a SISO system, the maximum sampling period can be obtained using Shannon sampling theorem. For a MIMO system, the following method can be used to obtain the upper bound. If the system feedback control law is given ahead, then $T^{\max}$ can be obtained by solving the following optimal problem:

$$\begin{aligned} &\max \quad T \\ &\text{s.t} \quad \left\| \text{eig}\left(e^{\mathbf{A}T} + \int_0^T e^{\mathbf{A}T} dt \mathbf{B}\mathbf{K}_0\right)\right\| < 1, \end{aligned} \quad (18)$$

where $\mathbf{A}$ is the system matrix and $\mathbf{B}$ is the control input matrix. $\mathbf{K}_0$ is the Kalman gain, which satisfies

$$\mathbf{Re}\left(\text{eig}\left(\mathbf{A} + \mathbf{B}\mathbf{K}_0\right)\right) < 0, \quad (19)$$

where $\mathbf{Re}(v)$ denotes the real part of v and eig($\mathbf{X}$) denotes the eigenvalues of matrix $\mathbf{X}$. Gain $\mathbf{K}_0$ can be determined by the pole assignment in the continuous time domain.

However, the above optimal problem is difficult to solve directly. The following iteration method can be used to obtain the approximate optimal value of $T^{\max}$:

Step 1. Let $q = 1$, and the initial value of $T^{\max}$ is $T^{\max}(q) = 2T^{\min}$. If the condition can satisfy the constraints of the optimal problem, go to Step 2; or else, go to Step 3.

Table 2: Wireless network parameters under 802.11b direct sequence spread spectrum.

Parameter	Value
R_t	11 Mbps
R_l	1 Mbps
T_{SIFS}, T_{DIFS}, T_{slot}	10, 50, 20 us
S_{MAC}, S_{PHY}	34, 24 bytes
S_{mc}	80 bytes
S_{ACK}	14 bytes + PHY header
$\text{CW}_{\min}$, $\text{CW}_{\max}$	32, 1024

Step 2. Let $q = q + 1$, and let $T^{\max}(q) = 2T^{\max}(q-1)$. If the condition can fulfill the constraints of the optimal problem, cycle Step 2; or else, end the iteration and then let $T^{\max} = T^{\max}(q-1)$.

Step 3. Let $T^{\max}(q) = (1 + (3/4)^q)T^{\min}$. If the condition still does not satisfy the constraints of the optimal problem, let $q = q + 1$ and cycle Step 3; or else end the iteration and let $T^{\max} = T^{\max}(q)$.

4. Modeling and Stability Analysis of Adaptive Sampling Period WNCS

4.1. Modeling of Adaptive Sampling Period WNCS. Considering the generality, one of the control loops in the WNCS is chosen as an example to illustrate the modeling approach. For the WNCS power consumption managed by algorithm in Section 2, the dynamics of the control system is time-varying. Since the sampling period varies among the M candidates, the system can be considered a switched system with M modes from the perspective of the switched control system scheme. Each switching mode is corresponded to one of the candidates. According to Assumption 1, the sensor and actuator nodes are assumed to be clock-driven. It results that the switching occurs at some of the sampling instants. Additionally, according to Assumption 3, the inevitable existence of network-induced delay is taken into account and it is less than one sampling period.

We consider a plant of control loop i in the WNCS with the following dynamics:

$$\begin{aligned} \dot{x}^i(t) &= \mathbf{A}^i x^i(t) + \mathbf{B}^i u^i(t) \\ y^i(t) &= \mathbf{C}^i x^i(t), \end{aligned} \quad (20)$$

where $x^i(t) \in \mathbf{R}^n$ is the plant state, $u^i(t) \in \mathbf{R}^m$ is the control input, and $y^i(t) \in \mathbf{R}^p$ is the plant output. $\mathbf{A}^i \in \mathbf{R}^{n\times n}$, $\mathbf{B}^i \in \mathbf{R}^{n\times m}$, and $\mathbf{C}^i \in \mathbf{R}^{p\times n}$ are the matrices of state, control input, and output matrices, respectively. Due to the generality of i, we omit the superscript i in the following model description and deduction.

Discretizing system (20) with sampling rate T_l and considering network-induced delay less than one sampling

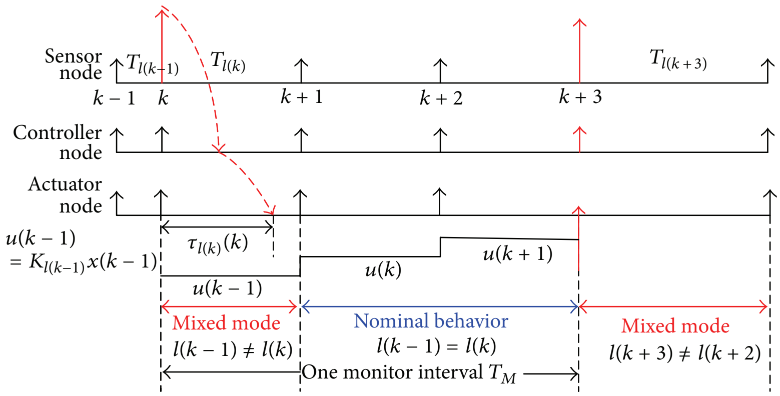

Figure 2: Evolution over one period of switched WNCS with two types of behavior.

period, the discrete dynamics of the open control loop can be described as

$$x(k+1) = \mathbf{\Phi}_{l(k)} x(k) + \mathbf{\Gamma}_{l(k)} u(k-1)$$
$$y(k) = \mathbf{C}x(k), \tag{21}$$

where $\mathbf{\Phi}_{l(k)} = e^{\mathbf{A}T_{l(k)}}$; $\mathbf{\Gamma}_l = \int_0^{T_{l(k)}} e^{\mathbf{A}t} dt\mathbf{B}$; and $l(k)$ is the identification of sampling period at the kth sampling instant, $l(k) \in \mathbb{Z} \rightarrow \ell = \{0, 1, \dots, M-1\}$.

For the discrete switched system (21), a switched state feedback controller is introduced in the following form:

$$u(k) = \mathbf{K}_{\gamma(k)} x(k), \tag{22}$$

where $\gamma(k) \in \mathbb{Z} \rightarrow \ell = \{0, 1, \dots, M-1\}$ denotes the switching signal used in the control.

Consequently, the closed-loop WNCS can be written as

$$\begin{bmatrix} x(k+1) \\ x(k) \end{bmatrix} = \begin{bmatrix} \mathbf{\Phi}_{l(k)} & \mathbf{\Gamma}_{l(k)}\mathbf{K}_{\gamma(k)} \\ \mathbf{I} & 0 \end{bmatrix} \begin{bmatrix} x(k) \\ x(k-1) \end{bmatrix}. \tag{23}$$

4.2. Stability Analysis of Adaptive Sampling Period WNCS. The control gains $\mathbf{K}_{\gamma(k)}$ are assumed to be designed in such a way that the closed-loop system is asymptotically stable when $\gamma(k) = l(k)$. Ideally, the switching signal used in control $\gamma(k)$ is the same as the real signal $l(k)$. However, this view is unrealistic in WNCS with network-induced delay, where $\gamma(k) = l(k-1)$. The evolution over one sampling period can be described by two distinct types of behavior: the nominal and mixed mode sampling periods, as shown in Figure 2.

(1) *Nominal sampling period* is when the system evolution uses the right switching information:

$$\gamma(k) = l(k-1), \qquad l(k) = l(k-1). \tag{24}$$

(2) *Mixed mode sampling period* is when the system command uses a wrong feedback gain

$$\gamma(k) = l(k-1), \qquad l(k) \neq l(k-1). \tag{25}$$

Denoting Δ^m as the samples spent in the mixed mode, since the delay is less than one sampling period, it follows that Δ^m has a range of $0 \leq \Delta^m \leq 1$. Moreover, we assume that the system is controlled using the right gains for at least Δ^n samples before another switching occurs.

The next thing we should do is to guarantee the closed-loop system remaining stable with the designed state feedback control gains when the switching signal is temporarily uncertain. Consider the scalars $\theta_n > 0$, $\theta_m > 0$ and the symmetric positive definite matrices $\mathbf{P}_l^n$, $\mathbf{P}_{(l,\gamma)}^m$ with $(l,\gamma) \in \ell \times \ell$, which satisfy the following matrix inequalities:

$$\overline{\mathbf{\Phi}}_{(l,\gamma)}^T \left(\mathbf{P}_{(l,\gamma)}^m\right)^{-1} \overline{\mathbf{\Phi}}_{(l,\gamma)} - \theta_m \mathbf{P}_{(l,\gamma)}^m < 0, \quad \forall (l,\gamma) \in \ell \times \ell$$
$$\overline{\mathbf{\Phi}}_{(l,l)}^T \mathbf{P}_l^n \overline{\mathbf{\Phi}}_{(l,l)} - \theta_n \mathbf{P}_l^n < 0, \quad \forall l \in \ell. \tag{26}$$

Moreover, consider the following two scalars,

$$\beta_n = \frac{\max_{l\in\ell} \mathrm{eig}_{\max}\left(\mathbf{P}_l^n\right)}{\min_{l\in\ell} \mathrm{eig}_{\min}\left(\mathbf{P}_l^n\right)},$$
$$\beta_m = \frac{\max_{(l,\gamma)\in\ell\times\ell} \mathrm{eig}_{\max}\left(\mathbf{P}_{(l,\gamma)}^m\right)}{\min_{(l,\gamma)\in\ell\times\ell} \mathrm{eig}_{\min}\left(\mathbf{P}_{(l,\gamma)}^m\right)}, \tag{27}$$

where $\mathrm{eig}_{\max}(\mathbf{X})$ and $\mathrm{eig}_{\min}(\mathbf{X})$ denote the maximum and the minimum eigenvalues of matrix $\mathbf{X}$, respectively.

Then, the stability of the closed-loop WNCS (23) can be guaranteed by the following theorem.

Theorem 5. *Let θ_n^*, θ_m^* be the solutions of the optimization problems $\theta_n^* = \min \theta_n$ and $\theta_m^* = \min \theta_m$ subject to matrix inequalities (26). Closed-loop system (23) is asymptotically stable if*

$$\beta_n \cdot \beta_m \cdot \left(\theta_n^*\right)^{\Delta^n} \cdot \theta_m^* < 1. \tag{28}$$

Proof. We consider the following Lyapunov functions:

$$V^n(k) = \overline{x}^T(k) \mathbf{P}_l^n \overline{x}(k), \qquad V^m(k) = \overline{x}^T(k) \mathbf{P}_{(l,\gamma)}^m \overline{x}(k). \tag{29}$$

Inequalities (13) show that

$$V^n(k_1) < \left(\theta_n^*\right)^{k_1-k_0} V^n(k_0). \tag{30}$$

$\forall k \in [k_0, k_1)$, if the right switching signal is used in the control, $l(k) = \gamma(k) = l(k_0)$, then

$$V^m(k_1) < (\theta_m^*)^{k_1-k_0} V^m(k_0). \tag{31}$$

$\forall k \in [k_0, k_1)$, if the switching signal in the control is not necessarily the same as the real signal, the pair $l(k)$, $\gamma(k)$ takes an arbitrary value $l(k_0)$, $\gamma(k_0)$ in $\ell \times \ell$.

Since the controller gains $\mathbf{K}_l$ are designed to make the matrices $\overline{\mathbf{\Phi}}_{(l,l)}$ stable, the scalar θ_n is smaller than one, $\theta_n < 1$. The scalar θ_m may be greater than one, $\theta_m > 1$, since the gains $\mathbf{K}_\gamma$ are not designed to stabilize combinations other than $\overline{\mathbf{\Phi}}_{(\gamma,\gamma)}$.

Combining inequalities (26) yield

$$\begin{gathered}
\min_{l\in\ell} \operatorname{eig}_{\min}(\mathbf{P}_l^n)\|\overline{x}(k_1)\|^2 \\
< (\theta_n^*)^{k_1-k_0}\max_{l\in\ell}\operatorname{eig}_{\max}(\mathbf{P}_l^n)\|\overline{x}(k_0)\|^2 \quad \forall l \in \ell \\
\min_{(l,\gamma)\in\ell\times\ell} \operatorname{eig}_{\min}\left(\mathbf{P}_{(l,\gamma)}^m\right)\|\overline{x}(k_1)\|^2 \\
< \max_{(l,\gamma)\in\ell\times\ell}\operatorname{eig}_{\max}\left(\mathbf{P}_{(l,\gamma)}^m\right)\|\overline{x}(k_0)\|^2 \quad \forall (l,\gamma) \in \ell\times\ell.
\end{gathered} \tag{32}$$

With the definitions of β_n and β_m, we can obtain the state vector norm decay or growth rate in a nominal regime and in an uncertain switching signal regime as follows:

$$\begin{gathered}
\|\overline{x}(k_1)\|^2 < \beta_n\cdot(\theta_n^*)^{k_1-k_0}\|\overline{x}(k_0)\|^2, \quad \forall l \in \ell \\
\|\overline{x}(k_1)\|^2 < \beta_m\cdot(\theta_m^*)^{k_1-k_0}\|\overline{x}(k_0)\|^2, \quad \forall (l,\gamma) \in \ell\times\ell.
\end{gathered} \tag{33}$$

Let k_s^m describe the instants when the closed-loop system jumps to a mixed mode with uncertain switching signal, and let k_s^n be the instance when the system enters into a normal regime. With definitions and bounds of Δ^m and Δ^n, it follows that

$$0 \le \Delta^m = k_s^n - k_s^m \le 1, \qquad k_{s+1}^m - k_s^n \le \Delta^n. \tag{34}$$

Without loss of generality, we assume that the system starts with a mixed-mode behavior, $k_s^m < k_s^n$. The system behavior in time interval $k \in [k_s^m, k_{s+1}^m)$ is then analyzed.

Given that $l(k) \ne \gamma(k)$, $\forall k \in [k_s^m, k_s^n)$ and $l(k) = \gamma(k)$, $\forall k \in [k_s^n, k_{s+1}^m)$, using inequalities (26), the norm of the state at the end of the sequence can be upper bounded asd

$$\begin{aligned}
\|\overline{x}(k_{s+1}^m)\|^2 &< \beta_m\cdot\beta_n\cdot(\theta_m^*)^{k_s^n-k_s^u}\cdot(\theta_n^*)^{k_{s+1}^m-k_s^n}\|\overline{x}(k_s^m)\|^2 \\
&< \|\overline{x}(k_{s+1}^m)\|^2 < \beta_m\cdot\beta_n\cdot\theta_m^*\cdot(\theta_n^*)^{\Delta^n}\|\overline{x}(k_s^m)\|^2.
\end{aligned} \tag{35}$$

It indicates that closed loop (16) will be asymptotically stable if condition (28) in Theorem 5 is satisfied. □

4.3. Choosing Rule of Update Period T_M

Theorem 6. *Consider the WNCS with adaptive sampling period rule* (3). *The WNCS can be stabilized by the switched state feedback controllers* (22)*, whereas the survival time can meet its expected value L_e, if the update period T_M satisfies the following conditions:*

$$\begin{aligned}
&(1)\ T_M \ge \max(\Delta_i^n + 1)\left[T_1^{\max}, T_2^{\max}, \ldots, T_n^{\max}\right] \\
&(2)\ \left\lfloor \frac{L_e}{T_M} \right\rfloor \cdot T_M \le \frac{E_{init}}{\overline{E}}\min\left\{T_1^{\min}, T_2^{\min}, \ldots, T_n^{\min}\right\},
\end{aligned} \tag{36}$$

where Δ_i^n is the least nominal sampling period of control loop i and the solution of Theorem 5, $[T_1^{\max}, T_2^{\max}, \ldots, T_n^{\max}]$, is the least common multiple of the maximum sampling period for all the n control loops in the WNCS.

Proof. According to Theorem 5, control loop i in the WNCS should stay at least Δ_i^n in a nominal sampling period in one updating interval for stability. With the consideration of $0 \le \Delta_i^m \le 1$, if the update period satisfies condition (1), all control loops in the WNCS will meet the demands of their least nominal sampling periods and will be stable. As a complete system, WNCS is composed of n control loops that will be stable when condition (1) is satisfied.

Condition (2) in Theorem 6 provides the upper bound of the updating period. For the power efficiency algorithm in Theorem 1, with the definition of $k_l(j)$, there exists

$$\sum_{l=1}^{M} k_l(j)\frac{T_M}{T_l} + \frac{T_M}{T_j} \le \left\lfloor \frac{L_e}{T_M} \right\rfloor \cdot \frac{T_M}{\min\left\{T_1^{\min}, T_2^{\min}, \ldots, T_n^{\min}\right\}}. \tag{37}$$

If condition (2) in Theorem 6 is satisfied, the item $((E_{\text{init}}/\overline{E}) - \sum_{l=1}^{M} k_l(j)(T_M/T_l) - (T_M/T_j))$ in the denominator of formula (3) will be greater than zero, which guarantees that formula (3) has physical meaning and is solvable. The survival time will, thus, reach the expected value by applying the power efficiency algorithm. □

5. Numerical Example

Simulation studies are performed on a WNCS closed by an IEEE 802.11b wireless network with two control loops sharing the network resources. The two control loops are assumed to have the same dynamics but with different initial conditions:

$$\begin{gathered}
\dot{x}^i(t) = \begin{bmatrix} -1 & -0.1 \\ 0 & 0.95 \end{bmatrix} x^i(t) + \begin{bmatrix} -0.15 \\ -0.43 \end{bmatrix} u^i(t) \\
y^i(t) = \begin{bmatrix} 1 & 1 \end{bmatrix} x^i(t), \\
i = 1, 2 \\
x^1(0) = \begin{bmatrix} -5 & 5 \end{bmatrix}^T, \qquad x^2(0) = \begin{bmatrix} -5 & 10 \end{bmatrix}^T.
\end{gathered} \tag{38}$$

The wireless network parameters are set as in Table 2. The time delays in both loops are less than one sampling period. Some other necessary parameters are given as shown in Table 2.

In Table 3, the minimum and maximum sampling periods are computed by the methods in Section 3. Solving

TABLE 3: Simulation parameters.

Parameter	Value
Initial energy of both sensors E_{init}	0.15 J
Sensor 1 expected survival time L_{e1}	75 s
Sensor 2 expected survival time L_{e2}	70 s
Unit transmission energy $\overline{E}$	25 dbm
Number of sampling period candidates M	10
The minimum sampling period of loop1 $T_1^{\min}$	1 ms
The maximum sampling period of loop1 $T_1^{\max}$	256 ms
The minimum sampling period of loop2 $T_2^{\min}$	1 ms
The maximum sampling period of loop2 $T_2^{\max}$	256 ms

TABLE 4: Controller gains of ten sampling modes.

Sampling period (/ms)	Controller gain
$T_0 = 1$	$K_0 = \begin{bmatrix}1117.6 & 1118.8\end{bmatrix}$
$T_1 = 29$	$K_1 = \begin{bmatrix}39.4837 & 40.5512\end{bmatrix}$
$T_2 = 58$	$K_2 = \begin{bmatrix}19.4678 & 20.4319\end{bmatrix}$
$T_3 = 86$	$K_3 = \begin{bmatrix}12.5668 & 13.4279\end{bmatrix}$
$T_4 = 114$	$K_4 = \begin{bmatrix}9.0353 & 9.7947\end{bmatrix}$
$T_5 = 143$	$K_5 = \begin{bmatrix}6.8663 & 7.5265\end{bmatrix}$
$T_6 = 171$	$K_6 = \begin{bmatrix}5.383 & 5.947\end{bmatrix}$
$T_7 = 199$	$K_7 = \begin{bmatrix}4.295 & 4.769\end{bmatrix}$
$T_8 = 227$	$K_8 = \begin{bmatrix}4.225 & 3.852\end{bmatrix}$
$T_9 = 256$	$K_9 = \begin{bmatrix}3.707 & 2.95\end{bmatrix}$

inequality (28) in Theorem 5, it yields $\Delta_1^n = \Delta_2^n = 8$, $\Delta^m = 1$. Also, the update period can be chosen by Theorem 6 as $T_M = 150$ ms.

Solving matrix inequalities (18) and (19), the controller gains of ten switching modes can be obtained as in Table 4.

With the above simulation parameters and controller gains, the curves of survival time prediction, power consumption, and control output of both control loops are shown in Figures 3 to 8.

Analyzing the simulation curves, we have the following results.

(1) Figures 3, 6, 4, and 7 imply that both sensor 1 and sensor 2 can meet their expected survival time requirements.

(2) The power consumption in three cases of minimum sampling, maximum sampling, and the proposed adaptive sampling is compared in Figures 4 and 7. It is obvious that the power is consumed much faster than the other two cases. In the case of the adaptive sampling, the power consumption varies according to both the requirements of the control performance and survival time. At the beginning, the power consumption curves vary quickly and more power are consumed because of the control systems not reaching stable yet. Then, after the control systems are settled, it tends to the minimum consumption rate which is corresponding to the maximum sampling period.

(3) Figures 5 and 8 are the control outputs of loop1 and loop2 in the three cases mentioned above. The figures show that the control systems can be stabilized through the proposed joint design methods. In three cases, the adaptive sampling can get the control performances closed to the case of minimum sampling.

(4) Combining Figures 4, 5, 7, and 8, it can be concluded that the proposed joint design method achieves a tradeoff between the performances of control and power efficiency.

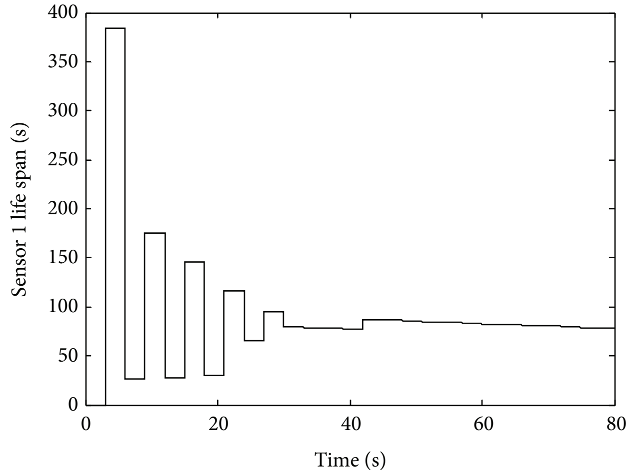

FIGURE 3: Sensor 1 survival time prediction.

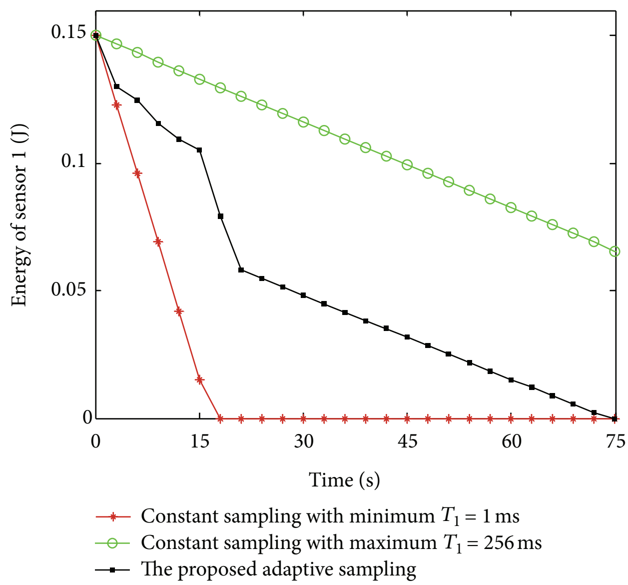

FIGURE 4: Sensor 1 power consumption comparison in three cases.

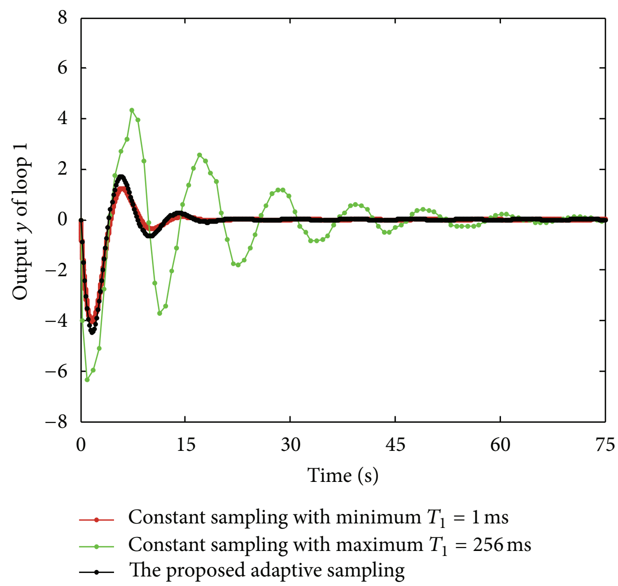

FIGURE 5: Control loop1 output comparison in three cases.

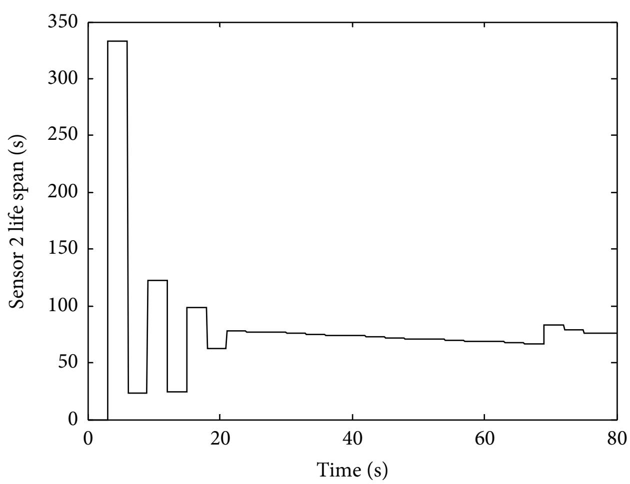

FIGURE 6: Sensor 2 survival time prediction.

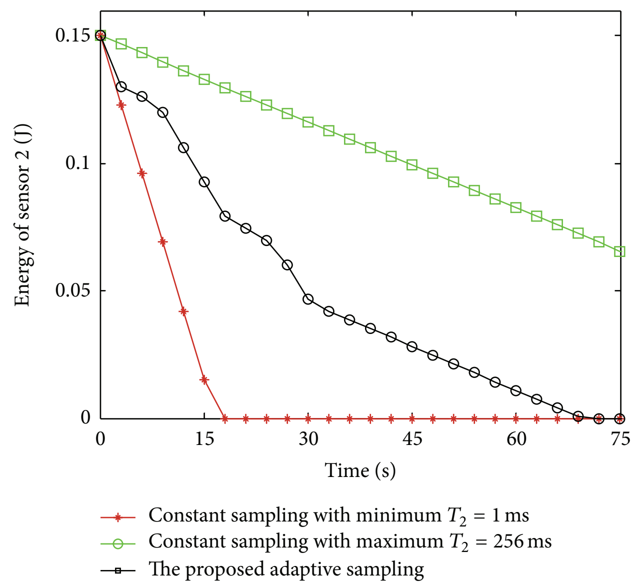

FIGURE 7: Sensor 2 power consumption comparison in three cases.

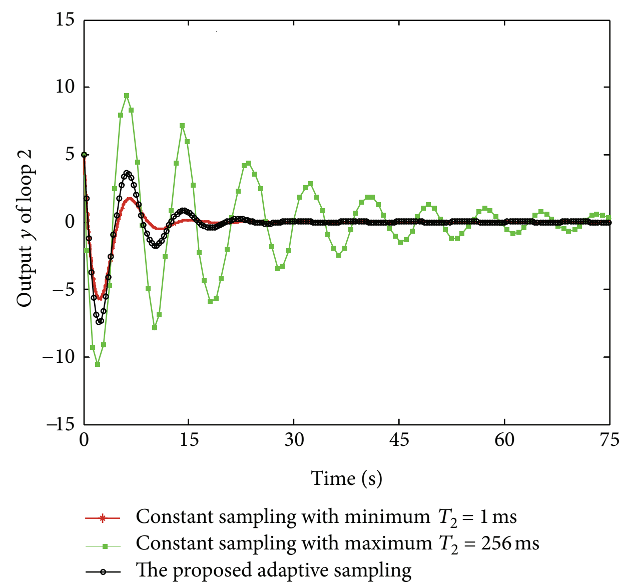

FIGURE 8: Control loop2 output comparison in three cases.

6. Conclusion

This paper presents a joint design method for wireless networked control systems with limited power constraint. A power efficiency algorithm based on the adaptive sampling period is put forward to satisfy the demands of sensor survival time and system stability. Then, the time-varying control system with transmission delay is modeled as a switched system with uncertain switching signals. A dwell-time-dependent control method is discussed to guarantee the stability of WNCS. Simulation results show the effectiveness of the proposed method and indicate that it can achieve good tradeoff performance. Methods by which to reduce power consumption from the aspect of a single node as well as balancing power consumption from the global network perspective are worthy of further exploration.

Conflict of Interests

The authors declare that there is no conflict of interests regarding the publication of this paper.

Acknowledgments

The working is sponsored by The NSFC (no. 61202473) and The Natural Science Foundation of Jiangsu Province (no. BK2012551).

References

[1] W. Dieterle, H. D. Kochs, and E. Dittmar, "Communication architectures for distributed computer control systems," *Control Engineering Practice*, vol. 3, no. 8, pp. 1171–1176, 1995.

[2] H. A. Thompson, "Wireless and Internet communications technologies for monitoring and control," *Control Engineering Practice*, vol. 12, no. 6, pp. 781–791, 2004.

[3] P. R. Kumar, "New technological vistas for systems and control," *IEEE Control Systems Magazine*, vol. 21, no. 1, pp. 24–37, 2001.

[4] X. Liu and A. Goldsmith, "Wireless medium access control in networked control systems," in *Proceedings of the American Control Conference (AAC '04)*, pp. 3605–3610, Boston, Mass, USA, July 2004.

[5] J. Colandairaj, G. W. Irwin, and W. G. Scanlon, "Wireless networked control systems with QoS-based sampling," *IET Control Theory and Applications*, vol. 1, no. 1, pp. 430–438, 2007.

[6] N. Israr, W. G. Scanlon, and G. W. Irwin, "A cross-layer communication framework for wireless networked control systems," in *Proceedings of the 1st International Conference on Wireless Communication, Vehicular Technology, Information Theory and Aerospace and Electronic Systems Technology (VITAE '09)*, pp. 577–581, Aalborg, Denmark, May 2009.

[7] S. Dai, H. Lin, and S. S. Ge, "Scheduling-and-control codesign for a collection of networked control systems with uncertain delays," *IEEE Transactions on Control Systems Technology*, vol. 18, no. 1, pp. 66–78, 2010.

[8] A. V. Savkin, "Analysis and synthesis of networked control systems: topological entropy, observability, robustness and optimal control," *Automatica*, vol. 42, no. 1, pp. 51–62, 2006.

[9] J. Z. Luo, F. Dong, and J. X. Cao, "A novel task scheduling algorithm based on dynamic critical path and effective duplication for pervasive computing environment," *Wireless Communications & Mobile Computing*, vol. 10, no. 10, pp. 1283–1302, 2010.

[10] X. Yin, X. Zhou, Z. Li, and S. Li, "Jint rate control and power control for lifetime maximization in Wreless Sensor Ntworks," *Journal of Internet Technology*, vol. 12, no. 1, pp. 69–78, 2011.

[11] M. Pajic, S. Sundaram, G. J. Pappas, and R. Mangharam, "The wireless control network: a new approach for control over networks," *IEEE Transactions on Automatic Control*, vol. 56, no. 10, pp. 2305–2318, 2011.

[12] J. Colandairaj, G. W. Irwin, and W. G. Scanlon, "A co-design solution for wireless feedback control," in *Proceeding of the International Conference on Networking, Sensing and Control (ICNSC '07)*, pp. 404–409, London, UK, April 2007.

[13] W. Liang and Y. Yang, "Maximizing battery life routing in wireless ad hoc networks," in *Proceedings of the 37th International Conference on System Sciences*, pp. 4739–4746, IEEE, Honolulu, Hawaii, USA, January 2004.

[14] K. Brian, J. Haberman, and W. Sheppard, *Overlapping Particle Swarms for Energy-Efficient Routing in Sensor Networks*, Wireless Network, Springer, 2011.

[15] D. Kim, K. Dantu, and M. Pedram, "Lifetime prediction routing in mobile Ad Hoc networks," in *Proceedings of the IEEE Wireless Communication and Networking Conference*, New York, NY, USA, 2003.

[16] L. Hetel, J. Daafouz, and C. Iung, "Stability analysis for discrete time switched systems with temporary uncertain switching signal," in *Proceedings of the 46th IEEE Conference on Decision and Control (CDC '07)*, pp. 5623–5628, New Orleans, Fla, USA, December 2007.

[17] S. Limin, *Wireless Sensor Network*, Tsinghua University Press, Beijing, China, 2006.

[18] Y. He, I. Lee, and L. Guan, "Distributed algorithms for network lifetime maximization in wireless visual sensor networks," *IEEE Transactions on Circuits and Systems for Video Technology*, vol. 19, no. 5, pp. 704–718, 2009.

[19] B. A. Bakr and L. Lilien, "A quantitative comparison of energy consumption and WSN lifetime for LEACH and LEACH-SM," in *Proceedings of the 31st International Conference on Distributed Computing Systems Workshops (ICDCSW '11)*, pp. 182–191, Minneapolis, Minn, USA, June 2011.

[20] C. Fischione, A. Bonivento, A. Sangiovanni-Vincentelli, F. Santucci, and K. H. Johansson, "Performance analysis of collaborative spatio-temporal processing for wireless sensor networks," in *Proceedings of the 3rd IEEE Consumer Communications and Networking Conference (CCNC '06)*, pp. 325–329, Las Vegas, Nev, USA, January 2006.

[21] Y. Iino, "Some considerations of wireless sensor network based control systems," in *Proceedings of the SICE Conference on Control Systems (CCS '07)*, Tokyo, Japan, 2007.

[22] Y. Iino, T. Hatanaka, and M. Fujita, "Event-predictive control for energy saving of wireless networked control system," in *Proceedings of the American Control Conference (ACC '09)*, pp. 2236–2242, St. Louis, Mo, USA, June 2009.

Hindawi Publishing Corporation
Mathematical Problems in Engineering
Volume 2014, Article ID 947164, 6 pages
http://dx.doi.org/10.1155/2014/947164

Research Article

Asymptotic Stabilization of Continuous-Time Linear Systems with Input and State Quantizations

Sung Wook Yun,[1] Sung Hyun Kim,[2] and Jin Young Park[1]

[1] *Technology Convergence R&BD Group, Korea Institute of Industrial Technology, Yuga-myeon, Dalseong-gun, Daegu 711-880, Republic of Korea*
[2] *Department of Electrical Engineering, University of Ulsan (UOU), Ulsan 680-749, Republic of Korea*

Correspondence should be addressed to Sung Hyun Kim; shnkim@ulsan.ac.kr

Received 5 May 2014; Revised 8 July 2014; Accepted 8 July 2014; Published 22 July 2014

Academic Editor: Xi-Ming Sun

This paper discusses the asymptotic stabilization problem of linear systems with input and state quantizations. In order to achieve asymptotic stabilization of such systems, we propose a state-feedback controller comprising two control parts: the main part is used to determine the fundamental characteristics of the system associated with the cost, and the additional part is employed to eliminate the effects of input and state quanizations. In particular, in order to implement the additional part, we introduce a quantizer with a region-decision making process (RDMP) for a certain linear switching surface. The simulation results show the effectiveness of the proposed controller.

1. Introduction

In the field of control systems, quantized feedback systems have attracted considerable attention because quantization errors in actuators and sensors have adverse effects on the general performance of systems; for example, they can affect the transient response, steady-state response, or stability. Among early studies on quantization, [1] studied the effect of quantization in a sampled data system, and [2] studied least-mean-squares state estimation in the presence of quantized outputs. More recently, many studies have focused on stabilization of quantized systems and can be divided into three branches: measurement quantization, input quantization, and combined quantization. The authors of [3–12] considered measurement (state or output) quantization. In [7, 8, 13–17], input quantization was considered. In addition, the authors of [18–24] handled both input and state (or output) quantizations.

In the framework of combined quantization, in particular, there are two main approaches for asymptotic stability of quantized feedback systems. The first approach is to employ logarithmic quantizers [23, 24]. Based on the assumption that logarithmic quantizers have an infinite number of quantization levels, [23] designed a guaranteed cost controller and [24] presented model predictive control of linear systems. However, it was practically difficult to achieve asymptotic stability in [23, 24] without the above assumption. The second approach is to employ quantizers with adjustable sensitivity (or zoom variable) [18, 21]. Based on the assumptions that the sensitivity can be changed dynamically and it approaches zero as time passes, [18, 21] achieved asymptotic stability. However, in the case of a finite set of possible values for the sensitivity, asymptotic stability could not be achieved. To the best of our knowledge, in the framework of combined quantization, no studies based on simple uniform quantizers have been performed. The goal of this paper is to develop a control policy without the aforementioned assumptions in order to achieve asymptotic stabilization of systems using combined quantization.

This paper deals with the asymptotic stabilization problem of linear systems with uniform input and state quantizations, where the quantization levels of the uniform quantizers are not design parameters but predetermined constants. For asymptotic stabilization of systems with input quantization, the authors in [15–17] proposed a simple yet powerful concept that required the exact state information in order to eliminate the effect of input quantization. Since the quantized state information rather than the exact state information was measurable in systems with state quantization, they could not handle systems with state quantization. However, this paper extends the previous studies to linear systems with not only input quantization, but also state quantization. In other words, to achieve asymptotic stabilization of such systems, we propose a state-feedback controller. Like the controllers in [15–17], the proposed controller consists of main and additional control parts. The former is responsible for determining the fundamental characteristics of the system associated with the cost and the latter is responsible for simultaneously eliminating the effects of input and state quantizations. Here, since each component of the latter part is designed as an integer multiple of the input quantization level, the decreasing property of a Lyapunov function associated with the cost can be maintained. In particular, in order to implement the latter part, we introduce a quantizer with a region-decision making process (RDMP), where the RDMP plays the role of determining where the state is located with respect to a certain linear switching surface. As mentioned above, since this paper focuses on asymptotic stabilization of linear systems using combined quantization rather than on communication constraints such as the communication rate and the channel capacity, it is not directly related to control with limited information but is included in the framework of combined quantization. The main contribution of this paper is the design of a novel RDMP quantizer-based state-feedback controller that achieves asymptotic stability for quantized feedback systems. Further, the merit of the proposed controller is that asymptotic stability can be achieved regardless of the assumptions such as adjustable sensitivity and an infinite number of quantization levels.

This paper is organized as follows. Section 2 provides a system description. Section 3 introduces an RDMP quantizer and a state-feedback controller for linear systems with input and state quantizations. Section 4 presents some simulation results for validating the proposed controller. Finally, Section 5 presents the conclusion along with a summary. The notations in this paper are consistent with those in [16] with the following additional notations. $\mathrm{sgn}(\sigma)$ is the sign of a scalar σ. For $x \in \mathbf{R}^n$, $[x]_i$ denotes the ith component of x. The inner product of x and y is denoted as $\langle x, y\rangle = x^T y$. Further, e_i is a unit vector with the ith nonzero entry; that is, $e_i \triangleq [0 \cdots \underbrace{1}_{i\text{th}} \cdots 0]^T$.

2. System Description

Consider the following continuous-time linear system with input and state quantizations:

$$\dot{x}(t) = Ax(t) + BQ_u(u(t)), \qquad u(t) = f(Q_x(x(t))), \tag{1}$$

where $x(t) \in \mathbf{R}^n$, $u(t) \in \mathbf{R}^m$, and $f(\cdot)$ are the state, control input, and mapping function from R^n to R^m, respectively. Further, the midtread uniform quantization operators $Q_u(\cdot)$ and $Q_x(\cdot)$ with respect to $u(t)$ and $x(t)$ are defined as

$$\begin{aligned} Q_u(u(t)) &\triangleq \varepsilon_u \text{ round}\left(\frac{u(t)}{\varepsilon_u}\right), \\ Q_x(x(t)) &\triangleq \varepsilon_x \text{ round}\left(\frac{x(t)}{\varepsilon_x}\right), \end{aligned} \tag{2}$$

where round$(\cdot)$ is a function that rounds to the nearest integer. Hereafter, we refer to the fixed values $\varepsilon_u(>0)$ and $\varepsilon_x(>0)$ as *quantizing levels* with respect to $u(t)$ and $x(t)$, respectively. Since this paper focuses on the steady-state performance (asymptotic stabilization) rather than the saturation level of the uniform quantizers, we assume that the saturation levels are sufficiently large. Based on this assumption, we note that the quantization errors $\nabla u(t)$ and $\nabla x(t)$ are defined as

$$\nabla u(t) \triangleq Q_u(u(t)) - u(t), \qquad \nabla x(t) \triangleq Q_x(x(t)) - x(t), \tag{3}$$

where each component of $\nabla u(t)$ and $\nabla x(t)$ at time t is bounded by $\varepsilon_u/2$ and $\varepsilon_x/2$, respectively; that is,

$$\|\nabla u(t)\|_\infty \le \frac{\varepsilon_u}{2}, \qquad \|\nabla x(t)\|_\infty \le \frac{\varepsilon_x}{2}. \tag{4}$$

3. Main Results

Before providing a state-feedback controller that can achieve asymptotic stabilization of system (1), let us first consider the following linear system:

$$\dot{x}(t) = Ax(t) + Bu(t), \qquad u(t) = Kx(t). \tag{5}$$

In addition to (5), choose the following cost:

$$\mathcal{J}(t) \triangleq \int_t^\infty \left\{x^T(\tau)\mathcal{Q}x(\tau) + x^T(\tau)K^T\mathcal{R}Kx(\tau)\right\}d\tau, \tag{6}$$

where $\mathcal{Q}$ and $\mathcal{R}$ are positive definite matrices.

Lemma 1. *For linear system* (5) *without input and state quantizations, suppose that there exist a symmetric positive definite matrix $\overline{P}$, a matrix $\overline{K}$, and a positive scalar γ such that*

$$0 > \begin{bmatrix} A\overline{P} + \overline{P}A^T + B\overline{K} + \overline{K}^T B^T & \overline{P} & \overline{K}^T \\ \overline{P} & -\mathcal{Q}^{-1} & 0 \\ \overline{K} & 0 & -\mathcal{R}^{-1} \end{bmatrix}, \tag{7}$$

$$0 < \begin{bmatrix} \gamma & x^T(0) \\ x(0) & \overline{P} \end{bmatrix}. \tag{8}$$

Then, the controller can be constructed as $u(t) = Kx(t)$, which makes the state $x(t)$ converge to the origin asymptotically, where $K \triangleq \overline{K}\,\overline{P}^{-1}$. Further, in order to obtain the minimum upper bound of the cost in (6)*, we minimize γ subject to* (7) *and* (8).

Proof. Consider the Lyapunov candidate $V(x(t)) = x^T(t)Px(t)$ with a positive definite matrix $P(=\overline{P}^{-1})$; $\dot{V}(x(t)) = 2x^T$

$(t)P(A + BK)x(t)$. If we assume that the upper bound of the cost in (6) is defined by the Lyapunov equation, then

$$\mathcal{J}(t) = \int_t^\infty \left\{x^T(\tau)\mathcal{Q}x(\tau) + x^T(\tau)K^T\mathcal{R}Kx(\tau)\right\}d\tau < V(x(t)). \quad (9)$$

This is ensured if $\dot{V}(x(t)) < \dot{\mathcal{J}}(t)$ holds when $\mathcal{J}(\infty) = V(x(\infty)) = 0$, which results in the relation

$$0 > PA + A^TP + PBK + K^TB^TP + \mathcal{Q} + K^T\mathcal{R}K. \quad (10)$$

Before and after multiplying both sides of (10) by $\overline{P}$ and using the Schur complement technique, we obtain (7). Relation (8) implies that $\mathcal{J}(0) < V(x(0)) = x^T(0)Px(0) \le \gamma$. □

Now, based on the solutions obtained from Lemma 1, we can construct a state-feedback controller for system (1) as

$$u(t) = f(Q_x(x(t))) + \overline{u}(t) = KQ_x(x(t)) + \overline{u}(t), \quad (11)$$

where $KQ_x(x(t))$ is the main control part used to achieve goals such as linear quadratic (LQ) regulation and pole assignment, and $\overline{u}(t)$ is the additional control part to simultaneously handle the input and state quantization errors. Here, we choose each component of $\overline{u}(t)$ to be the integer multiple of the input quantizing level ε_u, which results in the relation $Q_u(u(t)) = Q_u(KQ_x(x(t)) + \overline{u}(t)) = Q_u(KQ_x(x(t))) + \overline{u}(t)$. This relation enables us to divide the role of the controller in (11) into two parts: the main control part responsible for determining the fundamental characteristics of the system associated with the cost and the additional control part responsible for eliminating the effects of input and state quantizations.

The authors in [15–17] proposed a novel concept for asymptotic stabilization of systems with input quantization; however, since the exact state information is necessary to eliminate the effect of quantization, they could not handle systems with state quantization. To achieve asymptotic stabilization of systems with input and state quantizations, we introduce an RDMP quantizer that enables us to achieve the goal by using the quantized state information as follows. The overall closed-loop system to be considered is shown in Figure 1(a), where a midtread uniform quantizer $Q_u(\cdot)$ and an RDMP quantizer are employed in the input side and the state side, respectively. As described in Figure 1(b), the RDMP quantizer comprises a midtread uniform quantizer $Q_x(\cdot)$, a register, and the RDMP, where, based on the matrix P obtained from Lemma 1, the register stores PB. With respect to a linear switching surface $e_i^TB^TPx(t) = 0$, the RDMP plays the role of determining whether the state $x(t)$ lies in the region $\Omega_p = \{x(t) \mid e_i^TB^TPx(t) \ge 0\}$ or $\Omega_n = \{x(t) \mid e_i^TB^TPx(t) < 0\}$. As illustrated in Figure 1(c), the RDMP is designed using a midrise uniform quantizer $\overline{Q}_\eta(\cdot)$, amplifiers, adders, and so on. The operator $\overline{Q}_\eta(\cdot)$ is defined as $[\overline{Q}_\eta(\eta(t))]_i = \overline{Q}_\eta(\eta_i(t)) \triangleq \overline{\varepsilon}\,\{\text{floor}(\eta_i(t)/\overline{\varepsilon}) + 0.5\}$, where $\eta_i(t)$ is the ith component of $\eta(t)$, floor(σ) is the largest integer not greater than a scalar σ, and the fixed value $\overline{\varepsilon}(> 0)$ is a quantizing level. Further, for the sake of convenience, the saturation level of $\overline{Q}_\eta(\cdot)$ is set to ± 1, although it can be set to any value. Thus, the quantized measurement $x_q(t) \in \mathcal{R}^{n+m}$, that is, the output of the RDMP quantizer, is defined as $x_q(t) \triangleq [Q_x(x^T(t))\ \overline{Q}_\eta(\eta^T(t))]^T$, where $\eta(t) \in \mathcal{R}^m$ and $\eta_i(t) = e_i^TB^TPx(t)$. Therefore, the main control part $KQ_x(x(t))$ and the additional control part $\overline{u}(t)$ in (11) can be designed using the quantized measurements $Q_x(x(t))$ and $\overline{Q}_\eta(\eta(t))$, respectively.

Theorem 2. *For system* (1) *with input and state quantizations, suppose that there exist a symmetric positive definite matrix $\overline{P}$, a matrix $\overline{K}$, and a positive scalar γ such that* (7) *and* (8) *hold. Then, based on the RDMP quantizer shown in Figure 1, the controller can be constructed as $u(t) = KQ_x(x(t)) + \overline{u}(t)$ in* (11)*, which makes the state $x(t)$ converge to the origin asymptotically, where $K \triangleq \overline{K}\,\overline{P}^{-1}$ and the ith component of $\overline{u}(t)$ can be designed as*

$$\overline{u}_i(t) \triangleq -\varepsilon_u N \operatorname{sgn}\left(\overline{Q}_\eta(\eta_i(t))\right), \quad (12)$$

$N \triangleq \lceil(\varepsilon_u/2 + \varepsilon_x/2 \cdot \|e_i^TK\|_1)/\varepsilon_u\rceil$, $\eta_i(t) = e_i^TB^TPx(t)$, $P \triangleq \overline{P}^{-1}$, and the operator $\lceil\sigma\rceil$ is the smallest integer not less than a scalar σ. Further, in order to obtain the minimum upper bound of the cost in (6)*, we minimize γ subject to* (7) *and* (8).

Proof. Based on (3) and (11), the closed-loop system can be described as

$$\dot{x}(t) = (A + BK)x(t) + B(\overline{u}(t) + \nabla u(t) + K\nabla x(t)). \quad (13)$$

Let us consider the Lyapunov candidate $V(x(t)) = x^T(t)Px(t)$ with a positive definite matrix $P(=\overline{P}^{-1})$. Then, it follows that $\dot{V}(x(t)) = 2x^T(t)P(A + BK)x(t) + 2x^T(t)PB(\overline{u}(t) + \nabla u(t) + K\nabla x(t))$. From (4) and (12), the second term of $\dot{V}(x(t))$ becomes negative as follows:

$$\begin{aligned} &2x^T(t)PB(\overline{u}(t) + \nabla u(t) + K\nabla x(t)) \\ &= \sum_{i=1}^m 2x^T(t)PBe_i\left(\overline{u}_i(t) + e_i^T\nabla u(t) + e_i^TK\nabla x(t)\right) \\ &\le \sum_{i=1}^m \left\{2x^T(t)PBe_i\left(-\varepsilon_u N\operatorname{sgn}\left(e_i^TB^TPx(t)\right)\right)\right. \\ &\qquad\left. + \left|2x^T(t)PBe_i\right|\left(\frac{\varepsilon_u}{2} + \frac{\varepsilon_x}{2}\cdot\left\|e_i^TK\right\|_1\right)\right\} \\ &\le \sum_{i=1}^m \left\{-2\varepsilon_u N\left|e_i^TB^TPx(t)\right| + 2\varepsilon_u N\left|e_i^TB^TPx(t)\right|\right\} = 0, \end{aligned} \quad (14)$$

where $|e_i^TK\nabla x(t)| \le \|e_i^TK\|_1\|\nabla x(t)\|_\infty$, $\varepsilon_u/2 + \varepsilon_x/2 \cdot \|e_i^TK\|_1 \le \varepsilon_u N$, and $\operatorname{sgn}(\overline{Q}_\eta(e_i^TB^TPx(t))) = \operatorname{sgn}(e_i^TB^TPx(t))$, since $\overline{Q}_\eta(\cdot)$ is the midrise uniform quantizer. Therefore, $\dot{V}(x(t))$ can be rewritten as $\dot{V}(x(t)) \le 2x^T(t)P(A+BK)x(t)$. Finally, as shown in the proof of Lemma 1, if (7) and (8) hold, then $\mathcal{J}(0) <$

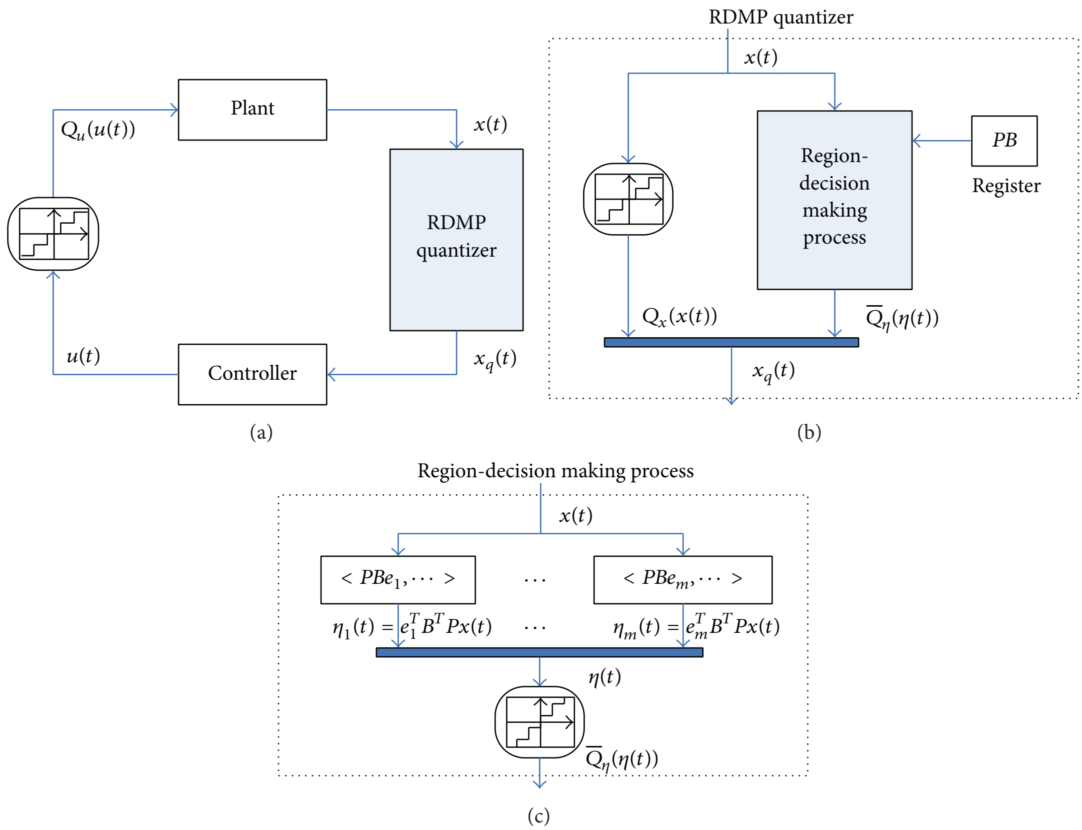

Figure 1: (a) Quantized feedback system; (b) RDMP quantizer; (c) region-decision making process in the RDMP quantizer.

$V(x(0)) = x^T(0)Px(0) \leq \gamma$. For more details, refer to the proof of Lemma 1. □

As shown in the proof of Theorem 2, we design $\overline{u}(t)$ as in (12) in order to eliminate the energy in the sense of Lyapunov caused by $\nabla u(t)$ and $\nabla x(t)$ and to maintain the decreasing property of a Lyapunov function associated with the cost. However, the chattering phenomenon may be caused by the proposed controller since the main control part employs $Q_x(x(t))$ and $\overline{u}(t)$ employs $\operatorname{sgn}(\sigma)$. In order to alleviate the chattering phenomenon without significant performance degradation, the continuous function $\tanh(\beta\sigma)$ can be employed in (12) instead of $\operatorname{sgn}(\sigma)$ [25]. Then, $\dot{V}(x(t))$ may not be negative for small σ. However, for any given δ, there exists a sufficiently large $\beta > 0$ such that $\dot{V}(x(t)) < 0$ for $|\sigma| > \delta$, and all trajectories enter the strip $|\sigma| < \delta$. This approximation steers the state into a neighborhood of $x(t) = 0$, and the size of the neighborhood shrinks as $\beta \to \infty$; on the other hand, as $\beta \to \infty$, the chattering phenomenon increases. That is, β is a trade-off parameter between the steady-state performance and the chattering phenomenon so that the maximum β in the practically allowable range is chosen.

Remark 3. The feature of this paper is that asymptotic stabilization of system (1) with input and state quantizations can be achieved even though coarse quantizers with large ε_x and ε_u are used instead of fine quantizers. Therefore, since we employ finite-level coarse quantizers with sufficiently large quantizing levels that enable us to avoid saturation, the assumption in Section 2 that the saturation levels of the quantizers are sufficiently large is indeed reasonable.

Remark 4. Here, a remarkable point is that if the information transmitted from the RDMP quantizer to the controller does not contain the sign of $\eta_i(t) = e_i^T B^T Px(t)$ but the information quantized by a midtread quantizer, it is almost impossible to completely reconstruct the sign of $\eta_i(t)$ on the controller side due to the presence of its quantization errors. Thus, it is certainly more desirable to transmit the sign of $\eta_i(t)$ to the controller side, instead of its quantized value. For this purpose, this paper has used the two regions $\Omega_p = \{x(t) \mid e_i^T B^T Px(t) \geq 0\}$ and $\Omega_n = \{x(t) \mid e_i^T B^T Px(t) < 0\}$ in the RDMP, which play an important role in determining the sign of $\eta_i(t) = e_i^T B^T Px(t)$. As a result, based on the sign assigned with the help of the two regions, we obtain the following relation:

$$\operatorname{sgn}\left(\overline{Q}_\eta\left(e_i^T B^T Px(t)\right)\right) = \operatorname{sgn}\left(e_i^T B^T Px(t)\right). \tag{15}$$

The above relation enables us to eliminate the energy in the sense of Lyapunov caused by $\nabla u(t)$ and $\nabla x(t)$.

Table 1: $\|x(t)\|_2$ in the steady state for different ε_x. ($\varepsilon_u = 1$).

ε_x	1	10^{-1}	10^{-2}	10^{-3}
Type-1	0.709	0.708×10^{-1}	0.505×10^{-1}	0.514×10^{-1}
Type-2	Up to a numerical precision $\simeq 10^{-5}$			

Table 2: $\|x(t)\|_2$ in the steady state for different ε_u. ($\varepsilon_x = 1$).

ε_u	1	10^{-1}	10^{-2}	10^{-3}
Type-1	0.709	0.705	0.704	0.704
Type-2	Up to a numerical precision $\simeq 10^{-5}$			

4. Simulation Results

In this section, we discuss the performance of the following three types of controllers: Type-1 controller is (11) with $\overline{u}_i(t) = 0$, Type-2 controller is (11) with $\overline{u}_i(t) = -\varepsilon_u N \operatorname{sgn}(\overline{Q}_\eta(\eta_i(t)))$, and Type-3 controller is (11) with $\overline{u}_i(t) = -\varepsilon_u N \tanh(\beta \overline{Q}_\eta(\eta_i(t)))$. The system parameters are given as follows: for $x(0) = [3 \quad 1]^T$, $\mathcal{Q} = I$, $\mathcal{R} = 0.01$, $\bar{\varepsilon} = 0.5$, $\beta = 1.1$,

$$A = \begin{bmatrix} 0 & 1 \\ -2 & 3 \end{bmatrix}, \qquad B = \begin{bmatrix} 0 \\ 1 \end{bmatrix}, \qquad \varepsilon_u = 1, \qquad \varepsilon_x = 0.1. \tag{16}$$

The solutions calculated using the Matlab 7.0.4 LMI toolbox are as follows:

$$P = \begin{bmatrix} 1.2021 & 0.0820 \\ 0.0820 & 0.1420 \end{bmatrix}, \qquad K = \begin{bmatrix} -8.1716 \\ -14.1610 \end{bmatrix}^T, \qquad N = 2, \tag{17}$$

and the minimized γ is 11.4534. Figure 2 illustrates the trajectories of the states for each controller, and Figure 3 shows $\|x(t)\|_2$ on a logarithmic scale. As shown in Figures 2 and 3, in the case of Type-1 controller, the state does not converge to the origin and remains around a certain region. However, in the case of Type-2 controller, the state converges to the origin asymptotically. Further, Tables 1 and 2 present $\|x(t)\|_2$ in the steady state for different values of ε_x and ε_u, respectively. As shown in the tables, in the case of Type-1 controller, $\|x(t)\|_2$ converges to a certain value due to the effects of input and state quantizations; however, in the case of Type-2 controller, $\|x(t)\|_2$ converges to zero (almost within the numerical precision $\simeq 10^{-5}$). That is, from the tables, we can clearly see that Type-2 controller achieves asymptotic stability for each of given ε_x and ε_u. Figures 3 and 4 show that Type-3 controller using $\tanh(\beta\sigma)$ in $\overline{u}(t)$ can alleviate the chattering phenomenon of Type-2 controller without significant performance degradation.

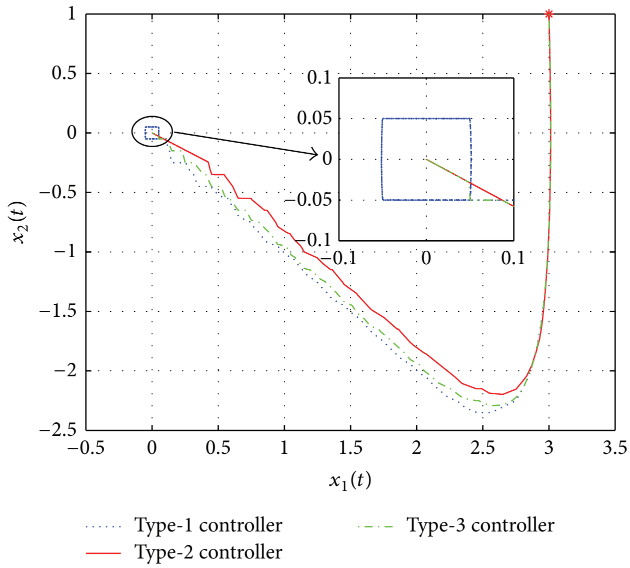

Figure 2: The trajectories of the states.

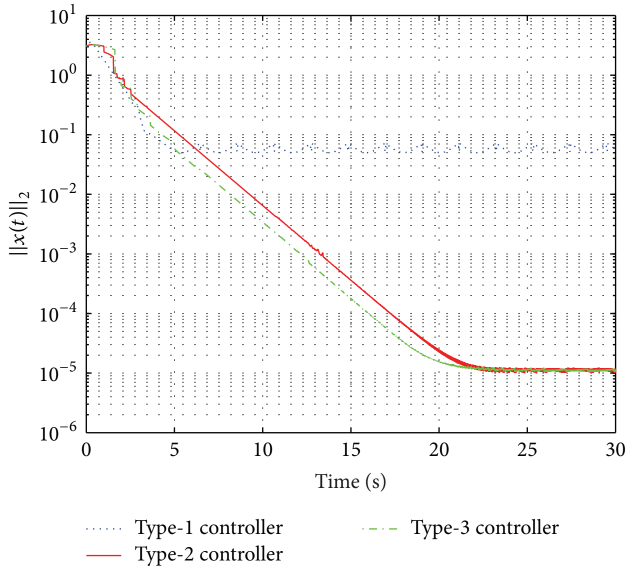

Figure 3: $\|x(t)\|_2$ on a logarithmic scale.

5. Conclusion

This paper addressed the asymptotic stabilization problem of linear systems with input and state quantizations. In order to achieve asymptotic stabilization of such systems, a state-feedback controller was proposed. For implementing the proposed controller, we introduced the RDMP quantizer that enabled us to eliminate the effects of input and state quantizations without the use of the exact state information and did not require assumptions such as adjustable sensitivity or an infinite number of quantizing levels. As shown in the simulation results, in the case of Type-1 controller, the state did not converge to the origin; however, in the case of Type-2 controller, the state converged to the origin despite input and state quantizations. Further, Type-3 controller alleviated the chattering phenomenon of Type-2 controller without significant performance degradation.

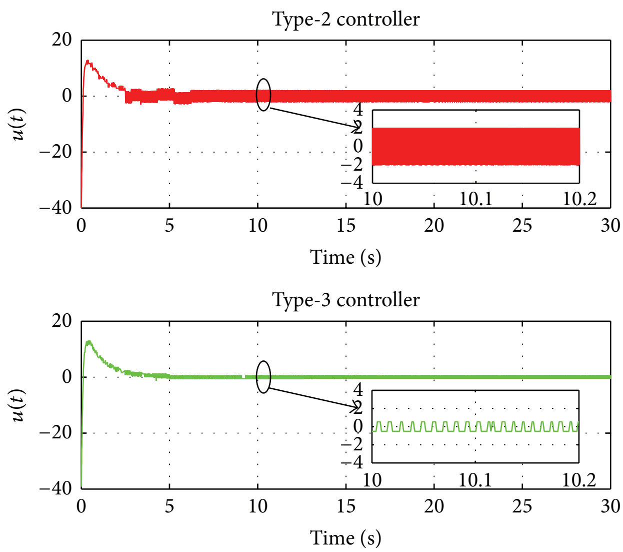

Figure 4: The trajectories of the inputs.

Conflict of Interests

The authors declare that there is no conflict of interests regarding the publication of this paper.

Acknowledgment

This work was supported by 2014 Research Funds of Hyundai Heavy Industries for University of Ulsan.

References

[1] R. E. Kalman, "Nonlinear aspects of sampled-data control systems," in *Proceedings of the Symposium on Nonlinear Circuit Theory*, pp. 273–313, Brooklyn, NY, USA, 1956.

[2] R. E. Curry, *Estimation and Control with Quantized Measurements*, MIT Press, Cambridge, Mass, USA, 1970.

[3] R. W. Brockett and D. Liberzon, "Quantized feedback stabilization of linear systems," *IEEE Transactions on Automatic Control*, vol. 45, no. 7, pp. 1279–1289, 2000.

[4] M. L. Corradini and G. Orlando, "Robust quantized feedback stabilization of linear systems," *Automatica*, vol. 44, no. 9, pp. 2458–2462, 2008.

[5] D. F. Delchamps, "Stabilizing a linear system with quantized state feedback," *IEEE Transactions on Automatic Control*, vol. 35, no. 8, pp. 916–924, 1990.

[6] N. Elia and S. K. Mitter, "Stabilization of linear systems with limited information," *IEEE Transactions on Automatic Control*, vol. 46, no. 9, pp. 1384–1400, 2001.

[7] M. Fu and L. Xie, "The sector bound approach to quantized feedback control," *IEEE Transactions on Automatic Control*, vol. 50, no. 11, pp. 1698–1711, 2005.

[8] M. Fu and L. Xie, "Quantized feedback control for linear uncertain systems," *International Journal of Robust and Nonlinear Control*, vol. 20, no. 8, pp. 843–857, 2010.

[9] H. Ishii and T. Başar, "Remote control of LTI systems over networks with state quantization," *Systems & Control Letters*, vol. 54, no. 1, pp. 15–31, 2005.

[10] L. A. Montestruque and P. J. Antsaklis, "Static and dynamic quantization in model-based networked control systems," *International Journal of Control*, vol. 80, no. 1, pp. 87–101, 2007.

[11] C. Peng and Y. Tian, "Networked H_∞ control of linear systems with state quantization," *Information Sciences*, vol. 177, no. 24, pp. 5763–5774, 2007.

[12] S. Wang, M. Yu, H. Wang, and W. Tan, "Switched quantization level control of networked control systems with packet dropouts," *Mathematical Problems in Engineering*, vol. 2014, Article ID 890543, 8 pages, 2014.

[13] Y. J. Choi, S. W. Yun, and P. Park, "Asymptotic stabilisation of system with finite-level logarithmic quantiser," *Electronics Letters*, vol. 44, no. 19, pp. 1117–1119, 2008.

[14] H. Gao and T. Chen, "A new approach to quantized feedback control systems," *Automatica*, vol. 44, no. 2, pp. 534–542, 2008.

[15] P. Park, Y. J. Choi, and S. W. Yun, "Eliminating effect of input quantisation in linear systems," *Electronics Letters*, vol. 44, no. 7, pp. 456–457, 2008.

[16] S. W. Yun, Y. J. Choi, and P. Park, "$\mathscr{H}_2$ control of continuous-time uncertain linear systems with input quantization and matched disturbances," *Automatica*, vol. 45, no. 10, pp. 2435–2439, 2009.

[17] S. W. Yun, Y. J. Choi, and P. Park, "Dynamic output-feedback guaranteed cost control for linear systems with uniform input quantization," *Nonlinear Dynamics*, vol. 62, no. 1-2, pp. 95–104, 2010.

[18] D. Liberzon, "Hybrid feedback stabilization of systems with quantized signals," *Automatica*, vol. 39, no. 9, pp. 1543–1554, 2003.

[19] B. Picasso and A. Bicchi, "On the stabilization of linear systems under assigned I/O quantization," *IEEE Transactions on Automatic Control*, vol. 52, no. 10, pp. 1994–2000, 2007.

[20] J. Raisch, "Simple hybrid control systems-continuous FDLTI plants with quantized control inputs and symbolic measurements," in *Proceedings of the llth International Conference on Analysis and Optimization of Systems*, G. Cohen and J-P. Quadrat, Eds., vol. 199 of *Lecture Notes in Computer Science*, pp. 359–376, Springer, Sophia-Antipolis, France, 1994.

[21] E. Tian, D. Yue, and C. Peng, "Quantized output feedback control for networked control systems," *Information Sciences*, vol. 178, no. 12, pp. 2734–2749, 2008.

[22] W. S. Wong and R. W. Brockett, "Systems with finite communication bandwidth constraints - II: stabilization with limited information feedback," *IEEE Transactions on Automatic Control*, vol. 44, no. 5, pp. 1049–1053, 1999.

[23] D. Yue, C. Peng, and G. Y. Tang, "Guaranteed cost control of linear systems over networks with state and input quantisations," *IEE Proceedings: Control Theory and Applications*, vol. 153, no. 6, pp. 658–664, 2006.

[24] X. Tang, H. Qu, H. Xie, and P. Wang, "Model predictive control of linear systems over networks with state and input quantizations," *Mathematical Problems in Engineering*, vol. 2013, Article ID 492804, 8 pages, 2013.

[25] H. G. Kwatny, C. Teolis, and M. Mattice, "Variable structure control of systems with uncertain nonlinear friction," *Automatica*, vol. 38, no. 7, pp. 1251–1256, 2002.

Hindawi Publishing Corporation
Mathematical Problems in Engineering
Volume 2014, Article ID 143938, 11 pages
http://dx.doi.org/10.1155/2014/143938

Research Article

Neighbor Constraint Assisted Distributed Localization for Wireless Sensor Networks

Longfei Wen, Lingguo Cui, Senchun Chai, and Baihai Zhang

School of Automation, Beijing Institute of Technology, Beijing 100081, China

Correspondence should be addressed to Lingguo Cui; cuilingguo@bit.edu.cn

Received 24 April 2014; Accepted 30 May 2014; Published 22 June 2014

Academic Editor: Jinhui Zhang

Localization is one of the most significant technologies in wireless sensor networks (WSNs) since it plays a critical role in many applications. The main idea in most localization methods is to estimate the sensor-anchor distances that are used by sensors to locate themselves. However, the distance information is always imprecise due to the measurement or estimation errors. In this work, a novel algorithm called neighbor constraint assisted distributed localization (NCA-DL) is proposed, which introduces the application of geometric constraints to these distances within the algorithm. For example, in the case presented here, the assistance provided by a neighbor will consist in formulating a linear equality constraint. These constraints can be further used to formulate optimization problems for distance estimation. Then through some optimization methods, the imprecise distances can be refined and the localization precision is improved.

1. Introduction

Wireless sensor networks (WSNs) composed of a large number of low-power sensors have been a subject of increased interest in recent years [1–3]. Location information of sensor nodes is vital for location-aware applications such as environmental monitoring, routing, and coverage control [4, 5]. Due to cost limitations and energy consumption, having each one of the sensors locate its position individually via GPS or other similar means is no longer a viable option. Hence, lots of works have focused on the localization algorithms for WSNs [6].

Based on the type of information they require, localization algorithms can be divided into two categories: (i) range-based and (ii) range-free [7–10]. For both categories of localization algorithms, the most crucial phase of the process lies in the determination of the distances between the sensor nodes which need to be located and the anchors. In range-based algorithms, the respective distances between sensors and anchors can be obtained via various ranging techniques such as time of arrival (TOA), time difference of arrival (TDOA), and received signal strength indication (RSSI). On the other hand, in range-free algorithms, distances can be estimated through topological or geometric information. DV-Hop is a classical distributed range-free algorithm which determines distances by hop counts [11]. By further combination with ranging techniques, DV-Hop can be extended in order to decrease its localization error; a noteworthy example of these methods is robust position [12–14]. However, no matter which method is used, the acquired distances information to the anchors is usually imprecise compared with the true distances because of ranging and estimation errors [15, 16]. The imprecise distances will result in poor localization performance. Actually, these imprecise distances can be refined since the true distances between nodes should satisfy the geometric relations. In other words, the localization precision can be improved with the help of some geometric constraints.

In this work, a novel algorithm called neighbor constraint assisted distributed localization (NCA-DL) is proposed which is effective in refining the distances required for localization. NCA-DL describes the geometric relations among the distances between sensor nodes and anchors as some equality constraints. The core idea behind NCA-DL is to use the *Cayley-Menger determinant* [17, 18] which will be defined in the following section. In NCA-DL, by using an adjacent neighbor which could be a mobile anchor, a linear equality constraint of distance estimation errors can be obtained. Through some optimal solution computation methods that are used to minimize the sum of the squared errors, the distances can be refined and the localization precision can be improved. The major contribution of this paper is twofold. First, the proposed algorithm is distributed so that sensor nodes can estimate their locations by themselves. Second, it introduces the idea of geometric constraints and decreases the distance estimation errors with the help of an adjacent neighbor. In general, the proposed method can largely improve the localization precision.

The layout of the paper is organized as follows. In Section 2, the preliminaries to the problem are introduced. In Section 3, the geometric relations among sensor nodes are formulated as constraints. In Section 4, the proposed distributed localization method will be described in detail. Section 5 presents the implementation and results of the numerical simulations that were performed to validate the method. Finally, conclusion will be drawn from this research in Section 6.

2. Preliminaries

Let us first consider $\{\mathbf{a}_1, \mathbf{a}_2, \dots, \mathbf{a}_n\}$ and $\{\mathbf{b}_1, \mathbf{b}_2, \dots, \mathbf{b}_n\}$ which represent a set of n distinct points, respectively. The *Cayley-Menger matrix* of these two sets can be defined as

$$C(\mathbf{a}_1, \mathbf{a}_2, \dots, \mathbf{a}_n; \mathbf{b}_1, \mathbf{b}_2, \dots, \mathbf{b}_n) \triangleq \begin{pmatrix} d^2(\mathbf{a}_1, \mathbf{b}_1) & d^2(\mathbf{a}_1, \mathbf{b}_2) & \cdots & d^2(\mathbf{a}_1, \mathbf{b}_n) & 1 \\ d^2(\mathbf{a}_2, \mathbf{b}_1) & d^2(\mathbf{a}_2, \mathbf{b}_2) & \cdots & d^2(\mathbf{a}_2, \mathbf{b}_n) & 1 \\ \vdots & \vdots & \ddots & \vdots & \vdots \\ d^2(\mathbf{a}_n, \mathbf{b}_1) & d^2(\mathbf{a}_n, \mathbf{b}_2) & \cdots & d^2(\mathbf{a}_n, \mathbf{b}_n) & 1 \\ 1 & 1 & \cdots & 1 & 0 \end{pmatrix}, \quad (1)$$

where $d(\mathbf{a}_i, \mathbf{b}_j)$; $\forall (i, j) \in \{1, 2, \dots, n\}$ denotes the Euclidean distance between the points $\mathbf{a}_i$ and $\mathbf{b}_j$.

The *Cayley-Menger bideterminant* of these two sequences of n points is defined as

$$D(\mathbf{a}_1, \mathbf{a}_2, \dots, \mathbf{a}_n; \mathbf{b}_1, \mathbf{b}_2, \dots, \mathbf{b}_n) \triangleq \det C(\mathbf{a}_1, \mathbf{a}_2, \dots, \mathbf{a}_n; \mathbf{b}_1, \mathbf{b}_2, \dots, \mathbf{b}_n). \quad (2)$$

The above determinant is widely used in distance geometry theory [17]. When the two sequences of points are the same, $D(\mathbf{a}_1, \mathbf{a}_2, \dots, \mathbf{a}_n; \mathbf{a}_1, \mathbf{a}_2, \dots, \mathbf{a}_n)$ is denoted for convenience by $D(\mathbf{a}_1, \mathbf{a}_2, \dots, \mathbf{a}_n)$ which is simply called a *Cayley-Menger determinant*.

A brief summary of the *Cayley-Menger determinant* is generalized as follows [19].

Theorem 1. *Consider an n-tuple of points $\mathbf{a}_1, \mathbf{a}_2, \dots, \mathbf{a}_n$ in m-dimensional space. If $n \geq m+2$, then the Cayley-Menger matrix $C(\mathbf{a}_1, \mathbf{a}_2, \dots, \mathbf{a}_n)$ is singular, namely,*

$$D(\mathbf{a}_1, \mathbf{a}_2, \dots, \mathbf{a}_n) = 0. \quad (3)$$

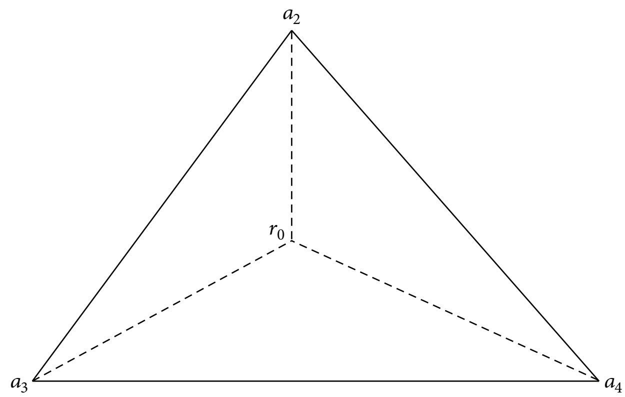

Figure 1: A regular node and the anchors.

Theorem 2 (Theorem 112.1 in Blumenthal [17]). *Consider an n-tuple of points $\mathbf{a}_1, \mathbf{a}_2, \dots, \mathbf{a}_n$ in m-dimensional space. If $n \geq m + 1$, the rank of Cayley-Menger matrix $C(\mathbf{a}_1, \mathbf{a}_2, \dots, \mathbf{a}_n)$ is at most $m + 1$.*

In a 2-dimensional Euclidean space, each node has a set of coordinates (x_i, y_i). The study of the localization problem applied to WSNs first requires some basic terminology and concepts to be defined.

Definition 3 (regular nodes). Most of the nodes in the network do not know their locations. The whole purpose of localization algorithms is to estimate the coordinates of these nodes.

Definition 4 (anchors). Some of the nodes can know their locations through manual placement or with the help of specific equipment such as GPS. The coordinates of these nodes are used as reference information to assist in the localization procedure.

According to the above theorems and definitions, an interesting development of localization is how to use the *Cayley-Menger determinant* to reduce the impact of distance measurement errors [20]. As shown in Figure 1, let $d_{ij} = d(\mathbf{a}_i, \mathbf{a}_j)$ denote the accurate Euclidean distance between anchors $\mathbf{a}_i$ and $\mathbf{a}_j$ with $i \neq j$, $(i, j = 1, 2, 3)$, which can be inferred from known anchor positions; $d_{0i} = d(\mathbf{r}_0, \mathbf{a}_i)$ denotes the accurate distances between the regular node $\mathbf{r}_0$ and node $\mathbf{a}_i$ with $i = 1, 2, 3$ and $\overline{d}_{0i}$ denotes the inaccurate distances acquired by either noisy range measurement or computations. Then the following equation is defined:

$$\overline{d}_{0i}^2 = d_{0i}^2 - \varepsilon_i. \quad (4)$$

Theorem 5. *The errors ε_i for $i = 1, 2, 3$ as defined immediately above satisfy a single algebraic equality which is quadratic though not homogeneous in the ε_i's:*

$$\boldsymbol{\varepsilon}^T \mathbf{A} \boldsymbol{\varepsilon} + \boldsymbol{\varepsilon}^T \mathbf{b} + c = 0, \quad (5)$$

where

$$\boldsymbol{\varepsilon} = [\varepsilon_1, \varepsilon_2, \varepsilon_3]^T$$

$$\mathbf{A} = \begin{pmatrix} 2d_{23}^2 & d_{12}^2 - d_{13}^2 - d_{23}^2 & d_{13}^2 - d_{23}^2 - d_{12}^2 \\ d_{12}^2 - d_{13}^2 - d_{23}^2 & 2d_{13}^2 & d_{23}^2 - d_{12}^2 - d_{13}^2 \\ d_{13}^2 - d_{12}^2 - d_{23}^2 & d_{23}^2 - d_{12}^2 - d_{13}^2 & 2d_{12}^2 \end{pmatrix}$$

$$\begin{aligned} b_1 &= 4d_{23}^2\overline{d}_{01}^2 + 2\left(d_{12}^2 - d_{13}^2 - d_{23}^2\right)\overline{d}_{02}^2 \\ &\quad + 2\left(d_{13}^2 - d_{12}^2 - d_{23}^2\right)\overline{d}_{03}^2 + 2d_{23}^2\left(d_{23}^2 - d_{12}^2 - d_{13}^2\right) \\ b_2 &= 4d_{13}^2\overline{d}_{02}^2 + 2\left(d_{12}^2 - d_{13}^2 - d_{23}^2\right)\overline{d}_{01}^2 \\ &\quad + 2\left(d_{23}^2 - d_{12}^2 - d_{13}^2\right)\overline{d}_{03}^2 + 2d_{13}^2\left(d_{13}^2 - d_{12}^2 - d_{23}^2\right) \\ b_3 &= 4d_{12}^2\overline{d}_{03}^2 + 2\left(d_{13}^2 - d_{12}^2 - d_{23}^2\right)\overline{d}_{01}^2 \\ &\quad + 2\left(d_{23}^2 - d_{12}^2 - d_{13}^2\right)\overline{d}_{02}^2 + 2d_{12}^2\left(d_{12}^2 - d_{13}^2 - d_{23}^2\right) \\ c &= 2d_{12}^2d_{13}^2d_{23}^2 + 2d_{23}^2\overline{d}_{01}^4 + 2d_{13}^2\overline{d}_{02}^4 + 2d_{12}^2\overline{d}_{03}^4 \\ &\quad + 2\left(d_{12}^2 - d_{13}^2 - d_{23}^2\right)\overline{d}_{01}^2\overline{d}_{02}^2 \\ &\quad + 2\left(d_{13}^2 - d_{12}^2 - d_{23}^2\right)\overline{d}_{01}^2\overline{d}_{03}^2 \\ &\quad + 2\left(d_{23}^2 - d_{12}^2 - d_{13}^2\right)\overline{d}_{02}^2\overline{d}_{03}^2 \\ &\quad + 2d_{23}^2\left(d_{23}^2 - d_{12}^2 - d_{13}^2\right)\overline{d}_{01}^2 \\ &\quad + 2d_{13}^2\left(d_{13}^2 - d_{12}^2 - d_{23}^2\right)\overline{d}_{02}^2 \\ &\quad + 2d_{12}^2\left(d_{12}^2 - d_{13}^2 - d_{23}^2\right)\overline{d}_{03}^2. \end{aligned} \tag{6}$$

Proof. According to Theorem 1, we know that $D(\mathbf{r}_0, \mathbf{a}_1, \mathbf{a}_2, \mathbf{a}_3) = 0$, namely,

$$\det \begin{pmatrix} 0 & d_{01}^2 & d_{02}^2 & d_{03}^2 & 1 \\ d_{01}^2 & 0 & d_{12}^2 & d_{13}^2 & 1 \\ d_{02}^2 & d_{12}^2 & 0 & d_{23}^2 & 1 \\ d_{03}^2 & d_{13}^2 & d_{23}^2 & 0 & 1 \\ 1 & 1 & 1 & 1 & 0 \end{pmatrix} = 0. \tag{7}$$

Suppose the anchors are nonlinear, $D(\mathbf{a}_1, \mathbf{a}_2, \mathbf{a}_3) \neq 0$. From (7), the following equation can be derived:

$$\begin{pmatrix} d_{01}^2 & d_{02}^2 & d_{03}^2 & 1 \end{pmatrix} \mathbf{E}^{-1} \begin{pmatrix} d_{01}^2 \\ d_{02}^2 \\ d_{03}^2 \\ 1 \end{pmatrix} = 0, \tag{8}$$

where

$$\mathbf{E} = \begin{pmatrix} 0 & d_{12}^2 & d_{13}^2 & 1 \\ d_{12}^2 & 0 & d_{23}^2 & 1 \\ d_{13}^2 & d_{23}^2 & 0 & 1 \\ 1 & 1 & 1 & 0 \end{pmatrix}. \tag{9}$$

Then according to (4), we can obtain

$$\begin{pmatrix} \overline{d}_{01}^2 + \varepsilon_1 & \overline{d}_{02}^2 + \varepsilon_2 & \overline{d}_{03}^2 + \varepsilon_3 & 1 \end{pmatrix} \mathbf{E}^{-1} \begin{pmatrix} \overline{d}_{01}^2 + \varepsilon_1 \\ \overline{d}_{02}^2 + \varepsilon_2 \\ \overline{d}_{03}^2 + \varepsilon_3 \\ 1 \end{pmatrix} = 0. \tag{10}$$

Multiplying both sides of (10) by the determinant of $\mathbf{E}^{-1}$, we can arrive at (5). This completes the proof. □

3. Geometric Relations with Neighbor Constraint

In this section, we will focus on the geometric relations among the distances between nodes, which can be transformed to an algebraic constraint of the distance estimation errors. At first, we define another basic term.

Definition 6 (neighbors). Each node in WSNs has a communication range. So, for a node i in network, the nodes which can communicate with node i directly are the neighbors of node i.

As shown in Figure 2, $\mathbf{r}(x_0, y_0)$ represents a regular node which needs to be located, $\mathbf{n}(x_1, y_1)$ represents a neighbor of node $\mathbf{r}'$ and $\mathbf{a}_i(x_i, y_i)$ represents the anchors with $i = 2, 3, 4$. Then Let $d_{ij} = d(\mathbf{a}_i, \mathbf{a}_j)$ denote the accurate Euclidean distance between anchors $\mathbf{a}_i$ and $\mathbf{a}_j$ with $i \neq j, i, j = 2, 3, 4$, $d_{1i} = d(\mathbf{n}, \mathbf{a}_i)$ denote the accurate distances between the neighbor node $\mathbf{n}$ and anchor $\mathbf{a}_i$ with $i = 2, 3, 4$, $d_{0i} = d(\mathbf{r}, \mathbf{a}_i)$ denote the accurate distances between the regular node $\mathbf{r}$ and anchor $\mathbf{a}_i$ with $i = 2, 3, 4$, and d_{01} denote the accurate distance between regular node $\mathbf{r}$ and its neighbor node $\mathbf{n}$.

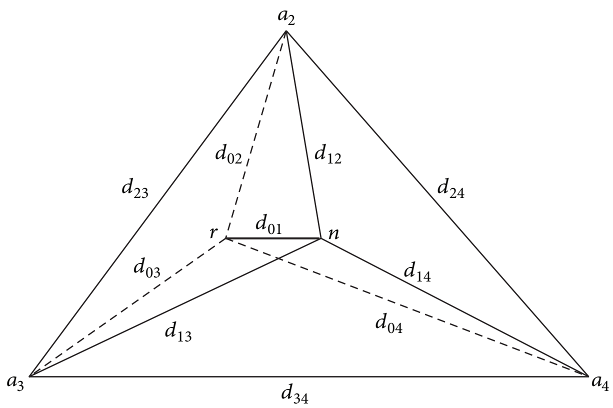

FIGURE 2: Anchors, a regular node, and its neighbor node.

In this case, suppose we know the accurate distances d_{1i} $(i = 2,3,4)$ and the accurate distance d_{01} by refinement or setting node $\mathbf{n}$ as a mobile anchor. Then $\overline{d}_{0i}^2 = d_{0i}^2 - \varepsilon_i$ denote the inaccurate distances squared between node $\mathbf{r}$ and anchor $\mathbf{a}_i$ with $i = 2,3,4$ for some error ε_i. That is to say, the true distances represented by the dotted line in Figure 2 cannot be obtained. In this work, we aim to refine these inaccurate distances to trend toward actual values.

Theorem 7. *The errors ε_i for $i = 2,3,4$ as defined immediately above satisfy an algebraic equality in the ε_i's, and whose coefficients are determined by d_{01}, $\overline{d}_{0i}$ for $i = 2,3,4$ and d_{ij} for $i,j = 1,2,3,4$ and $i \neq j$:*

$$\alpha\varepsilon_2 + \beta\varepsilon_3 + \gamma\varepsilon_4 + \delta = 0, \tag{11}$$

where

$$\begin{aligned}
\alpha &= d_{34}^2\left(d_{23}^2 + d_{24}^2 - d_{34}^2\right) - 2d_{34}^2 d_{12}^2 \\
&\quad + d_{13}^2\left(d_{24}^2 - d_{23}^2 + d_{34}^2\right) + d_{14}^2\left(d_{23}^2 - d_{24}^2 + d_{34}^2\right) \\
\beta &= d_{24}^2\left(d_{23}^2 - d_{24}^2 + d_{34}^2\right) - 2d_{24}^2 d_{13}^2 \\
&\quad + d_{12}^2\left(d_{24}^2 - d_{23}^2 + d_{34}^2\right) + d_{14}^2\left(d_{23}^2 + d_{24}^2 - d_{34}^2\right) \\
\gamma &= d_{23}^2\left(d_{24}^2 - d_{23}^2 + d_{34}^2\right) - 2d_{23}^2 d_{14}^2 \\
&\quad + d_{12}^2\left(d_{23}^2 - d_{24}^2 + d_{34}^2\right) + d_{13}^2\left(d_{23}^2 + d_{24}^2 - d_{34}^2\right) \\
\delta &= \overline{d}_{02}^2\left(d_{34}^2\left(d_{23}^2 + d_{24}^2 - d_{34}^2\right) - 2d_{34}^2 d_{12}^2\right. \\
&\qquad \left. + d_{13}^2\left(d_{24}^2 - d_{23}^2 + d_{34}^2\right) + d_{14}^2\left(d_{23}^2 - d_{24}^2 + d_{34}^2\right)\right) \\
&\quad + \overline{d}_{03}^2\left(d_{24}^2\left(d_{23}^2 - d_{24}^2 + d_{34}^2\right) - 2d_{24}^2 d_{13}^2\right. \\
&\qquad \left. + d_{12}^2\left(d_{24}^2 - d_{23}^2 + d_{34}^2\right) + d_{14}^2\left(d_{23}^2 + d_{24}^2 - d_{34}^2\right)\right) \\
&\quad + \overline{d}_{04}^2\left(d_{23}^2\left(d_{24}^2 - d_{23}^2 + d_{34}^2\right) - 2d_{23}^2 d_{14}^2\right. \\
&\qquad \left. + d_{12}^2\left(d_{23}^2 - d_{24}^2 + d_{34}^2\right) + d_{13}^2\left(d_{23}^2 + d_{24}^2 - d_{34}^2\right)\right) \\
&\quad + d_{23}^2 d_{14}^2\left(d_{24}^2 - d_{23}^2 + d_{34}^2\right) + d_{24}^2 d_{13}^2\left(d_{23}^2 - d_{24}^2 + d_{34}^2\right) \\
&\quad + d_{34}^2 d_{12}^2\left(d_{23}^2 + d_{24}^2 - d_{34}^2\right) - 2d_{23}^2 d_{24}^2 d_{34}^2 \\
&\quad + d_{01}^2\left(d_{23}^4 + d_{24}^4 + d_{34}^4 - 2d_{23}^2 d_{24}^2 - 2d_{23}^2 d_{34}^2 - 2d_{24}^2 d_{34}^2\right).
\end{aligned} \tag{12}$$

Proof. According to Theorem 1, we know that $D(\mathbf{r}, \mathbf{n}, \mathbf{a}_2, \mathbf{a}_3, \mathbf{a}_4) = 0$, namely,

$$\det\begin{pmatrix}
0 & d_{01}^2 & d_{02}^2 & d_{03}^2 & d_{04}^2 & 1 \\
d_{01}^2 & 0 & d_{12}^2 & d_{13}^2 & d_{14}^2 & 1 \\
d_{02}^2 & d_{12}^2 & 0 & d_{23}^2 & d_{24}^2 & 1 \\
d_{03}^2 & d_{13}^2 & d_{23}^2 & 0 & d_{34}^2 & 1 \\
d_{04}^2 & d_{14}^2 & d_{24}^2 & d_{34}^2 & 0 & 1 \\
1 & 1 & 1 & 1 & 1 & 0
\end{pmatrix} = 0. \tag{13}$$

One can then obtain,

$$\det\begin{pmatrix} \mathbf{B}_{11} & \mathbf{B}_{12} \\ \mathbf{B}_{12}^T & \mathbf{B}_{22} \end{pmatrix} = 0, \tag{14}$$

where

$$\mathbf{B}_{11} = \begin{pmatrix} 0 & d_{01}^2 \\ d_{01}^2 & 0 \end{pmatrix} \qquad \mathbf{B}_{12} = \begin{pmatrix} d_{02}^2 & d_{03}^2 & d_{04}^2 & 1 \\ d_{12}^2 & d_{13}^2 & d_{14}^2 & 1 \end{pmatrix}$$

$$\mathbf{B}_{22} = \begin{pmatrix} 0 & d_{23}^2 & d_{24}^2 & 1 \\ d_{23}^2 & 0 & d_{34}^2 & 1 \\ d_{24}^2 & d_{34}^2 & 0 & 1 \\ 1 & 1 & 1 & 0 \end{pmatrix}. \tag{15}$$

Suppose the anchors are nonlinear; $D(\mathbf{a}_2, \mathbf{a}_3, \mathbf{a}_4) \neq 0$, so $\mathbf{B}_{22}$ is nonsingular. From (14), the following equation can be derived:

$$\det\left(\mathbf{B}_{11} - \mathbf{B}_{12}\mathbf{B}_{22}^{-1}\mathbf{B}_{12}^T\right)\det\mathbf{B}_{22} = 0. \tag{16}$$

That is,

$$\det\begin{pmatrix} 0-\left(\mathbf{b}_{120}^{T}\mathbf{B}_{22}^{-1}\mathbf{b}_{120}\right) & d_{01}^{2}-\left(\mathbf{b}_{120}^{T}\mathbf{B}_{22}^{-1}\mathbf{b}_{121}\right) \\ d_{01}^{2}-\left(\mathbf{b}_{121}^{T}\mathbf{B}_{22}^{-1}\mathbf{b}_{120}\right) & 0-\left(\mathbf{b}_{121}^{T}\mathbf{B}_{22}^{-1}\mathbf{b}_{121}\right) \end{pmatrix}=0, \tag{17}$$

where

$$\begin{aligned} \mathbf{b}_{120} &= \left(d_{02}^{2} \quad d_{03}^{2} \quad d_{04}^{2} \quad 1\right)^{T} \\ \mathbf{b}_{121} &= \left(d_{12}^{2} \quad d_{13}^{2} \quad d_{14}^{2} \quad 1\right)^{T}. \end{aligned} \tag{18}$$

According to the proof procedure of Theorem 5, we can obtain $\mathbf{b}_{120}^{T}\mathbf{B}_{22}^{-1}\mathbf{b}_{120} = \mathbf{b}_{121}^{T}\mathbf{B}_{22}^{-1}\mathbf{b}_{121} = 0$. Then from (17), we obtain

$$\mathbf{b}_{120}^{T}\mathbf{B}_{22}^{-1}\mathbf{b}_{121} = \mathbf{b}_{121}^{T}\mathbf{B}_{22}^{-1}\mathbf{b}_{120} = d_{01}^{2}. \tag{19}$$

This yields

$$\left(\overline{d}_{02}^{2}+\varepsilon_2 \quad \overline{d}_{03}^{2}+\varepsilon_3 \quad \overline{d}_{04}^{2}+\varepsilon_4 \quad 1\right)\mathbf{B}_{22}^{-1}\begin{pmatrix} d_{12}^{2} \\ d_{13}^{2} \\ d_{14}^{2} \\ 1 \end{pmatrix} = d_{01}^{2}. \tag{20}$$

Multiplying both sides of (20) by the determinant of $\mathbf{B}_{22}$, we obtain

$$\begin{aligned} &\left(\overline{d}_{02}^{2}+\varepsilon_2 \quad \overline{d}_{03}^{2}+\varepsilon_3 \quad \overline{d}_{04}^{2}+\varepsilon_4 \quad 1\right)\mathbf{B}_{22}^{*}\begin{pmatrix} d_{12}^{2} \\ d_{13}^{2} \\ d_{14}^{2} \\ 1 \end{pmatrix} \\ &\quad = d_{01}^{2}\times\det\left(\mathbf{B}_{22}\right), \end{aligned} \tag{21}$$

where

$$\mathbf{B}_{22}^{*} = \begin{pmatrix} 2d_{34}^{2} & d_{23}^{2}-d_{24}^{2}-d_{34}^{2} & d_{24}^{2}-d_{23}^{2}-d_{34}^{2} & d_{34}^{2}\left(d_{34}^{2}-d_{23}^{2}-d_{24}^{2}\right) \\ d_{23}^{2}-d_{24}^{2}-d_{34}^{2} & 2d_{24}^{2} & d_{34}^{2}-d_{23}^{2}-d_{24}^{2} & d_{24}^{2}\left(d_{24}^{2}-d_{23}^{2}-d_{34}^{2}\right) \\ d_{24}^{2}-d_{23}^{2}-d_{34}^{2} & d_{34}^{2}-d_{23}^{2}-d_{24}^{2} & 2d_{23}^{2} & d_{23}^{2}\left(d_{23}^{2}-d_{24}^{2}-d_{34}^{2}\right) \\ d_{34}^{2}\left(d_{34}^{2}-d_{23}^{2}-d_{24}^{2}\right) & d_{24}^{2}\left(d_{24}^{2}-d_{23}^{2}-d_{34}^{2}\right) & d_{23}^{2}\left(d_{23}^{2}-d_{24}^{2}-d_{34}^{2}\right) & 2d_{23}^{2}d_{24}^{2}d_{34}^{2} \end{pmatrix}. \tag{22}$$

According to (21), we can get (11). This completes the proof. □

4. Neighbor Constraint Assisted Distributed Localization

Based on the algebraic constraints mentioned in the previous sections, a neighbor constraint assisted distributed localization algorithm (NCA-DL) is hereby proposed as a means of improving the localization precision. The main idea behind NCA-DL is to refine the distances to anchors using a neighbor node. In NCA-DL, the regular nodes estimate the initial distances to the anchors using the method similar to DV-Hop [11]. Then according to the algebraic constraints of the distance estimation errors, Lagrangian multiplier method is introduced in order to obtain the optimal errors and refine the distances. The following section will give a full description of the principles and performance analysis of this novel NCA-DL algorithm.

4.1. Principles of the Algorithm. Initially, anchors (set A) are deployed in the sensing field with the regular nodes (set R). We assume each node has the ability of ranging, and for simplicity, the number of the anchors is set to 3. The whole process of NCA-DL is divided into four phases.

(A) Distance Estimation. Each regular node is supposed to obtain initial distance estimation to the anchors. So two times of flooding are required to accomplish the process of distance estimation. In the first flooding, the anchors start by propagating their location information. Then all nodes receive the location information from every anchor as well as the hop count to these anchors. When an anchor node receives location information from other anchors, it can calculate the average size of a hop based on their locations and the hop count among them. In the second flooding, the average size of a hop is transmitted in a controlled manner into the network as a correction factor. When a regular node receives the correction, it can be able to estimate the distances to the anchors using the correction and the hop count information received in the previous flooding.

(B) Neighbor Node Election. The main purpose of this phase is to choose a proper neighbor for each regular node to assist distance refinement in the next phase. For most ranging technology, when sensors are closer, the distance estimations are more accurate. According to the requirement of Theorem 7, in order to obtain the constraint equation of the distance estimation errors, it is fundamental to choose an adjacent neighbor because the distance between the regular node and its neighbor can be measured accurately. Meanwhile, the distances among the neighbor and the anchors also should satisfy geometry relationship, that is to say, the distances should be refined by the method in [20]. So in this phase, the nearest node of each regular node is chosen as an assistant neighbor and its distances to the anchors obtained in the previous phase are supposed to be refined using Theorem 5.

To improve the localization precision of the regular node further, the distances between the neighbor and the anchors need to be estimated accurately. Though the imprecise distances can be refined through Theorem 5 which can meet the requirement of Theorem 7, the distances are still imprecise. So in this phase, with the growing research for the mobility of sensors [21], a mobile anchor also can be used to be a "neighbor" of each regular node. The distances between this "neighbor" and the other static anchors can be accurately calculated by the coordinates of these anchors, which definitely meets the requirement of Theorem 7. In this case, the mobile anchor is supposed to move in the sensing field. The aim is just to assist the regular node with localization through the constraint defined in Theorem 7 and it does not need to consider the collinear problems of the anchors. So SCAN [22] could be used for the path planning method, which is the most straightforward one.

(C) Distance Refinement. The algebraic equalities that define the errors and relate the distances to the anchors for each regular node have now been fully determined from the previous two phases, as described in Theorems 5 and 7. The next step of the algorithm attempts to quantify these errors in the inaccurate distance estimations between regular nodes and anchors. Let ε_i ($\forall i \in \{2,3,4\}$) as defined in (4) be the error in the estimated squared distances between a regular node and the anchors. The goal here is to minimize the sum of the squared errors:

$$J = \varepsilon_2^2 + \varepsilon_3^2 + \varepsilon_4^2. \tag{23}$$

In (23), J is subjected to a quadratic equality constraint defined in (5) and a linear equality constraint defined in (11). So, to solve the optimization problem with constraints, Lagrangian multiplier method has been implemented in the algorithm. It is a mathematical method used to solve the optimization problem, which can convert the constraints to the seeking of extreme values with the help of Lagrangian multipliers. We can get the following Lagrangian multiplier form:

$$\begin{aligned} &H(\varepsilon_2,\varepsilon_3,\varepsilon_4,\lambda_1,\lambda_2) \\ &\quad = \sum_{i=2}^{4}\varepsilon_i^2 + \lambda_1 f_1(\varepsilon_2,\varepsilon_3,\varepsilon_4) + \lambda_2 f_2(\varepsilon_2,\varepsilon_3,\varepsilon_4), \end{aligned} \tag{24}$$

where λ_1, λ_2 are the Lagrangian multipliers and f_1, f_2 are the functions of $\varepsilon_2, \varepsilon_3, \varepsilon_4$, whose coefficients can be obtained in (5) and (11).

By differentiating the Lagrangian H with respect to ε_i ($i = 2,3,4$) and λ_i ($i = 1,2$) and equating the result to zero, five equations can be obtained. Solving these five algebraic equations numerically and discarding all the nonoptimal stationary-point solutions, $\varepsilon_2, \varepsilon_3, \varepsilon_4$ can be solved. Then the distances to the anchors for the regular node are refined. The below example demonstrates the steps in this phase.

The simplest scenario as depicted in Figure 2 is considered, where node $\mathbf{r}$ is the regular node that needs to be located. Node $\mathbf{r}$ can measure its distances to three anchors $\mathbf{a}_2, \mathbf{a}_3, \mathbf{a}_4$ whose coordinates are (10, 10), (90, 10), and (50, 90), respectively. The noisy distance measurements acquired by node $\mathbf{r}$ are $\overline{d}_{02} = 56.3$, $\overline{d}_{03} = 65.7$, and $\overline{d}_{04} = 41.6$. The distances between the neighbor node $\mathbf{n}$ and other nodes are estimated in the previous phase as $d_{01} = 5$, $d_{12} = 56.6$, $d_{13} = 56.6$, and $d_{14} = 40$. In this case, the goal is to obtain the estimation errors $\varepsilon_2, \varepsilon_3, \varepsilon_4$ and refine $\overline{d}_{02}, \overline{d}_{03}$, and $\overline{d}_{04}$.

Firstly, two equality constraints as described by (5) and (11) will be determined:

$$\begin{aligned} 0 &= f_1(\varepsilon_2,\varepsilon_3,\varepsilon_4) \\ &= \big(-2.5\varepsilon_2^2 - 2.5\varepsilon_3^2 - 2\varepsilon_4^2 + 3\varepsilon_2\varepsilon_3 + 2\varepsilon_2\varepsilon_4 + 2\varepsilon_3\varepsilon_4 \\ &\qquad + 16597\varepsilon_2 + 7341\varepsilon_3 + 27262\varepsilon_4 + 14159000\big) \times (25600)^{-1} \\ 0 &= f_2(\varepsilon_2,\varepsilon_3,\varepsilon_4) \\ &= 0.25\varepsilon_2 + 0.25\varepsilon_3 + 0.5\varepsilon_4 + 310.6. \end{aligned} \tag{25}$$

To determine the optimal values for $\varepsilon_2, \varepsilon_3, \varepsilon_4$, the following problem needs to be solved:

$$\begin{aligned} \min \quad & \varepsilon_2^2 + \varepsilon_3^2 + \varepsilon_4^2 \\ \text{s.t.} \quad & f_1(\varepsilon_2,\varepsilon_3,\varepsilon_4) = 0 \\ & f_2(\varepsilon_2,\varepsilon_3,\varepsilon_4) = 0. \end{aligned} \tag{26}$$

By differentiating the Lagrangian H defined in (24), we obtain

$$\begin{aligned} \frac{\partial H}{\partial \varepsilon_2} &= 2\varepsilon_2 + 0.25\lambda_2 \\ &\quad + \lambda_1\left(\frac{3}{25600\varepsilon_3} - \frac{\varepsilon_2}{5120} + \frac{\varepsilon_4}{12800} + 0.65\right) = 0 \\ \frac{\partial H}{\partial \varepsilon_3} &= 2\varepsilon_3 + 0.25\lambda_2 \\ &\quad + \lambda_1\left(\frac{3}{25600\varepsilon_2} - \frac{\varepsilon_3}{5120} + \frac{\varepsilon_4}{12800} + 0.28\right) = 0 \end{aligned}$$

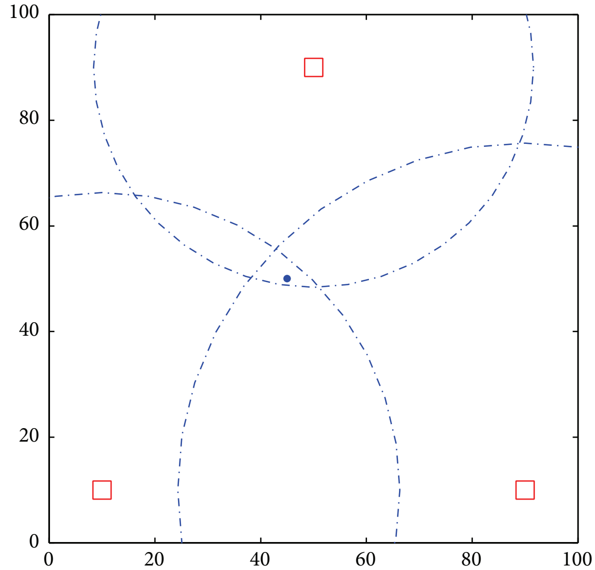

(a) Performance of noisy distances

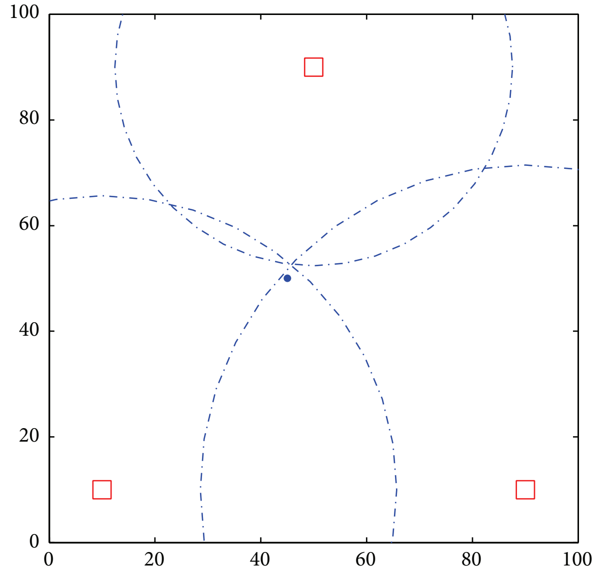

(b) Performance of refined distances

Figure 3: Locations of anchors and the regular node.

$$\frac{\partial H}{\partial \varepsilon_4} = 2\varepsilon_4 + 0.5\lambda_2 + \lambda_1\left(\frac{\varepsilon_2}{12800} + \frac{\varepsilon_3}{12800} - \frac{\varepsilon_4}{6400} + 1.06\right) = 0$$

$$\frac{\partial H}{\partial \lambda_1} = f_1(\varepsilon_2, \varepsilon_3, \varepsilon_4) = 0, \qquad \frac{\partial H}{\partial \lambda_2} = f_2(\varepsilon_2, \varepsilon_3, \varepsilon_4) = 0. \tag{27}$$

Solving the above five algebraic equations above, we get,

$$\varepsilon_2^* = -67.39, \qquad \varepsilon_3^* = -545.76, \qquad \varepsilon_4^* = -314.59. \tag{28}$$

Correspondingly, the refined distances between regular node $\mathbf{r}$ and the three anchors are

$$\begin{aligned} \widehat{d}_{02} &= \sqrt{\overline{d}_{02}^2 + \varepsilon_2^*} = 55.6 \\ \widehat{d}_{03} &= \sqrt{\overline{d}_{03}^2 + \varepsilon_3^*} = 61.4 \\ \widehat{d}_{04} &= \sqrt{\overline{d}_{04}^2 + \varepsilon_4^*} = 37.6. \end{aligned} \tag{29}$$

As shown in Figure 3, "·" represents the regular node, "□" represents the anchor, and the radius of the circle is the estimated distance between the regular node and the anchor. In Figure 3(b), the three circles intersect in one point, which proves that the refined distances satisfy the geometric constraints.

(D) Localization. So far, regular nodes have known the refined distances to the anchors according to (29). Based on the above refinement scheme, we know that the refined distances satisfy the geometric constraints. Localization can be carried out by the least square method. $r(x, y)$ represents the regular node, $a(x_i, y_i)$ $(i = 2, 3, 4)$ represent the locations of the anchors, and $\widehat{d}_{02}, \widehat{d}_{03}, \widehat{d}_{04}$ represent the refined distances between the regular node and the anchors. The coordinate of the regular node can be estimated by

$$\widehat{X} = \left(\mathbf{A}^T\mathbf{A}\right)^{-1}\mathbf{A}^T b, \tag{30}$$

where

$$\mathbf{A} = \begin{pmatrix} 2(x_2 - x_4) & 2(y_2 - y_4) \\ 2(x_3 - x_4) & 2(y_3 - y_4) \end{pmatrix}, \qquad X = \begin{pmatrix} x \\ y \end{pmatrix}$$
$$b = \begin{pmatrix} x_2^2 - x_4^2 + y_2^2 - y_4^2 + \widehat{d}_{04}^2 - \widehat{d}_{02}^2 \\ x_3^2 - x_4^2 + y_3^2 - y_4^2 + \widehat{d}_{04}^2 - \widehat{d}_{03}^2 \end{pmatrix}. \tag{31}$$

Figure 4 illustrates the localization of the computational example above with both noisy and refined distances. "∗" represents the calculated location. The localization errors in Figures 4(a) and 4(b) are 0.67 m and 0.55 m, respectively.

4.2. Communication Cost Analysis. For energy cost of NCA-DL, the communication consumption is mainly considered in the distance estimation and refinement phases. n represents the number of the sensors and n_A represents the number of the anchors. Then for the two flooding processes in the distance estimation phase, it gives a bound of $O(2\times n_A\times n)$ to the communication cost in this process. While in the refinement phase, each node needs to communicate with its neighbors so the communication cost is $O(n)$. The total communication complexity is $O(n \times (2 \times n_A + 1))$. It is known that the communication complexity of DV-Hop is $O(2 \times n_A \times n)$.

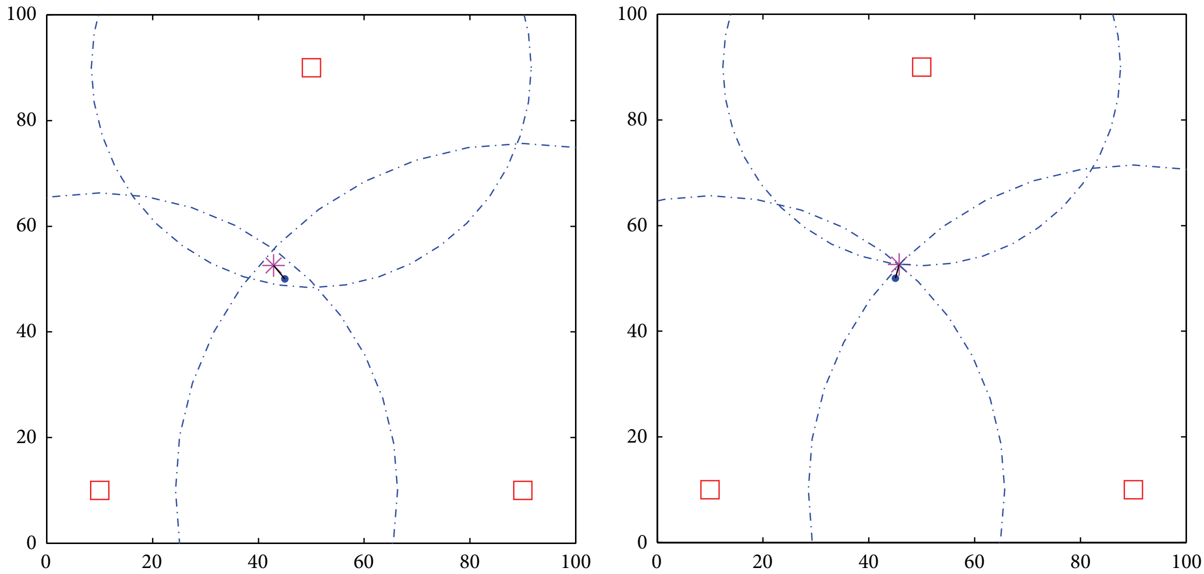

(a) Localization with noisy distances

(b) Localization with refined distances

Figure 4: Localization effect of noisy distances and refined distances.

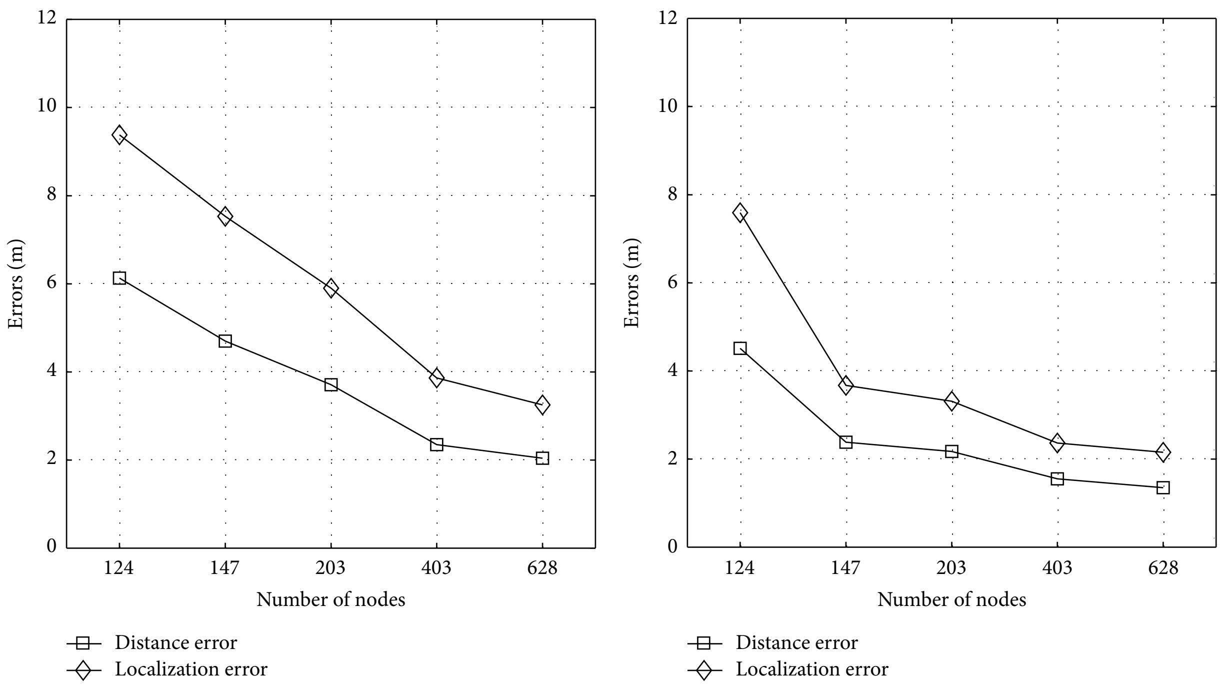

(a) Random placement model

(b) Perturbed grid model

Figure 5: Distance estimation and localization error of NCA-DL.

Since the method proposed in [20] is just to refine distance estimations with additional calculation, its communication complexity is the same as DV-Hop. So the cost of NCA-DL is in the same order of magnitude as other algorithms while it can largely improve the localization performance.

5. Numerical Results

This section we will describe the implementation of the NCA-DL algorithm and evaluate its performance through extensive simulations. The results obtained from these simulations will focus on analysing the distance estimation errors and

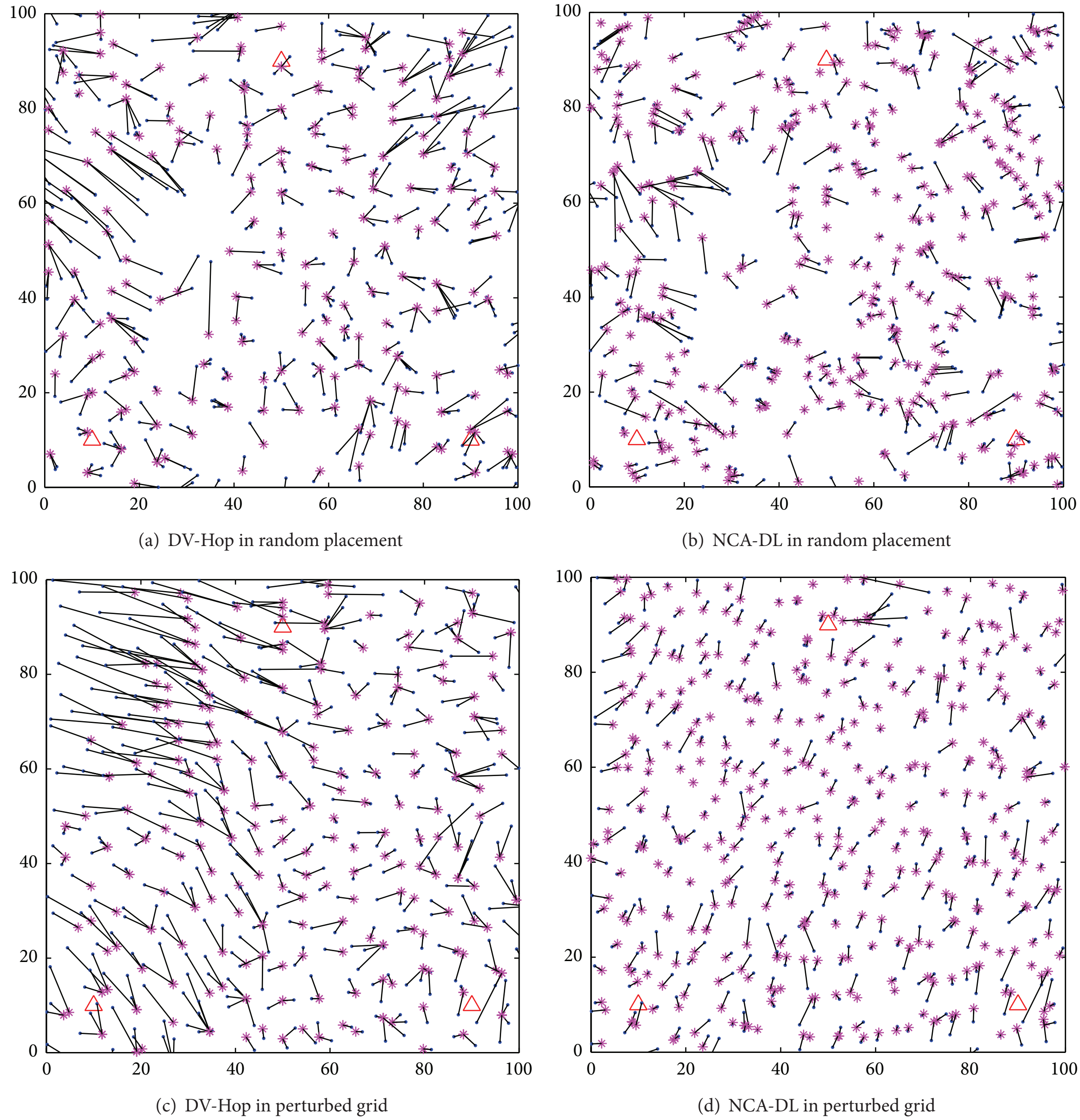

Figure 6: Localization effect in both deployment models.

localization errors and further compare results obtained by NCA-DL, DV-Hop, robust position, and the method proposed in [20] which have been mentioned above.

5.1. Simulation Configuration. The basic network setup area is considered to be a 100 m × 100 m square field. The communication radius of the nodes is set to 10 m. In our simulations, sensor nodes are deployed using two models: (i) random placement and (ii) perturbed grid. In the random placement model, sensor nodes are randomly deployed in the network by dropping from an airplane or some other methods. In this case, the topology of the network is likely to be irregular. In the second model, nodes are deployed using perturbed grid where the nodes are perturbed with a random shift from grid. In this situation, nodes will tend to uniformly occupy the field avoiding large concentration of nodes, which also guarantee the regularity of the topology of the network.

In all cases, regular nodes have the ability of ranging and the results are averaged over 10 trails. The average localization error is defined as follows:

$$\text{error} = \frac{1}{n}\sum_{i=1}^{n} \left\| \mathbf{x}_i - \overline{\mathbf{x}}_i \right\| \times \frac{1}{r}, \qquad (32)$$

where n is the number of the regular nodes, $\mathbf{x}_i$ is the actual location of regular node i, $\overline{\mathbf{x}}_i$ is the estimated location of regular node i, and r is the communication radius.

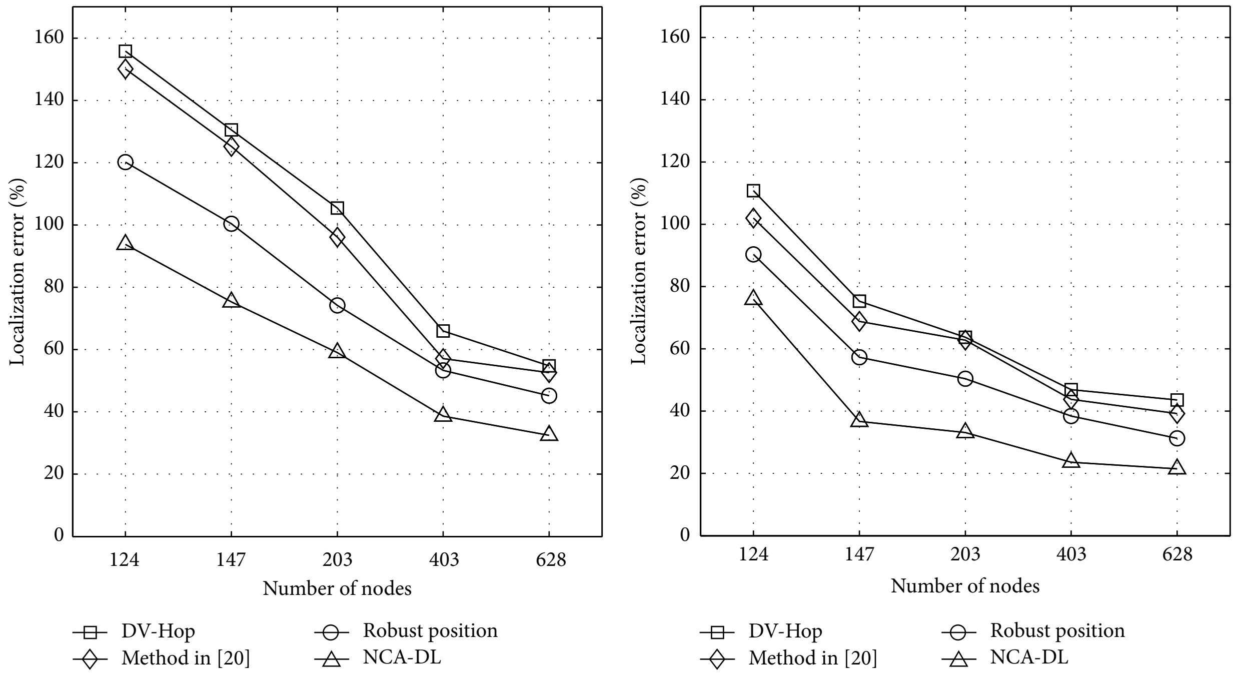

(a) Random placement model

(b) Perturbed grid model

Figure 7: Localization error against number of nodes.

Table 1: Average distance estimation error.

Number of nodes (Avg. degree)	Avg. distance estimation error (m)			
	Random placement		Perturbed grid	
	DV-Hop	NCA-DL	DV-Hop	NCA-DL
124 (4.8)	12.32	6.13	6.15	4.51
147 (5.8)	8.28	4.70	4.01	2.38
203 (7.5)	5.43	3.71	3.92	2.17
403 (11.1)	3.39	2.35	2.99	1.55
628 (14.2)	3.06	2.04	2.72	1.35

5.2. NCA-DL Performance. At first, we focus on the distance estimation error between regular nodes and anchors. In this set of simulations, we varied the number of the nodes (avg. degree) from 124 (4.8) to 628 (14.2). The number of the anchors is set to 3. The average distance estimation errors obtained from these simulations are stated in Table 1.

As indicated in Table 1, we can observe that the distance estimation error of both DV-Hop and NCA-DL under perturbed gird deployment is smaller than that of these two algorithms under random placement. With the increase of the number of nodes (avg. degree), both DV-Hop and NCA-DL can improve the ranging effectiveness. Moreover, DV-Hop suffers large ranging error when the average degree is low while NCA-DL has smaller errors for divers network scales.

Now, it has been proved that the NCA-DL algorithm can significantly decrease the distance estimation errors with the help of a collaborating neighbor; both initial deployment model conditions were therefore simulated in order to graphically verify their respective localization performance.

Figure 5 exemplifies the distance estimation and localization error of NCA-DL against number of nodes in both deployment models. It is demonstrated that the distance estimation error in NCA-DL can be decreased with the increase of the number of nodes. As shown in Figure 5(b), the localization error decreases more obviously when the distance estimation error drops below a critical value (around 2 m).

Figure 6 exemplifies the localization performance of DV-Hop and NCA-DL. "Δ" represents the anchors, "." represents the true location, "∗" represents the calculated location, and the line between them represents the localization error. In this set of simulations, the number of deployed nodes (avg. degree) is set to 403 (11.1) and the number of the anchors is set to 3. According to the definition of localization error in (32), in the random placement deployment, the average localization error resulting form DV-Hop is around 66% while the error goes down to around 46% in perturbed grid deployment, as shown in Figures 6(a) and 6(c). In Figures 6(b) and 6(d), we can see that NCA-DL decreases the localization error to 38% and 23%, respectively, in the two deployment models. In general, NCA-DL can increase the localization precision about 40% compared with DV-Hop under such network environment.

Figure 7 illustrates the localization error in both random placement and perturbed grid models. Compared with the other algorithms, NCA-DL has much lower localization error. With the increase of number of nodes, the performance of all the algorithms upgrades. It is also demonstrated that the NCA-DL algorithm can achieve high localization precision in the perturbed grid deployment model when the density of sensors is high, as shown by Figure 7(b).

6. Conclusions

Location information of sensors is vital in wireless sensor networks. In this paper, a novel distributed localization algorithm called NCA-DL is proposed, which introduces the *Cayley-Menger determinant* as an important tool for formulating the distances between pairs of regular nodes and anchors to algebraic constraints. In NCA-DL, an adjacent neighbor is chosen for each regular node to establish constraint equations. Then the imprecise distances can be refined by using these constraints and an appropriate objective function. Finally, the localization precision is improved.

The set of numerical simulations carried out to validate this method demonstrate the scalability of NCA-DL over a range of node numbers. Comparisons have been performed with other known localization algorithms, which show that NCA-DL can largely reduce the localization errors displayed by existing methods. In the considered sensor network cases initialized under random deployment conditions, the NCA-DL algorithm has proven to increase the localization precision by up to 30% compared with the method proposed in [20] and 40% compared with DV-Hop.

Conflict of Interests

The authors declare that there is no conflict of interests regarding the publication of this paper.

Acknowledgments

This work was supported by National Defense Advanced Research Project of China (Grants nos. 104080 and 40405020401), National Natural Science Foundation of Youth Science Fund (no. 61203144), and Research Fund for the Doctoral Program of Higher Education of China (no. 20121101110032).

References

[1] G. Han, H. Xu, T. Q. Duong, J. Jiang, and T. Hara, "Localization algorithms of wireless sensor networks: a survey," *Telecommunication Systems*, vol. 52, no. 4, pp. 2419–2436, 2013.

[2] Y. Hu, Y. Ding, and K. Hao, "An immune cooperative particle swarm optimization algorithm for fault-tolerant routing optimization in heterogeneous wireless sensor networks," *Mathematical Problems in Engineering*, vol. 2012, Article ID 743728, 19 pages, 2012.

[3] Y. Tian, Y. Ou, H. R. Karimi, Y. T. Liu, and J. Q. Han, "Distributed multitarget probabilistic coverage control algorithm for wireless sensor networks," *Mathematical Problems in Engineering*, vol. 2014, Article ID 421753, 8 pages, 2014.

[4] Z. Liu, Q. Zheng, L. Xue, and X. Guan, "A distributed energy-efficient clustering algorithm with improved coverage in wireless sensor networks," *Future Generation Computer Systems*, vol. 28, no. 5, pp. 780–790, 2012.

[5] Z. Liu, L. Dai, Y. Yuan, and J. Wang, "Distributed joint optimal control of power and rate with clustered routing protocol in wireless sensor networks," *Communications in Computer and Information Science*, vol. 334, pp. 325–334, 2013.

[6] G. Mao, B. Fidan, and B. D. O. Anderson, "Wireless sensor network localization techniques," *Computer Networks*, vol. 51, no. 10, pp. 2529–2553, 2007.

[7] J. Shen, A. F. Molisch, and J. Salmi, "Accurate passive location estimation using TOA measurements," *IEEE Transactions on Wireless Communications*, vol. 11, no. 6, pp. 2182–2192, 2012.

[8] P. K. Sahu, E. H.-K. Wu, and J. Sahoo, "DuRT: dual RSSI trend based localization for wireless sensor networks," *IEEE Sensors Journal*, vol. 13, no. 8, pp. 3115–3123, 2013.

[9] J. Lee, W. Chung, and E. Kim, "A new range-free localization method using quadratic programming," *Computer Communications*, vol. 34, no. 8, pp. 998–1010, 2011.

[10] C.-C. Chen, C.-Y. Chang, and Y.-N. Li, "Range-free localization scheme in wireless sensor networks based on bilateration," *International Journal of Distributed Sensor Networks*, vol. 2013, Article ID 620248, 10 pages, 2013.

[11] D. Niculescu and B. Nath, "Ad hoc positioning system (APS)," in *IEEE Global Telecommunicatins Conference (GLOBECOM '01)*, pp. 2926–2931, San Antonio, Tex, USA, November 2001.

[12] C. Savarese, J. Rabaey, and K. Langendoen, "Robust positioning algorithms for distributed ad-hoc wireless sensor networks," in *USENIX Annual Technical Conference*, pp. 317–327, Monterey, Calif, USA, June 2002.

[13] Q. Qian, X. Shen, and H. Chen, "An improved node localization algorithm based on DV-Hop for wireless sensor networks," *Computer Science and Information Systems*, vol. 8, no. 4, pp. 953–972, 2011.

[14] S. Kumar and D. K. Lobiyal, "An advanced DV-Hop localization algorithm for wireless sensor networks," *Wireless Personal Communications*, vol. 71, no. 2, pp. 1365–1385, 2013.

[15] M. Li and Y. Liu, "Rendered path: range-free localization in anisotropic sensor networks with holes," *IEEE/ACM Transactions on Networking*, vol. 18, no. 1, pp. 320–332, 2010.

[16] U. A. Khan, S. Kar, and J. M. F. Moura, "DILAND: an algorithm for distributed sensor localization with noisy distance measurements," *IEEE Transactions on Signal Processing*, vol. 58, no. 3, pp. 1940–1947, 2010.

[17] L. M. Blumenthal, *Theory and Applications of Distance Geometry*, The Clarendon Press, Oxford, UK, 1953.

[18] M. Cao, C. Yu, and B. D. O. Anderson, "Formation control using range-only measurements," *Automatica*, vol. 47, no. 4, pp. 776–781, 2011.

[19] L. Yang, "Solving geometric constraints with distance-based global coordinate system," in *International Workshop on Geometric Constraint Sloving*, Beijing, China, 2003.

[20] M. Cao, B. D. O. Anderson, and A. S. Morse, "Sensor network localization with imprecise distances," *Systems and Control Letters*, vol. 55, no. 11, pp. 887–893, 2006.

[21] C.-H. Ou, "A localization scheme for wireless sensor networks using mobile anchors with directional antemnas," *IEEE Sensor Journal*, vol. 11, no. 7, pp. 1607–1616, 2011.

[22] D. Koutsonikolas, S. M. Das, and Y. C. Hu, "Path planning of mobile landmarks for localization in wireless sensor networks," *Computer Communications*, vol. 30, no. 13, pp. 2577–2592, 2007.

Hindawi Publishing Corporation
Mathematical Problems in Engineering
Volume 2014, Article ID 367629, 5 pages
http://dx.doi.org/10.1155/2014/367629

Research Article

Temperature Control of Gas Chromatograph Based on Switched Delayed System Techniques

Xiao-Liang Wang, Ming-Xu Zhang, Kun-Zhi Liu, and Xi-Ming Sun

The School of Control Science and Engineering, Dalian University of Technology, Dalian 116024, China

Correspondence should be addressed to Kun-Zhi Liu; kunzhiliu1989@163.com

Received 10 April 2014; Accepted 10 May 2014; Published 26 May 2014

Academic Editor: Yun-Bo Zhao

We address the temperature control problem of the gas chromatograph. We model the temperature control system of the gas chromatograph into a switched delayed system and analyze the stability by common Lyapunov functional technique. The PI controller parameters can be given based on the proposed linear matrix inequalities (LMIs) condition and the designed controller can make the temperature of gas chromatograph track the reference signal asymptotically. An experiment is given to illustrate the effectiveness of the stability criterion.

1. Introduction

Gas chromatograph can separate the mixture by using chromatographic column and then the components of the mixture can be analyzed qualitatively. At present, gas chromatograph has been widely used in medicine, food safety, petrochemical [1], environmental science [2], and many other fields.

However, with gas chromatograph applied to process analysis [3], quality testing [4], environment online monitoring [5], and sudden emergency monitoring, the contradiction between non-real-time measurement and the demand of the real-time measurement in various fields is becoming more and more obvious. Therefore, the application of gas chromatograph into the field of measure is restricted. Recently, the contradiction is solved partly by improving the speed of temperature programming of chromatographic column or by improving the column flow velocity, as well as by reducing the chromatographic column inner diameter [6]. Among these approaches, the first method, that is, by improving the speed of temperature programming of chromatographic column, seems more effective. As demonstrated in the paper [7], the analysis time can be shortened to 10 percent by improving the speed of temperature programming. Since the temperature of the chromatograph column affects directly the gas chromatograph column efficiency, separation selectivity, and the sensitivity and the stability of detector, therefore the accurate temperature control for the thermostated oven is very important and is our main attention in this paper. In general, the thermostated oven works at 0°C~400°C. Since heating process of the thermostated oven is essentially a heat transfer process, time delay phenomena are inevitable. In the meanwhile, the parameters of the thermostated oven system model change with the variation of the temperature. Therefore, the controller design and stability analysis for this kind of system are complicated extremely, and to the best of the authors' knowledge, there are few works available in the existing literature till now. In this paper, in order to track the reference temperature signal, a switching controller is introduced, whose parameters can change with the variation of the temperature. We model the temperature control system as a switched delayed system [8]. Based on such a switched delayed system model, stability of gas chromatograph can be analyzed by the common Lyapunov functional [9], and the PI controller parameters can be given such that the temperature of the gas chromatograph tracks the reference signal asymptotically. An experiment is given to illustrate the effectiveness of the stability.

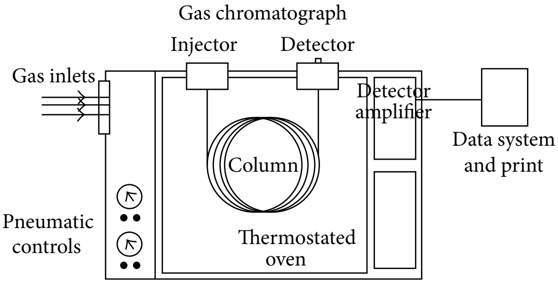

Figure 1: Structure diagram of gas chromatograph.

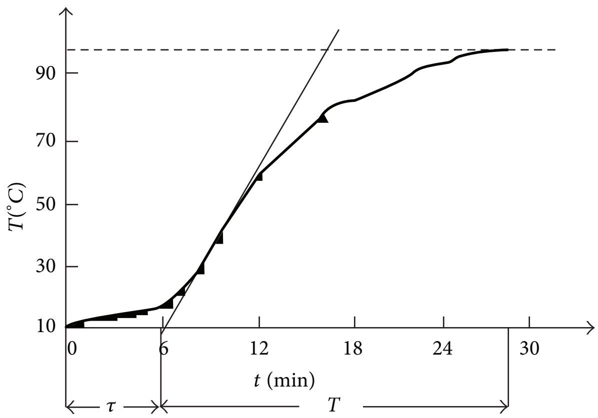

Figure 2: Illustration of ascending curve method.

2. Modeling Based on Switched Delayed System

Gas chromatograph consists of several parts as shown in Figure 1. The mixture to be detected is firstly gasified and then goes into the chromatographic column through injector. The temperature programming of the thermostated oven is executed by the electrical control equipment. The model can be described by the following transfer function:

$$G(s) = \frac{Ke^{-\tau s}}{1+Ts}, \tag{1}$$

where T and K are, respectively, the constant parameters and τ is the transmission delays. These parameters can be obtained by analyzing ascending curve as shown in Figure 2. Specifically, $K = y(\infty)/\Delta U$, where $y(\infty)$ is the steady state value of the step response and ΔU is the difference of a given step signal. PI controller is adopted to control the temperature system as follows:

$$P(t) = K_p e(t) + K_i \int_0^t e(t)\,dt, \tag{2}$$

where K_p is the proportion coefficient, K_i is the integral coefficient, and $e(t)$ is the error between the reference and output. Figure 3 is the control block diagram.

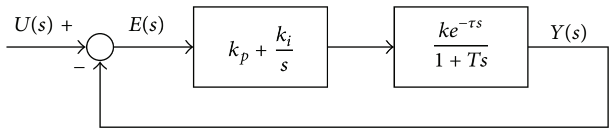

Figure 3: Signal flow graph.

The transfer function of the whole system can be given as follows:

$$\frac{E(s)}{U(s)} = 1 - \frac{KK_p s e^{-\tau s} + KK_i e^{-\tau s}}{Ts^2 + s + KK_p s e^{-\tau s} + KK_i e^{-\tau s}}. \tag{3}$$

Let $M(s)/U(s) = 1/(Ts^2 + s + KK_p s e^{-\tau s} + KK_i e^{-\tau s})$ and $Z(s)/M(s) = KK_p s e^{-\tau s} + KK_i e^{-\tau s}$, where M is intermediate variable; then, we have

$$\begin{aligned} u &= T\ddot{m}(t) + \dot{m}(t) + KK_p \dot{m}(t-\tau) + KK_i m(t-\tau), \\ z &= KK_p \dot{m}(t-\tau) + KK_i m(t-\tau), \\ e &= u - z. \end{aligned} \tag{4}$$

Set $x_1 = m$ and $x_2 = \dot{m}$; then, the system's state space equation can be written as follows:

$$\begin{aligned} \dot{x}_1 &= x_2, \\ \dot{x}_2 &= -\frac{1}{T}x_2 - \frac{KK_i}{T}x_1(t-\tau) - \frac{KK_p}{T}x_2(t-\tau) + \frac{1}{T}u, \\ e &= u - KK_p x_2(t-\tau) - KK_i x_1(t-\tau), \end{aligned} \tag{5}$$

where x_1 and x_2 are the system state. Denote $x = [x_1 \;\; x_2]^T$ and $x(t-\tau) = [x_1(t-\tau) \;\; x_2(t-\tau)]^T$; then, (5) can be reformulated as follows:

$$\begin{aligned} \dot{x} &= \begin{bmatrix} 0 & 1 \\ 0 & -\frac{1}{T} \end{bmatrix} x + \begin{bmatrix} 0 & 0 \\ -\frac{KK_i}{T} & -\frac{KK_p}{T} \end{bmatrix} x(t-\tau) + \begin{bmatrix} 0 \\ \frac{1}{T} \end{bmatrix} u, \\ e &= u - [KK_i \;\; KK_p]\, x(t-\tau). \end{aligned} \tag{6}$$

Set $u(t) = r$. Let $\overline{x} = x - cr$, where $c = \begin{bmatrix} 1/KK_i \\ 0 \end{bmatrix}$; then, we have

$$\begin{aligned} \dot{\overline{x}} &= \begin{bmatrix} 0 & 1 \\ 0 & -\frac{1}{T} \end{bmatrix} \overline{x} + \begin{bmatrix} 0 & 0 \\ -\frac{KK_i}{T} & -\frac{KK_p}{T} \end{bmatrix} \overline{x}(t-\tau), \\ e &= -[KK_i \;\; KK_p]\, \overline{x}(t-\tau). \end{aligned} \tag{7}$$

When the thermostated oven temperature varies from 0°C to 120°C, the system model is given as follows:

$$G(s) = \frac{K_1 e^{-\tau s}}{1 + T_1 s}. \tag{8}$$

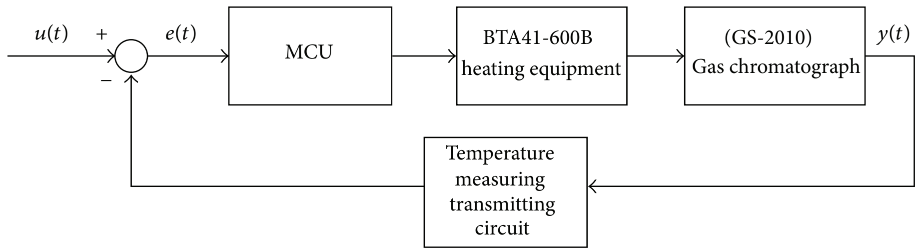

Figure 4: Temperature control system.

The corresponding PI controller parameters are K_{pi} and K_{i1}. The obtained temperature control subsystem is given as follows:

$$\dot{\overline{x}} = \begin{bmatrix} 0 & 1 \\ 0 & -\dfrac{1}{T_1} \end{bmatrix} \overline{x} + \begin{bmatrix} 0 & 0 \\ -\dfrac{K_1 K_{i1}}{T_1} & -\dfrac{K_1 K_{p1}}{T_1} \end{bmatrix} \overline{x}(t-\tau), \quad (9)$$
$$e = -\begin{bmatrix} K_1 K_{i1} & K_1 K_{p1} \end{bmatrix} \overline{x}(t-\tau).$$

When the thermostated oven temperature varies from 120°C to 260°C, the parameters of the thermostated oven temperature system are K_2 and T_2. The corresponding PI controller parameters are K_{p2} and K_{i2}. The obtained temperature control subsystem is given as follows:

$$\dot{\overline{x}} = \begin{bmatrix} 0 & 1 \\ 0 & -\dfrac{1}{T_2} \end{bmatrix} \overline{x} + \begin{bmatrix} 0 & 0 \\ -\dfrac{K_2 K_{i2}}{T_2} & -\dfrac{K_2 K_{p2}}{T_2} \end{bmatrix} \overline{x}(t-\tau), \quad (10)$$
$$e = -\begin{bmatrix} K_2 K_{i2} & K_2 K_{p2} \end{bmatrix} \overline{x}(t-\tau).$$

When the thermostated oven temperature varies from 260°C to 400°C, the parameters of the temperature system are T_3 and K_3 and the parameters of the corresponding PI controller are K_{p3} and K_{i3}. The state space equation for the temperature control subsystem can be written as follows:

$$\dot{\overline{x}} = \begin{bmatrix} 0 & 1 \\ 0 & -\dfrac{1}{T_3} \end{bmatrix} \overline{x} + \begin{bmatrix} 0 & 0 \\ -\dfrac{K_3 K_{i3}}{T_3} & -\dfrac{K_3 K_{p3}}{T_3} \end{bmatrix} \overline{x}(t-\tau), \quad (11)$$
$$e = -\begin{bmatrix} K_3 K_{i3} & K_3 K_{p3} \end{bmatrix} \overline{x}(t-\tau).$$

We model the whole temperature control system to be a switched delayed system as follows:

$$\dot{x}(t) = A_{q(t)} x(t) + F_{q(t)} x(t-\tau), \quad (12)$$

$$e(t) = C_{q(t)} x(t-\tau), \quad (13)$$

where $x \in \mathbb{R}^2$ is the state, $\tau \geq 0$ is the delay, $q(t) : \mathbb{R}_{\geq 0} \to \{1,2,3\}$, $A_q = \begin{bmatrix} 0 & 1 \\ 0 & -1/T_q \end{bmatrix}$, $F_q = \begin{bmatrix} 0 & 0 \\ -K_q K_{iq}/T_q & -K_q K_{pq}/T_q \end{bmatrix}$, and $C_q = -\begin{bmatrix} K_q K_{iq} & K_q K_{pq} \end{bmatrix}$. The switched delayed system consists of three subsystems. Denote the continuous function space from $[-\tau, 0]$ to $\mathbb{R}^2$ by C_τ. Let $\Omega_1 = \{(\phi_1,\phi_2)^T \in C_\tau \mid 0 \leq KK_i\phi_1(-\tau) + KK_p\phi_2(-\tau) \leq 120\}$, $\Omega_2 = \{(\phi_1,\phi_2)^T \in C_\tau \mid 120 < KK_i\phi_1(-\tau)+KK_p\phi_2(-\tau) \leq 260\}$, and $\Omega_3 = \{(\phi_1,\phi_2)^T \in C_\tau \mid 260 < KK_i\phi_1(-\tau)+KK_p\phi_2(-\tau) \leq 400\}$. The system (12) is switched to subsystem $q \in \{1,2,3\}$ when $x_t \in \Omega_q$, where x_t is defined as $x_t(s) = x(t+s)$, $s \in [-\tau, 0]$.

3. Stability Analysis

Next, we will give a theorem guaranteeing the uniformly globally asymptotical stability of system (12).

Theorem 1. *The switched delayed system* (12) *is uniformly globally asymptotically stable for any large delay τ and for any switching signal $q(t)$ if there exist positive definite matrices P and Q such that for all $q \in \{1,2,3\}$, the following LMI holds:*

$$\begin{bmatrix} A_q^T P + PA_q + Q & PF_q \\ * & -Q \end{bmatrix} < 0. \quad (14)$$

Proof. Choose Lyapunov functional $V(x_t) = x^T(t)Px(t) + \int_{t-\tau}^{t} x^T(s)Qx(s)ds$. Taking derivative of $V(x_t)$ along the solution of system (12) leads to

$$\begin{aligned} \dot{V}(x_t) &= x^T(t)\left(A_q^T P + PA_q\right)x(t) + 2x^T(t)PF_q x(t-\tau) \\ &\quad + x^T(t)Qx(t) - x^T(t-\tau)Qx(t-\tau) \\ &= \xi^T \begin{bmatrix} A_q^T P + PA_q + Q & PF_q \\ * & -Q \end{bmatrix} \xi < 0, \end{aligned} \quad (15)$$

where $\xi(t) = \left[x^T(t) \;\; x^T(t-\tau)\right]^T$. Thus $V(x_t) \to 0$ as $t \to +\infty$. Uniformly globally asymptotical stability is guaranteed. □

Corollary 2. *If the controller parameters K_q and K_{iq} ($q \in \{1,2,3\}$) are chosen such that the condition of Theorem 1 is satisfied, then the output of the temperature control system Figure 4 can track the reference signal $u(t)$ asymptotically.*

Theorem 1 gives the sufficient condition to guarantee the stability of system (12) by common Lyapunov functional, while the obtained LMI condition is delay-independent, which is usually conservative. Next we will give LMI condition depending on the delay bound τ to guarantee the stability of system (1).

Theorem 3. *The switched delayed system* (12) *is asymptotically stable if there exist symmetric positive definite matrices* $P = P^T > 0$, $Q = Q^T \geq 0$, *and* $Z = Z^T > 0$, *a symmetric semipositive definite matrix* $X = \left[\begin{smallmatrix} X_{11} & X_{12} \\ X_{12}^T & X_{22} \end{smallmatrix}\right]$, *and any appropriately dimensioned matrices* Y *and* N *such that for all* $q \in \{1, 2, 3\}$, *the following LMIs hold:*

$$\Phi = \begin{bmatrix} \Phi_{11} & \Phi_{12} & \tau A_q^T Z \\ \Phi_{12}^T & \Phi_{22} & \tau F_q^T Z \\ \tau Z A_q & \tau Z F_q & -\tau Z \end{bmatrix} < 0,$$
$$\Psi = \begin{bmatrix} X_{11} & X_{12} & Y \\ X_{12}^T & X_{22} & N \\ Y^T & N^T & Z \end{bmatrix} \geq 0, \tag{16}$$

where

$$\begin{aligned} \Phi_{11} &= PA_q + A_q^T P + Y + Y^T + Q + \tau X_{11}, \\ \Phi_{12} &= PF_q - Y + N^T + \tau X_{12}, \\ \Phi_{22} &= -N - N^T - Q + \tau X_{22}. \end{aligned} \tag{17}$$

Proof. The main argument is based on Theorem 2 in [10]. Choose Lyapunov functional as follows:

$$\begin{aligned} V(x_t) = {} & x^T(t) P x(t) + \int_{t-\tau}^{t} x^T(s) Q x(s)\, ds \\ & + \int_{-\tau}^{0} \int_{t+\theta}^{t} \dot{x}^T(s) Z \dot{x}(s)\, ds\, d\theta. \end{aligned} \tag{18}$$

Combining Theorem 2 in [10] and conditions in Theorem 3, we have that $V(x_t)$ is a common Lyapunov functional for switched delayed system (12). Thus system (12) is asymptotically stable. □

Corollary 4. *If the controller parameters* K_q *and* K_{iq} $(q \in \{1, 2, 3\})$ *are chosen such that the condition of Theorem 3 is satisfied, then the output of the temperature control system Figure 4 can track the reference signal* $u(t)$ *asymptotically.*

4. Experiment

Figure 4 is the illustration of the experiment. By the ascending curve method, the parameters of the temperature system of the thermostated oven are measured as follows: $K_1 = 1$, $T_1 = 420$, $K_2 = 1.4$, $T_2 = 424$, $K_3 = 1.4$, and $T_3 = 426$. The corresponding PI controller parameters are chosen as $K_{p1} = 8.7$, $K_{i1} = 0.30$, $K_{p2} = 9$, $K_{i2} = 0.32$, $K_{p3} = 9.2$, and $K_{i3} = 0.35$.

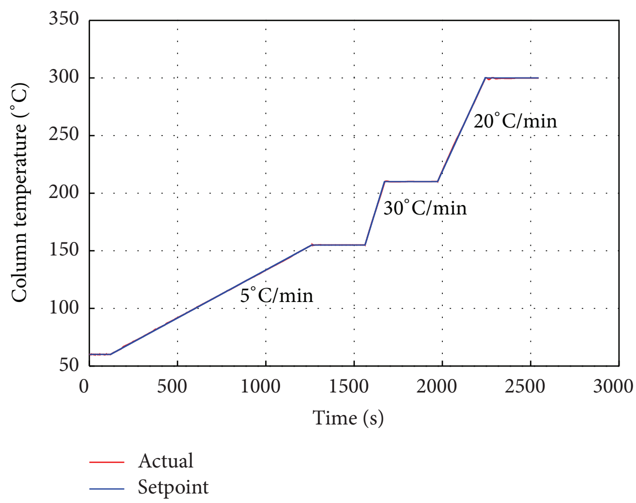

Figure 5: Experiment of the control thermostated oven temperature.

Then we have

$$\begin{gathered} A_1 = \begin{bmatrix} 0 & 1 \\ 0 & -\frac{1}{420} \end{bmatrix}, \qquad F_1 = \begin{bmatrix} 0 & 0 \\ -\frac{1}{1400} & -\frac{29}{1400} \end{bmatrix}, \\ C_1 = -[0.3 \quad 8.7], \\ A_2 = \begin{bmatrix} 0 & 1 \\ 0 & -\frac{1}{424} \end{bmatrix}, \qquad F_2 = \begin{bmatrix} 0 & 0 \\ -\frac{7}{6625} & -\frac{63}{2120} \end{bmatrix}, \\ C_2 = -[0.448 \quad 12.6], \\ A_3 = \begin{bmatrix} 0 & 1 \\ 0 & -\frac{1}{426} \end{bmatrix}, \qquad F_3 = \begin{bmatrix} 0 & 0 \\ -\frac{49}{42600} & -\frac{161}{5325} \end{bmatrix}, \\ C_3 = -[0.49 \quad 12.88]. \end{gathered} \tag{19}$$

Applying Corollary 4, it is concluded that the switched delayed system is stable. Figure 5 shows the practical tracking curve of the temperature control system of the thermostated oven. It can be seen from Figure 5 that the temperature control system can track the reference accurately.

5. Conclusion

In this paper, we address the temperature tracking problem of the gas chromatograph. We model the temperature control system into a switched delayed system. By the common Lyapunov functional technique, stability of the temperature control system is derived and the PI controller parameters can be given based on the LMIs conditions. An experiment is given to illustrate the effectiveness of the proposed criterion.

Conflict of Interests

The authors declare that there is no conflict of interests regarding the publication of this paper.

Acknowledgment

This work was supported by the National Natural Science Foundation of China under Grant nos. 61174058 and 61325014.

References

[1] A. B. Littlewood, *Gas Chromatography: Principles, Techniquesm and Applications*, Academic Press, New York, NY, USA, 1962.

[2] F. J. Santos and M. T. Galceran, "The application of gas chromatography to environmental analysis," *TrAC: Trends in Analytical Chemistry*, vol. 21, no. 9-10, pp. 672–685, 2002.

[3] Y. Liu, N. Grinberg, K. C. Thompson et al., "Evaluation of a C18 hybrid stationary phase using high-temperature chromatography," *Analytica Chimica Acta*, vol. 554, no. 1-2, pp. 144–151, 2005.

[4] D. N. Thanh, S. L. Byung, R. L. Bo, M. L. Dae, and G.-H. Lee, "A multiresidue method for the determination of 109 pesticides in rice using the Quick Easy Cheap Effective Rugged and Safe (QuEChERS) sample preparation method and gas chromatography/mass spectrometry with temperature control and vacuum concentration," *Rapid Communications in Mass Spectrometry*, vol. 21, no. 18, pp. 3115–3122, 2007.

[5] P. A. Smith, "Person-portable gas chromatography: rapid temperature program operation through resistive heating of columns with inherently low thermal mass properties," *Journal of Chromatography A*, vol. 1261, pp. 37–45, 2012.

[6] M. van Deursen, J. Beens, C. A. Cramers, and H.-G. Janssen, "Possibilities and limitations of fast temperature programming as a route towards fast GC," *Journal of High Resolution Chromatography*, vol. 22, no. 9, pp. 509–513, 1999.

[7] M. van Lieshout, R. Derks, H.-G. Janssen, and C. A. Cramers, "Fast capillary gas chromatography: comparison of different approaches," *Journal of High Resolution Chromatography*, vol. 21, no. 11, pp. 583–586, 1998.

[8] X.-M. Sun, J. Zhao, and D. J. Hill, "Stability and L2-gain analysis for switched delay systems: a delay-dependent method," *Automatica*, vol. 42, no. 10, pp. 1769–1774, 2006.

[9] J. Hale and S. V. Lunel, *Introduction to Functional Differential Equations*, Springer, New York, NY, USA, 1993.

[10] M. Wu, Y. He, J.-H. She, and G.-P. Liu, "Delay-dependent criteria for robust stability of time-varying delay systems," *Automatica*, vol. 40, no. 8, pp. 1435–1439, 2004.